DEVELOPMENT OF A NEW HIGH PERFORMANCE SYNTHETIC FIBER FOR CONCRETE REINFORCEMENT

by

Shannon O'Connell

Submitted in partial fulfilment of the requirements
for the degree of Master of Applied Science

at

Dalhousie University
Halifax, Nova Scotia
July 2011

DALHOUSIE UNIVERSITY

DEPARTMENT OF CIVIL AND RESOURCE ENGINEERING

The undersigned hereby certify that they have read and recommend to the Faculty of Graduate Studies for acceptance a thesis entitled “Development of a New High Performance Synthetic Fiber for Concrete Reinforcement” by Shannon O’Connell in partial fulfilment of the requirements for the degree of Master of Applied Science.

Dated: July 5, 2011

Supervisor: _____

Readers: _____

_____

_____

DALHOUSIE UNIVERSITY

DATE: July 5, 2011

AUTHOR: Shannon O'Connell

TITLE: Development of a New High Performance Synthetic Fiber for Concrete Reinforcement

DEPARTMENT OR SCHOOL: Department of Civil and Resource Engineering

DEGREE: MASc CONVOCATION: October YEAR: 2011

_____

Signature of Author

For Mom & Mel

TABLE OF CONTENTS

LIST OF TABLES

LIST OF FIGURES

ABSTRACT

The research objective was to develop a new competitively priced, high strength macrosynthetic fiber for concrete reinforcement. Mechanical bond properties were examined through aligned and inclined pullout testing. Variables involved in optimizing these properties included materials, fiber cross section, and other changes made through manufacturing processes. In addition to extensive pullout testing, improvements to fiber properties were explored through tensile testing, creep testing, and fiber performance in concrete mixtures. Practical considerations were also made, such as manufacturing processes, cost, and workability. Properties of synthetic microfibers were also considered for use in engineered cementitious composites. Synthetic macrofibers containing PVDF demonstrated high bond strength in pullout testing. Fibers demonstrating the highest performance in FRC testing were those with additional mechanical anchorage such as fibrillation or embossment. EVA as an additive did not exhibit increased interfacial bond, but further research was recommended. Further research on deformed fibers containing PVDF was also recommended.

LIST OF SYMBOLS AND ABBREVIATIONS

ACI – America Concrete Institute

AFMA – American Fiber Manufacturers Association

AFT – Atlantic Fiber Technologies Limited

ASTM – American Society for Testing and Materials

CH – Calcium hydroxide

CSH – Calcium silicate hydrate

ECC – Engineered cementitious composite

EVA – Ethylene vinyl acetate

FRC – Fiber reinforced concrete

HDPE – High density polyethylene

ITZ – Interfacial transition zone

LVDT – Linear variable displacement transducer

MAH – Melaic anhydride

PDDA – Performance driven design approach

PP – Polypropylene

PVA – Polyvinyl alcohol

PVC – Polyvinyl chloride

PVDF – Poly(vinylidene fluoride)

RSI – Residual strength index

SCC – Self-compacting concrete

SOG – Slab on grade

UHPFRC – Ultra-high-performance fiber reinforced composites

W/C – Water cement ratio

WWF – welded wire fabric

A = Cross sectional area of the filament (mm^2)

a_o = Initial flaw size distribution

b = Sample width (mm)

d = Sample height (mm)

d_{eq} = Equivalent fiber diameter (mm)

d_f = Fiber diameter (mm)

E_c = Elastic modulus of composite (GPa)

E_f = Elastic modulus of fiber (GPa)

E_m = Elastic modulus of matrix (GPa)

F = Applied force (N)

f = Snubbing friction coefficient

f_1 = First peak strength (MPa)

f_p = Peak strength (MPa)

f_{150}^D = Residual strength at net deflection of L/150 (MPa)

f_{600}^D= Residual strength at net deflection of L/600 (MPa)

f' = Apparent fiber strength reduction factor

$\hat{f}$ = Apparent fiber strength reduction factor normalized with respect to matrix strength

G_c = Shear modulus of composite (GPa)

G_d = Chemical bond energy (J/m^2)

K_m = Fracture toughness of matrix ($MPa\sqrt{m}$)

L = Span length (mm)

l_a = Minimum allowable fiber length based on desired aspect ratio (mm)

l_c = Critical fiber length (mm)

l_e = Embedded length of fiber (mm)

l_f = Fiber length (mm)

l_1 = Pullout length at given incline angle (mm)

P = Pullout force (N)

P_a = Maximum load before load drop, illustrated in Figure 3.11, (N)

P_{avg} = Average load corresponding to 0.5, 0.75, 1.00 and 1.25 mm deflection (N)

P_b = Load value immediately after load drop, illustrated in Figure 3.11 (N)

P_{crit} = Critical load at which fiber will rupture, found using a tensile test performed at the same speed as the pullout test (N)

P_{max} = Maximum pullout load (N)

P_P = Peak load (kN)

P_T = Maximum tensile load (N)

P_{600}^{D} = Residual load at net deflection of L/600 (kN)

P_{150}^{D} = Residual load at net deflection of L/150 (kN)

P_0 = Peak pullout load on an incline angle of 0° (N)

P_1 = First peak load (kN)

$\widehat{P}$ = Normalized pullout load per unit pullout length (N)

P_ϕ = Predicted peak pullout load on given incline angle (N)

Q = Coefficient used in Q test to determine outliers in a data set

Q_c = Critical value of Q beyond which outliers are rejected

Q_{exp} = Experimental value of Q to compare to Q_{crit} in Q test

R = Reaction force (N)

RSI = Residual strength index (MPa)

R^* = Effective radius of matrix cylinder containing fiber (mm)

r = Fiber radius (mm)

S = Fiber slip (mm)

S_v = Shear force (N)

t = Fiber thickness (mm)

T_{150}^{D}= Toughness, taken as area under load vs. deflection curve between a net deflection of 0 and L/150 (Joules)

U_P = Pullout energy (N-mm)

V_f = Fiber fraction (% or kg/m^3)

V_m = Volume fraction of matrix

w = Fiber width (mm)

β = Slip hardening parameter

δ = Displacement of fiber from initial center line (mm)

δ_a = Initial distance between two markers, as illustrated in Figure 2.22 (mm)

δ_b = Distance travelling marker moved over time, as illustrated in Figure 2.22 (mm)

δ_P = Net deflection at peak load (mm)

δ_1 = Net deflection at first peak load (mm)

$\left(\frac{\Delta P}{\Delta S_i}\right)$ = Initial slope of pullout load vs. slip curve as S' approaches 0

ϵ = Fiber strain at present load, taken from tensile test conducted at same speed (mm/mm)

ϵ_{10} = Strain corresponding to σ_{10} (mm/mm)

ϵ_{30} = Strain corresponding to σ_{30} (mm/mm)

η_τ = Fiber efficiency (%)

ϕ = Inclined angle of fiber pullout (radians)

σ_a = Apparent fiber strength, determined from the load at which fibers rupture during inclined pullout testing (MPa)

σ_f = tensile strength of fiber (MPa)

σ_{fu} = Ultimate tensile strength of fiber (MPa)

σ_{fu}^{n} = Nominal fiber tensile strength, determined through aligned pullout testing (MPa)

σ_{10} = Stress at 10% of the ultimate tensile stress (MPa)

σ_{30} = Stress at 30% of the ultimate tensile stress (MPa)

τ = Elastic shear stress at interface (MPa)

τ_c = Critical bond strength (MPa)

τ_{fu} = Interfacial bond strength (MPa)

τ_{max} = Maximum interfacial bond strength, determined through pullout testing (MPa)

τ_o = Interfacial frictional stress at the onset of slip (MPa)

τ_s = Chemical bond strength stress at the onset of slip (MPa)

ACKNOWLEDGEMENTS

First and foremost, thank you to Dr. Dean Forgeron for his supervision and support throughout this research. Thank you to Atlantic Fiber Technologies for financial support as well as the use of their facilities. Thank you to my supervisory committee, Dr. John Newhook and Dr. George Jarjoura. Thank you to all the faculty and staff of the Civil & Resource Engineering Department, especially Tanya Timmins and Shelley Parker.

Thank you to my family and friends for tolerating my incessant excuses of “but I’m so busy” throughout my schooling. After 21 years of school, you can have all of my attention now.

Thank you especially to my mother, Christine, for life, guidance and good genes. Thank you also to my sister Melanie. You two are the inspiration for all of my achievements.

CHAPTER 1 INTRODUCTION

1.1 FIBER REINFORCED CONCRETE

Concrete is a brittle material with low tensile strength, known to crack under low tensile strains. To overcome this limitation, concrete has traditionally been reinforced, commonly with steel rebar, to increase its tensile strength capacity. Over the past four decades the use of fiber reinforced concrete (FRC) and engineered cementitious composites (ECC) have been expanding steadily. Fiber reinforced concrete commonly uses hydraulic cement, water, fine and coarse aggregates, and short, discrete, randomly distributed fibers. ECC commonly uses the same ingredients, with the exception of coarse aggregate. A wide variety of fibers have been developed with varying materials, lengths, and cross sections.

Although FRC has been used in practice by the construction community since the 1980's, uses are often limited to non-structural applications, partially due to limited performance and lack of complete design guidelines (Li, Wang, & Wu, 2001). Although the fibers cannot yet directly replace rebar, and only cause a modest increase in strength, the fibers can be used to control cracking behavior, as well as improve impact resistance, toughness and other mechanical properties.

Fibers increase mechanical properties of FRC by intersecting the cracks and transferring load across them through the pullout process. Pullout resistance is fundamental to fiber performance in FRC. Steel fibers in FRC use mechanical anchorage, such as hooked ends, to resist pullout, whereas synthetic fibers can use materials that form a chemical bond with the matrix itself. Mineral admixtures such as fly ash and silica fume can improve fiber-matrix bond strength by changing the matrix structure, and are often used in conjunction with fibers to create "high performance" concrete.

Typical fibers used in FRC are discrete and randomly distributed. These fibers may be further classified into macro or microfibers, based on the fiber aspect ratios. Aspect

ratio is defined as the fiber length divided by the fiber diameter. Microfibers are typically less than 0.5 mm in diameter, and can range from 1 to 50 mm in length. Microfibers are primarily used to reduce plastic drying shrinkage, and are commonly used in ECC. This is because microfibers are known to intercept and arrest microcracks during early stages of concrete curing and to provide high early tensile strength. Microfibers are typically added at low dosage volumes, between 0.08 and 0.2%. However newer synthetic microfibers are added at increasing volumes to provide mechanical improvements in ECC.

Macrofibers have larger dimensions and are typically produced in lengths ranging from 12 to 60 mm. Macrofibers are primarily used in FRC to enhance the post cracking behavior and are typically added at higher dosage volumes, between 0.2 and 2%. Macrofibers control larger cracks caused by dynamic loads, impact, or fatigue (Banthia & Mindess, 1995), by bridging the cracks and resisting pullout. Ideally, macrofibers will slip shortly before rupture, and thus absorb a maximum amount of energy in the process. Several varieties of fibers may be combined to utilize the benefits of both macro and microfibers. These are known as hybrid FRC mixtures.

The first clear example of a fiber reinforced building material was the use of straw to reinforce clay bricks 3000 years ago. Throughout the past four decades steel has been the primary fiber material used for concrete reinforcement. From 1950 - 1970 commonly used fibers changed from primarily smooth steel and glass to deformed steel and polymeric. At the time it was thought that fibers could not replace rebar and only added a modest increase to strength. The fibers were primarily used to control the development of cracks.

Steel fibers have been used extensively due to their high modulus and availability. Steel fibers today can be used as the sole means of reinforcement in slabs on grade, precast concrete, shotcrete, and even in elevated slabs. Because of this, the majority of existing research on FRC has been focused on steel fibers. The result of such extensive research is that steel fibers have been integrated into structural design codes.

Synthetic fibers primarily consist of polymeric fibers. They offer several benefits over steel fibers, mainly that they are essentially corrosion-free. They are commonly used in slabs on grade, shotcrete, and precast architectural structures as they do not leave surface stains from rust. Synthetic fibers have also been used in elevated metal composite slabs and "steel-free" bridge decks, for example, the Salmon River Bridge in Nova Scotia (Newhook & Mufti, 1996). Synthetic fibers are cost competitive when compared to steel fibers and can reduce equipment wear due to the material flexibility. Due to the number of polymeric materials that exist, synthetic fibers can be customized for a variety of applications.

Fiber-matrix interfacial bond is considered the governing factor in improving the mechanical properties of synthetic fiber reinforced concrete. Bond components are classified as physical or chemical adhesion, friction, mechanical anchorage or fiber-to-fiber interlock (Naaman & Najm, 1991). In addition to varying materials or increasing fiber cross sections to take advantage of adhesion, manufacturing innovations include fibrillation and embossed surfaces to improve the fiber-matrix bond.

1.2 PROJECT OBJECTIVES

This research is part of a larger program aimed at developing a new competitively priced high strength and high stiffness synthetic macrofiber for concrete. The research goal is to produce a new fiber exceeding the properties of existing commercial synthetic fibers, thus expanding the use of synthetic fibers in structural applications. Additionally, properties of synthetic microfibers will also be investigated.

More specifically, this research focuses on understanding the behavior of synthetic fibers in pullout testing. In addition to the extensive pullout testing program, improvements to fiber properties are explored through tensile testing, fiber performance in flexural FRC, and creep testing. Practical considerations are also made, such as manufacturing processes, costs, and workability in concrete.

The mechanical properties of fiber-matrix interfacial bond of synthetic fibers are examined through pullout testing. The variables involved in optimizing these properties include the material or combination of materials used, size and cross section of the fiber, and other changes that can be made throughout the manufacturing process. Effects of these variables on fiber properties are discussed. Specifically, the mechanics of the additional bond created due to a change in particular properties, such as fiber stretch ratio or the addition of PVDF to the fiber, are discussed. A variety of synthetic materials were tested to compare properties and to narrow the search for a new fiber.

CHAPTER 2 BACKGROUND

In order to investigate fiber optimization, it was necessary to understand the developments in FRC throughout history. This chapter will provide the necessary background information to understand this research, including advancements in fibers and synthetic fiber applications. Additionally, in order to test synthetic fibers in pullout it was necessary to develop appropriate test methods, as standards do not currently exist for single fiber pullout testing. Consequently, test methods used for fiber pullout in previous literature will be compared and discussed. Background information on test methods for synthetic fibers in tensile testing, tensile creep testing, and FRC performance testing will also be presented.

2.1 STEEL FIBER REINFORCED CONCRETE

In 1964, Romualdi and Mandel investigated the resulting improvement in concrete's tensile strength by the addition of short lengths of steel wire, uniformly distributed through the matrix. This was one of the first investigations into steel FRC. Since then, the increase caused by steel fibers to the tensile strength of concrete has been proven repeatedly through continued research. Steel fibers have been found to decrease crack spacing and crack width (Vandewalle, 2000), increase concrete's performance under dynamic loads (Katzensteiner, Mindess, Fliatrault, & Banthia, 1994), enhance fatigue resistance (Ramakrishnan, Gollapudi, & Zellers, 1987), and can even successfully replace shear stirrups in beams (Altoubat, Yazdanbakhsh, & Rieder, 2009).

High strength concrete is often used in high rise structures, where the columns on the lower floors may be too large. High strength concrete allows for a decrease in the required size of these columns and therefore offers an increase in floor space. However, high strength concrete, while stronger in compression, is less ductile than weaker concrete (Tasdemir, Tasdemir, Lydon, & Barr, 1996). As discrete steel fibers have been shown to increase ductility (Hsu & Hsu, 1994), steel fibers can be added to high strength

concrete to maintain the increase in compressive strength without sacrificing ductility.

Steel fibers have also been used in slabs to effectively replace welded wire fabric (WWF) and rebar. This not only decreases the cost of labor to install the WWF reinforcement, but also decreases the required slab thickness by negating the minimum cover requirements and significantly improving mechanical properties. When used along with rebar, steel fibers minimize the development of corrosion in concrete members, both through minimizing the formation of cracks (where chlorides are allowed to enter and reach the reinforcement), and through having discrete reinforcement (corrosion is not passed through the member, but ends with the exposed fiber).

While smooth, rounded steel fibers have been proven to benefit concrete, they do not demonstrate significant bond strength. To overcome this, hooked end steel fibers are commonly used. The end hook creates an additional mechanical bond to the matrix. Markovich, van Mier and Walraven in 2001 described the phases a hooked end steel fiber undergoes during pullout. Initially, there is a short phase of debonding between the fiber and the surrounding matrix. This is followed by a longer phase of plastic deformation, as illustrated in Figure 2.1. As shown in Figure 2.1 a and b, the bent portion of the fiber is undergoing plastic deformation. Figure 2.1 c shows the portion labeled 2 being bent again at the location that portion 1 had initially been. Figure 2.1 d shows the fiber having finally been straightened, and is then completely pulled out of the hole formed in the matrix.

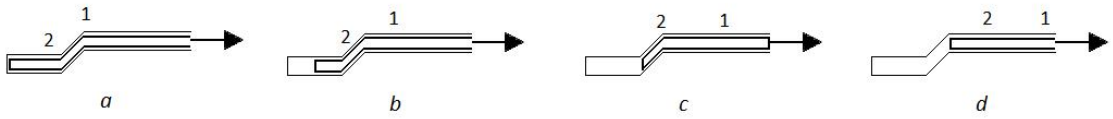

Figure 2.1 - Stages in the plastic deformation of a steel fiber hook (Markovich, van Mier, & Walraven, 2001)

Similarly, other types of deformed steel fibers have been used to create additional mechanical bond, such as crimped fibers, or “bow ties” which have flattened ends. Figure 2.2 illustrates various shapes of deformed steel fibers available.

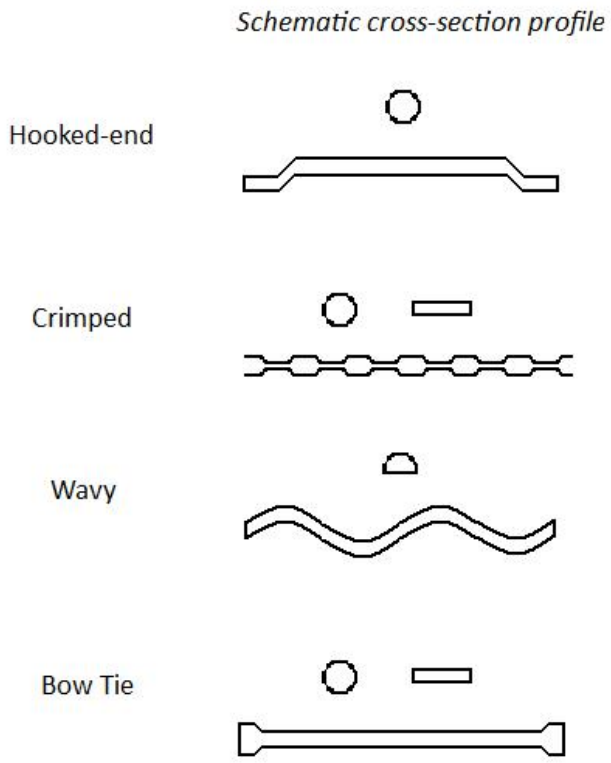

Figure 2.2 - Typical Deformed Steel Fibers (Bentur & Mindess, 1990)

Steel fibers have a high tensile strength and modulus of elasticity, typically around 1160 MPa and 210 GPa, respectively (Bekaert, 2005). Carbon and glass fibers have ultimate tensile strengths of 2555 MPa, and 2480 MPa, respectively, however their dimensions are considerably smaller and their length must be short to prevent balling during concrete mixing. These tensile strength values vary with manufacturing methods and purity of composition (Hua & Zhou, 2009). Although glass and carbon fibers have extremely high tensile strengths, the high cost of these materials is typically prohibitive, making steel the preferred option. Additionally, glass fibers can suffer deterioration in

the extremely basic environment in concrete, even treated glass fibers. Steel fibers are also ductile, making them more useful for increasing the ductility of concrete when compared with brittle materials such as glass fibers.

Some standards have been updated to reflect the research continuously supporting the effectiveness of steel fibers as reinforcement in concrete. ACI 318-08, Section 11.4.6.1, allows for the exemption of minimum shear reinforcement for specific beams, including those constructed using steel fibers (ACI Committee 318, 2008). Also, the ASTM standard "ASTM 820-06 Standard Specification for Steel Fibers for Fiber-Reinforced Concrete" contains detailed specifications for steel fibers used in fiber reinforced concrete.

While steel fibers are successful at concrete reinforcement, there is little room left for advancement. This invites innovation for other materials with properties that can be tailored for specific applications, such as synthetic fibers.

2.2 SYNTHETIC FIBER REINFORCED CONCRETE

Synthetic fiber reinforced concrete offers many of the benefits of steel FRC, including decreased labor costs for installation, decreased slab thicknesses, and increased ductility. Synthetic FRC is more corrosion resistant than steel FRC because synthetic fibers do not corrode when exposed to chlorides, oxygen and water. This makes synthetic fibers desirable for architectural applications, as they do not rust if exposed at the concrete surface. However certain synthetic materials could corrode in the alkali environment of concrete throughout the life of the composite. Therefore, the lifespan of the material is one consideration in the development of a new synthetic fiber.

Synthetic fibers are polymeric and are commonly categorized into low and high modulus fibers, as well as macro and microfibers. Because this class of fibers includes so many different materials and manufacturing methods, the properties of synthetic fibers vary greatly. Synthetic fibers such as polypropylene or nylon typically have a low modulus of

elasticity, and contribute primarily to reinforcing the concrete under dynamic loads, as well as improving crack control, ductility and material toughness (Bentur & Mindess, 1990). Conversely, fibers such as carbon, polyvinyl alcohol (PVA) and asbestos have a higher modulus of elasticity, and contribute to the strength and stiffness of the concrete when added at high volume fractions, up to 4% (Manolis, Gareis, Tsonos, & Neal, 1997). Figure 2.3 shows three types of synthetic fibers of varying materials and shapes.

Figure 2.3 - Three varieties of synthetic fibers; (a) blended polypropylene, polyethylene fibrillated macrofibers, (b) straight polyolefin macrofibers, and (c) polyester microfibers

The variety of properties of synthetic fibers allows them to be tailored to specific applications by varying the cross sections, materials, and manufacturing methods. Because of this, there is currently a rush for continued improvement in the synthetic fiber industry, and therefore many recent advancements are proprietary. As a result of the variety in developments, it has been difficult for industry standards to specifically address design issues without exempting certain materials. Therefore, the development of useful North American standards for synthetic fibers is still ongoing, but has growing demand (Francis, 2005).

While synthetic fibers such as polypropylene, polyethylene, nylon, or PVA are readily available commercially, there are also fibers containing combinations of materials, for

example blended polypropylene/polyethylene fibers. These materials are blended together from individual resins during the manufacturing process, and fibrillate during mixing. Fiber fibrillation occurs when the materials partially split to form fibrils, increasing surface area exposed to the matrix and thus increasing bond strength through mechanical anchorage (Trottier & Mahoney, 2001). Combinations of materials can be used to optimize both cost and mechanical properties. Polypropylene and polyethylene also blend effectively because they have similar melting points, which allows them to be formed together from resins. However many other synthetic materials with differing melting points cannot be effectively blended together without resulting in degrading one component or clogging the manufacturing line by not fully melting a material.

While many synthetic fibers have a lower modulus than steel fibers, they are more effective at increasing the ductility of concrete, and thus are more desirable for certain applications. These applications will be discussed in Section 2.2.2.

2.2.1 Synthetic Fiber Manufacturing Processes

The primary production method for synthetic fibers is extrusion. The fiber material begins as beads of resin, as shown in Figure 2.4. The resin is converted to a viscous fluid through melting or being dissolved in a solvent, and is forced through a spinneret and formed into continuous filaments. For melt extrusion, the material is driven through a heated chamber by a screw. Temperatures and speeds throughout the screw chamber are varied based on the material and the desired properties of the extruded filaments. A gear pump is commonly used to control the pressure on the material as it reaches the spinneret. Varying the pump speeds can be used to vary the cross sectional dimensions of the resulting fibers.

Figure 2.4 - Polyethylene resin

The spinneret contains many small holes which the material passes through. The spinneret can have between one or several hundred holes. These holes can vary in cross section and depth, which can be used to tailor the size and geometric shape of the resulting fibers as well as the number of fibers. It is important that the spinneret be free of defects as these defects can show in the surface of the final fiber product. Because of this, spinnerets are made of high strength, corrosion free materials and are cleaned regularly. Figure 2.5 shows a spinneret used in the production of polyolefin fibers.

Figure 2.5 - Spinneret extruding polyolefin material

From the spinneret the filaments are a semi-solid polymer, and become a solid through a process called spinning. There are four methods of spinning; wet spinning, dry spinning, gel spinning, and melt spinning. These methods vary in economics and materials used.

Wet spinning uses materials that have been dissolved in a solvent. The spinneret is immersed in a chemical bath and the filaments precipitate from the solution and form a solid as they are extruded. Wet spinning is commonly used for acrylic, aramid and spandex fibers (American Fiber Manufacturers Association , 2011).

Dry spinning is similar to wet spinning, in that it uses materials that have been dissolved in solvents, however the spinneret is not immersed in a chemical solution. Instead the extruded filaments solidify by being passed through a stream of air or inert gas. Dry spinning is commonly used for acrylic, spandex or acetate fibers.

Gel spinning is often the most expensive method used in fiber extrusion. During gel spinning the polymer is not in a true liquid state, but bound together in liquid crystal form. The liquid crystals become aligned with a high degree of orientation, which gives the resulting filament increased tensile strengths (AFMA, 2011). Gel spinning is used to obtain high strength fibers such as high strength polyethylene, aramid, or PVA.

Melt spinning is a more common method and is used for materials that are melted before passing through the spinneret. The material then solidifies by cooling through air or a water bath. Melt spinning is commonly used for polyester, polyolefin, or nylon fibers. Recent advancements indicate that with proper material selection, tensile strengths approaching those reached using gel spinning are attainable using melt spinning.

The fibers developed for this project were produced using melt spinning primarily due to the economics of the fibers produced. A schematic of the extrusion line is presented in Figure 2.6. Figure 2.7 shows filaments passing shortly through air, then through a water bath after emerging from the spinneret in a melt spinning process.

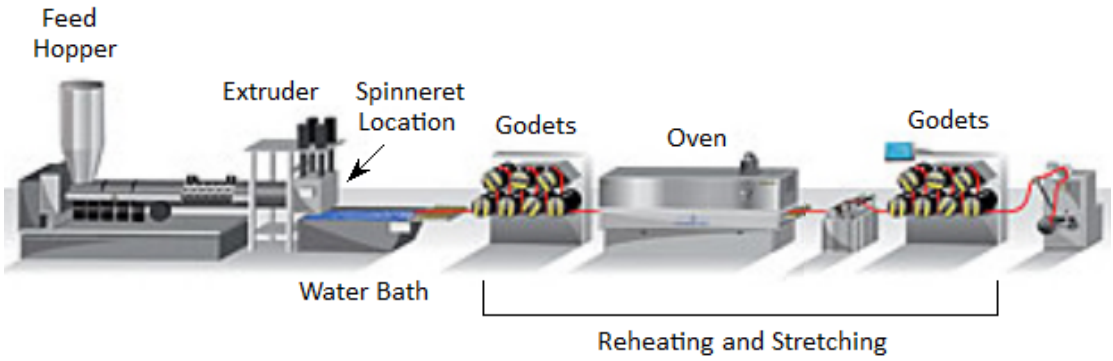

Figure 2.6 - Extrusion line using melt spinning process (Reimotec, 2011)

Figure 2.7 - Filament extrusion using melt spinning

The continuous filaments produced from the spinning process then pass through spindles and ovens where they are drawn and reheated. The fibers can be heated in air or water within the ovens. Figure 2.8 shows the spindles, known as godets, which are located on either side of the oven. The speed between the godets can be varied to stretch the filaments within the oven. The ratio between the final and initial length of the filaments is called the stretch ratio, or draw ratio, and is determined by the godet

speeds. This process gives the filaments a high degree of uniaxial molecular orientation, and thus increased tensile strength (Lin & Argon, 1994). Filaments can then pass through an additional oven without being stretched. This is called annealing and is intended to reduce the residual internal stresses caused by stretching.

Figure 2.8 - Godets used to stretch filaments on an extrusion line

A balance is often sought between maximizing the fiber stretch ratio without rupturing the filaments on the extrusion line. If a fiber ruptures during production the entire manufacturing line has to be stopped and restrung if the individual filament is unable to be restrung alone. This is unacceptable for efficient and cost effective manufacturing, as it can take hours to properly restring a large extrusion line. During this project the researchers had the benefit of using a smaller “experimental line”, developed for trials of newly developed fibers.

When the filaments exit the extrusion line they are often wound on to spindles or bobbins for future use. For use in concrete, fibers must be cut to specific lengths, which vary depending on the application. A fiber cutter unwinds the filaments from the bobbin and cuts them to a specified length by varying the blade distances. The cut fibers are then collected on a conveyor and bagged for use in concrete mixing.

2.2.2 Current applications of Synthetic Fiber Reinforced Concrete

Slab on Grade

The use of synthetic fibers in slab on grade (SOG) applications has been thoroughly researched and practiced regularly for over a decade. Synthetic microfibers have been shown to reduce up to 90% of plastic shrinkage cracks, which form while the concrete is in the early plastic stage of curing. As plastic shrinkage cracks can easily develop into macrocracks throughout the life of the composite, fibers can increase the service life. Synthetic fibers have also been shown to significantly decrease drying shrinkage cracking in concrete SOG's (Senthilkumar & Natesan, 2004).

External applications such as sidewalks or pavement are ideal for synthetic FRC because they can resist cracking caused by humidity and temperature variations, in addition to resisting corrosion from chlorides that would commonly be used to deice pavements (Costa & Appleton, 1999).

Synthetic FRC is excellent for use in indoor SOG's such as those in industrial applications. Synthetic macrofibers have been used to reduce slab thickness and have been shown to successfully replace reinforcement and steel fibers in heavy load applications (Trottier, Mahoney, & Forgeron, 2002). Synthetic fibers can resist impact loading and fatigue caused by heavy industrial equipment travelling repeatedly across the slabs. Thus synthetic FRC increases the service life and decreases required maintenance to the structure. This offers a life cycle cost saving in addition to the material and labor cost savings often associated with FRC (Francis, 2005).

Marine Structures

Synthetic fibers also offer improved performance in marine applications, where concrete would be regularly exposed to salt-water environments. The main cause of distress in marine structures is reinforcement corrosion due to chloride attack (Costa & Appleton, 1999). Synthetic fibers reduce surface cracking and thus reduce corrosion caused by chlorides penetrating the structure through the cracks. Synthetic macrofibers

reduce skin reinforcement requirements, thus moving the reinforcement further from the surface and reducing cracking potential. This results in an increase in service life of marine structures such as wharfs and boat ramps when compared to steel reinforcement.

Shotcrete

Synthetic fibers are used regularly in shotcrete applications, such as tunnel linings for mining. Shotcrete is sprayed from a hose, as pictured in Figure 2.9, directly on to tunnel walls using a portable on-site mixer and pump.

In mining applications, large deflections must be allowed due to high local deformations from earth pressure or water leakage. Synthetic FRC is most suitable for this application because synthetic fibers can allow high strains without rupturing (Won, Park, Lee, Jang, & Kim, 2009). Synthetic fibers can be easier on equipment such as hoses when compared with steel fibers as they are less sharp and more flexible.

Synthetic fibers are an alternative to welded wire mesh to reinforce shotcrete in tunnel linings (Trottier, Mahoney, & Forgeron, 2002). This decreases labor and material costs as no mesh installation is required and cover requirements are negated. More importantly, potential voids behind the mesh are eliminated, which decreases potential spalling and therefore increases safety (Won, Park, Lee, Jang, & Kim, 2009)

Figure 2.9 - Operation of a shotcrete hose

In addition to high local deformations, mining applications require resistance to high local loads. Because synthetic fibers are load rate dependent (meaning they exhibit a higher ultimate tensile strength at higher loading rates), they have been shown to improve resistance to impact loads better than steel fibers (Manolis, Gareis, Tsonos, & Neal, 1997). This is particularly useful in mining applications where rock bursts may occur regularly. Increased impact resistance is also of significant benefit to structures located in earthquake zones.

Engineered Cementitious Composites

Synthetic fibers are also commonly used in ECCs. ECCs such as ultra-high-performance fiber reinforced composites (UHPFRC) can have compressive strengths ranging from 80 MPa to 200 MPa and beyond (Graybeal & Davis, 2008). UHPFRC also has excellent mechanical properties such as high tensile strength, strain hardening, and dense microstructure, leading to low permeability. These qualities make UHPFRC useful for rehabilitating existing structures (Habel, Denarie, & Bruhwiler, 2007).

UHPFRCs and ECCs are often used for thin walled panels where steel rebar may either not fit or cannot be placed properly due to the size and shape of the structural member. ECCs are also commonly used in precast panels due to the improvements in crack control, and decreases in labor requirements and member sizes. Some specific precast applications include structural elements, thin walled panels, septic tanks, catch basins, crash barriers, and concrete pipelines (Pelisser, Barros, Lebre, & Caldras, 2010).

Steel Free Bridge Decks – The Salmon River Bridge

Much research was performed throughout the 1980's and 1990's on Canadian requirements for the design of bridge decks. It was found that the primary cause of failure and maintenance of bridge decks in Canada was due to the corrosion of steel reinforcement. This was attributed to the repetitive freeze-thaw cycles and frequent use of deicing salts throughout Canada. Research began to focus on the design of a steel free bridge deck that would take advantage of the internal arching action of concrete in

bridge decks and eliminate the need for internal reinforcement. The result of this was the design described by Newhook and Mufti in 1996, a steel free bridge deck containing synthetic macrofibers as the only internal reinforcement, working compositely with external steel strapping. The design concept is illustrated in Figure 2.10.

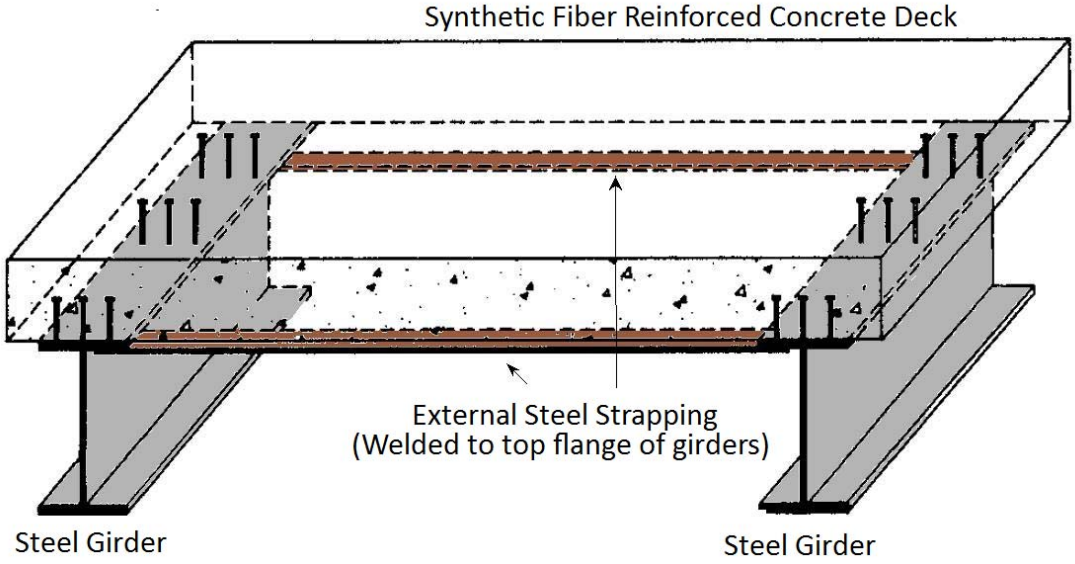

Figure 2.10 - Synthetic fiber reinforced concrete bridge deck design concept (after Newhook & Mufti, 1996)

In 1995 a two span bridge, with one span using the steel free bridge deck design, was constructed for use in Nova Scotia. This was the Salmon River Bridge, and was the first of its kind in the world (Newhook & Gaudet, 2006). The synthetic fibers used in the bridge were 32 mm long, homopolymer, twisted and fibrillated. The bridge was constructed and opened in December 1995 for use to highway traffic including heavy truck traffic in a location where it would be regularly exposed to deicing salts. Regular monitoring occurred throughout the first several years of the bridge life.

Figure 2.11 - View of the underside of the Salmon River steel-free bridge deck (Newhook & Gaudet, 2006)

In 2006, Newhook and Gaudet published a 10 year review of the field performance of the Salmon River Bridge. It was found that longitudinal and transverse cracks visible on the underside of the bridge deck remained largely unchanged since they were observed during the first six months of the bridge life. By measuring crack widths it was concluded that the bridge had significant fatigue life remaining before reaching the unstable cracking zone (Newhook & Gaudet, 2006). Additional strain measurements further confirmed that the superstructure response was virtually unchanged after ten years. It was concluded that this design can be expected to satisfy the 100 year design life required by the Canadian Highway Bridge Design Code, with minimal maintenance. This design has since been used in several bridges across Canada.

2.2.3 Performance-Driven Design-Approach (PDDA)

Li, *et al*. in 2001 discussed the performance-driven design-approach (PDDA) as illustrated in Figure 2.12. This design philosophy takes the approach that links exist between structural performance, composite behavior and material microstructure.

Micromechanics is emphasized as the link between mechanical properties and the microstructure of materials (Li, Wang, & Wu, 2001). Through this method, a specific application is considered, and the desired mechanical properties of ECC are selected based on the application. From there, analytical models focusing on micromechanics can be of great use. Microstructural tailoring is the next step, where the tailoring of synthetic fiber properties is of significant importance. Processing is the final consideration in this approach.

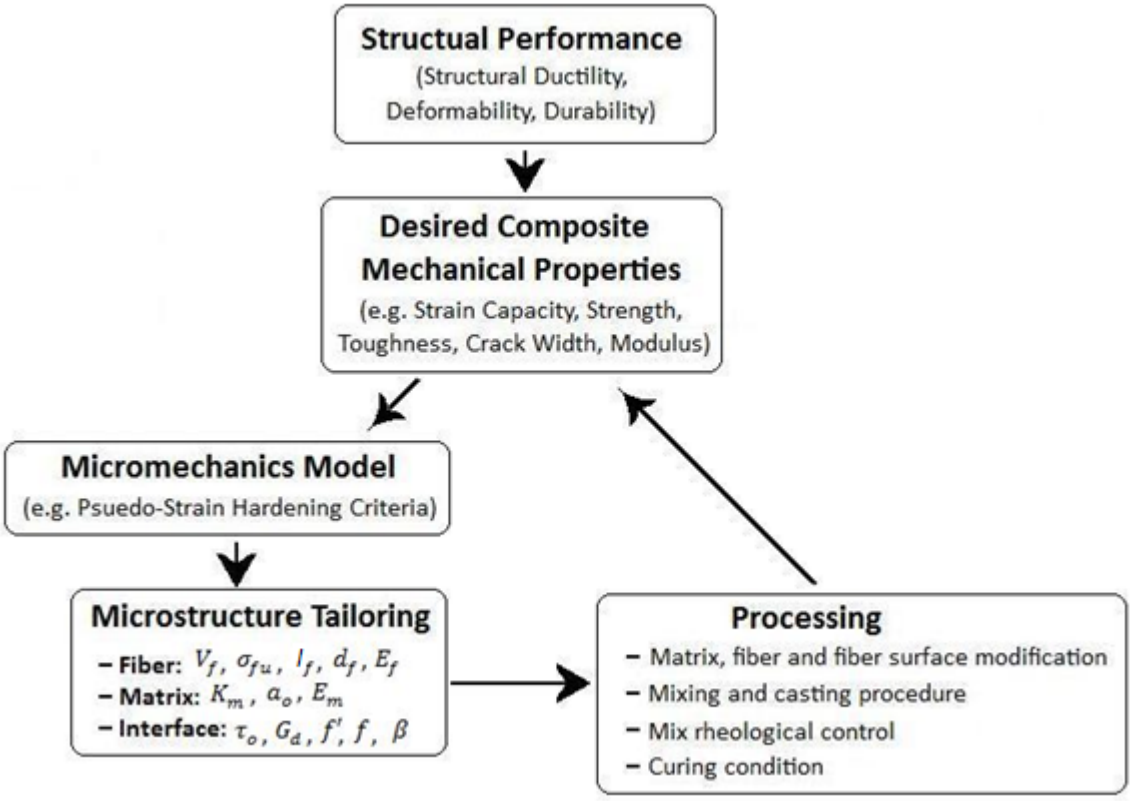

Figure 2.12 - Performance-driven design-approach for a synthetic fiber reinforced engineered cementitious composite (after Li, Wang, & Wu, 2001)

Where,

V_f = Fiber fraction (% or kg/m^3)

σ_{fu} = Ultimate tensile strength of fiber (MPa)

l_f = Fiber length (mm)

d_f = Fiber diameter (mm)

E_f = Elastic Modulus of fiber (GPa)

K_m = Fracture toughness of matrix (MPa$\sqrt{m}$)

a_o = Initial flaw size distribution

E_m = Elastic modulus of matrix (GPa)

τ_o = Interfacial frictional stress (MPa)

G_d = Chemical bond energy (J/m^2)

f' = Apparent fiber strength reduction factor

f = Snubbing friction coefficient

β = Slip hardening parameter

The greater objective of this research is to improve bond strength through synthetic fiber tailoring, based on the fiber cross section and desired length. This is a crucial step in PDDA. The variables defined for Figure 2.12, with the exception of those regarding the matrix properties, can be tailored using properties of synthetic fibers as discussed throughout Section 2.2, particularly within the manufacturing processes. Additionally, micromechanical models can be formed from parameters derived from single fiber pullout testing.

2.3 FIBER TENSILE TEST

Tensile testing is performed on synthetic fibers to determine their ultimate tensile strength and elastic modulus. These are primary properties used for the comparison of different fiber types and for marketing of commercial fibers.

ASTM D683-08 is intended to be used to determine the tensile properties of plastics by stretching dog bone shaped specimens to rupture. However, because of the molecular alignment and varying parameters associated with the manufacturing processes of synthetic fibers, dog bone specimens produced by the same material would not exhibit the same tensile properties as the extruded filaments.

Tensile testing on synthetic fibers is commonly performed according to two standards. These are “ASTM D2256-09 Standard Test Method for Tensile Properties of Yarns by the Single-Strand Method”, and “EN 14880-2:2006 Fibres for Concrete – Part 2: Polymer Fibres – Definitions, Specifications and Conformity”. Because synthetic fiber producers often sell the same product in both European and North American markets, both standards need to be simultaneously satisfied.

Establishing a consistent testing rate is key because the tensile properties of many synthetic fibers, for example polypropylene, are load rate dependent (Manolis, Gareis, Tsonos, & Neal, 1997). This means that an increase in testing speed could result in a falsely high reported modulus of elasticity.

To test the tensile properties of synthetic fibers, filament samples are taken during manufacturing before the fibers are cut. This is because a length of the filament much greater than that of the cut fibers is required for the testing process. EN 14889-2:2006 specifies a minimum of three measurements of the filament cross section be taken before tensile testing.

ASTM D2256-09 Standard Test Method for Tensile Properties of Yarns by the Single-Strand Method specifies a constant rate of testing that results in fiber rupture within a time of 20 s ± 3 s. ASTM D2256-09 states that the tolerance of 3 s is wide enough to allow convenient adjusting of the testing rate, while still being narrow enough to ensure proper agreement between test results. However, ASTM D2256 does specify that other operating rates may be used, such as 120 ± 5 % of the sample length per minute. For example, a sample length of 165 mm would allow an acceptable testing rate of 198 ± 8 mm/min.

The maximum tensile force applied to the specimen before rupture is recorded. This is used to calculate the ultimate tensile strength as shown in Equation 2-1.

$$\sigma_{fu} = \frac{P_T}{A} \quad \textbf{2-1}$$

Where,

σ_{fu} = Ultimate tensile strength of fiber (MPa)

P_T = Maximum tensile load (N)

A = Cross sectional area of the filament (mm^2)

A stress-strain curve is plotted from the measurements recorded throughout the test. While ASTM D2256-09 recommends the initial elastic modulus be taken from the resulting stress-strain plot at a tangent to the maximum slope, this is not necessarily a representative modulus for synthetic fibers. Some synthetic fiber materials can have varying slopes throughout a tension test, however a fiber in concrete may never reach its maximum elongation, and may pullout of the matrix before rupturing. Therefore, the elastic modulus is taken in the same manner recommended by ASTM D2256-09 for the chord modulus, that is, by selecting two specific points on the plot and calculating the slope of the line between these two points. It is recommended that the elastic modulus be taken at low values of strain (under 30% of the ultimate tensile capacity) because Hooke's law is valid only for cases where elastic behavior is maintained. This satisfies EN 14889-2:2006, which specifies that the modulus of elasticity be calculated using the stress and deformation at 10% and 30% of the maximum tensile strength. The modulus is calculated according to Hooke's law, shown in Equation 2-2, and illustrated in Figure 2.13:

$$E_f = \frac{\sigma}{\epsilon} = \frac{\Delta\sigma}{\Delta\epsilon} = \frac{\sigma_{30} - \sigma_{10}}{\epsilon_{30} - \epsilon_{10}} \quad \textbf{2-2}$$

Where,

E_f = Elastic modulus of the fiber (GPa)

σ_{30} = Stress at 30% of the ultimate tensile stress (MPa)

σ_{10} = Stress at 10% of the ultimate tensile stress (MPa)

ϵ_{30} = Strain corresponding to σ_{30} (mm/mm)

ϵ_{10} = Strain corresponding to σ_{10} (mm/mm)

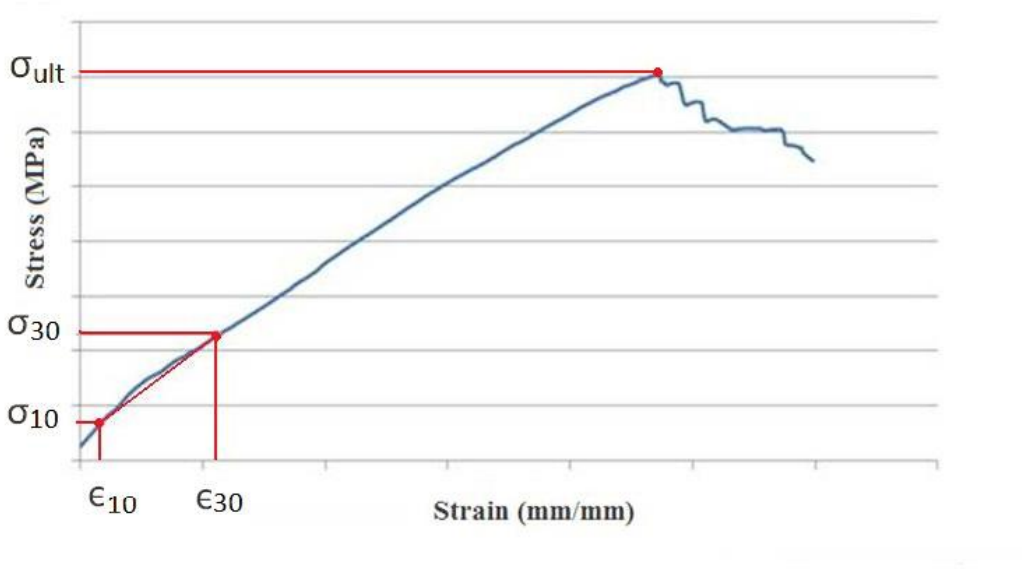

Figure 2.13 - Stress-strain curve resulting from a filament tensile test

2.4 SINGLE FIBER PULLOUT TEST

Assessing the bond properties between the fiber-matrix interface can be done using single fiber pullout testing, that is, pulling a single fiber from the surrounding matrix. Pullout testing is not a regularly used test method for FRC, however, it is an essential test for fiber interface tailoring. There is currently no known standard for testing single fibers in pullout; however, several authors have successfully developed their own methods.

Most fiber pullout tests collect data to plot a curve of pullout load vs. fiber slip. The purpose of pullout testing is to determine the fiber bond strength using parameters such as chemical bond energy, G_d (J/m^2), frictional bond strength, τ_o (MPa), and slip hardening coefficient, β, as well as to characterize the pullout behavior of different fiber types. For example, fibers can debond and then pullout, while some fibers rupture before complete pullout can occur. Characterizing the pullout behavior of a fiber is necessary to tailor the fiber for a particular application.

2.4.1 Fiber Placing and Casting Methods

Historically, the majority of pullout testing has been performed on steel fibers of various shapes, as discussed in section 2.1. In the majority of setups for steel fiber pullout testing, a mortar mix is cast in a mold and the steel fiber is placed into the mortar mixture with additional fixtures to allow for the desired angles and embedment lengths, as illustrated in Figure 2.14. The stiffness of steel fibers allows this type of placement without concern that the embedded end of the fiber could become bent.

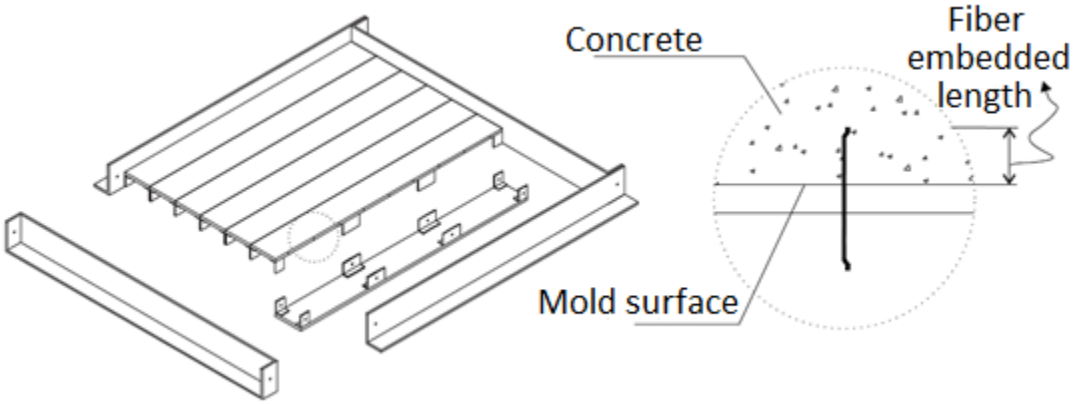

Figure 2.14 - Pullout specimen casting method for steel fibers used by Cunha, Barros & Sena-Cruz, 2010

In the case of polymeric synthetic fibers, such a process is not possible due to their flexibility, and they require a different casting method. Redon *et al.* in 2001 cast continuous PVA fibers through a mortar mixture in a rectangular prism mold, then cut the samples from the hardened mortar to the desired embedment length of 0.8 mm, as illustrated in Figure 2.15. This method of cutting through the mortar was necessary for an embedment length this small. Properly compacting a sample of such small dimensions could be difficult and cause voids. Specimens were then further cut to create individual pullout specimens containing a single fiber each. It is important to note that the fibers were aligned horizontally to the mortar casting direction. This ensured that any mild segregation of the mortar did not affect the results when testing varying fiber embedment lengths.

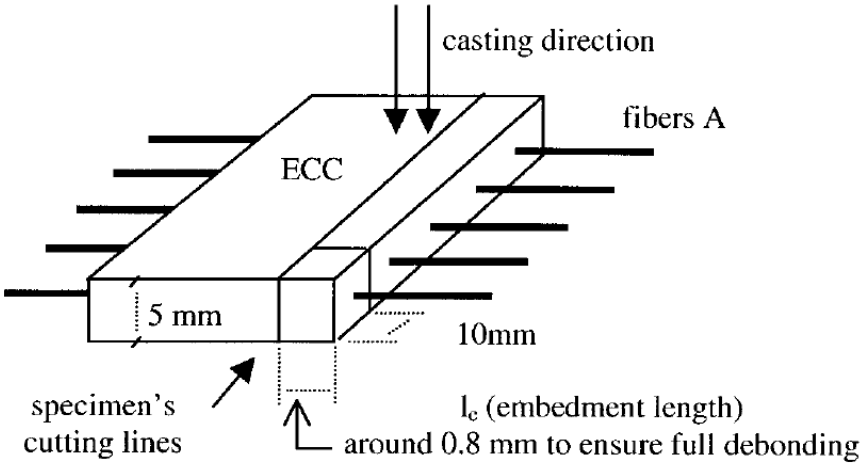

Figure 2.15 - Pullout specimen casting method used by Redon, Li, Wu, Hoshiro, Saito & Ogawa, 2001

A similar casting method was used by Rathod & Patodi in 2010 when they tested polyester-type fibers in single fiber pullout. Specimens were cast in a continuous mold and fibers were aligned to the loading direction for samples tested at 0 degree fiber inclination, as illustrated in Figure 2.16. Fibers were also cast directly in the specimen at inclines to the loading direction. Four different mortar mixtures with varying sand to

cement ratios were used to examine the effect on the fiber-matrix bond. Similar to Redon *et al.*, the casting direction was perpendicular to the fiber direction, to prevent any discrepancies in the matrix from affecting the fiber-matrix bond results.

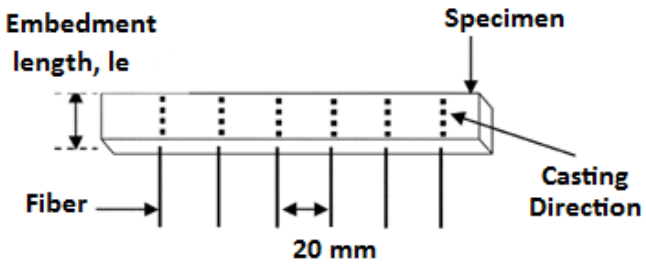

Figure 2.16 - Pullout specimen casting method used by Rathod & Patodi, 2010

2.4.2 Test Setup and Fiber Restraint Methods

Markovich *et al.*, 2001, gave special attention to the state of stresses around the fiber when designing the pullout test setup for a steel fiber. It was proposed that setups using a steel ring restraining the top of the specimen could cause lateral confinement around the fiber within the specimen, as illustrated in Figure 2.17, giving falsely high bond strength results. Instead Markovich *et al.* glued the sample to the bottom plate, as shown in Figure 2.18.

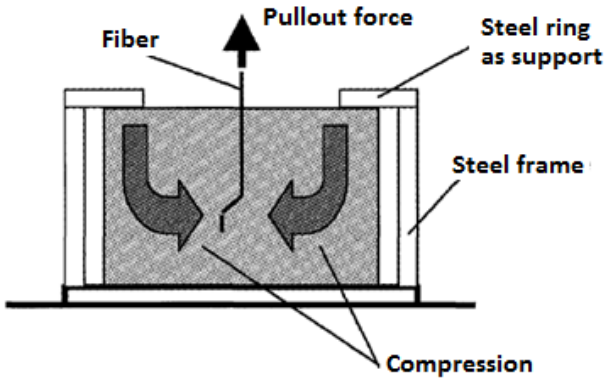

Figure 2.17 - Pullout test setup causing additional compressive strength of the matrix around the fiber (Markovich, van Mier, & Walraven, 2001)

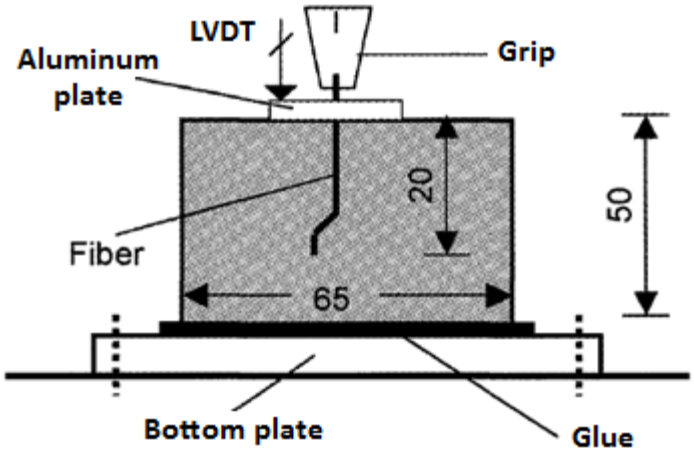

Figure 2.18 - Fiber pullout test setup used by Markovich, van Mier & Walraven, 2001 for steel fibers

A similar experimental setup was used by Redon *et al.* in 2001 to test PVA fibers in single fiber pullout. Specimens were glued to the testing equipment to ensure no additional compressive strength was developed around the fiber by the matrix. However, the test setup for pullout of synthetic fibers has some added considerations over that of steel fibers. First, the fiber gripping method is of concern. For a steel fiber, the fiber can easily be gripped in a pneumatic grip. However, for a synthetic fiber, which can stretch much more readily than a steel fiber, care must be taken to account for any elastic strain in the fiber. This strain must not contribute to the measured fiber slip within the pullout specimen. Redon *et al.* accounted for this by minimizing the fiber free length, that is, the length of the fiber between the clamping mechanism and the point of intersection with the matrix. The free length was minimized to 1 mm, which can be considered negligible as the stretching at peak load was less than 0.1% of the fiber free length (Redon, Li, Wu, Hoshiro, Saito, & Ogawa, 2001).

An additional concern with the fiber gripping method is that grips may pinch synthetic fibers causing damage to the fiber at the grip location. If the fiber ruptures it may be difficult to determine the rupture was at the matrix surface due to bond strength, and

not due to damage caused by the clamp. Redon *et al.* accounted for this by casting the free end of the fiber and gluing the specimen directly to the testing mount, as shown in Figure 2.19.

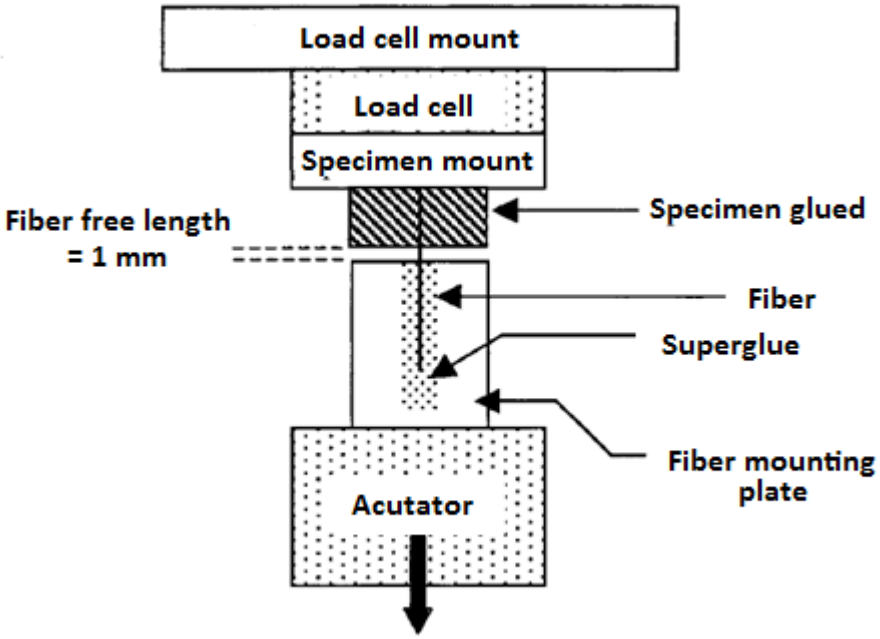

Figure 2.19 - Fiber pullout test setup used by Redon, Li, Wu, Hoshiro, Saito & Ogawa, 2001

Rathod & Patodi, 2010 used a pneumatic grip to secure the fiber and a mechanical grip to hold the specimen, as shown in Figure 2.20. This setup had several issues. First, the mechanical grip used to hold the specimen was using only lateral confinement, and thus would cause increased compression around the fiber and therefore inflate results, as proposed by Markovich, *et al.*, 2001. The scale of inflation of bond strength would be dependent on how tightly the mechanical grip was adjusted for each sample. The second problem with this setup was with the pneumatic grip holding the fiber. Rathod & Patodi stated that the pneumatic grip was carefully placed to grip the fiber at the surface of the sample to ensure there was no free fiber length, as this would prevent elastic stretching of the fiber; however, elastic stretching of the fiber is something that

can be easily accounted for using data from tensile tests conducted at the same speed. The combination of zero free fiber length and a pneumatic grip meant that if the fiber ruptured, it was not possible to tell visibly if the fiber ruptured due to bond strength or from the damage to the fiber at the grip location.

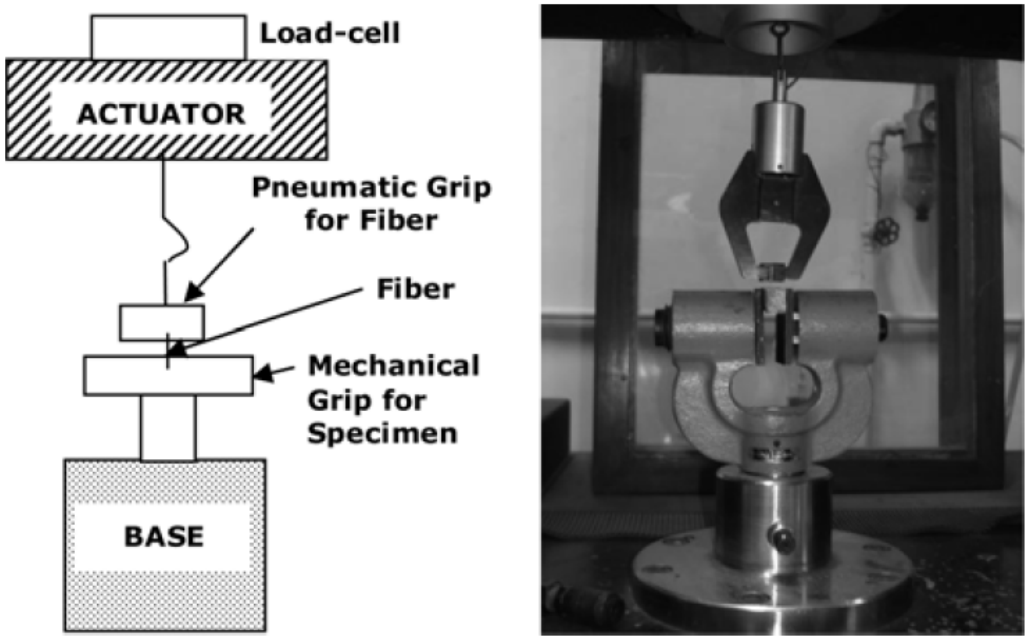

Figure 2.20 - Single fiber pullout test setup used by Rathod & Patodi, 2010

2.4.3 Accounting for Elastic Strain Contribution

If fiber free length is allowed, the elastic strain contribution over the free length has to be subtracted from the measured slip of the fiber (Banholzer, Brameshuber, & Jung, 2006). The ease of accounting for the stretch in the fiber depends on the method of measuring displacement. In fiber pullout test setups such as those used by Redon, *et al.* in 2001 or by Rathod & Patodi in 2010, the free fiber length was of concern because the fiber slip was being measured by the displacement of the actuator. Another method of measuring displacement is a "video-extensiometer", as used by Banholzer, *et al.* in 2006, as illustrated in Figure 2.21. This device measures the displacement between two

markers on the fiber. While this setup was unnecessarily complicated for measuring the pullout of steel fibers, it would be ideal for synthetic fibers.

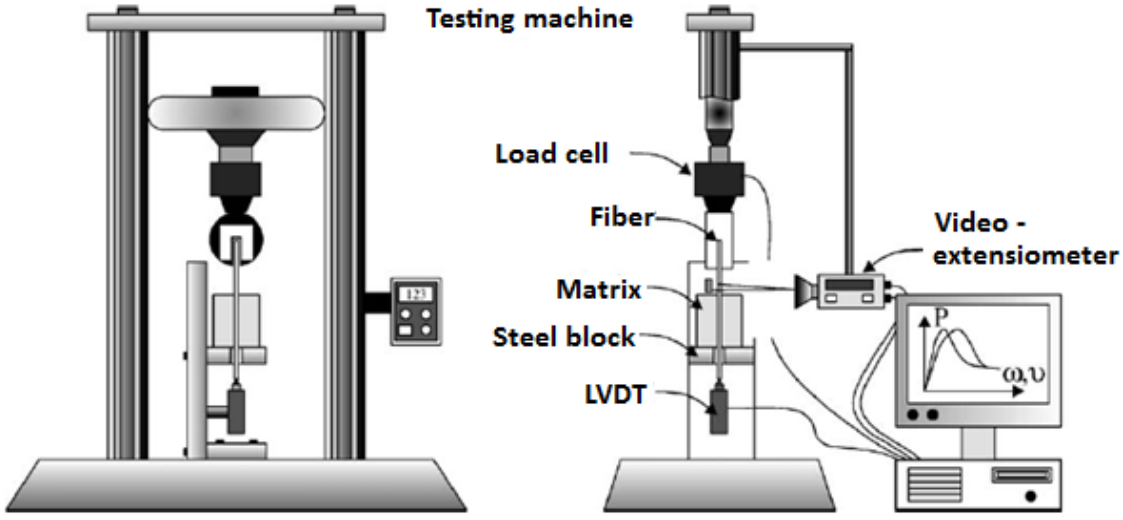

Figure 2.21 - Fiber pullout test setup used by Banholzer, *et al.* in 2006 for steel fibers

Measuring the displacement between two markers on the fiber using a laser extensometer, as was done in this study, would provide the opportunity to remove elastic fiber strain from the measurement of fiber slip in a pullout test. If the distance between a point on the fiber and the fiber at the matrix surface is tracked, a known fiber strain can be applied and subtracted from that measurement, as illustrated in Figure 2.22. Equation 2-3 would be applied to calculate elastic losses.

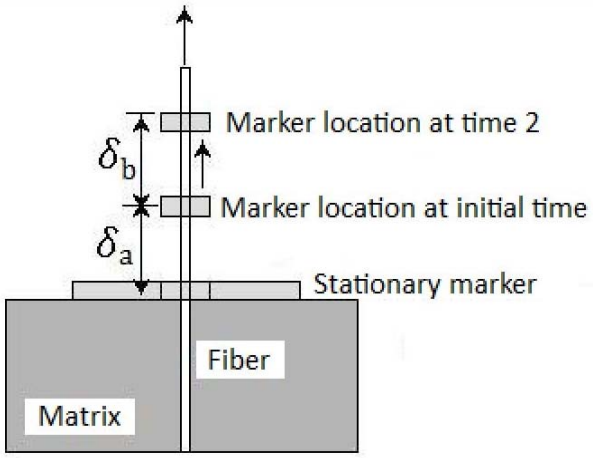

Figure 2.22 - Method for measuring fiber slip with fiber free length

$$S = \delta_b - \epsilon\delta_a \qquad \textbf{2-3}$$

Where,

S = Fiber slip (mm)

δ_a = Initial distance between two markers, as illustrated in Figure 2.22 (mm)

δ_b = Distance travelling marker moved over time, as illustrated in Figure 2.22 (mm)

ϵ = Fiber strain at present load, taken from tensile test conducted at same speed (mm/mm)

2.4.4 Effect of Strain Rate on Fiber Pullout Behavior

Most single fiber pullout tests are conducted using displacement controlled machines. The testing rate used by researchers has varied from 0.06 mm/min to 1080 mm/min, with the majority of tests being conducted in the range of 1 to 10 mm/min. A slower testing speed is preferred in order to capture data from critical stages of the test, and to represent the static loading fibers undergo within a concrete composite.

Kim, *et al.* in 2008 examined the effect of loading rate on the pullout behavior of deformed steel fibers. The loading rates used varied from 1.08 mm/min (representing static loading) to 1080 mm/min (representing seismic loading). Using both hooked end and twisted steel fibers in varying matrix strengths, they determined that while the pullout strength of both fiber types was dependent on the matrix strength, only the twisted fiber was dependent on the loading rate. This was attributed to microcracking being distributed relatively evenly around twisted fibers during pullout, while being localized to the area around the hook of a hooked end fiber. This is due to the differing mechanisms responsible for the pullout process of each fiber; hooked fibers deform during pullout while twisted fibers result in matrix failure immediately surrounding the fiber.

Loading rates have also varied depending on the fiber type. Markovich, *et al.*, 2001, used a pullout testing speed of 300 mm/min. While they were using steel fibers, this was still a high loading ratio and essential transition data could have been missed. Loading rates used for synthetic fibers have historically been much lower. Redon *et al.* used a displacement rate of 1.2 mm/min on PVA fibers, and Rathod & Patodi in 2010 used a displacement rate of 2 mm/min on polyester type fibers. As previously discussed, the tensile strength of synthetic fibers is load rate dependent; therefore a fast loading rate could cause non-representative results in pullout testing.

In 2006 Yang and Li examined the loading rate dependence of the behavior of high performance fiber reinforced cementitious composites in tension by using ECC reinforced with PVA fibers. They conducted both uniaxial tensile testing on the composite material, as well as pullout testing on the PVA fibers themselves. Single fiber pullout tests were conducted at displacement speeds between 0.06 mm/min up to 600 mm/min. These displacement rates were selected to correspond with the cross head rates used in the composite uniaxial tensile tests. Yang and Li found that the chemical bond energy, G_d, at the highest pullout speed was up to 5 times higher than the

chemical bond strength associated with the lowest pullout speed (0.06 mm/min). However, they also found that pullout speed had no significant effect on the results of frictional bond strength, τ_o, or the slip hardening coefficient, β.

2.4.5 Testing for Compressive Strength of Mortar Matrix

For the purposes of comparing fiber pullout tests conducted from differing mortar mixtures, mortar cubes must be cast along with the pullout specimens. The mortar cubes are used to determine the compressive strength of the matrix. Mortar cube specimens are cast and tested according to "ASTM C109-08 Standard Test Method for Compressive Strength of Hydraulic Cement Mortars (Using 2-in or [50 mm] Cube Specimens)".

2.5 FRC Performance Testing

To characterize the performance of a fiber type within a composite, several testing methods are used; compressive strength testing, flexural testing using beams to characterize the contribution of fibers to first peak strength and residual strength as well as toughness, and flexural testing using round panels to characterize the fibers contribution to flexural toughness). These testing methods and associated calculations are described in this section.

The first peak strength characterizes the flexural behavior of FRC at the initiation of a crack, whereas residual strength characterizes the capacity of the FRC to maintain load carrying capacity after cracking. Flexural toughness is expressed as the area under a load-deflection curve from flexural testing and is an indicator of the energy absorption capacity of the test specimen (ASTM International, 2010).

It is common for macrofibers to improve the residual strength and toughness while having little to no effect on the first peak strength when compared to concrete with no

fibers. In contrast, microfibers commonly improve the first peak strength while having little effect on the flexural toughness of the concrete.

2.5.1 Fiber Reinforced Concrete Compressive Strength Test

The compressive strength of FRC is determined using ASTM C39-10 “Standard Test Method for Compressive Strength of Cylindrical Concrete Specimens”. During this test a compressive axial load is applied to molded cylinders until failure occurs.

Sample sizes are commonly 100 mm diameter cylinders, with a height of 200 mm. The specimen is placed in the testing machine where a compressive axial load is applied at a constant rate. As mentioned in section 2.3, the capacity of synthetic fibers is load rate dependent, and a varying load rate could affect the results of a compressive strength test on a synthetic FRC cylinder. Therefore, it is important that consistent loading rates be maintained between tests. The load is applied until the load decreases steadily and the sample shows a defined fracture pattern. Figure 2.23 shows a fiber reinforced concrete cylinder with sulfur caps in the testing machine post rupture.

Figure 2.23 - Cylinder failed in compression in testing machine

The maximum load is noted along with a brief description of the fracture pattern. A sketch or photo is taken as well. The compressive strength of the concrete is determined by dividing the maximum load applied to the sample by the cross sectional area of the cylinder.

2.5.2 Fiber Reinforced Concrete Flexural Strength Tests

Synthetic macrofibers primarily contribute to the flexural toughness or residual strength of concrete members tested in flexure. There are three standard test methods used to characterize the contribution of fibers to the flexural performance in concrete. These are "ASTM C1609-10 Standard Test Method of Flexural Performance of Fiber-Reinforced Concrete (Using Beam with Third-Point Loading)", "ASTM C1399-10 Standard Test Method for Obtaining Residual-Strength of Fiber-Reinforced Concrete", and "ASTM C1550-10 Standard Test Method for Flexural Toughness of Fiber Reinforced Concrete Using Centrally Loaded Round Panel".

Flexural Performance Testing (ASTM C1609-10)

Testing FRC specimens using ASTM C1609-10 allows fiber performance to be characterized using first peak strength, residual strength, and flexural toughness. Specimens are typically rectangular beams measuring 150 x 150 x 500 mm. Figure 2.24 shows the setup required for flexural testing using third-point loading. The load and deflection undergone by the specimen throughout the test are recorded using a data acquisition system, and the resulting load-deflection curve is used to determine various specimen parameters, as illustrated in Figure 2.25.

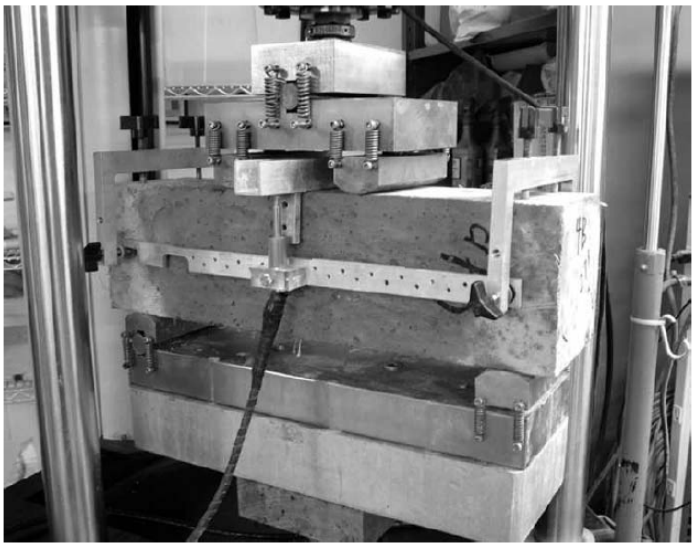

Figure 2.24 - Typical setup for ASTM C1609-10 testing (ASTM International, 2010)

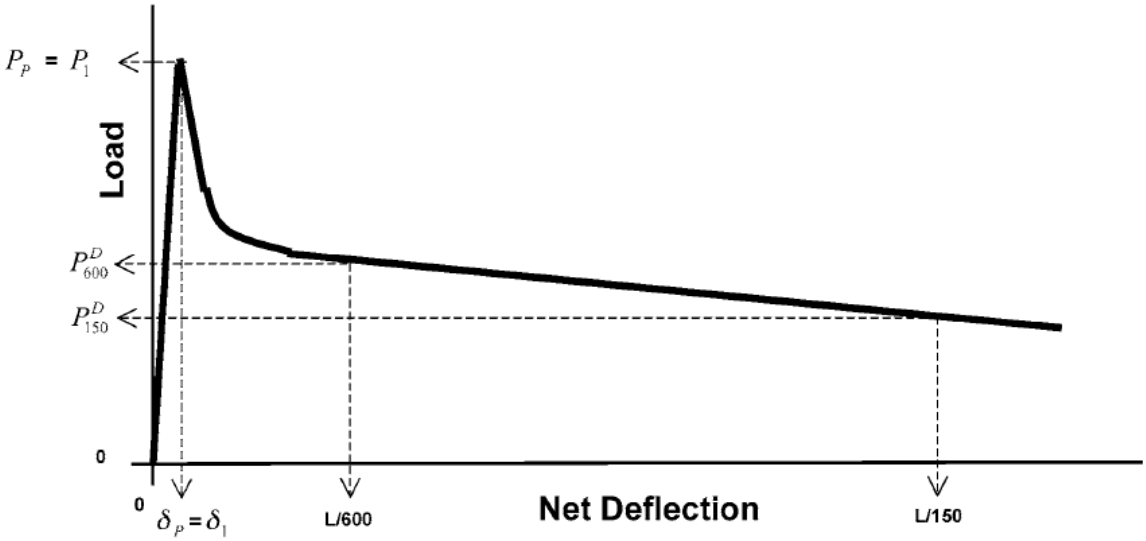

Figure 2.25 - Example of parameters taken from load-deflection curve (ASTM International, 2010)

Using the parameters from the load vs. net deflection curve, the strengths (f_x) are calculated using Equation 2-4.

$$f_x^D = \frac{P_x^D L}{bd^2} \quad \textbf{2-4}$$

Where,

L = Span length (mm)

b = Sample width (mm)

d = Sample height (mm)

P_1 = First peak load (kN)

P_P = Peak load (kN)

δ_1 = Net deflection at first peak load (mm)

δ_P = Net deflection at peak load (mm)

f_1 = First peak strength (MPa)

f_p = Peak strength (MPa)

P_{600}^D = Residual load at net deflection of L/600 (kN)

f_{600}^D= Residual strength at net deflection of L/600 (MPa)

P_{150}^D = Residual load at net deflection of L/150 (kN)

f_{150}^D = Residual strength at net deflection of L/150 (MPa)

T_{150}^D= Toughness, taken as area under load vs. deflection curve between a net deflection of 0 and L/150 (Joules)

Residual Strength Testing (ASTM C1399-10)

Testing to quantify the contribution of fibers to the residual strength of concrete is commonly done using ASTM C1399-10. This standard provides a good measure of the post-cracking strength of a FRC sample. Figure 2.26 shows a typical setup for a specimen undergoing this test.

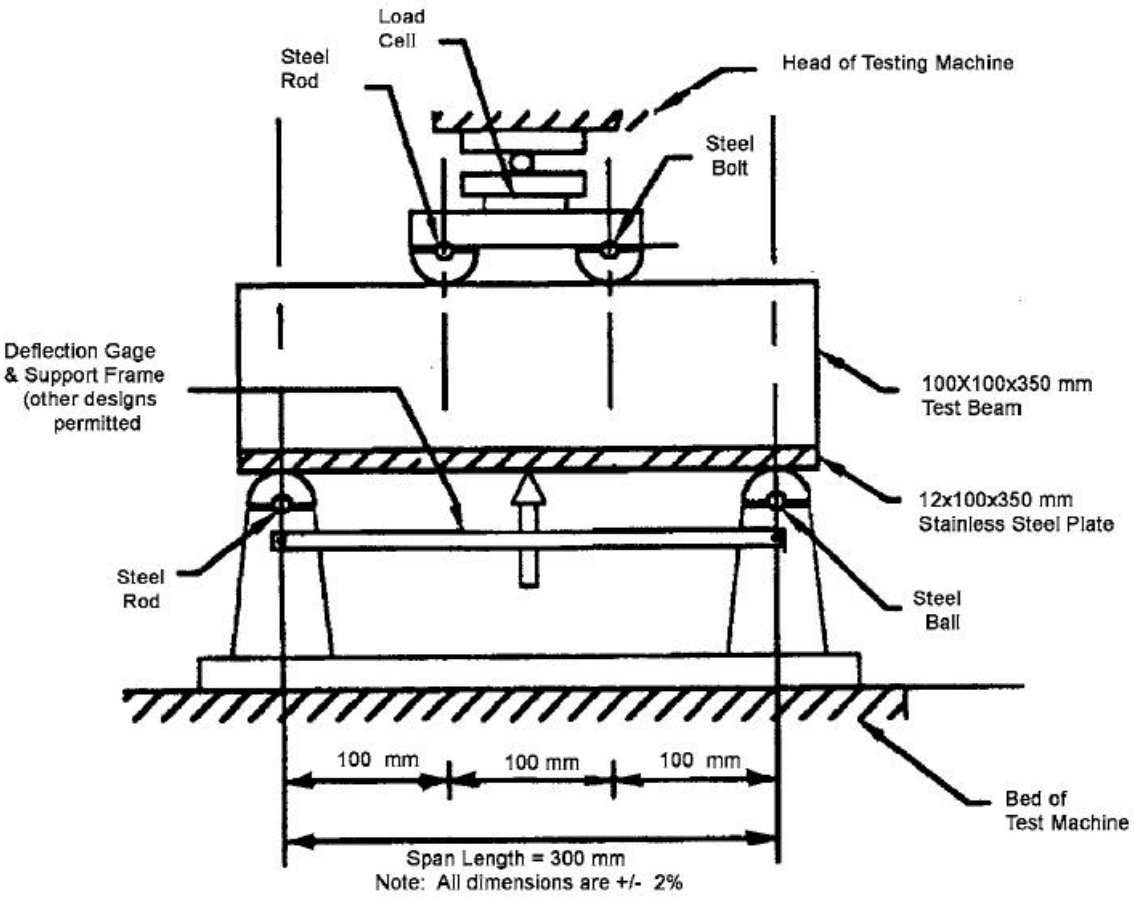

Figure 2.26 - Pre-crack setup for ASTM C1399-10 testing (ASTM International, 2010)

Specimens used for ASTM C1399-10 are typically rectangular beams, measuring 100 x 100 x 350 mm, but this test is not recommended for use with relatively rigid or stiff fibers measuring 40 mm or greater in length in molded specimens. This is because casting processes in molded beams can cause unrepresentative fiber alignment along the walls of the mold (ASTM International, 2010). To prevent this, ASTM C1399-10 recommends samples with macrofibers greater than 40 mm be saw cut to the required dimensions from larger molded samples.

From this testing a load deflection curve is created using data stored by a data acquisition system. The residual strength index (RSI) is calculated according to Equation 2-5.

$$RSI = \frac{P_{avg}\, L}{bd^2} \qquad \textbf{2-5}$$

Where,

RSI = Residual strength index (MPa)

P_{avg} = Average load corresponding to 0.5, 0.75, 1.00 and 1.25 mm deflection (N)

L = Sample length (mm)

b = Sample width (mm)

d = Sample height (mm)

This test is commonly used in conjunction with ASTM 1609-10 to characterize fiber performance, because this test is not ideal for reporting results of relatively stiff synthetic fibers over 40 mm in length in molded specimens.

Flexural Toughness Testing Using Round Panels (ASTM C1550-10)

Testing FRC specimens using ASTM C1550-10 Standard Test Method for Flexural Toughness of Fiber Reinforced Concrete Using Centrally Loaded Round Panel allows fiber performance to be characterized using flexural toughness by quantifying the energy absorbed between initial loading and specific values of central deflection. Central deflection is defined as the net deflection at the center of a panel measured relative to a plane defined by the three pivots used to support the panel. In this test the FRC specimen is a molded round panel, 75 mm thick and 800 mm in diameter, that is centrally loaded up to a central deflection of 40 mm. Figure 2.27 and Figure 2.28 show a typical setup and measurement methods for ASTM C1550-10.

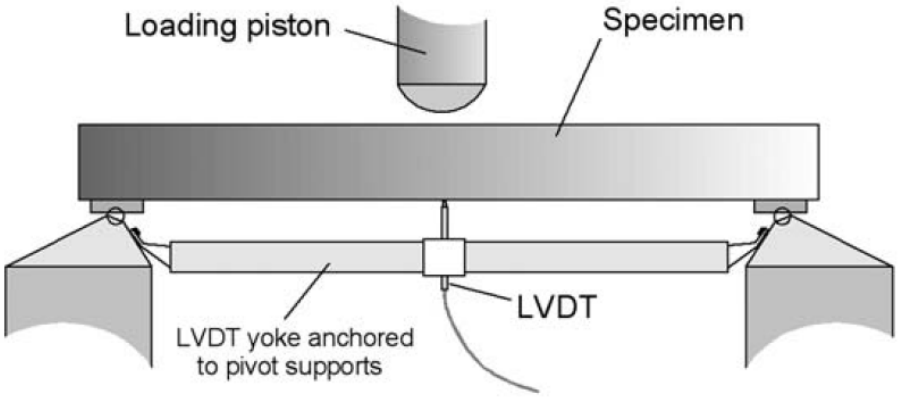

Figure 2.27 - Suggested method of deflection measurement using linear variable deflection transducers (LVDT) (ASTM International, 2010)

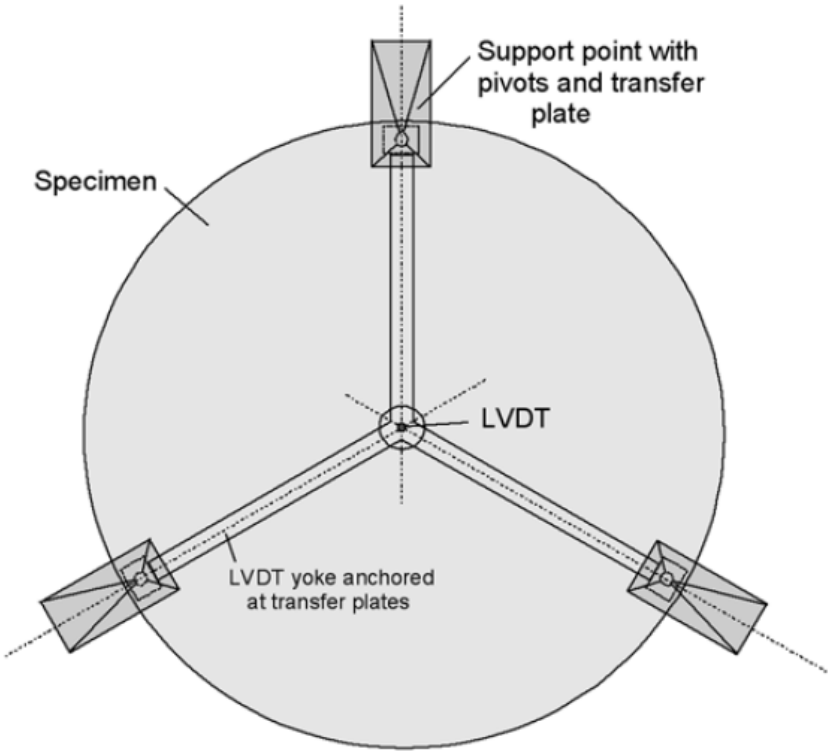

Figure 2.28 - Plan view of suggested method of deflection measurement using LVDT (ASTM International, 2010)

Energy absorption, or toughness, is reported in joules, and is taken as the area under the load vs. central deflection curve, with corrections, between 0 and 40 mm deflection. The peak load and number of radial cracks observed are also reported. Figure 2.29 shows the typical fracture pattern resulting from flexural toughness testing on round panels.

Figure 2.29 - Typical fracture pattern of round panels after testing

ASTM C1550-10 provides a good representation of the deflection behavior of a plate-like FRC structural member, as it exhibits similar failure modes to an *in situ* structure. This test is ideal for fiber reinforced shotcrete samples because a sample this size is simple to form using shotcrete. Also, because the energy absorption up to a central deflection of 40 mm is used, this test is representative of typical shotcrete applications such as tunnel linings, where large deflections and therefore large crack openings would be expected.

2.6 FIBER TENSILE CREEP TEST

Testing the tensile creep behavior of synthetic fibers in the form of filaments is another method of characterizing different fiber types. This testing is useful because fibers

bridging cracks in a structural member may experience tensile loads over an extended period of time. Therefore, it is useful to compare the effectiveness of different fiber types in creep testing.

“ASTM D2990-09 Standard Test Methods for Tensile, Compressive, and Flexural Creep and Creep Rupture of Plastics” outlines the testing of plastics in creep. Similarly to tensile testing, dog bone specimens produced by the same material would not exhibit the same tensile properties as the extruded filaments. This is due to the molecular alignment and varying parameters associated with the manufacturing processes of synthetic fibers.

There is currently no standard for testing extruded synthetic filaments in tensile creep, however several authors have had success with their own methods. In 1981 Takaku examined the effect of stretch ratio on creep fracture of polypropylene filaments produced from melt extrusion, by attaching a weight to the lower end of a filament hung in an oven. Takaku used filaments of varying stretch ratios as well as one unstretched filament. It was found that creep rates were independent of stretch ratios. However it was also found that higher stretch ratios result in higher breaking stresses during the creep testing. This can be expected, since higher stretch ratios increase the tensile strength of polymeric fibers by increasing the uniaxial molecular alignment (Lin & Argon, 1994).

Cochrane, in 2003, investigated the effects of elevated temperatures on tensile creep of synthetic filaments using a frame made from polyvinyl chloride (PVC) piping with filaments hanging from the frame and weights attached to the bottom of the filaments. Care was taken not to induce stress concentrations where the filament was attached to the weights or the frame. During daily measurements a ruler was used to measure the displacement between marks placed on the filaments, and a wire attached horizontally to the frame. This setup is illustrated in Figure 2.30. It was found that the filaments loaded at 20% or greater of their tensile strength demonstrated increased creep strains at elevated temperatures when compared with room temperature. However, Cochrane

admitted that a greater number of test specimens and a method of measurement more reliable than a hand held ruler would yield more confident results.

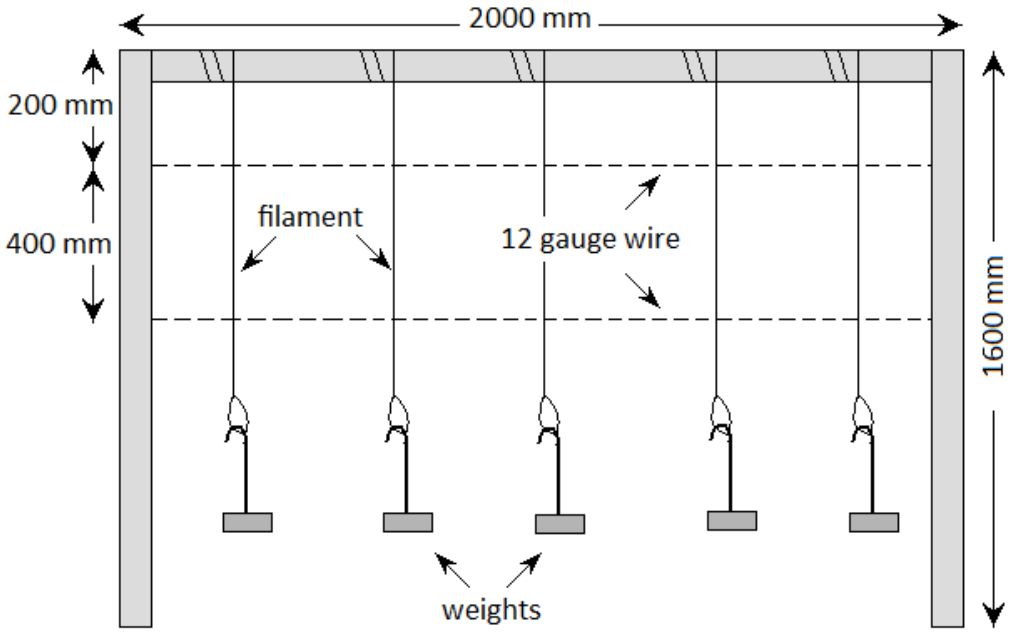

Figure 2.30 - Setup for testing filament tensile creep (after Cochrane, 2003)

While filament tensile creep testing is an effective way of comparing creep behavior of different fiber types, it does not account for many of the complexities associated with the behavior of fibers in a concrete matrix such as fiber alignment or pullout. Therefore, when developing a new synthetic fiber, additional creep testing on synthetic FRC beam samples using the same fibers would verify the performance of fibers under sustained loads within FRC.

Creep testing on cracked FRC composites has been conducted and connections have been found between creep performance and the fiber-matrix bond. In 2000 Kurtz & Balaguru investigated the creep-time behavior of cracked polymeric FRC beams under sustained flexural loading. This investigation used specimens containing fibrillated polypropylene fiber and specimens containing nylon fibers. Applied loads ranged from

22% to 88% of the average residual strength of the samples, found using ASTM C1399-10. The setup used for loading creep specimens is illustrated in Figure 2.31.

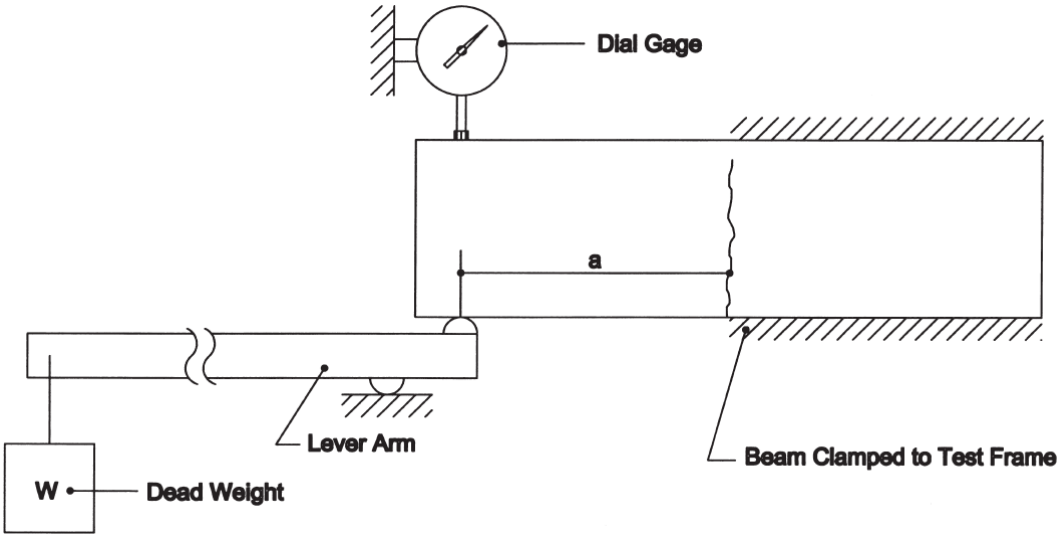

Figure 2.31 - FRC beam creep test setup used by Kurtz & Balaguru, 2000

It was found that the maximum sustainable stress for the polypropylene samples was 24.9% of the average residual stress, and 38.3% for the nylon samples. Nylon FRC was found to creep considerably faster than the polypropylene FRC, but for less time, resulting in similar net levels of creep deformation for both groups. This was attributed to the fibrillation of the polypropylene fibers, which results in increased bond strength compared to nylon fibers and can sustain slip without a complete loss of bond. Similar results were found by MacKay & Trottier in 2004. These authors showed that sustained loads up to 40% are possible using the AFT commercially available fiber Tuf-Strand SF, a fibrillated polypropylene/polyethylene blend. Continued testing on the same samples demonstrated these loads were still sustained over ten years.

CHAPTER 3 LITERATURE REVIEW

In order to evaluate the performance of different synthetic fibers for use in FRC, an understanding of synthetic fibers and pullout processes was necessary. This chapter will present a review of existing literature on synthetic fiber behavior in pullout, as well as currently available materials used for synthetic fibers.

3.1 FIBER MATRIX INTERFACE

The capacity of a fiber's contribution to the mechanical properties of concrete is highly dependent on the ability of the matrix to transfer load to the fiber. This transfer occurs at the interfacial transition zone (ITZ), which is the volume of the matrix surrounding either the fiber or coarse aggregate. Scrivener *et al.* (2004) described the ITZ as follows:

> "...the region of the cement paste around the aggregate particles, which is perturbed by the presence of the aggregate. Its origin lies in the packing of the cement grains against the much larger aggregate, which leads to a local increase in porosity and predominance of smaller cement particles in this region."

The microstructure of the matrix in the ITZ is significantly different from that of the bulk matrix. The thickness of the ITZ depends on what is perturbing it. Discrete cement particles, on the scale of 10 μm in size in the fresh mix, form calcium silicate hydrate (CSH) particles and calcium hydroxide (CH) crystals upon hydration. These two layers of CSH and CH particles form a duplex film, approximately 1 μm thick, immediately around the fiber (Geng & Leung, 1996). This, combined with bleeding and entrapment of water and inefficient packing of cement grains, forms water-filled spaces immediately around the fiber, as illustrated in Figure 3.1 (Bentur & Mindess, 1990). The microstructure of the ITZ has an effect on the mechanics of the fiber-matrix bond and the material properties such as strength and permeability of the concrete.

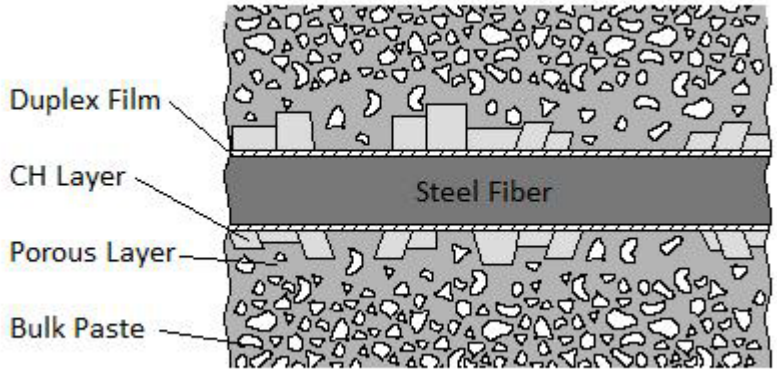

Figure 3.1 - Interfacial transition zone around a steel fiber (after Bentur & Mindess, 1990)

Although the ITZ is referred to as a zone, it is highly transitional and its thickness cannot be clearly defined. Hu *et al.* investigated the properties of this zone in 2004 and found that a natural phenomenon in the ITZ is size segregation, which leads to different gradients in porosity and particle size at various distances from the aggregate or fiber. Therefore, the ITZ microstructure can be improved by varying the particle size of the cementitious materials to even finer grains through the addition of mineral admixtures. Previous experiments using silica fume (Detwiler & Mehta, 1989), fly ash (Carette, Bilodeau, Chevrier, & Malhotra, 1993), and even rice husk ash (Bui, 2001) have supported this theory. The smaller particle size of these mineral admixtures allows them to fill in porous areas of the ITZ, increasing the bond between the matrix and the fiber or aggregate. Table 3.1 shows typical particle sizes of common cementitious materials (Habeeb & Faayadh, 2009). It should be noted that particle sizes of these materials vary based on manufacturing processes.

Mineral admixtures are typically industrial by-products and thus are both inexpensive and environmentally friendly. This has resulted in the increased use of supplementary cementing materials in concrete, particularly silica fume, fly ash, blast furnace slag and ground limestone. Blended cements containing one or more of these mineral

admixtures are common, and have the potential to impact the quality and composition of the ITZ. Since any fiber developed in this program will be used in conjunction with one or more of these materials, it is important that their effect be considered.

Table 3.1 - Typical particle sizes of common cementitious materials

Material	Typical Particle Size	Citation
Cement	10 - 40 µm	Habeeb & Faayadh, 2009
Fly Ash	0.5 µm to 100 µm	Davison, *et al.*, 1974
Silica Fume	0.05 to 0.5 µm	Diamond & Sahu, 2006
Rice Husk Ash	20 - 60 µm	Habeeb & Faayadh, 2009

3.2 FIBER BOND AND PULLOUT BEHAVIOR

While stress is transferred to fibers even in an uncracked matrix, the initiation of fiber pullout processes occur only after the matrix has cracked. As a crack is initiated, load is transferred to the fiber in the immediate area. This relieves the stress on the surrounding matrix and slows the propagation of the crack. As the applied load further increases, fibers may bridge the crack depending on their bond strength, or multiple cracks may form throughout the matrix. The mechanisms through which this occurs are described in this section.

3.2.1 Elastic Stress Transfer in an Uncracked Composite

Elastic stress transfer is the dominant mechanism before formation of the first crack. At this point the fiber and matrix still behave compositely. A non-uniform shear stress develops at the fiber matrix interface, transferring the load from the matrix to the fiber itself. Because the elastic modulus of the matrix differs from that of the fiber, the shear stress developed is such that the strain in both materials is kept the same (Bentur & Mindess, 1990).

Most models representing the elastic shear stress transfer between the fiber-matrix interface use shear lag theories to analyze the stress field deformation immediately around the fiber. This deformation is illustrated in Figure 3.2.

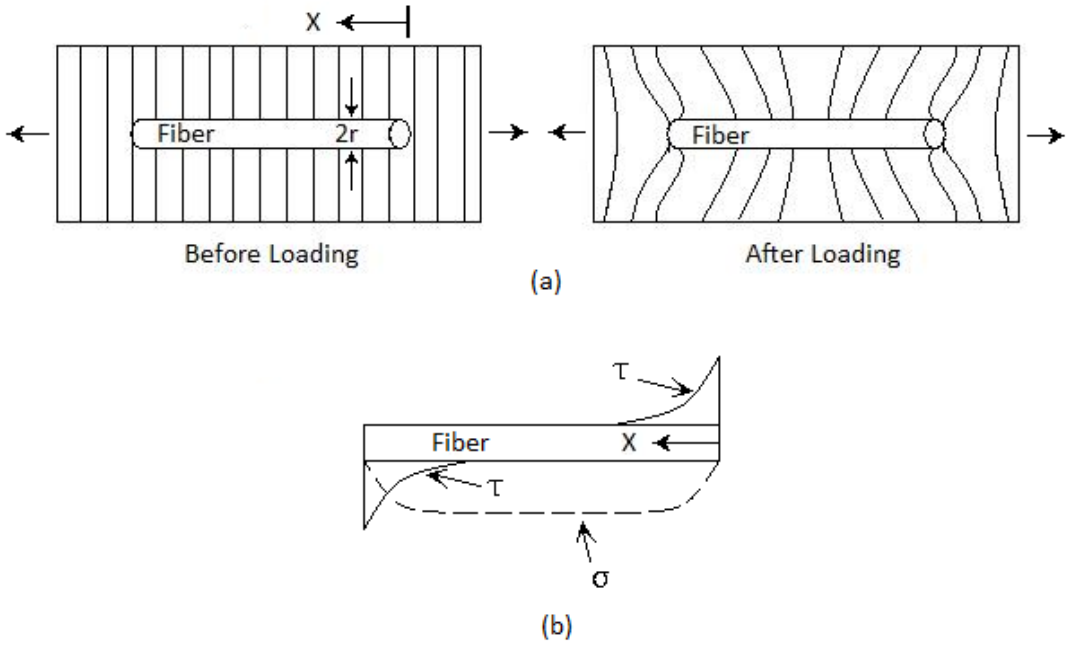

Figure 3.2 - Schematic description of a fiber embedded in a matrix, and the deformation and stress fields around it: (a) deformation in the matrix around the fiber prior to and after loading; (b) elastic shear stress distribution at the interface (τ) and tensile stress distribution of the fiber (σ) (Bentur & Mindess, 1990)

The shear stress felt by the fiber is greatest at the fiber ends and zero at the middle. In the middle, the stress is transferred from the matrix to the fiber, growing gradually with increased load as the adhesional shear stress threshold is approached.

Adhesional shear bond can be described as either physical, or chemical adhesion. Frictional shear stress transfer is considered physical adhesion, and is exhibited in most synthetic fibers. Chemical adhesion is rarer in synthetic fibers, but has been strongly

observed in hydrophilic fibers such as PVA (Redon, Li, Wu, Hoshiro, Saito, & Ogawa, 2001). While bond strength is improved with increased physical and chemical adhesion, typical fiber dosages are too low to effect the composite of the FRC.

3.2.2 Elastic and Frictional Stress Transfer in an Uncracked Composite

Depending on the efficiency of the fiber, debonding may occur before the fiber is fully utilized. If there is not a complete loss of bond, the frictional resistance mechanism will be activated as the fiber attempts to slip in the debonded zone (Bentur & Mindess, 1990). A debonded zone of length a, is formed as the interfacial shear stress resulting from load P exceeds the adhesional shear stress. This is illustrated in Figure 3.3. As the external load, P, increases, so does the debonded zone until the fiber has fully debonded or ruptured. It should be noted that the strains in an uncracked matrix are often not sufficient to cause fiber bond failure, and this mechanism is likely only for very small fibers with low bond strength.

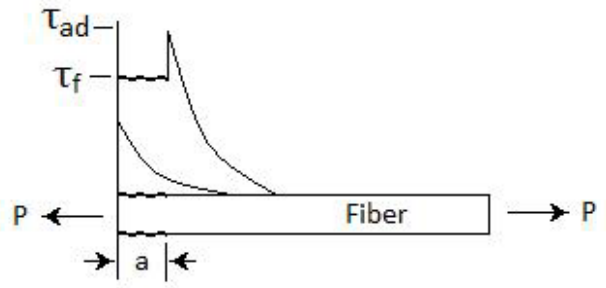

Figure 3.3 - Distribution of interfacial shear stresses in zones of combined elastic and frictional shear stress transfer (Bentur & Mindess, 1990)

3.2.3 Fiber Matrix Debonding in a Cracked Composite

In most FRC composite applications, macrofibers are activated after cracking, when fibers can bridge cracks that have propagated through the matrix. Single fiber pullout

testing is used to simulate this behavior in a controlled environment. Stress transfer mechanisms in a cracked matrix are similar to those in an uncracked matrix (combinations of adhesional shear stress and frictional stress). However in a cracked matrix the maximum interfacial shear stress occurs at the face of the crack, as opposed to the ends of the fiber in an uncracked matrix. If debonding occurs before crack formation, the shear stress will be a combination of adhesional shear stress and frictional shear stress, as illustrated in Figure 3.4. If debonding has not occurred before crack formation, the shear stress will be as illustrated in Figure 3.5, until the interfacial shear stress exceeds the adhesional shear stress and debonding occurs.

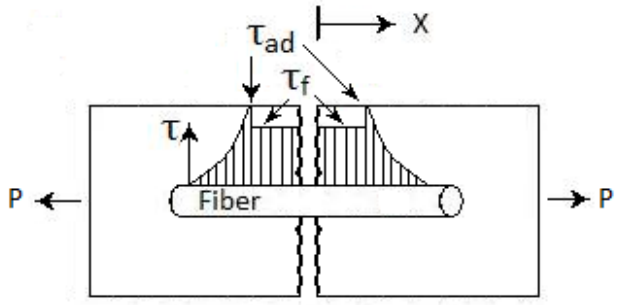

Figure 3.4 - Interfacial shear stress distribution where debonding has preceded cracking (Bentur & Mindess, 1990)

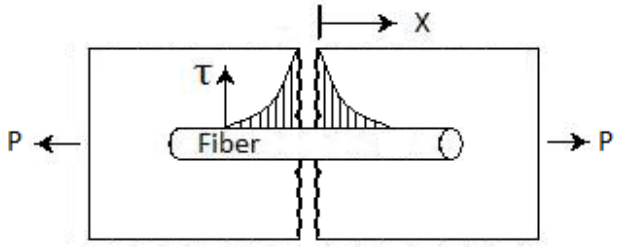

Figure 3.5 - Interfacial shear stress distribution immediately after cracking where no debonding has occurred prior to cracking (Bentur & Mindess, 1990)

3.2.4 Other Fiber-Matrix Interface Interactions

The interfacial damage mechanisms of polymeric fibers differ from that of steel fibers. Baggot & Gandhi (1981) found that polypropylene fibers experience surface damage during pullout, such as the chiseling out of long shavings of polypropylene by a matrix particle, as shown in Figure 3.6.

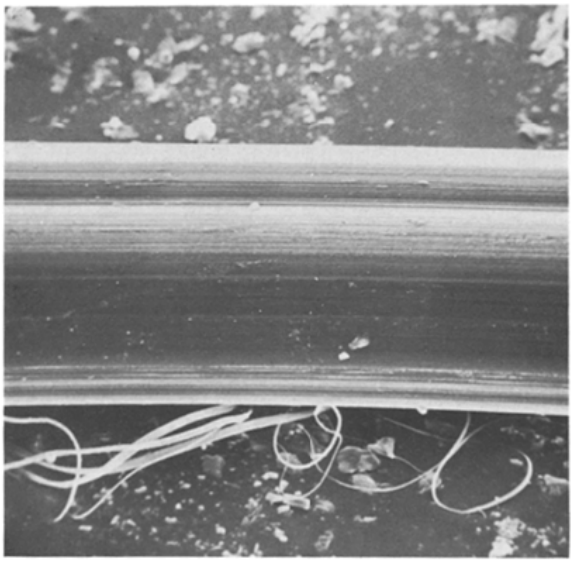

Figure 3.6 - Shaving produced from a polypropylene fiber during pullout (Baggot & Ghandi, 1981)

Geng & Leung in 1996 had similar findings using both nylon and polypropylene fibers. After total debonding, cement particles in the stiffer matrix surface can tear into the fiber and cause peeling. The shavings increase frictional shear stress at the interface and thus increase the fiber-matrix bond strength in a cracked composite. It was proposed that the hydrophilic nature of the nylon fibers caused water to penetrate into the fiber surface causing swelling, which in turn increased fiber peeling and thus increased the pullout load after debonding (Geng & Leung, 1996).

The Poisson effect on a fiber undergoing pullout is not considered to effect frictional stresses. When a fiber bridges a crack, the tensile strain of the fiber is greater than that

of the matrix, causing the fiber to shrink radially. This may reduce frictional stress and the effectiveness of the fiber, however, Baggot & Ghandi, 1981, found that the high Poisson's ratio contraction of polypropylene fibers could be negated by asperities in the fiber surface and misalignments of the fiber relative to the crack. Therefore, a slight increase in inclination angle may be enough to negate the Poisson's effect. As randomly distributed fibers in a matrix are rarely aligned perpendicular to a crack face, the Poisson's effect can generally be negated in modeling fiber pullout from composites.

Geng & Leung, 1996, observed holes on the surface of a polypropylene fiber after undergoing pullout. These holes formed from the surface ligaments thinning and pulling apart, as shown in Figure 3.7. Geng & Leung attributed this to the Poisson's effect. Under the low pullout rate and long pullout distance the fiber undergoes creeping, due to the existing molecular alignment. The result is a pseudo volumetric increase, and small holes are formed to maintain a constant volume.

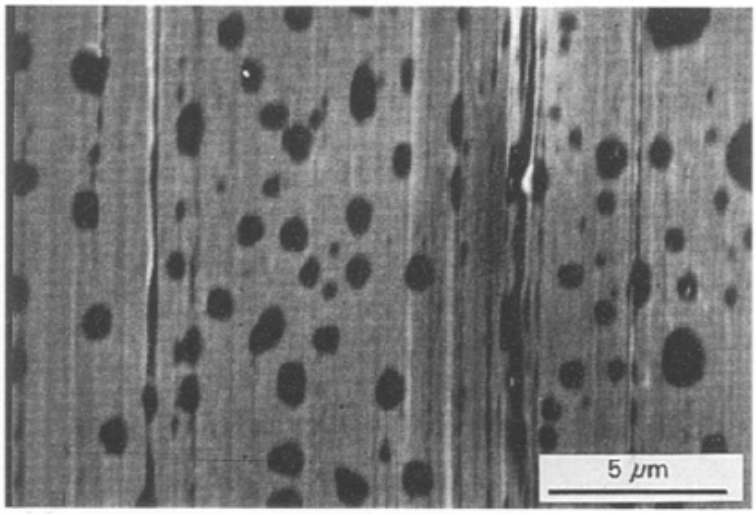

Figure 3.7 - Holes formed on the surface of a polypropylene fiber after pullout (Geng & Leung, 1996)

3.2.5 Effect of Fiber Inclination Angle

Single fiber pullout testing commonly simulates the fiber being aligned with the applied load, as well as the face of the crack being smooth, straight and normal to the direction of fiber protrusion. The reality of FRC is that cracks are quite irregularly shaped, and randomly distributed fibers can bridge cracks at any angle between 0 and 90 degrees. The behavior of fiber pullout at various angles can vary greatly. In an attempt to simulate fiber pullout more realistically, some researchers have conducted pullout testing on specimens loaded at an angle to the direction of fiber protrusion.

In 1990, Li, *et al.* investigated the effect of pullout angle on both polypropylene and nylon fibers in a mortar matrix. Fibers were cast at embedment lengths of 25 mm in two mortar mixtures, one considered normal strength, and one considered high strength (80 MPa). The loading setup of the specimen is as illustrated in Figure 3.8. Specimens were tested at inclined angles of ϕ = 0°, 15°, 30°, 45°, 60° and 75°. It was found that the maximum pullout load increased with an increase in ϕ for the range of 0° through 45°. However for the higher inclined angles, 60° and 75°, the data was scattered and in some cases the maximum pullout load decreased with an increase in ϕ. Similar trends were found for pullout energy (taken as the area under the pullout load vs. fiber slip curve). This was attributed to the sharper "matrix wedge" formed at higher angles, which can be weaker. In this case matrix wedges spall off causing sudden drops in pullout load, as shown in Figure 3.9. It was also found that the specimens prepared with the high strength mortar had equivalent pullout loads when compared with the normal strength mortar at 0° inclinations, suggesting that the mortar strength has little effect on the fiber matrix bond strength. However, specimens prepared with the high strength mortar had increased pullout loads compared to the normal strength mortar when higher angles were compared, due to the higher resistance to matrix spalling.

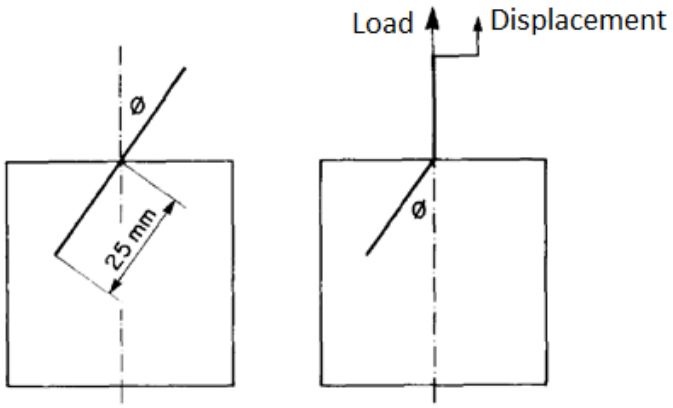

Figure 3.8 - Inclined angle pullout test setup used by Li, Wang & Backer, 1990

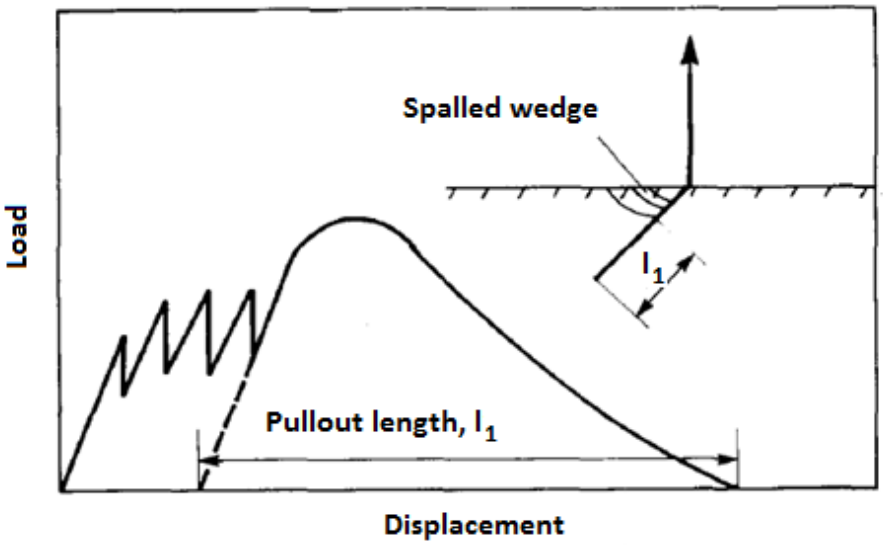

Figure 3.9 - Pullout load vs. displacement curve illustrating load drops caused by matrix spalling (Li, Wang, & Backer, 1990)

Leung & Li in 1992 described the additional forces on a stiff, brittle fiber when not perpendicular to the crack plane. The opening of a crack may produce additional shear and fiber bending, as well as the debonding forces, as shown in Figure 3.10. Leung & Li proposed that the crack bridging force of a fiber can be broken down to two

components; the fiber-matrix interfacial stress along the axis of the fiber, and the reactions due to the fiber bending against the matrix. Using pullout results from 0° inclination, the interfacial shear stress component can be obtained. The bridging force would be the vector sum of the two components, and the composite crack bridging stress can be taken as the product of the bridging force per fiber and the number of fibers per unit crack area.

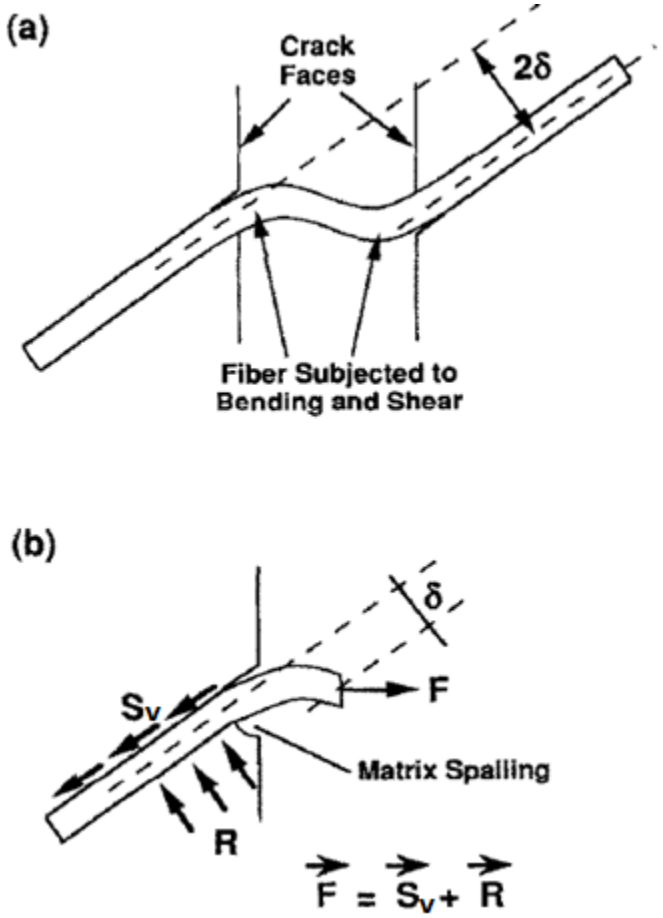

Figure 3.10 - (a) Bending and shear of fiber bridging a crack; (b) Components of force during crack bridging (Leung & Li, Effect of fiber inclination on crack bridging stress in brittle fiber reinforced brittle matrix composites, 1992)

Where,

F = Applied force (N)

R = Reaction force (N)

S_v = Shear force (N)

δ = Displacement of fiber from initial center line (mm)

Leung & Li's hypothesis was for a stiff, brittle fiber. For a flexible fiber being pulled out on an incline, the bending component becomes negligible compared to the interfacial debonding component (Leung & Ybanez, 1997). Li *et al*., in 1990, proposed that the case of a flexible fiber undergoing inclined pullout could be treated as a flexible string passing over a pulley, and a "snubbing friction coefficient", *f*, was proposed. This snubbing friction coefficient is used to relate the inclined peak pullout load to the pullout load at $\phi = 0°$, according to Equation 3-1, and is favored due to its simplicity.

$$P_\phi = P_0 \exp(f\phi) \qquad \textbf{3-1}$$

Where,

P_ϕ = Predicted peak pullout load on given incline angle (N)

P_0 = Peak pullout load on an incline angle of 0° (N)

f = Snubbing friction coefficient

In 2002, Zhang & Li examined the effect of angle inclination on the fiber rupture load. Since a fiber experiences increased shear and bending forces during inclined pullout, it can be assumed that higher stresses will be experienced by the fiber as well. By conducting pullout testing on synthetic fibers at inclined angles, Zhang & Li found that the fiber rupture load decreases with increasing ϕ. This decreased rupture load divided by the cross sectional area is referred to as 'fiber apparent strength' (Kanda & Li, 1998). Because of the fiber apparent strength decreases with increased ϕ, the critical fiber

embedment length is shortened.

3.2.6 Analysis of Pullout Curves

In modeling FRC composites, the fiber-matrix bond is often over simplified by assuming a uniform shear bond stress reported in terms of average strength over the embedded surface area of the fiber (Wang, Li, & Backer, 1988). While this was somewhat accurate for aligned smooth steel fibers, it becomes inaccurate for synthetic fibers offering other contributions to bond such as chemical adhesion or the accumulation of shavings from matrix damage during pullout and the snubbing effect. Pullout curves may exhibit very different trends for different fibers (Geng & Leung, 1996).

Fiber pullout curves typically use pullout load (N) plotted against fiber slip (mm). Pullout curves have been characterized using the parameters interfacial frictional stress at the onset of slip, τ_o, chemical bond, G_d, snubbing friction coefficient, f, and slip-hardening parameter, β. The strength reduction factor, f', is also used to characterize pullout curves produced from an inclined pullout test.

Figure 3.11 illustrates a pullout curve broken into three stages, as described by Redon *et al*., 2001 for a PVA microfiber. Initially, a stable fiber debonding process occurs along the fiber-matrix interface. Pullout load continues to increase up to a value P_a, and the embedment length, l_e, is unchanged, while the debonded length increases until it is equal to l_e. In the second stage, the load progresses from P_a to P_b. A sharp drop between P_a and P_b indicates the breaking of a chemical bond between the fiber and the matrix. In the third stage, frictional resistance is the dominant force. It is in this stage that the fiber-matrix interface can exhibit slip-hardening, constant friction, or slip-softening characteristics.

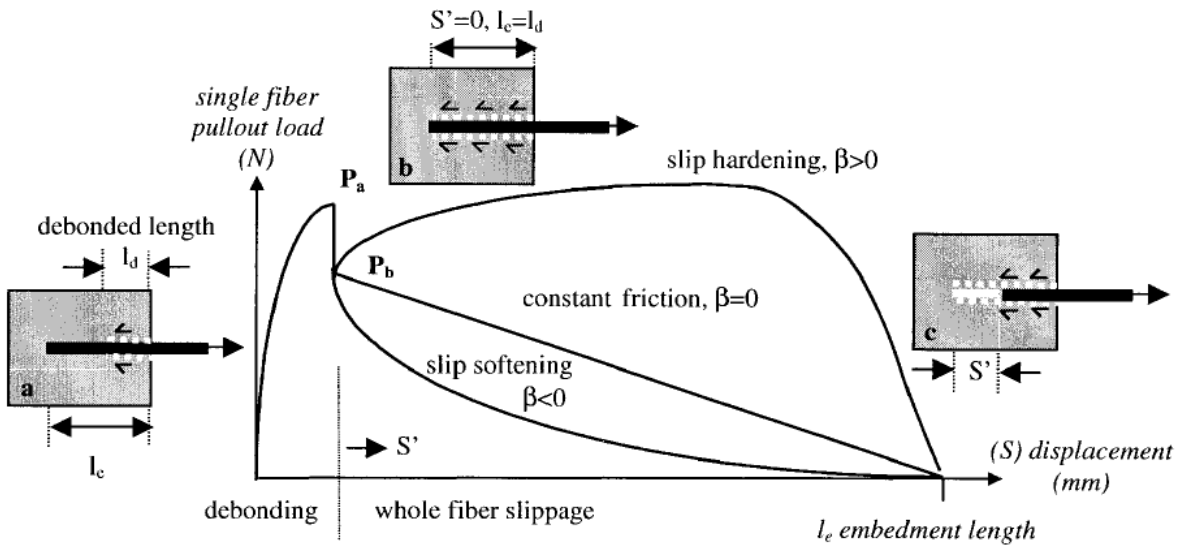

Figure 3.11 - General profile of a single fiber pullout curve (Redon, Li, Wu, Hoshiro, Saito, & Ogawa, 2001)

The value of slip, S, corresponding with pullout load P_b is considered the onset of full fiber slip, S' (Redon, Li, Wu, Hoshiro, Saito, & Ogawa, 2001). Thus the frictional bond strength at the onset of slip can be calculated according to Equation 3-2.

$$\tau_o = \frac{P_b}{\pi d_f l_e} \qquad \textbf{3-2}$$

Where,

τ_o = Interfacial frictional stress at the onset of slip (MPa)

P_b = Load value immediately after load drop, illustrated in Figure 3.11 (N)

d_f = Fiber diameter (mm)

l_e = Embedded length of fiber (mm)

Chemical Adhesion

Leung & Li in 1991 proposed Equation 3-3 be used to calculate the chemical bond strength, τ_s, at the fiber-matrix interface.

$$\left[\left(\frac{\tau_s}{\tau_o}\right)^2 - \left(\frac{\tau_s}{\tau_o}\right)\right]^{1/2} - \cosh^{-1}\left(\frac{\tau_s}{\tau_o}\right)^{1/2} = \left(\frac{P_a}{P_b} - 1\right)\frac{2\rho l_f}{d_f} \quad \textbf{3-3}$$

Where,

$$\rho^2 = \frac{2G_c E_c}{\left[V_m E_m E_f \log\frac{2R^*}{d_f}\right]} \quad \textbf{3-4}$$

τ_s = Chemical bond strength stress at the onset of slip (MPa)

τ_o = Interfacial frictional stress at the onset of slip (MPa)

P_a = Maximum load before load drop, illustrated in Figure 3.11 (N)

P_b = Load value immediately after load drop, illustrated in Figure 3.11 (N)

d_f = Fiber diameter (mm)

l_f = Fiber length (mm)

G_c = Shear modulus of composite (GPa)

E_c = Elastic modulus of composite (GPa)

V_m = Volume fraction of matrix

E_m = Elastic modulus of matrix (GPa)

E_f = Elastic modulus of fiber (GPa)

R^* = Effective radius of matrix cylinder containing fiber (mm)

These equations involve several variables that are difficult to determine such as R^*, the effective radius of the cylinder containing the fiber. Many of these variables cannot be determined using a single fiber pullout test alone.

A more applicable equation was proposed by Redon *et al.* in 2001. The chemical bond energy can be calculated according to Equation 3-5 using the difference between P_a and P_b, obtained from the pullout curves.

$$G_d = \frac{2(P_a - P_b)^2}{\pi^2 E_f {d_f}^3} \quad \textbf{3-5}$$

Where,

G_d = Chemical bond energy (J/m^2)

P_a = Maximum load before load drop, illustrated in Figure 3.11, (N)

P_b = Load value immediately after load drop, illustrated in Figure 3.11 (N)

E_f = Elastic modulus of fiber (GPa)

d_f = Fiber diameter (mm)

By approaching the chemical bond parameter as an energy value, rather than a shear strength, this equation provides an excellent method for quantifying the chemical bond of a synthetic fiber.

Slip Hardening Parameter

Redon *et al.* proposed the slip hardening coefficient can be calculated using the slope of the pullout load vs. slip curve at the onset of slip, S', according to Equation 3-6. This slope is based on the assumption of a linear slip dependence of friction, and is illustrated in Figure 3.12. The slip hardening parameter can apply to slip hardening, constant friction and slip softening. The slip hardening parameter would be positive, zero or negative in these cases, respectively.

$$\beta = \left(\frac{d_f}{l_f}\right)\left[\left(\frac{1}{\tau_o \pi d_f}\right)\left(\frac{\Delta P}{\Delta S'}\right)_{S' \to 0} + 1\right] \quad \textbf{3-6}$$

Where,

β = Slip hardening parameter

d_f = Fiber diameter (mm)

l_f = Fiber length (mm)

τ_o = Interfacial frictional stress at the onset of slip (MPa)

$\left(\frac{\Delta P}{\Delta S'}\right)$ = Initial slope of pullout load vs. slip curve as S' approaches 0

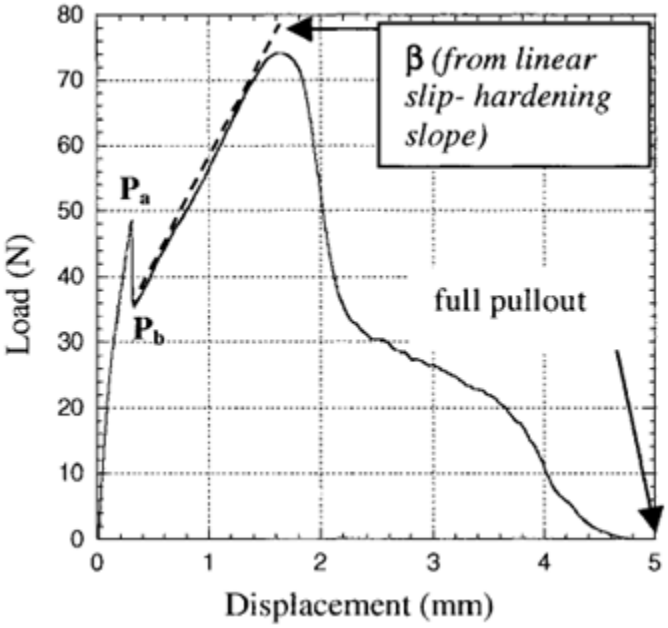

Figure 3.12 - Pullout curve illustrating calculation of β for slip-hardening with full fiber pullout (Redon, Li, Wu, Hoshiro, Saito, & Ogawa, 2001)

Using β, for small values of S', the pullout load, P, can be predicted according to Equation 3-7, as proposed by Redon, *et al.*, 2001.

$$P = \tau_o \pi d_f \left[l_e + S \left(\beta \frac{l_e}{d_f} - 1 \right) \right] \quad \textbf{3-7}$$

Where,

P = Pullout force (N)

τ_o = Interfacial frictional stress at the onset of slip (MPa)

d_f = Fiber diameter (mm)

l_e = Embedded length of fiber (mm)

S = Fiber slip (mm)

β = Slip hardening parameter

In pullout tests resulting in slip hardening, the peak pullout load is achieved after the initial debonding stage, as illustrated in Figure 3.13. When a fiber demonstrates slip hardening, it can be assumed that the fiber used in large volume fractions would result in strain hardening in an ECC. This is desirable for structural applications where an increase in concrete strength is desired without the addition of steel reinforcement. Hydrophilic fibers such as nylon and PVA have been found to exhibit slip hardening in pullout testing and subsequently strain hardening in ECC's (Geng & Leung, 1996), (Li, Wang, & Wu, 2001).

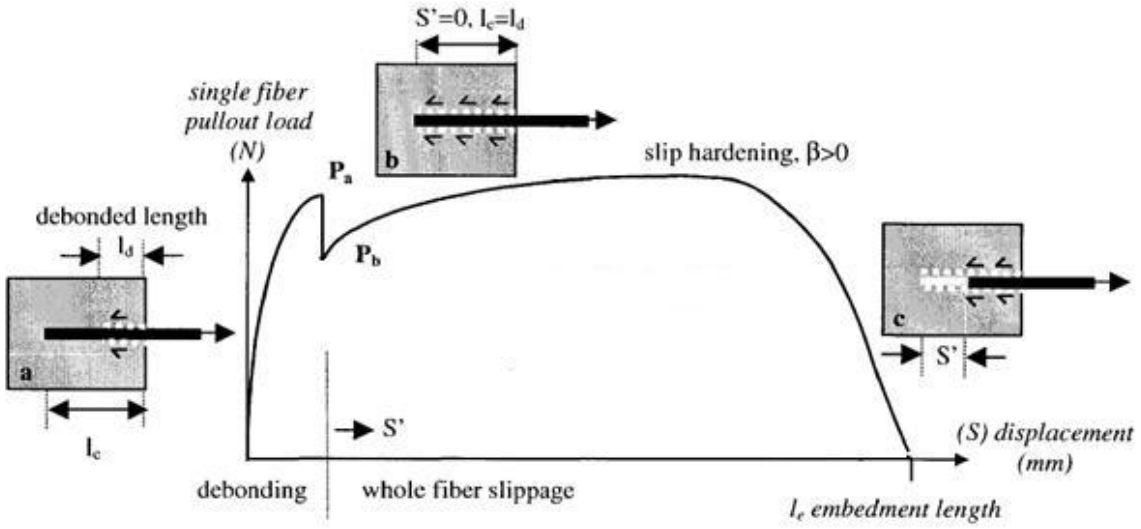

Figure 3.13 - Pullout curve resulting from slip-hardening (Redon, Li, Wu, Hoshiro, Saito, & Ogawa, 2001)

Constant Friction

A fiber exhibits constant friction behavior when the curve after initial debonding is not concave, but is linear, showing a constant load decrease with continued fiber slip. This is illustrated in Figure 3.14. Such linear behavior is rare in fiber pullout testing, as other factors such as the buildup of surface shavings would contribute to changes in frictional stress, and thus pullout load, as fiber slip progresses.

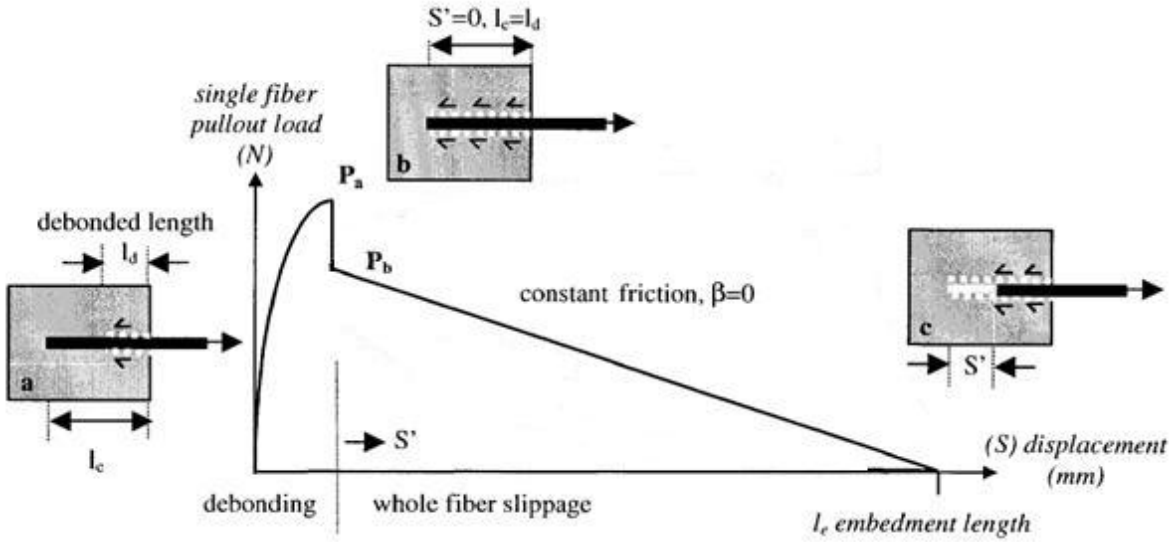

Figure 3.14 - Pullout curve resulting from constant friction pullout (Redon, Li, Wu, Hoshiro, Saito, & Ogawa, 2001)

Slip Softening

A fiber exhibits slip softening behavior when the pullout curve decays at an increasing rate after initial debonding, with pullout load decreasing with continued fiber slip, as illustrated in Figure 3.15. Slip softening is more likely to occur with hydrophobic fibers that do not contribute significant chemical bond strength. Fibers that exhibit slip softening in pullout testing can be expected to exhibit strain softening in an ECC.

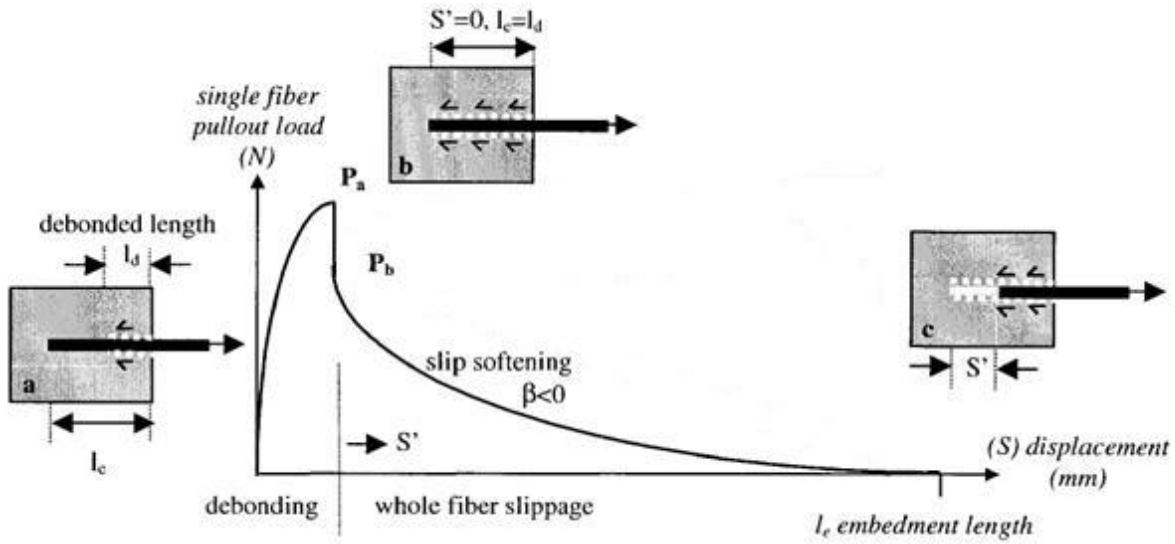

Figure 3.15 - Pullout curve resulting from slip-softening (Redon, Li, Wu, Hoshiro, Saito, & Ogawa, 2001)

Pullout Energy

Rathod & Patodi in 2010 used pullout energy as a parameter to directly compare the pullout performance of different synthetic fibers. Pullout energy, U_P (N-mm), is taken as the area under a pullout load vs. slip curve from a single fiber pullout test.

Pullout energy is an excellent method to quantify fiber performance in pullout tests because it accounts for factors which peak pullout strength may not include, such as fiber rupture. While a strong fiber-matrix interfacial bond is desired, if the bond is too strong, as is sometimes the case with PVA fibers, the fiber can rupture well before pullout. Consider the areas under the pullout curves illustrated in Figure 3.16. The fiber having the peak pullout load ruptures and results in low pullout energy when compared with the fiber exhibiting slip softening over the entire embedment length.

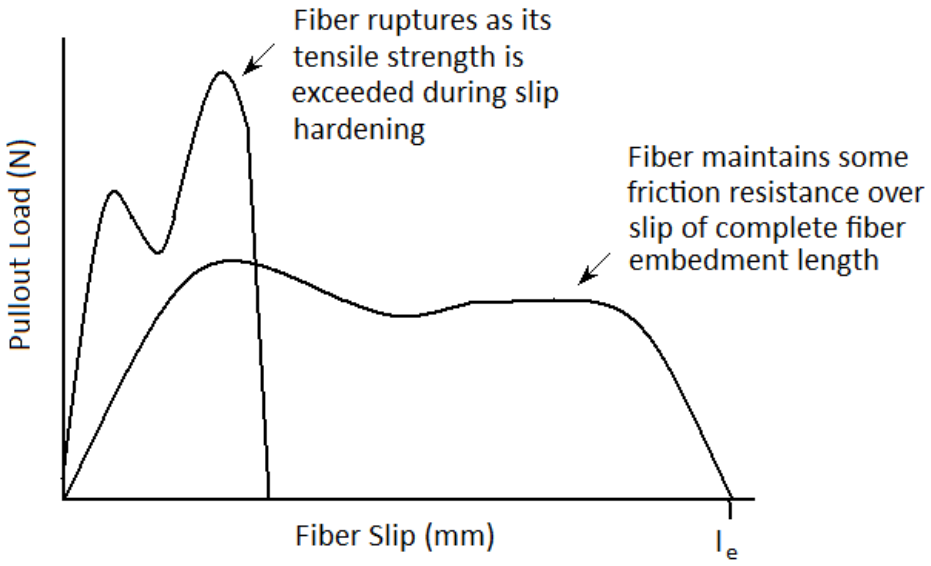

Figure 3.16 - Pullout curves resulting from slip-hardening with fiber rupture and slip softening

Matrix Spalling and Snubbing

When inclined pullout testing is conducted, matrix spalling is a common result, as discussed in Section 3.2.5. The effects of matrix spalling are easily visible in a pullout load vs. slip curve, as illustrated in Figure 3.17.

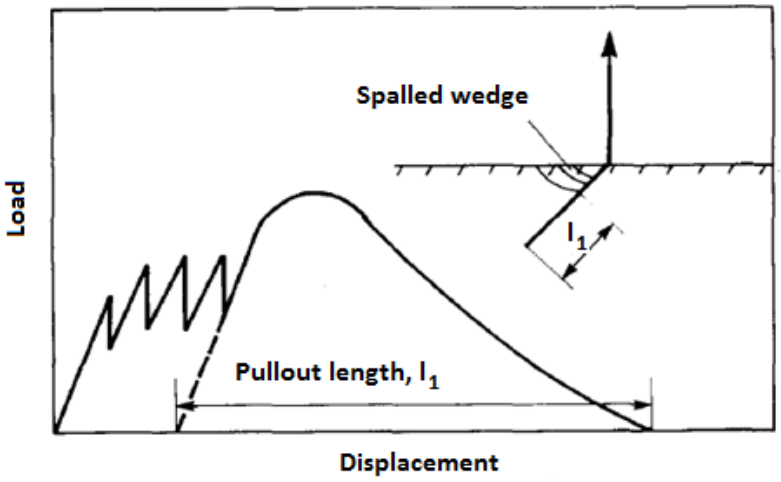

Figure 3.17 - Pullout curve illustrating matrix spalling (Li, Wang, & Backer, 1990)

Li *et al*. in 1990 proposed normalizing the pullout load per unit pullout length with respect to inclined angle, using Equation 3-8. This is reasonable because the effective fiber pullout length decreases as inclined angle increases.

$$\widehat{P} = \frac{(P_{max}/l_1)_{\emptyset}}{(P_{max}/l_1)_{\emptyset=0}} \quad \textbf{3-8}$$

Where,

$\widehat{P}$ = Normalized pullout load per unit pullout length (N)

P_{max} = Maximum pullout load (N)

l_1 = Pullout length at given incline angle (mm)

ϕ = Inclined angle of fiber pullout (radians)

Li *et al.* goes on to propose that the $\widehat{P}$ - ϕ relationship is a function of the snubbing friction coefficient, *f*, according to Equation 3-9, and Equation 3-10. The increase in $\widehat{P}$ with ϕ is due to the frictional force at the fiber exit point.

$$\hat{P} = e^{f\emptyset} \quad \textbf{3-9}$$

Which can also be written as:

$$f = \frac{1}{\emptyset}\ln \hat{P} \quad \textbf{3-10}$$

Where,

$\widehat{P}$ = Normalized pullout load per unit pullout length (N)

f = Snubbing friction coefficient

ϕ = Inclined angle of fiber pullout (radians)

Leung & Ybanez used the snubbing friction coefficient to predict the peak pullout load at any angle according to Equation 3-11.

$$P_\phi = P_0 \exp(f\phi) \quad \textbf{3-11}$$

Where,

P_ϕ = Peak pullout load on given incline angle (N)

P_0 = Peak pullout load on an incline angle of 0° (N)

f = Snubbing friction coefficient

ϕ = Inclined angle of fiber pullout (radians)

The snubbing friction effect depends directly on the matrix interface properties (Li, Wang, & Backer, 1991), and may be dependent on the matrix strength more than fiber characteristics. In 1998, Kanda & Li defined "apparent strength" of a fiber in an inclined pullout test. Because synthetic fibers are typically manufactured to maximize tensile strength, they may be significantly weaker when subjected to compressive strengths from bending moments. Thus, a fiber may rupture at a lower strength during an inclined pullout test than in an aligned pullout test. This lowered fiber strength is known as the "apparent strength" of the fiber and can be calculated using Equation 3-12.

$$\sigma_a = \sigma_{fu}^n \, e^{-f'\phi} \quad \textbf{3-12}$$

Where,

σ_a = Apparent fiber strength (MPa)

σ_{fu}^n = Nominal fiber tensile strength, determined through aligned pullout testing (MPa)

f' = Apparent fiber strength reduction factor

The strength reduction factor, f' is necessary to account for the reduction in fiber strength when pulled out on an incline (Li, Wang, & Wu, 2001). This reduced strength can then be used to compare the effectiveness of synthetic fibers in FRC.

Fiber Efficiency

Another method of characterizing fiber performance in pullout testing is to calculate the efficiency of the fiber in pullout, η. Bentur & Mindess, 1990, proposed Equation 3-13 to determine the strength efficiency for bond, η_τ.

$$\eta_\tau = \begin{cases} \frac{\left(\frac{1}{2}\right)\tau}{\tau_c}, & \tau < \tau_c \\ 1 - \frac{\left(\frac{1}{2}\right)\tau_c}{\tau}, & \tau > \tau_c \end{cases} \quad \textbf{3-13}$$

Where,

$$\tau_c = \frac{\sigma_f r}{l_e} \quad \textbf{3-14}$$

And,

τ_c = Critical bond strength (MPa)

η_τ = Fiber efficiency (%)

τ = Elastic shear stress at interface (MPa)

σ_f = Tensile strength of fiber (MPa)

r = Fiber radius (mm)

l_e = Embedded length of fiber (mm)

The factor of two in Equation 3-13 accounts for the two sides of a fiber bridging a crack each having equal pullout resistance. Therefore, assuming a circular fiber cross section, for a single fiber pullout test, which simulates only one side of the crack, Equation 3-13 can be reduced to Equation 3-15, for cases of $\tau < \tau_c$.

$$\eta_\tau = \frac{P_{max}}{P_{crit}} \quad \textbf{3-15}$$

Where,

η_τ = Fiber efficiency (%)

P_{max} = Maximum pullout load (N)

P_{crit} = Critical load at which fiber will rupture, found using a tensile test performed at the same speed as the pullout test (N)

It is often useful to determine a critical fiber length to maximize efficiency. The critical fiber length, l_c is the minimum fiber length for which the full strength of the fiber, σ_{fu} can be transferred to the matrix through interfacial bond strength, τ_{fu}. Equation 3-16 as described by Kauffman, *et al.* in 2007, allows a critical fiber length to be found for a cylindrical fiber. A fiber longer than l_c can be prone to rupture when tension levels exceed σ_{fu} (Kaufmann, Lubben, & Schwitter, 2007).

$$l_c = \frac{\sigma_{fu} r}{2\tau_{fu}} \qquad \textbf{3-16}$$

Where,

l_c = Critical fiber length (mm)

σ_{fu} = Ultimate tensile strength of fiber (MPa)

r = Fiber radius (mm)

τ_{fu} = Interfacial bond strength (MPa)

Using the parameters discussed, as determined from single fiber pullout tests, the performance of differing synthetic fibers can be directly compared. These parameters can also be used in micromechanical models to determine the fiber performance in FRC composites.

3.3 RHEOLOGY OF SYNTHETIC FIBER REINFORCED CONCRETE

Rheology is the study of the flow of matter and is used to refer to the ability of fresh concrete to flow without segregation. Superplasticizers are commonly used to increase the flow of fresh concrete without compromising the strength of the hardened concrete with additional water. In practice, superplasticizers are very frequently used with synthetic FRC to maintain workability.

3.3.1 Fiber Aspect Ratio vs. Workability

The fiber aspect ratio is defined as the fiber length divided by the fiber diameter. Equivalent diameter, d_{eq}, is defined as the diameter of a round fiber having the same cross sectional area as the fiber being considered. This is used to normalize fiber dimensions for fibers with different cross sections. While an increase in fiber length provides a greater surface area for the matrix to bond to, it has negative side effects:

> "There is an inherent contradiction between the fiber geometry required to allow easy handling of the fresh FRC, and that required for maximum efficiency in the hardened composite. Longer fibers of smaller diameter will be more efficient in the hardened FRC, but will make the fresh FRC more difficult to handle". (Banthia & Mindess, 1995)

This was supported by Grunewald & Walraven (2001) who found that each concrete mixture has a "maximum fiber content" beyond which the workability is compromised. This maximum fiber content is inversely proportional to the aspect ratio of the fiber used. While it is tempting to maximize the aspect ratio of a fiber to increase fiber-matrix bond, this decreases concrete workability. Therefore, a balance must be sought when tailoring the aspect ratio of a new fiber. In the past, increasing fiber surface area was among the only ways to increase fiber matrix bond strength without mechanical anchorage. This research investigates methods to increase chemical bond as a means of improving interfacial bond.

3.3.2 Fiber Bundling

Fiber bundling has also been observed with synthetic fibers. Fiber bundling is the tendency for certain types of synthetic fibers, particularly glass fibers, to clump together within the matrix. This is especially a concern for fibers with high aspect ratios, or fibrillated fibers. Poor mixing of fresh synthetic FRC also contributes to fiber bundling. Fiber bundling reduces the number of individual fibers directly interacting with the matrix, weakening the composite (Li, Wang, & Backer, 1990). It also introduces a weak zone where fibers are in contact with each other and not the matrix.

The effect of fiber bundling is difficult to quantify due to unknown parameters such as the compaction density of the fiber bundles, the degree of cement penetration into the fiber bundles, and bundle size distribution. Li *et al.* in 1990 investigated the effect of fiber bundling on the strength of synthetic FRC composites. Using glass, aramid and nylon fibers, bundles were tested in pullout from a cement matrix. It was found that the fibers having lower bond strength with the matrix, nylon and glass, were infiltrated by cement slurry due to non-ideal packing. This caused inflated results, as more fiber surface was allowed to bond with the matrix. For the aramid fibers, only the fibers on the outside layer developed full bond with the matrix, while the fibers inside the bundle were pulled out with little resistance (Li, Wang, & Backer, 1990).

While a bundle of fibers has a higher pullout resistance than a singular fiber, this is an inefficient use of fibers as more material would be required within a composite using fiber bundles. Individual fibers should be randomly distributed throughout the matrix for greater efficiency. Fiber bundling can often be avoided with careful mixing to ensure proper fiber dispersion.

3.3.3 Self-Compacting Fiber Reinforced Concrete

Self-compacting concrete (SCC) is concrete that in its fresh state is able to flow enough to fill form work while passing obstacles such as rebar, as well as consolidate under the action of its own weight, all without segregating (Pereira, Barros, & Camoes, 2008). The development of SCC has resulted in great increases in productivity, as labor required to compact the concrete is reduced or eliminated.

When designing a SCC mix using synthetic fiber, it is important to provide enough cement paste to allow free movement of the coarse aggregate and fibers past one another as the mixture flows, while maintaining adequate yield stress to prevent segregation. Super plasticizer is an admixture commonly used to increase the fluidity of concrete, however too much can cause segregation and bleeding of the cement paste, (Forgeron & Omer, 2010). A balance is required to maintain the stability of the mixture while increasing fluidity. An increase in fiber content requires a reduction in coarse aggregate or additional paste content to coat the increased fiber surface area. However, a reduction in coarse aggregate could affect the mechanical properties of the hardened concrete.

Typical testing methods for SCC include “ASTM C1621-09b Standard Test Method for Passing Ability of Self-Consolidating Concrete by J-Ring”, and “ASTM C1611-09be1 Standard Test Method for Slump Flow of Self-Consolidating Concrete”, commonly referred to as the J-ring test and slump flow test, respectively. In addition to these standards, “EFNARC Guidelines – The European Guidelines for Self-Compacting Concrete: Specification, Production and Use” is also commonly used, which outlines the V-funnel test and the L-box test. These tests, pictured in Figure 3.18, are used to determine the segregation resistance and the passing ability of a SCC mixture.

Figure 3.18 - Testing methods for SCC. From left: Slump flow, L-box, J-Ring and V-funnel tests (Forgeron & Omer, 2010), (ASTM International, 2009)

In 2010 Buratti, *et al.* investigated the long term behavior of beams constructed from fiber reinforced SCC and compared these with beams constructed from SCC and steel reinforcing bars. Steel and synthetic fibers were used. Buratti, *et al.* tested the long term flexural performance and crack resistance of the beams, as well as the segregation resistance and passing ability of the mixtures using the Slump flow, V-Funnel and J-Ring Tests. While the lowest long term damage was found in the beams using a mixture of steel and synthetic fibers, the reported properties of the fresh concrete were poor. Three of the five fiber reinforced SCC mixtures, including the one containing synthetic fibers, failed at one of the three SCC test methods due to the buildup of fibers, disqualifying these mixtures as self-compacting.

Forgeron & Omer, 2010, characterized the flow of SCC containing fibrillated synthetic macrofibers of 38 mm and 50 mm in length. 20 mixes were tested containing fiber contents of 0.20%, 0.25%, 0.30%, 0.35%, 0.40% and 0.50%, as well as a control concrete mix containing no fibers. The water cement ratio was also varied to test the effect of volume of paste content on the flow characteristics of the mixes. The slump flow, filling capacity, L-box and V-funnel tests were used to test the flow characteristics. The mixes containing higher paste content performed better in the L-box tests. Acceptable slump flows were achieved for all mixes proving that synthetic self-fibrillating macrofibers can

be used with fiber volumes up to 0.4% by volume in self-compacting concrete mixtures using only ternary blend cement and high range water reducing admixtures. However the mixes containing the 50 mm fibers were unsuccessful at the L-Box and V-Funnel tests. While the fibers were tested at two different lengths, and therefore different aspect ratios, the fiber cross section was unchanged. Therefore the surface area of fibers in mixtures having the same fiber content was identical. This indicated that fiber aspect ratio has a stronger influence on flow characteristics than the number of synthetic fibers in the mixture (Forgeron & Omer, 2010). Mechanical properties of the hardened concrete were also tested and fibers were found to improve cracking resistance for all mixes.

When developing a synthetic fiber for use in FRC, variables such as aspect ratio and paste content of the mix (based on intended application) should be considered in order to maintain the balance between workability and concrete strength. The ability to not only control cross section but also bond strength, as is the attempt with this research, is novel, and will provide more flexibility for optimizing a newly developed fiber.

3.4 CURRENT SYNTHETIC FIBER MATERIALS

When comparing different materials for the development of a new synthetic fiber, it is useful to consider the properties of synthetic fibers currently available. Table 3.2 lists important properties of materials considered for use in synthetic fibers. It should be noted that the values in Table 3.2 can vary based on factors such as manufacturing process, material source, and market fluctuations. The values shown are meant to be representative of typical values for each fiber material. It should also be noted that PVA, carbon, aramid and glass are typically only produced as microfibers and therefore may not be useful for the same applications as several of the other materials listed.

Table 3.2 - Comparison of select properties of some common fibers used as concrete reinforcement (after Bentur & Mindess, 1990)

Fiber Material	SG	σ_f (MPa)	E_f (GPa)	Relative Bond Strength	Alkali Resistance	Approx. Cost (US/kg)
Tuf-Strand SF	0.92	650-750	9.5	Very High	High	$ 8.50
High Density Polyethylene	0.96	400	5-6	Low	High	$ 2.00
Polypropylene	0.90	500-750	5-7	Low	High	$ 3.00
Poly(vinylidene fluoride)	1.78	350	2	High	High	$ 32.00
Nylon	1.14	900	5	Low	High	$ 5.50
Polyvinyl alcohol	1.30	20-25	1.2-1.5	Very High	High	$ 6.00
Carbon	1.90	2500-3000	230	Moderate	High	$ 46.00
Aramid	1.45	3600	65-133	Moderate	Moderate	$ 33.00
Glass	2.60	2000-4000	70-80	Moderate	Low	$12.00
Polyester	1.34	900-1100	17	Low	Low	$ 2.20
Acrylic	1.18	400-1000	14-19.5	High	High	$ 4.00

Properties to consider when selecting a material for use as a synthetic fiber include tensile strength, elastic modulus, and bond strength. These properties determine the fibers contribution to the mechanical properties of FRC. Melt temperature and specific gravity are important properties for the purpose of manufacturing the fibers. Another consideration is the material resistance to alkali degradation. Concrete is a harsh alkaline environment and some materials, specifically glass, can dissolve within the matrix over time, reducing the strength of the concrete rather than strengthening it. Cost is also an important consideration. A material must be have a superior cost to performance ratio than currently available alternatives to justify manufacturing.

3.4.1 Tuf-Strand Synthetic Fiber

In 2001 a blended fiber, Tuf-Strand SF, containing 77% polypropylene and 23% high density polyethylene, was developed by Trottier *et al.* for use as concrete reinforcement. This fiber is self-fibrillating, providing a significant mechanical bond with the concrete matrix. Tuf-Strand SF is produced through melt extrusion and exhibits high tensile properties when compared with pure HDPE or polypropylene fibers. The fiber is produced by AFT and is sold commercially by Euclid Chemical Company. Due to its commercial success and proven performance in FRC (Trottier, Mahoney, & Forgeron, 2002), Tuf-Strand SF has been used as the benchmark for this research.

3.4.2 High Density Polyethylene

High density polyethylene (HDPE) is one of least expensive materials used for synthetic fibers. Its remarkable deformability and toughness allows HDPE to undergo very high permanent strains, through molecular alignment and thus increasing tensile strength (Lin & Argon, 1994). HDPE is stable in an alkaline environment, however it is hydrophobic, meaning it repels water and thus is poor at forming a chemical bond with the matrix. Mechanical alterations to the fiber surface can compensate for this by increasing frictional bond.

The effect of varying extrusion parameters on different commercially available HDPE resins was investigated to produce fibers for use in FRC (Trottier A. M., 2009). It was found that by using a medium molecular weight grade HDPE resin and high draw ratios, fibers were produced having tensile strengths greater than that of Tuf-Strand SF fibers. High molecular weight grade HDPE can also reach very high tensile strengths, but gel spinning is required. Recent advancements in resin manufacturing and processing have allowed melt extrusion to produce HDPE filaments with tensile strengths of over 1000 MPa, well above the 400 MPa reached conventionally. The high tensile properties coupled with the low material cost make HDPE a good candidate material for future

synthetic fibers.

3.4.3 Polypropylene

Polypropylene is very commonly used for synthetic fibers. It is a relatively low cost material, with high tensile properties when produced using melt extrusion. It is also heat resistant and exhibits excellent resistance to degradation in alkaline environments. While polypropylene is also hydrophobic, polypropylene fibers have a tendency to form surface deformations during pullout (Geng & Leung, 1996). These flaws can form a mechanical bond with the matrix by increasing frictional resistance. This allows untreated polypropylene fibers to perform successfully in FRC.

3.4.4 Poly(vinylidene fluoride)

Poly(vinylidene fluoride), (PVDF), resin has typically been used in chemical industry applications as an anti-corrosion material, as well as in electrical applications as an insulation material. PVDF has not been thoroughly investigated as a material for synthetic fibers, however research suggests the potential for good performance in FRC. PVDF can be used in the melt extrusion process, and is alkali resistant. PVDF has the potential to be blended with other polymers to create blended synthetic fibers (Li & Kaito, 2003).

PVDF has a higher specific gravity than most polymeric materials used for synthetic fibers. This helps with concrete mixing and placement, as lighter fibers often float and segregate from the fresh mixture. Also, in concrete applications where processes are in place for reclamation of aggregate and mixing water, a fiber that floats would clog water reclamation pumps. A fiber that sinks with the aggregate can be reclaimed and recycled in future mixes.

The chemical interactions at the interface of PVDF powder and white cement were investigated using different methods of spectroscopy (MacDonald, 2010). It was observed that PVDF reacted chemically with the cement in powder form, indicating that blended fibers containing PVDF could create a strong chemical bond with the concrete matrix.

The tensile properties and molecular orientation of PVDF for use as concrete reinforcement when produced using melt extrusion have also been investigated (Trottier A. M., 2009). It was found that the elastic modulus and tensile strength of the material generally increased as the draw ratio increased. Trottier concluded that pure PVDF fibers did not exhibit tensile strengths high enough to compete with currently available synthetic fibers.

3.4.5 Nylon

Nylon is the generic name for polyamide materials. This material is frequently used in the textile industry, and is relatively low cost. Nylon fibers have high tensile strengths and are stable in alkaline and heated environments. They are hydrophilic in nature, and can swell from water, mildly increasing the frictional resistance in pullout from concrete (Geng & Leung, 1996). Despite this, nylon fibers have historically demonstrated low bond strength, (Wang, Li, & Backer, 1988).

3.4.6 Polyvinyl Alcohol

PVA is a commonly used material for synthetic fibers in FRC because of its high tensile properties and high bond strength. It is also alkali resistant and has a high melting point. PVA fibers cannot be produced using melt spinning, but require gel spinning. This increasing PVA fiber production costs.

PVA is hydrophilic and creates a strong chemical bond between the fiber and the surrounding matrix. Unfortunately, the PVA fiber-matrix bond is so strong that the fiber often ruptures before pulling out of the matrix. In addition to this, PVA fibers have low lateral resistance and thus are more likely to fracture during inclined pullout (Li, Wang, & Wu, 2001). While this improves the ductility of the composite, it reduces the toughness.

To decrease the fiber-matrix bond to a more suitable strength, PVA fibers are sometimes coated with an oiling agent (Li V. , Wu, Wang, Ogawa, & Saito, 2002). It has also been shown that the presence of admixtures such as fly ash in PVA reinforced ECCs can also decrease the bond strength to a useful limit (Redon, Li, Wu, Hoshiro, Saito, & Ogawa, 2001).

3.4.7 Other Commercially Available Fibers

Some other commercially available synthetic fiber materials include carbon, aramid, glass, polyester and acrylic. While these fibers have been used in concrete composites, they were too expensive for their potential performance, and thus were not a material used in this research. Therefore, they will only be briefly discussed in this section.

Carbon

Carbon fibers are highly resistant to corrosion and have a very high elastic modulus, making them stiffer than steel fibers. However they are more brittle than polymeric fibers and also do not exhibit high bond strength without surface alterations (Reda Taha & Shrive, 1998). The primary drawback for carbon fibers is the high cost; in fact, carbon fibers have the highest cost of the fibers discussed.

Aramid

Aramid fibers are commercially known as Kevlar, and are manufactured by Dupont. While these fibers have a very high tensile strength, elastic modulus, and thermal stability, they have been shown to exhibit significant increases in creep under transient moisture conditions (Wang, Dillard, & Ward, 1992). Aramid fibers cannot be produced by melt extrusion, which contributes to the high cost of the fibers.

Glass

Glass fibers have a high tensile strength and are reasonably priced when compared with carbon or aramid fibers. However they are very brittle and do not increase ductility in FRC composites as successfully as polymeric fibers. Another sinificant drawback with glass fibers is the very low alkali resistance. Surface treatments have been invented to produce “alkali resistant” glass fibers, however long term degradation still occurs (Purnell & Beddows, 2005).

Polyester

Polyester fibers are low cost and relatively high tensile strength. They are hydrophobic, but often have a silicon outer layer that increases polarity and slightly improves the bond with the matrix (Rathod & Patodi, 2010). However they have low alkali resistance, making them unsuitable for concrete reinforcement.

Acrylic

Acrylic fibers are used extensively in the textile industry, primarily for clothing. These fibers have high bond strength and high alkali resistance. Acrylic fibers also have the potential for high tensile strengths; however this cannot be done using melt spinning, making this material not cost effective for use as fiber reinforcement.

3.5 ALTERATIONS TO IMPROVE FIBER-MATRIX BOND

There are many alterations that can improve the fiber-matrix bond, both by altering frictional bond strength and chemical bond strength. One way to improve fiber-matrix bond strength is to narrow the interfacial transition zone of the matrix by using fine cementitious materials such as fly ash or silica fume. However, as this research aims to develop a new synthetic fiber for commercial use, the concrete mix proportions cannot be dictated. Thus, this section will focus on alterations to the fiber itself.

3.5.1 Mechanical Alterations

For hydrophobic synthetic fibers, which do not usually exhibit high chemical bond strength, mechanical alterations can be made to improve frictional resistance using mechanical anchorage.

Fiber Deformation

Deforming the surface of synthetic fibers has been accomplished in various ways, all with the intention of increasing the frictional resistance at the fiber-matrix interface. Fiber deformation is primarily performed on macrofibers, because the fine diameter of microfibers makes this type of mechanical alteration difficult. One commonly used and cost efficient method is crimping, shown in Figure 3.19. Synthetic fibers can be easily crimped by being passed through loosely engaged gears on the extrusion line.

Figure 3.19 - Crimped synthetic fiber for use in FRC (Propex Concrete Systems, 2007)

Won, *et al.*, 2006, used single fiber pullout testing to investigate the bond behavior of six types of deformed and one straight mono-filament polypropylene macrofiber. The deformed shapes used are as illustrated in Figure 3.20. It was found that the double deformed and enlarged end (button end) geometries exhibit a sudden loss of interface toughness after fracture of the deformed fiber parts, while the hooked and sinusoidal end fibers failed by pullout. The straight fiber had the lowest pullout strength. This proved that mechanical deformation can increase the fiber-matrix bond. The crimped fibers exhibited significantly higher pullout load and interface toughness than the other fibers. Using these findings, the optimum height and amplitude for crimped polypropylene fibers was determined to be 1.8 mm and 6 mm, respectively. While mechanically optimum, these dimensions are large compared to typical fiber sizes, and could be difficult to produce on an extrusion line.

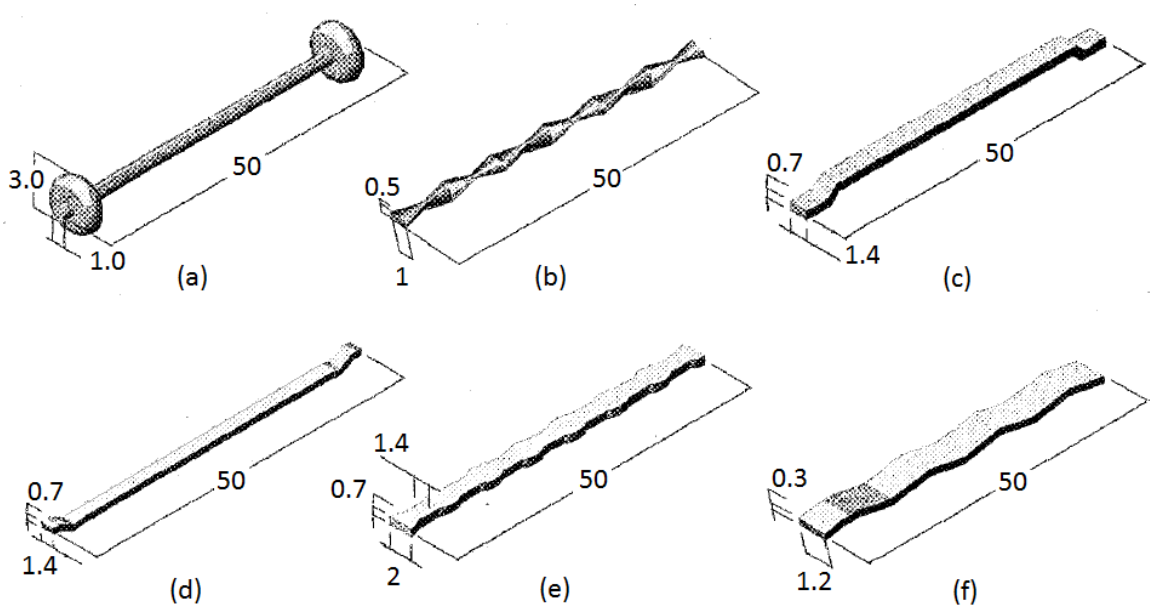

Figure 3.20 - Deformed shape of synthetic macrofibers (dimensions in mm): (a) button end; (b) twisted; (c) hooked end; (d) sinusoidal ends; (e) double deformed; (f) crimped (Won, Park, Lee, Jang, & Kim, 2009)

Embossment is another method of fiber deformation that has been successfully used on synthetic fibers. Embossment involves stamping a pattern on to the fibers on the extrusion line. Figure 3.21 shows a commercially available synthetic fiber with an embossed cross pattern.

Figure 3.21 - Embossed pattern on "Bar Chip" brand polyolefin fiber

In 2008 Kim, *et al.* investigated the effect of fiber deformations on shrinkage cracking in fiber reinforced ECCs. They tested straight, crimped and embossed polyolefin fibers. The embossed fibers are shown in Figure 3.22. It was concluded that all other variables being equal, such as fiber quantity, length and diameter, the fiber geometry does affect the mechanical bond and thus the plastic shrinkage of the composites. The embossed fibers were found to have the greatest performance. However, it was found that once the fiber volume fraction exceeds 0.5% plastic shrinkage was fully controlled and so fiber geometry had no further effect.

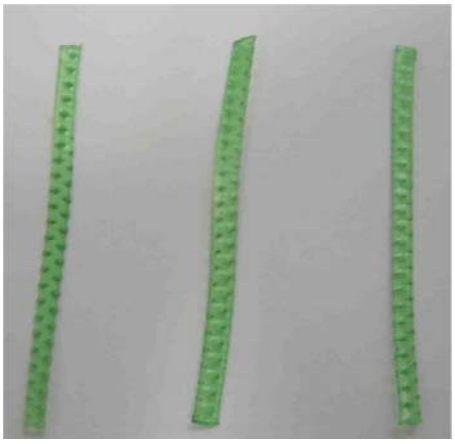

Figure 3.22 - Geometry of embossed recycled polyolefin fiber (Kim, El-Tawil, & Naaman, 2008)

It should be noted that these mechanical alterations to synthetic fibers could decrease the tensile strength of the fiber. Also, crimping and embossing can be difficult to achieve economically on a melt extrusion line. A decrease in the rate at which filaments are produced would be required for these mechanical alterations to be incorporated in manufacturing, thus increasing the production cost. Therefore, to justify these methods the increase in interfacial bond must be sufficient to overcome the loss in tensile properties and increase in production costs.

Fibrillation

Polypropylene fibers are known to fibrillate slightly after mixing when knife cuts are included in the production process, and this has been proven to increase the bond strength of these fibers (Geng & Leung, 1996). Polypropylene fibrillation has been used to produce mesh-like fibers, as illustrated in Figure 3.23. The fibers appear as a fine bundled fiber, but separate into a mesh after mixing. This increases the fiber surface area available to bond with the matrix.

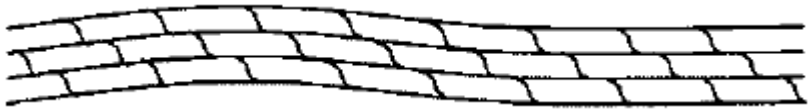

Figure 3.23 - Fibrillated mesh polypropylene fibers (Trottier, Mahoney, & Forgeron, 2002)

In 2001 Trottier, *et al.* developed a blended fiber containing 77% polypropylene and 23% high density polyethylene that was self-fibrillating. The fibers undergo fibrillation after mixing due to the immiscibility of the two materials. The cross sections of fibrillated fibers both before and after mixing are illustrated in Figure 3.24. Fibrillation allows the fiber to maintain its macrofiber behavior to prevent balling while mixing, but contribute properties similar to that of microfibers in FRC performance due to the fibrils. Fibrillation increases the fiber surface area by approximately 20% while also creating significant mechanical anchorage. Both of these qualities increase the frictional resistance of the fiber to pullout. Fibrillated fibers have been proven to successfully replace welded wire fabric in slabs on grade (Trottier, Mahoney, & Forgeron, 2002).

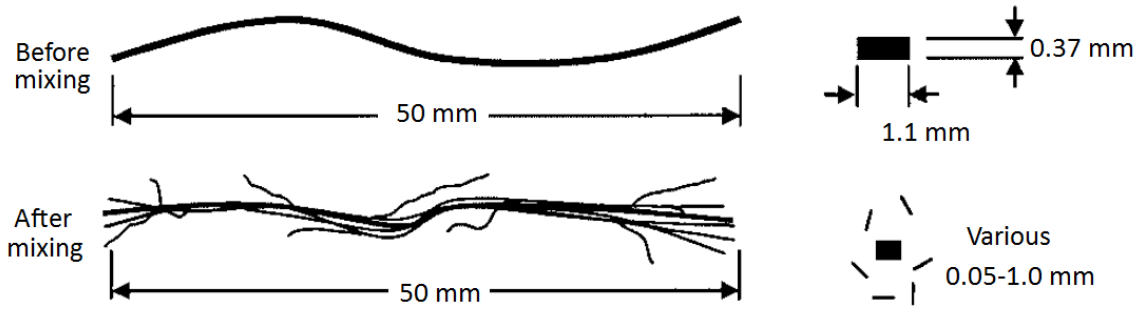

Figure 3.24 - Fiber fibrillation and change in dimensions before and after mixing (after Trottier, *et al.*, 2002)

Cross Sectional Geometry

An increase in fiber surface area has been shown to improve fiber-matrix bond strength, however, this can sometimes decrease fiber workability, as discussed in Section 3.3.1. One way to increase fiber surface area without compromising workability is to manipulate the cross sectional geometry of the fiber. For fibers produced using melt spinning, changing the cross sectional geometry can be achieved during manufacturing using the spinneret.

The extrusion die on the spinneret determines the cross section of the fiber by extruding the fibers in the shape of the spinneret holes. A schematic of the extrusion die is shown in Figure 3.25. The die head on the spinneret can be replaced, meaning several die heads can be produced with varying shapes for spinneret holes. However, the production of high quality die heads can be expensive, and testing a variety of geometries may not be economically feasible. The spinneret holes can produce simple cross sections, such as circular, rectangular, or more intricate cross sections, such as a star shape with many points or a trilobal shape, as pictured in Figure 3.26. A fiber with a more intricate cross section, such as trilobal, has a greater surface area than a circular fiber of similar dimensions, thus allowing a greater area to bond with the matrix.

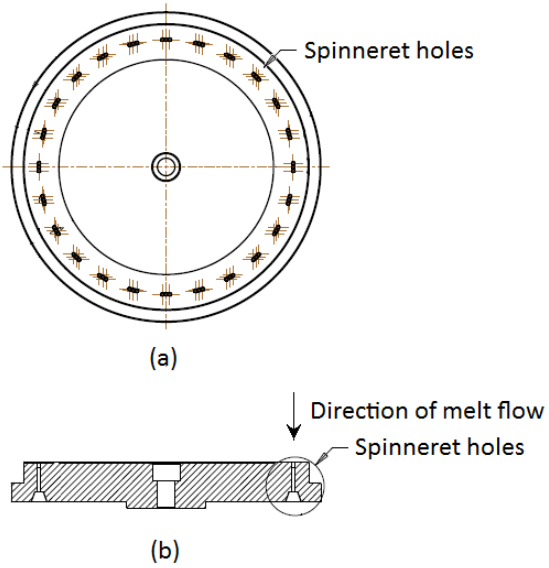

Figure 3.25 - Extrusion di: (a) plan view (b) profile view

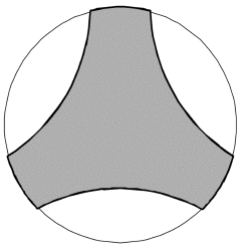

Figure 3.26 - Trilobal shaped cross section of polyester fiber (Rathod & Patodi, 2010)

3.5.2 Chemical Alterations

Alterations to improve the chemical bond strength of fibers can include both admixtures and chemical surface treatments. “Admixtures” in this case refers to materials being added directly to the synthetic resins as the fiber is being produced to change the chemical properties of the entire fiber. Chemical surface treatments have been used to either increase or decrease the chemical bond strength as necessary for the desired applications.

Ethylene Vinyl Acetate

Ethylene vinyl acetate (EVA) is a resin commonly sold as an adhesive. In both rubber and plastic copolymer states, EVA has been shown to improve toughness in nylon when blended in quantities as low as 15% (Zhang, Yu, & Ren, 2009). EVA has a low melt temperature and therefore can be easily added to the melt extrusion process.

In 2009, MacDonald used nuclear magnetic resonance spectroscopy to investigate the behavior of poly(ethylene vinyl acetate) in white cement. Results indicated the potential for EVA to form a chemical bond with cement powder. This indicates that EVA, when used as an additive to synthetic fibers, could potentially increase the chemical bond at the fiber-matrix interface.

Melaic Anhydride

Melaic anhydride (MAH) is a polymer used as an adhesive and polymer compatibilizer. It was designed as a blend component for unmodified polyethylene, and is known to promote adhesion between polyolefins (Yu, Zhang, & Ren, 2009). Therefore, MAH can be used to blend two polymeric materials that would not normally blend, for example to take advantage of the tensile strength of one material while incorporating the chemical bond strength of the other. MAH has a density of 0.96 and a melting point of 130°C (Dow Chemical Company, 2011).

Oiling Agents

As previously discussed, some hydrophilic fibers, such as PVA, have interfacial bonds so strong that fibers rupture before achieving pullout, decreasing the toughness of the composite. To decrease the fiber-matrix bond to a more useful strength, PVA fibers are sometimes coated with an oiling agent.

Li, *et al.* in 2002 investigated the effect of using an oiling agent on PVA fibers. The research goal was to illustrate the importance of interface tailoring on the performance of ECCs. Using the micromechanics model for the parameters τ_o, G_D, and β described by

Lin, *et al.* in 1999, the authors determined target values for interface tailoring to achieve an increase in strain capacity of the composite. Using single fiber pullout testing and uniaxial testing on the composite, the amount of oiling agent was added to the fibers to achieve the desired parameter values. The oil agent used is known to bond strongly with the fiber, and so no oil would be expected to be lost during concrete mixing. The authors concluded that proper interface tailoring can achieve tensile strain hardening with strain capacity above 4% for PVA reinforced ECCs, and that an oiling agent content of 1.2% was optimum for their purposes.

Other Chemical Alterations

Bicomponent fibers, consisting of a core such as polypropylene with a sheath of a differing material, have recently been produced using a "co-extrusion" process. These fibers have the strength of the core material while taking advantage of the bond strength of the sheath material (Kaufmann, Lubben, & Schwitter, 2007). Other chemical alterations to increase bond strength of synthetic fibers have included chemical surface treatments such as oxyflourination, surface oxidation, bromination, fluorocarbon, and even plasma treatments (Li, Wu, & Chan, 1996). However, many of these treatment processes are not cost effective, nor can they be used in the melt extrusion process.

The following chapter describes the testing program including the sample preparation, testing methods, and the fiber types evaluated and other materials used for each test.

CHAPTER 4 TESTING PROGRAM

To fully compare and characterize different synthetic fibers, several tests were conducted. These are divided into fiber extrusion, fiber tensile testing, single fiber pullout testing, testing of fiber performance in FRC mixtures, and tensile creep testing. The following section describes the numerous trials of fiber production using the melt extrusion process. This process varied settings on the extrusion line, as well as materials and combinations of materials used. This was followed by tensile testing, which involves determining the tensile strength and elastic modulus of the extruded fibers. Tensile testing was followed by pullout testing to characterize the interfacial bond properties of the fibers. Select macrofibers were then chosen for FRC performance testing, to characterize the contribution of fibers to the flexural performance in a concrete mixture. Tensile creep testing was also conducted to characterize the ability of fibers to maintain sustained loading.

4.1 FIBER EXTRUSION

The fibers for these experiments are produced by melt extrusion on an “experimental line” for AFT in Sydney, Nova Scotia. The primary variables investigated to produce the fiber with the highest tensile strength were cross sectional dimensions, stretch ratios, and materials mixed.

The screw speed and temperatures within the melt screw chamber were set according to the melting temperatures of varying materials. The pump speed and stretch ratio were varied to achieve the desired cross sectional size. Stretch ratios were then increased slowly and samples were taken until the fibers began to break on the line. Stretch ratios varied from 5.0 to 16.21, depending on the materials and fiber geometry. Filament samples were taken throughout this process to investigate the effect of stretch ratio on tensile strength and elastic modulus, and to compare tensile properties with the benchmark fiber, Tuf-Strand SF.

A target cross section of 1.0 mm width and 0.3 mm thickness for macrofibers, and 0.3 mm diameter for microfibers was set. Figure 4.1 shows the shapes and profile views of the die head holes in the spinneret. Microfibers were circular in geometry, produced using the cross section shown in Figure 4.1 (a). Initially fiber cross sectional geometry for macrofibers was produced according to Figure 4.1 (b). This is the same geometry used for Tuf-Strand self-fibrillating fibers. As testing continued on materials not meant for fibrillation, a new die head was produced using the geometry shown in Figure 4.1 (c).

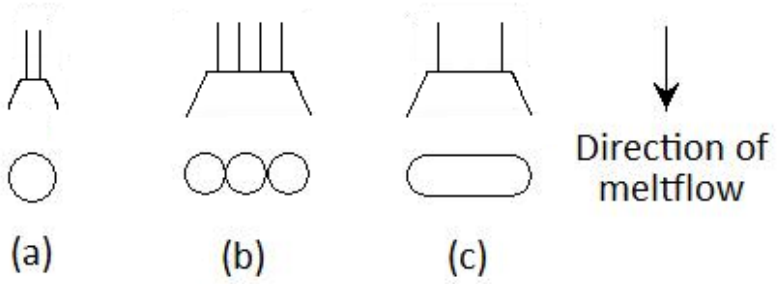

Figure 4.1 - Holes in spinneret die head controlling cross section of fibers for (a) microfibers, (b) fibrillating macrofibers, (c) monofilament macrofibers

The materials used in the production of prototype fibers included HDPE, polypropylene (PP), PVDF, EVA, and MAH. In addition to these materials, existing commercially available synthetic fibers were also tested for comparison. These fibers were Tuf-Strand SF, Nylon (BASF brand), PVA (Kuralon brand), another polypropylene/polyethylene blend called Strux 85/50, and an embossed polypropylene fiber called BASF MasterFiber MAC 470.

The filaments were extruded in a series of seven separate trials over two year time period. The complete list of extruded filaments is included in Appendix A. The first trial produced filaments made from pure PVDF. During this trial, settings such as oven temperatures and stretch ratios were varied. Based on the initial results of this trial it was determined that PVDF filaments had unsatisfactory tensile strengths to be used as

the primary material in a successful fiber. However it was hypothesized that the addition of PVDF to other materials could increase the fiber-matrix chemical bond. The sample from this trial with the highest elastic modulus was selected for pullout testing.

The second trial involved adding PVDF to PP in the ratios of 78% PP and 22% PVDF. Filaments containing HDPE and PVDF in the ratios of 82% HDPE and 18% PVDF were also extruded. These ratios were chosen to create a fiber with a specific gravity greater than 1, thus the fiber would sink. PP and HDPE were chosen as the primary materials in this trial based on previous performance. As discussed in Section 3.4, these materials have been shown to have high tensile strength properties and low cost. During this trial, it was found that mixtures containing PVDF showed evidence of a buildup around the di holes, shown in Figure 4.2. As the extrusion line ran, this buildup continued to increase until pieces detached from the die head and were carried on the filaments down the extrusion line. This caused irregularities on the fibers. Samples of the buildup were sent to a chemical lab and were determined to be PVDF. It was proposed that because PP and HDPE are hydrophobic and PVDF is hydrophilic, the materials are separating within the mixing chamber.

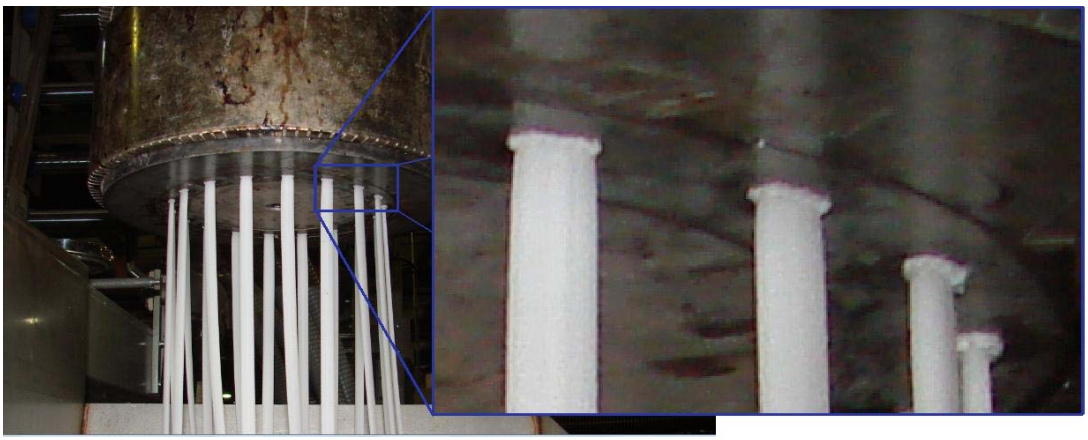

Figure 4.2 - Buildup of PVDF on holes of spinneret die head

The third trial involved extruding filaments of an HDPE resin from a new supplier. This resin is referred to as HDPE 5906. Samples were taken at increasing stretch ratios. Initial testing indicated promising results when using this resin. During this trial another attempt was made to blend PP and PVDF with little success.

The fourth trial used HDPE 5906 to produce microfibers, having circular cross sections and diameters under 0.6 mm. Initial testing on these fibers indicated very high tensile strengths. This resulted in continued use of HDPE 5906 throughout future trials.

The fifth trial focused on new methods to blend PVDF with HDPE 5906. To prevent PVDF buildup on the die head, MAH was proposed as an additive. Because MAH is a copolymer stabilizer, it was used to allow the HDPE and PVDF resins to mix without separating during melt extrusion. It was observed that while the PVDF buildup did not seem to occur at PVDF contents below 3%, the problem became magnified as the PVDF content was increased, and more MAH was required. EVA was also introduced to HDPE 5906 as an additive to increase fiber-matrix bond. This material was added in the form of resins containing 90% polyethylene filler and 10% pure EVA. During this trial the fibers produced were microfibers having diameters less than 0.5 mm.

The sixth trial investigated another HDPE resin referred to as HDPE 1288. Filaments produced in this trial were also microfibers with circular cross sections less than 0.35 mm in diameter.

The seventh and final trial was a culmination of previous trials. Fibers produced in this trial included successful blends of HDPE 5906, PVDF and MAH in varying ratios, to determine the effect of PVDF addition on fiber properties. In addition, fibers containing blends of PP, HDPE 5906, and EVA were also produced. Filaments for tensile testing and pullout testing were produced, as well as cut fibers for use in performance testing.

4.2 FIBER TENSILE TEST

All filament samples taken from the experimental line were first tested in tension to determine the tensile strength and elastic modulus. Before testing, cross sectional measurements were taken on ten samples of each filament. Tensile testing was conducted according to ASTM D2256-10 and EN 14880-2:2006, as described in Section 2.3. Testing was conducted using an Instron 8501 machine with a 500 kN load cell and an Instron 8500+ controller. A load was applied by stretching the fiber at a constant rate of 200 mm/min.

Specimens were handled in a careful manner to ensure no twisting or stretching of the filament took place during setup. The filament was restrained using two custom made fixtures, containing two stationary spindles which the filament was looped around, before being clamped at each end by a small wing nut as shown in Figure 4.3. This was to reduce local stresses around the clamped section of the filament. A very small initial tension was applied to ensure no slack or kinks were present in the sample.

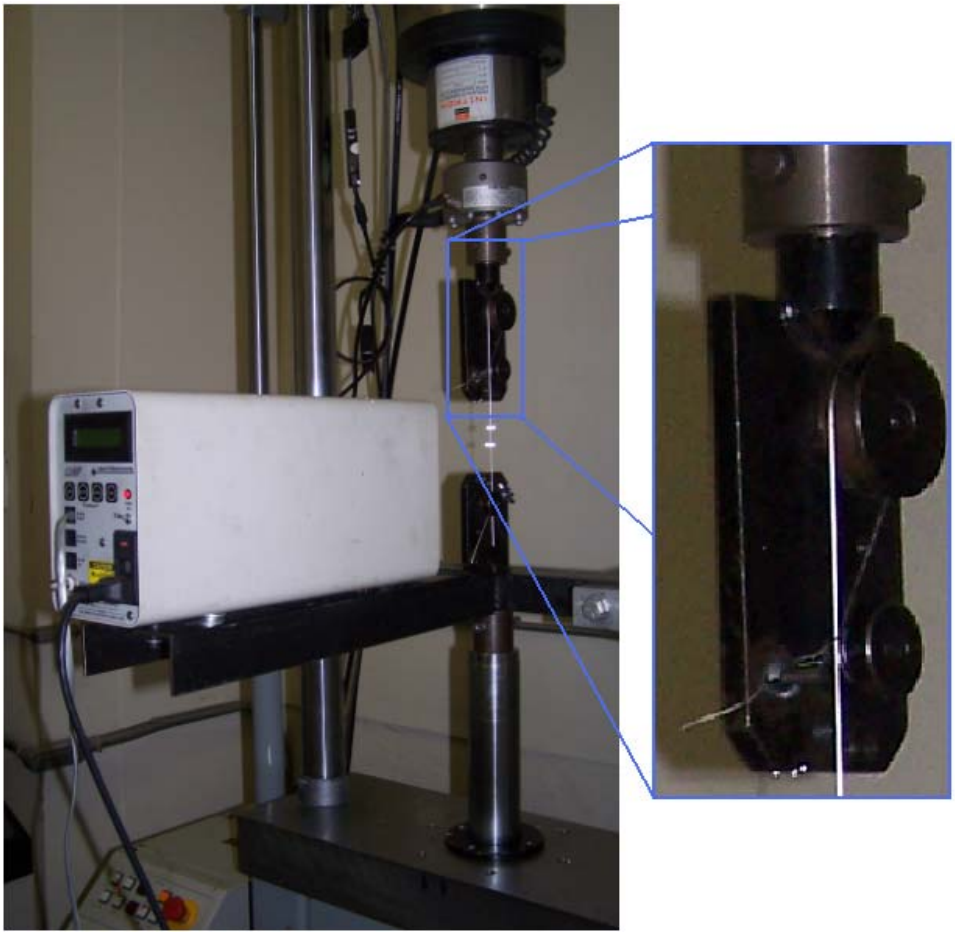

Figure 4.3 - Setup for tensile testing of filaments with close-up of restraining fixture

Elongation of the specimen was measured using a laser extensometer, pictured in Figure 4.4, and two pieces of reflective tape set at 40 mm apart on the specimen between the restraining fixtures. EN 14889-2:2006 recommends the initial distance between the two tapes be greater than 20 mm to avoid increasing measurement uncertainty. The elongation between the reflective tapes was recorded throughout the test, while the load cell tracked the tensile load applied to the specimen. A data acquisition system recorded the tensile load and the distance between the reflective tapes throughout the test.

Figure 4.4 - Laser extensometer

Testing was conducted at a constant rate of displacement until fiber rupture. The machine was then stopped and reset to the initial gauge length, in accordance with ASTM D2256-10. The test results were recorded to within three significant figures. During testing the break location was observed in accordance with ASTM D2256-10. If the filament broke at the clamp the test was considered invalid and was repeated.

158 different filament types were tested in tension. Tests on approximately 10 samples of each filament type were conducted and the results were averaged. The data provided the ultimate tensile strength as well as the elastic modulus of the samples. The elastic modulus is taken between 10% and 30% of the ultimate tensile capacity, in accordance with the standards. Fiber cross sections were measured using digital calipers. Ten measurements each were taken for both fiber width and thickness.

In addition to the samples taken from the experimental line, filament samples of commercially available nylon, PVA, and Tuf-Strand SF were also tested in tension for comparison.

4.3 SINGLE FIBER PULLOUT TEST

4.3.1 Materials

After tensile testing results were compared, filaments exhibiting high tensile strengths were selected for single fiber pullout testing. The fibers tested in pullout are listed in Table 4.1 for macrofibers and Table 4.2 for microfibers, along with the casted inclination angles and embedment lengths. These particular fibers were chosen for their tensile properties, and to compare the fiber-matrix bond strength of different materials in varying proportions. At least ten samples were produced for each inclination angle and embedment length. Embedment lengths were chosen based on typical values used commercially for macrofibers and microfibers. Microfibers use smaller embedment lengths than macrofibers due to restrictions to fiber aspect ratios, as discussed in Section 3.3.1.

Table 4.1 - Macrofibers used in single fiber pullout testing

Fiber Description	Inclination Angle (degrees)	Embedment Length (mm)
100 % HDPE	0, 15, 30, 45 and 60	25.4 and 22.23
HDPE, 1% PVDF	0, 15, 30, 45 and 60	
HDPE, 3% PVDF	0, 15, 30, 45 and 60	
HDPE, 5% PVDF, 10% MAH	0, 15, 30, 45 and 60	
HDPE, 7% PVDF, 10% MAH	0, 15, 30, 45 and 60	
HDPE, 9% PVDF, 10% MAH	0, 15, 30, 45 and 60	
HDPE, 11% PVDF, 20% MAH	0, 15, 30, 45 and 60	
100% PVDF	0	
HDPE, 10% EVA	0, 15, 30, 45 and 60	
80% PP, 10% HDPE, 10% EVA	0, 15 and 30	
Tuf-Strand SF	0, 15, 30, 45 and 60	

Table 4.2 - Microfibers used in single fiber pullout testing

Fiber Description	Inclination Angle (degrees)	Embedment Length (mm)
HDPE 5906	0	19.05 and 15.88
HDPE 1288	0	
HDPE, 10% PVDF, 20% MAH	0, 15, 30, 45 and 60	
HDPE, 10% EVA	0, 15, 30, 45 and 60	
Nylon	0, 15 and 30	
PVA	0	

The concrete matrix for pullout specimens was prepared using the mortar mixture shown in Table 4.3. This mixture was used because the water/cement ratio and cement content was representative of real world applications. Mortar mixtures were prepared in 0.005 m^3 batches. Cement used was ASTM Type 1 Portland Cement, produced in Joliette, Quebec and supplied by Holcim Canada. The fine aggregate used was Nova Scotia sourced river sand supplied by Shaw Resources, with a fineness modulus of 2.72. A sieve analysis was performed on the fine aggregate according to ASTM C136-06 "Standard Test Method for Sieve Analysis of Fine and Coarse Aggregates". The resulting aggregate gradation curve falls within the limits set by ASTM C33-11 "Standard Specification for Concrete Aggregates" for grain size distribution, as shown in Figure 4.5. The superplasticizer used was Plastol 5000 High Range Water Reducing Admixture, supplied by The Euclid Chemical Company.

Table 4.3 - Mortar mixture used for pullout specimens

Material	Quantity (kg/m3)
Cement	400
Fine Aggregate	1200
Water	160
Superplasticizer	as necessary

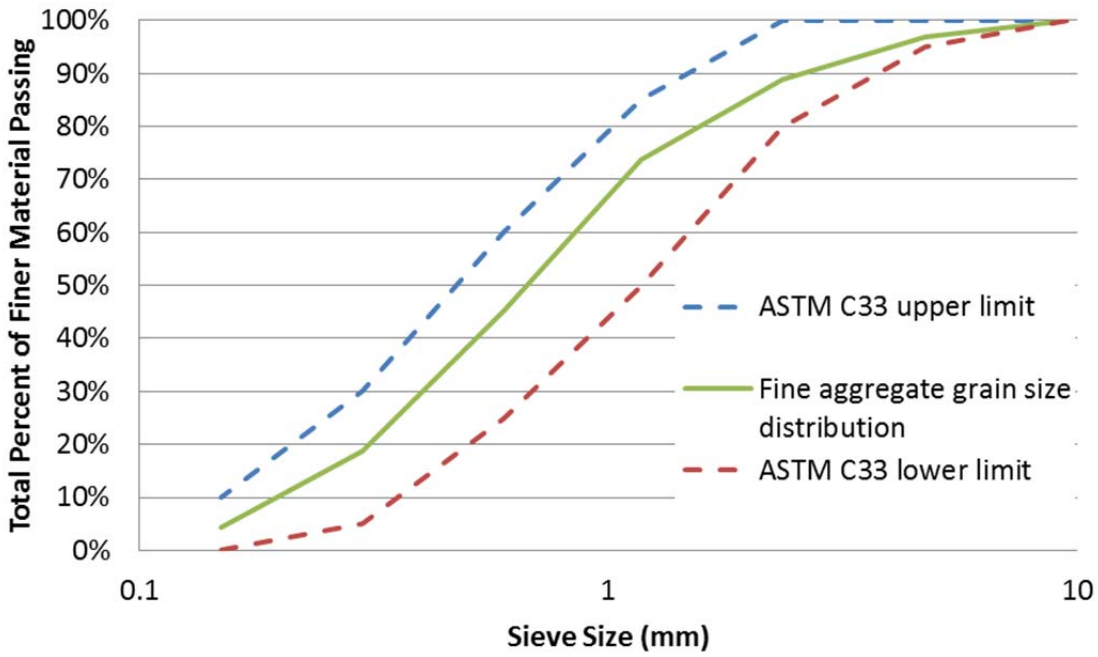

Figure 4.5 - Fine aggregate gradation for mortar mixture used in pullout specimens

4.3.2 Specimen Preparation

Molds were specially made for the pullout specimens using polyvinyl chloride. A total of five molds were constructed; four used to cast pullout specimens and one used to cast cubes of the mortar mixture alone, as shown in Figure 4.6. The molds were constructed as ten cubes measuring 50 mm x 50 mm x 50 mm, with a center insert. Four 9.5 mm (3/8 in) diameter threaded bolts were used in each mold to adjust the location of the center insert and thus adjust the fiber embedment length in the sample, as shown in Figure 4.7. The purpose of four pullout molds was to allow one fiber type to be cast at four different embedment lengths simultaneously, using the same mortar batch, producing ten samples each.

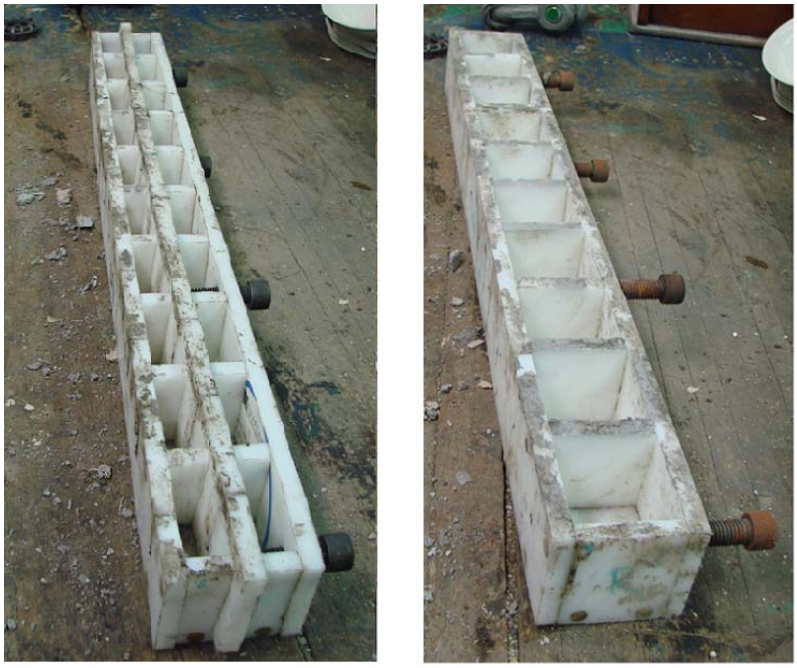

Figure 4.6 - Molds for pullout specimens and mortar cubes

Selected embedment lengths were 16 mm, 19 mm, 22.2 mm and 25 mm, (5/8 in, 3/4 in, 7/8 in and 1 in, respectively). These distances were selected because they correspond to 50% of 32 mm, 38 mm, 45 mm and 50 mm fiber lengths. The greatest active embedment length of a full fiber bridging a crack would be 50% of its total length.

Initially, holes were drilled through the molds and the fibers were threaded through. However, due to the varying fiber diameters, this method allowed mortar to fill the holes surrounding the fiber, sealing it into the mold after curing. This resulted in damaging the fiber upon removal of the pullout specimens from the molds. To prevent fiber damage, slots were cut in the upper portion of the mold fronts and center inserts, as shown in Figure 4.7. This allowed the fibers to be slid into place before casting, and easily removed from the molds after curing.

Figure 4.7 - Mold used for pullout specimen

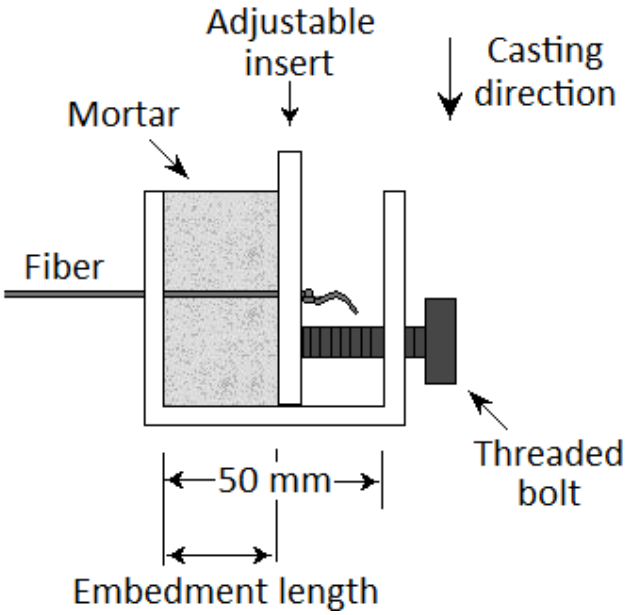

Figure 4.8 - Casting method used for pullout specimens

The casting method for pullout samples is illustrated in Figure 4.8. The center insert was adjusted to the desired embedment length and secured using the threaded bolts. Filaments were handled carefully to ensure no twisting or kinks of the fiber were present within the embedment length. A knot was formed to secure the fibers against the adjustable insert. The fibers were placed into molds via the slots. Fibers were

secured to a flat surface outside the mold using tape to prevent kinking or twisting during casting. Form release oil was then applied to the cube molds and pullout molds with extreme care not to contact the fibers.

The mortar mixture was prepared using a steel mixing bowl. Sand and cement were mixed by hand in the bowl. Water was then added slowly. A mixing attachment on a power drill was used to thoroughly mix the mortar. If deemed necessary based on visual inspection, superplasticizer was added in 5 mL increments, up to 10 mL maximum.

The mortar was placed in the molds in 2 lifts, each lift being tamped with a small tamping rod to ensure no voids in the mortar surrounding the fiber. Tamping can potentially bring bleed water to the surface and cause a slightly weaker plain at the lift interface. Therefore, the lift interface was set below the fiber level, to ensure there was no effect on the fiber matrix interface due to bleeding caused from tamping. The mortar casting direction was as shown in Figure 4.8. This is to ensure no inconsistencies in pullout results would be caused by possible segregation of the mixture. Similarly, the cube molds were filled in two lifts, each lift tamped to ensure there were no voids in the mortar.

Samples were then covered with plastic and allowed to harden at room temperature in the molds for 24 hours. The knotted end of the filament was cut for removal from the molds, and any additional fiber protrusion was cut flush with the mortar face on one specimen side. The samples were then removed from the molds and placed in a moist curing room to cure for a minimum of 28 days to ensure a percentage of hydration similar to that of the FRC samples had taken place. Hardened mortar cubes and pullout specimens are shown in Figure 4.9.

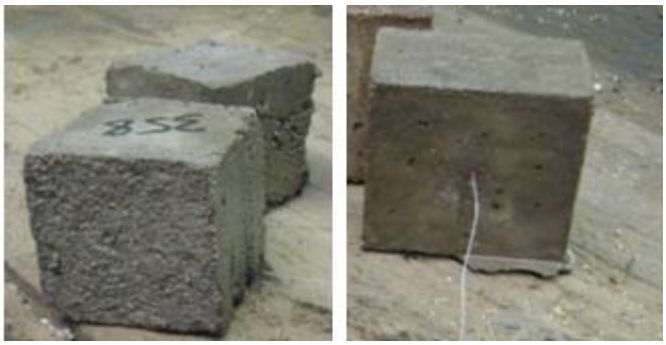

Figure 4.9 - Mortar cubes and pullout specimens after demolding, before moist curing

4.3.3 Pullout Testing Apparatus and Implementation

Similarly to tensile testing, pullout testing was conducted using an Instron 8501 machine with a 5 kN load cell and an Instron 8500+ controller. Before testing, the thickness of each specimen was measured to determine the exact embedment length. The loose end of the filament was restrained using the same custom made fixture described in 4.2, to reduce local stresses around the clamped section of the filament. The pullout specimens were restrained using a custom made fixture, pictured in Figure 4.10.

Figure 4.10 - Pullout specimen undergoing testing

The bottom plate of the fixture was attached to a threaded rod to allow adjustments for varying specimen sizes. The threaded rod was adjusted so that the specimen meets the upper restraining plate but not so tight as to induce compression. The fixture was designed to restrain the specimen with minimal addition of lateral compressive forces around the fiber, as illustrated in Figure 4.11.

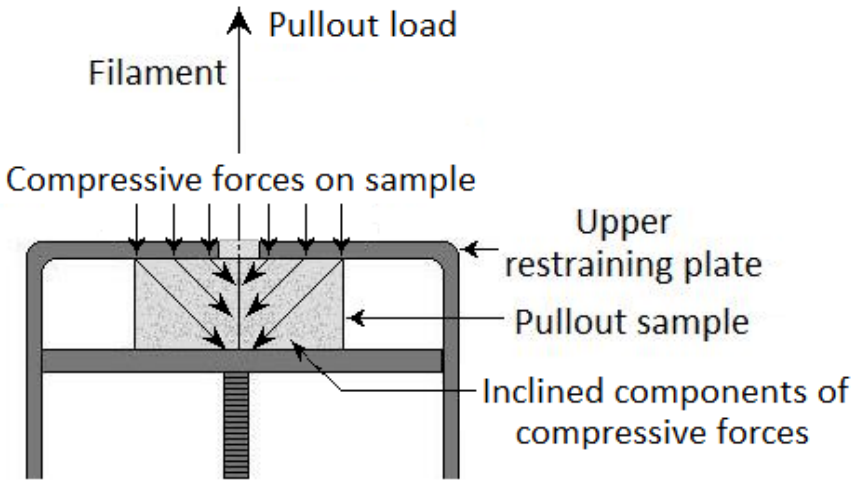

Figure 4.11 - Minimized compressive forces on sample

A removable aluminum fixture with reflective tape was placed on top of the specimen, as pictured in Figure 4.12 and illustrated in Figure 4.13. This is to provide a stationary reading flush with the surface of the sample. The reflective tape cannot be placed on the block itself, because the laser extensometer measures distances in plane. Therefore the aluminum fixture was constructed as thin as possible to increase accuracy.

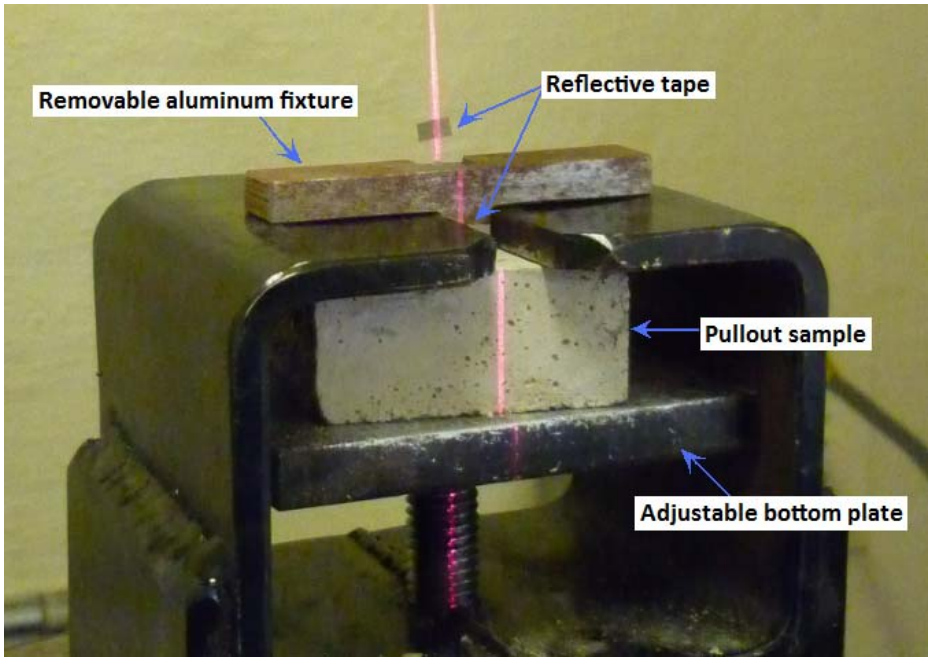

Figure 4.12 - Pullout specimen and removable aluminum fixture

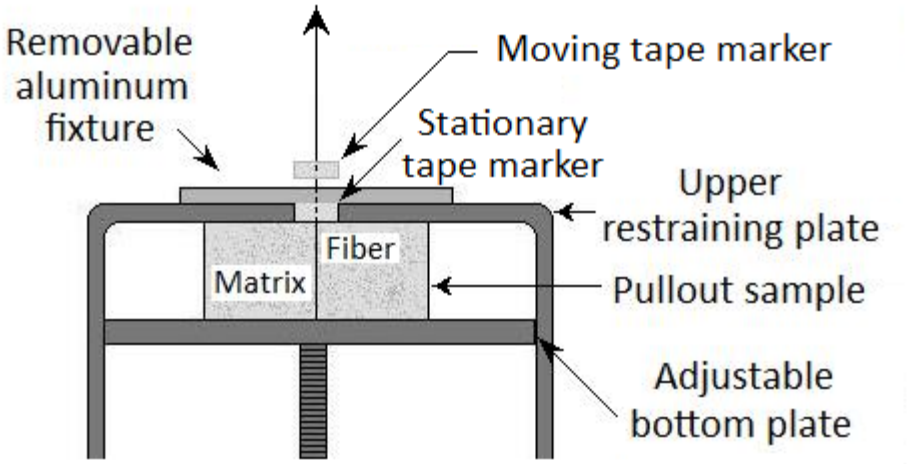

Figure 4.13 - Schematic of single fiber pullout test setup

Specimens were handled in a careful manner to ensure no twisting or stretching took place during setup. A very small initial tension was applied to ensure no slack or kinks were present in the sample. Based on the review literature, pullout testing was conducted at a constant actuator displacement rate of 5 mm/min. This rate can reasonably represent static loading (Kim, *et al*. 2008).

Elongation of the specimen was measured using a laser extensometer and two pieces of reflective tape, one placed on the aluminum fixture as a stationary reading, and the other placed directly on the filament, as close to the aluminum fixture as possible to minimize error. The elongation between the reflective tapes was recorded throughout the test, while the load cell tracked the tensile load applied to the specimen. A data acquisition system recorded the tensile load and the distance between the reflective tapes throughout the test. The complete pullout test setup is shown in Figure 4.14.

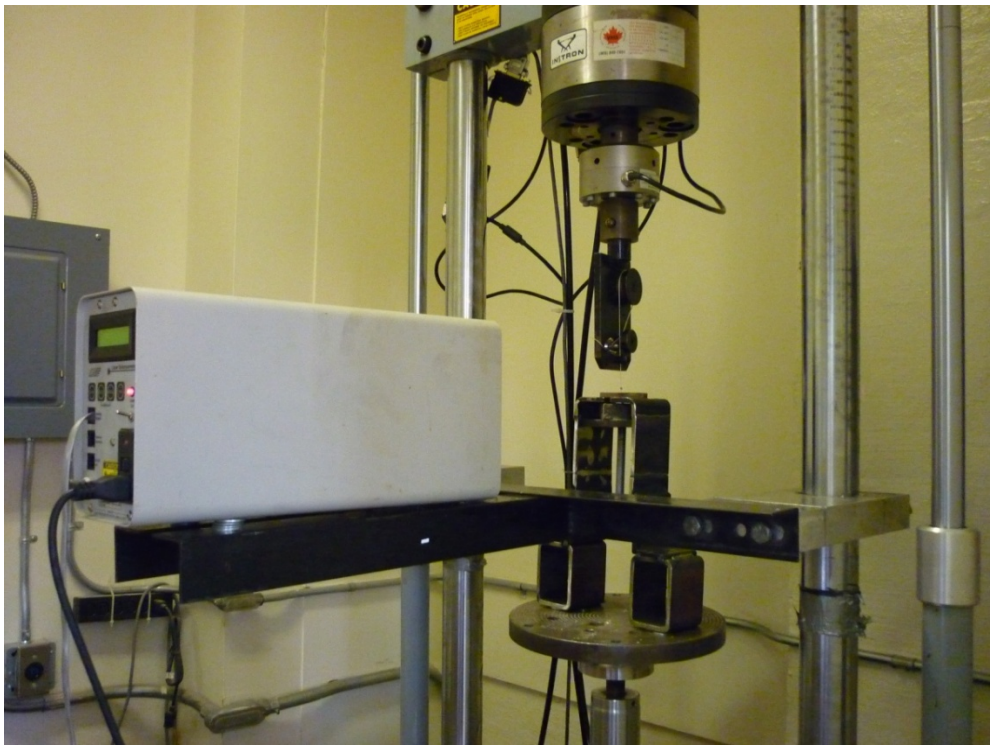

Figure 4.14 - Single fiber pullout test setup and laser extensometer

The primary data extracted from single fiber pullout testing is pullout load vs. fiber slip curves. As discussed in Section 2.4.3, fiber slip was calculated by removing the elastic strain contribution. To do this, filaments were also tested in tension at a constant displacement rate of 5 mm/min, and strains at equivalent loads were subtracted from the pullout data displacement, as illustrated in Figure 4.15. Equation 4-1 was applied to remove the elastic strain contribution from the filament.

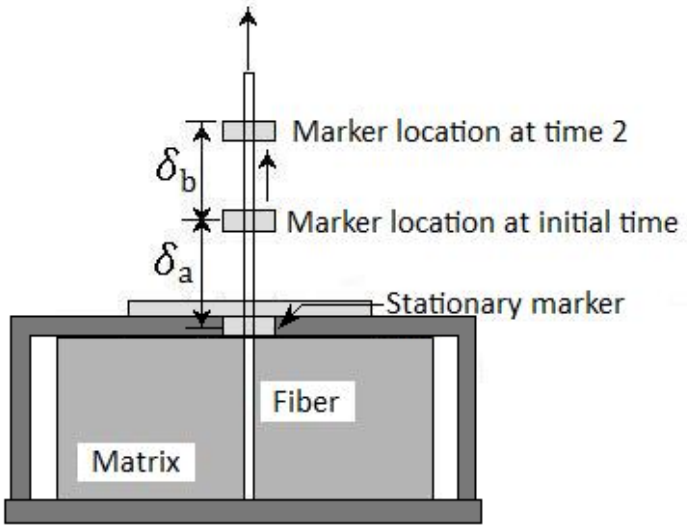

Figure 4.15 - Method for measuring fiber slip, accounting for elastic strain

$$S = \delta_b - \epsilon\delta_a \qquad \textbf{4-1}$$

Where,

S = Fiber slip (mm)

δ_a = Initial distance between two markers, as illustrated in Figure 4.15 (mm)

δ_b = Distance travelling marker moved over time, as illustrated in Figure 4.15 (mm)

ϵ = Fiber strain at present load, taken from tensile test conducted at same speed (mm/mm)

One source of error in this test was that the calculation of slip does not account for possible strain taking place within the concrete sample. While recognizing that there are several minute sources of error, for the purposes of comparing different fiber types and manufacturing methods to develop a synthetic fiber, the test setup used was deemed more than adequate.

4.3.4 Inclined Pullout Testing

As discussed in Section 3.2.5, single fiber pullout testing commonly simulates the fiber being aligned with the applied load, which is often not the reality of randomly distributed fibers bridging cracks in FRC. To characterize the behavior of fibers undergoing inclined pullout, specimens were tested on varying inclined angles. Randomly distributed fibers can bridge cracks at any angle between 0 and $\pi/2$. Therefore, pullout specimens were tested at 15, 30, 45 and 60 degree inclinations. Inclines were achieved using wedge inserts in the pullout testing setup. Figure 4.16 shows the wedge inserts used. Figure 4.17 shows a pullout specimen undergoing inclined pullout testing.

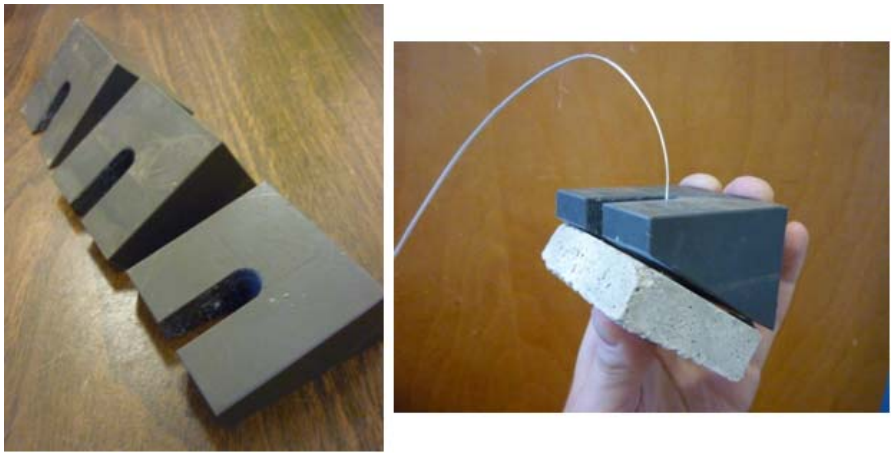

Figure 4.16 - Angled wedge inserts used for inclined pullout test

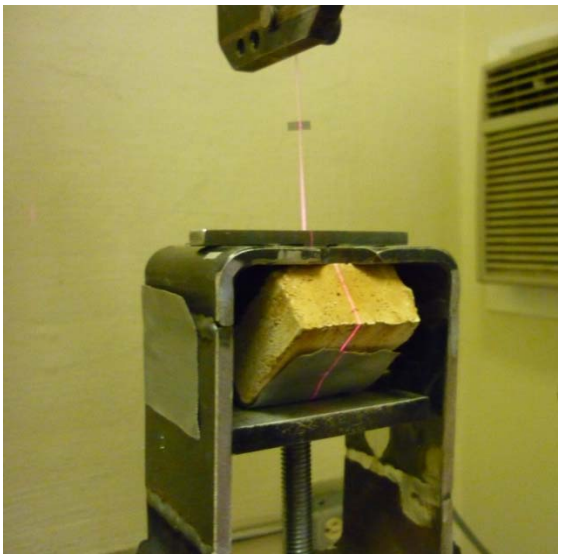

Figure 4.17 - Pullout specimen undergoing inclined pullout

4.3.5 Testing for Compressive Strength of Mortar Matrix

To account for possible dependence on matrix strength, each set of pullout samples were cast along with ten mortar cubes to determine the compressive strength of the matrix. Figure 4.18 shows the test setup used for testing the compressive strength of the mortar. Before testing, the faces of each cube were measured. Compressive strength testing of the mortar was conducted in accordance with ASTM C109-08 "Standard Test Method for Compressive Strength of Hydraulic Cement Mortars (Using 2-in. or [50-mm] Cube Specimens)". The specimen and a 100 kN load cell, shown in Figure 4.19, were placed in a Forney testing machine where a compressive axial load was applied at a constant rate until a maximum load was reached and fracture occurred. The compressive strength of the mortar was determined by dividing the maximum load applied to the sample by the cross sectional area of the cube face.

Figure 4.18 - Test setup for compression of mortar cube

Figure 4.19 - Load cell and readout used for compression testing of mortar cubes

4.4 FRC PERFORMANCE TESTING

4.4.1 Materials

The fibers used in performance testing are listed in Table 4.4. These were nine prototype fibers and three commercially available synthetic macrofibers. The prototype fibers were chosen based on initial results of tensile testing and pullout testing. The commercial fibers were Tuf-Strand SF, Strux 85/50, a polypropylene/polyethylene blend, and BASF MasterFiber MAC470, an embossed polypropylene fiber as shown in Figure 4.20. The selected prototype fibers were cut to 50 mm lengths in the production plant. The Tuf-Strand and Strux 85/50 fibers were 50 mm in length, and the BASF fiber was 47 mm in length. Only macrofibers were used in performance testing in order to compare hardened properties with commercially available macrofibers in a typical FRC mixture. Where microfibers would be commonly used in ECCs with no coarse aggregate, a different concrete mixture would be required and thus these fibers were not included in this series of testing.

Table 4.4 - Fibers used in FRC performance testing

Fiber Description	Width (mm)	Thick (mm)
100 % HDPE	1.39	0.25
HDPE, 1% PVDF	1.41	0.27
HDPE, 3% PVDF	1.42	0.25
HDPE, 5% PVDF, 10% MAH	1.26	0.26
HDPE, 7% PVDF, 10% MAH	1.28	0.27
HDPE, 9% PVDF, 10% MAH	1.28	0.27
HDPE, 11% PVDF, 20% MAH	1.51	0.29
HDPE, 10% EVA	1.55	0.29
80% PP, 10% HDPE, 10% EVA	1.31	0.25
Tuf-Strand SF	1.05	0.34
BASF - MasterFiber MAC470	1.64	0.80
Strux 85/50	0.98	0.35

Figure 4.20 - BASF MasterFiber MAC470 embossed fibers

The concrete used for performance testing was prepared using the mixture shown in Table 4.5. This mixture was used because the water/cement ratio (0.44), cement content and aggregate contents are representative of real world applications. The fiber dosages of 3 kg/m^3 were selected as these are typical dosages used in field applications that could be expected to provide an improvement in FRC performance while maintaining suitable workability. This mixture was designed for a target compressive strength of 40 MPa.

The cement used was ASTM Type 1 Portland Cement, produced in Joliette, Quebec and supplied by supplied by Holcim Canada. The fine aggregate used was Nova Scotia sourced river sand supplied by Shaw Resources, with a fineness modulus of 2.72. The coarse aggregate was gravel with a nominal size of 19 mm, sourced from Rocky Lake Quarry in Nova Scotia. A sieve analysis was performed on the fine and coarse aggregate in accordance with ASTM C136-06 “Standard Test Method for Sieve Analysis of Fine and Coarse Aggregates”. The resulting aggregate gradation curves fall within the limits set by ASTM C33-11 “Standard Specification for Concrete Aggregates” for grain size distribution, as shown in Figure 4.21. The superplasticizer used was Eucon SPC High Range Water Reducer - Superplasticizer, supplied by The Euclid Chemical Company.

Table 4.5 - Concrete mixture used for FRC specimens

Material	Quantity (kg/m3)
Cement	373
Fine Aggregate	850
Coarse Aggregate	860
Water	163
Fiber	3
Superplasticizer	40-100 mL

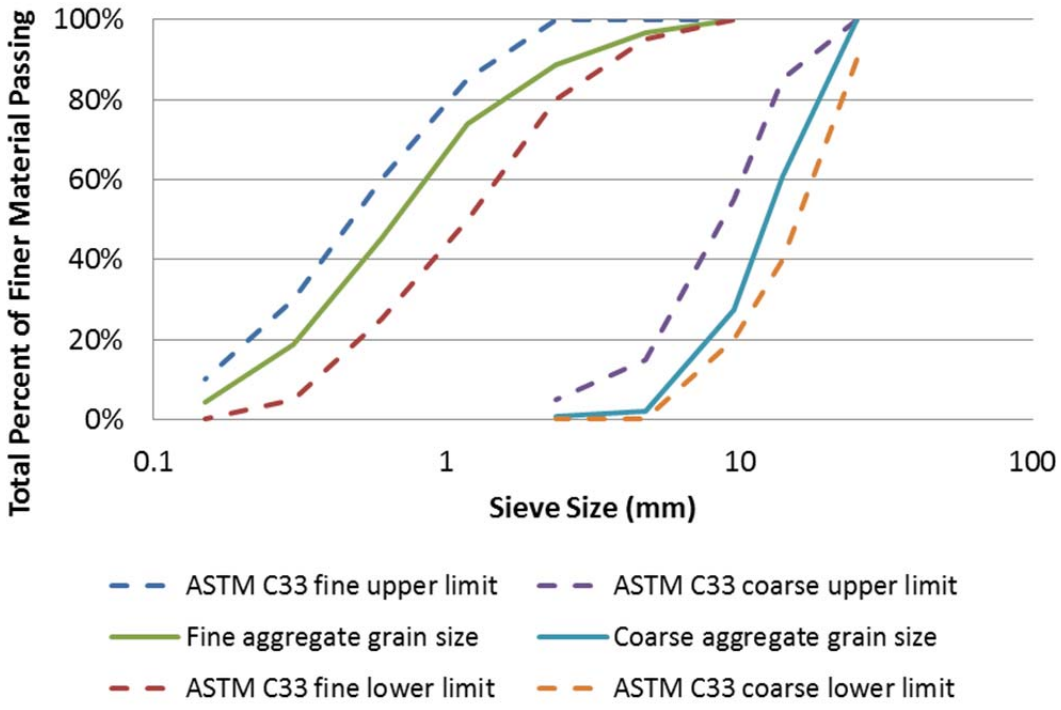

Figure 4.21 - Gradation curve for fine and coarse aggregate

4.4.2 Mixing Procedure

One batch of concrete was mixed for each fiber type used in performance testing. A batch size of 0.175 m^3 was used in order to produce four beams for ASTM C1399-10,

five beams for ASTM C1609-10, three cylinders for ASTM C39-10, and one round panel for ASTM C1550-10.

A drum type mixer was used throughout the trials. Moisture contents were measured on both the fine and coarse aggregate, and corrections were made to the amount of mixing water as necessary. Fine and coarse aggregate were added to the drum first and mixed for 30 seconds. Next the cement was added, and mixed for one minute. Water was then added and mixed for three minutes.

A slump test was then performed according to ASTM C143-10 “Standard Test Method for Slump of Hydraulic-Cement Concrete”. The target compressive strength for these mixtures was 40 MPa, and the appropriate water content should result in a slump of 150-175 mm before the addition of superplasticizer and fibers. Aggregate moisture content changed throughout the trials, therefore water contents were affectively controlled by targeting slump. Once the desired slump was achieved, a density measurement was taken according to ASTM C138-10 “Standard Test Method for Density (Unit Weight), Yield, and Air Content (Gravimetric) of Concrete” to ensure the concrete density was within the desired range of 2350-2400 kg/m^3.

Superplasticizer was added based on visual inspection and previous experience. The mixture was then mixed for an additional two minutes to allow the superplasticizer to take effect. Fibers were added next and mixed for four minutes to allow typical fiber surface damage to occur. An additional slump test was taken to approximate the decrease in workability caused by fiber addition. Washout samples, shown in Figure 4.22, were also taken after the addition of fibers. Washout samples were conducted by filling a bucket with fresh FRC, and flushing with water. A handful of fibers was separated from the mixture and stored in plastic. The purpose of a washout sample was to visibly inspect the fibers for fibrillation after mixing.

Figure 4.22 - A washout sample showing visible fibrillation

Beams, cylinders, and round panel specimens were cast in accordance with ASTM 1609-10, ASTM 1399-10, ASTM C39-10, and ASTM C1550-10 respectively. The samples were placed on a vibrating table and cast in two lifts. The samples were covered with plastic and allowed to harden at room temperature for 24 hours before the forms were removed. The samples were then allowed to cure in a moist curing room for a minimum of 28 days, until testing.

4.4.3 FRC Compressive Strength Test

Compressive strength testing of FRC cylinder samples was conducted according to ASTM C39-10. Three 100 mm x 200 mm cylinder samples were taken for each FRC mix. Testing was conducted using a Forney testing machine, pictured in Figure 2.23. Before testing, the samples were capped using a sulfur compound to ensure there were no defects in the surface area to which the load was applied. Specimens were tested after 32 days of curing. Ideally the specimens would have been tested after 28 days of curing, but there was a delay in testing due to testing equipment failure. Photos of cylinders were taken to later inspect the fracture pattern if necessary.

4.4.4 FRC Flexural Performance Test (ASTM C1609-10) and FRC Residual Strength Test (ASTM C1399-10)

Five 150 mm x 150 mm x 550 mm beam specimens for each mix were tested for flexural strength in accordance with ASTM C 1609-10. Four 100 mm x 100 mm x 350 mm beam specimens for each mix were tested for residual strength in accordance with ASTM C1399-10. These test setups are shown in Figure 4.23 and Figure 4.24.

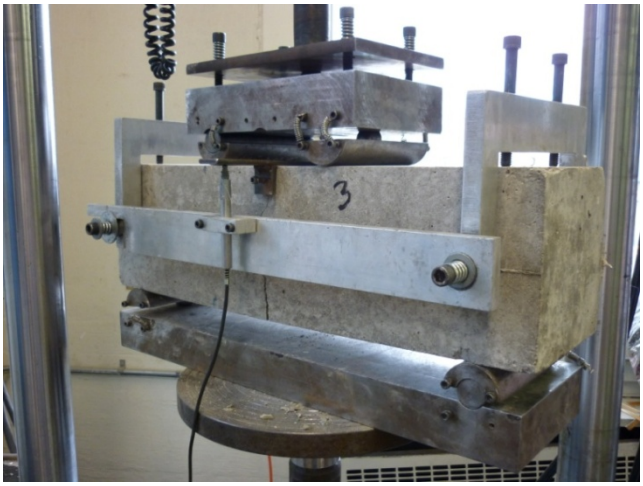

Figure 4.23 - Test setup for ASTM C1609-10

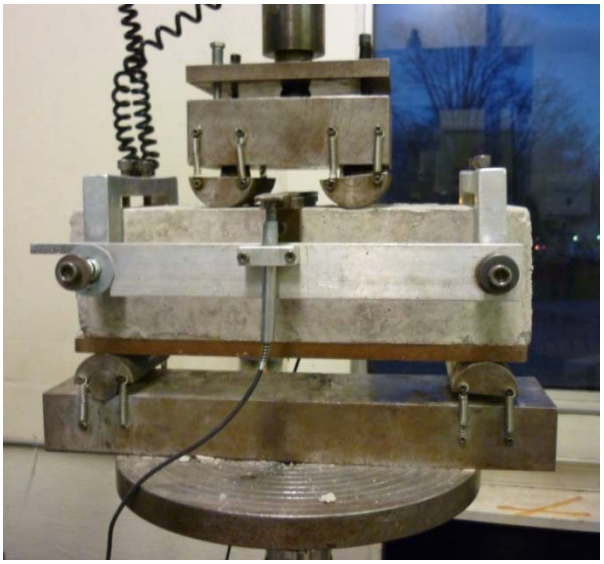

Figure 4.24 - Instron 8501 and test setup for ASTM C1399-10

Testing for both residual strength testing and flexural strength testing was conducted using an Instron 8501 machine, pictured in Figure 4.24, with a 100 kN load cell and an Instron 8500+ controller, pictured in Figure 4.25. The test was run using the program "Wave Maker", shown in Figure 4.26. Data was collected using this program as well.

Figure 4.25 - Instron 8500+ controller panel

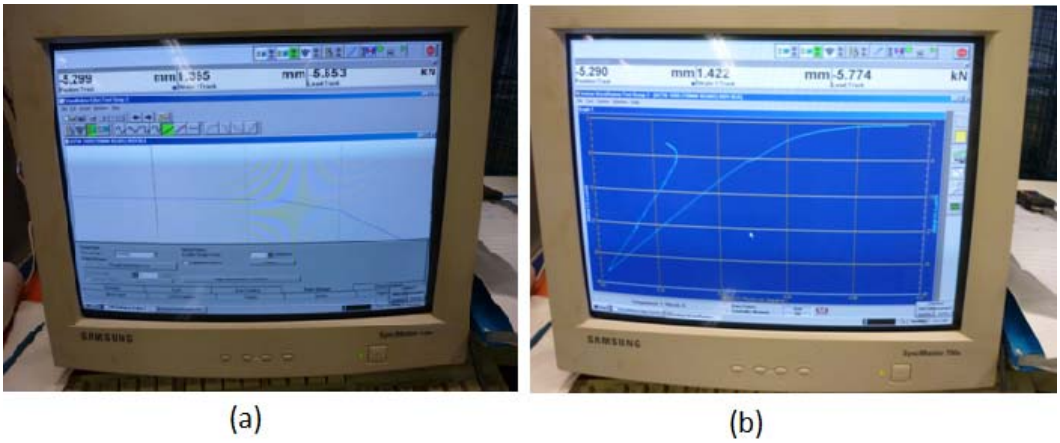

Figure 4.26 - Wave Maker Program (a) Wave Maker program editor (b) test plot of applied load vs. actuator position

Before testing, each specimen was measured in three places along both width and depth. An average of these measurements was used as the true cross section measurements in order to ensure accuracy of the results. Specimens were tested after 32 days of curing. After testing, the beams were fully broken, as shown in Figure 4.27, and photos of the break face were taken to allow for visual inspection of fiber distribution.

Figure 4.27 - Fully broken beam specimens

4.4.5 FRC Flexural Toughness Testing Using Round Panels (ASTM C1550-10)

One 75 mm thick, 800 mm diameter round panel specimen for each mix was tested for flexural toughness in accordance with ASTM C1550-10. While a minimum of three specimens are recommended in ASTM C1550-10, due to material restrictions, only one specimen each could be taken. However, ASTM C1550-10 states the following regarding repeatability of this testing:

> "Studies in repeatability of energy absorption up to 40 mm central displacement observed within one laboratory indicate single-operator values of the one-sigma within-batch limit (1s%) of 6%. Therefore, results from two properly conducted tests by the same operator on specimens made from the same batch of concrete are not expected to differ from each other by more than 17%."

While three specimens are ideal for this test, given the repeatability of this test and the wide scope of additional performance testing in this research, the samples were deemed suitable for adding to the comparisons of the performance of different fibers in FRC.

Before testing, the cross sectional height of the panels was measured. A custom made testing frame meeting the restrictions set out in ASTM C1550-10 was used, as shown in Figure 4.28. The panel was loaded using a piston up to a central deflection of 45 mm. A data acquisition system was used to plot the applied load vs. the central deflection of the specimen throughout testing. After failure specimens were fully broken and photos of the break face were taken to allow for visual inspection of fiber distribution, as shown in Figure 4.29.

Figure 4.28 - Test setup for ASTM C1550-10

Figure 4.29 - Fully broken round panel specimen

4.5 FIBER TENSILE CREEP TEST

The fibers used in tensile creep testing are listed in Table 4.6. These fibers were chosen based on initial results of tensile testing and pullout testing. Four filaments of each fiber type were used. The applied weights were selected to be 5%, 10%, 20% and 40% of the maximum tensile strength of the fiber.

Table 4.6 - Fibers used in tensile creep testing

Fiber Description	Width (mm)	Thick (mm)
100 % HDPE (Thick)	1.41	0.42
100 % HDPE	1.39	0.25
HDPE, 1% PVDF	1.41	0.27
HDPE, 3% PVDF	1.42	0.25
HDPE, 11% PVDF, 20% MAH	1.51	0.29
100% PVDF	1.76	0.47
HDPE, 10% EVA	1.55	0.29
80% PP, 10% HDPE, 10% EVA	1.31	0.25
Tuf-Strand SF	1.05	0.34
100% HDPE 5906 (Micro)	0.29	0.30
HDPE, 10% PVDF, 20% MAH (Micro)	0.25	0.25
HDPE, 10% EVA (Micro)	0.28	0.27

After the fibers were selected and an appropriate spacing was chosen, a frame was constructed using two 38 mm diameter circular hollow steel sections, 2.5 mm in thickness, which the fibers would hang from. Vertical supports were constructed using 25 x 25 mm square hollow steel sections, 3 mm in thickness. The frame was connected to the wall to maintain stability. The test setup is shown in Figure 4.30. Fibers were wrapped around the top steel bar five times to decrease local stresses at the location of attachment, and then connected to the frame supports using bow knots.

Figure 4.30 - Test setup for fiber tensile creep testing

To allow the weight to hang from the fiber without causing large local stresses, several ideas were tested. First, clamps intended for airplane wires were used, with rubber buffers where the fiber would otherwise contact the steel. A loop was formed at the bottom and passed through the wire clamps, as shown in Figure 4.31 (a). This was modeled after the test setup used by Cochrane in 2003. However, for microfibers and smooth macrofibers, the loops slipped from the clamp when weights were applied. To correct this, wire clamps were not used and a bow knot was selected instead, as shown in Figure 4.31 (b). Bow knots do not slip, but can increase local stresses around the fiber, causing breaks at the knot location when weight was applied. For heavier weights, a nail knot was used, shown in Figure 4.31 (c). A nail knot would not slip but would also decrease local stresses on the fiber around the knot location, when compared with a bow knot.

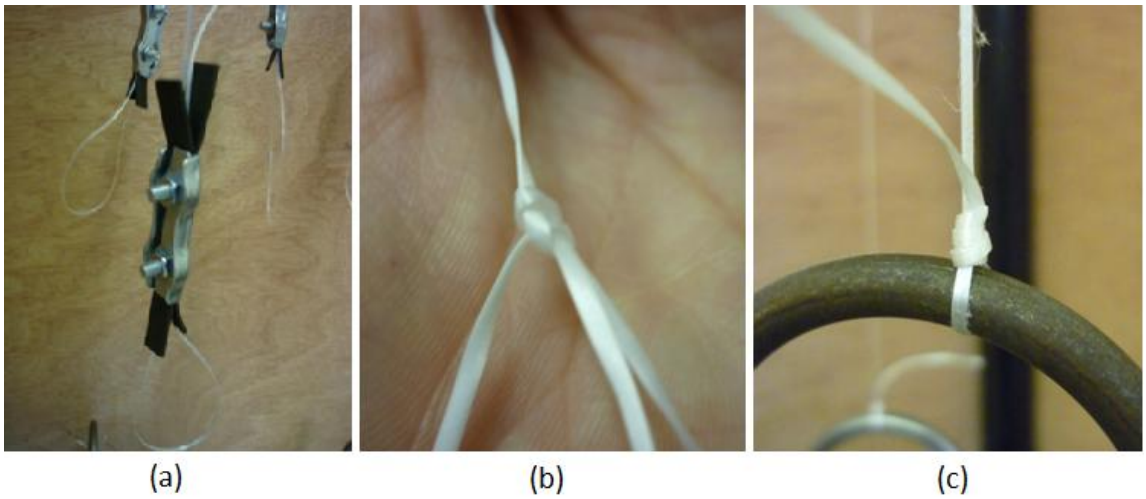

Figure 4.31 - Loop restraints: (a) wire clamps, (b) bow knot, (c) nail knot

Weights were cut from 50 mm diameter and 100 mm diameter solid steel. The weights were sized at 5%, 10%, 20% and 40% of the maximum tensile capacity of each fiber. To increase accuracy, multiple measurements were desired. Therefore, three sets of reflective tape were placed along each filament, as shown in Figure 4.30. The distances between the reflective tapes were measured using a laser extensometer on a dolly of adjustable heights, shown in Figure 4.32.

Figure 4.32 - Laser extensometer on adjustable dolly

Initial measurements were taken both before and immediately after the weights were applied. Measurements were then taken daily for thirty days, after which measurements were taken every second day up to 60 days, then three times per week until the final analysis for this research was completed, providing 104 days of tensile creep. Creep strain was taken as the change in distance between the pieces of reflective tape, divided by the initial gauge length. Instantaneous strain was removed from calculations to account for elastic strain and therefore record creep strain only. The three measurements taken on each filament were averaged for accuracy. Resulting creep strain was plotted against elapsed time in days to investigate the creep behavior of fibers under tensile loading.

CHAPTER 5 RESULTS AND DISCUSSION

The results of the testing program are presented and discussed in this section. The results and discussion of the following will be presented: tensile testing on various extruded filaments, single fiber pullout testing on selected filaments, FRC performance testing using cut fibers, and tensile creep testing on selected filaments.

5.1 TENSILE STRENGTH AND MODULUS OF ELASTICITY RESULTS

The materials used in the melt extrusion and subsequent tensile testing include HDPE, polypropylene (PP), PVDF, EVA, and MAH. A representative stress vs. strain diagram from tensile testing is shown as Figure 5.1. Additionally, commercially available fibers such as PVA, Tuf-Strand SF, and two types of nylon fibers were tested. A complete list of the fibers tested and the resulting tensile strength and elastic modulus, along with the stretch ratios, fiber dimensions and equivalent diameters, are presented in Appendix A.

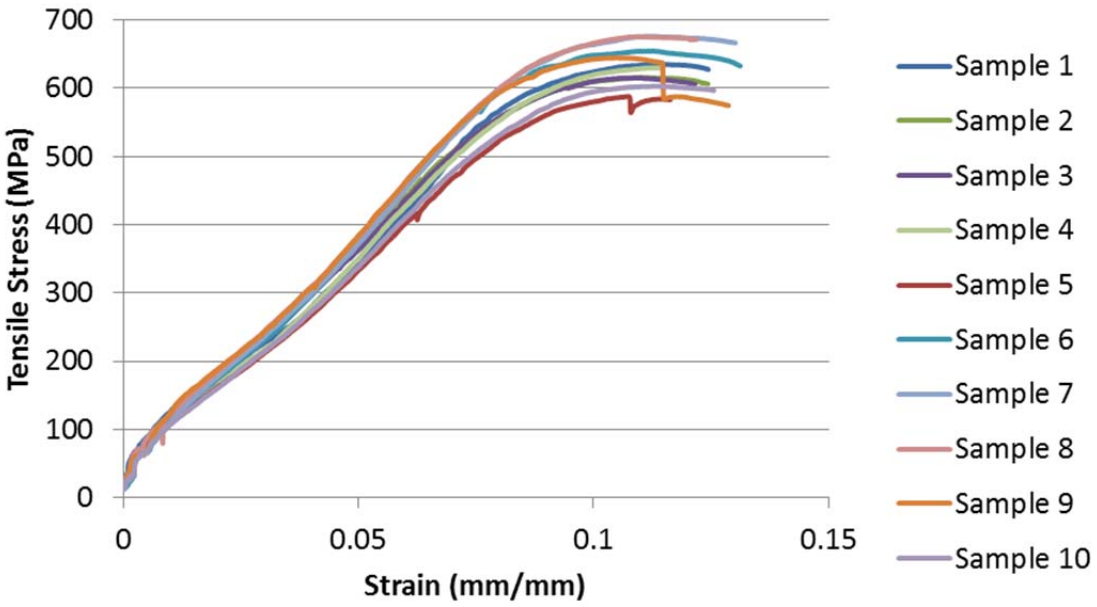

Figure 5.1 - Stress vs. strain curves for 10 samples of the same prototype fiber containing HDPE 5906, 5% PVDF and 10% MAH

5.1.1 Materials

The geometric and material properties of some prototype macrofibers and microfibers are shown in Table 5.1 and Table 5.2, respectively. It should be noted that these properties are significantly affected by extrusion settings. The values in this table are presented to provide a comparison between materials only. Extrusion settings and their effect on tensile properties will be further discussed in Sections 5.1.2 and 5.1.3.

Table 5.1 - Tensile properties of some prototype macrofibers and Tuf-Strand SF

Fiber Description	Width (mm)	Thickness (mm)	σ_f (MPa)	E_f (GPa)	d_{eq} (mm)
100% HDPE	1.39	0.25	673	6.13	0.651
80% PP, 20% HDPE	1.30	0.27	704	10.77	0.658
HDPE, 1% PVDF	1.41	0.27	709	6.34	0.676
HDPE, 3% PVDF	1.42	0.25	749	7.01	0.659
HDPE, 5% PVDF, 10% MAH	1.26	0.26	779	9.25	0.636
HDPE, 7% PVDF, 10% MAH	1.28	0.27	764	9.10	0.643
HDPE, 9% PVDF, 10% MAH	1.28	0.27	731	8.17	0.650
HDPE, 11% PVDF, 20% MAH	1.51	0.29	559	5.79	0.727
100% PVDF	1.76	0.47	527	3.44	0.996
HDPE, 10% EVA	1.55	0.29	595	5.67	0.738
80% PP, 10% HDPE, 10% EVA	1.31	0.25	718	10.93	0.633
Tuf-Strand SF	1.05	0.34	646	9.53	0.650

Table 5.2 - Tensile properties of some prototype microfibers and commercial microfibers

Fiber Description	Width (mm)	Thickness (mm)	σ_f (MPa)	E_f (GPa)	d_{eq} (mm)
HDPE (5906)	0.29	0.28	1391	15.93	0.286
HDPE (1288)	0.19	0.20	1842	28.47	0.192
HDPE (5906), 5% EVA	0.27	0.29	1236	12.56	0.281
HDPE (5906), 10% EVA	0.25	0.26	1448	19.75	0.253
HDPE (5906), 10% PVDF, 20% MAH	0.25	0.25	1420	18.93	0.247
PVA (Kuralon)	0.12	0.12	2092	28.66	0.122
Nylon (PA66)	0.14	0.15	2323	5.70	0.145
Nylon (Co-polymide Ultramid C4Q42)	0.15	0.15	2023	6.91	0.149

It was found during the extrusion trials and initial testing that PVDF filaments, when used as the primary material, had unsatisfactory tensile properties. The elastic modulus of PVDF fibers was below 3.5 GPa, significantly less than the commercially available Tuf-Strand SF, which has an elastic modulus of 9.5 GPa. Also, the raw material cost for PVDF is ten times that of Tuf-strand SF ($32.00/kg vs. $2.80/kg), meaning commercializing a purely PVDF fiber would not be economical. PVDF was therefore used as an additive to other materials to increase fiber-matrix bond strength. To allow PVDF to fully blend with HDPE and PP, MAH was added as a stabilizer in quantities of 20% or less.

EVA was also introduced as an additive to increase fiber-matrix bond. The tensile testing results shown in Table 5.2 indicate that EVA can be successfully used as an additive without significant decreases in tensile properties. Quantification of the influence of EVA addition on interfacial bond strength was part of this investigation and is discussed in Section 5.2.

Two resins of HDPE were also investigated; these were HDPE 5906 and HDPE 1288. Both resins were found to have excellent tensile properties. HDPE 5906 was selected as the primary material for macrofibers combined with either PVDF or EVA due to the superior

properties found through initial extrusion runs. Later trials showed that at some extrusion settings HDPE 1288 produced superior tensile properties to the HDPE 5906. These combinations produced several prototype macrofibers that achieved higher tensile strengths than Tuf-Strand SF.

While the prototype microfibers achieved impressive tensile properties, they did not surpass the tensile properties of the commercially available microfibers made from nylon and PVA at the diameters used. It should be noted that the commercially available fibers are not formed through melt extrusion but through significantly more costly methods such as gel spinning. Therefore, these prototype microfibers could potentially be an economically viable product.

Effect of PVDF Addition on Tensile Properties

The effect of the addition of PVDF on fiber tensile properties was investigated using the prototype fibers listed in Table 5.3. The fibers were primarily HDPE 5906, but contained PVDF added in various quantities, as well as MAH added as necessary for the materials to blend. These fibers have similar cross sectional dimensions as well as similar stretch ratios. Figure 5.2 and Figure 5.3 illustrate the effect of PVDF and MAH addition on tensile strength and elastic modulus respectively.

Table 5.3 - Prototype fibers containing PVDF

Fiber Description	Width (mm)	Thickness (mm)	σ_f (MPa)	E_f (GPa)	HDPE content
100% HDPE	1.40	0.25	673	6.13	100%
HDPE, 1% PVDF	1.41	0.27	709	6.34	99%
HDPE, 3% PVDF	1.42	0.25	749	7.01	97%
HDPE, 5% PVDF, 10% MAH	1.26	0.26	779	9.25	85%
HDPE, 7% PVDF, 10% MAH	1.28	0.27	764	9.10	83%
HDPE, 9% PVDF, 10% MAH	1.28	0.27	731	8.17	81%
HDPE, 11% PVDF, 20% MAH	1.51	0.29	559	5.79	69%

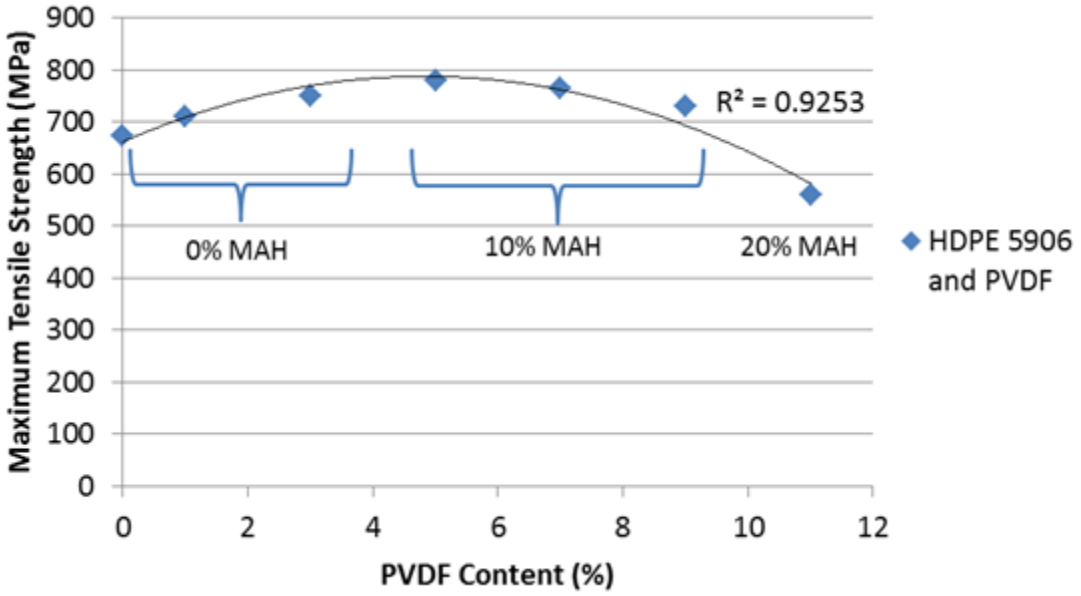

Figure 5.2 - Tensile strength vs. PVDF content

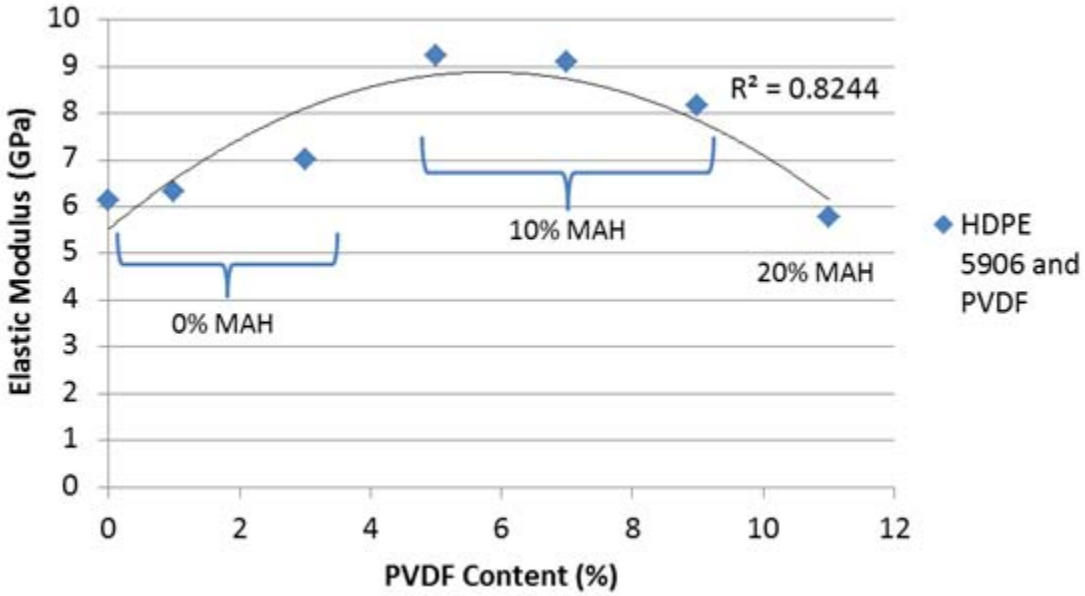

Figure 5.3 - Elastic modulus vs. PVDF content

As previously discussed, PVDF was not suitable as the sole material for a new synthetic fiber, because the resin in pure form cannot be stretched sufficiently to produce the desired tensile properties, without breaking on the extrusion line. By adding PVDF to HDPE, higher stretch ratios were achieved than with PVDF alone. Therefore, PVDF addition slightly improved the tensile properties of the fiber, as shown in Figure 5.2 and Figure 5.3. It can be concluded that the addition of less than 10% PVDF does not cause a loss in tensile properties and may result in a slight improvement.

As PVDF was continually increased, greater proportions of MAH were required for blending; 20% MAH was required for the addition of 11% PVDF. This reduced the overall tensile properties of the fiber. This can be attributed to HDPE 5906 typically being the strongest of the three materials, whereas MAH was used as a copolymer stabilizer only and was not meant to be used as a polymer under tension.

5.1.2 Effect of Stretch Ratio on Tensile Properties

The effect of the stretch ratio on fiber tensile properties was investigated by grouping prototype fibers as macrofibers or microfibers. Figure 5.4 and Figure 5.5 illustrate the effect of stretch ratio on macrofiber tensile strength and elastic modulus, respectively, for the prototype fibers listed in Table 5.1. Tuf-Stand SF is shown on these figures for comparison, as it was used as the benchmark for this research. Figure 5.6 and Figure 5.7 illustrate the effect of stretch ratio on microfiber tensile strength and elastic modulus, respectively for the prototype fibers listed in Table 5.2.

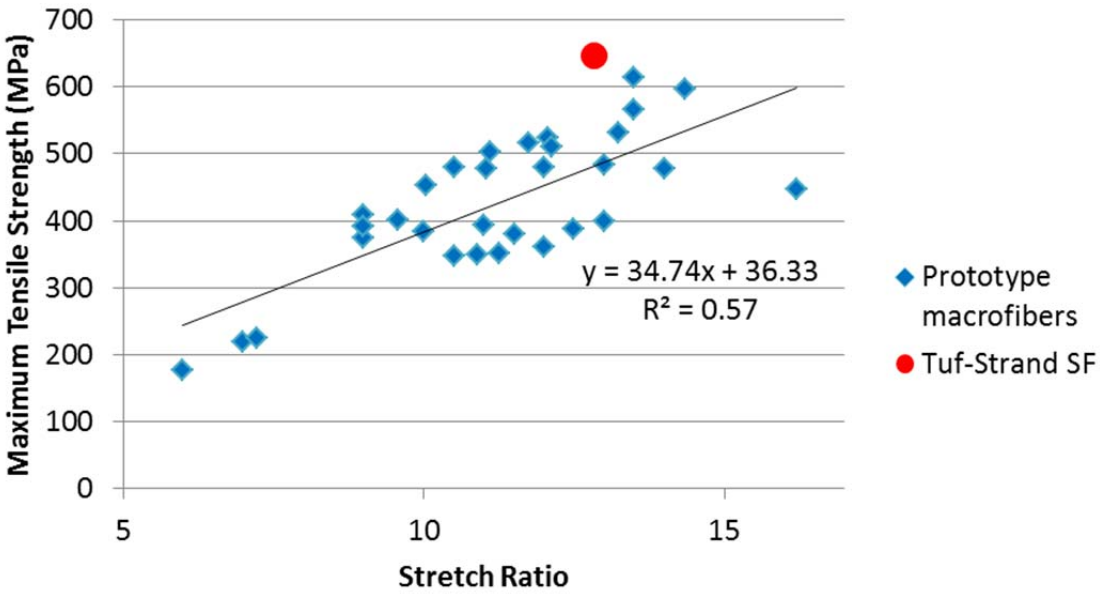

Figure 5.4 - Maximum tensile strength vs. stretch ratio for macrofibers

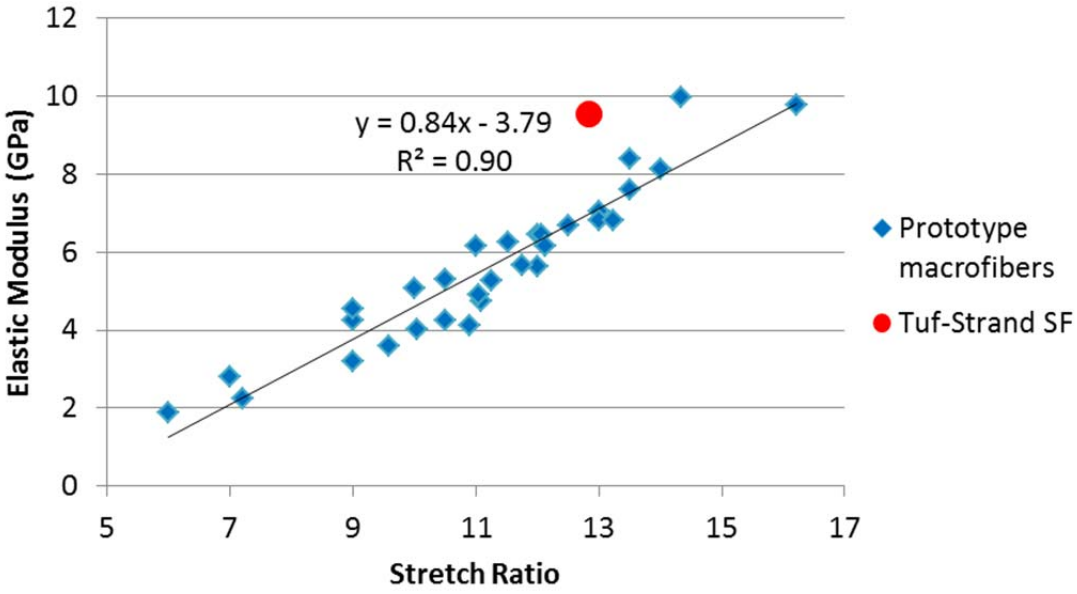

Figure 5.5 - Elastic modulus vs. stretch ratio for macrofibers

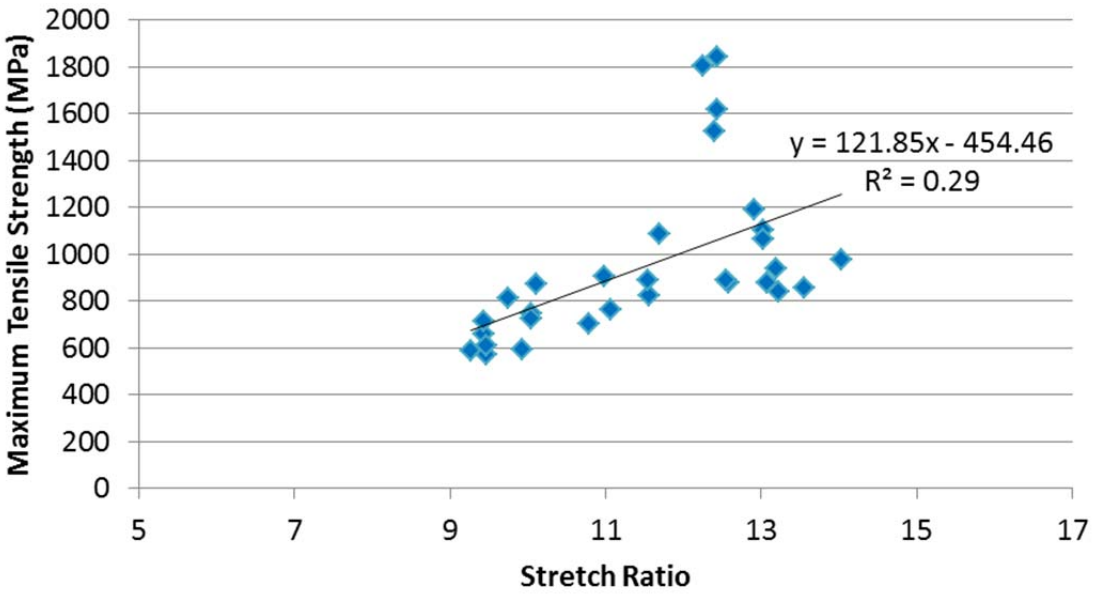

Figure 5.6 - Maximum tensile strength vs. stretch ratio for microfibers

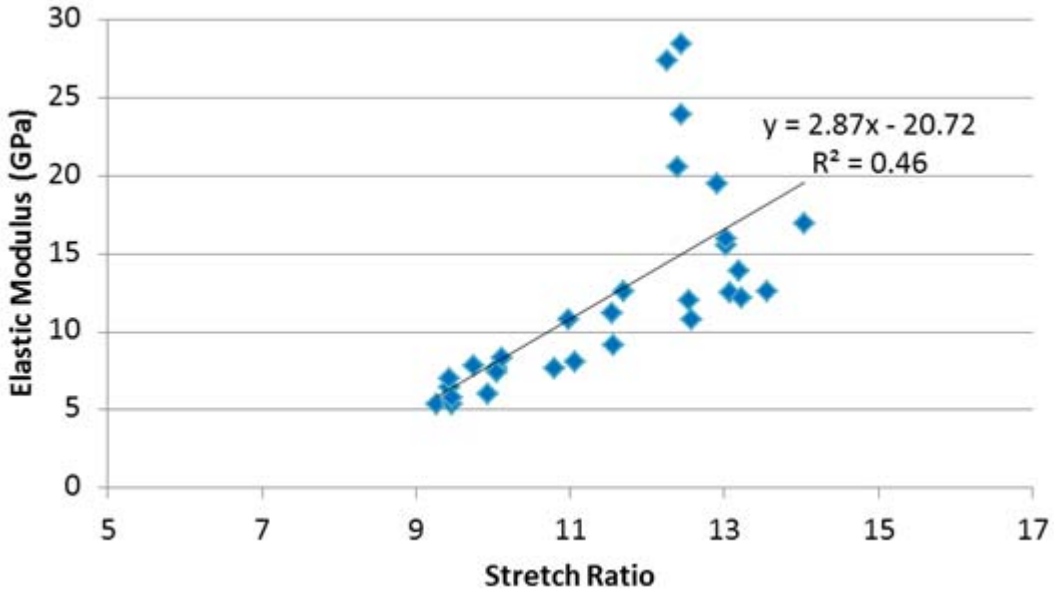

Figure 5.7 - Elastic modulus vs. stretch ratio for microfibers

A trend of increasing tensile strength and elastic modulus with increasing stretch ratio was observed. This was attributed to the increased molecular alignment associated with increasing stretch ratios. It has been shown that an increase in the alignment of molecular chains in a material can significantly improve the tensile properties of the resulting filament (Lin & Argon, 1994). Variation from the fitted line are due to the wide variety of extrusion parameters and material compositions of the filaments that make up each data set.

For macrofibers, an increase in stretch ratio from 9 to 12 resulted in a 30% increase in tensile strength and a 67% increase in elastic modulus. Similarly, for microfibers, an increase in stretch ratio from 9 to 12 resulted in a 56% increase in tensile strength and 168% increase in elastic modulus. For both micro and macrofibers stretch ratio has a more significant effect on elastic modulus than tensile strength. The influence of stretch ratio on elastic modulus was greater for microfibers. This was attributed to the smaller fiber diameter of microfibers. During extrusion fiber stretch typically occurs during entrance to the ovens. Smaller diameter fibers allowed a larger percentage of their cross section to be heated and thus more effectively align the molecular chains at a specific stretch ratio. The effect of fiber diameter on tensile properties is further discussed in Section 5.1.3.

Material blends with similar extrusion settings were then compared to more closely examine the effects of stretch ratio. The resulting charts are shown as Figure 5.8 and Figure 5.9 for tensile strength and elastic modulus, respectively.

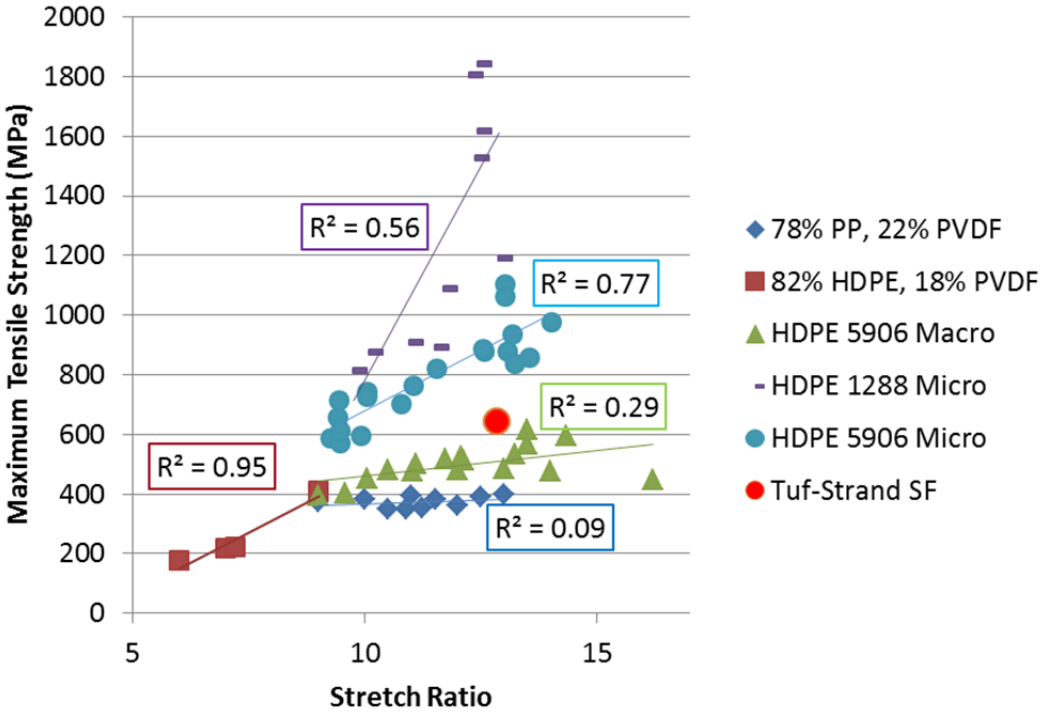

Figure 5.8 - Maximum tensile strength vs. stretch ratio for similar grouped fiber types

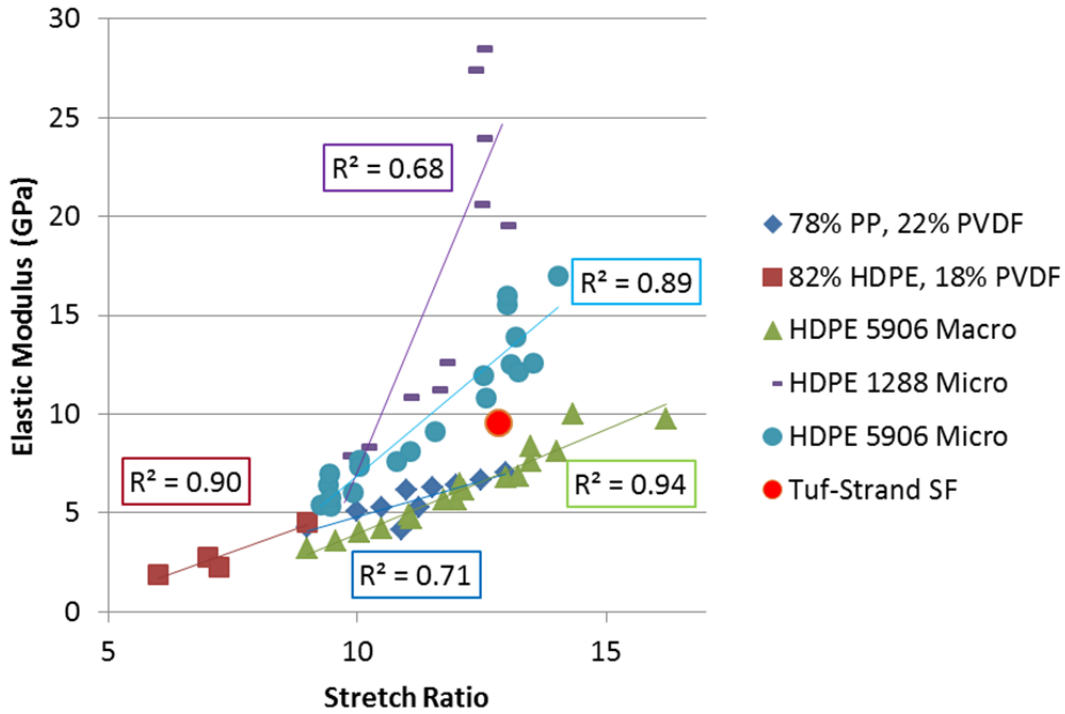

Figure 5.9 - Elastic modulus vs. stretch ratio for similar grouped fiber types

An increase in stretch ratio resulted in an increase in tensile strength and elastic modulus for varying materials; however the impact varied between materials. Of note is the variation in trend line slope between HDPE 5906 macrofibers and microfibers, indicating that the behavior of the same material in different configurations can still vary. This can again be attributed to the change in fiber dimensions.

While increasing stretch ratio resulted in improved tensile properties, when the stretch ratio was increased too far, filaments tended break on the extrusion line, reducing manufacturing efficiency. Therefore, other methods increasing tensile properties must be utilized in conjunction with increased stretch ratios.

5.1.3 Effect of Equivalent Diameter on Tensile Properties

The effect of fiber size using equivalent diameter on fiber tensile properties was investigated. The equivalent diameter, and consequently the cross sectional area of a fiber is affected by the stretch ratio. An increase in stretch ratio results in a decrease in equivalent diameter. However equivalent diameter can also be controlled by the spinneret die head design and the pump speeds on the extrusion line. Figure 5.10 and Figure 5.11 illustrate the effect of equivalent diameter on the fiber tensile strength and elastic modulus, respectively, for all fiber prototypes. The data was grouped by trial to illustrate variations according to similar materials and extrusion settings. A trend of increasing tensile strength and elastic modulus with decreasing equivalent diameter was observed. This can be attributed to the smaller fiber allowing heat to reach the fiber core more effectively during stretching, as discussed in Section 5.1.2.

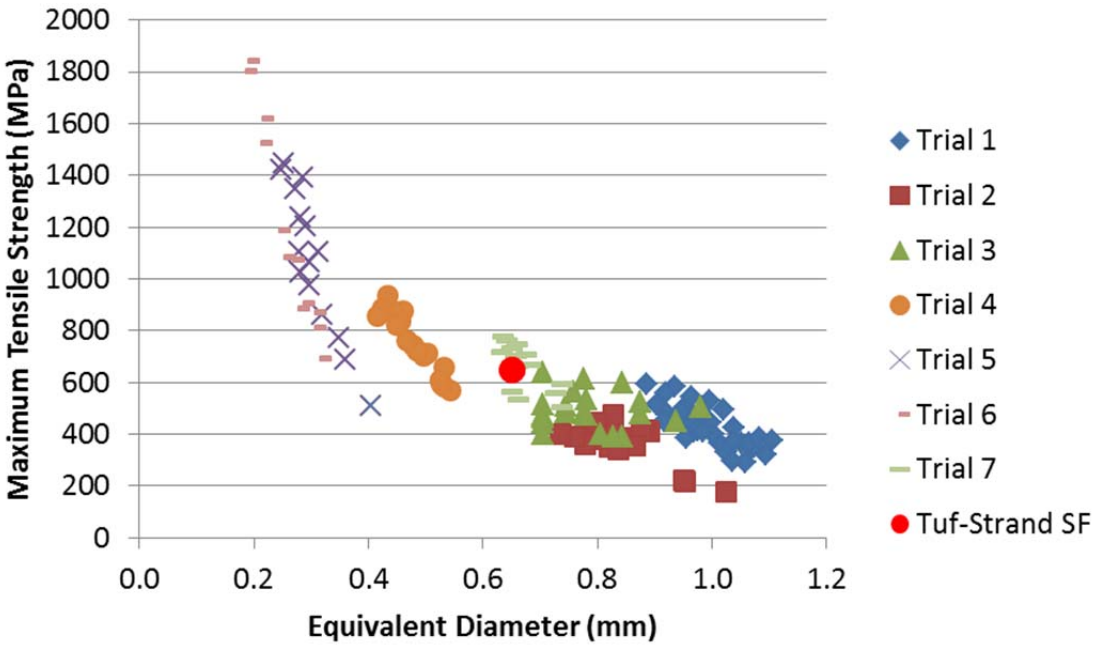

Figure 5.10 - Maximum tensile strength vs. equivalent diameter for all prototype fibers

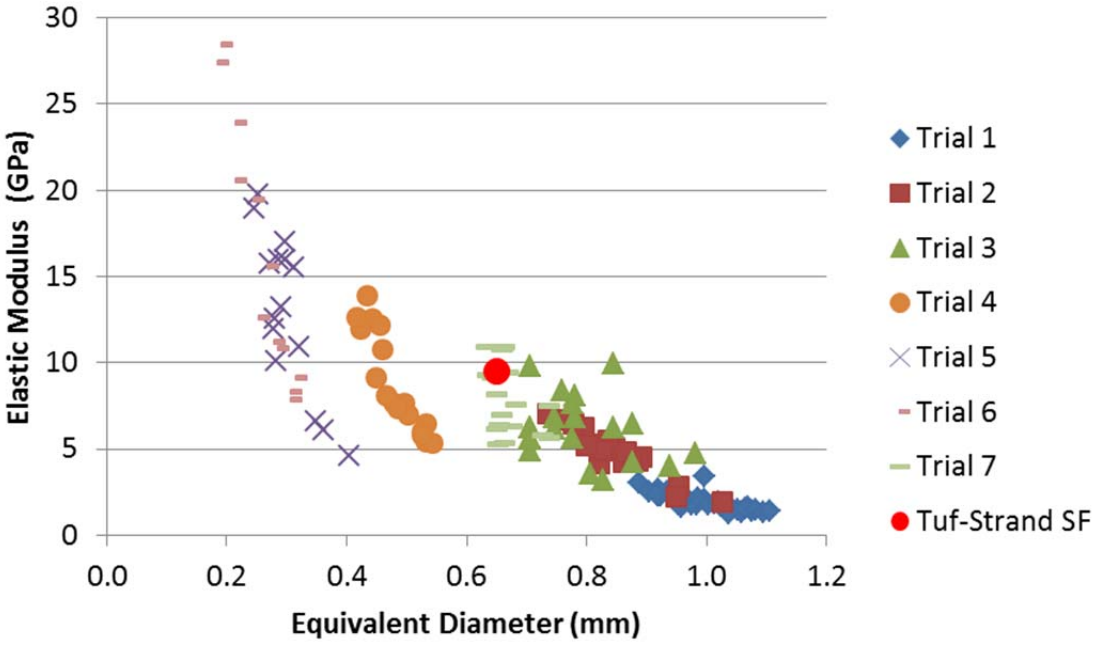

Figure 5.11 - Elastic modulus vs. equivalent diameter for all prototype fibers

The same results were shown for macrofibers in Figure 5.12 and Figure 5.13, and for microfibers in Figure 5.14 and Figure 5.15. The influence of equivalent diameter on tensile properties was greatest for microfibers. This can again be attributed to the smaller fiber diameter allowing oven heat to more effectively penetrate the fiber and allow a larger percentage of the cross section to be aligned.

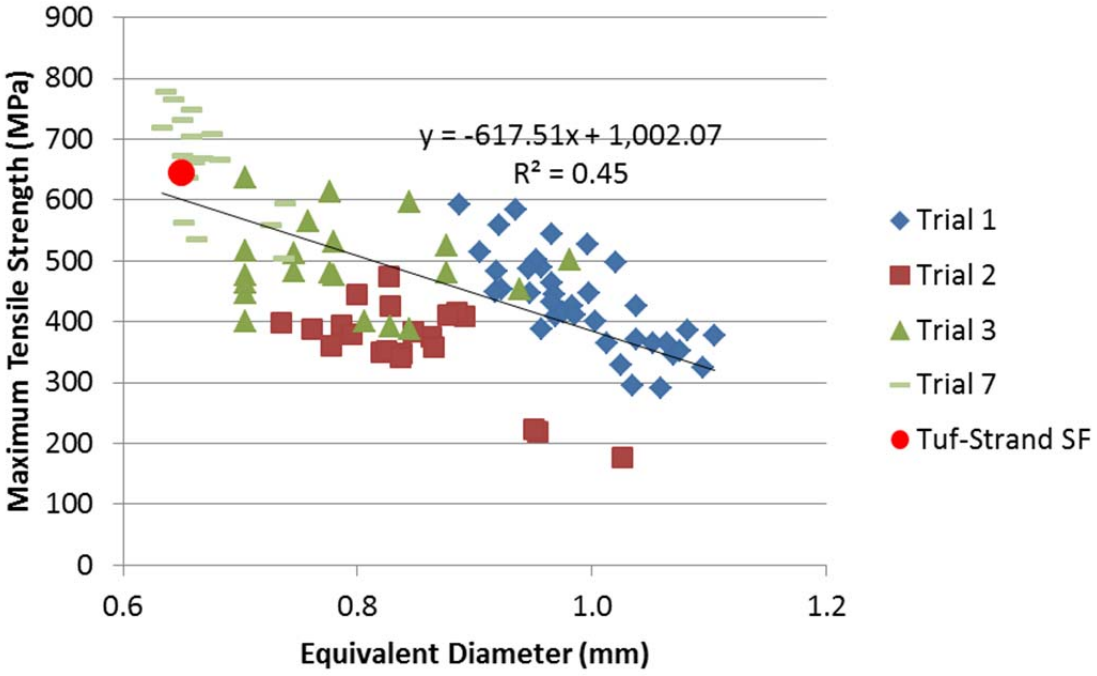

Figure 5.12 - Maximum tensile strength vs. equivalent diameter for macrofibers

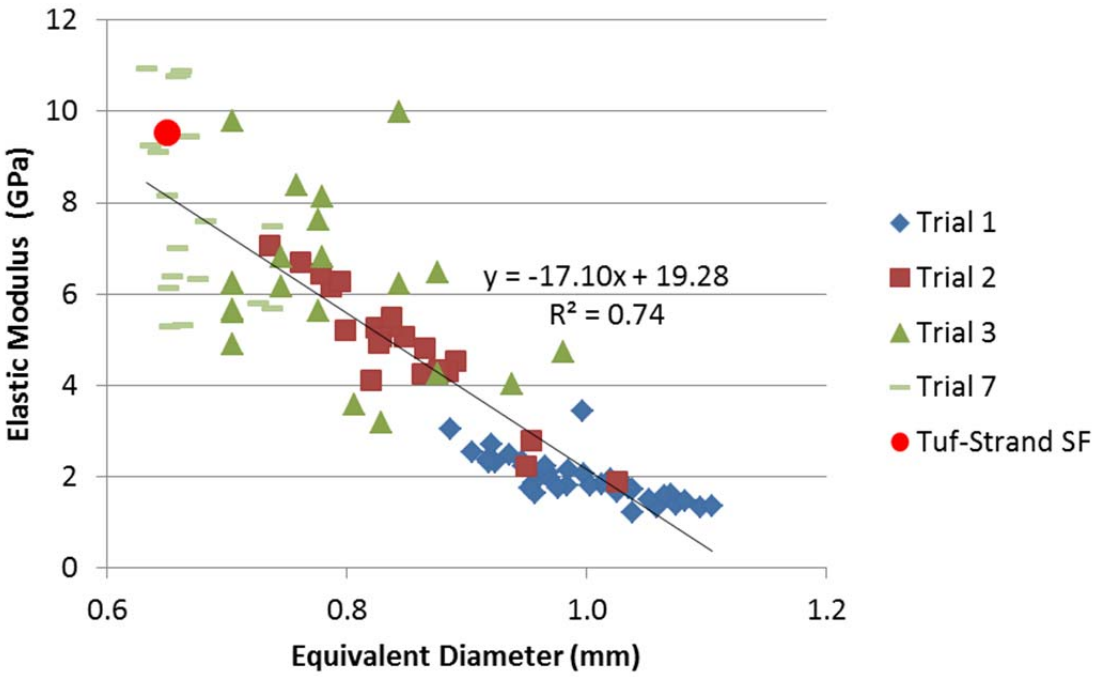

Figure 5.13 - Elastic modulus vs. equivalent diameter for macrofibers

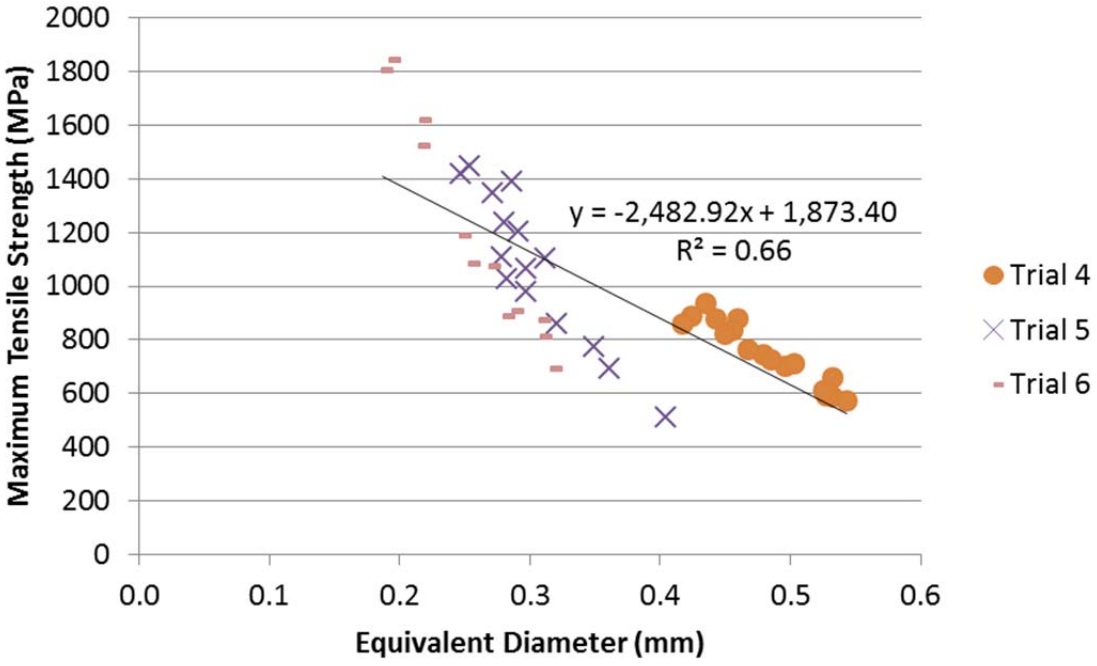

Figure 5.14 - Maximum tensile strength vs. equivalent diameter for microfibers

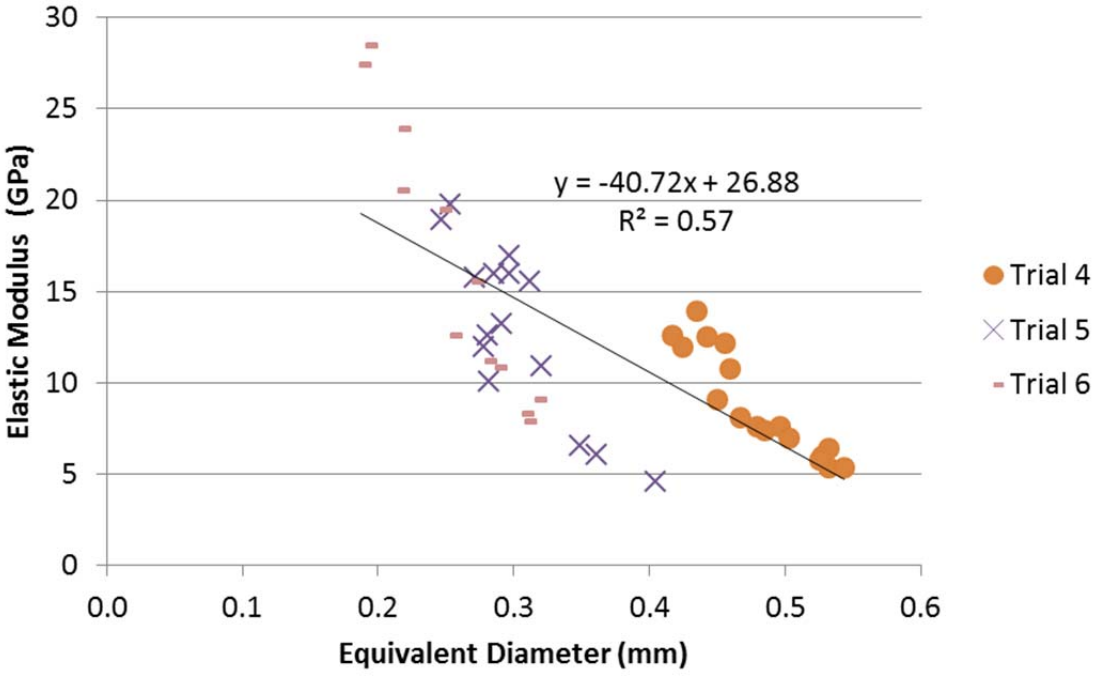

Figure 5.15 - Elastic modulus vs. equivalent diameter for microfibers

There are limitations to the strength and stiffness improvements possible by reducing the effective diameter. As discussed in Section 3.3.1, suitable aspect ratios must be maintained to provide sufficient surface area for the matrix to bond to and to minimize the potential for fibers to tangle during concrete mixing.

Therefore, balance must be achieved which maximizes stretch ratio without breaking the fibers whilst controlling the fiber dimensions using different spinneret die heads and pump speeds. More research should be performed on the effect of varying die head designs to control fiber dimensions and resulting tensile properties.

5.2 FIBER BOND AND PULLOUT RESULTS

The results of single fiber pullout tests were analyzed both to characterize the behavior of fibers in pullout, as well as to compare the performance of various prototype synthetic fibers. Pullout load vs. slip curves were plotted for each sample and summary charts were created by plotting the average load vs. slip curve, the 95% confidence interval, and the envelope in which all samples fell for that set (*i.e.* having the same fiber, inclination angle and embedment length). An example of a summary chart is shown as Figure 5.16. The summary chart for each set of pullout samples is presented in Appendix B. Results and discussion of aligned pullout testing are presented, followed by results of inclined pullout testing.

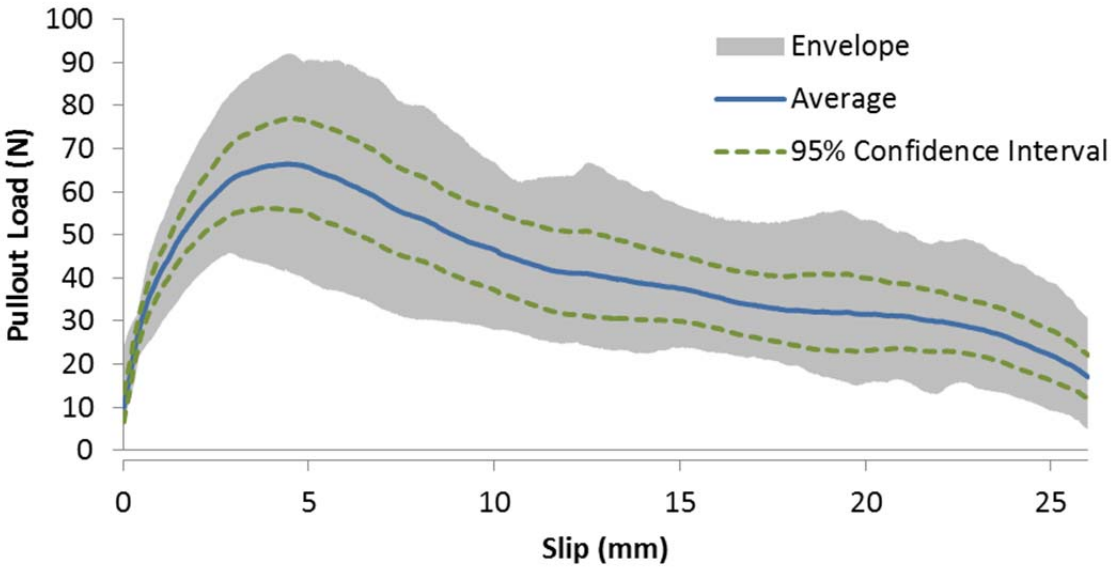

Figure 5.16 - Summary pullout chart for prototype fiber containing HDPE, 9% PVDF, and 10% MAH, tested at 0 degree inclination, 25 mm embedment length

5.2.1 Analysis of Pullout Curves

Initial visual assessments of fiber pullout curves, (using 25 mm embedment lengths for macrofibers and 15.9 mm embedment lengths for microfibers), indicated that nylon fibers demonstrated very poor pullout performance. These fibers were consequently excluded from further investigation. The remaining fibers included 12 macrofibers (11 prototypes and 1 commercially available fiber, Tuf-Strand SF), and 5 microfibers (4 prototypes and 1 commercially available fiber, PVA), to investigate.

Chemical Bond Energy and Slip Hardening Parameter

According to previous literature primarily focusing on PVA microfibers, a drop in the pullout load at low values of slip indicates a broken chemical bond with the matrix. Equation 5-1 and Equation 5-2 were used by Redon, *et al.*, 2001 to calculate the chemical bond energy and slip hardening parameter, respectively, of pullout curves for PVA fibers.

$$G_d = \frac{2(P_a - P_b)^2}{\pi^2 E_f {d_f}^3} \quad \textbf{5-1}$$

$$\beta = \left(\frac{d_f}{l_f}\right)\left[\left(\frac{1}{\tau_o \pi d_f}\right)\left(\frac{\Delta P}{\Delta S'}\right)_{S' \to 0} + 1\right] \quad \textbf{5-2}$$

Equation 5-1 is derived from the area under the load vs. slip curve illustrated in Figure 5.17. The significant drop in load is the indication this chemical bond has been broken. The slope of the pullout curve after debonding indicates if the fiber exhibits slip hardening, slip softening, or a constant friction mechanism, and is used to calculate the slip hardening parameter, β.

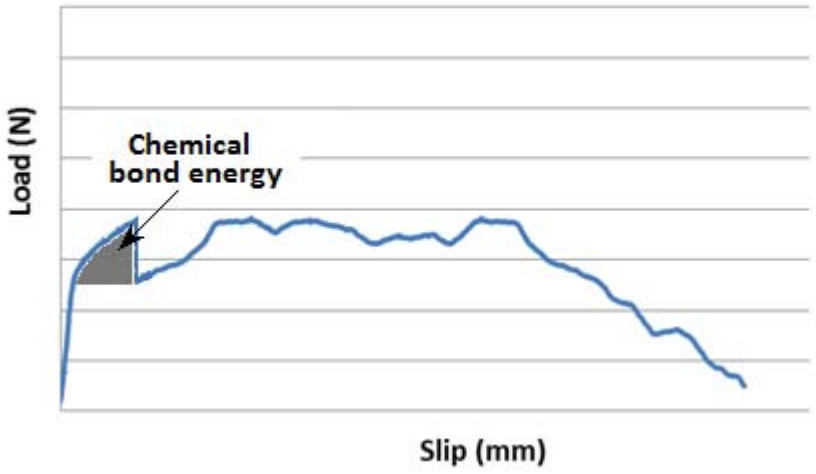

Figure 5.17 - Illustrative pullout load vs. slip curve showing chemical bond energy

This method is useful for PVA fibers, which exhibit a much stronger chemical bond with the matrix than frictional shear during pullout. However, for many other materials exhibiting low chemical bond strength, frictional shear is the dominant resistance mechanism. Chemical energy does not release over the whole fiber length instantaneously, rather chemical debonding and frictional shear act simultaneously during debonding. Therefore, when inspecting pullout curves for fibers with significant frictional shear resistance, there is no noticeable drop in the pullout load. Instead there is a gradual change in slope. This may be observed in the summary curve shown in Figure 5.16.

Pullout testing on the prototype fibers showed that the drop indicating chemical bond could not be detected due to the effective frictional shear resistance that is initiated during debonding of these fibers. Thus, it is difficult to determine the proportion of energy attributed to chemical bond using these methods. Pullout energy, U_P, taken as the area under the pullout curve up to a specified length of slip, as well as interfacial shear stress, τ_{max}, were used instead to quantify fiber performance.

The slip hardening parameter was also difficult to quantify using these methods. However, conclusions could still be drawn as to whether or not fiber types demonstrate slip hardening, slip softening, or constant friction mechanisms, based on the pullout curve shape. The following section discusses the pullout curve shapes associated with different fiber types.

Inspection of Pullout Curve Shapes

Figure 5.18 through Figure 5.23 illustrate representative curve shapes from a single sample of each set of pullout tests at 0 degree inclination angle and 25.4 mm and 15.9 mm embedment length for macrofibers and microfibers, respectively. It should be noted that these curves were selected for their representative shape, and peak values shown may not represent the average from the complete set of ten samples.

Figure 5.18 shows a load vs. slip curve for the prototype macrofiber containing 100% HDPE. The pullout curve showed no sudden drop in load to indicate a significant chemical bond formed with the matrix. After debonding, the curve has a slight concave down shape, indicating a slip hardening mechanism. The first peak load was not reached until beyond 5 mm slip, indicating that debonding had already occurred. The peak load can be attributed to frictional shear after debonding has occurred.

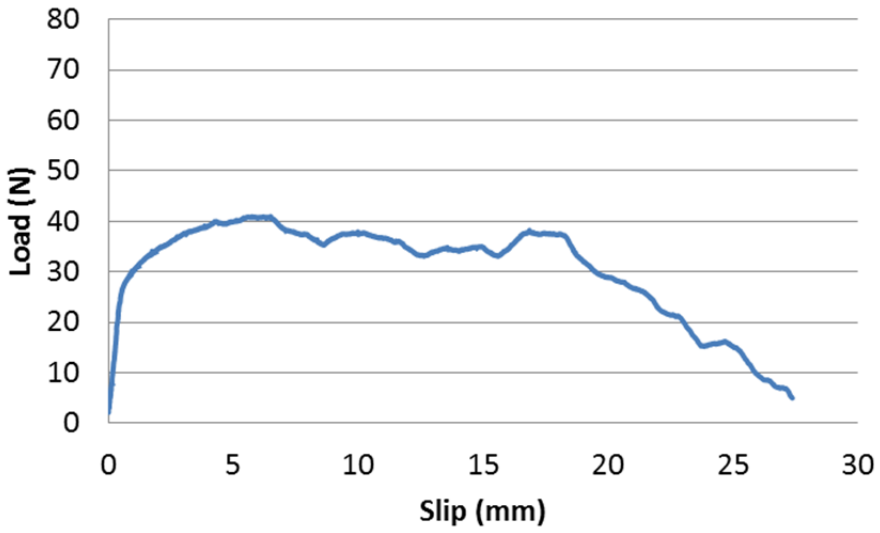

Figure 5.18 - Pullout load vs. slip curve for 100% HDPE macrofiber

Figure 5.19 shows load vs. slip curves for the prototype macrofibers containing HDPE with various quantities of PVDF and MAH. The pullout curve shows the peak load achieved at early slip values, followed by a steady decrease in load when the fiber has fully debonded, indicating a constant friction mechanism. The load decreases more quickly than with the 100% HDPE fiber, which could be attributed to the larger peak loads, which would be more difficult to sustain as slip increases. As the PVDF content was increased, there was an increase in the peak load. There was also a tendency for the peak load to occur at a greater slip with increased PVDF content. This shift can be attributed to the increase in chemical bond acting along with frictional shear, because PVDF has been shown to have good chemical bond with the matrix (MacDonald, 2010).

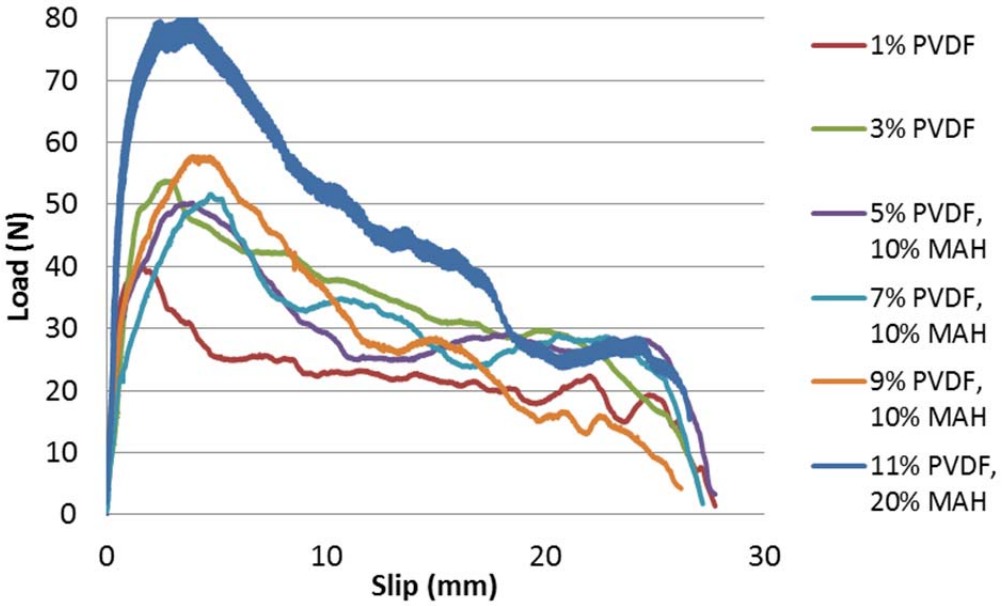

Figure 5.19 - Pullout load vs. slip curves for HDPE based macrofibers with gradual PVDF and MAH addition

Figure 5.20 displays a load vs. slip curve for the prototype macrofiber containing 100% PVDF. The pullout curve showed no drop when the pullout curve attains peak load, however there was a sharp change in the slope of the curve, indicating a chemical bond formed with the matrix. After the initial change in slope, there was a gradual increase in load until the peak load occurred at 17.4 mm slip, indicating a strong slip hardening mechanism.

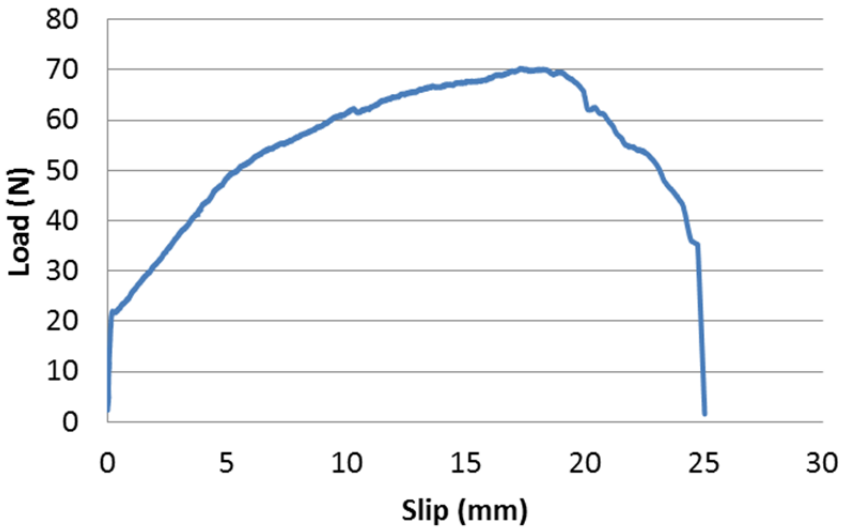

Figure 5.20 - Pullout load vs. slip curve for 100% PVDF macrofiber

Figure 5.21 displays load vs. slip curves for Tuf-Strand SF, the prototype macrofiber containing HDPE and 10% EVA, and the macrofiber containing PP, 10% HDPE and 10% EVA. The load vs. slip curve for the HDPE and 10% EVA macrofiber showed a steady decrease in load after debonding occurred, indicating a constant friction mechanism.

The load vs. slip curve for Tuf-Strand SF showed several peaks and valleys within the first several mm of slip, indicating a chemical bond existed with the matrix. When the fiber debonded there was a slight concave down shape, indicating a slip hardening mechanism.

The load vs. slip curve for the PP, 10% HDPE and 10% EVA macrofiber also showed multiple peaks at low slip values, indicating chemical bond. A second peak in load occurred towards the end of the pullout process, which indicated slip hardening behavior. This was an unusual trend for synthetic fibers in pullout, as typically a concave upward pullout curve would not peak again before complete pullout. This behavior can be attributed to the fact that this fiber would fibrillate if it were mixed in concrete. Small fibrils caused by slight splitting of the fiber along the embedded length caused more material to shear off and collect in the matrix cavity during pullout. This would decrease the diameter of the cavity thus increasing frictional shear resistance during pullout.

The pullout curves for Tuf-Strand SF and the prototype macrofiber containing PP, 10% HDPE and 10% EVA were not accurate representations of fiber behavior in FRC. Fibers used in pullout testing were carefully handled and undamaged, while fibrillation would occur in these fibers during concrete mixing, improving frictional bond. Testing was conducted in this manner to evaluate the contribution of EVA to pullout resistance. Fiber performance in FRC testing was also performed and these results are discussed in Section 5.3. If pullout testing incorporated fibrillation, the pullout curves would be expected to demonstrate increased slip hardening.

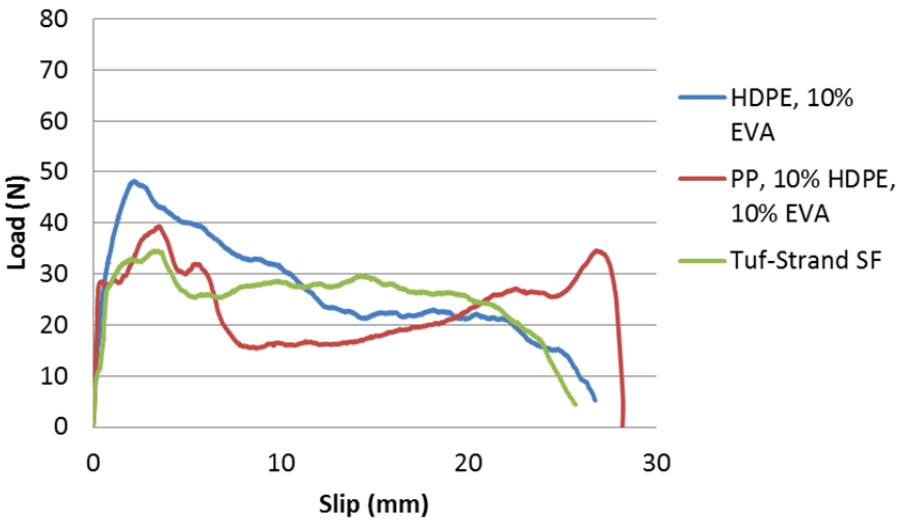

Figure 5.21 - Pullout load vs. slip curves for Tuf-Strand SF, and macrofibers containing EVA

Figure 5.22 displays a load vs. slip curve for the microfibers tested in pullout. The load vs. slip curves for the HDPE 5906 and the HDPE 1288 microfiber were similar. Both displayed a linear increase up to the peak load at less than 1 mm slip. When the fibers were fully debonded the load gradually decreased until the pullout process was complete, indicating little chemical bond strength with the matrix and a constant friction mechanism.

The pullout curves for the prototype microfibers containing HDPE, 10% PVDF and 20% MAH, and containing HDPE and 10% EVA had similar shapes to that of the HDPE microfibers, but the peak load for these microfibers occurred at a larger slip than with the HDPE fibers. This indicated that the presence of PVDF and EVA result in a higher chemical bond then the HDPE microfibers, occurring along with frictional shear. The nylon fiber achieved a very low peak load and gradually decreased in load until complete pullout, indicating very little chemical or frictional bond.

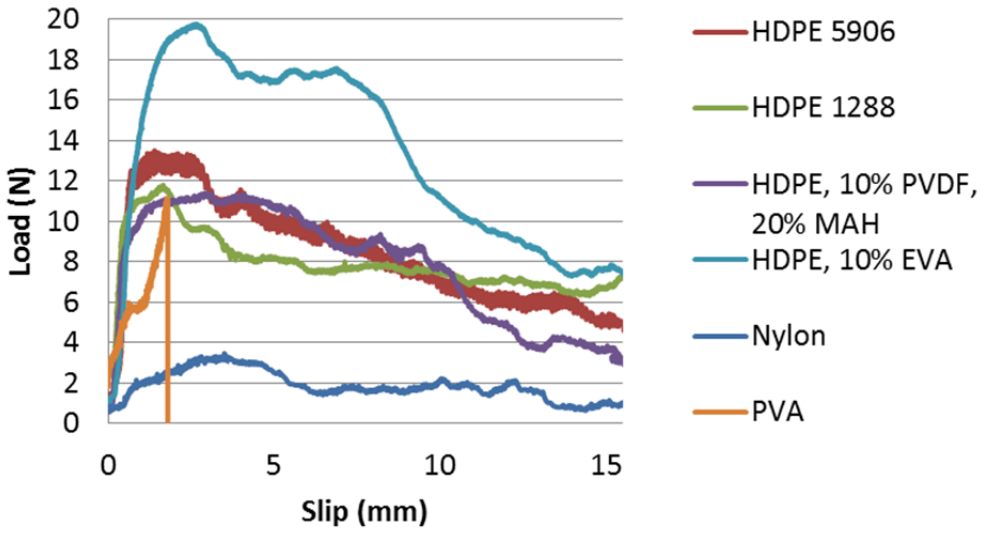

Figure 5.22 - Pullout load vs. slip curves for microfibers

Figure 5.23 displays the microfiber load vs. slip curves on a finer scale to examine the behavior at slip values less than 3.5 mm. For the PVA load vs. slip curve, there was a change in slope at approximately 1 mm slip, indicating a chemical bond with the matrix. The load continued to increase until fiber rupture, indicating a slip hardening mechanism. This behavior was consistent for the PVA samples, and matched findings in previous literature investigating PVA fibers in pullout. This sample shows the utility of using pullout energy to gauge synthetic fiber pullout performance. A fiber which ruptures at low values of slip absorbs significantly less energy than a fiber which sustains loads throughout the pullout process.

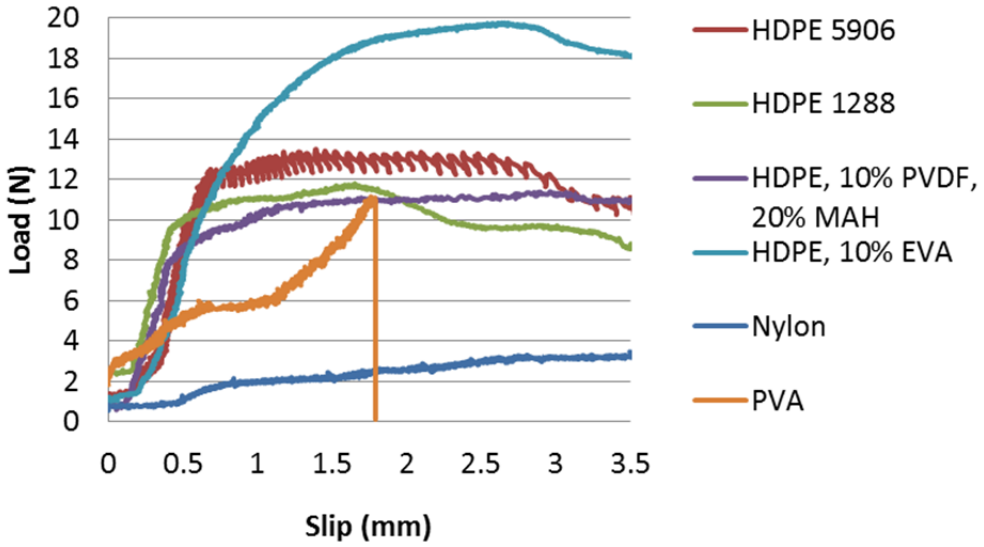

Figure 5.23 - Pullout load vs. slip curves for microfibers up to 5 mm slip

Table 5.4 and Table 5.5 summarize the pullout mechanisms identified by the load vs. slip curve shapes.

Table 5.4 - Pullout mechanisms for macrofibers

Fiber Description	Pullout Mechanism
100 % HDPE	Slip Hardening
HDPE, 1% PVDF	Constant Friction
HDPE, 3% PVDF	Constant Friction
HDPE, 5% PVDF, 10% MAH	Constant Friction
HDPE, 7% PVDF, 10% MAH	Constant Friction
HDPE, 9% PVDF, 10% MAH	Constant Friction
HDPE, 11% PVDF, 20% MAH	Constant Friction
100% PVDF	Slip Hardening
HDPE, 10% EVA	Constant Friction
80% PP, 10% HDPE, 10% EVA	Slip Hardening
Tuf-Strand SF	Slip Hardening

Table 5.5 - Pullout mechanisms for microfibers

Fiber Description	Pullout Mechanism
HDPE 5906	Constant Friction
HDPE 1288	Constant Friction
HDPE 5906, 10% PVDF, 20% MAH	Constant Friction
HDPE 5906, 10% EVA	Constant Friction
PVA	Slip Hardening

Pullout Energy and Interfacial Shear Stress

Fiber efficiency, η_τ, maximum interfacial shear stress, τ_{max}, and pullout energy, U_P, were calculated for 0 degree inclination angles using the methods outlined in Section 3.2.6. This was in order to quantitatively compare fiber performance in pullout testing. The results are presented in Table 5.6 for macrofibers and in Table 5.7 for microfibers. This data confirmed the negligible bond strength of nylon fibers.

Table 5.6 - Results of aligned pullout testing on macrofibers at 25 mm embedment length

Fiber Description	d_{eq} (mm)	σ_f (MPa)	η_τ	U_P at 10 mm slip (N-mm)	τ_{max} (MPa)
100 % HDPE	0.65	673	24.0%	338	0.83
HDPE, 1% PVDF	0.68	709	18.7%	240	0.70
HDPE, 3% PVDF	0.66	749	23.6%	363	0.92
HDPE, 5% PVDF, 10% MAH	0.66	779	26.7%	387	1.08
HDPE, 7% PVDF, 10% MAH	0.66	764	26.2%	453	1.12
HDPE, 9% PVDF, 10% MAH	0.68	731	31.9%	547	1.25
HDPE, 11% PVDF, 20% MAH	0.73	595	39.3%	660	1.40
100% PVDF	1.00	527	17.8%	438	0.89
HDPE, 10% EVA	0.74	595	22.1%	336	0.80
80% PP, 10% HDPE, 10% EVA	0.63	718	20.4%	270	0.73
Tuf-Strand SF	0.65	646	16.1%	218	0.61

Table 5.7 - Results of aligned pullout testing on microfibers at 15.8 mm embedment length

Fiber Description	d_{eq} (mm)	σ_f (MPa)	η_τ	U_P at 3.5 mm slip (N-mm)	τ_{max} (MPa)
HDPE 5906	0.30	1062	28.5%	39	0.94
HDPE 1288	0.20	1842	29.9%	30	1.14
HDPE 5906, 10% PVDF, 20% MAH	0.25	1420	49.6%	44	1.63
HDPE 5906, 10% EVA	0.28	1107	40.0%	53	1.34
PVA	0.12	2092	65.7%	14	2.11

A 50 mm fiber length is typically used for commercial macrosynthetic fibers. For a 50 mm fiber length, the maximum embedment length of a fiber bridging a crack is 25 mm. However, a crack opening in typical FRC applications using macrosynthetic fibers, such

as slabs or tunnel linings, would seldom be greater than 10 mm. Therefore, it is representative of field conditions to compare macrofibers using the pullout energy from 0 to 10 mm of slip. Microfibers are typically used in engineered cement composites and other applications where crack widths would be minimal. Therefore, microfibers were compared using pullout energy from 0 to 3.5 mm of slip. Pullout energy, taken as the area under a pullout load vs. slip curve, is a very useful parameter for directly comparing synthetic fibers in pullout because it accounts for factors such as fiber rupture, which is not represented by chemical bond strength.

The maximum interfacial shear stress, τ_{max}, is also a useful parameter for comparing synthetic fiber behavior in pullout. τ_{max} considers the maximum pullout load achieved and therefore can incorporate both chemical and frictional bond. It can also be used to predict a critical fiber length, beyond which fiber rupture becomes a concern. Maximum interfacial shear strength was calculated according to Equation 5-3.

$$\tau_{max} = \frac{P_{max}}{\pi d_{eq} l_e} \quad \textbf{5-3}$$

Where,

τ_{max} = Maximum interfacial bond strength determined through pullout testing (MPa)

P_{max} = Maximum pullout load (N)

d_{eq} = Equivalent diameter of fiber (mm)

l_e = Embedded length of fiber (mm)

In cases where the peak pullout load is reached towards the end of the pullout process, the value of τ_{max} may not accurately represent fiber behavior in FRC because the maximum shear resistance cannot be achieved at typical crack sizes. For example, Figure 5.24 illustrates the pullout curve for a sample of the prototype microfiber containing PVDF, tested at 0 degree inclination angle and 25 mm embedment length. In most cases, the first peak pullout load is also the maximum pullout load, but for this sample

the maximum pullout load occurs towards the end of the pullout process. The resulting value of τ_{max} would not be expected to be reached during typical cracking in FRC, due to the large slip distance at which it occurs. Therefore, it would be more useful to compare τ_{max} resulting from the peak pullout load achieved in the same window of slip values as used for pullout energy comparisons.

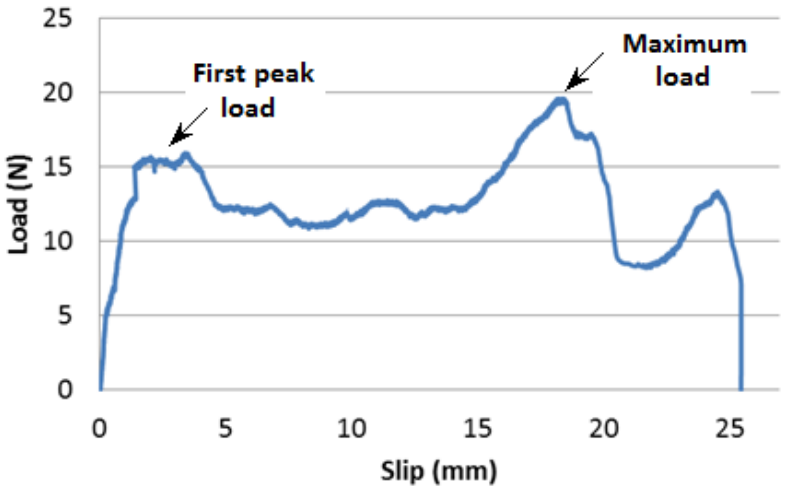

Figure 5.24 - Pullout load vs. slip curve for microfibers containing HDPE, 10% PVDF and 20% MAH, illustrating maximum pullout load occuring well after first peak load

Fiber efficiency, η_τ, calculated according to Equation 5-4, is not a particularly useful parameter for directly comparing fiber pullout performance. It is more useful for illustrating how much of the fibers inherent tensile strength can be utilized during pullout testing. Since a significant part of the fiber development process was maximizing the fibers tensile strength, low efficiency during pullout testing indicates a poor balance between bond strength and tensile strength. Fibers with low efficiency during pullout testing were HDPE and 1% PVDF, 100% PVDF, and Tuf-Strand SF for macrofibers, and nylon for microfibers. Mixing of fibers in FRC can increase fiber roughness and thus reduce tensile strength and increase frictional pullout resistance, effectively increasing the fiber efficiency. For example, while Tuf-Strand SF had low efficiency in pullout, it can be expected to perform well in FRC due to fibrillation.

$$\eta_\tau = \frac{P_{max}}{P_{crit}} \quad \textbf{5-4}$$

Where,

η_τ = Fiber efficiency (%)

P_{max} = Maximum pullout load from single fiber pullout test (N)

P_{crit} = Critical load at which fiber will rupture, found using a tensile test performed at the same speed as the pullout test (N)

Macrofiber Pullout Results

Table 5.8 presents the results of pullout testing on macrofibers of 25 mm embedment length, in order of decreasing τ_{max}. Interfacial shear was used instead of pullout energy for comparison between different sized fibers because the calculation incorporated the fiber diameter. A fiber with a larger diameter offers a greater surface area to bond with the matrix, which is not accounted for using pullout energy. This is particularly notable with the 100% PVDF fiber, which had the largest equivalent diameter, and therefore demonstrated a high value of pullout energy, but had a low value of interfacial shear.

The results in Table 5.8 show that the fibers with the highest interfacial shear strength were the prototype fibers with higher PVDF contents. The addition of EVA did not cause significant improvement to fiber-matrix bond in pullout testing. The fiber with the lowest interfacial shear strength was Tuf-Strand SF, however this fiber generally performs well in FRC due to the fiber fibrillating during concrete mixing. Therefore, pullout testing is useful for qualifying the behavior of synthetic fiber materials which do not depend on mixing action such as fibrillation. If fibrillation could be incorporated into pullout testing, Tuf-Strand SF and the fiber containing PP, 10% HDPE, and 10% EVA could be expected to perform significantly better in pullout due to the additional mechanical anchorage caused by fibrillation.

Table 5.8 - Results of aligned pullout testing for macrofibers

Fiber Description	d_{eq} (mm)	σ_f (MPa)	η_τ	U_P at 10 mm slip (N-mm)	τ_{max} (MPa)
HDPE, 11% PVDF, 20% MAH	0.73	595	39.3%	660	**1.40**
HDPE, 9% PVDF, 10% MAH	0.68	731	31.9%	547	**1.25**
HDPE, 7% PVDF, 10% MAH	0.66	764	26.2%	453	**1.12**
HDPE, 5% PVDF, 10% MAH	0.66	779	26.7%	387	**1.08**
HDPE, 3% PVDF	0.66	749	23.6%	363	**0.92**
100% PVDF	1.00	527	17.8%	438	**0.89**
100 % HDPE	0.65	673	24.0%	338	**0.83**
HDPE, 10% EVA	0.74	595	22.1%	336	**0.80**
80% PP, 10% HDPE, 10% EVA	0.63	718	20.4%	270	**0.73**
HDPE, 1% PVDF	0.68	709	18.7%	240	**0.70**
Tuf-Strand SF	0.65	646	16.1%	218	**0.61**

Figure 5.25 illustrates the effect of PVDF addition on both the interfacial shear stress and the pullout energy up to 10 mm slip. An increase in PVDF content resulted in a direct increase in both of these parameters. Therefore, PVDF does add an improvement to the fiber-matrix bond when added to HDPE based fibers. These results support the findings by MacDonald in 2010, who found that PVDF demonstrated chemical bond with a white cement mortar matrix. However, additional bond strength may be limited, as evidenced by the 100% PVDF fiber not exhibiting the highest bond. The equations of the trend lines in Figure 5.25 could be used in future extrusion trials to predict fiber properties based on PVDF content when using similar cross sections and extrusion settings.

From these results it can be concluded that of the fibers containing PVDF and MAH, the fiber containing HDPE, 11% PVDF and 20% MAH produced the highest bond strength. Thus this is the only PVDF containing macrofiber that will be included in the discussion of inclined pullout testing in Section 5.2.2. The performance of these fibers in FRC will be compared in Section 5.3.

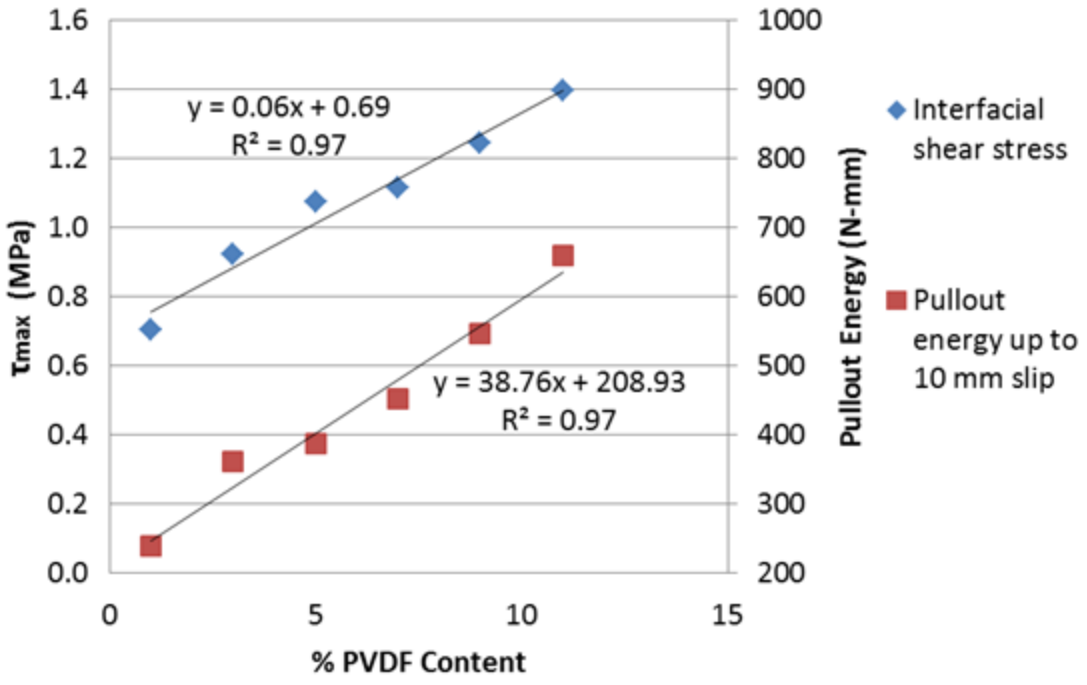

Figure 5.25 - Maximum interfacial shear stress vs. PVDF content and pullout energy up to 10 mm slip vs. PVDF content

Based on the results of the gradual addition of PVDF to HDPE based fibers, it would be expected that the 100% PVDF fiber would exhibit the highest fiber-matrix bond. Instead, the 100% PVDF fiber had lower interfacial shear resistance than the HDPE/PVDF blends, with the exception of the fiber containing HDPE and 1% PVDF. This can be explained by interfacial damage mechanisms during pullout.

To further investigate this theory, fibers were visually inspected at 10x magnification using an optical microscope. Both virgin fibers and fibers damaged during pullout were inspected. Figure 5.26 and Figure 5.27 show the magnified surface of the fiber containing HDPE, 7% PVDF and 10% MAH, and the 100% PVDF fiber, respectively. Figure 5.26 (a) shows striations existing on the surface of the virgin fiber containing HDPE, 7% PVDF, and 10% MAH, indicating surface roughness. These imperfections catch on cement particles during pullout, which causes peeling on the fiber surface, increasing

interfacial shear stress through frictional resistance. Figure 5.26 (b) shows surface damage on the fiber containing HDPE, 7% PVDF and 10% MAH after undergoing pullout. This matches findings by Baggot & Gandhi, 1981, and by Geng & Leung, 1996, who found similar shavings on polypropylene fibers after pullout resulted in increased pullout resistance in a cracked composite.

Figure 5.27 (a) shows a virgin 100% PVDF fiber. This fiber has noticeably less surface roughness than the fiber in Figure 5.26. Figure 5.27 (b) shows the same fiber type after undergoing pullout, with very little visible surface damage. Similar surface striations to the fiber containing HDPE, 7% PVDF and 10% MAH were visible in other PVDF containing fibers, with more striations being visible as PVDF content decreased. The magnified photos are useful as a way to validate findings obtained through other testing means, but are a poor indicator of bond strength by themselves.

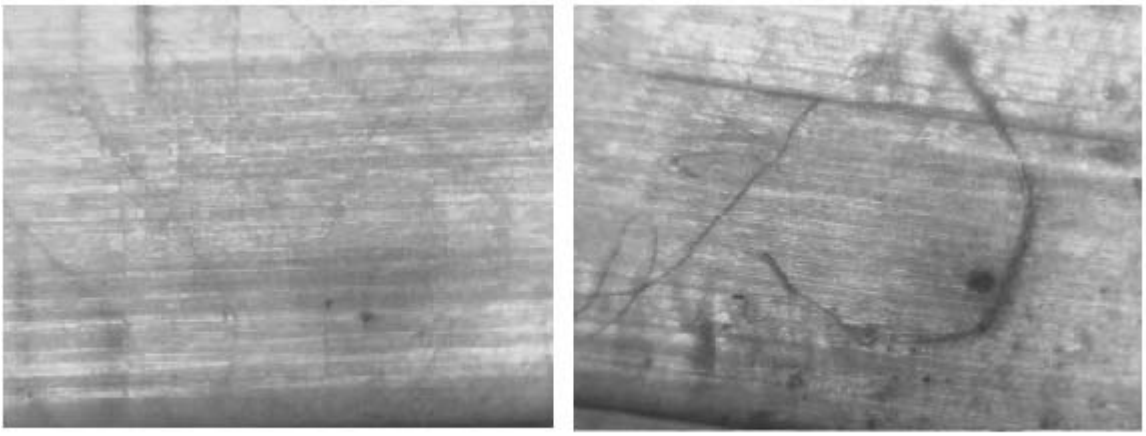

Figure 5.26 - HDPE, 7% PVDF fiber at 10x magnification (a) undamaged (b) damaged during pullout

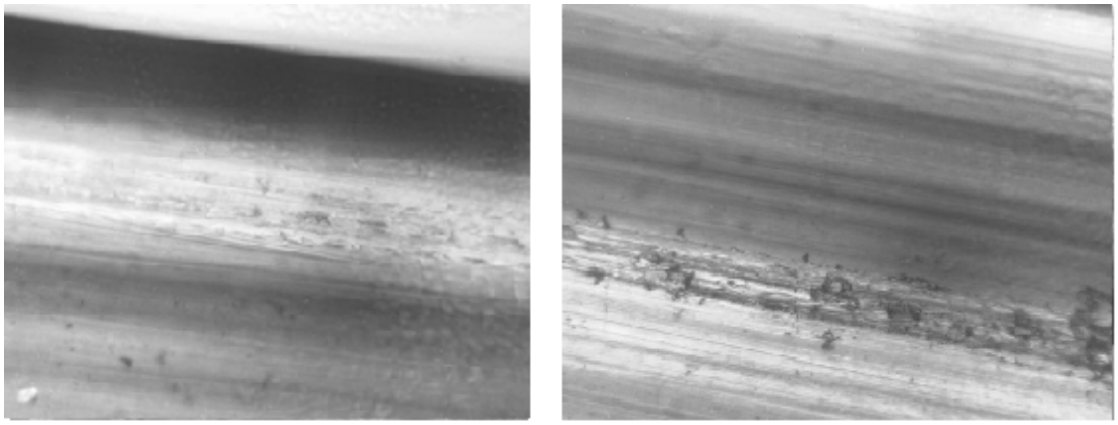

(a) (b)

Figure 5.27 - 100% PVDF fiber at 10x magnification (a) undamaged, (b) damaged during pullout

Microfiber Pullout Results

Table 5.9 presents the results of pullout testing on microfibers of 15.9 mm embedment length, in order of decreasing τ_{max}. The PVA demonstrated the highest interfacial shear and the lowest value of pullout energy of the microfibers. This is because many of the PVA samples ruptured at low values of slip during fiber pullout. This can be attributed to the significant chemical bond strength between PVA and the cement matrix, as found by Li, *et al.* in 2001.

Table 5.9 - Results of aligned pullout testing for microfibers

Fiber Description	d_{eq} (mm)	σ_f (MPa)	η_τ	U_P at 3.5 mm slip (N-mm)	τ_{max} (MPa)
PVA	0.12	2092	65.7%	14	**2.11**
HDPE 5906, 10% PVDF, 20% MAH	0.25	1420	49.6%	44	**1.63**
HDPE 5906, 10% EVA	0.28	1107	40.0%	53	**1.34**
HDPE 1288	0.20	1842	29.9%	30	**1.14**
HDPE 5906	0.30	1062	28.5%	39	**0.94**

From the results in Table 5.9 it can be seen that there is no significant difference between the HDPE 1288 and the HDPE 5906 prototype fibers in pullout testing. Also, while the macrofiber bond results did not conclusively show that the addition of EVA caused an improvement to fiber-matrix bond, this improvement was shown from the microfiber testing. The microfiber containing HDPE 5906 and 10% EVA demonstrated greater interfacial shear stress and pullout energy at 3.5 mm slip than both the HDPE 1288 and the HDPE 5906 microfibers. This is consistent with the findings by MacDonald in 2010, who showed that EVA demonstrated a chemical bond with mortar using white cement. These results were not consistent with the macrofiber pullout results, which did not demonstrate increased chemical bond with the addition of EVA. This may be attributed to surface roughness playing a larger role than chemical bond in macrofiber pullout than microfiber pullout due to increased surface areas of larger fibers.

Similar to the macrofiber results, the addition of PVDF and MAH demonstrated increased fiber-matrix bond in microfiber pullout testing. The fiber containing HDPE, 10% PVDF and 20% MAH demonstrated superior performance to the fiber containing HDPE and 10% EVA. The fiber containing PVDF had a higher value of interfacial shear stress but a lower value of pullout energy than the fiber containing EVA. This can be attributed to 3 of the 10 samples rupturing during pullout testing on the fiber containing PVDF.

Critical Fiber Length

Using the interfacial shear strength and the equation developed by Kaufmann *et al.*, 2007, shown as Equation 5-5, a critical fiber length, l_c, can be determined.

$$l_c = \frac{\sigma_{fu} d_{eq}}{4\tau_{max}} \quad \textbf{5-5}$$

Where,

l_c = Critical fiber length (mm)

σ_{fu} = Ultimate tensile strength of fiber, based on rate of testing simulating static loading (MPa)

d_{eq} = Equivalent fiber diameter (mm)

τ_{max} = Maximum interfacial bond strength, determined through pullout testing (MPa)

This critical fiber length is the minimum length for which the full strength of the fiber, (determined using the tensile strength at 5 mm/min testing rates), can be transferred to the matrix. A greater fiber length than this would be prone to rupture during pullout, and thus would not utilize the fiber efficiency. Table 5.10 and Table 5.11 present the critical fiber lengths for macro and microfibers, respectively.

Table 5.10 - Critical fiber length results based on aligned pullout testing for macrofibers

Fiber Description	Critical fiber length, *l*c (mm)
100 % HDPE	102
HDPE, 1% PVDF	130
HDPE, 3% PVDF	104
HDPE, 5% PVDF, 10% MAH	91
HDPE, 7% PVDF, 10% MAH	92
HDPE, 9% PVDF, 10% MAH	76
HDPE, 11% PVDF, 20% MAH	50
100% PVDF	135
HDPE, 10% EVA	110
80% PP, 10% HDPE, 10% EVA	119
Tuf-Strand SF	147

Table 5.11 - Critical fiber length results based on aligned pullout testing for microfibers

Fiber Description	Critical fiber length, *l*c (mm)
HDPE 5906	55
HDPE 1288	53
HDPE 5906, 10% PVDF, 20% MAH	32
HDPE 5906, 10% EVA	40
PVA	25

Aspect ratios, defined as the ratio of fiber length to fiber diameter, (Equation 5-6), for synthetic fibers are typically limited to 100. An aspect ratio greater than this is likely to cause "balling" and difficulty with concrete workability.

$$Aspect\ ratio = l_a/d_{eq} \quad \textbf{5-6}$$

Where,

l_a = Minimum allowable fiber length based on desired aspect ratio (mm)

d_{eq} = Equivalent fiber diameter (mm)

The smallest d_{eq} for the prototype macrofibers was 0.633 mm. Using a maximum aspect ratio of 100, this sets the minimum allowable fiber length to 63.3 mm for the macrofibers. Synthetic macrofibers are typically produced at lengths no greater than 50 mm. Critical fiber lengths for the microfibers were found to be 50 mm or greater. The smallest d_{eq} for the prototype microfibers was 0.195 mm. Using a maximum aspect ratio of 100, this sets the minimum allowable fiber length to 19.5 mm for the microfibers. Synthetic microfibers are typically produced at lengths much shorter than macrofibers, sometimes as small as 12 mm. Critical fiber lengths for the prototype microfibers were found to be 32 mm or greater.

These results indicate that for the prototype macro and microfibers, rupture would not be of immediate concern. It should be noted that this critical fiber length is a non-

conservative estimate because it is based on values from aligned pullout testing, an ideal situation that rarely occurs within FRC. Fibers undergoing inclined pullout would fracture at lower strengths due to increased stresses from bending and friction against crack face edges. This is called apparent fiber strength and is discussed in Section 5.2.2.

5.2.2 Inclined Pullout Results

Inclined pullout testing was conducted at 15, 30, 45 and 60 degree angles. The summary charts including the pullout load vs. displacement curves for inclined pullout testing are included in Appendix B. Results presented in this section are for 25.4 mm embedment lengths for macrofibers and 15.9 mm embedment lengths for microfibers.

Table 5.12 shows the inclined pullout testing results of specific fibers, including peak pullout load, efficiency and pullout energy up to full embedment length. The complete data tables for inclined pullout testing results are included in Appendix B. Fibers tested in pullout but not tested on inclines were PVA, HDPE 5906, and HDPE 1288 for microfibers, and 100% PVDF for macrofibers. The prototype fiber containing HDPE, 11% PVDF and 20% MAH exhibited the greatest interfacial bond strength of the macrofibers containing gradual additions of PVDF and MAH, and therefore will be the only fiber of this type discussed.

The results in Table 5.12 indicate that maximum pullout load, pullout energy, and fiber efficiency tended to increase with increased inclination angle for the fiber types being investigated. This is consistent with the findings by Li *et al.* in 1990.

Table 5.12 - Results of inclined pullout testing for select fiber types

Fiber Description	ϕ (degrees)	Matrix Strength (MPa)	P_{max} (N)	U_P (N-mm)	η_τ
100 % HDPE	0	37.6	43.0	779	24.0%
	15	34.3	44.1	816	24.6%
	30	34.3	60.7	903	33.9%
	45	35.7	51.5	979	28.8%
	60	35.7	57.6	942	32.2%
HDPE, 11% PVDF, 20% MAH	0	47.3	81.1	1312	39.3%
	15	37.9	75.8	1281	36.7%
	30	37.9	117.7	1180	57.0%
	45	35.2	126.3	849	61.2%
	60	35.2	119.5	728	57.9%
HDPE, 10% EVA	0	53.6	47.0	636	22.1%
	15	36.4	53.6	857	25.2%
	30	36.4	81.5	1204	38.4%
	45	29.3	70.7	1070	33.3%
	60	29.3	77.4	975	36.4%
80% PP, 10% HDPE, 10% EVA	0	38.3	37.1	599	20.4%
	15	38.3	43.1	832	23.7%
	30	33.7	50.2	937	27.6%
Tuf-Strand SF	0	46.9	31.9	509	16.1%
	15	54.0	31.9	517	16.1%
	30	53.2	40.1	639	20.2%
	45	54.2	40.5	585	20.4%
	60	37.6	50.7	889	25.6%
HDPE (5906), 10% PVDF, 20% MAH (Micro)	0	34.2	20.2	221	49.6%
	15	58.5	15.4	138	37.9%
	30	53.7	31.1	263	76.4%
	45	49.9	35.9	125	88.3%
	60	54.3	30.0	109	73.8%
HDPE (5906), 10% EVA (Micro)	0	50.8	18.7	210	40.0%
	15	51.7	14.9	200	31.9%
	30	50.2	18.9	225	40.3%
	45	46.2	27.5	248	58.7%
	60	53.6	32.5	157	69.3%

Snubbing Friction Coefficient

Table 5.13 presents the results of the inclined pullout testing analysis to determine snubbing friction coefficients of select fibers. Snubbing friction coefficients, *f*, were determined using Equation 5-7 and Equation 5-8 as proposed by Li *et al.* in 1990:

$$\widehat{P} = \frac{(P_{max}/l_1)_{\emptyset}}{(P_{max}/l_1)_{\emptyset=0}} \quad \textbf{5-7}$$

And,

$$f = \frac{1}{\emptyset}\ln \hat{P} \quad \textbf{5-8}$$

Where,

$\widehat{P}$ = Normalized pullout load per unit pullout length (N)

P_{max} = Maximum pullout load (N)

l_1 = Pullout length at given incline angle (mm)

f = Snubbing friction coefficient

ϕ = Inclined angle of fiber pullout (radians)

The peak pullout loads at angles were then predicted using the snubbing friction coefficient, according to Equation 5-9 as proposed by Leung & Ybanez:

$$P_{\phi} = P_0 \exp(f\phi) \quad \textbf{5-9}$$

Where,

P_{ϕ} = Predicted peak pullout load on given incline angle (N)

P_0 = Peak pullout load on an incline angle of 0° (N)

f = Snubbing friction coefficient

ϕ = Inclined angle of fiber pullout (radians)

Table 5.13 - Snubbing friction coefficients and predicted loads for inclined pullout testing of select fiber types

Fiber Description	ϕ (degrees)	P_{max} (N)	$\widehat{P}$	f	Predicted P_{ϕ} (N)
100 % HDPE	0	43.0	1.00	0.30	43.0
	15	44.1	1.00		46.5
	30	60.7	1.40		50.4
	45	51.5	1.15		54.5
	60	57.6	1.33		59.0
HDPE, 11% PVDF, 20% MAH	0	81.1	1.00	0.23	81.1
	15	75.8	0.94		86.1
	30	117.7	1.47		91.4
	45	126.3	1.50		97.0
	60	119.5	1.47		103.0
HDPE, 10% EVA	0	47.0	1.00	0.39	47.0
	15	53.6	1.07		52.1
	30	81.5	1.66		57.8
	45	70.7	1.44		64.0
	60	77.4	1.58		71.0
80% PP, 10% HDPE, 10% EVA	0	37.1	1.00	0.51	37.1
	15	43.1	1.22		42.4
	30	50.2	1.39		48.5
Tuf-Strand SF	0	31.9	1.00	0.31	31.9
	15	31.9	1.01		34.6
	30	40.1	1.22		37.6
	45	40.5	1.24		40.8
	60	50.7	1.49		44.3
HDPE (5906), 10% PVDF, 20% MAH (Micro)	0	20.2	1.00	0.46	20.2
	15	15.4	0.76		22.8
	30	31.1	1.54		25.7
	45	35.9	1.78		29.0
	60	30.0	1.49		32.8
HDPE (5906), 10% EVA (Micro)	0	18.7	1.00	0.28	18.7
	15	14.9	-		-
	30	18.9	0.94		22.7
	45	27.5	1.39		24.4
	60	32.5	1.67		26.3

Microfibers had higher snubbing coefficients than macrofibers. This is due to the smaller cross sections of microfibers, which resulted in decreased bending resistance. The predicted peak pullout loads were a reasonable match to the experimental values. This is also illustrated in Figure 5.28 for Tuf-Strand SF. This is consistent with the findings of Kanda & Li in 1998, who found that snubbing friction coefficients could be used to estimate the peak pullout load at any inclination angle. This can be used to predict fiber behavior at a variety of angles and could potentially be used in modeling fiber behavior in synthetic FRC.

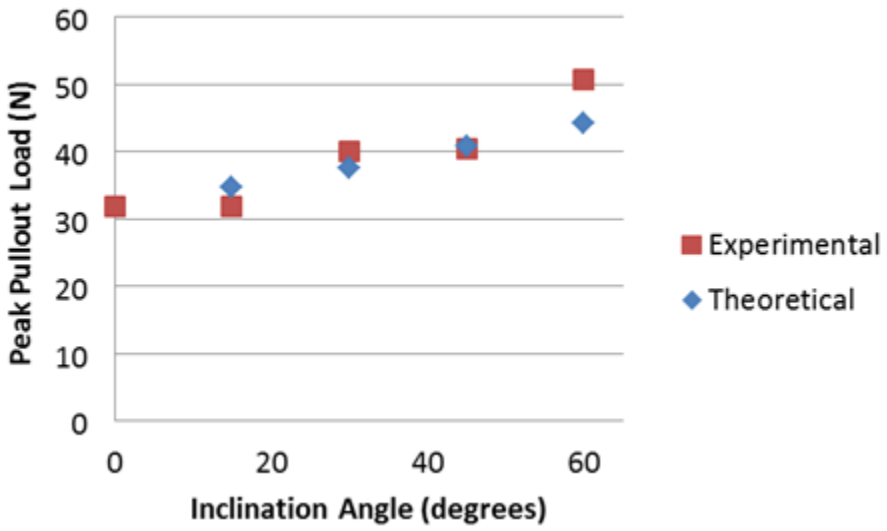

Figure 5.28 - Comparison of pullout load between experimental and theoretical predictions using snubbing friction coefficient for Tuf-Strand SF

The two microfibers had a greater variation between experimental and predicted values of peak pullout load than the macrofibers, due to larger variations in experimental values. This could be attributed to the greater prevalence of tensile rupture seen in the microfibers. A small variation in pullout load is exaggerated due to the low values of maximum load. While this is not typically an issue when comparing stresses, it results in some dubious values of snubbing coefficient. For example, the snubbing coefficient for the prototype microfiber containing HDPE and 10% EVA at 15 degrees was found to be a

large negative number. This caused the average snubbing friction coefficient for that fiber to be a negative number as well, implying that the pullout load decreased as pullout inclination angles increased, which was clearly erroneous. As the other values for inclined pullout increased with increasing angles, the 15 degree value was taken as an outlier and was removed from the calculation of snubbing friction coefficient for this fiber.

Apparent Fiber Strength Reduction

Apparent fiber strength, σ_a, is the stress value at which a fiber will rupture during inclined pullout testing. It is typically lower than the nominal tensile fiber strength due to additional bending stresses acting on the fiber during inclined pullout testing. The fiber strength reduction factor, f', accounts for the reduction in fiber strength when pulled out on an incline. f' was determined for select fibers using Equation 5-10 as proposed by Kanda & Li in 1998.

$$\sigma_a = \sigma_{fu}^n \, e^{-f'\phi} \qquad \textbf{5-10}$$

Where,

σ_a = Apparent fiber strength, determined from the load at which fibers rupture during inclined pullout testing (MPa)

σ_{fu}^n = Nominal fiber tensile strength, determined through aligned pullout testing (MPa)

f' = Apparent fiber strength reduction factor

Because apparent fiber strength is calculated using loads at which fibers rupture during pullout, the strength reduction factors could only be calculated for fibers that experienced rupture during inclined pullout testing. The relevant fibers that did not experience rupture during pullout testing were Tuf-Strand SF and the prototype fiber containing PP, 10% HDPE and 10% EVA. The apparent fiber strengths and calculated fiber strength reduction factors are presented in Table 5.14 for select fibers.

In order to account for the effect of the compressive strength of the matrix, the fiber strength reduction factor was normalized with respect to the matrix compressive strength, by dividing by f by the matrix strength. This value is presented as $\hat{f}$ and can be used to directly compare the fiber strength reduction effect felt by inclined fibers, regardless of matrix compressive strength.

Table 5.14 - Apparent fiber strength results for fibers with ruptured samples

Fiber Description	ϕ (degrees)	Number of Ruptures	σ_a (MPa)	f'	$\hat{f}$
100 % HDPE	0	-	517	0.85	2.45
	30	2	299		
	60	1	259		
HDPE, 11% PVDF, 20% MAH	0	-	384	0.32	0.88
	30	7	300		
	45	7	319		
	60	9	294		
HDPE, 10% EVA	0	-	477	0.88	2.76
	30	1	277		
	45	3	230		
	60	4	238		
HDPE (5906), 10% PVDF, 20% MAH (Micro)	0	3	167	0.18	0.28
	15	1	118		
	30	5	179		
	45	7	197		
	60	6	156		
HDPE (5906), 10% EVA (Micro)	0	-	789	1.98	4.09
	45	3	128		
	60	7	141		

The pullout loads at which ruptures occurred are consistent with the findings of Kanda & Li in 1998, who found that fibers tend to rupture at lower stresses as ϕ increases. A positive fiber strength reduction factor implies that fiber strength will be reduced as

inclination angle increases. Based on the values presented in Table 5.14, the fibers containing PVDF experienced the least reduction in apparent fiber strength.

There were some significant sources of error with these calculations. Apparent fiber strength reduction factors are meant to be calculated using the rupture loads at 0 degree embedment lengths. The majority of fibers tested did not experience rupture at 0 degrees. Instead the tensile strength when tested at 5 mm/min was used for these calculations, as this value was considered a close approximation of fiber rupture strength during pullout testing. Only one fiber type (the HDPE, 10% PVDF, 20% MAH microfiber) experienced rupture at 0 degrees, thus it was the only fiber type with an accurately calculated value of fiber strength reduction factor. If pullout rupture stresses were used instead of ultimate tensile stresses, it would be expected that the fiber strength reduction factor would be lower, implying the fibers maintain more of their strength during inclined pullout than shown here. Therefore, the values shown in Table 5.14 are conservative estimates.

In order to more accurately investigate apparent fiber strength reductions, pullout tests at 0 degrees that end in fiber rupture must be performed. This could be achieved using samples cast at embedment lengths significantly greater than the critical embedment lengths calculated in Section 5.2.1.

5.3 FRC Performance Results

A total of 12 mixes were cast to characterize fiber behavior in FRC performance testing; nine mixes using prototype macrofibers and three mixes using commercially available macrofibers. All mixes used fiber volumes of 3.0 kg/m^3. This section describes the fresh properties as well as the results and effect of fibers on compressive and flexural strength of the FRC mixtures.

5.3.1 Fresh Properties

The fibers cast, along with the fresh properties of the mixtures, are presented in Table 5.15. The fresh properties measured were slump and density. Densities were taken before fiber addition. These properties were tracked during the FRC trials to ensure consistency between mixes. This ensured that only the fiber properties varied. The results of the FRC fresh properties indicated that consistency was successfully maintained between mixes.

Table 5.15 - Fresh properties of FRC

Fiber	Slump (mm)		Density (kg/m^3)	Fibrillation Evident?
	Before Fiber Addition	After Fiber and Super Plasticizer Addition		
HDPE, 1% PVDF	175	175	2366	No
HDPE, 3% PVDF	180	110	2397	No
HDPE, 5% PVDF, 10% MAH	180	140	2410	No
HDPE, 7% PVDF, 10% MAH	125	110	2390	No
HDPE, 9% PVDF, 10% MAH	160	160	2386	No
HDPE, 11% PVDF, 20% MAH	160	150	2400	No
100% HDPE	200	140	2377	No
HDPE, 10% EVA	180	160	2387	Yes
80% PP, 10% PE, 10% EVA	175	110	2400	Yes
BASF - MasterFiber MAC470	160	180	2377	No
Strux 85/50	180	200	-	Yes
Tuf-Strand SF	150	100	2393	Yes

Washout samples were also taken from the fresh concrete to determine if fibrillation was evident after mixing. The complete set of fibrillation photos, along with photos of the undamaged cut fibers, are presented in Appendix C for the prototype fibers and Tuf-Strand SF. Visual inspection of washout samples and the fibers during mixing indicated fibrillation occurred for Tuf-Strand SF, Strux 85/50, and the prototype fiber containing

PP, 10% HDPE and 10% EVA. This was expected as these fibers contain blends of both PP and polyethylene, which are materials known to separate and cause fibrillation. Figure 5.29 (a) shows a washout sample for the prototype fiber containing PP, 10% HDPE and 10% EVA. The frayed ends and splitting fibers indicate fibrillation. In contrast, Figure 5.29 (b) shows the prototype fiber containing HDPE and 3% PVDF. The fibers have maintained their cross sectional shape and no fibrillation is evident.

(a) (b)

Figure 5.29 - Washout samples of prototype fibers containing (a) PP, 10% HDPE and 10% EVA, illustrating fibrillation and (b) HDPE and 3% PVDF, illustrating no fibrillation

Visible fiber splitting was also found in the washout sample from the prototype fiber containing HDPE and 10% EVA, shown in Figure 5.30. This was not expected as EVA is an adhesive and HDPE is not known to fibrillate individually. This splitting was caused by a flaw in the di head used for this prototype fiber, due to restrictions of milling equipment during production of the di head. This flaw resulted in an inconsistency in the fiber cross section as illustrated in Figure 5.31. Similar splitting was not found for other prototype fibers produced using the same di head. This fiber splitting would be expected to improve flexural performance of FRC, as it could possibly behave as a form of mechanical anchorage in a similar manner to fibrillation.

Figure 5.30 - Washout sample of fiber containing HDPE and 10% EVA

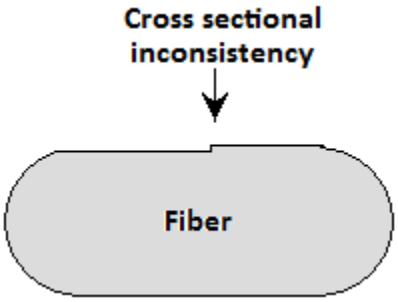

Figure 5.31 - Inconsistency in cross section of fiber containing HDPE and 10% EVA, resulting in fiber splitting

5.3.2 Compressive Strengths

Compressive strength specimens were tested after 28 days. Results of the compressive strength testing on FRC samples are presented in Table 5.16. A complete table of the individual specimen results is included in Appendix C. The targeted compressive strength of the FRC was 40 MPa. Macrofiber addition is known to decrease the compressive strength of concrete, as the fibers themselves are intended to perform in tension, and thus take up volume that would otherwise have been filled by the higher

strength concrete. (Manolis, Gareis, Tsonos, & Neal, 1997). The compressive strength results indicate the FRC mixtures were successful at relatively achieving the targeted compressive strengths.

Table 5.16 - Results for compressive strength of FRC mixes

Fiber	Average Compressive Strength, f'_c (MPa)
100% HDPE	41.6
HDPE, 1% PVDF	43.9
HDPE, 3% PVDF	44.9
HDPE, 5% PVDF, 10% MAH	41.7
HDPE, 7% PVDF, 10% MAH	46.5
HDPE, 9% PVDF, 10% MAH	37.4
HDPE, 11% PVDF, 20% MAH	42.5
HDPE, 10% EVA	39.9
80% PP, 10% HDPE, 10% EVA	41.2
Tuf-Strand SF	32.2
BASF - MasterFiber MAC470	39.0
Strux 85/50	36.1

5.3.3 Flexural Strength and Toughness of FRC

Flexural and residual strength and toughness of the FRC mixtures were tested using ASTM C1609, ASTM C1399 and ASTM C1550. The following section presents the results and discussion of FRC performance in flexural testing.

Q-Test

The Q test, (also known as Dixon's Q test), was used for the elimination of outliers for the FRC performance results. This test is a simple way to identify and eliminate outliers, and can only be applied to a set of data once. A value of Q, $Q_{exp,}$ is calculated using

Equation 5-11 and compared to a critical value of Q, Q_c. Critical values of Q for different data quantities and confidence levels are shown in Table 5.17. If $Q_{exp} > Q_c$ then the outlier is rejected from the data set for that confidence level.

Table 5.17 - Critical values for Q test

Number of Values	Confidence Level		
	$Q_{90\%}$:	$Q_{95\%}$:	$Q_{99\%}$:
3	0.941	0.970	0.994
4	0.765	0.829	0.926
5	0.642	0.710	0.821
6	0.560	0.625	0.740
7	0.507	0.568	0.680
8	0.468	0.526	0.634
9	0.437	0.493	0.598
10	0.412	0.466	0.568

An example of the application of the Q test is shown below. Table 5.18 shows the RSI values resulting from ASTM 1399 testing on four samples of the HDPE, 7% PVDF and 10% MAH fiber. The value for sample 1 was suspected of being an outlier.

$$Q_{exp} = \frac{(suspected\ outlier - \ nearest\ value)}{(maximum\ value - minimum\ value)} \quad \textbf{5-11}$$

$$Q_{exp} = \frac{(0.99 - 0.59)}{(0.99 - 0.50)} = 0.816$$

From Table 5.17, Q_c = 0.765 for four samples, 90% confidence level. $Q_{exp} > Q_c$ for this sample, therefore it was removed from the data as an outlier. Visual inspection of the break face for this sample, shown in Figure 5.32 further confirmed the error in this sample. A collection of fibers was visible close to the tension face of the beam. This would provide a falsely high RSI value for this sample.

Table 5.18 - Residual strength index results for HDPE, 7% PVDF, 20% MAH FRC

Sample ID	RSI (MPa)
HDPE, 7% PVDF, 20% MAH-3.0-1	0.99
HDPE, 7% PVDF, 20% MAH-3.0-2	0.53
HDPE, 7% PVDF, 20% MAH-3.0-3	0.59
HDPE, 7% PVDF, 20% MAH-3.0-4	0.50

Figure 5.32 - Break face of outlier sample from ASTM C1399 testing for fiber containing HDPE, 7% PVDF and 10% MAH

The Q test was applied to the data sets for ASTM 1690 test results and for ASTM 1399 test results. One sample was removed from the ASTM 1609 test results for the Strux 85/50 fiber with 99% confidence. One sample each for the mixtures containing the HDPE, 7% PVDF and 10% MAH fiber, the HDPE and 1% PVDF fiber, and the HDPE and 10% EVA fiber, were removed with 90% confidence from the ASTM 1399 test results.

ASTM C1609 Flexural Toughness Results

Toughness and first peak flexural strength using the three point bending test results of ASTM C1609 testing are shown in Table 5.19. Complete tables of the individual test results for ASTM C1609 testing are included in Appendix D. Curves of applied load vs. deflection were plotted for each sample. The average curves are presented in

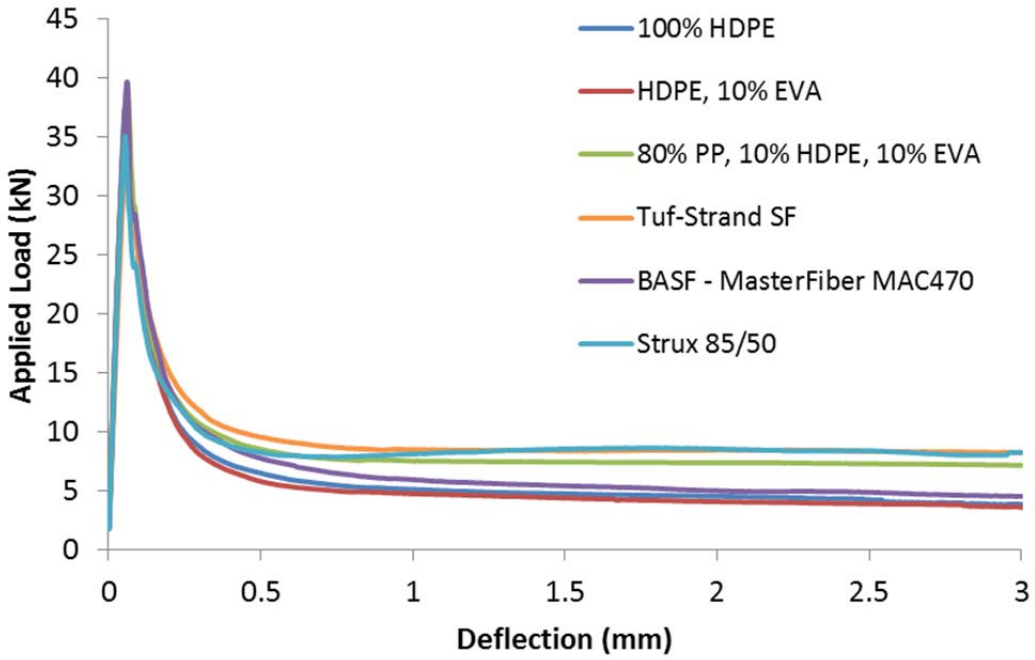

Figure 5.33 and Figure 5.34. Complete curves resulting from the individual ASTM C1609 testing are included in Appendix D.

Table 5.19 - Results for flexural strength and toughness from ASTM C1609 testing

Fiber	First Peak Strength, f_p, (MPa)	T_{150}^{150} (J)
100% HDPE	4.94	17.88
HDPE, 1% PVDF	4.63	21.66
HDPE, 3% PVDF	4.50	18.76
HDPE, 5% PVDF, 10% MAH	5.10	19.73
HDPE, 7% PVDF, 10% MAH	4.74	19.02

HDPE, 9% PVDF, 10% MAH	4.71	18.91
HDPE, 11% PVDF, 20% MAH	4.54	17.41
HDPE, 10% EVA	4.77	17.06
80% PP, 10% HDPE, 10% EVA	5.01	25.92
BASF - MasterFiber MAC470	5.00	20.95
Strux 85/50	4.50	23.09
Tuf-Strand SF	4.45	28.87

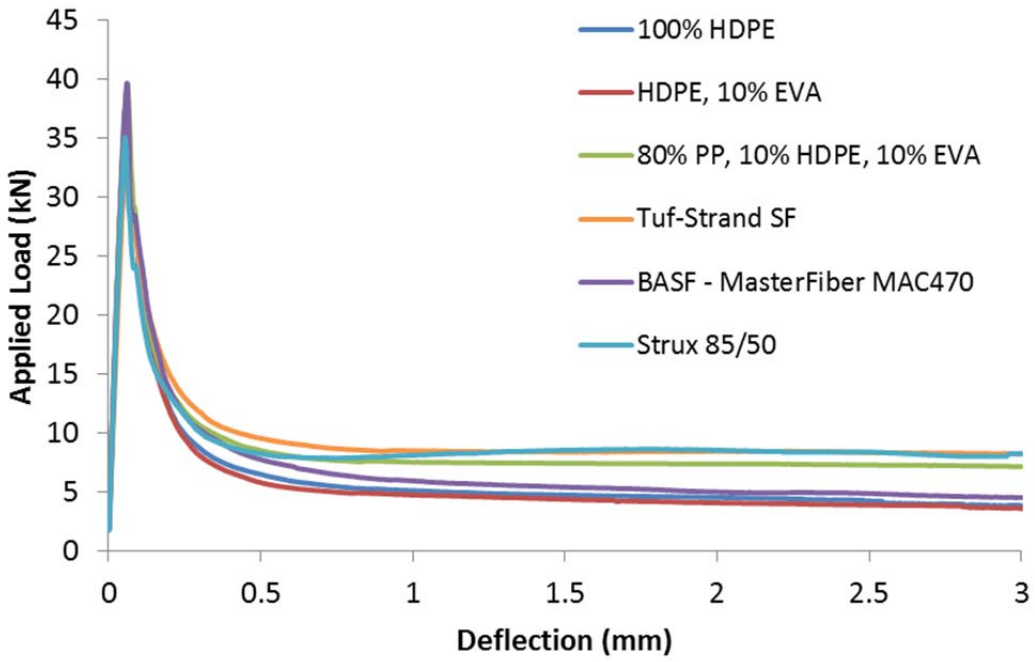

Figure 5.33 - Load vs. deflection curve for ASTM C1609 testing for commercial fibers and some prototype fibers

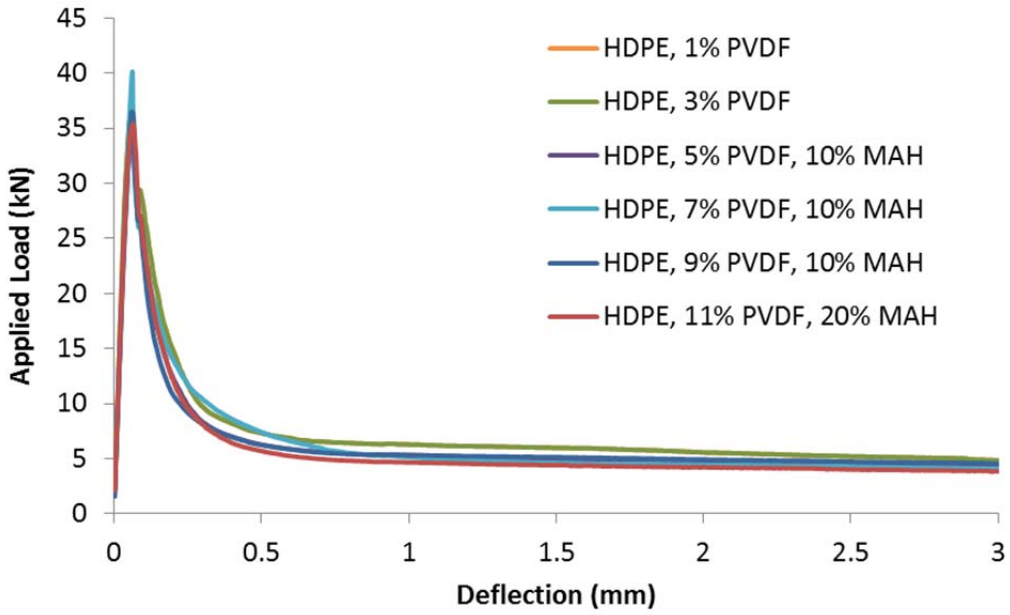

Figure 5.34 - Load vs. deflection curve for ASTM C1609 testing for prototype fibers containing PVDF

The results presented for ASTM C1609 testing show that the FRC mixtures with the largest toughness values are Tuf-Strand SF, the prototype fiber containing PP, 10% HDPE and 10% EVA, Strux 85/50 and the BASF fiber. These results were expected, as these are the four fibers with a form of additional mechanical anchorage. These fibers undergo fibrillation during mixing, with the exception of BASF fibers, which are embossed. Fibrillation and embossment are forms of mechanical anchorage and thus increase pullout resistance. These results indicate that some form of mechanical anchorage is important for improving FRC toughness.

The other prototype fibers were all found to have very similar values of toughness, despite the fiber splitting that was visible in the washout sample of the prototype fiber containing HDPE and 10% EVA. No single material, such as EVA or PVDF additions, improved the first peak strength or toughness significantly during ASTM C1609 testing. The exception to this is the prototype fiber containing HDPE and 1% PVDF. During ASTM C1609 testing, equipment malfunctions occurred on three of the five samples. The curves for these samples were plotted up to the point of equipment failure, as indicated

by * in Figure 5.35. The samples that were not tested to completion could not be included in results, as data was not captured up to 3 mm of deflection. These samples were all visibly lower than the two samples reported in results, and thus would have lowered the average. Therefore, the toughness value being reported for the fiber containing HDPE and 1% PVDF is falsely inflated and not representative of this fibers performance in FRC.

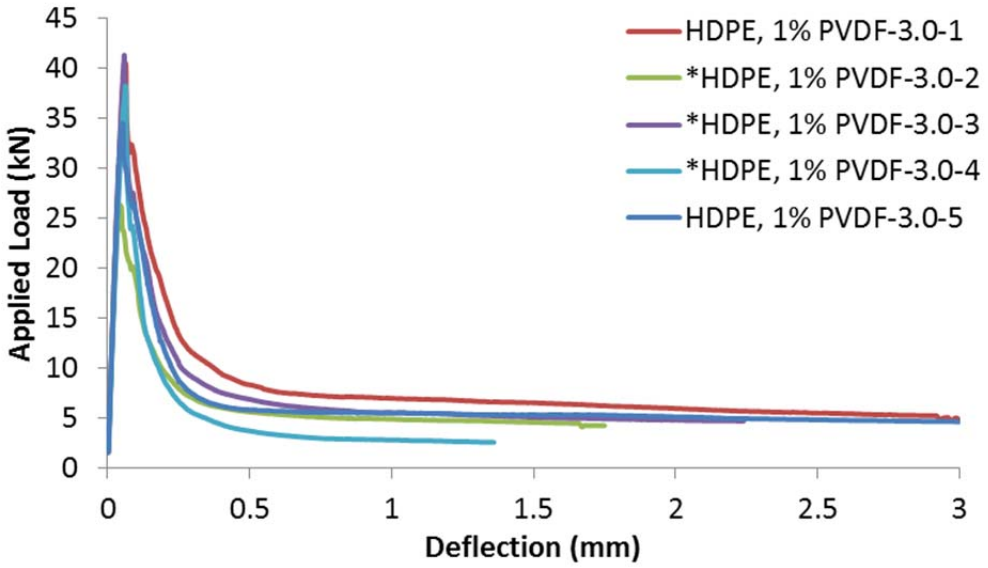

Figure 5.35 - Applied load vs. deflection curve for individual ASTM C 1609 samples for the prototype fiber containing HDPE and 1% PVDF

Figure 5.36 illustrates the effect of PVDF addition on FRC flexural toughness normalized with respect to fiber d_{eq}. No significant effect was observable with increased PVDF content. This is not consistent with results of pullout testing, which indicated that as PVDF content increased, interfacial bond strength increased as well. This is attributed to the number of fibers in each mixture, shown in Table 3.1. The density of PVDF is almost twice that of HDPE, (1.78 g/cm^3 and 0.96 g/cm^3, respectively). Because fibers were added based on weight, (3 kg/m^3 of concrete), the denser fibers resulted in less fibers in the FRC mixtures. For example, the FRC mix containing the 11% PVDF prototype fiber

had 25% less fibers than the FRC mix containing the 1% PVDF fiber. Because these fibers exhibited similar results with fewer fibers, it can be concluded that the addition of PVDF to prototype fibers does improve flexural toughness in FRC mixtures on an individual fiber basis. Figure 5.37 illustrates this effect by presenting the ASTM C1609 toughness results normalized with respect to the number of fibers in a 3 kg mixture. A trend of increasing toughness with increasing PVDF content is observable. To account for this effect, fibers should be dosed based on volumes if these prototype fibers were sold commercially.

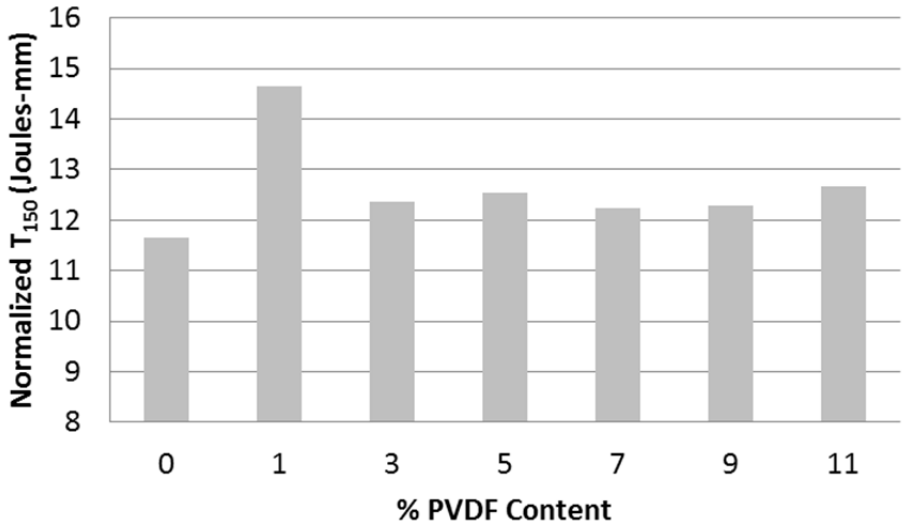

Figure 5.36 - ASTM C1609 toughness normalized with respect to equivalent diameter vs. PVDF content

Table 5.20 - Number of fibers in FRC mixtures resulting from gradual addition of PVDF to prototype fibers

Fiber Description	Density (g/cm3)	Volume of fibers in 3 kg (mm3*10^6)	Volume per single fiber (mm3)	Number of Fibers in 3 kg (*10^3)
100 % HDPE (5906)	0.96	3.13	16.64	188

HDPE, 1% PVDF	0.97	3.10	17.94	173
HDPE, 3% PVDF	0.98	3.05	17.05	179
HDPE, 5% PVDF, 10% MAH	1.00	3.00	17.26	174
HDPE, 7% PVDF, 10% MAH	1.02	2.95	16.85	175
HDPE, 9% PVDF, 10% MAH	1.03	2.91	18.30	159
HDPE, 11% PVDF, 20% MAH	1.05	2.86	20.50	140

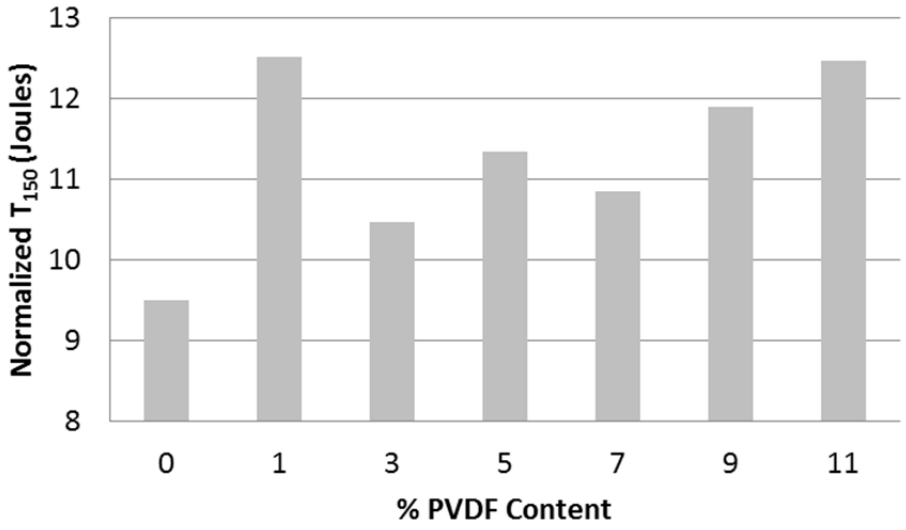

Figure 5.37 - ASTM C1609 toughness normalized with respect to number of fibers vs. PVDF content

ASTM C1399 Residual Strength Results

The residual strength index results from ASTM C1399 testing are shown in Table 5.21. Complete tables of the individual test results for ASTM C1399 testing are included in Appendix E. Curves of stress vs. deflection were plotted for each sample. The average curves are presented in

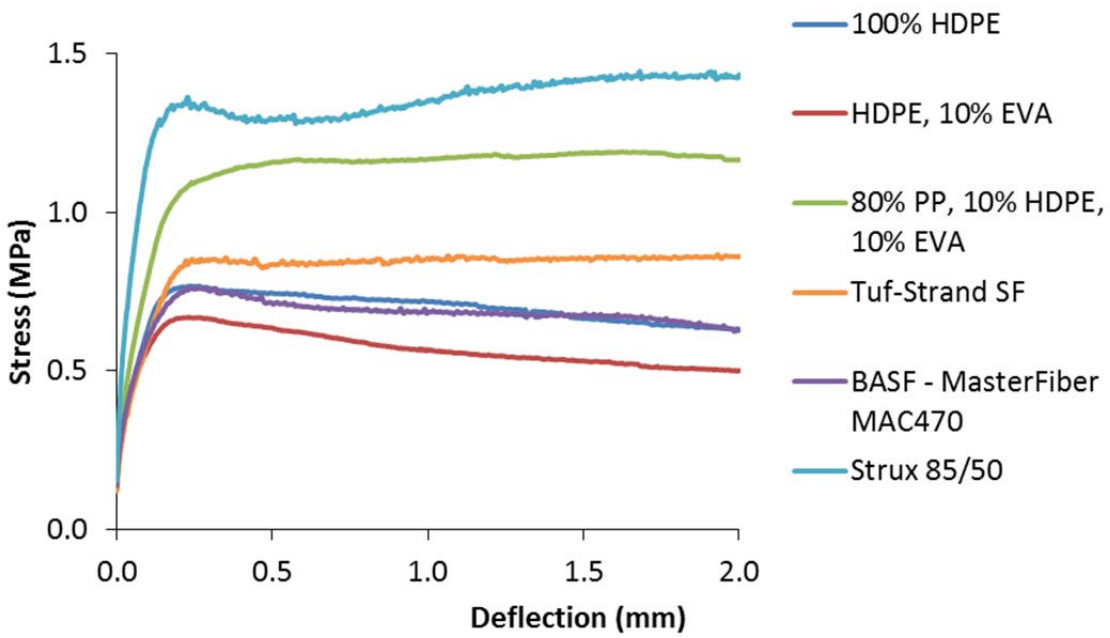

Figure 5.38 and Figure 5.39. Complete curves resulting from the individual ASTM C1399 testing are included in Appendix E.

Table 5.21 - Residual strength index results from ASTM C1399 testing

Fiber	RSI (MPa)
100% HDPE	0.72
HDPE, 1% PVDF	0.94
HDPE, 3% PVDF	0.82
HDPE, 5% PVDF, 10% MAH	0.84
HDPE, 7% PVDF, 10% MAH	0.54
HDPE, 9% PVDF, 10% MAH	0.83
HDPE, 11% PVDF, 20% MAH	0.71

HDPE, 10% EVA	0.59
80% PP, 10% HDPE, 10% EVA	1.17
Tuf-Strand SF	0.85
BASF - MasterFiber MAC470	0.69
Strux 85/50	1.34

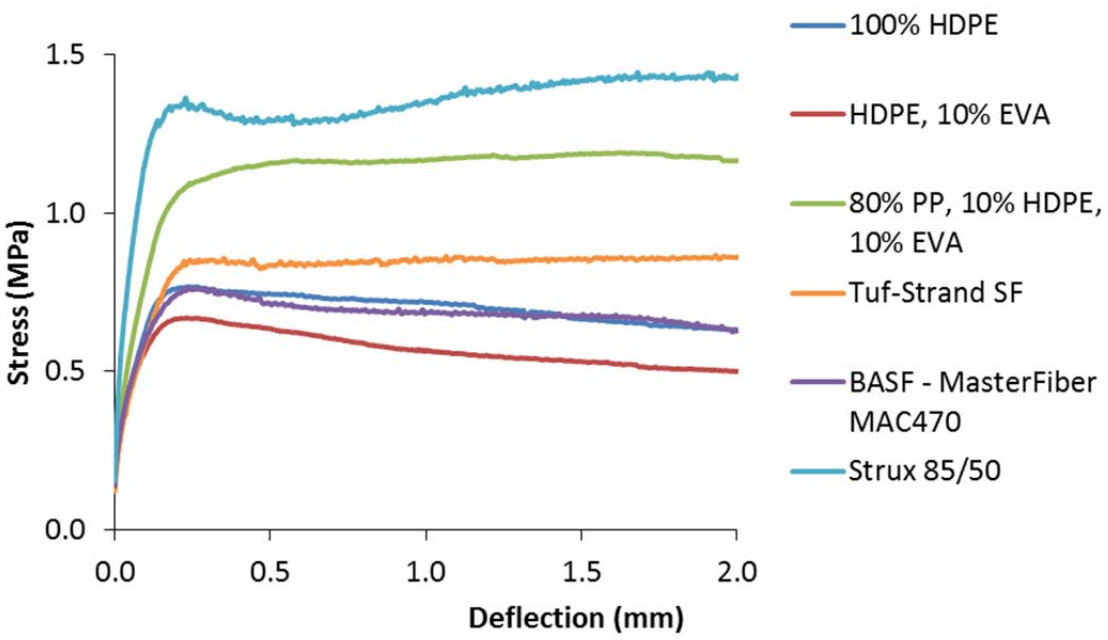

Figure 5.38 - Stress vs. deflection curves from ASTM C1399 testing for commercial fibers and some prototype fibers

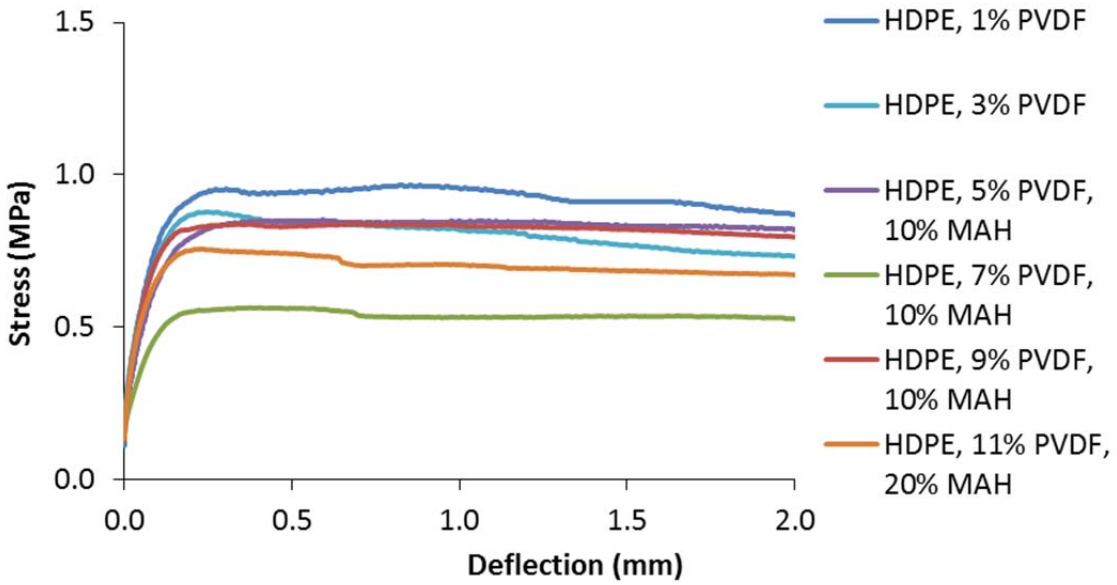

Figure 5.39 - Stress vs. deflection curves from ASTM C1399 testing for prototype fibers containing PVDF

The results presented for ASTM C1399 testing show that the FRC mixtures with the largest RSI values are Strux 85/50, and the prototype fiber containing PP, 10% HDPE and 10% EVA. These results were consistent with the results of ASTM C1609 testing. However the remaining results for ASTM C1399 testing were inconsistent with the ASTM C1609 testing results.

ASTM C1399 testing was conducted as a means of supporting the ASTM C1609 testing results. As described in ASTM 1399-10, in molded specimens, this test is not recommended for use with relatively rigid or stiff fibers measuring 40 mm or greater in length. This is because casting processes in molded beams can cause unrepresentative fiber alignment along the walls of the mold (ASTM International, 2010). The fibers used in this testing were all relatively stiff 50 mm length macrofibers cast into molds, thus exacerbating unrealistic fiber alignments along mold walls. This likely produced unrepresentative results in residual strength testing.

ASTM C1550 Results of Flexural Toughness Using Round Panels

The peak load and energy results of ASTM C1550 testing are presented in Table 5.22. Complete tables of the individual test results for ASTM C1550 testing are included in Appendix F. Curves of applied load vs. center deflection were plotted for each sample. The average curves are presented in Figure 5.40 and Figure 5.41. Complete curves resulting from the individual ASTM C1550 testing are included in Appendix F. Toughness values for ASTM C1609 testing and energy values for ASTM C1550 testing had a correlation value of 0.914.

Table 5.22 - Results of ASTM C1550 testing

Fiber	Thickness (mm)	Peak Load (kN)	Corrected Energy at 40 mm Center Deflection (J)	Number of Radial Cracks
100% HDPE	84.3	39.6	150	3
HDPE, 1% PVDF	82.7	35.8	160	3
HDPE, 3% PVDF	77.7	31.4	146	3
HDPE, 5% PVDF, 10% MAH	83.7	35.7	173	3
HDPE, 9% PVDF, 10% MAH	83.3	33.8	168	3
HDPE, 11% PVDF, 20% MAH	81.0	32.7	172	3
HDPE, 10% EVA	78.3	33.0	142	3
80% PP, 10% HDPE, 10% EVA	81.7	33.9	244	2
Tuf-Strand SF	78.3	28.0	281	3
BASF - MasterFiber MAC470	84.0	30.8	149	3
Strux 85/50	81.7	30.5	215	3

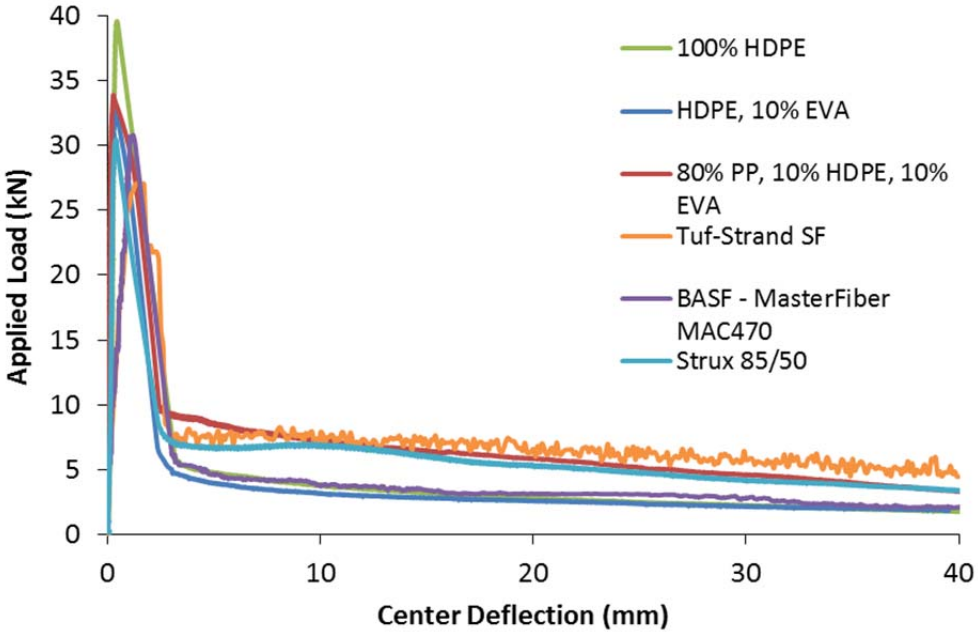

Figure 5.40 - Applied load vs. center deflection curves from ASTM C1550 testing for commercial fibers and some prototype fibers

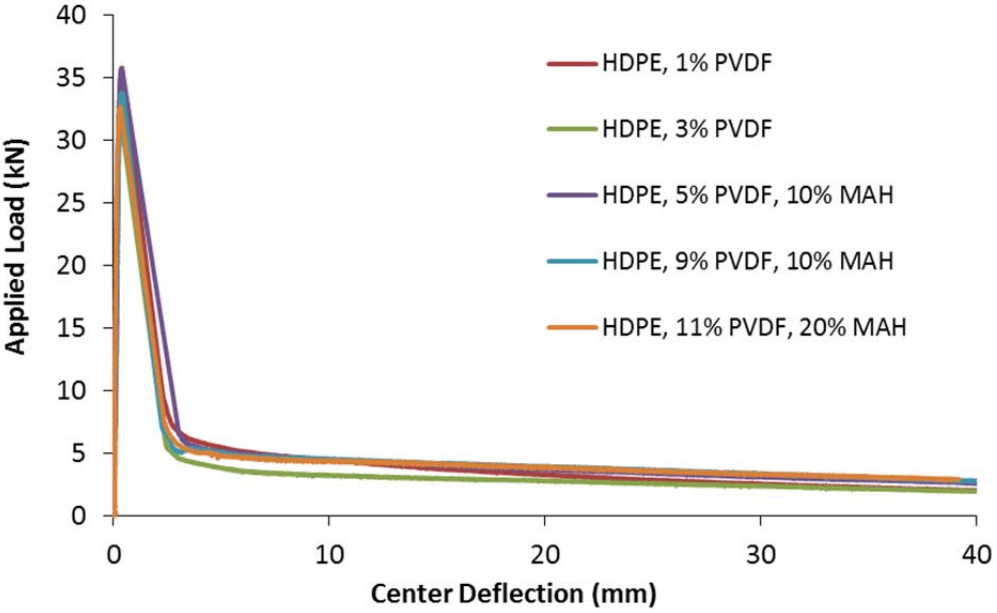

Figure 5.41 - Applied load vs. center deflection curves from ASTM C1550 testing for prototype fibers containing PVDF

During testing, the FRC mixture for the prototype fiber containing HDPE, 7% PVDF and 10% MAH experienced unstable failure and critical data was missed. This unstable failure was due to poor control of the testing apparatus speed by the test operator. Therefore, the ASTM C1550 test results for this mixture could not be included.

The results presented for ASTM C1550 testing show that the FRC mixtures with the largest energy values used Tuf-Strand SF, the prototype fiber containing PP, 10% HDPE and 10% EVA, and Strux 85/50. These were the three fibers that demonstrated fibrillation during FRC mixing, and so had increased mechanical anchorage and therefore increased pullout resistance. These results were consistent with ASTM C1609 results. The other prototype fibers were all found to have very similar values of toughness. No single material, such as EVA or PVDF additions, significantly improved the energy absorbed during ASTM C1550 testing. This indicated that some form of mechanical anchorage is important for improving FRC toughness, and can outperform fibers having superior interfacial shear strength alone.

Figure 5.42 illustrates the effect of PVDF addition on FRC flexural toughness normalized with respect to fiber equivalent diameter. Similar to ASTM C1609 test results, no significant effect was observable with increased PVDF content. This is again attributed to the number of fibers in each mixture. The increased fiber density with increased PVDF addition resulted in less fibers in the FRC mixtures when dosed by weight. As found with ASTM C1609 testing, the FRC mixtures containing fibers with increased PVDF contents exhibited similar results with fewer fibers. Figure 5.43 illustrates this effect by presenting the corrected energy results normalized with respect to the number of fibers in a 3 kg mixture. A trend of increasing energy absorption with increasing PVDF content is observable. Therefore, it can be concluded that the addition of PVDF to prototype fibers does improve flexural toughness in FRC mixtures on an individual fiber basis. This is consistent with the results demonstrated during pullout testing.

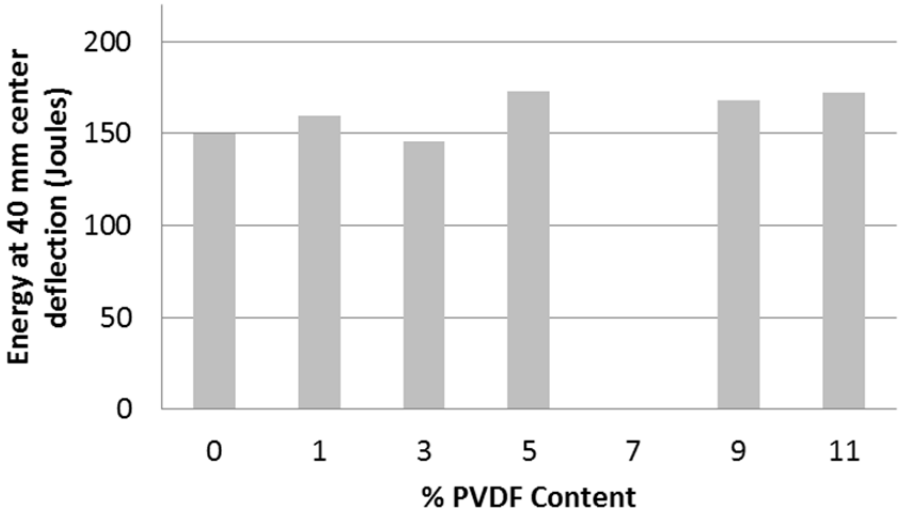

Figure 5.42 - Energy at 40 mm center deflection vs. PVDF content for ASTM C1550 testing

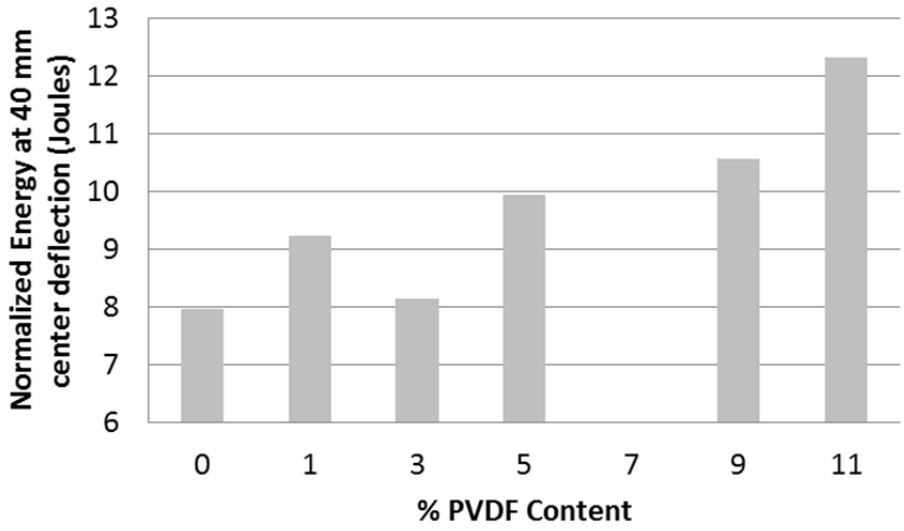

Figure 5.43 - Energy at 40 mm center deflection normalized with respect to number of fibers vs. PVDF content for ASTM C1550 testing

5.4 TENSILE CREEP RESULTS

The results of filaments undergoing tensile creep were compiled using plots of creep strain vs. elapsed time. Figure 5.44 illustrates the resulting graph for Tuf-Strand SF samples. The complete plots for each fiber type tested in tensile creep are included in Appendix G. The data used for this analysis spanned up to 104 elapsed days of sustained load.

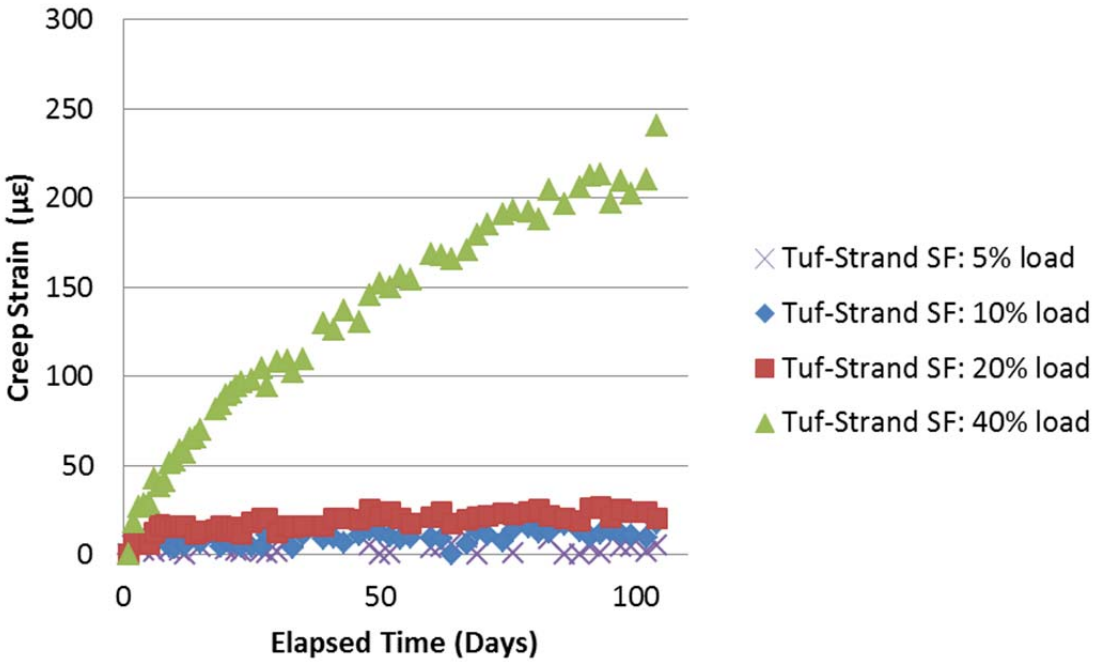

Figure 5.44 - Creep Strain vs. Elapsed time results for Tuf-Strand SF samples

Several fibers ruptured during tensile creep testing. Table 5.23 presents the elapsed time at which rupture occurred for each sample. As the fibers ruptured it was evident that the fibers broke above the location of the knot, as shown in Figure 5.45. Therefore, the fibers did not break due to local stresses formed at the knot location. This indicates the test method was successful at distributing the load throughout the length of the fiber.

Table 5.23 - Time at which samples experienced creep rupture

Fiber Description	5% load	10% load	20% load	40% load
100 % HDPE (Thick)	-	-	14 days	1 day
100 % HDPE	-	-	-	2 days
HDPE, 1% PVDF	-	-	-	1 day
HDPE, 3% PVDF	-	-	-	1 day
HDPE, 11% PVDF, 20% MAH	-	-	-	1 day
100% PVDF	-	-	-	-
HDPE, 10% EVA	-	-	79 days	5 days
80% PP, 10% HDPE, 10% EVA	-	-	-	-
Tuf-Strand SF	-	-	-	-
100% HDPE 5906 (Micro)	-	-	10 days	1 day
HDPE (5906), 10% PVDF, 20% MAH (Micro)	-	-	7 days	1 day
HDPE, 10% EVA (Micro)	-	-	31 days	1 day

Figure 5.45 - Ruptured filament and weight

From the resulting creep strain plots it can be seen that the fiber with the least creep strain of the samples was 100% PVDF. Fibers containing PP or PVDF as the primary material were the only samples that did not rupture at 40% load. The fibers containing HDPE as the primary material experienced significant creep at low loads, and ruptured at loads above 20%, indicating that HDPE behaves poorly under sustained tensile loads. Based on pullout results, the HDPE based fibers reach maximum pullout loads at less than 10 mm slip for both aligned and inclined pullout. Also, the pullout efficiency of these fibers is typically between 20% and 40%. Therefore these fibers could be expected to reach maximum pullout loads if sustained structural loading at typical crack openings is expected. This is the most significant finding from this creep testing, because the development of a new fiber had been heading towards HDPE as the primary material, due to its high strength and cost effectiveness. Due to the materials poor performance in creep testing, the fiber materials may be reconsidered if sustained structural loads are expected.

The results of the creep testing imply there is a threshold for loads that can be sustained. Of the twelve fibers tested, all but three ruptured under the 40% load, and half (six) of the samples ruptured under the 20% load. All but two of the samples that ruptured did so within the first two weeks. For the HDPE based samples, the shapes of the curves were primarily linear until rupture. Several of the curves appeared to be bilinear, with the initial steep curve transitioning to a lesser slope, which indicated a lower creep rate. Figure 5.46 displays the clearest example of this behavior. This behavior only occurred under higher loads, and therefore was only observed for the PP and PVDF samples. The percent elongation at which this transition occurred varied between samples and applied loads, and tended to occur within the first two weeks. This suggests that materials that do not rupture within the first two weeks have the potential to sustain long term loads. However this data only considered the first 104 days of testing. Longer term sampling would provide further insight into long-term creep performance.

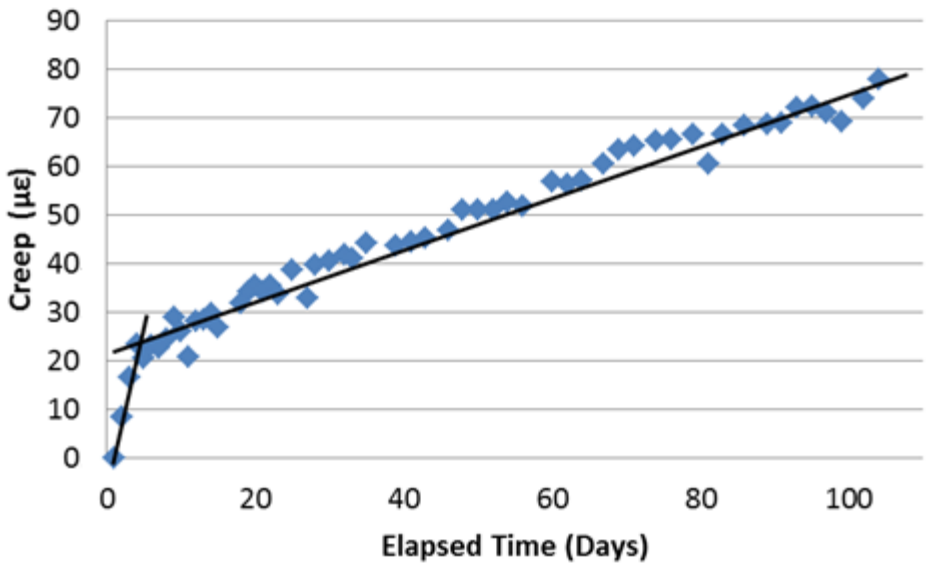

Figure 5.46 - 80% PP, 10% HDPE, 10% EVA prototype fiber displaying bilinear behavior under 40% load

For fibers undergoing very small creep strains, the accuracy of the measurements became a concern. One source of error resulted from the inconsistent surface of the concrete floor that the laser dolly moved across. This affected the level of the laser during some measurements. Also, for some fibers the weights spun slightly such that the reflective tape no longer faced the laser extensometer. This was particularly a problem for the microfibers which, because of the elliptical cross section, did not lay flat over the circular steel section they were hung from. This resulted in slight inaccuracies due to the variations in tape distance from the laser. While these slight inaccuracies were not problematic for samples with large strains, they became noticeable in the remaining samples. For example the 100% PVDF sample at 5% load did not stretch more than 0.35 mm over the 104 days of sampling, as illustrated in Figure 5.47. Because the laser extensometer can only be read visually up to 0.01 mm, the change between daily measurements was difficult to detect.

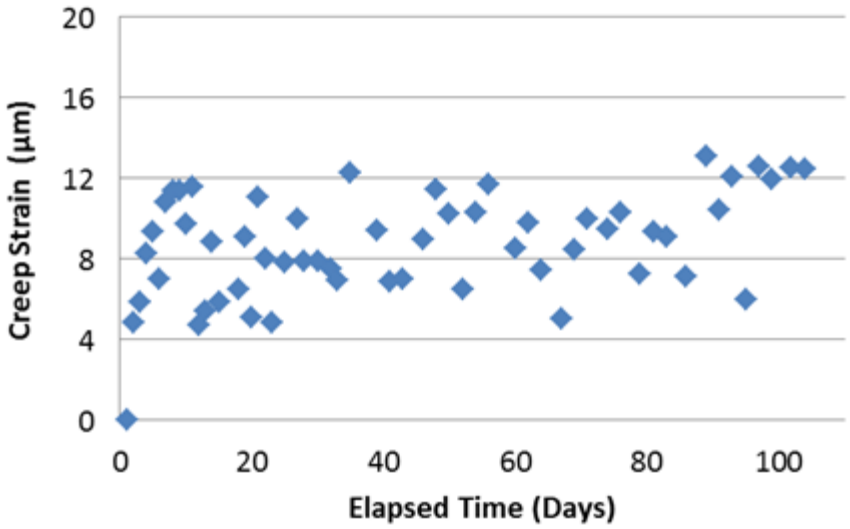

Figure 5.47 - Creep Strain vs. Elapsed Time data for 100% PVDF fiber, under 5% load

5.5 SUMMARY OF RESULTS

The following section outlines the findings resulting from this research. Table 5.24 and Table 5.25 present a summary of selected results for macrofibers and microfibers of interest.

Table 5.24 - Summary of Results for tests using macrofibers of interest

	100% HDPE	HDPE, 11% PVDF, 20% MAH	100 % PVDF	HDPE, 10% EVA	80% PP, 10% HDPE, 10% EVA	Tuf-Strand SF
Width (mm)	1.39	1.51	1.76	1.55	1.31	1.05
Thickness (mm)	0.25	0.29	0.47	0.29	0.25	0.34
σ_f (MPa)	673	559	527	595	718	646
E_f (GPa)	6.13	5.79	3.44	5.67	10.93	9.53
d_{eq} (mm)	0.65	0.73	1.00	0.74	0.63	0.65
Pullout Mechanism	Slip Hardening	Constant Friction	Slip Hardening	Constant Friction	Slip Hardening	Slip Hardening
η_τ	24.0%	39.3%	17.8%	22.1%	20.4%	16.1%
U_P at 10mm slip (N-mm)	338	660	438	336	270	218
τ_{max} (MPa)	0.83	1.4	0.89	0.8	0.73	0.61
***l*c (mm)**	102	50	135	110	119	147
f	0.3	0.23	-	0.39	0.51	0.31
$\hat{f}$	2.45	0.88	-	2.76	-	-
Fibrillation Evident?	No	No	-	Yes	Yes	Yes
C1609 f_p, (MPa)	4.94	4.54	-	4.77	5.01	4.45
C 1609 T_{150}^{150} (J)	17.88	17.41	-	17.06	25.92	28.87
C1550 Energy (J)	150	172	-	142	244	215

Table 5.25 - Summary Results for tests using microfibers of interest

	HDPE (5906)	HDPE (1288)	HDPE (5906), 10% EVA	HDPE (5906), 10% PVDF, 20% MAH	PVA
Width (mm)	0.29	0.19	0.25	0.25	0.12
Thickness (mm)	0.28	0.2	0.26	0.25	0.12
σ_f (MPa)	1391	1842	1448	1420	2092
E_f (GPa)	15.93	28.47	19.75	18.93	28.66
d_{eq} (mm)	0.29	0.19	0.25	0.25	0.12
Pullout Mechanism	Constant Friction	Constant Friction	Constant Friction	Constant Friction	Slip Hardening
η_τ	28.5%	29.9%	49.6%	40.0%	65.7%
U_P at 3.5 mm slip (N-mm)	39	30	44	53	14
τ_{max} (MPa)	0.94	1.14	1.63	1.34	2.11
***l*c (mm)**	55	53	32	40	25
f	-	-	0.28	0.46	-
$\hat{f}$	-	-	4.09	0.28	-

The following sections outline findings for the main tests in the research program.

5.5.1 Tensile Testing Summary

Comparisons of different synthetic material combinations and manufacturing settings on fiber tensile properties were made throughout Section 5.1, “Tensile Strength and Modulus of Elasticity Results”. The following results were found:

- EVA may be successfully used as an additive to HDPE without causing significant decreases to tensile strength or elastic modulus.
- Tensile properties of prototype microfibers were found to be commercially viable, as the production method is much less costly than that of the commercial microfibers compared. Based on trends observed, tensile strengths equivalent to commercial fibers are attainable with smaller cross sections.
- An addition of less than 10% PVDF to HDPE did not cause a loss in tensile strength or elastic modulus. However an addition of over 10% PVDF required up to 20% MAH to properly blend with HDPE, thus reducing tensile strength.
- An increase in stretch ratio was shown to increase tensile strength and elastic modulus for both micro and macrofibers. This was attributed to the increased molecular alignment associated with increasing stretch ratios. The impact of stretch ratio on these properties varied with each material.
- For both micro and macrofibers, a change in stretch ratio had a greater effect on elastic modulus than on tensile strength.
- A decrease in equivalent diameter was shown to increase tensile strength and elastic modulus of synthetic fibers. This was attributed to a smaller fiber diameter, which allowed heat to reach the fiber core more effectively during stretching.
- The most effective fibers may be produced by maximizing stretch ratio whilst controlling fiber dimensions using spinneret die head designs and pump speeds.
- The average standard deviation was 65 MPa for maximum tensile strength and 0.9 GPa for fiber elastic modulus, indicating an acceptable level of consistency for tensile testing results and consistency of manufacturing methods.

5.5.2 Fiber Bond and Pullout Testing Summary

Comparisons of the interfacial bond properties of several synthetic prototype micro and macrofibers, as well as several commercially available synthetic fibers, were made

throughout Section 5.2 based on results of single fiber pullout tests. The following results were found:

- Commercially available nylon fibers exhibited very poor fiber-matrix bond strength.
- Chemical bond energy and slip hardening parameters could not be quantified using methods described in previous literature, as these methods applied specifically to PVA microfibers and were not applicable to other synthetic fibers.
- Pullout curve shapes were used to identify fibers as demonstrating slip hardening, slip softening, or constant friction mechanisms during pullout. Prototype fibers exhibited primarily slip hardening and constant friction mechanisms.
- Pullout energy and interfacial shear strength were the most useful parameters to quantify fiber-matrix bond performance, as they accounted for factors such as fiber rupture.
- The macrofibers that demonstrated the highest interfacial bond strength were the prototype fibers with high PVDF contents. This was attributed to the increased chemical bond strength, in addition to fiber roughness.
- The macrofiber that demonstrated the lowest interfacial bond strength was Tuf-Strand SF. Fibers that fibrillated did not exhibit interfacial shear resistance in pullout testing, which would otherwise be exhibited in FRC performance testing, due to the absence of fibrillation in pullout testing specimens.
- The gradual addition of PVDF to HDPE was shown to increase the fiber-matrix bond for both micro and macrofibers.
- The 100% PVDF macrofiber did not demonstrate greater pullout resistance than most HDPE/PVDF blends. Visual inspection of fibers under magnification indicated this was due to increased surface roughness with HDPE/PVDF blends compared to the smooth 100% PVDF fiber, due to incompatibility of the two materials.

- The addition of EVA did not produce an improvement in interfacial bond strength of HDPE for macrofibers. However, it did provide some improvement with microfiber pullout testing.
- The majority of PVA microfibers fibers ruptured during pullout testing.
- Using interfacial shear strength, a critical fiber length was predicted for fibers. The critical fiber length was 50 mm or greater for macrofibers, and 25 mm or greater for microfibers. These lengths were above the typical length of commercial fibers for each.
- Snubbing friction coefficients were calculated using results of inclined fiber pullout testing, and were used to predict peak pullout loads for fibers at any angle. The predicted loads correlated well with experimental data, although less so for microfibers than for macrofibers, due to the low rupture loads of microfibers.
- Microfibers had higher snubbing coefficients than macrofibers. This is due to the smaller cross sections of microfibers, which resulted in decreased bending resistance.
- Apparent fiber strength reduction factors were calculated for fibers experiencing rupture during pullout. Results indicated fibers containing PVDF had low apparent fiber strength reduction factors. Further sampling is necessary to properly quantify this factor.

5.5.3 FRC Performance Testing Summary

Several synthetic prototype and commercially available macrofibers were tested in FRC mixtures, and their performance was compared throughout Section 5.3. The following results were found:

- Washout samples indicated fibrillation occurred in four of the twelve fibers tested in FRC. This was expected with the PP/HDPE blended fibers; however, the

fiber containing HDPE and 10% EVA also showed fiber splitting, but this did not result in a performance improvement.

- Slump, density and compressive strength testing was all within targeted range, indicating consistency between concrete mixes.
- ASTM C1609 test results indicated that the fibers that result in the greatest toughness, (energy absorption), were those that had forms of mechanical anchorage such as fibrillation or embossment. These fibers had superior FRC performance, despite performing poorly in pullout testing. These results were consistent with those of the ASTM C1550 testing.
- Fibers without an additional form of mechanical anchorage did not show significant variation in FRC performance results. The fiber containing HDPE and 10% EVA did not show improved performance over 100% HDPE for both ASTM C1609 and ASTM C1550 testing.
- The addition of PVDF to HDPE did not provide an improvement to FRC performance results, despite the improvement in bond strength observed in pullout testing. This was attributed to increased densities with increasing PVDF content, which resulted in fewer fibers in each mixture, as they were dosed by weight.
- The standard deviation of ASTM C1609 toughness results ranged from 0.4-3.8 Joules, with an average of 2.1 Joules, indicating acceptable repeatability of results.
- From the ASTM C1399 test results it was concluded that fiber alignment occurred along the walls of the mold during testing causing unrepresentative results. This is known to occur with molded ASTM C1399 specimens using relatively stiff or rigid fibers 40 mm or longer. As a result, the results of the ASTM C1399 testing did not correlate with the ASTM C1609 testing nor the ASTM C1550 testing.

5.5.4 Tensile Creep Testing Summary

Several synthetic prototype micro and macrofibers, as well as the commercially available synthetic fiber Tuf-Strand SF, were tested for creep under sustained tensile loads for 104 days. Comparisons of the fiber resistance to tensile creep were made throughout Section 5.4. The following results were found:

- 104 elapsed days of creep data showed that the fiber containing 100% PVDF performed well under sustained creep loading and experienced the least creep strain of the fibers tested. HDPE based fibers performed poorly, with larger creep strain.
- The tensile creep testing results indicated that a threshold exists beyond which loads cannot be sustained. The majority of fibers experiencing rupture did so under sustained loads of 40% of the maximum tensile strength, usually within the first two weeks of testing. Beyond this point there was a tendency for creep strain to stabilize.

The following chapter outlines the overall general conclusions of this research and recommendations for future work, including a prototype macrofiber design proposal.

CHAPTER 6 CONCLUSION

A research program was executed to characterize the behavior of prototype synthetic fibers in pullout testing, as well as FRC performance testing. The objective of this research was to develop a novel, competitively priced, high strength and high stiffness macrosynthetic fiber for concrete. Additionally, properties of synthetic microfibers were also investigated. Improvements to fiber properties were examined through tensile testing, flexural FRC testing, and creep testing. The mechanical properties of bond by synthetic fibers to the cementitious matrix were examined through pullout testing. Practical considerations were also made, such as manufacturing processes, costs, and workability in concrete. Recommendations for future research, including modifications to the testing program and a prototype design, are discussed in the following section.

6.1 RECOMMENDATIONS

6.1.1 Testing Program Modifications

Based on the results of the testing program, further modifications are recommended for the experimental apparatus, as well as the fibers themselves.

Pullout Testing

Results of the testing program showed that fibrillated fibers had the highest performance in FRC testing, but low performance in pullout testing. This was because fibrillation did not occur in the filament samples used in pullout testing. It is recommend that a method simulating the roughening that fibers would undergo in concrete mixing be incorporated into pullout testing. This would result in pullout testing more accurately representing fiber behavior in a concrete mixture. In addition, embossed fibers should also be tested in pullout to verify the findings of the FRC testing: that mechanical anchorage outperforms adhesional bond strength for synthetic macrofibers due to increased pullout resistance.

Adjustments should also be made to inclined pullout testing. In order to more accurately investigate apparent fiber strength reductions, 0 degrees fiber ruptures are necessary. This could be achieved using samples cast at embedment lengths greater than the critical embedment lengths calculated in Section 5.2.1.

Performance Testing

It is recommended that FRC performance testing be completed on macrofibers of interest by dosing fibers based on volume percentage instead of weight. This would allow a more effective comparison of differing fiber materials due to the differences in fiber density. Macrofibers should also be tested in a "ready-mix" concrete plant setting to accurately represent the field conditions FRC would be used in. It is also recommended that performance testing of microfibers in ECC mixes be tested to further characterize their performance.

Tensile Creep Testing

Tensile creep should testing be continued to verify the conclusions drawn from 104 days of creep data. Regarding additional creep testing, variations should be made to the sustained loads, as it was found that the majority of fibers could not sustain 40% of their critical tensile strength for longer than two weeks. A finer gradation of load should be applied to fibers of interest to more thoroughly characterize fiber creep behavior. In addition, when a fiber type is selected for commercial distribution, creep testing on FRC samples is recommended to fully characterize fiber performance.

6.1.2 Additional Recommendations

While EVA as an additive to HDPE based macrofibers did not readily show an increase in interfacial bond strength, this could be attributed to the contents of the EVA resin used. The primary resin contents are low grade polyethylene. Pure EVA can be purchased in powder form. Pullout testing using HDPE fibers that are heated and dipped in this

powder is recommended to indicate if this would increase interfacial bond strength. If so, this process could be incorporated into the melt extrusion line. There is continued interest in EVA as a chemical bond strengthening additive due to its low material cost and the recognized bond between pure EVA and a cement matrix (MacDonald, 2010).

Tensile testing results showed that higher fiber tensile properties result from a decrease in equivalent diameter and an increase in stretch ratio. Therefore, fiber dimensions should be controlled using the spinneret die head and varying pump speeds, while stretch ratio is maximized without fiber rupture. In addition to this, die head design can be used to manipulate fiber cross sections to achieve increased interfacial bond. Varying the fiber cross section to increase available fiber surface area could increase adhesional bond for some fiber types. Therefore more research is recommended on spinneret die head design to potentially increase both tensile and bond strength.

Blended cements containing one or more mineral admixtures are common, and have the potential to impact the quality and composition of the ITZ. Since any fiber developed in this program could potentially be used in conjunction with one or more of these materials, it is important that their impact be considered in future research. Specifically, fibers containing EVA or PVDF as an additive should be tested in pullout using mortar mixtures containing combinations of fly ash, blast furnace slag or silica fume to determine if similar performance would be achieved based on the differing chemical reactions with these materials.

6.1.3 Prototype Macrofiber Design Proposal

The objective of this research was to develop a competitively priced, high strength and synthetic macrofiber for concrete. Therefore the conclusions drawn from this research were applied to propose the design of a prototype synthetic macrofiber for commercial production.

Fiber pullout testing results indicated that the prototype fiber containing HDPE, 11% PVDF and 20% MAH demonstrated the greatest resistance to pullout under the testing conditions used. This prototype fiber also had a low apparent fiber strength reduction factor, suggesting the fiber may sustain inclined pullout loads successfully. However, because this fiber is for commercial production, cost is a primary concern. As shown in Table 6.1, the material cost of PVDF is significantly larger than the other materials considered. The result is that the prototype fibers containing HDPE, 11% PVDF and 20% MAH has a raw material cost of $5.20/kg. This is a high cost when compared with that of Tuf-Strand SF; $2.80/kg. Due to this, a prototype fiber containing HDPE, 5% PVDF and 10% MAH is proposed, as it has an acceptable material cost of $3.41/kg and also demonstrated sufficient bond strength during pullout testing.

Table 6.1 - Cost for synthetic fiber materials

Material	Approximate Cost (US$/kg)
HDPE	2.00
PP	3.00
PVDF	32.00
MAH	1.50
EVA	1.80

The next major consideration in the design of a prototype fiber was tensile strength. A target tensile strength of 730 MPa was selected, as it is an increase over the tensile strength of Tuf-Strand SF; approximately 650 MPa. Using the trends found during tensile testing and the trend line equation from Figure 5.12, an equivalent diameter of 0.44 mm is recommended to achieve the target tensile strength.

In order to minimize balling and workability issues in fresh concrete, the fiber aspect ratio was limited to 100. To maintain this aspect ratio and the target equivalent

diameter, fiber length is limited to 44 mm. Fibers are typically cut to 5 mm increments, therefore a fiber length of 40 mm is recommended. This provides a fiber aspect ratio of 90, and also results in more efficient ratio of fibers produced to material used. The critical fiber length for the prototype fiber containing HDPE, 5% PVDF and 10% MAH was 90 mm. The proposed production fiber has a smaller equivalent diameter than the prototype tested, and therefore would be expected to have a critical fiber length above 90 mm. Therefore a fiber length of 40 mm was acceptable.

The next consideration was fiber cross section. Using a change in the di head design, a flatter fiber cross section can be achieved, as shown in Figure 6.1. By decreasing the thickness but maintaining a similar fiber width, a larger equivalent diameter would be achieved, while maintaining a similar surface area for interfacial bond. A target width of 1.1 mm is recommended, as this is the typical width of a Tuf-Strand SF fiber. Using this width and maintaining the equivalent diameter, a target thickness of 0.14 mm was determined according to Equation 6-1. During the extrusion process, the proposed fiber should be stretched as much as possible before rupture, and the gear pump and screw speed should be adjusted to target the recommended fiber dimensions.

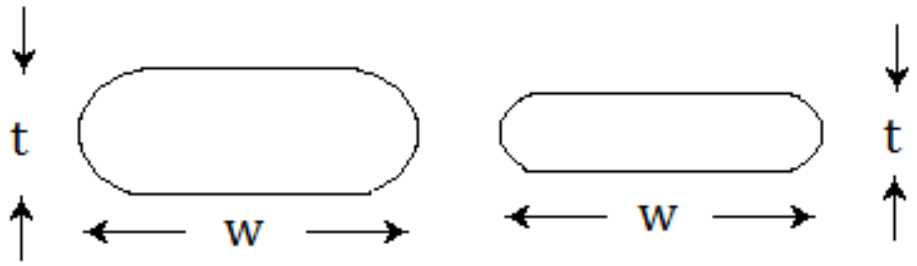

Figure 6.1 - Recommended change in cross section using a new di head design

$$d_{eq} = \frac{2\sqrt{(w-t)t + \pi(\frac{t}{2})^2}}{\pi} \quad \text{6-1}$$

Where,

d_{eq} = Equivalent fiber diameter (mm)

w = Fiber width (mm)

t = Fiber thickness (mm)

The toughness per fiber for both Tuf-Strand SF and the prototype fiber containing HDPE, 5% PVDF and 10% MAH were determined using the results of FRC performance testing and normalizing with respect to fiber cross sectional area. Given the smaller cross section and fiber length, a greater number of fibers would be contained in a 3 kg/m^3 fiber dosage in FRC, providing an equivalent cost per performance to Tuf-Strand SF. Table 6.2 shows a comparison between Tuf-Strand SF and the proposed prototype fiber.

Table 6.2 - Cost per performance comparison for Tuf-Strand SF and the proposed prototype fiber

Property	Tuf-Strand SF	Proposed Prototype: HDPE, 5% PVDF, 10% MAH
Material cost	$2.80/kg	$3.41/kg
Toughness per fiber	0.147 J	0.072 J
Number of fibers in 3 kg	196	491
Predicted performance per kg	9.63 J	11.74 J
Cost per performance	$2.91	$2.91

While Tuf-Strand SF had the largest critical fiber length of the macrofibers, the fibrillating nature of this fiber increased the fiber surface area and consequently increased the required paste content to fully coat the fiber. A fiber that does not fibrillate but still demonstrates high bond strength, such as the proposed prototype, could require less paste content and thus be more efficient in FRC. The performance of Tuf-Strand SF is sensitive to fibrillation occurring and therefore requires proper mixing. The proposed prototype would be less sensitive to changes in mix time, and therefore could have more consistent field performance results than Tuf-Strand SF.

The results of FRC performance testing indicated that the fibers with the highest performance were those having a means of mechanical anchorage, such as embossment or fibrillation. Therefore it is recommended that twisting be applied to the proposed prototype, as this production method is already in place in the AFT plant, where this prototype would be extruded. While fiber twisting is normally used as a method of ensuring adequate fiber dispersion without balling in fresh concrete, it is a simple method of fiber deformation that could increase mechanical anchorage within the matrix. Fiber embossment should also be tested to determine if the production cost per performance ratio is acceptable. However it should be ensured that embossment does not compromise the tensile properties of the fiber significantly.

Table 6.3 summarizes the recommendations for the design of a prototype synthetic macrofiber. With the combination of increased surface roughness and chemical bond offered by a fiber containing PVDF, as well as the possible additional mechanical anchorage caused by twisting, such a fiber could offer an alternative to Tuf-Strand SF for applications requiring increased workability, SCC mixtures, or mixtures that do not produce significant abrasion and result in little fiber fibrillation. It is recommended that this fiber be tested at varying dosages to fully characterize fiber behavior in FRC and to target a specific performance as necessary.

Table 6.3 - Summary of recommendations for prototype fiber design

Property	Target
Material content	HDPE, 5% PVDF, 10% MAH
Material cost	$2.80/kg
Tensile strength	730 MPa
Equivalent diameter	0.44 mm
Aspect ratio	90
Fiber length	40 mm
Fiber width	1.1 mm
Fiber thickness	0.14 mm
Cross section	Ribbon
Deformation	Twisting

REFERENCES

ACI Committee 318. (2008). *Building Code Requirments for Structural Concrete (ACI 318-08) and Commentary.* Famington Hills, MI: American Concrete Institute.

Altoubat, S., Yazdanbakhsh, A., & Rieder, K.-A. (2009). Shear behavior of macro-synthetic fiber-reinforced concrete beams without stirrups. *ACI Materials Journal*, 381-389.

American Concrete Institute. (2008). *ACI 544.3R-08 Guide for Specifying, Proportioning, and Production of Fiber-Reinforced Concrete.* Farmington Hills, MI: American Concrete Institute.

American Fiber Manufacturers Association . (2011, March). *Manufacturing: Synthetic and Cellulosic Fiber Formation Technology*. Retrieved March 8, 2011, from Fibersource: http://www.fibersource.com/f-tutor/techpag.htm

ASTM International. (2006). *ASTM A820-06 Standard Specification for Steel Fibers for Fiber-Reinforced Concrete.* West Conshohocken, PA: ASTM International.

ASTM International. (2006). *ASTM C136-06 Standard Specification for Air-Entraining Admixtures for Concrete.* West Conshohocken, PA: ASTM international.

ASTM International. (2006). *ASTM C136-06 Standard Test Method for Sieve Analysis of Fine and Coarse Aggregates .* West Conshohocken, PA: ASTM International.

ASTM International. (2008). *ASTM C109-08 Standard Test Method for Compressive Strength of Hydraulic Mortars (Using 2-in. or [50-mm] Cube Specimens).* West Conshohocken, PA: ASTM International.

ASTM International. (2008b). *ASTM C618-08a Standard Specification for Coal Fly Ash and Raw or Calcined Natural Pozzolan for Use in Concrete.* West Conshohocken, PA: ASTM International.

ASTM International. (2009). *ASTM C1611-09be1 Standard Test Method for Slump Flow of Self-Consolidating Concrete.* West Conshohocken, PA: ASTM International.

ASTM International. (2009). *ASTM C1621 -09b Standard Test Method for Passing Ability of Self-Consolidating Concrete by J-Ring.* West Conshohocken, PA: ASTM International.

ASTM International. (2009). *ASTM D2990-09 Standard Test Method for Tensile, Compressive, and Flexural Creep and Creep Rupture of Plastics.* West Conshohocken, PA: ASTM International.

ASTM International. (2010). *ASTM C1116-10 Standard Specification for Fiber-Reinforced Concrete.* West Conshohocken, PA: ASTM International.

ASTM International. (2010). *ASTM C1240-10 Standard Specification for Silica Fume Used in Cementitious Mixtures.* West Conshohocken, PA: ASTM International.

ASTM International. (2010). *ASTM C138-10 Standard Test Method for Density (Unit Weight), Yield, and Air Content (Gravimetric) of Concrete.* West Conshohocken, PA: ASTM International.

ASTM International. (2010). *ASTM C1399-10 Standard Test Method for Obtaining Average Residual-Strength of Fiber-Reinforced Concrete.* West Conshohocken, PA: ASTM International.

ASTM International. (2010). *ASTM C143-10 Standard Test Method for Slump of Hydraulic-Cement Concrete.* West Conshohocken, PA: ASTM International.

ASTM International. (2010). *ASTM C1550-10 Standard Test Method for Flexural Toughness of Fiber Reinforced Concrete Using Centrally Loaded Round Panel.* West Conshohocken, PA: ASTM International.

ASTM International. (2010). *ASTM C1609-10 Standard Test Method for Flexural Performance of Fiber-Reinforced Concrete (Using Beam with Third-Point Loading).* West Conshohocken, PA: ASTM International.

ASTM International. (2010). *ASTM C39-10 Standard Test Method for Compressive Strength of Cylindrical Concrete.* West Conshohocken, PA: ASTM International.

ASTM International. (2010). *ASTM C494-10 Standard Specification for Chemical Admixtures for Concrete.* West Conshohocken, PA: ASTM international.

ASTM International. (2010). *ASTM D2256-10 - Standard Test Method for Tensile Properties of Yarns by the Single-strand Method.* West Conshohocken, PA: ASTM International.

ASTM International. (2011). *ASTM C33-11 Standard Specification for Concrete Aggregates.* West Conshohocken, PA: ASTM International.

Baggot, R., & Ghandi, D. (1981). Multiple cracking in aligned polypropylene fibre reinforced cement composites. *Journal of materials Science*, 65-74.

Banholzer, B., Brameshuber, W., & Jung, W. (2006). Analytical evaluation of pull-out tests - The inverse problem. *Cement and Concrete Composites*, 564-571.

Banthia, N., & Gupta, R. (2004). Hybrid fiber reinforced concrete (HyFRC): fiber synergy in high strength matrices. *Materials and Structures, Vol. 37*, 707-716.

Banthia, N., & Mindess, S. (1995). *Fiber Reinforced Concrete Modern Developments.* Vancouver: The University of British Columbia.

Bekaert. (2005, February). Dramix RL-45-50-BN Product Data Sheet. Zwevegem, Belgium: Bekaert.

Bentur, A., & Mindess, S. (1990). *Fibre reinforced cementitious composites.* London: Elsevier Applied Science.

Bui, D. D. (2001). *Rice husk ask as a mineral admixture for high performance concrete.* Delft, Netherlands: Ph.D. Thesis, Delft University Press.

Buratti, N., Mazzotti, C., & Savoia, M. (2010). Long-term behavior of fiber-reinforced self-compacting concrete beams. In K. Khayat, & D. Feys, *Design, Production and Placement of Self-Consolidating Concrete, RILEM Bookseries 1* (pp. 439-450). Montreal: Springer.

Carette, G., Bilodeau, A., Chevrier, R., & Malhotra, V. M. (1993). Mechanical properties of concrete incorporating high volume of fly ash from sources in the U.S. *ACI Materials Journal*, 535-544.

Cochrane, J. T. (2003). *Flexural Creep Behavior of Fiber Reinforced Concrete Under High Temperatures (Thesis).* Halifax, Nova Scotia: Dalhousie University.

Costa, A., & Appleton, J. (1999). Chloride penetration into concrete in marine environment - Part 1: Main parameters affecting chloride penetration. *Materials and Structures*, 252-259.

Cunha, V., Barros, J., & Sena-Cruz, J. (2008). Bond-slip mechanisms of hooked-end steel fibers in self-compacting concrete. *Materials Science Forum*, 877-881.

Cunha, V., Barros, J., & Sena-Cruz, J. (2010). Pullout behavior of steel fibers in self-compacting concrete. *Journla of Materials in Civil Engineering*, 1-9.

Davison, R. L., Natusch, D. F., & Wallace, J. R. (1974). Trace elements in fly ash - dependence of concentration on particle size. *Environmental Science and Technology*, 1107-1113.

Detwiler, R. J., & Mehta, P. K. (1989). Chemical and physical effects of silica fume on the mechanical behavior of concrete. *ACI Material Journal 86*, 609-614.

Diamond, S., & Sahu, S. (2006). Densified silica fume: Particle size and dispersion in concrete. *Materials and Structures* , 849-859.

Dow Chemical Company. (2011). Amplify GR 205 - Functional Polymer - Melaic Anhydride. *Dow Chemical Company Product Technical Information*. Dow Chemical Company.

EFNARC. (2005, May). *The European Guidelines for Self-Compacting Concrete: Specification, Production and Use.* Retrieved March 18, 2011, from EFNARC Publications: http://www.efnarc.org/

Eren, O., & Celik, T. (1997). Effect of silica fume and steel fibers on some properties of high-strength concrete. *Construction and Building Materials, Vol. 11*, 373-382.

European Committee for Standardization. (2006). *EN 14889-2:2006 Fibres for concrete - Part 2: Polymer fibres - Definitions, specifications and conformity.* Brussels, Belgium: European Committee for Standardization.

Forgeron, D., & Omer, A. (2010). Flow characterisitics of macro-synthetic fiber-reinforced self-consolidating concrete. *Fiber Reinforced Self-Consolidating Concrete: Research and Applications* (pp. 1-14). American Concrete Institute.

Francis, J. (2005). Synthetic fibre-reinforced concrete for external applications. *Concrete*, 40-41.

Geng, Y., & Leung, C. (1996). A microstructural study of fibre/mortar interfaces during fibre depbonding and pull-out. *Journal of Materials Science*, 1285-1294.

Graybeal, B., & Davis, M. (2008). Cylinder or cube: Strength testing of 80 to 200 MPa (11.6 to 29 ksi) ultra-high-performance fiber-reinforced concrete. *ACI Materials Journal*, 603-609.

Grunewald, S., & Walraven, J. C. (2001). Parameter-study on the influence of steel fibers and coarse aggregate content on the fresh properties of self-compacting concrete. *Cement and Concrete Research 31*, 1793-1798.

Habeeb, G. A., & Faayadh, M. M. (2009). Rice husk ash concrete : the effect of RHA average particle size on mechanical properties and Drying Shrinkage. *Australian Journal of Basic and Applied Science*, 1616-1622.

Habel, K., Denarie, E., & Bruhwiler, E. (2007). Experimental investigation of composite ultra-high-performance fiber-reinforced concrete and conventional concrete

members. *ACI Structural Journal*, 93-101.

Hsie, M., Tu, C., & Song, P. S. (2008). Mechanical properties of polypropylene hybrid fiber-reinforced concrete. *Materials Science and Engineering A 494*, 153-157.

Hsu, L. S., & Hsu, C. T. (1994). Complete stress-strain behavior of high-strength concrete under compression. *Magazine of Concrete Research*, 301-312.

Hu, J., & Stroeven, P. (2004). Properties of the interfacial transition zone in model concrete. *Interface Science 12*, 389-397.

Hua, Y., & Zhou, T. (2009). Experimental study of the mechanical properties of hybrid fiber reinforced concrete. *Materials Science Forum Vols. 610-613*, 69-75.

International Organizationf for Standardization. (2009). *ISO 6892-1 :Metallic materials tensile testing part 1: method of test at room temperature.* Brussels, Belgium: International Organizationf for Standardization.

Kanda, T., & Li, V. (1998). Interface property and apparent strength of high-strength hydrophilic fiber in cement matrix. *Journla of materials in Civil Engineering*, 5-13.

Katzensteiner, B., Mindess, S., Fliatrault, A., & Banthia, N. (1994). Dynamic tests of steel-fiber reinforced concrete frames. *Concrete International*, 57-60.

Kaufmann, J., Lubben, J., & Schwitter, E. (2007). Mechanical reinforcement of concrete with bi-component fibers. *Composites: Part A: Applied Science and Manufacturing*, 1975-1984.

Kim, D. J., El-Tawil, S., & Naaman, A. E. (2008). Loading rate effect on pullout behavior of deformed steel fibers. *ACI Materials Journal*, 576-584.

Kim, J., Park, C., Lee, S.-W., Lee, S.-W., & Won, J. (2007). Effects of the geometry of recycled PET fiber reinforcement on shrinkage cracking of cement-based composites. *Composites: Part B: Engineering*, 442-450.

Kim, N.-W., Saeki, N., & Horiguchi, T. (1999). Crack and strength properties of hybrid

reinforced concrete at early ages. *Transactions of the Japan Concrete Institute, Vol. 21*, 241-246.

Kurtz, S., & Balaguru, P. (2000). Postcrack creep of polymeric fiber-reinforced concrete in flexure. *Cement and Concrete Research*, 183-190.

Lawler, J. S., Zampini, D., & Shah, S. P. (2005). Microfiber and macrofiber hybrid fiber-reinforced concrete. *Journal of Materials in Civil Engineering, Vol. 17, No. 5*, 595-604.

Leung, C., & Li, V. (1991). New strength-based model for the debonding of discontinuous fibres in an eleastic matrix. *Journal of Materials Science*, 5996-6010.

Leung, C., & Li, V. (1992). Effect of fiber inclination on crack bridging stress in brittle fiber reinforced brittle matrix composites. *Journal of the Mechanics and Physics of Solids*, 1333-1362.

Leung, C., & Ybanez, N. (1997). Pullout of inclined flexible fiber in cementitious composite. *Journal of Engineering Mechanics*, 239-246.

Li, V. C., Wang, S., & Wu, C. (2001). Tensile strain-hardening behavior of polyvinyl alcohol engineered cementitious composite (PVA-ECC). *ACI Materials Journal*, 483-492.

Li, V. C., Wang, Y., & Backer, S. (1990). Effect of inclining angle, bundling, and surface treatment on synthetic fibre pull-out from a cement matrix. *Composites*, 132-140.

Li, V., Wang, Y., & Backer, S. (1991). A micromechanical model of tension-softening and bridging touchening of short random fiber reinforced brittle matrix composties. *Journal of the Mechanics and Physics of Solids*, 607-625.

Li, V., Wu, C., Wang, S., Ogawa, A., & Saito, T. (2002). Interface tailoring for strain-hardening polyvinyl alcohol - engineered cementitious composites. *ACI Materials Journal*, 463-472.

Li, V., Wu, H., & Chan, Y. (1996). Effect of plasma treatment of polyethylene fibers on interface and cementitious compostie properties. *Journal of the American Ceramic Society*, 700-704.

Li, Y., & Kaito, A. (2003). Crystallization and orientation behaviors of poly(vinylidene flouride) in the oriented blend with nylon 11. *Polymer*, 8167-8176.

Lin, L., & Argon, A. (1994). Review: Structure and plastic deformation of polyethylene. *Journal of Materials Science*, 294-323.

Lin, Z., Kanda, T., & Li, V. (1999). On interface property characterization and performance of fiber-reinforced cementitious composites. *Concrete Science and Engineering*, 173-174.

MacDonald, J. L. (2010). *Doctorate thesis: A study of the chemical interaction at the polymeric powder and fibre white cement interface.* Halifax, Nova Scotia: Dalhousie University.

MacKay, J., & Trottier, J. (2004). Post-crack creep behavior of steel and synthetic FRC under flexural loading. In E. S. Bernard, *Shotcrete: More Engineering Developments* (pp. 183-187). London: Taylor & Francis Group.

Manolis, G. D., Gareis, P. J., Tsonos, A. D., & Neal, J. A. (1997). Dynamic properties of polypropylene fiber-reinforced concrete slabs. *Cement and Concrete Composites*, 340-349.

Markovich, I., van Mier, J. G., & Walraven, J. C. (2001). Single fiber pullout from hybrid fiber reinforced concrete. *Heron*, 1991-2000.

Mindess, S., Young, J. F., & Darwin, D. (2002). *Concrete, Second Edition.* Upper Saddle River, NJ: Prentice Hall.

Mufti, A. A., Newhook, J. P., & Mahoney, M. (1999). Salmon River Bridge Field Assessment. *Proceedings of the Canadian Society for Civil Engineering Annual Conference.* Regina: Canadian Society for Civil Engineering.

Mufti, A., Newhook, J., & Mahoney, M. (1999). Salmon River bridge field assessment. *Proceedings, Annual Conference - Canadian Society for Civil Engineering* (pp. 51-60). Canadian Society for Civil Engineering.

Naaman, A. (1998). New fiber technology. *Concrete International*, 57-62.

Naaman, A. E., & Najm, H. (1991). Bond-slip mechanisms of steel fibers in concrete. *ACI Materials Journal*, 135-145.

Newhook, J., & Gaudet, J. (2006). Salmon River steel-free bridge deck - 10 year review of field performance. *Proceedings of the 3rd International Conference on Bridge Maintenance, Safety and Management*, (pp. 991-992). Portugal.

Newhook, J., & Mufti, A. (1996). Synthetic fiber-reinforced concrete bridge decks: Redefining bridge deck design and behavior. *Transportation Research Record*, 21-26.

Pelisser, F., Barros, A., Lebre, H., & Caldras, R. (2010). Effect of the addition of synthetic fibers to concrete thin slabs on plastic shrinkage cracking. *Construction and Building Materials*, 2171-2176.

Pereira, E., Barros, J., & Camoes, A. (2008). Steel fiber-reinforced celf-compacting concrete - experimental research and numerical simulation. *Journal of Structural Engineering*, 1310-1321.

Propex Concrete Systems. (2007, October 7). *Enduro 600 Product Data Sheet.* Retrieved March 31, 2010, from Propex Concrete Systems Corporation product website: http://fibermesh.com/downloads/Enduro%20600.pdf

Purnell, P., & Beddows, J. (2005). Durability and simulated ageing of new martix glass fibre reinforced concrete. *Cement and Concrete Composites*, 875-884.

Qi, H. B., Hua, Y., Jiang, Z. Q., Huang, S. Z., & Zhang, S. B. (2000). Microstructure of the carbon and the polypropylene hybrid fiber reinforced concrete acted by bending and tensile stresses. *Key Engineering Materials Vols. 183-187*, 881-886.

Rafeeq, A. S., Ashok, G., & Krishnamoorthy, S. (1999). Influence of steel fibers in fatigure resistance of concrete in direct compression. *Journal of Materials in Civil Engineering*, 172-179.

Ramakrishnan, V., Gollapudi, S. P., & Zellers, R. C. (1987). Performance characterisitics and fatigue strength of polypropylene fiber reinforced concrete. *Fiber Reinforced Concrete Properties and Application, ACI Special Publication SP105-09* (pp. 159-177). Detroit, Michigan: American Concrete Institute.

Rathod, J. D., & Patodi, S. C. (2010). Interface tailoring of polyester-type fiber in engineered cementitious composite matrix against pullout. *ACI Materials Journal*, 114-122.

Reda Taha, M. M., & Shrive, N. G. (1998). Enhancing fracture toughness of high-performance carbon fiber cement composites. *ACI Materials Journal*, 168-178.

Redon, C., Li, V. C., Wu, C., Hoshiro, H., Saito, T., & Ogawa, A. (2001). Measuring and modifying interface properties of PVA fibers in ECC matrix. *Journal of Materials in Civil Engineering*, 299-406.

Reimotec. (2011, March). *PP Strapping Tape Line*. Retrieved March 12, 2011, from Reimotec.com: http://www.reimotec.com/REIMOTEC/en/Products___Services/PP_strapping_tape

Romualdi, J. P., & Mandel, J. A. (1964). Tensile strength of concrete affected by uniformly distributed closely spaced short lengths of wire reinforcement. *Journal of American Concrete Institute*, 657-671.

Scrivener, K. L., Crumbie, A. K., & Laugesen, P. (2004). The interfacial transition zone (ITZ) between cement paste and aggregate in concrete. *Interface Science 12*, 411-421.

Senthilkumar, S., & Natesan, S. (2004). Effect of polypropylene fibre addition on

restrained plastic shrinkage cracking of cement composites. *Journal of the Institution of Engineers*, 100-106.

Sujivorakul, C., Waas, A. M., & Naaman, A. E. (2000). Pullout response of a smooth fiber with an end anchorage. *Journal of Engineering Mechanics*, 986-993.

Takaku, A. (1981). Effect of drawing on creep fracture of polypropylene fibers. *Journal of Applied Polymer Science*, 3565-3573.

Tasdemir, C., Tasdemir, M. A., Lydon, F. D., & Barr, B. (1996). Effects of silica fume and aggregate size on the brittleness of concrete. *Cement and Concrete Research*, 63-68.

Toutanji, H. A. (1998). Influence of air entrainment on the properties of silica fume concrete. *Advances in Cement Research, v 10, n 3*, 135-139.

Trottier, A. M. (2009). *Masters thesis: Development and optimization of synthetic fibres for reinforcement of concrete.* Halifax, Nova Scotia: Dalhousie University.

Trottier, J. F., & Mahoney, M. (2001). Innovative synthetic fibers. *Concrete International*, 23-28.

Trottier, J. F., Mahoney, M., & Forgeron, D. (2002). Can synthetic fibers replace welded wire fabric in slabs on ground. *Concrete International*, 59-68.

Trottier, J., & Mahoney, M. (2001). Innovative synthetic fibers. *Concrete International*, 23-28.

Vandewalle, L. (2000). Cracking behavior of concrete beams reinforced with a combination of ordinary reinforcement and steel fibers. *Materials and Structures*, 164-170.

Vandewalle, L. (2007). Postcracking behavior of hybrid steel fiber reinforced concrete. *Fracture Mechanics of Concrete and Concrete Structures - High-Performance Concrete, Brick-Masonry and Environmental Aspects*, 1367-1375.

Wang, J., Dillard, D., & Ward, T. (1992). Temperature and stress effects in the creep of aramid fibers under transient moisture conditions and discussions on the mechanisms. *Journal of Polymer Science: Part B: Polymer Physics*, 1391-1400.

Wang, Y., Li, V., & Backer, S. (1988). Modelling of fibre pull-out from a cement matrix. *The International Journal of Cement Composites and Lightweight Concrete*, 143-149.

Won, J., Lim, D., & Park, C. (2006). Bond behavior and flexural performance of structural synthetic fibre-reinforced concrete. *Magazine of Concrete Research*, 401-410.

Won, J., Park, C., Lee, S., Jang, C., & Kim, H. (2009). Performance of synthetic macrofibres in reinforced concerete for tunnel linings. *Magazine of Concrete Research*, 165-172.

Yang, E., & Li, V. (2005). Rate dependence in engineered cementitious composites. *Proceedings of the HPFRCC RILEM Conference.* Hawaii.

Yu, H., Zhang, Y., & Ren, W. (2009). Toughening effect of ethylene-vinyl acetate rubber on nylon 1010 compatibilized by maleated ethylene-vinyl acetate copolymers. *Journal of Polymer Science: Part B: Polymer Physics*, 434-444.

Zhang, J., & Li, V. (2002). Effect of inclination angle on fiber rupture load in fiber reinforced cementitious composites. *Composites Science and Technology*, 775-781.

Zhang, Y., Yu, H., & Ren, W. (2009). Ethylene-vinyl acetate copolymers toughen nylon 1010. *Society of Plastics Engineers*, 1-3.

APPENDIX A - ADDITIONAL TABLES AND PLOTS FOR TENSILE TESTING RESULTS

Table A-1 - Properties of filaments from extrusion trials - 1 of 8

Production Date	Material	Stretch Ratio	Width (mm)	Thickness (mm)	σ_f (MPa)		E_f (GPa)		Designation	d_{eq}
					Avg	St. Dev	Avg	St. Dev		
Dec-08	PVDF	5.00	1.70	0.57	346	91	1.61	0.08	Macro fiber	1.07
Dec-08	PVDF	6.00	1.85	0.46	364	111	1.82	0.05	Macro fiber	1.01
Dec-08	PVDF	6.20	1.77	0.44	409	91	1.98	0.17	Macro fiber	0.97
Dec-08	PVDF	5.00	1.72	0.55	291	28	1.33	0.07	Macro fiber	1.06
Dec-08	PVDF	6.00	1.75	0.46	426	12	1.80	0.11	Macro fiber	0.98
Dec-08	PVDF	6.31	1.65	0.43	453	132	2.30	0.23	Macro fiber	0.92
Dec-08	PVDF	5.00	1.69	0.58	352	51	1.40	0.13	Macro fiber	1.08
Dec-08	PVDF	6.00	1.67	0.50	447	120	2.07	0.14	Macro fiber	1.00
Dec-08	PVDF	6.32	1.79	0.49	329	104	1.67	0.18	Macro fiber	1.03
Dec-08	PVDF	6.38	1.76	0.47	527	73	3.44	0.37	Macro fiber	1.00
Dec-08	PVDF	5.00	1.70	0.55	364	36	1.50	0.05	Macro fiber	1.05
Dec-08	PVDF	6.00	1.69	0.46	464	123	2.11	0.29	Macro fiber	0.97
Dec-08	PVDF	6.62	1.69	0.43	585	52	2.49	0.16	Macro fiber	0.94
Dec-08	PVDF	5.00	1.71	0.56	364	65	1.58	0.09	Macro fiber	1.06
Dec-08	PVDF	6.00	1.60	0.47	447	64	2.22	0.16	Macro fiber	0.95
Dec-08	PVDF	6.76	1.67	0.42	483	69	2.32	0.11	Macro fiber	0.92
Dec-08	PVDF	6.85	1.73	0.44	490	101	1.63	0.51	Macro fiber	0.96
Dec-08	PVDF	5.00	1.71	0.53	426	54	1.71	0.08	Macro fiber	1.04

Table A-2 - Properties of filaments from extrusion trials - 2 of 8

Production Date	Material	Stretch Ratio	Width (mm)	Thickness (mm)	σ_f (MPa)		E_f (GPa)		Designation	d_{eq}
					Avg	St. Dev	Avg	St. Dev		
Dec-08	PVDF	6.00	1.60	0.48	387	64	1.85	0.06	Macro fiber	0.96
Dec-08	PVDF	6.83	1.64	0.43	559	80	2.70	0.20	Macro fiber	0.92
Dec-08	PVDF	5.00	1.71	0.58	386	44	1.48	0.19	Macro fiber	1.08
Dec-08	PVDF	6.00	1.66	0.51	401	63	1.81	0.15	Macro fiber	1.00
Dec-08	PVDF	6.76	1.56	0.42	591	134	3.03	0.16	Macro fiber	0.89
Dec-08	PVDF	6.88	1.62	0.42	515	107	2.55	0.27	Macro fiber	0.90
Dec-08	PVDF	7.00	1.70	0.41	449	84	2.36	0.33	Macro fiber	0.92
Dec-08	PVDF	6.00	1.58	0.50	446	70	2.08	0.25	Macro fiber	0.97
Dec-08	PVDF	6.00	1.56	0.49	502	91	1.76	0.36	Macro fiber	0.95
Dec-08	PVDF	6.00	1.60	0.49	433	123	2.05	0.40	Macro fiber	0.97
Dec-08	PVDF	6.00	1.55	0.52	414	96	1.74	0.29	Macro fiber	0.98
Dec-08	PVDF	6.00	1.54	0.49	486	73	2.35	0.18	Macro fiber	0.95
Dec-08	PVDF	5.00	1.79	0.50	295	74	1.76	0.24	Macro fiber	1.04
Dec-08	PVDF	5.41	1.80	0.50	371	53	1.23	0.10	Macro fiber	1.04
Dec-08	PVDF	5.00	1.99	0.50	324	67	1.34	0.09	Macro fiber	1.09
Dec-08	PVDF	6.00	1.84	0.47	497	72	1.93	0.13	Macro fiber	1.02
Dec-08	PVDF	5.00	1.99	0.51	376	39	1.37	0.06	Macro fiber	1.11
Dec-08	PVDF	6.00	1.79	0.45	411	96	2.14	0.10	Macro fiber	0.99
Dec-08	PVDF	6.30	1.69	0.46	544	110	2.23	0.25	Macro fiber	0.97

Table A-3 - Properties of filaments from extrusion trials - 3 of 8

Production Date	Material	Stretch Ratio	Width (mm)	Thickness (mm)	σ_f (MPa)		E_f (GPa)		Designation	d_{eq}
					Avg	St. Dev	Avg	St. Dev		
6-Mar-09	78% PP 22% PVDF	9.00	1.39	0.45	375	27	4.24	0.58	Macro fiber	0.86
6-Mar-09	78% PP 22% PVDF	10.00	1.34	0.45	384	33	5.06	0.68	Macro fiber	0.85
6-Mar-09	78% PP 22% PVDF	10.50	1.36	0.44	348	55	5.29	1.45	Macro fiber	0.84
6-Mar-09	78% PP 22% PVDF	10.90	1.35	0.42	349	32	4.11	1.67	Macro fiber	0.82
6-Mar-09	78% PP 22% PVDF	11.00	1.32	0.40	394	37	6.15	0.46	Macro fiber	0.79
6-Mar-09	78% PP 22% PVDF	11.25	1.36	0.42	352	30	5.26	0.74	Macro fiber	0.82
6-Mar-09	78% PP 22% PVDF	11.52	1.33	0.40	380	24	6.27	1.52	Macro fiber	0.80
6-Mar-09	78% PP 22% PVDF	12.00	1.31	0.39	360	19	6.44	0.95	Macro fiber	0.78
6-Mar-09	78% PP 22% PVDF	12.50	1.24	0.40	389	36	6.69	0.79	Macro fiber	0.76
6-Mar-09	78% PP 22% PVDF	13.00	1.22	0.37	398	10	7.05	2.38	Macro fiber	0.74
5-Mar-09	82 % PP 18% PVDF	9.00	1.43	0.47	409	53	4.54	0.31	Macro fiber	0.89
5-Mar-09	83 % PP 17% PVDF	9.03	1.46	0.45	415	28	4.30	0.48	Macro fiber	0.88
5-Mar-09	84 % PP 16% PVDF	10.00	1.34	0.43	426	18	5.08	0.28	Macro fiber	0.83
5-Mar-09	85% PP 15% PVDF	9.00	1.43	0.45	411	19	4.34	0.62	Macro fiber	0.88
5-Mar-09	100% PP	9.00	1.35	0.47	358	82	4.82	0.87	Macro fiber	0.87
5-Mar-09	100% PP	9.00	1.33	0.45	341	112	5.49	2.09	Macro fiber	0.84
5-Mar-09	100% PP	10.00	1.32	0.44	473	24	4.91	0.20	Macro fiber	0.83
5-Mar-09	100% PP	11.00	1.28	0.42	445	37	5.21	0.78	Macro fiber	0.80
5-Mar-09	82 % HDPE 18% PVDF	6.00	1.53	0.59	177	4	1.89	0.15	Macro fiber	1.03
5-Mar-09	82 % HDPE 18% PVDF	7.00	1.39	0.56	219	13	2.79	0.46	Macro fiber	0.95

Table A-4 - Properties of filaments from extrusion trials - 4 of 8

Production Date	Material	Stretch Ratio	Width (mm)	Thickness (mm)	σ_f (MPa)		E_f (GPa)		Designation	d_{eq}
					Avg	St. Dev	Avg	St. Dev		
5-Mar-09	82 % HDPE 18% PVDF	7.22	1.42	0.54	224	2	2.23	0.21	Macro fiber	0.95
7-May-09	HDPE (5906)	10.50	1.47	0.44	480	88	4.24	0.78	Macro fiber	0.88
7-May-09	HDPE (5906)	12.00	1.20	0.43	480	57	5.63	1.58	Macro fiber	0.78
7-May-09	HDPE (5906)	13.00	1.15	0.41	484	45	6.81	1.70	Macro fiber	0.75
7-May-09	HDPE (5906)	14.00	1.24	0.42	477	75	8.13	0.68	Macro fiber	0.78
7-May-09	80% PP, 20% PVDF	10.00	1.41	0.42	389	19	6.22	2.02	Macro fiber	0.84
19-May-09	HDPE (5906)	9.00	2.47	0.22	392	17	3.18	0.19	Macro fiber	0.83
19-May-09	HDPE (5906)	9.58	2.37	0.22	401	14	3.59	0.15	Macro fiber	0.81
19-May-09	HDPE (5906)	10.04	2.56	0.28	452	19	4.03	0.29	Macro fiber	0.94
19-May-09	HDPE (5906)	11.10	2.66	0.29	502	40	4.74	0.15	Macro fiber	0.98
19-May-09	HDPE (5906)	12.07	1.47	0.44	524	54	6.46	1.08	Macro fiber	0.88
19-May-09	HDPE (5906)	13.50	1.20	0.43	614	39	7.61	0.81	Macro fiber	0.78
19-May-09	HDPE (5906)	12.14	1.15	0.41	511	83	6.15	0.96	Macro fiber	0.75
19-May-09	HDPE (5906)	13.24	1.24	0.42	532	93	6.82	2.09	Macro fiber	0.78
19-May-09	HDPE (5906)	14.34	1.41	0.42	597	92	9.98	1.91	Macro fiber	0.84
19-May-09	HDPE (5906)	16.21	1.08	0.39	447	71	9.78	2.84	Macro fiber	0.70
19-May-09	HDPE (5906)	11.04	1.08	0.39	477	39	4.89	0.38	Macro fiber	0.70
19-May-09	HDPE (5906)	11.75	1.08	0.39	516	30	5.65	0.46	Macro fiber	0.70
20-May-09	50% PP, 50% HDPE (5906)	13.01	1.08	0.39	464	44	6.25	0.65	Macro fiber	0.70
20-May-09	60% PP, 40% HDPE (5906)	13.01	1.08	0.39	400	32	6.20	1.00	Macro fiber	0.70

Table A-5 - Properties of filaments from extrusion trials - 5 of 8

Production Date	Material	Stretch Ratio	Width (mm)	Thickness (mm)	σ_f (MPa)		E_f (GPa)		Designation	d_{eq}
					Avg	St. Dev	Avg	St. Dev		
19-May-09	HDPE (5906)	13.50	1.23	0.40	566	103	8.38	1.12	Macro fiber	0.76
Sep-09	HDPE (5906)	9.27	0.51	0.56	586	33	5.39	0.46	Micro fiber	0.53
Sep-09	HDPE (5906)	9.43	0.51	0.56	657	60	6.43	0.55	Micro fiber	0.53
Sep-09	HDPE (5906)	9.47	0.52	0.57	571	33	5.32	0.35	Micro fiber	0.54
Sep-09	HDPE (5906)	9.93	0.51	0.54	593	70	6.01	0.20	Micro fiber	0.53
Sep-09	HDPE (5906)	9.47	0.51	0.54	610	39	5.78	0.58	Micro fiber	0.53
Sep-09	HDPE (5906)	10.79	0.49	0.50	702	58	7.62	0.28	Micro fiber	0.50
Sep-09	HDPE (5906)	12.58	0.46	0.46	876	37	10.79	0.71	Micro fiber	0.46
Sep-09	HDPE (5906)	13.08	0.45	0.44	878	98	12.53	0.53	Micro fiber	0.44
Sep-09	HDPE (5906)	13.19	0.42	0.45	937	85	13.92	1.67	Micro fiber	0.43
Sep-09	HDPE (5906)	13.23	0.44	0.47	837	157	12.17	1.03	Micro fiber	0.46
Sep-09	HDPE (5906)	9.44	0.48	0.52	712	54	7.00	0.59	Micro fiber	0.50
Sep-09	HDPE (5906)	10.05	0.46	0.50	744	76	7.64	0.61	Micro fiber	0.48
Sep-09	HDPE (5906)	10.05	0.48	0.49	725	64	7.38	0.70	Micro fiber	0.48
Sep-09	HDPE (5906)	11.06	0.46	0.48	763	47	8.09	0.82	Micro fiber	0.47
Sep-09	HDPE (5906)	11.56	0.44	0.46	822	58	9.11	0.39	Micro fiber	0.45
Sep-09	HDPE (5906)	12.55	0.41	0.44	887	109	11.98	0.91	Micro fiber	0.42
Sep-09	HDPE (5906)	13.55	0.42	0.42	858	88	12.60	1.98	Micro fiber	0.42
Sep-09	HDPE (5906)	13.02	0.31	0.32	1103	41	15.53	1.30	Micro fiber	0.31

Table A-6 - Properties of filaments from extrusion trials - 6 of 8

Production Date	Material	Stretch Ratio	Width (mm)	Thickness (mm)	σ_f (MPa)		E_f (GPa)		Designation	d_{eq}
					Avg	St. Dev	Avg	St. Dev		
Sep-09	HDPE (5906)	13.02	0.29	0.30	1062	93	15.95	1.79	Micro fiber	0.30
Sep-09	HDPE (5906)	14.04	0.29	0.31	977	103	16.97	1.30	Micro fiber	0.30
Sep-09	82 % HDPE 18% PVDF	11.98	0.41	0.40	512	102	4.57	1.37	Micro fiber	0.40
Sep-09	82 % HDPE 18% PVDF	11.98	0.35	0.37	690	15	6.06	0.35	Micro fiber	0.36
Sep-09	82 % HDPE 18% PVDF	11.98	0.34	0.36	773	17	6.58	0.33	Micro fiber	0.35
Sep-09	82 % HDPE 18% PVDF	11.98	0.31	0.33	861	32	10.90	0.62	Micro fiber	0.32
04-Feb-10	HDPE (5906)	11.70	0.29	0.28	1391	61	15.93	2.12	Micro fiber	0.29
04-Feb-10	HDPE (5906), 5% EVA	11.70	0.29	0.29	1201	122	13.25	2.58	Micro fiber	0.29
04-Feb-10	HDPE (5906), 10% EVA	11.70	0.27	0.30	1027	90	10.06	1.06	Micro fiber	0.28
04-Feb-10	HDPE (5906), 10% EVA	11.76	0.28	0.27	1107	61	11.93	1.42	Micro fiber	0.28
05-Feb-10	HDPE (5906), 5% EVA	11.70	0.27	0.29	1236	133	12.56	1.01	Micro fiber	0.28
05-Feb-10	HDPE (5906)	11.70	0.26	0.28	1348	171	15.76	3.72	Micro fiber	0.27
05-Feb-10	HDPE (5906), 10% PVDF, 20% MAH	11.96	0.25	0.25	1420	59	18.93	1.89	Micro fiber	0.25
04-Feb-10	HDPE (5906), 10% EVA	13.38	0.25	0.26	1448	63	19.75	2.08	Micro fiber	0.25
22-Feb-10	HDPE (1288)	11.54	0.26	0.30	888	49	11.18	1.35	Micro fiber	0.28
22-Feb-10	HDPE (1288)	11.70	0.26	0.25	1086	51	12.60	1.60	Micro fiber	0.25
22-Feb-10	HDPE (1288)	12.26	0.17	0.20	1803	155	27.38	4.35	Micro fiber	0.19
22-Feb-10	HDPE (1288)	12.44	0.19	0.20	1842	132	28.47	4.19	Micro fiber	0.19
22-Feb-10	HDPE (1288)	12.44	0.21	0.22	1617	103	23.92	4.36	Micro fiber	0.22
23-Feb-10	HDPE (1288)	12.40	0.24	0.20	1524	139	20.56	2.19	Micro fiber	0.22

Table A-7 - Properties of filaments from extrusion trials - 7 of 8

Production Date	Material	Stretch Ratio	Width (mm)	Thickness (mm)	σ_f (MPa)		E_f (GPa)		Designation	d_{eq}
					Avg	St. Dev	Avg	St. Dev		
23-Feb-10	HDPE (1288)	12.91	0.26	0.23	1190	64	19.49	4.56	Micro fiber	0.25
23-Feb-10	HDPE (1288)	9.75	0.30	0.32	811	36	7.86	0.92	Micro fiber	0.31
23-Feb-10	HDPE (1288)	10.11	0.29	0.32	873	59	8.30	0.71	Micro fiber	0.31
23-Feb-10	HDPE (1288)	10.98	0.28	0.30	907	56	10.82	0.95	Micro fiber	0.29
24-Feb-10	HDPE (5906), 10% PVDF, 20% MAH	11.96	0.31	0.33	693	34	9.11	0.56	Micro fiber	0.32
24-Feb-10	HDPE (5906), 10% PVDF, 20% MAH	11.96	0.23	0.31	1072	184	15.56	1.85	Micro fiber	0.27
	PVA		0.12	0.12	2092	115	28.66	2.15	Macro fiber	0.12
	Nylon (PA66)		0.14	0.15	2323	430	5.70	0.59	Macro fiber	0.14
	Nylon (Co-polymide Ultramid C4Q42)		0.15	0.15	2023	393	6.91	2.86	Macro fiber	0.15
15-Feb-10	TUF STRAND SF	12.84	1.05	0.34	646	34	9.53	1.78	Macro fiber	0.65
04-Jun-10	HDPE (5906)	10.41	1.39	0.25	673	68	6.13	0.60	Macro fiber	0.65
04-Jun-10	HDPE (5906), 10% EVA	10.41	1.55	0.29	595	40	5.67	0.26	Macro fiber	0.74
04-Jun-10	HDPE (5906), 1% PVDF	10.40	1.41	0.27	709	14	6.34	0.38	Macro fiber	0.68
04-Jun-10	HDPE (5906), 3% PVDF	10.39	1.42	0.25	749	44	7.01	0.44	Macro fiber	0.66
04-Jun-10	HDPE (5906), 11% PVDF, 20% MAH	10.32	1.51	0.29	559	26	5.79	0.35	Macro fiber	0.73
29-Jun-10	80% PP, 20% HDPE	12.80	1.30	0.27	704	40	10.77	0.87	Macro fiber	0.66
29-Jun-10	80% PP, 10% HDPE, 10% EVA	13.20	1.31	0.35	504	29	7.47	1.24	Macro fiber	0.74
29-Jun-10	80% PP, 20% HDPE	12.55	1.29	0.29	669	38	9.44	0.91	Macro fiber	0.67

Table A-8 - Properties of filaments from extrusion trials - 8 of 8

Production Date	Material	Stretch Ratio	Width (mm)	Thickness (mm)	σ_f (MPa)		E_f (GPa)		Designation	d_{eq}
					Avg	St. Dev	Avg	St. Dev		
29-Jun-10	80% PP, 10% HDPE, 10% EVA	13.47	1.31	0.25	718	43	10.93	0.68	Macro fiber	0.63
29-Jun-10	80% PP, 10% HDPE, 10% EVA	14.12	1.33	0.27	669	31	10.89	1.05	Macro fiber	0.66
29-Jun-10	80% PP, 20% HDPE	13.19	1.32	0.27	663	42	10.81	1.00	Macro fiber	0.66
15-Sep-10	100% HDPE	9.31	1.24	0.28	562	60	5.28	0.78	Macro fiber	0.65
15-Sep-10	HDPE (5906), 5% PVDF, 10% MAH	9.31	1.34	0.27	536	83	5.31	1.14	Macro fiber	0.66
15-Sep-10	HDPE (5906), 5% PVDF, 10% MAH	10.51	1.31	0.27	636	32	6.39	0.54	Macro fiber	0.66
15-Sep-10	HDPE (5906), 5% PVDF, 10% MAH	11.74	1.30	0.30	666	29	7.60	0.52	Macro fiber	0.68
15-Sep-10	HDPE (5906), 5% PVDF, 10% MAH	12.05	1.26	0.26	779	36	9.25	0.40	Macro fiber	0.64
15-Sep-10	HDPE (5906), 7% PVDF, 10% MAH	12.04	1.28	0.27	764	36	9.10	0.37	Macro fiber	0.64
15-Sep-10	HDPE (5906), 9% PVDF, 10% MAH	12.06	1.28	0.27	731	18	8.17	0.45	Macro fiber	0.65

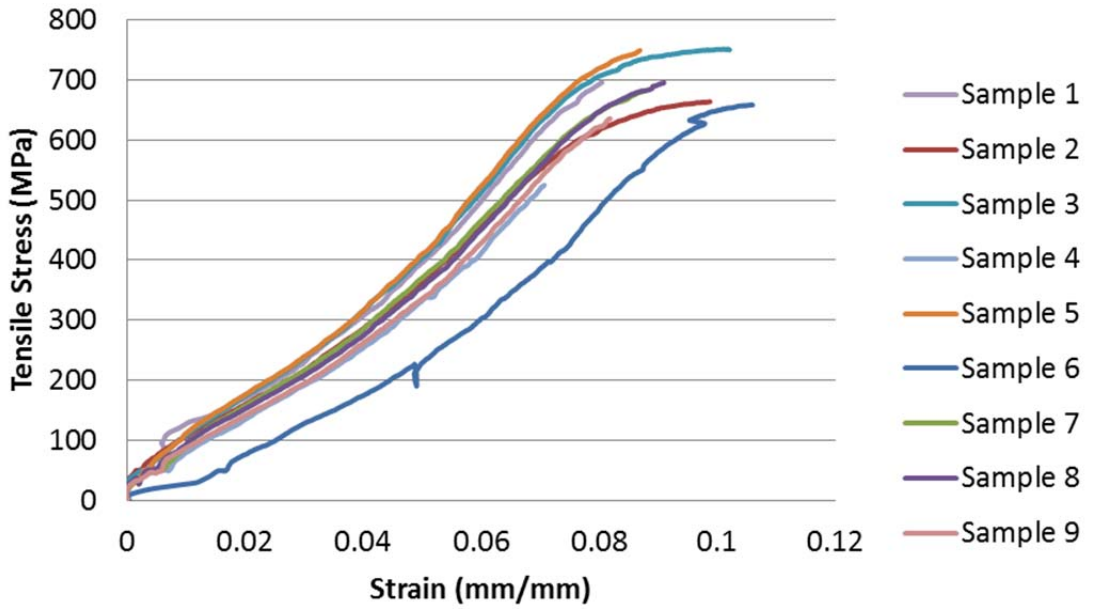

Figure A-1 - Stress vs. Strain curves for prototype macrofiber containing 100% HDPE 5906

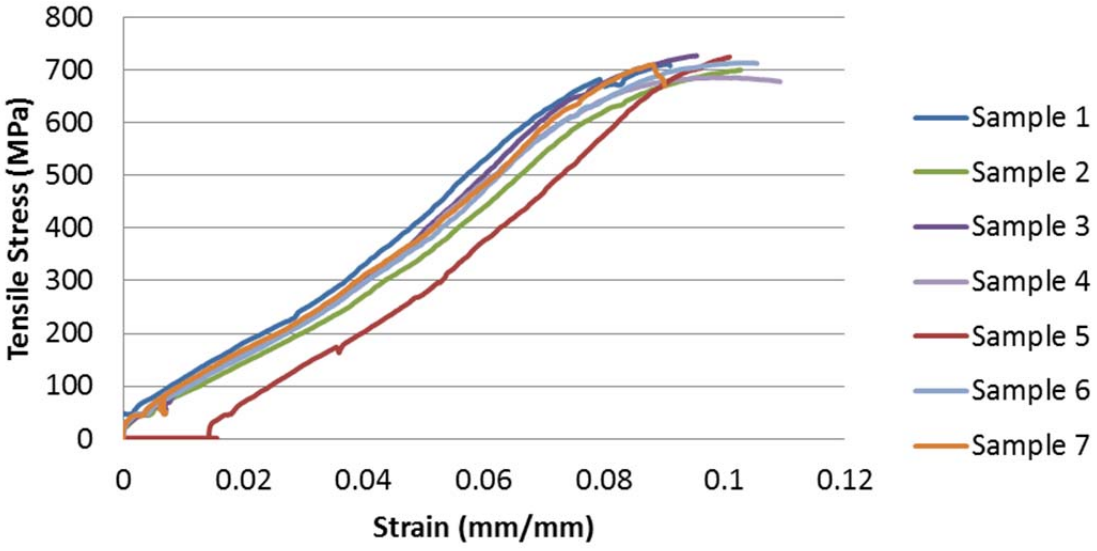

Figure A-2 - Stress vs. Strain curves for prototype macrofiber containing HDPE and 1% PVDF

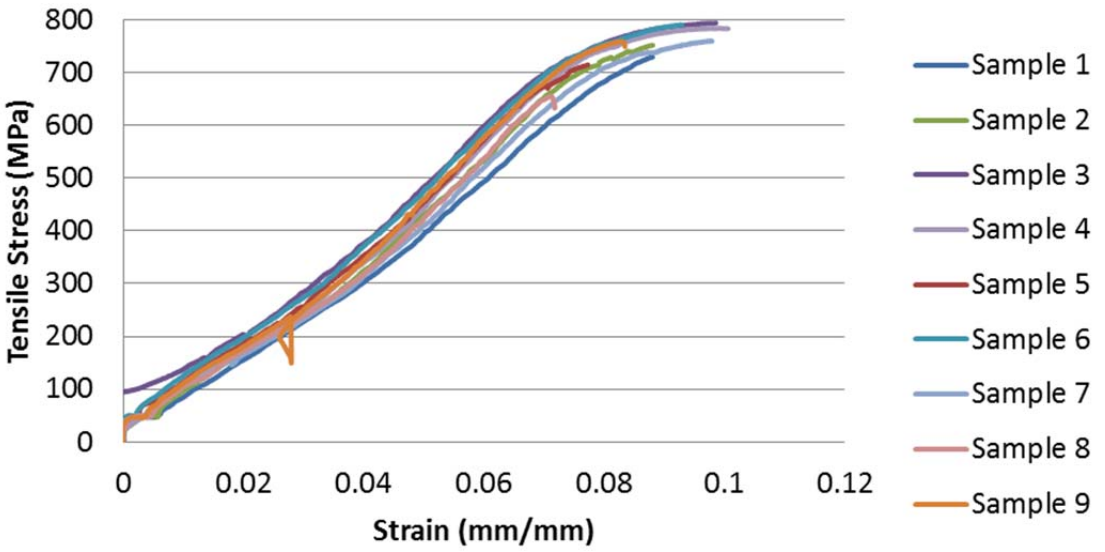

Figure A-3 - Stress vs. Strain curves for prototype macrofiber containing HDPE and 3% PVDF

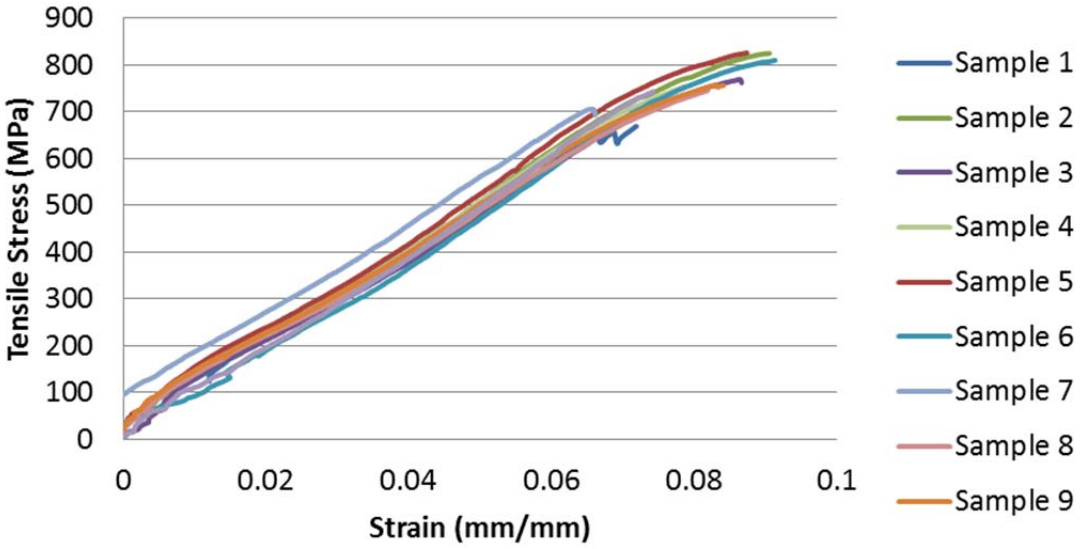

Figure A-4 - Stress vs. Strain curves for prototype macrofiber containing HDPE, 5% PVDF and 10% MAH

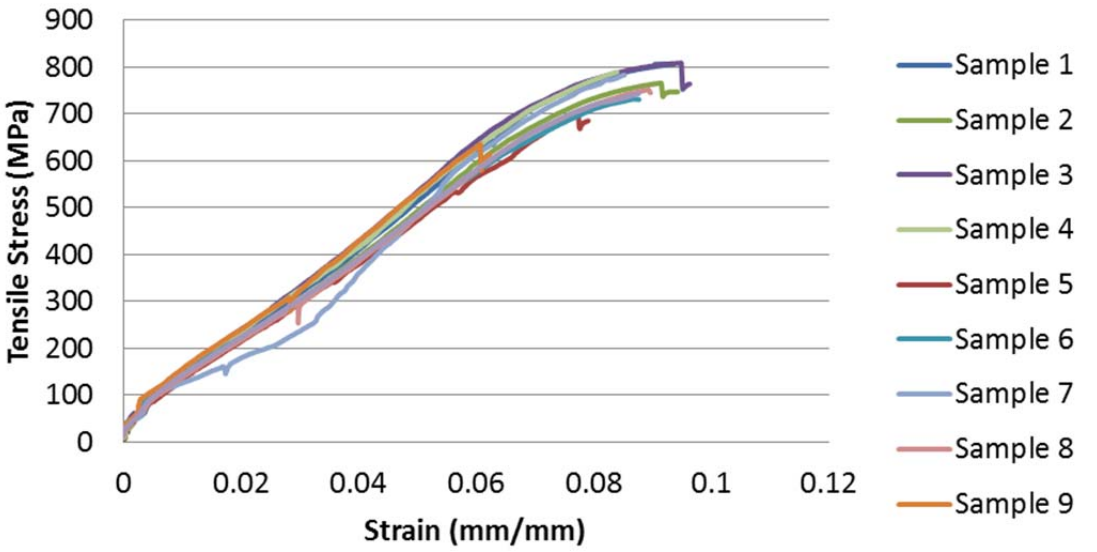

Figure A-5 - Stress vs. Strain curves for prototype macrofiber containing HDPE, 7% PVDF and 10% MAH

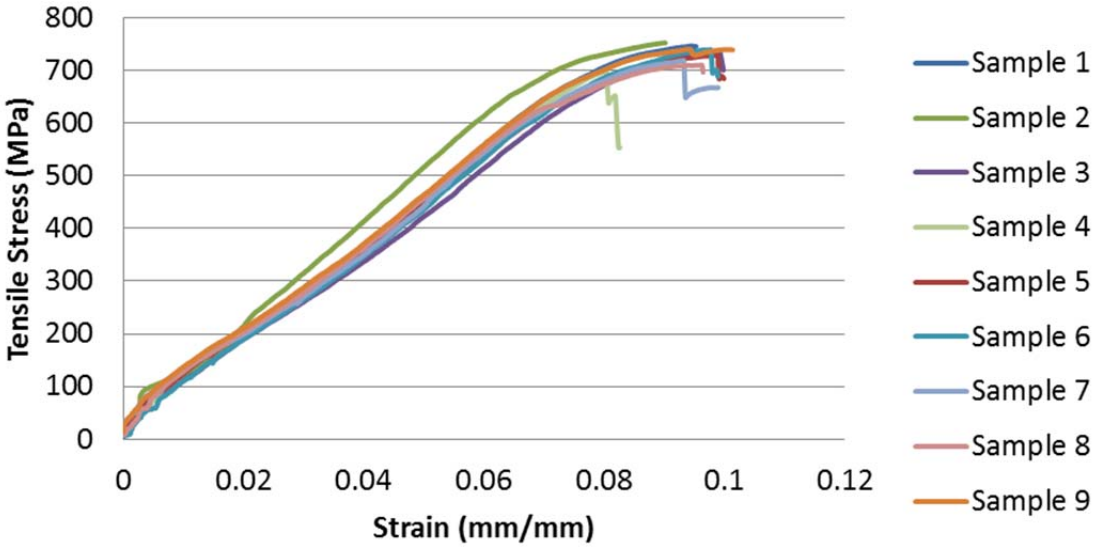

Figure A-6 - Stress vs. Strain curves for prototype macrofiber containing HDPE, 9% PVDF and 10% MAH

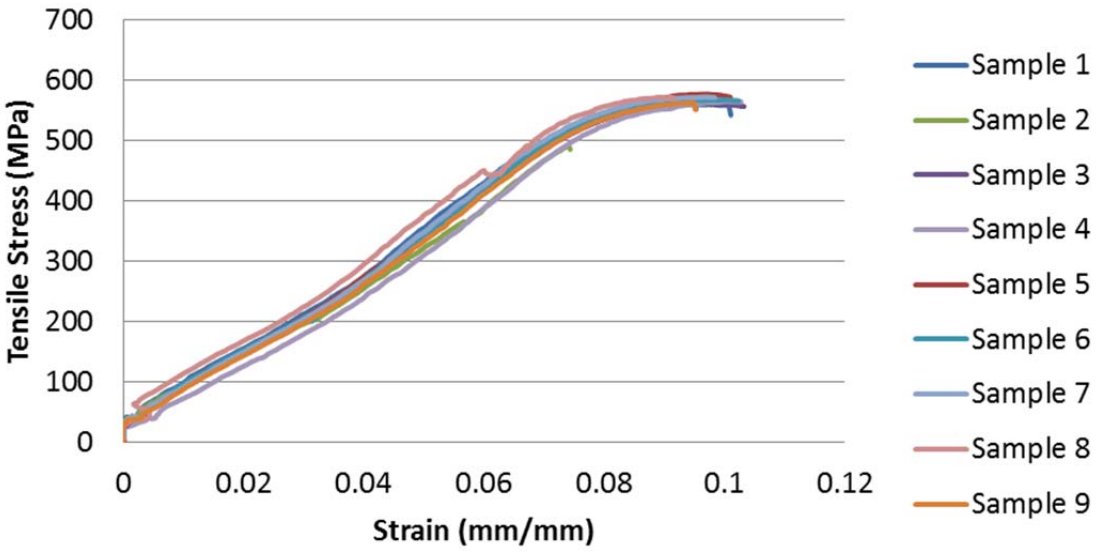

Figure A-7 - Stress vs. Strain curves for prototype macrofiber containing HDPE, 11% PVDF and 20% MAH

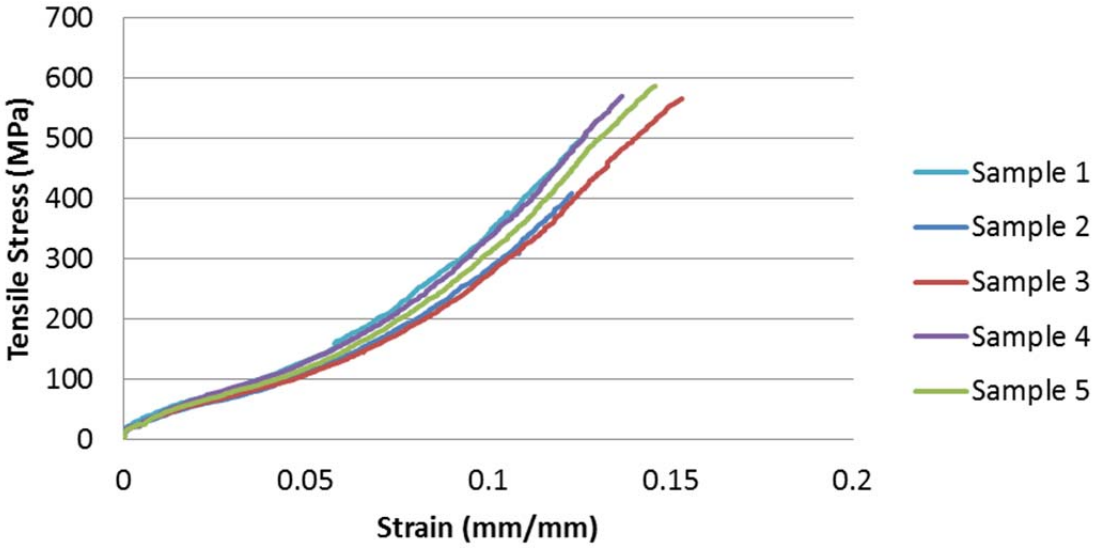

Figure A-8 - Stress vs. Strain curves for prototype macrofiber containing 100% PVDF

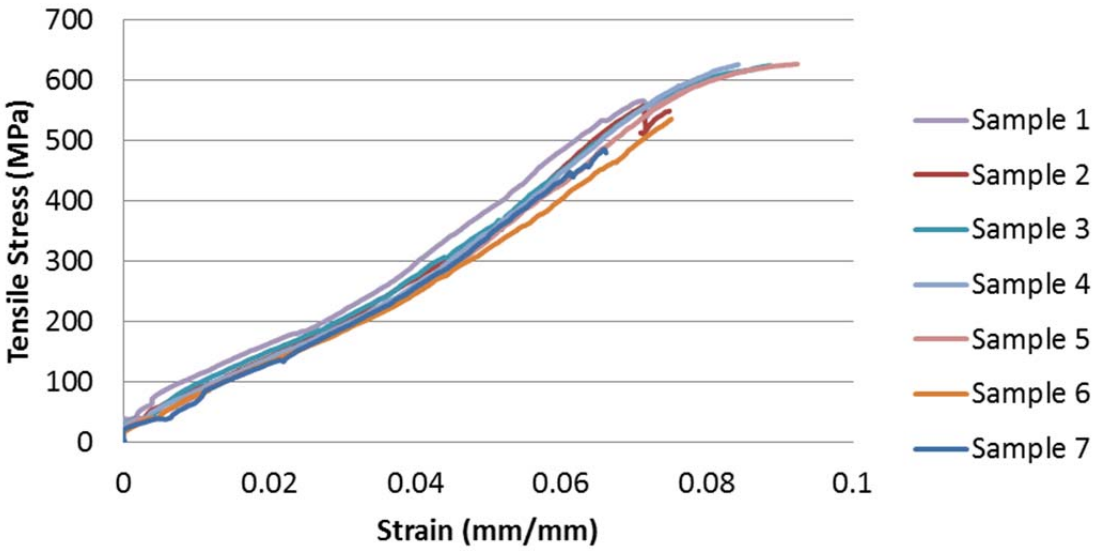

Figure A-9 - Stress vs. Strain curves for prototype macrofiber containing HDPE and 10% EVA

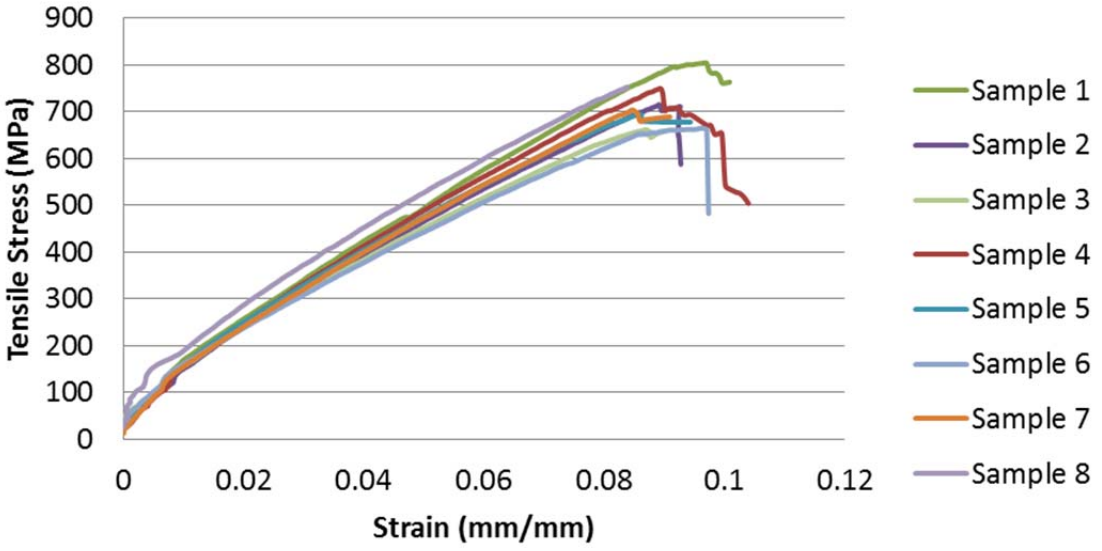

Figure A-10 - Stress vs. Strain curves for prototype macrofiber containing PP, 20% HDPE and 10% EVA

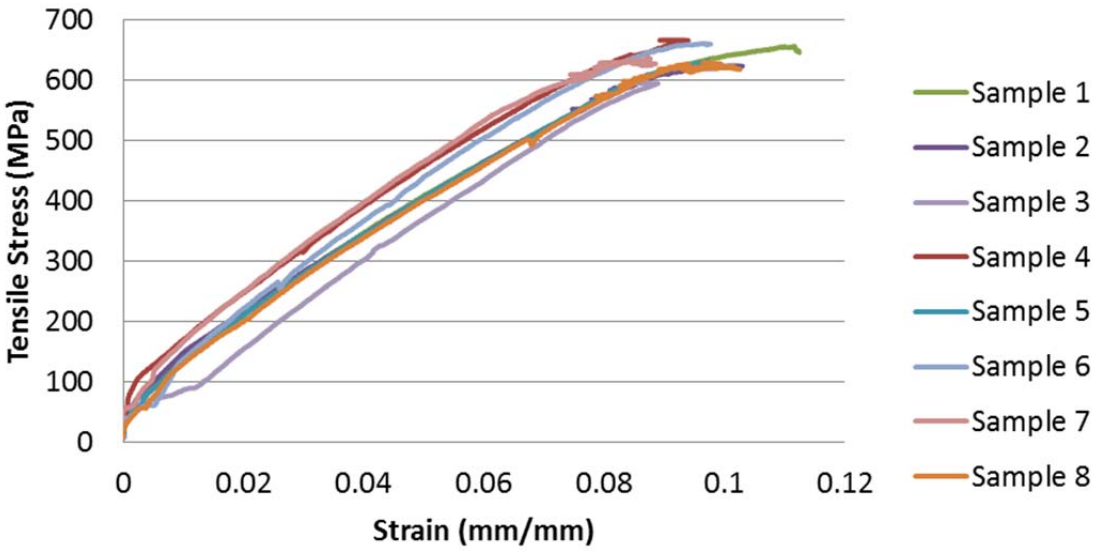

Figure A-11 - Stress vs. Strain curves for Tuf-Strand SF

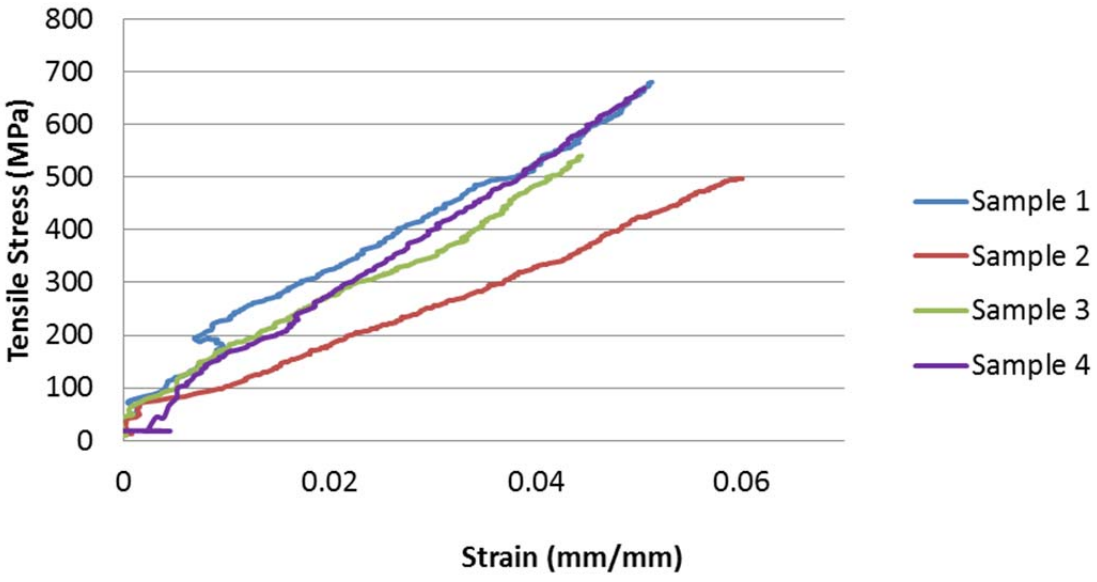

Figure A-12 - Stress vs. Strain curves for prototype macrofiber containing 100% HDPE 5906 (thick)

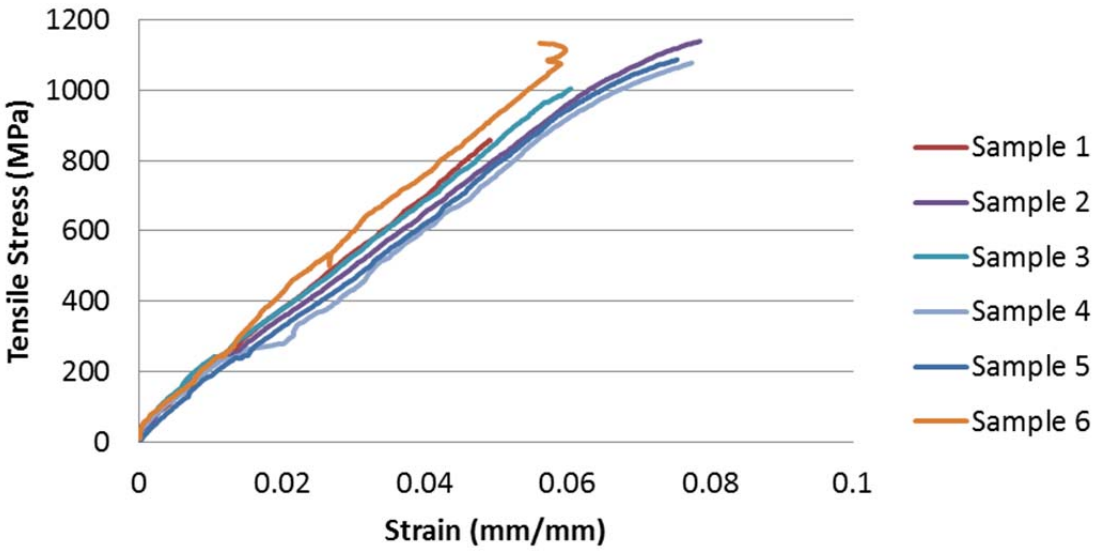

Figure A-13 - Stress vs. Strain curves for prototype microfiber containing 100% HDPE 5906

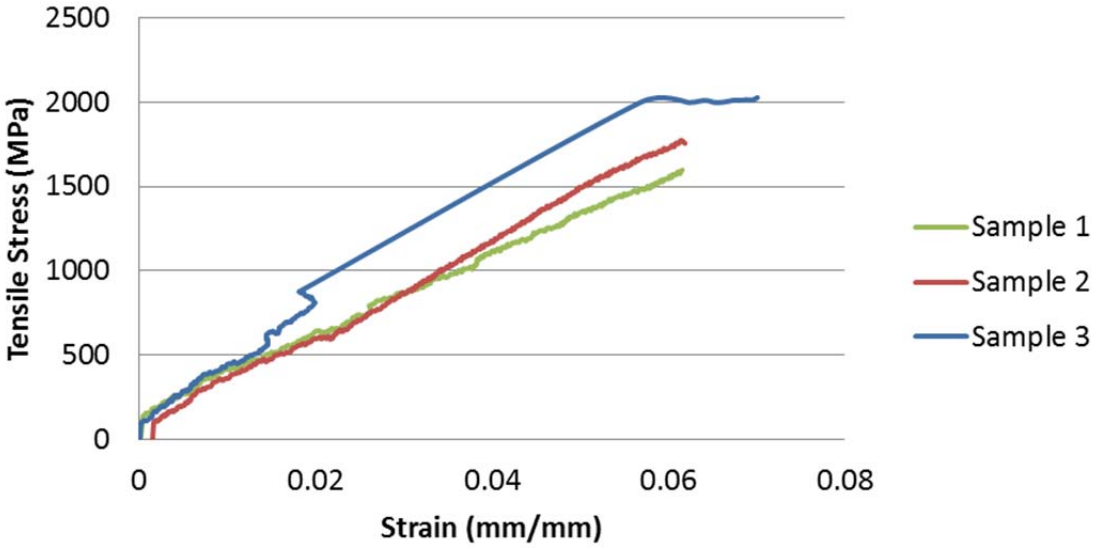

Figure A-14 - Stress vs. Strain curves for prototype microfiber containing 100% HDPE 1288

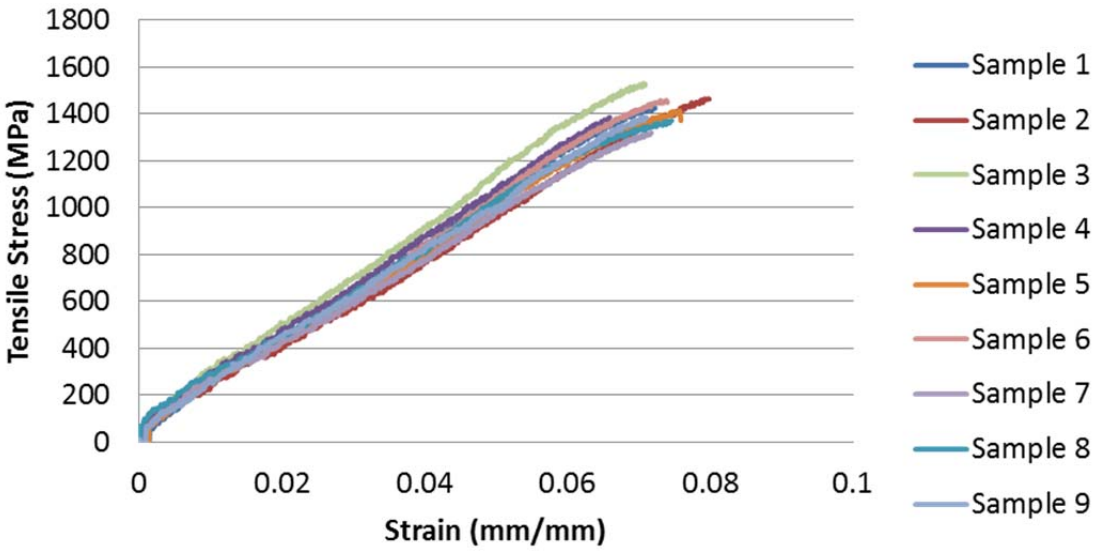

Figure A-15 - Stress vs. Strain curves for prototype microfiber containing HDPE, 10% PVDF and 20% MAH

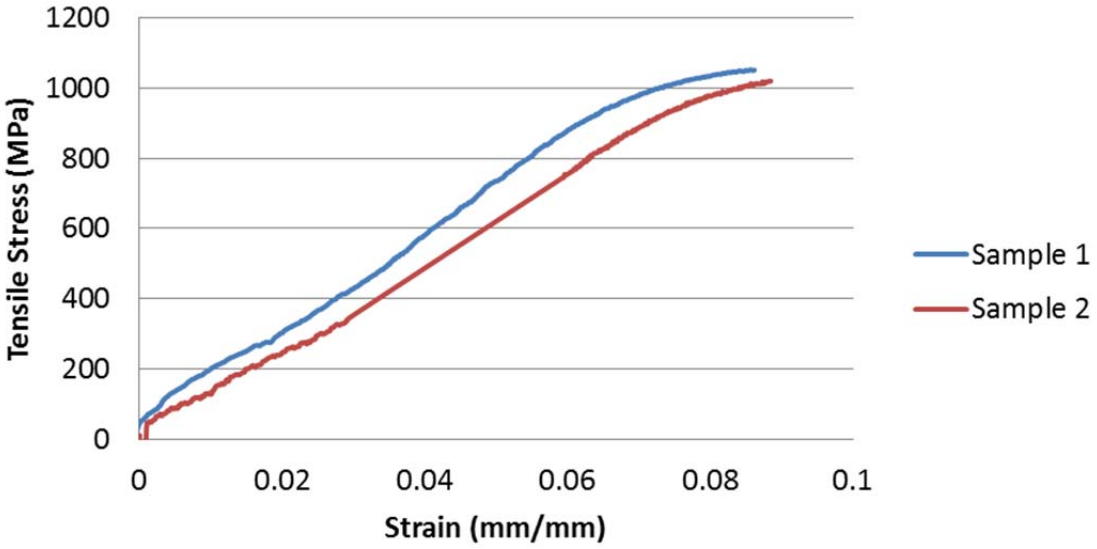

Figure A-16 - Stress vs. Strain curves for prototype microfiber containing HDPE and 10% EVA

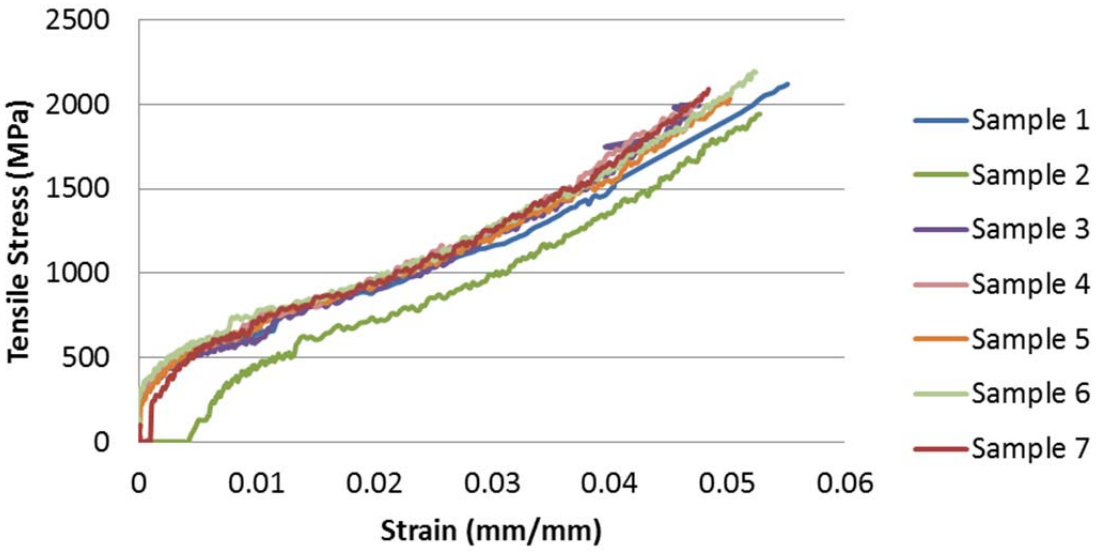

Figure A-17 - Stress vs. Strain curves for PVA microfiber

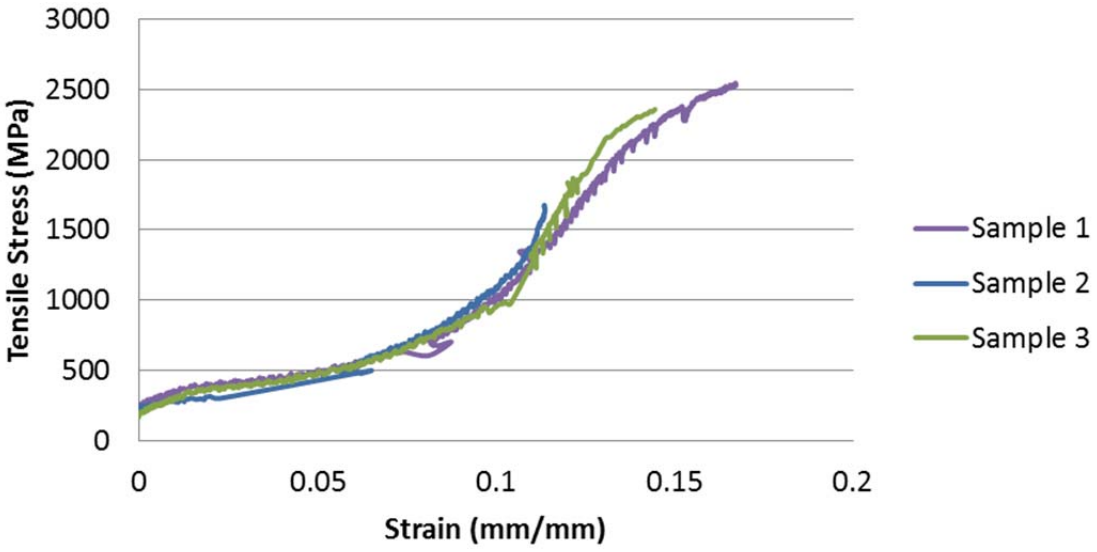

Figure A-18 - Stress vs. Strain curves for nylon microfibers

APPENDIX B - ADDITIONAL TABLES AND PLOTS FOR RESULTS OF PULLOUT TESTING

B.1 - Tables of Pullout Results

Table B-9 - Macrofiber pullout testing results - 1 of 5

Fiber Description	Width (mm)	Thick (mm)	σ_f (MPa)	E_f (GPa)	ϕ (degrees)	Embedment Length (mm)	Matrix Strength (MPa)	P_{max} (N)	U_p (N-mm)	η_τ
100% HDPE	1.39	0.25	673	6.13	0	25.40	37.6	43.0	779	24.0%
						22.23	37.6	42.1	602	23.5%
					15	25.40	34.3	44.1	816	24.6%
						22.23	34.3	43.4	682	24.2%
					30	25.40	34.3	60.7	903	33.9%
						22.23	34.3	44.9	766	25.1%
					45	25.40	35.7	51.5	979	28.8%
						22.23	34.3	48.9	608	27.3%
					60	25.40	35.7	57.6	942	32.2%
						22.23	35.7	52.3	717	29.3%
HDPE, 1% PVDF	1.41	0.27	709	6.34	0	25.40	52.1	37.6	499	18.7%
						22.23	52.1	37.3	482	18.5%
					15	25.40	38.0	43.2	714	21.5%
						22.23	38.0	39.4	619	19.6%
					30	25.40	38.0	45.0	670	22.3%
						22.23	38.0	45.1	731	22.4%
					45	25.40	37.0	76.5	1150	38.0%
						22.23	37.0	59.2	880	29.4%
					60	25.40	37.0	92.4	907	45.9%
						22.23	37.0	68.5	987	34.1%

Table B-10 - Macrofiber pullout testing results - 2 of 5

Fiber Description	Width (mm)	Thick (mm)	σ_f (MPa)	E_f (GPa)	ϕ (degrees)	Embedment Length (mm)	Matrix Strength (MPa)	P_{max} (N)	U_p (N-mm)	η_τ
HDPE, 3% PVDF	1.42	0.25	749	7.01	0	25.40	51.2	48.5	787	23.6%
						22.23	51.2	47.3	629	23.0%
					15	25.40	43.0	46.1	839	22.4%
						22.23	43.0	43.5	584	21.1%
					30	25.40	43.0	57.6	811	28.0%
						22.23	43.0	49.2	716	23.9%
					45	25.40	38.2	61.4	1011	29.9%
						22.23	38.2	58.6	841	28.5%
					60	25.40	38.2	64.7	881	31.5%
						22.23	38.2	58.3	651	28.4%
HDPE, 5% PVDF, 10% MAH	1.34	0.27	779	9.25	0	25.40	33.7	56.9	792	26.7%
						22.23	33.7	52.8	712	24.7%
					15	25.40	29.9	51.4	870	24.1%
						22.23	29.9	47.1	661	22.1%
					30	25.40	29.9	63.9	908	29.9%
						22.23	29.9	66.0	1034	30.9%
					45	25.40	30.4	92.9	1242	43.5%
						22.23	30.4	61.1	871	28.6%
					60	25.40	30.4	89.0	997	41.7%
						22.23	30.4	74.6	936	34.9%

Table B-11 - Macrofiber pullout testing results - 3 of 5

Fiber Description	Width (mm)	Thick (mm)	σ_f (MPa)	E_f (GPa)	ϕ (degrees)	Embedment Length (mm)	Matrix Strength (MPa)	P_{max} (N)	U_p (N-mm)	η_τ
HDPE, 7% PVDF, 10% MAH	1.31	0.27	764	9.10	0	25.40	30.1	58.4	852	26.2%
						22.23	30.1	55.9	641	25.1%
					15	25.40	30.1	67.7	1055	30.4%
						22.23	30.1	58.0	797	26.0%
					30	25.40	37.0	87.5	1297	39.3%
						22.23	37.0	64.4	816	28.9%
					45	25.40	37.0	99.2	1221	44.6%
						22.23	37.0	99.2	1023	44.6%
					60	25.40	33.5	113.4	873	51.0%
						22.23	33.5	64.0	743	28.8%
HDPE, 9% PVDF, 10% MAH	1.30	0.30	731	8.17	0	25.40	33.5	67.8	1010	31.9%
						22.23	33.5	66.0	944	31.0%
					15	25.40	29.9	58.2	841	27.4%
						22.23	29.9	46.0	648	21.6%
					30	25.40	29.9	60.2	913	28.3%
						22.23	29.9	53.3	799	25.0%
					45	25.40	36.8	115.6	769	54.3%
						22.23	36.8	115.3	756	54.2%
					60	25.40	36.8	121.3	646	57.0%
						22.23	36.8	102.8	656	48.3%

Table B-12 - Macrofiber pullout testing results - 4 of 5

Fiber Description	Width (mm)	Thick (mm)	σ_f (MPa)	E_f (GPa)	ϕ (degrees)	Embedment Length (mm)	Matrix Strength (MPa)	P_{max} (N)	U_p (N-mm)	η_τ
HDPE, 11% PVDF, 20% MAH	1.51	0.29	595	5.67	0	25.40	47.3	81.1	1312	39.3%
						22.23	47.3	82.2	927	39.8%
					15	25.40	37.9	75.8	1281	36.7%
						22.23	37.9	61.0	885	29.6%
					30	25.40	37.9	117.7	1180	57.0%
						22.23	37.9	106.6	1027	51.7%
					45	25.40	35.2	126.3	849	61.2%
						22.23	35.2	115.5	749	56.0%
					60	25.40	35.2	119.5	728	57.9%
						22.23	35.2	128.9	470	62.5%
HDPE, 10% EVA	1.55	0.29	595	5.67	0	25.40	53.6	47.0	636	22.1%
						22.23	48.7	52.2	707	24.6%
					15	25.40	36.4	53.6	857	25.2%
						22.23	36.4	50.8	743	23.9%
					30	25.40	36.4	81.5	1204	38.4%
						22.23	36.4	57.9	808	27.2%
					45	25.40	29.3	70.7	1070	33.3%
						22.23	29.3	71.7	1084	33.7%
					60	25.40	29.3	77.4	975	36.4%
						22.23	29.3	72.5	872	34.1%

Table B-13 - Macrofiber pullout testing results - 5 of 5

Fiber Description	Width (mm)	Thick (mm)	σ_f (MPa)	E_f (GPa)	ϕ (degrees)	Embedment Length (mm)	Matrix Strength (MPa)	P_{max} (N)	U_p (N-mm)	η_τ
100% PVDF	1.76	0.47	527	3.44	0	25.40	47.2	70.6	1033	17.8%
						22.23	47.2	52.8	824	13.3%
PP, 10% HDPE, 10% EVA	1.31	0.25	718	10.93	0	25.40	38.3	37.1	599	20.4%
						22.23	38.3	34.9	573	19.2%
					15	25.40	38.3	43.1	832	23.7%
						22.23	38.3	37.8	621	20.8%
					30	25.40	33.7	50.2	937	27.6%
						22.23	33.7	45.3	807	24.9%
Tuf-Strand SF	1.05	0.34	643	9.53	0	25.40	46.9	31.9	509	16.1%
						22.23	46.9	31.0	428	15.7%
					15	25.40	54.0	31.9	517	16.1%
						22.23	54.0	31.0	451	15.6%
					30	25.40	53.2	40.1	639	20.2%
						22.23	53.2	37.1	610	18.7%
					45	25.40	54.2	40.5	585	20.4%
						22.23	54.2	39.2	556	19.8%
					60	25.40	37.6	50.7	889	25.6%
						22.23	37.6	38.5	560	19.4%

Table B-14 - Microfiber pullout testing results - 1 of 2

Fiber Description	Width (mm)	Thick (mm)	σ_f (MPa)	E_f (GPa)	ϕ (degrees)	Embedment Length (mm)	Matrix Strength (MPa)	P_{max} (N)	U_p (N-mm)	η_τ
HDPE 5906	0.29	0.30	1062	15.95	0	19.05	46.8	11.3	127	23.8%
						15.88	57.1	13.6	152	28.5%
HDPE 1288	0.19	0.20	1841	28.47	0	19.05	47.7	20.2	220	55.8%
						15.88	47.7	10.8	114	29.9%
HDPE (5906), 10% PVDF, 20% MAH	0.25	0.25	1419	18.93	0	19.05	34.2	18.3	228	45.0%
						15.88	34.2	20.2	221	49.6%
					15	19.05	58.5	19.7	224	48.4%
						15.88	58.5	15.4	138	37.9%
					30	19.05	53.7	34.2	192	84.1%
						15.88	53.7	31.1	263	76.4%
					45	19.05	49.9	36.7	116	90.2%
						15.88	49.9	35.9	125	88.3%
					60	19.05	54.3	29.1	124	71.5%
						15.88	54.3	30.0	109	73.8%

Table B-15 - Microfiber pullout testing results - 2 of 2

Fiber Description	Width (mm)	Thick (mm)	σ_f (MPa)	E_f (GPa)	ϕ (degrees)	Embedment Length (mm)	Matrix Strength (MPa)	P_{max} (N)	U_p (N-mm)	η_τ
HDPE 5906, 10% EVA	0.28	0.27	1106	11.93	0	19.05	50.8	19.6	251	41.7%
						15.88	50.8	18.7	210	40.0%
					15	19.05	51.7	15.0	181	32.0%
						15.88	51.7	14.9	200	31.9%
					30	19.05	50.2	19.4	207	41.3%
						15.88	50.2	18.9	225	40.3%
					45	19.05	46.2	24.5	219	52.4%
						15.88	46.2	27.5	248	58.7%
					60	19.05	53.6	29.0	145	61.8%
						15.88	53.6	32.5	157	69.3%
Nylon	0.14	0.15	2322	5.70	0	19.05	42.1	4.0	34	13.7%
						15.88	42.1	3.8	39	13.1%
					15	19.05	42.1	8.9	65	30.5%
						15.88	42.1	6.9	64	23.7%
					30	19.05	47.7	8.5	95	29.2%
						15.88	47.7	5.9	88	20.2%
PVA	0.12	0.12	2092	28.66	0	19.05	49.0	14.7	15	74.0%
						15.88	49.0	13.1	13	65.7%

B.2 - 100% HDPE PULLOUT CURVES

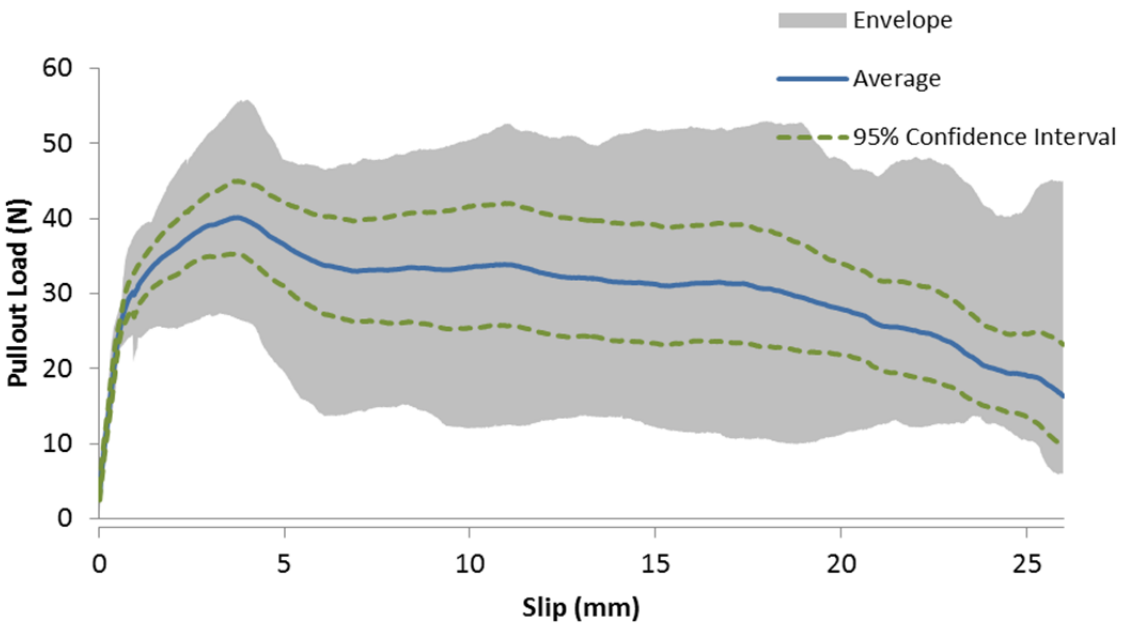

Figure B-19 - Load vs. slip curve for prototype macrofiber containing 100% HDPE: 0 degree inclination angle, 25.4 mm embedment length

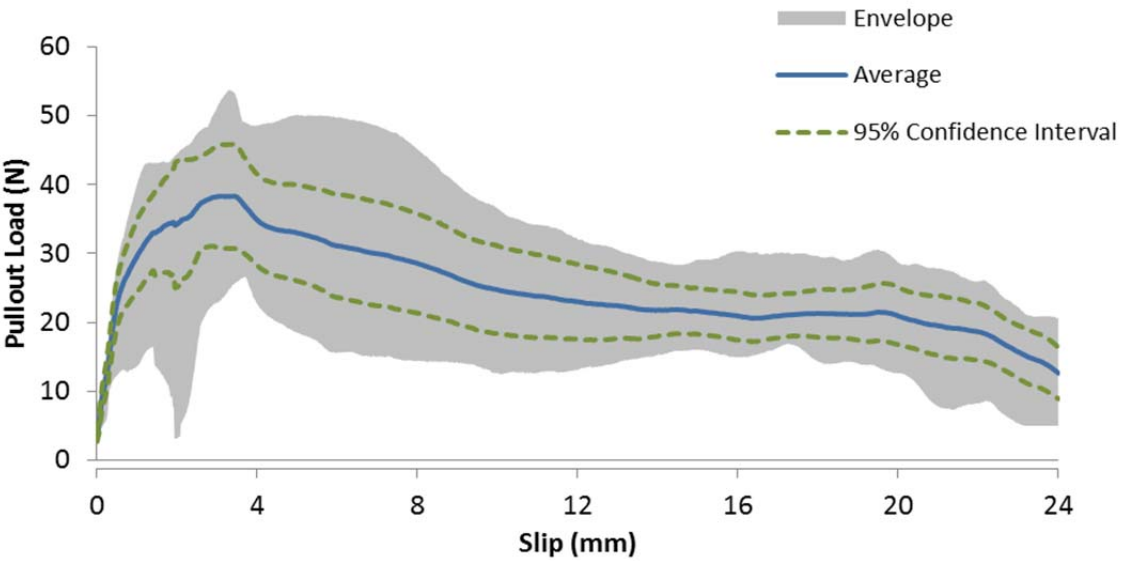

Figure B-20 - Load vs. slip curves for prototype macrofiber containing 100% HDPE: 0 degree inclination angle, 22.2 mm embedment length

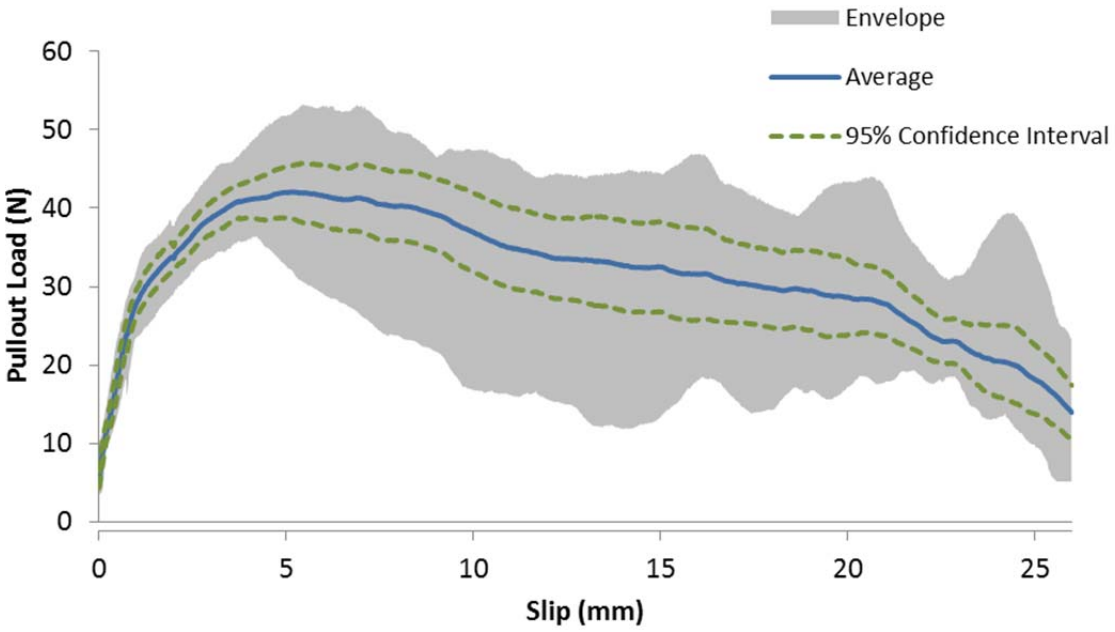

Figure B-21 - Load vs. slip curve for prototype macrofiber containing 100% HDPE: 15 degree inclination angle, 25.4 mm embedment length

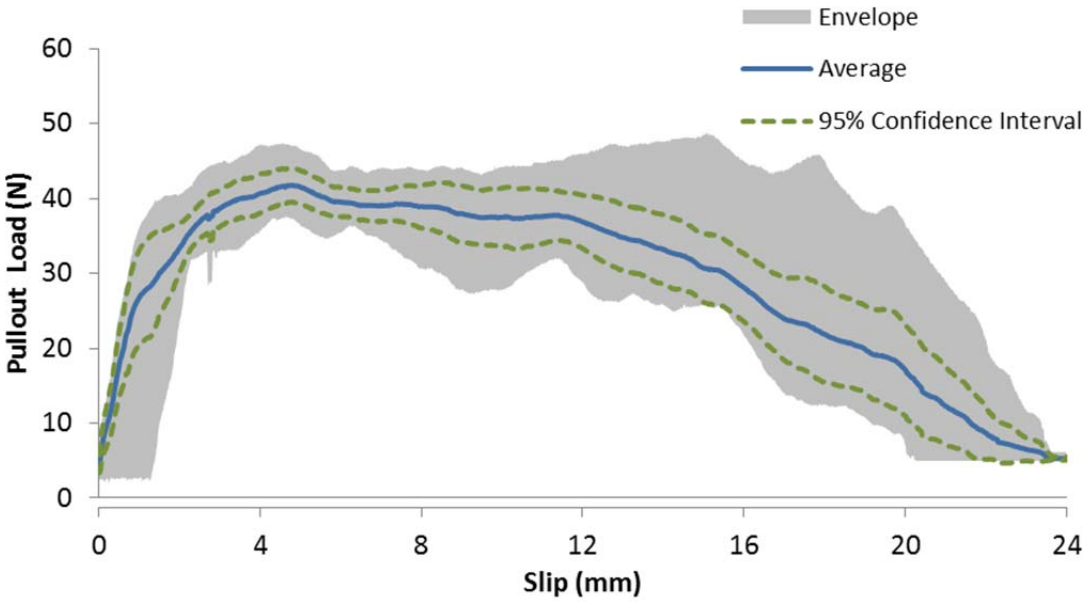

Figure B-22 - Load vs. slip curves for prototype macrofiber containing 100% HDPE: 15 degree inclination angle, 22.2 mm embedment length

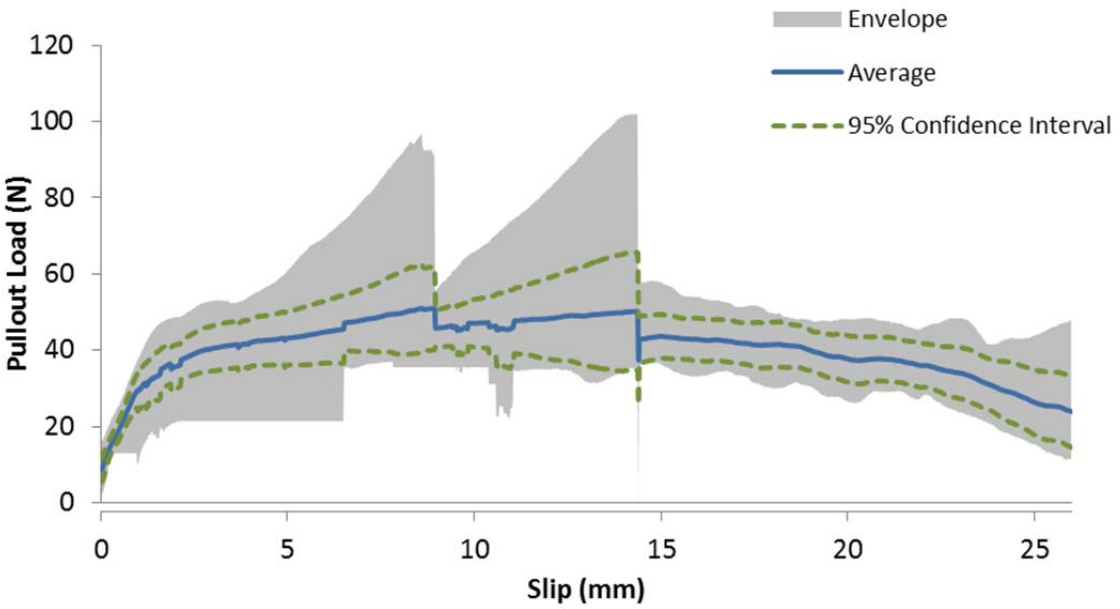

Figure B-23 - Load vs. slip curve for prototype macrofiber containing 100% HDPE: 30 degree inclination angle, 25.4 mm embedment length

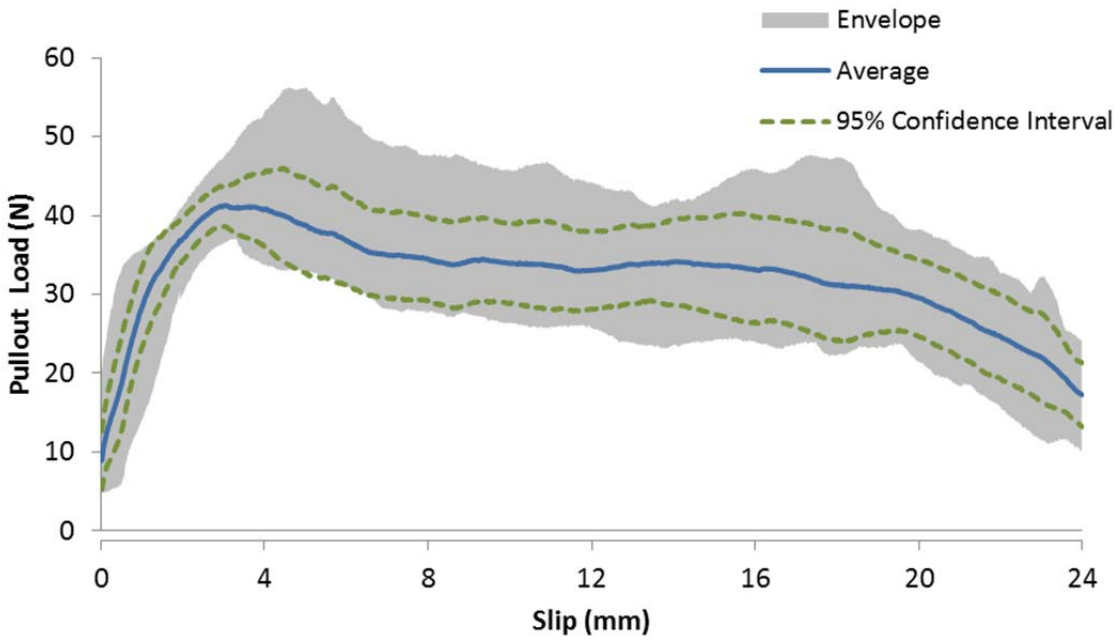

Figure B-24 - Load vs. slip curves for prototype macrofiber containing 100% HDPE: 30 degree inclination angle, 22.2 mm embedment length

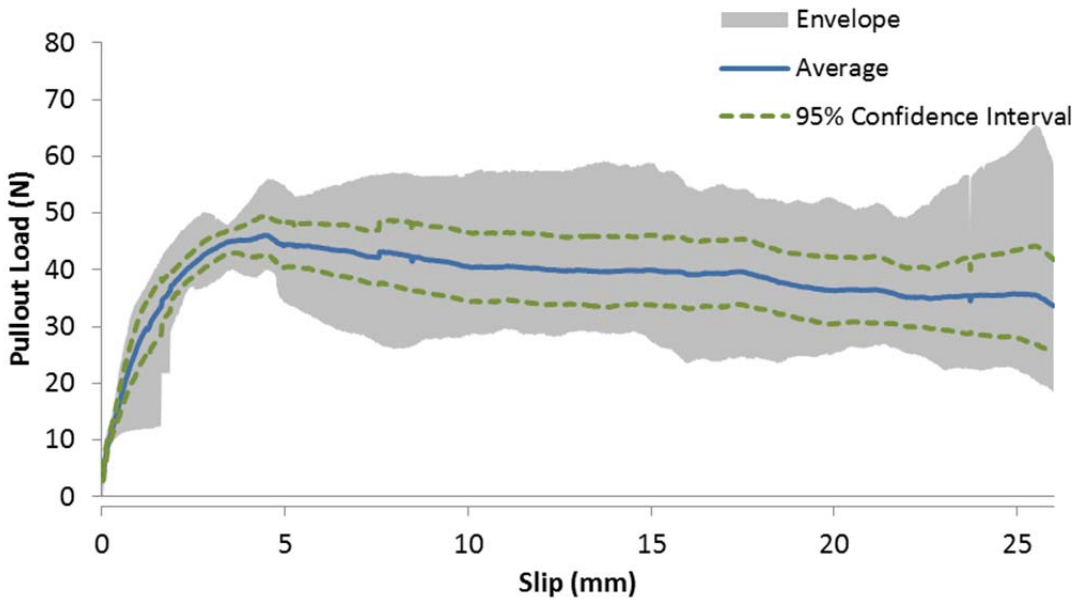

Figure B-25 - Load vs. slip curve for prototype macrofiber containing 100% HDPE: 45 degree inclination angle, 25.4 mm embedment length

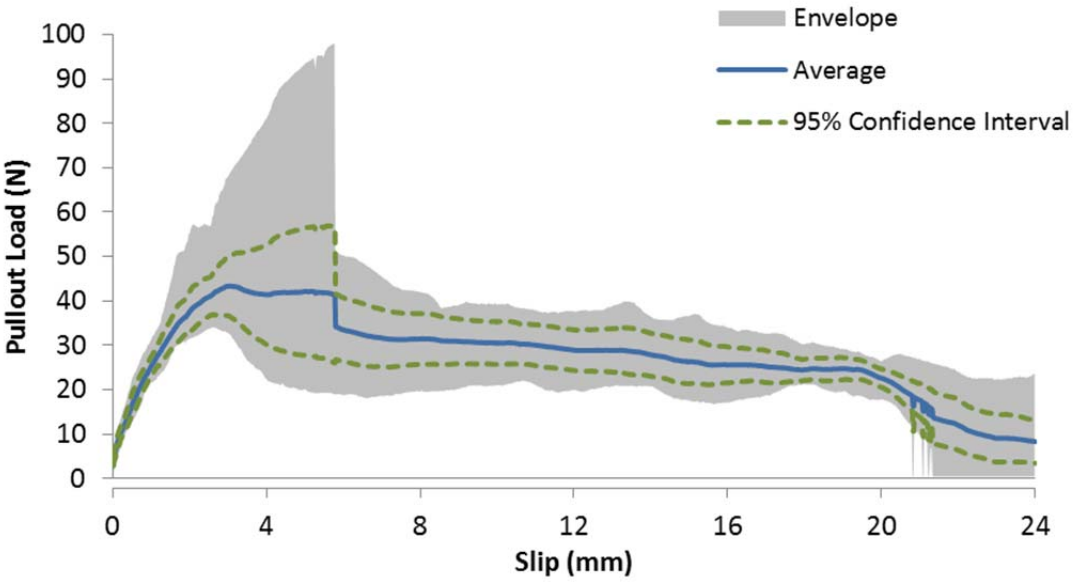

Figure B-26 - Load vs. slip curves for prototype macrofiber containing 100% HDPE: 45 degree inclination angle, 22.2 mm embedment length

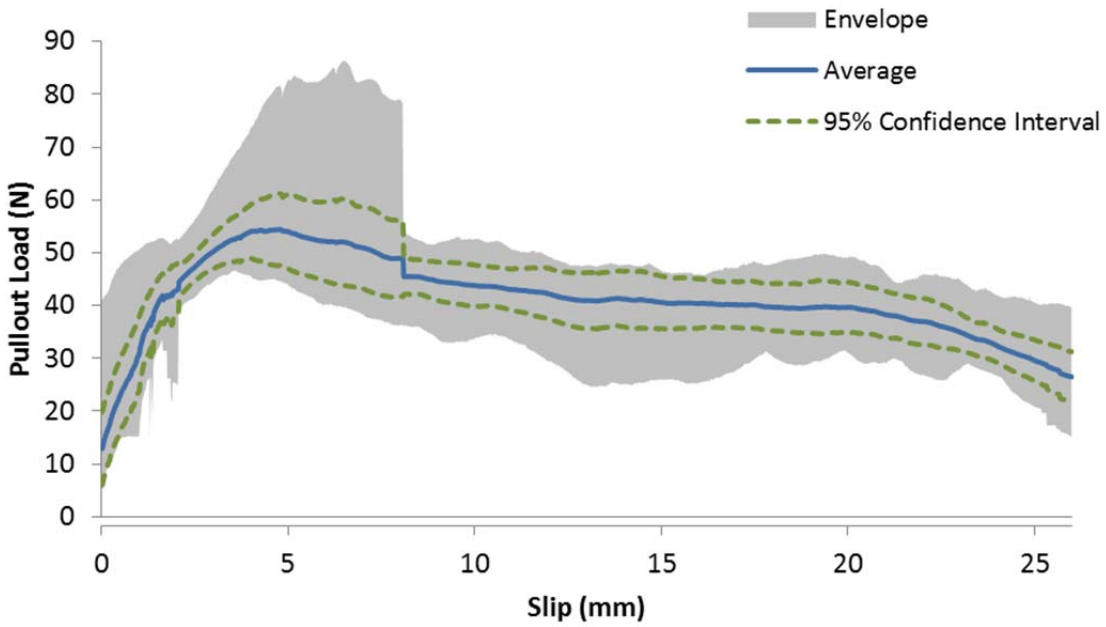

Figure B-27 - Load vs. slip curve for prototype macrofiber containing 100% HDPE: 60 degree inclination angle, 25.4 mm embedment length

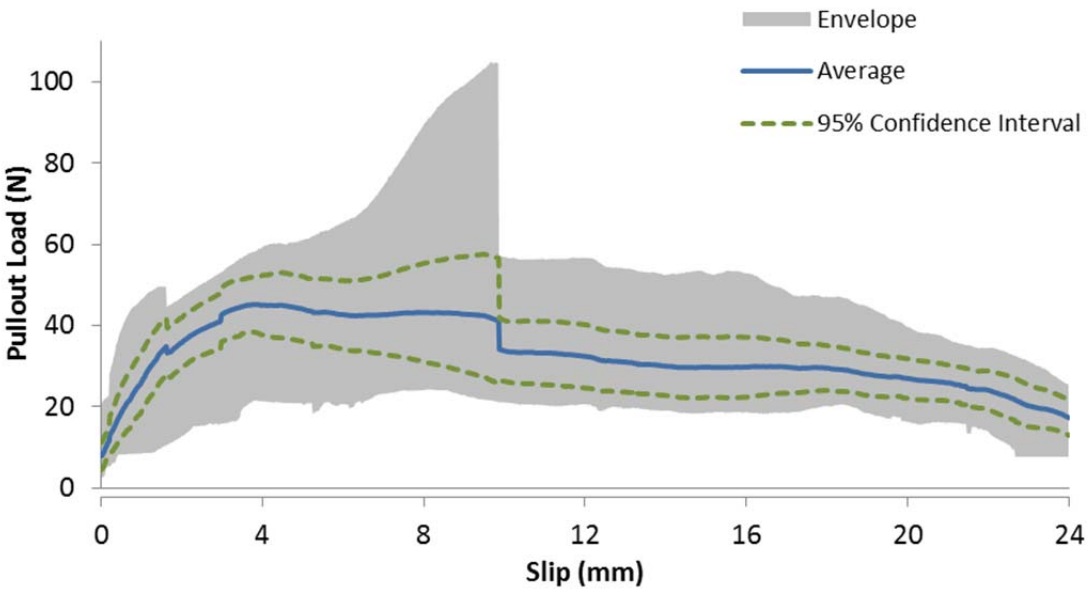

Figure B-28 - Load vs. slip curves for prototype macrofiber containing 100% HDPE: 60 degree inclination angle, 22.2 mm embedment length

B.3 - HDPE, 1% PVDF PULLOUT CURVES

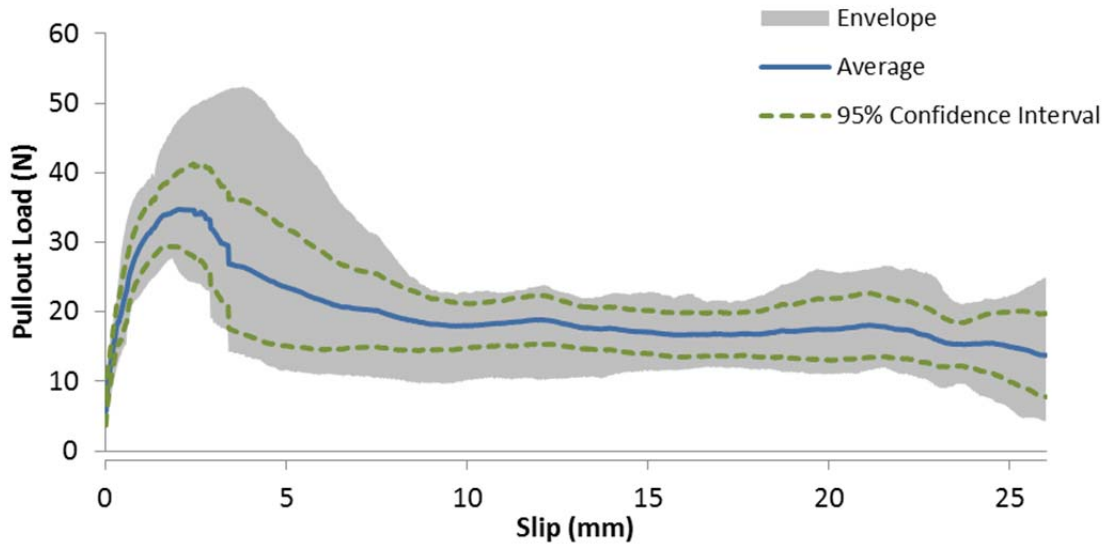

Figure B-29 - Load vs. slip curve for prototype macrofiber containing HDPE and 1% PVDF: 0 degree inclination angle, 25.4 mm embedment length

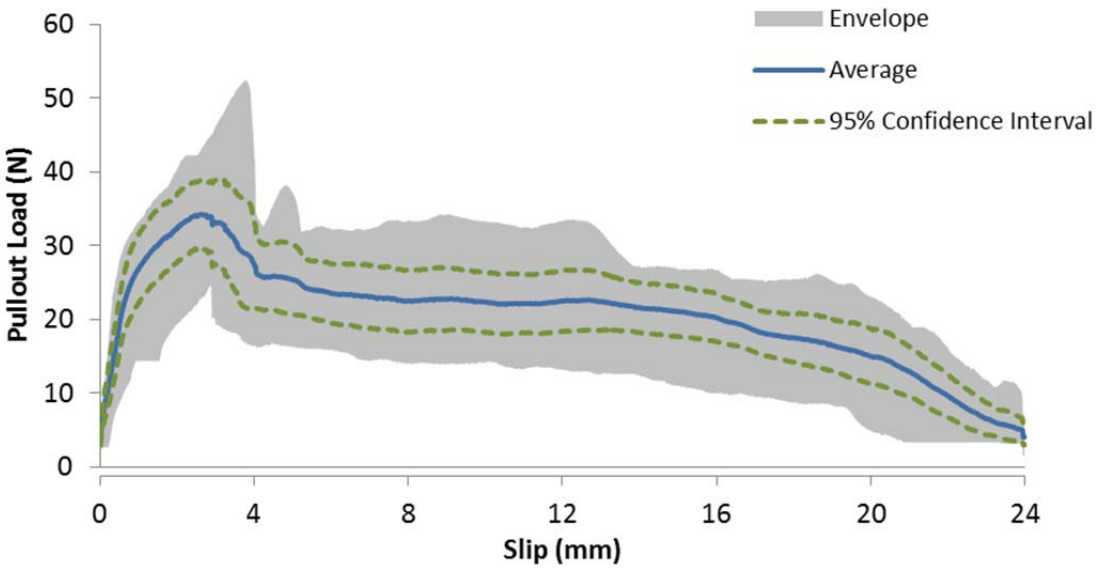

Figure B-30 - Load vs. slip curves for prototype macrofiber containing HDPE and 1% PVDF: 0 degree inclination angle, 22.2 mm embedment length

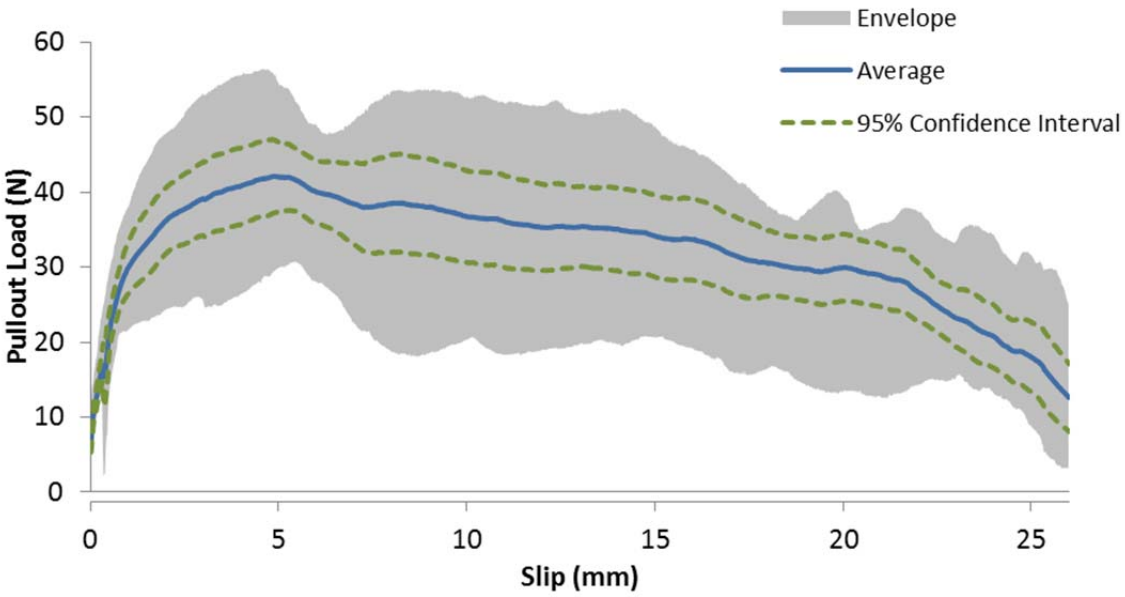

Figure B-31 - Load vs. slip curve for prototype macrofiber containing HDPE and 1% PVDF: 15 degree inclination angle, 25.4 mm embedment length

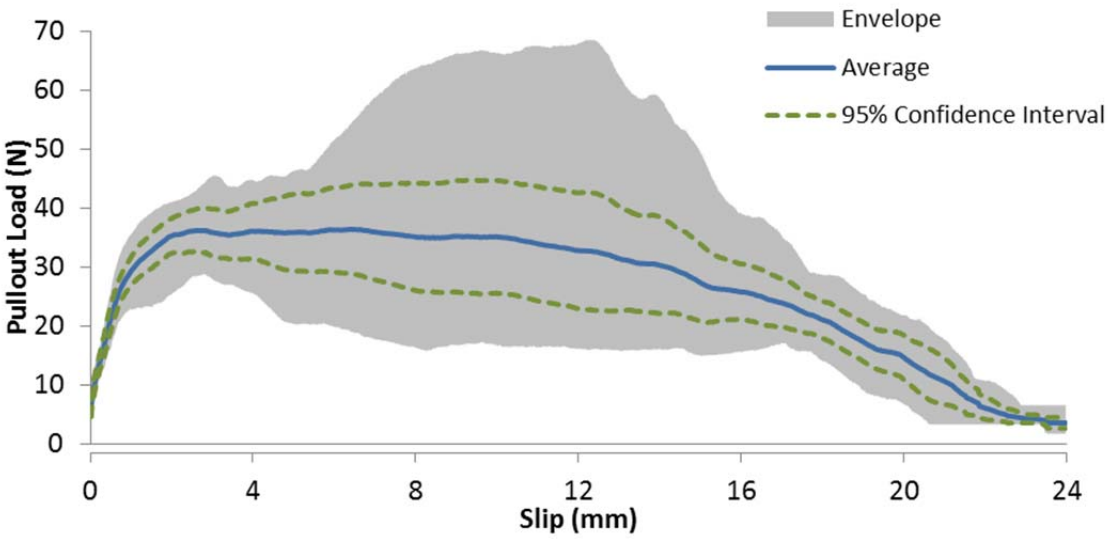

Figure B-32 - Load vs. slip curves for prototype macrofiber containing HDPE and 1% PVDF: 15 degree inclination angle, 22.2 mm embedment length

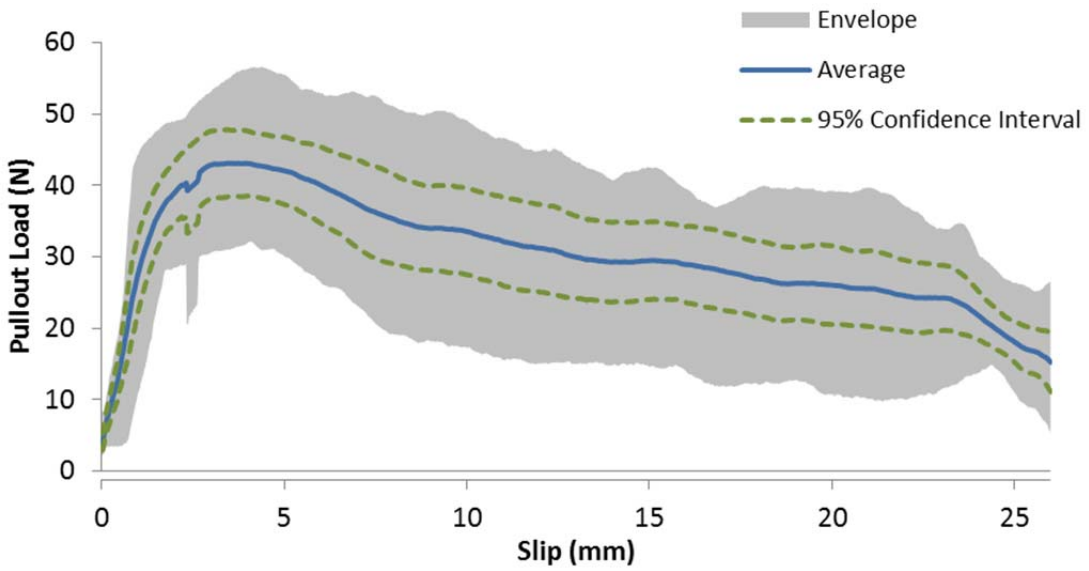

Figure B-33 - Load vs. slip curve for prototype macrofiber containing HDPE and 1% PVDF: 30 degree inclination angle, 25.4 mm embedment length

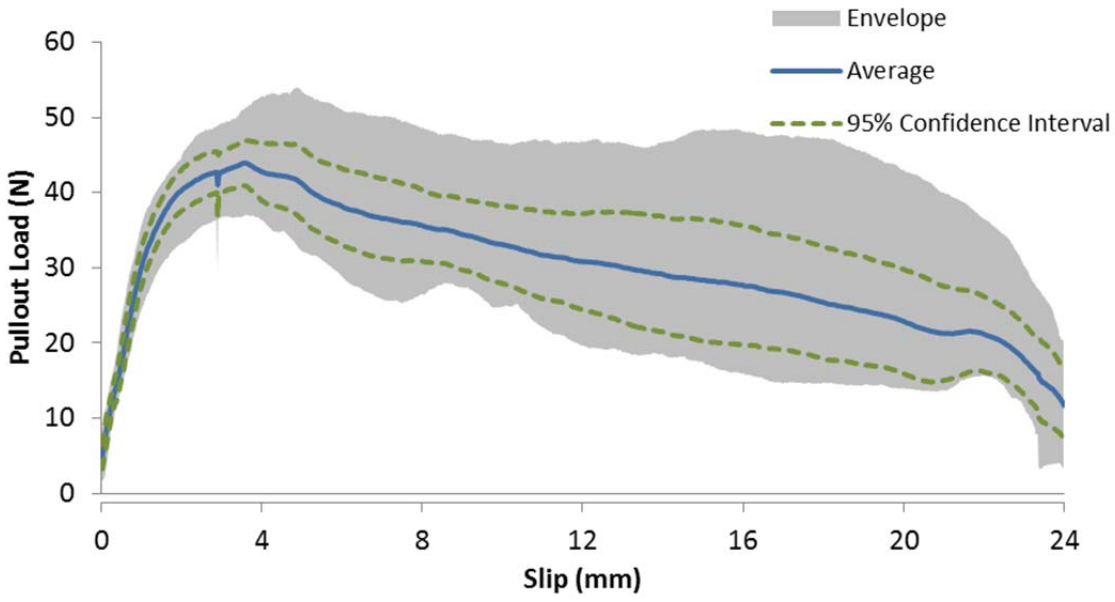

Figure B-34 - Load vs. slip curves for prototype macrofiber containing HDPE and 1% PVDF: 30 degree inclination angle, 22.2 mm embedment length

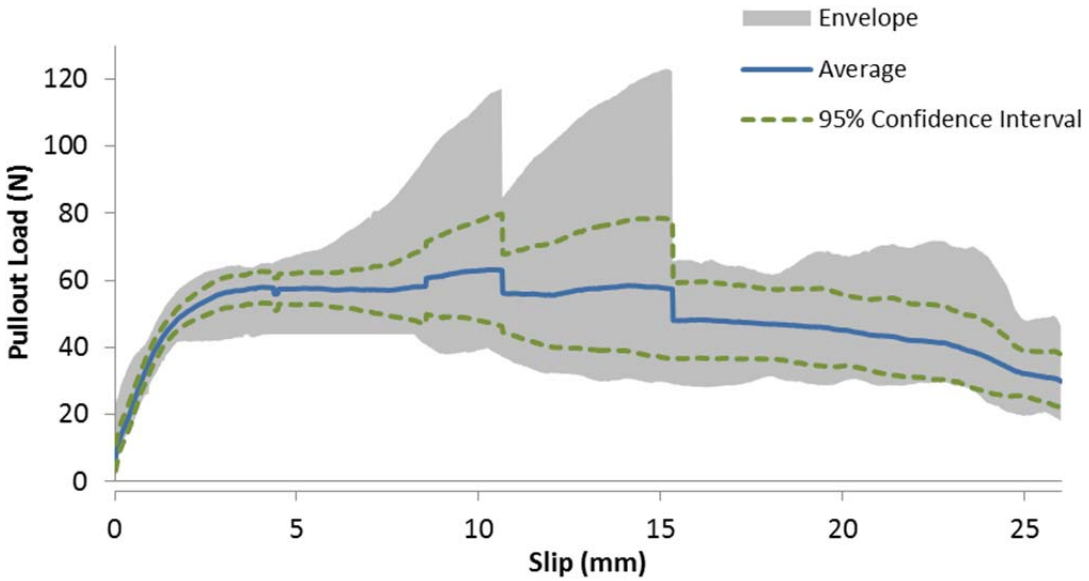

Figure B-35 - Load vs. slip curve for prototype macrofiber containing HDPE and 1% PVDF: 45 degree inclination angle, 25.4 mm embedment length

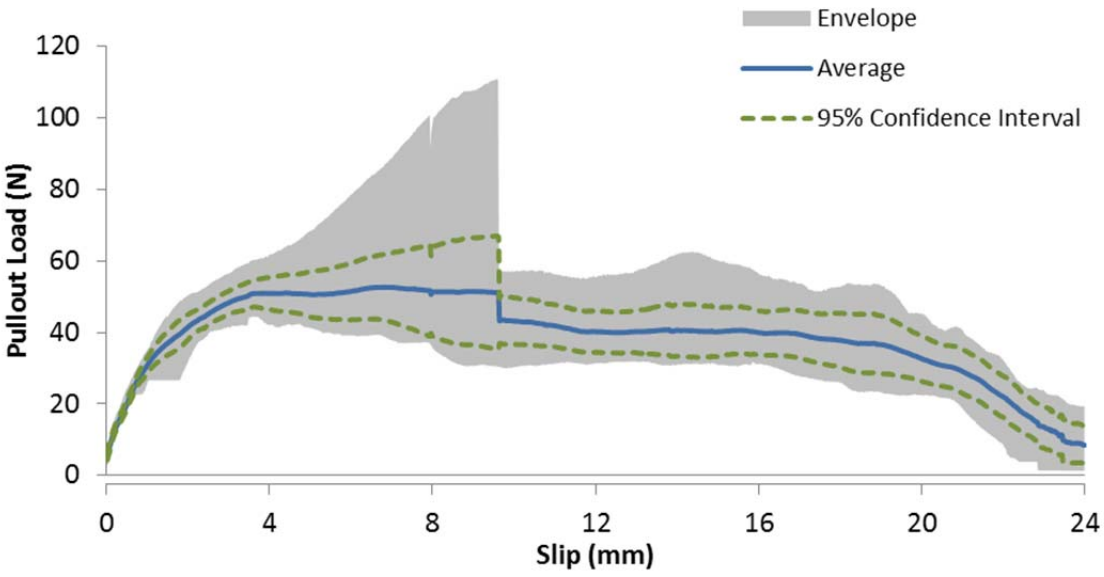

Figure B-36 - Load vs. slip curves for prototype macrofiber containing HDPE and 1% PVDF: 45 degree inclination angle, 22.2 mm embedment length

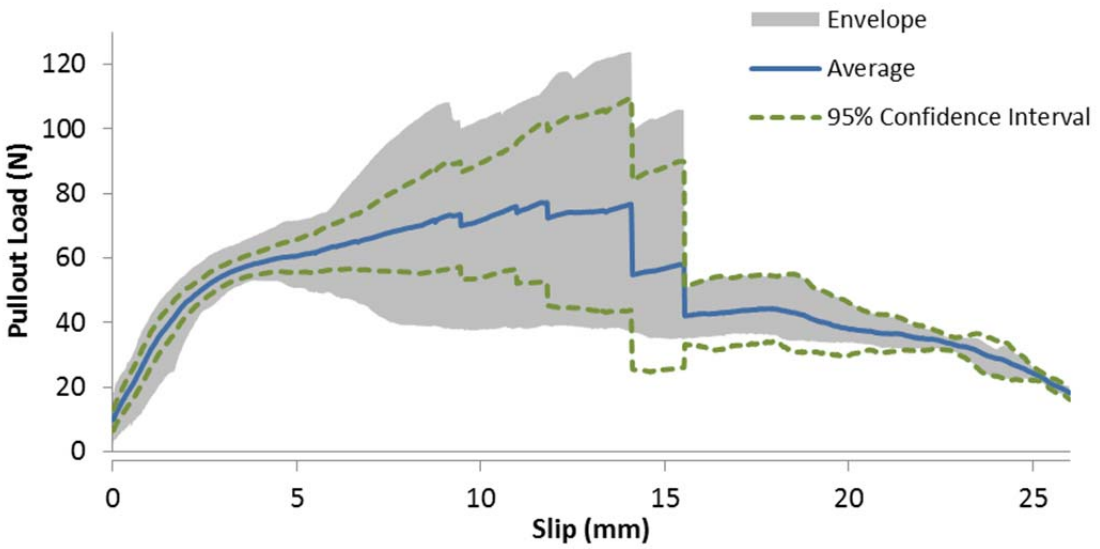

Figure B-37 - Load vs. slip curve for prototype macrofiber containing HDPE and 1% PVDF: 60 degree inclination angle, 25.4 mm embedment length

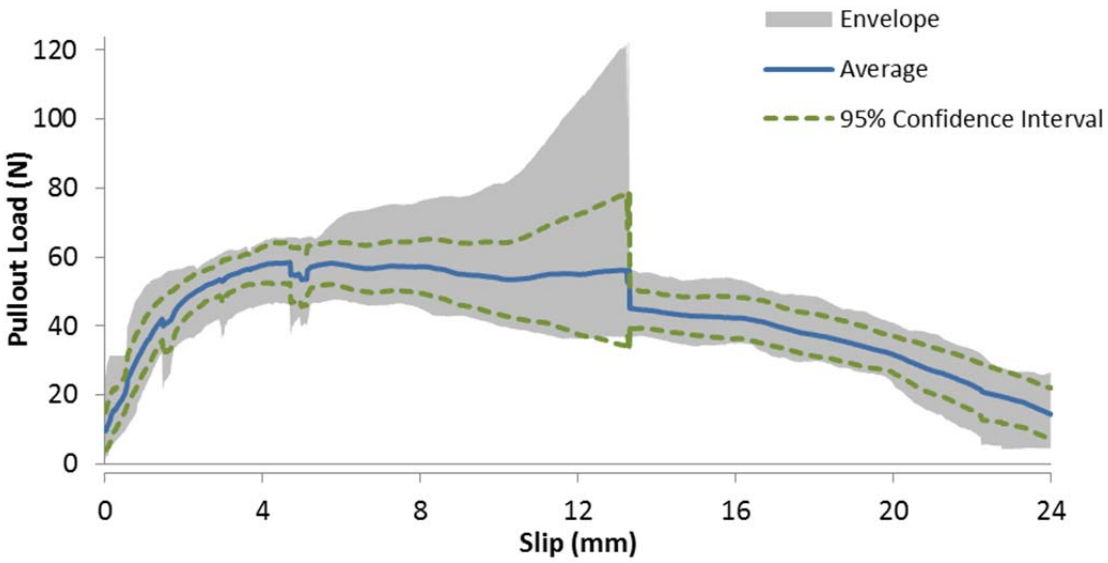

Figure B-38 - Load vs. slip curves for prototype macrofiber containing HDPE and 1% PVDF: 60 degree inclination angle, 22.2 mm embedment length

B.4 - HDPE, 3% PVDF PULLOUT CURVES

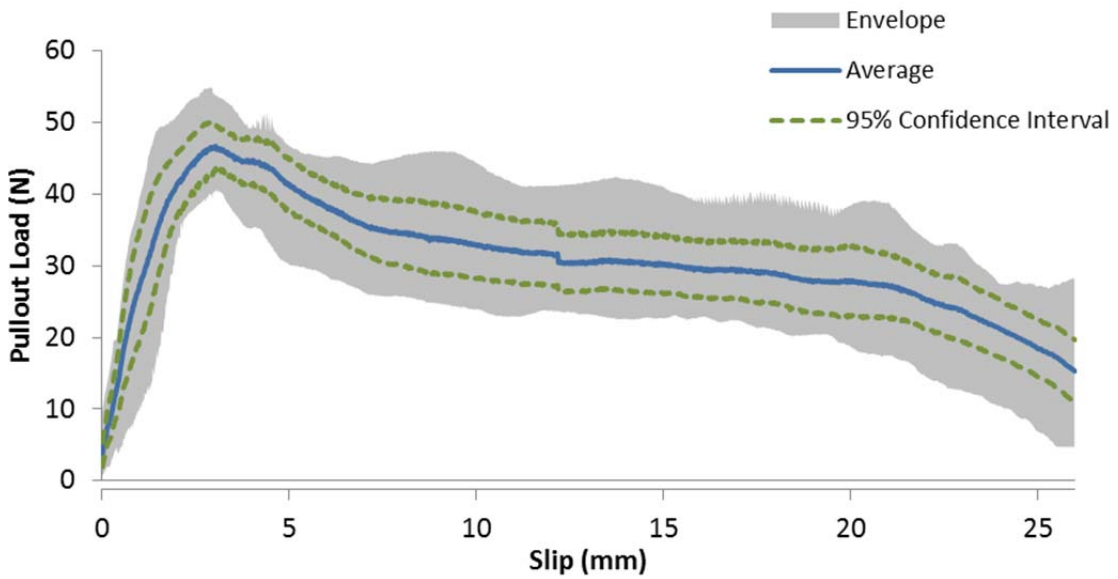

Figure B-39 - Load vs. slip curve for prototype macrofiber containing HDPE and 3% PVDF: 0 degree inclination angle, 25.4 mm embedment length

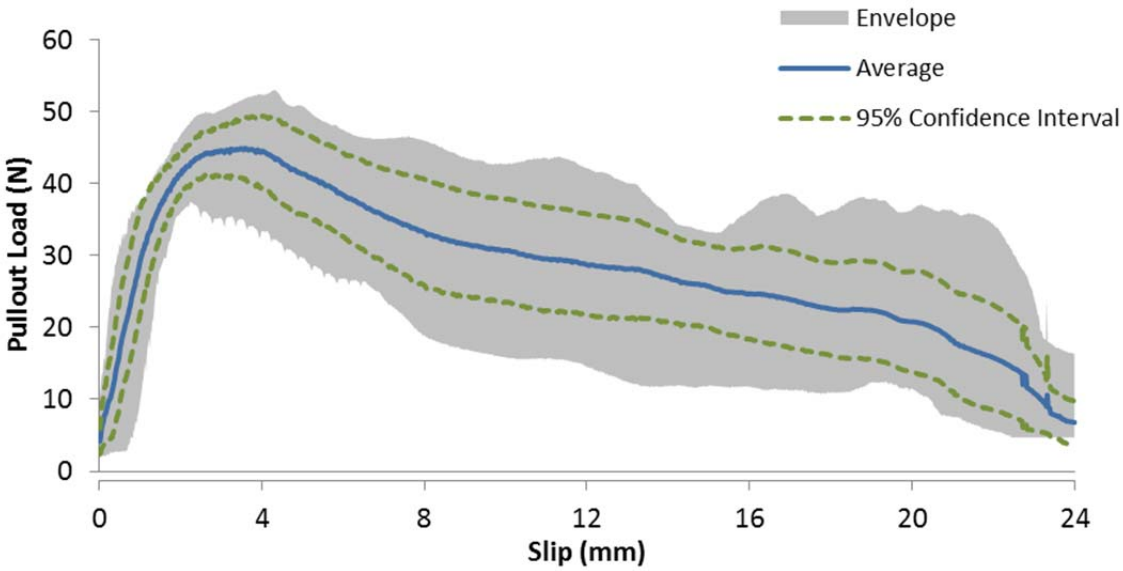

Figure B-40 - Load vs. slip curves for prototype macrofiber containing HDPE and 3% PVDF: 0 degree inclination angle, 22.2 mm embedment length

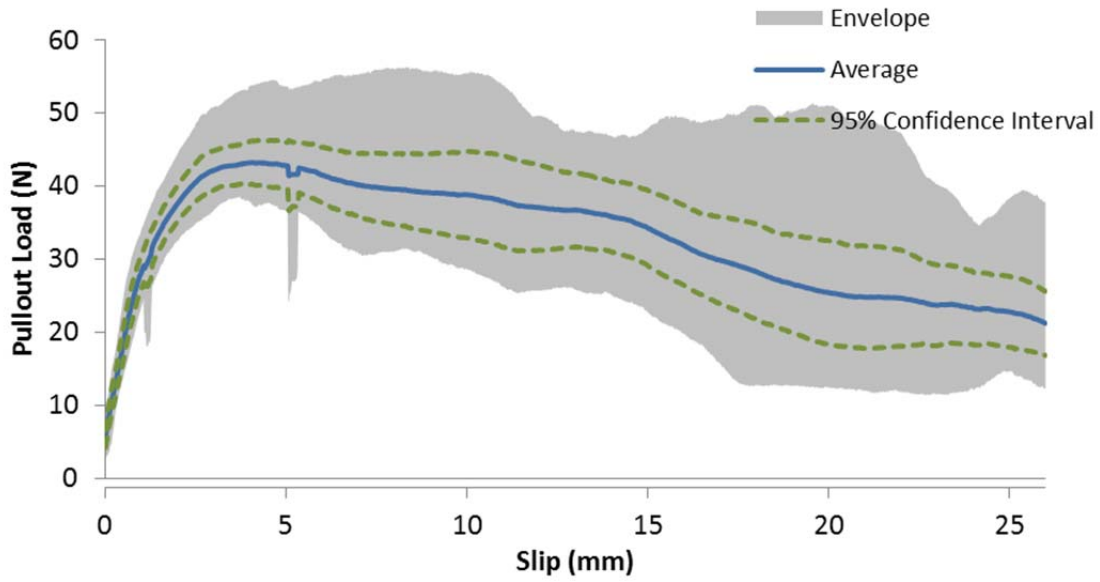

Figure B-41 - Load vs. slip curve for prototype macrofiber containing HDPE and 3% PVDF: 15 degree inclination angle, 25.4 mm embedment length

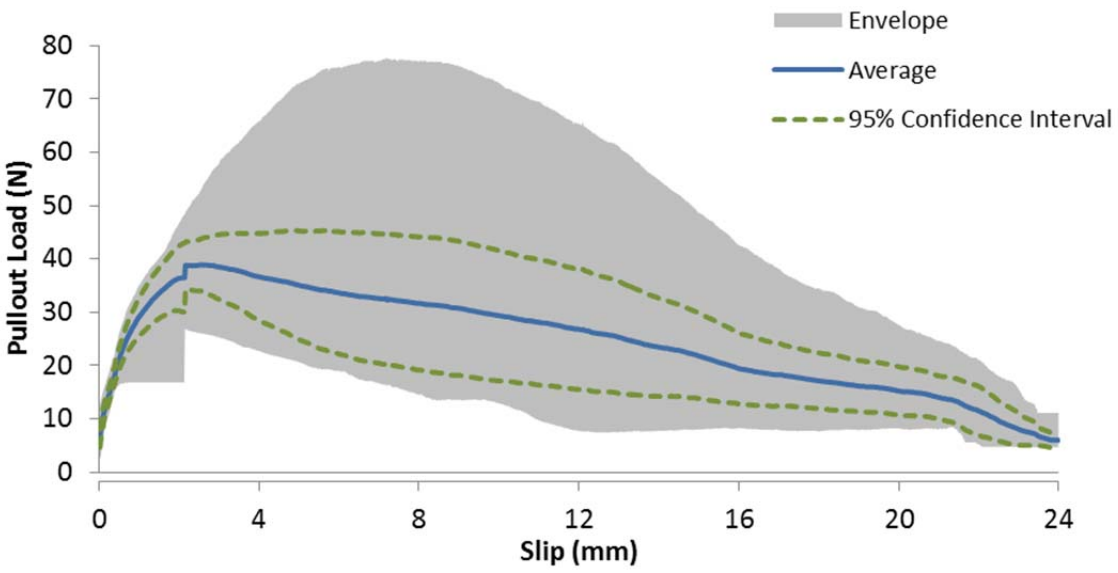

Figure B-42 - Load vs. slip curves for prototype macrofiber containing HDPE and 3% PVDF: 15 degree inclination angle, 22.2 mm embedment length

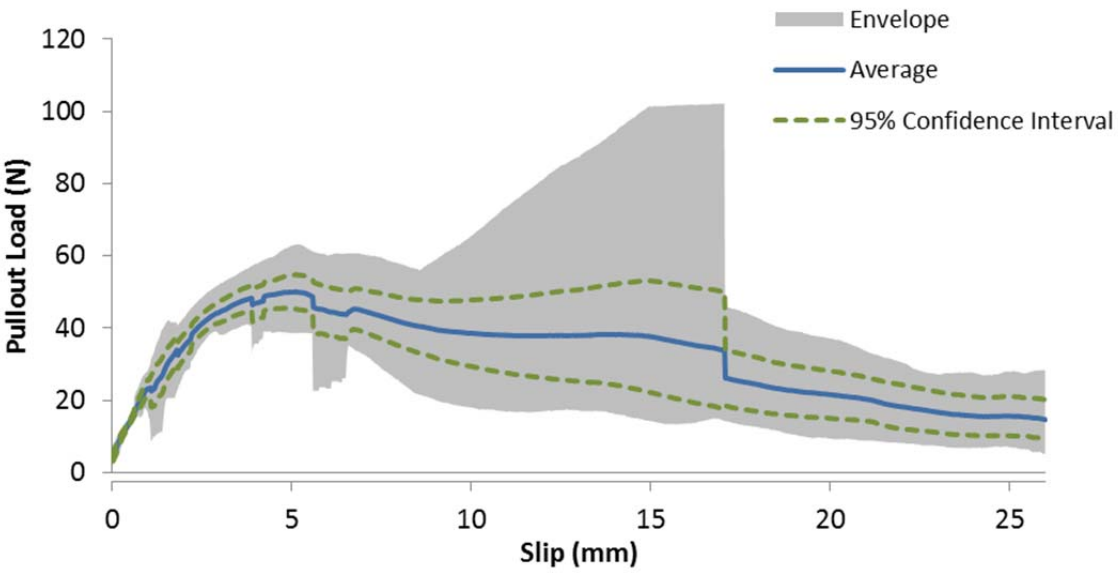

Figure B-43 - Load vs. slip curve for prototype macrofiber containing HDPE and 3% PVDF: 30 degree inclination angle, 25.4 mm embedment length

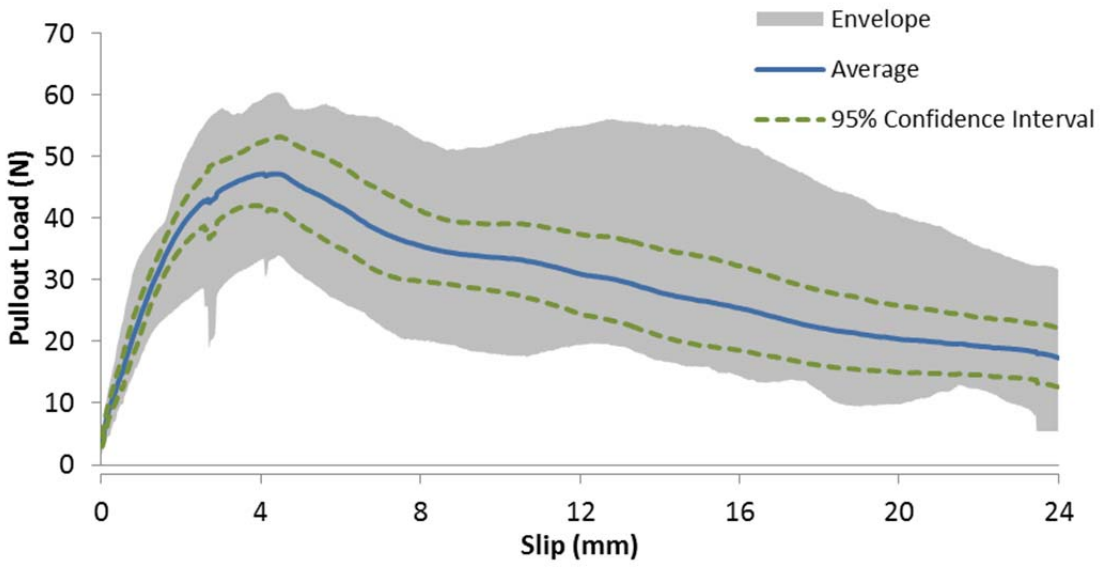

Figure B-44 - Load vs. slip curves for prototype macrofiber containing HDPE and 3% PVDF: 30 degree inclination angle, 22.2 mm embedment length

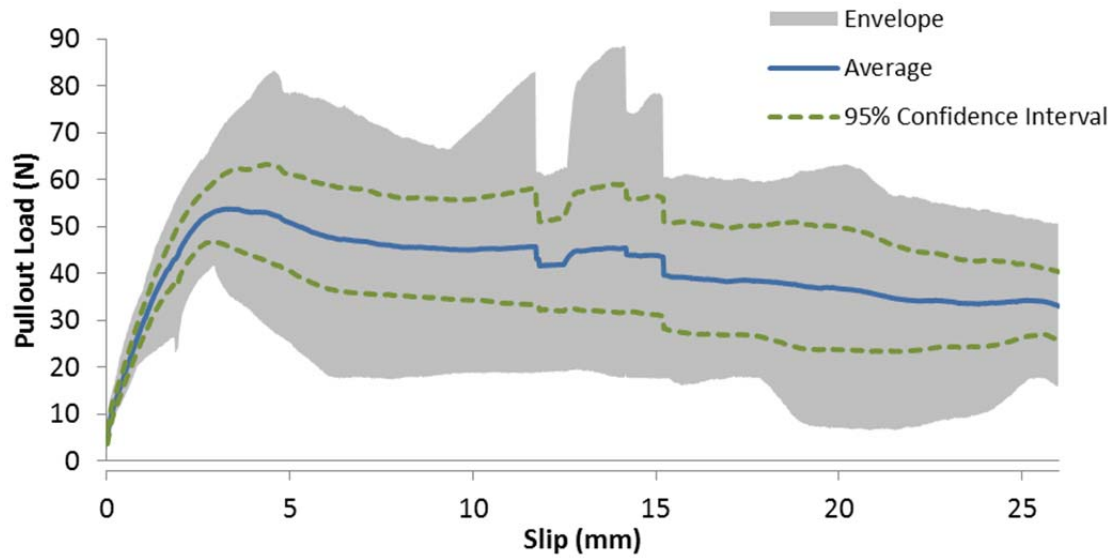

Figure B-45 - Load vs. slip curve for prototype macrofiber containing HDPE and 3% PVDF: 45 degree inclination angle, 25.4 mm embedment length

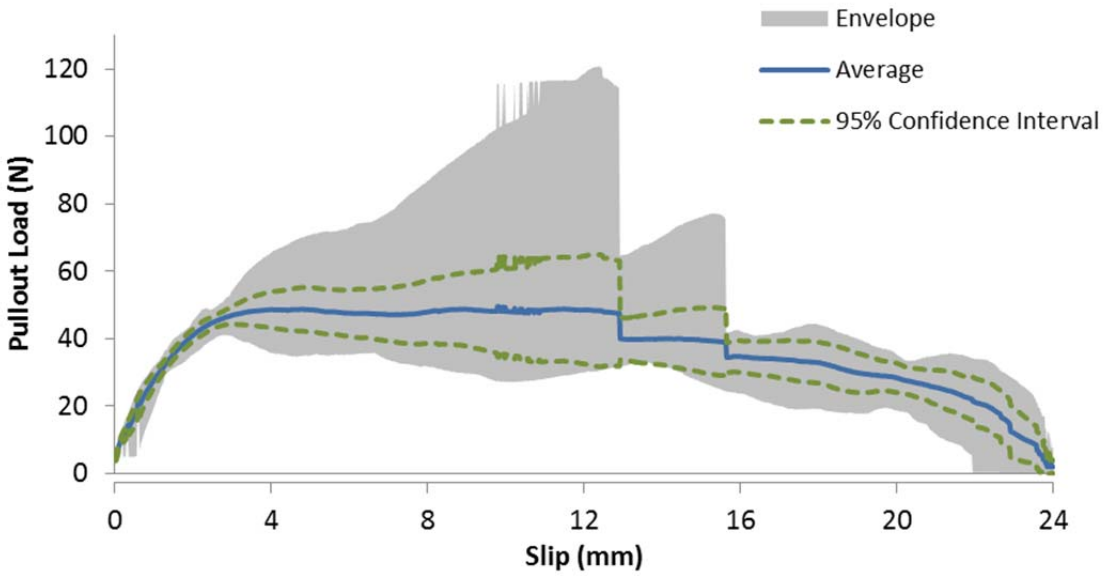

Figure B-46 - Load vs. slip curves for prototype macrofiber containing HDPE and 3% PVDF: 45 degree inclination angle, 22.2 mm embedment length

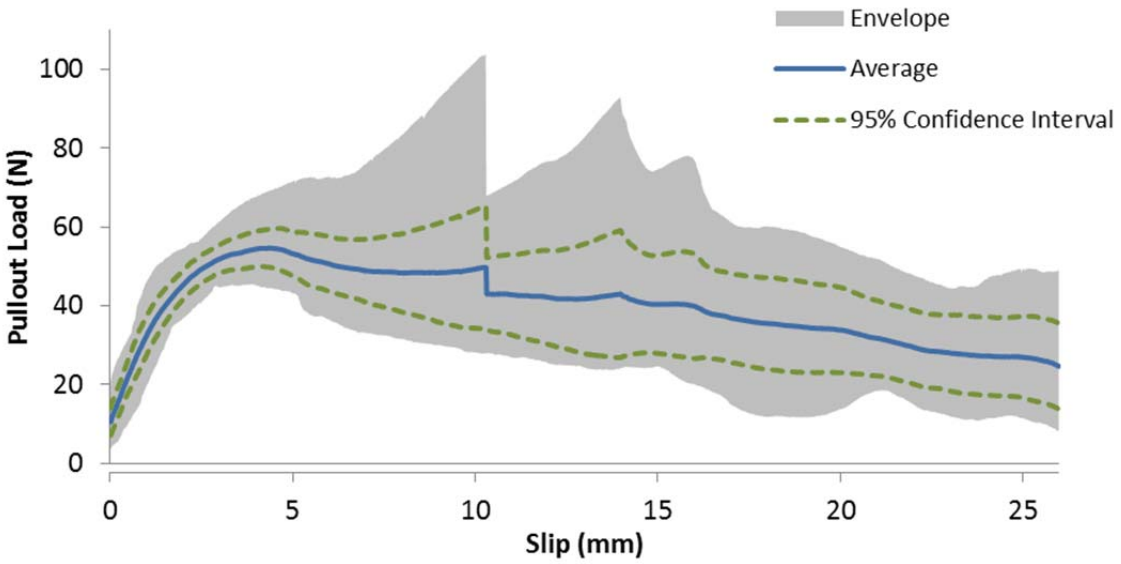

Figure B-47 - Load vs. slip curve for prototype macrofiber containing HDPE and 3% PVDF: 60 degree inclination angle, 25.4 mm embedment length

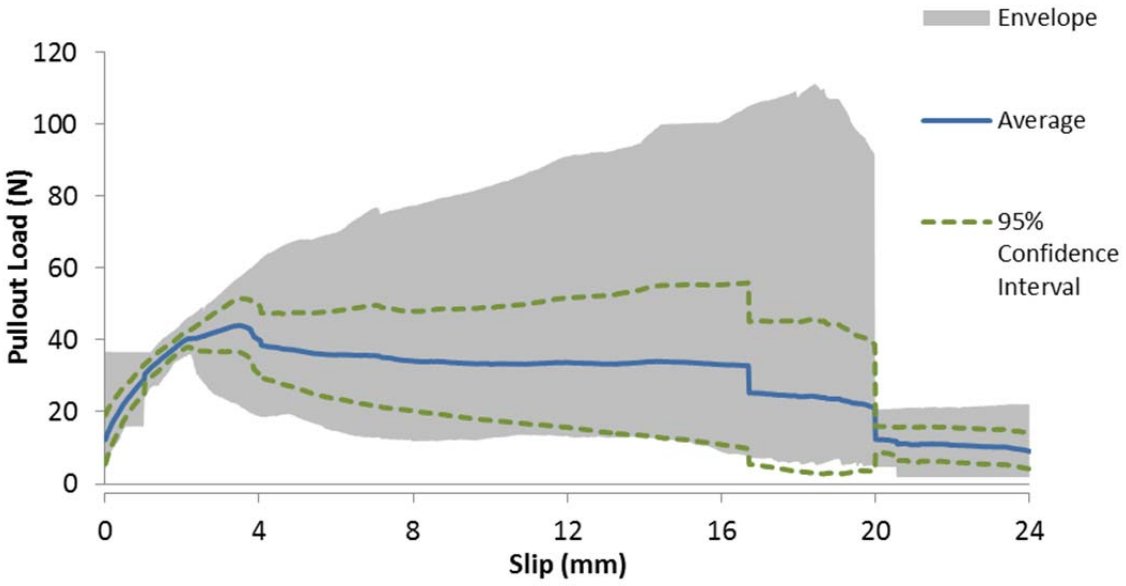

Figure B-48 - Load vs. slip curves for prototype macrofiber containing HDPE and 3% PVDF: 60 degree inclination angle, 22.2 mm embedment length

B.5 - HDPE, 5% PVDF, 10% MAH PULLOUT CURVES

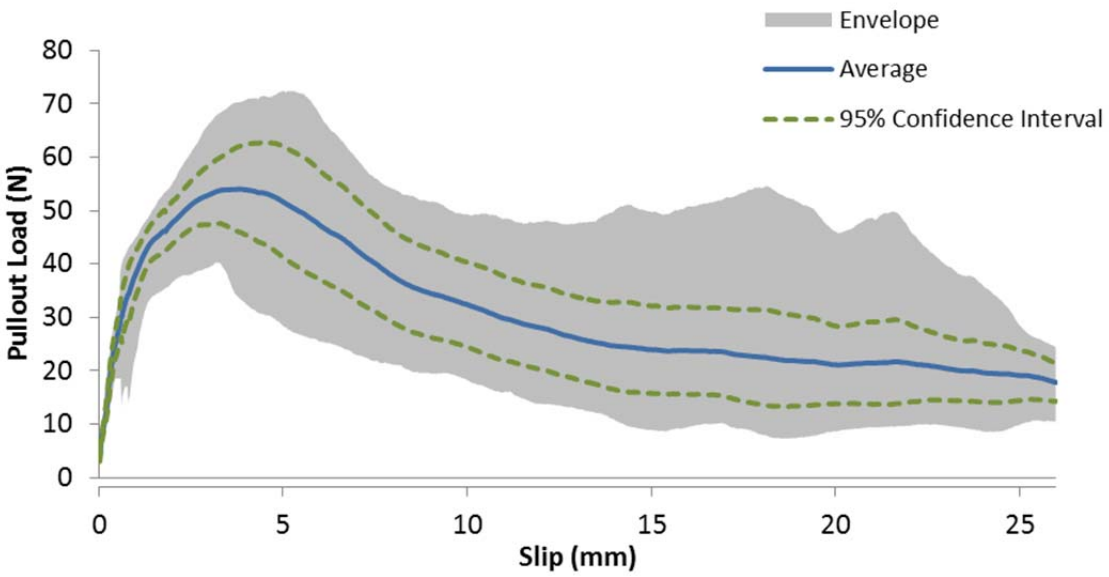

Figure B-49 - Load vs. slip curve for prototype macrofiber containing HDPE, 5% PVDF and 10% MAH: 0 degree inclination angle, 25.4 mm embedment length

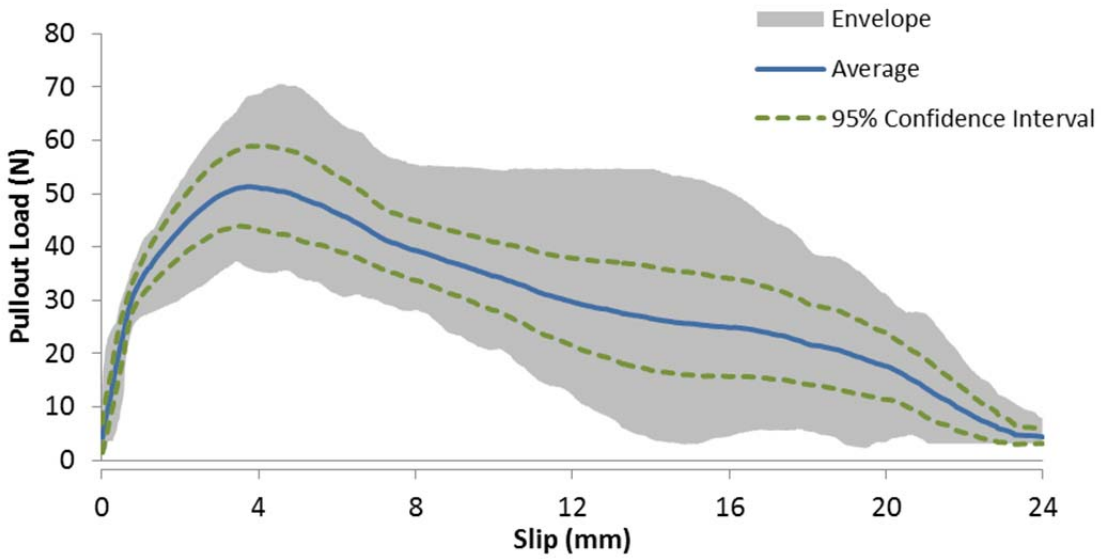

Figure B-50 - Load vs. slip curves for prototype macrofiber containing HDPE, 5% PVDF and 10% MAH: 0 degree inclination angle, 22.2 mm embedment length

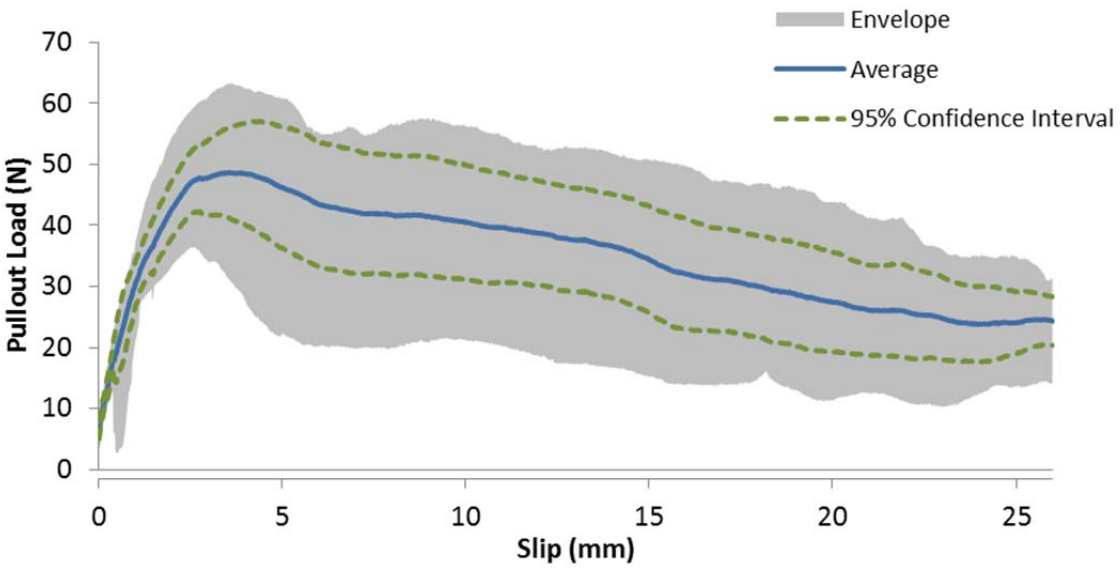

Figure B-51 - Load vs. slip curve for prototype macrofiber containing HDPE, 5% PVDF and 10% MAH: 15 degree inclination angle, 25.4 mm embedment length

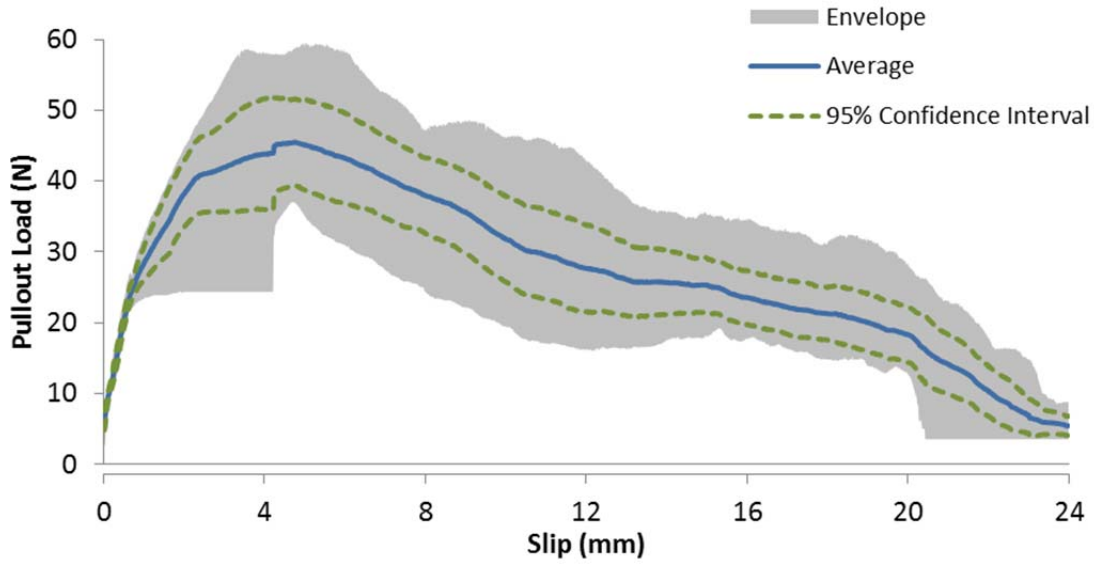

Figure B-52 - Load vs. slip curves for prototype macrofiber containing HDPE, 5% PVDF and 10% MAH: 15 degree inclination angle, 22.2 mm embedment length

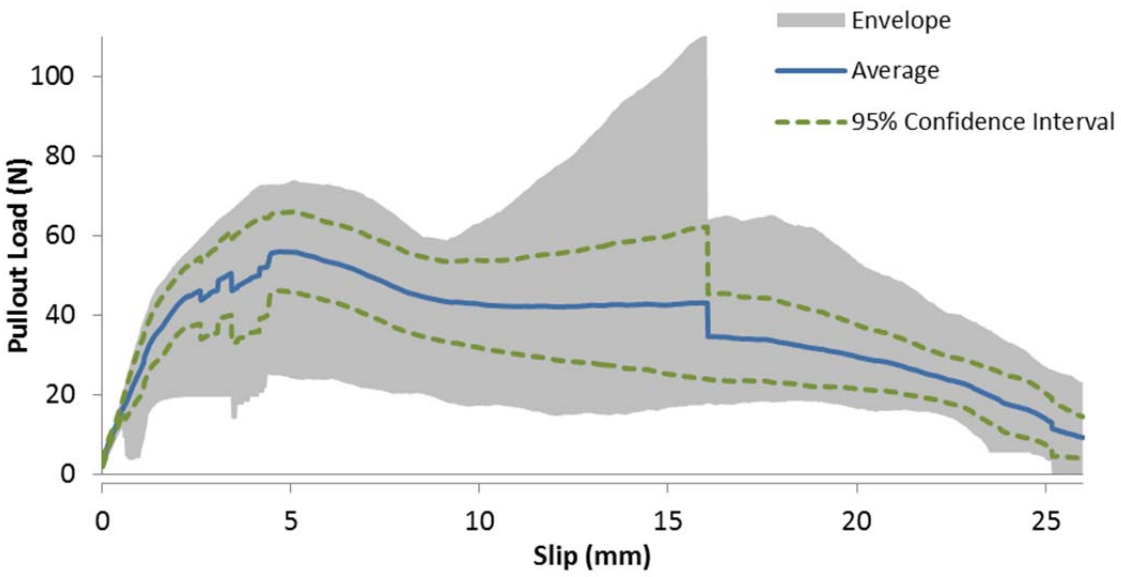

Figure B-53 - Load vs. slip curve for prototype macrofiber containing HDPE, 5% PVDF and 10% MAH: 30 degree inclination angle, 25.4 mm embedment length

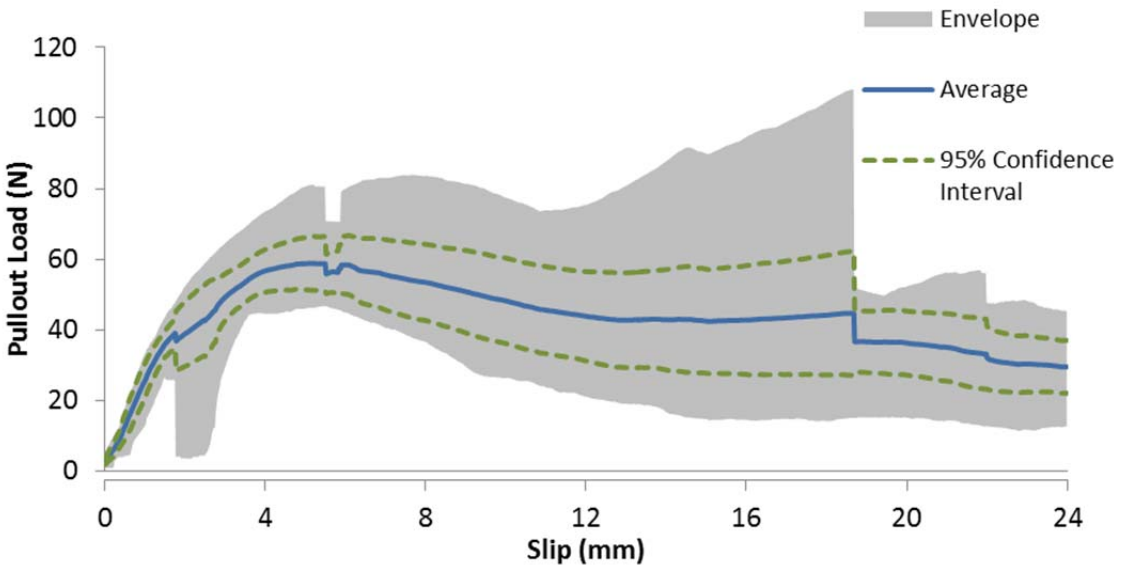

Figure B-54 - Load vs. slip curves for prototype macrofiber containing HDPE, 5% PVDF and 10% MAH: 30 degree inclination angle, 22.2 mm embedment length

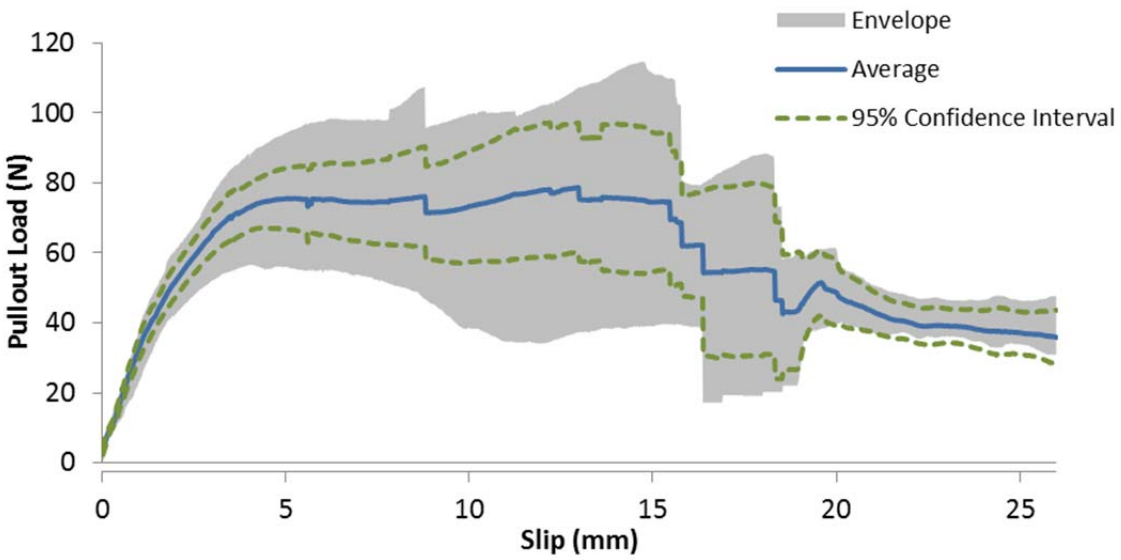

Figure B-55 - Load vs. slip curve for prototype macrofiber containing HDPE, 5% PVDF and 10% MAH: 45 degree inclination angle, 25.4 mm embedment length

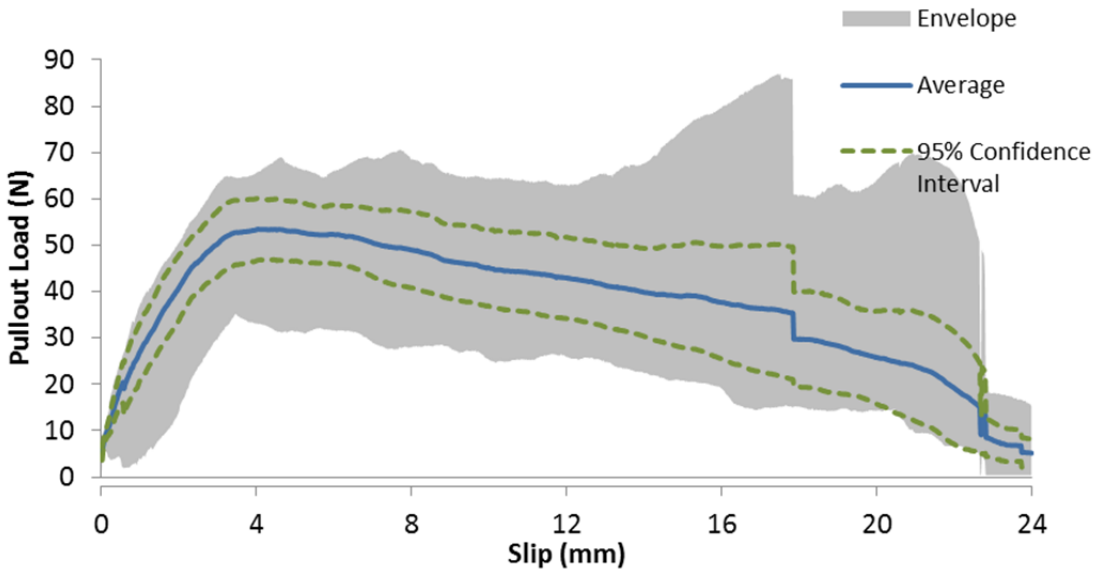

Figure B-56 - Load vs. slip curves for prototype macrofiber containing HDPE, 5% PVDF and 10% MAH: 45 degree inclination angle, 22.2 mm embedment length

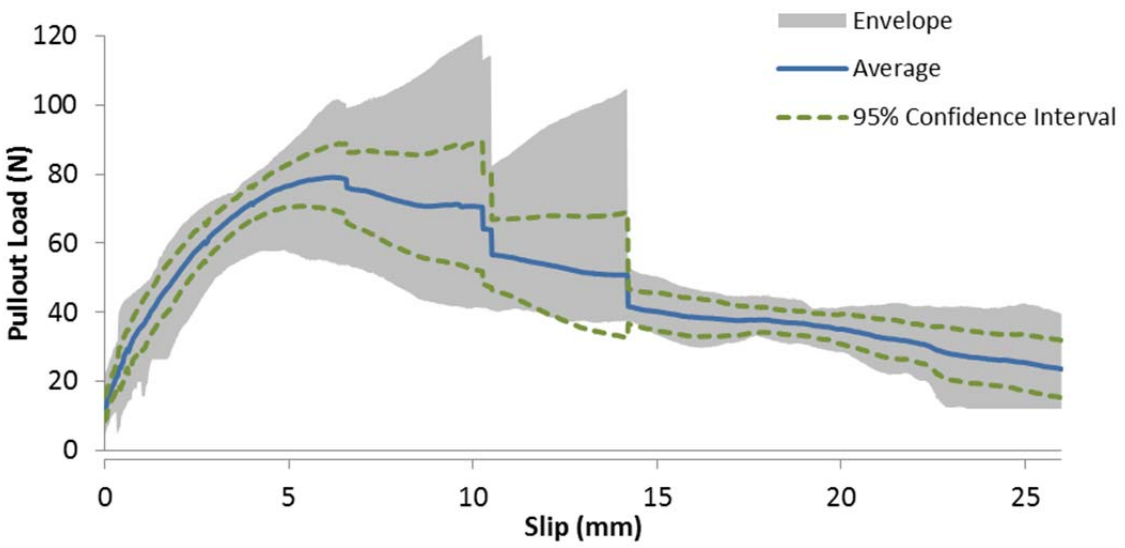

Figure B-57 - Load vs. slip curve for prototype macrofiber containing HDPE, 5% PVDF and 10% MAH: 60 degree inclination angle, 25.4 mm embedment length

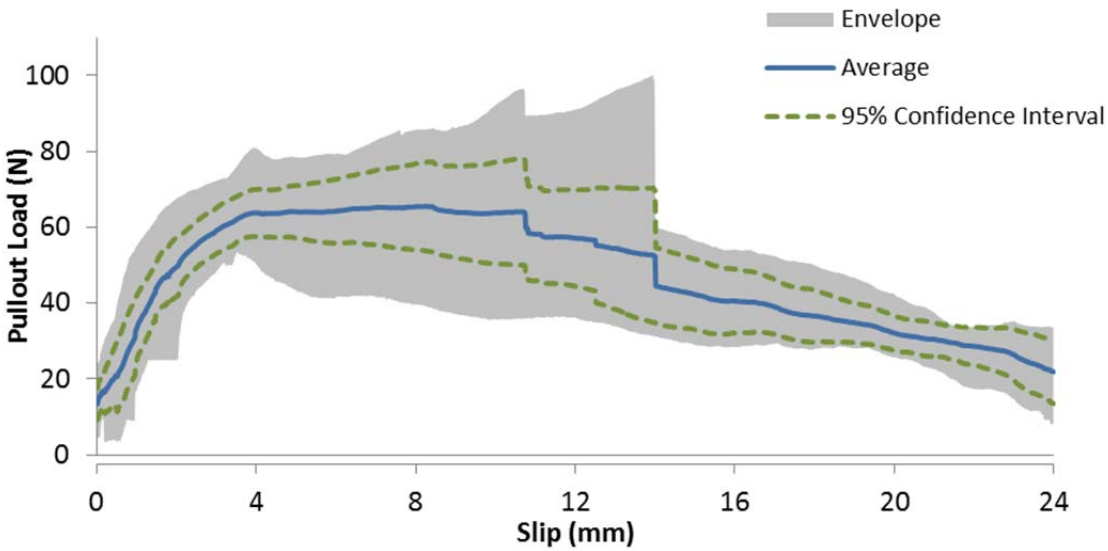

Figure B-58 - Load vs. slip curves for prototype macrofiber containing HDPE, 5% PVDF and 10% MAH: 60 degree inclination angle, 22.2 mm embedment length

B.6 - HDPE, 7% PVDF, 10% MAH PULLOUT CURVES

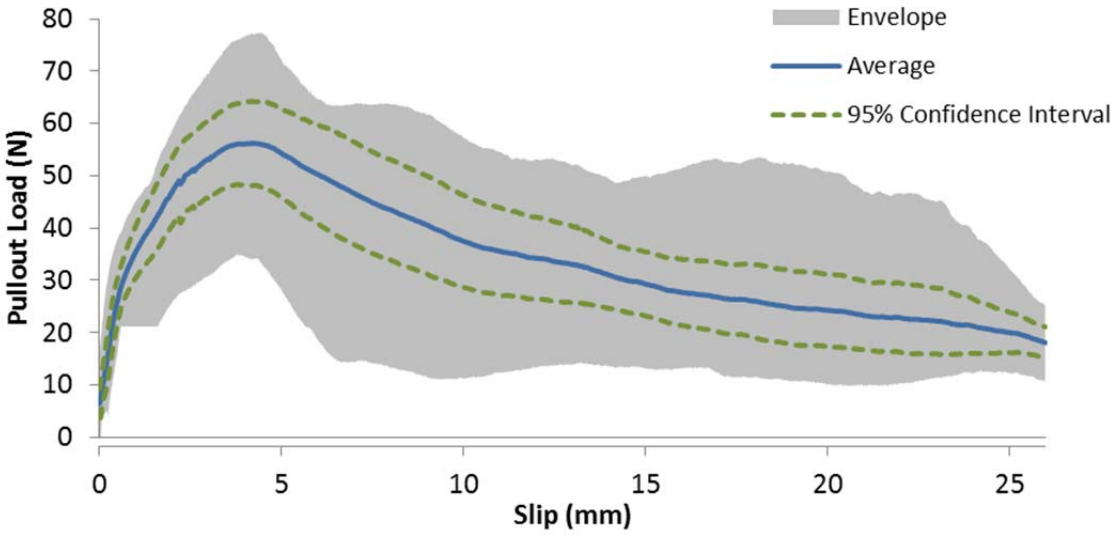

Figure B-59 - Load vs. slip curve for prototype macrofiber containing HDPE, 7% PVDF and 10% MAH: 0 degree inclination angle, 25.4 mm embedment length

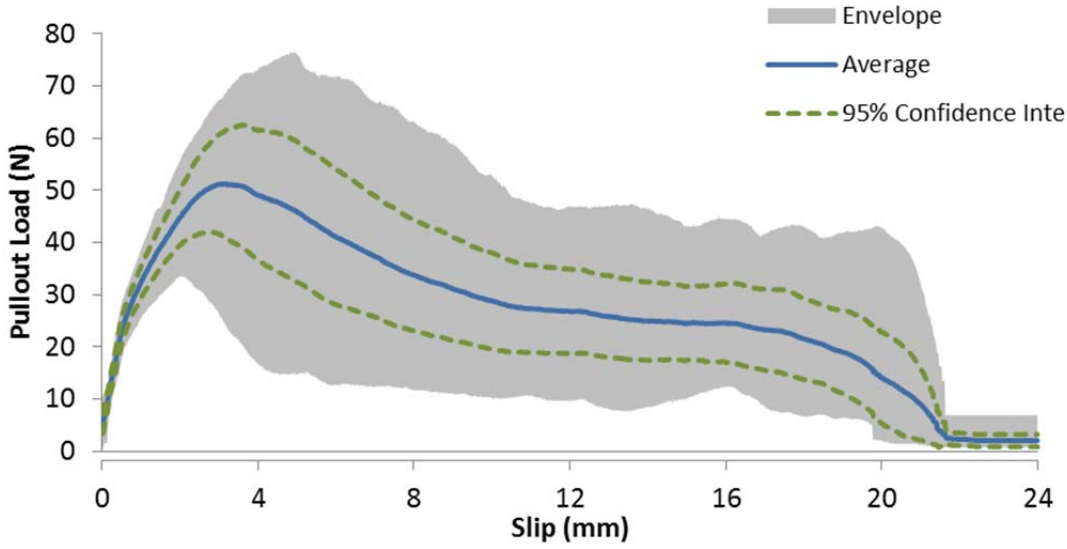

Figure B-60 - Load vs. slip curves for prototype macrofiber containing HDPE, 7% PVDF and 10% MAH: 0 degree inclination angle, 22.2 mm embedment length

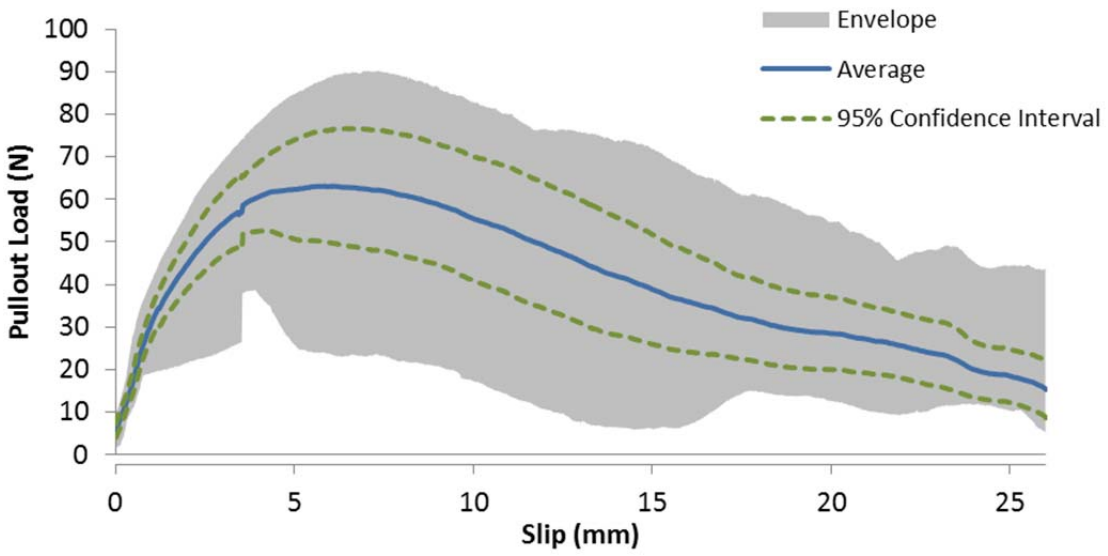

Figure B-61 - Load vs. slip curve for prototype macrofiber containing HDPE, 7% PVDF and 10% MAH: 15 degree inclination angle, 25.4 mm embedment length

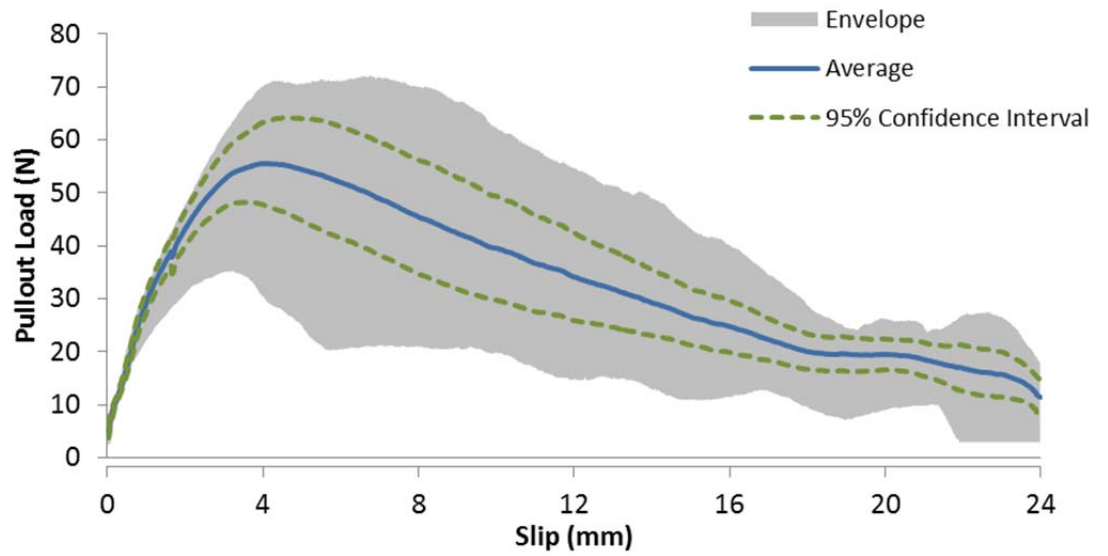

Figure B-62 - Load vs. slip curves for prototype macrofiber containing HDPE, 7% PVDF and 10% MAH: 15 degree inclination angle, 22.2 mm embedment length

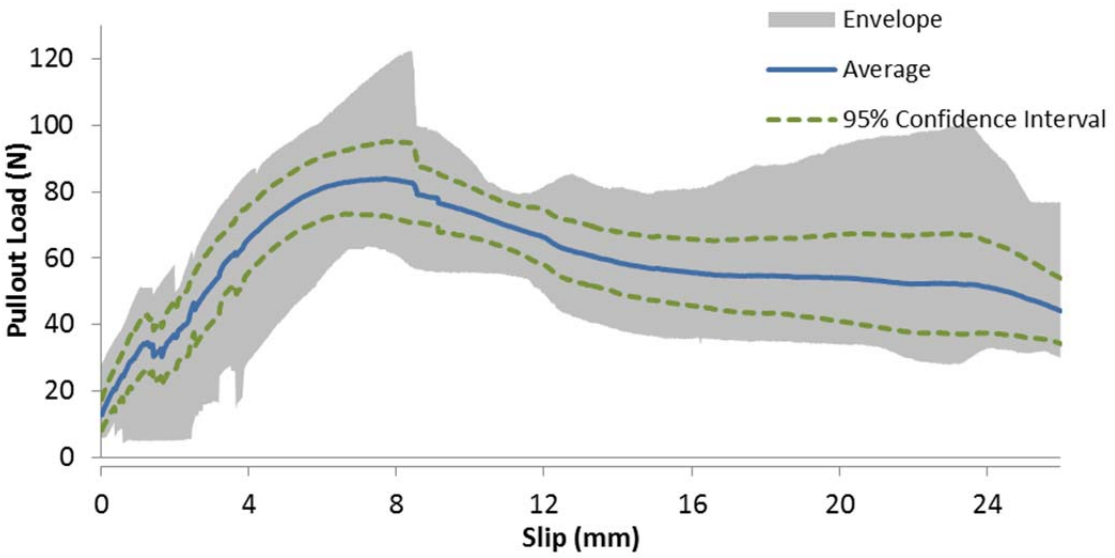

Figure B-63 - Load vs. slip curve for prototype macrofiber containing HDPE, 7% PVDF and 10% MAH: 30 degree inclination angle, 25.4 mm embedment length

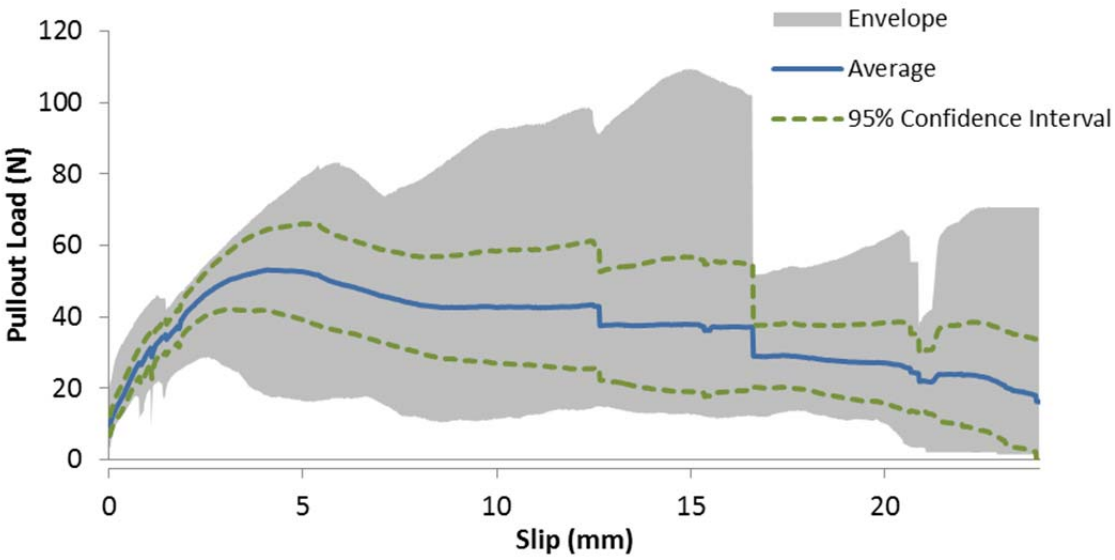

Figure B-64 - Load vs. slip curves for prototype macrofiber containing HDPE, 7% PVDF and 10% MAH: 30 degree inclination angle, 22.2 mm embedment length

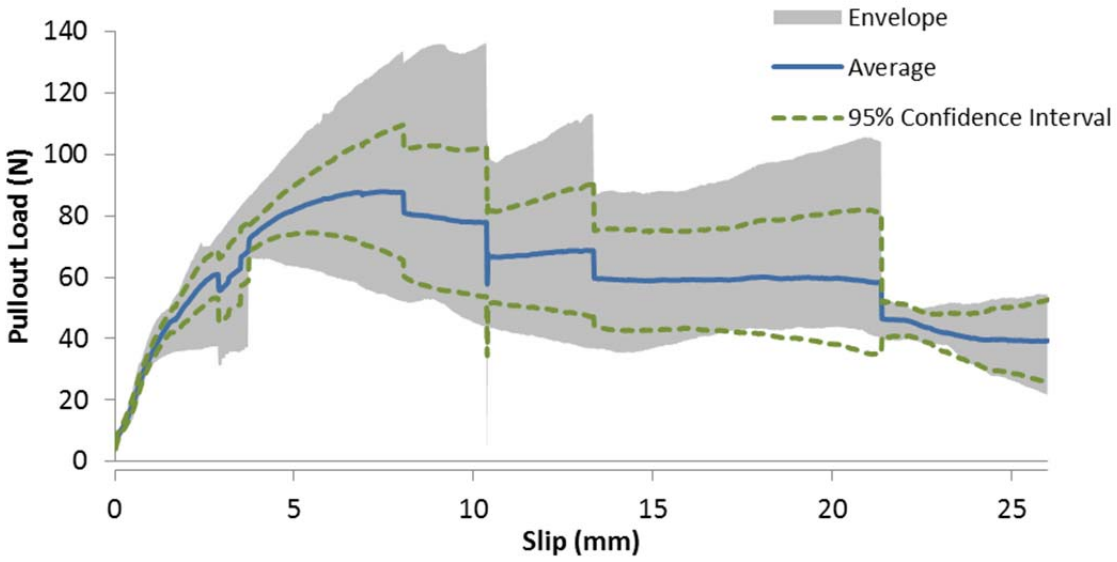

Figure B-65 - Load vs. slip curve for prototype macrofiber containing HDPE, 7% PVDF and 10% MAH: 45 degree inclination angle, 25.4 mm embedment length

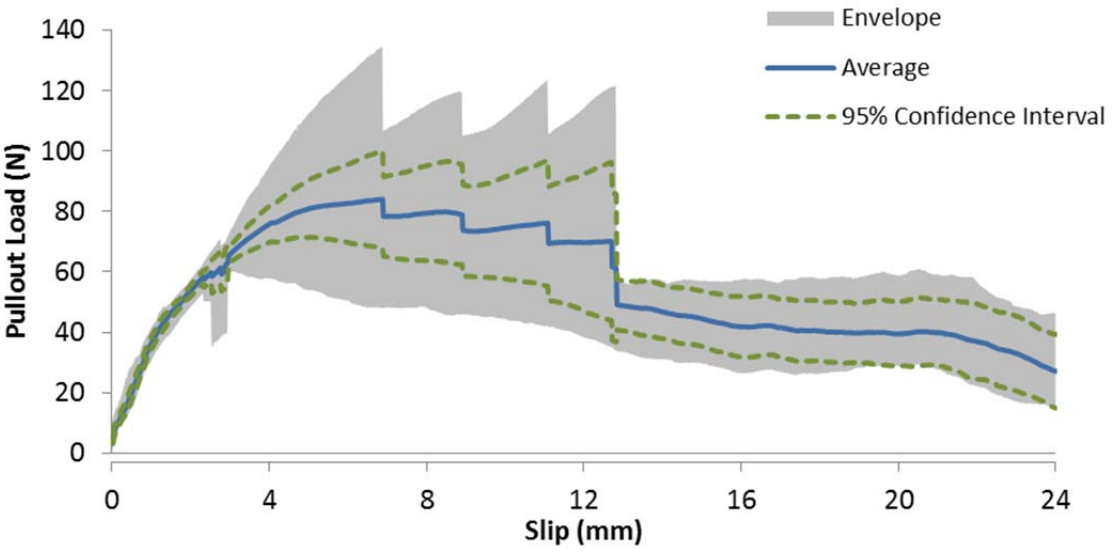

Figure B-66 - Load vs. slip curves for prototype macrofiber containing HDPE, 7% PVDF and 10% MAH: 45 degree inclination angle, 22.2 mm embedment length

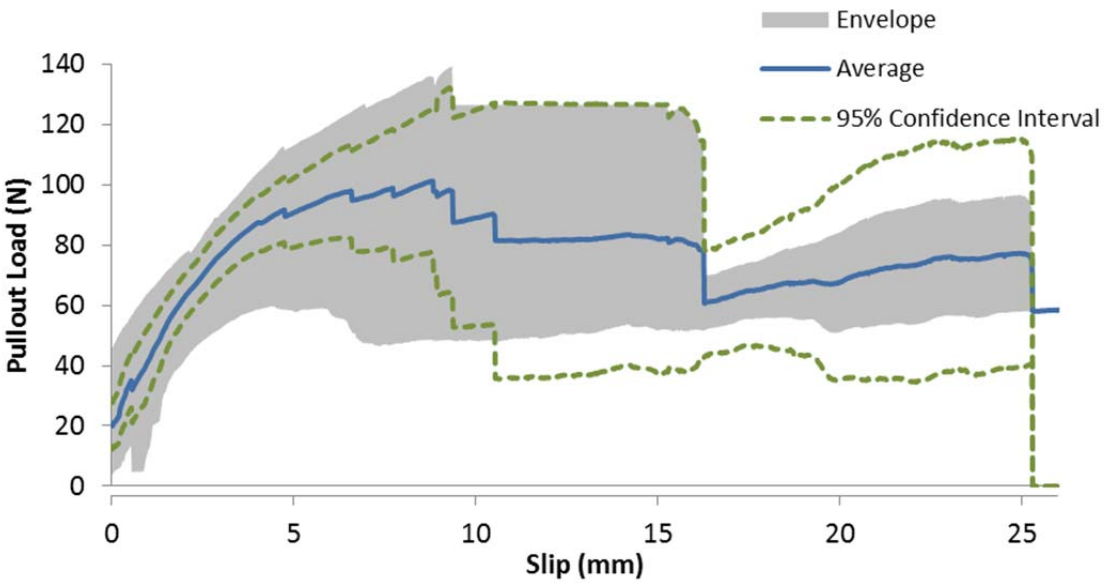

Figure B-67 - Load vs. slip curve for prototype macrofiber containing HDPE, 7% PVDF and 10% MAH: 60 degree inclination angle, 25.4 mm embedment length

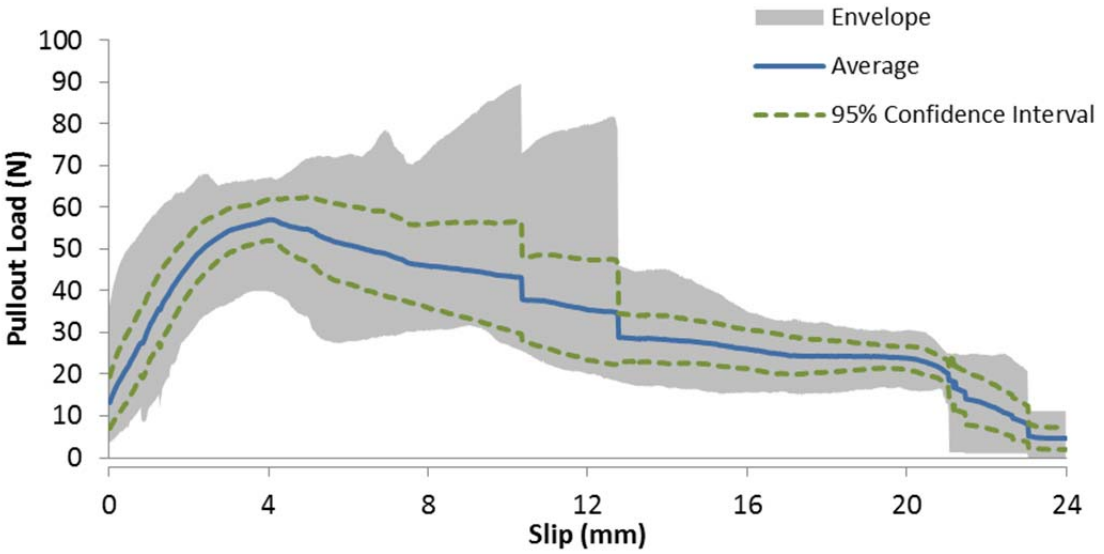

Figure B-68 - Load vs. slip curves for prototype macrofiber containing HDPE, 7% PVDF and 10% MAH: 60 degree inclination angle, 22.2 mm embedment length

B.7 - HDPE, 9% PVDF, 10% MAH PULLOUT CURVES

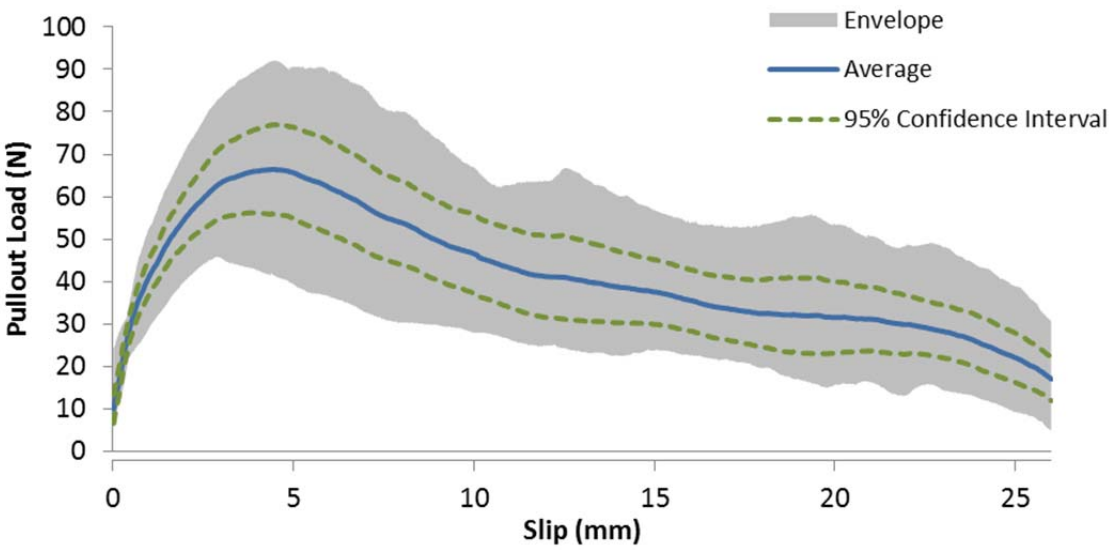

Figure B-69 - Load vs. slip curve for prototype macrofiber containing HDPE, 9% PVDF and 10% MAH: 0 degree inclination angle, 25.4 mm embedment length

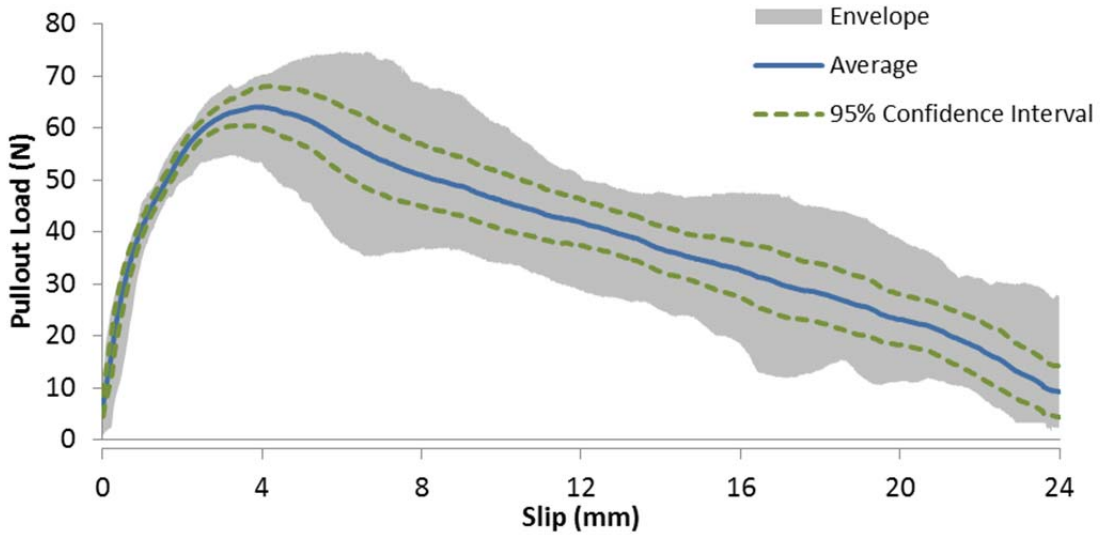

Figure B-70 - Load vs. slip curves for prototype macrofiber containing HDPE, 9% PVDF and 10% MAH: 0 degree inclination angle, 22.2 mm embedment length

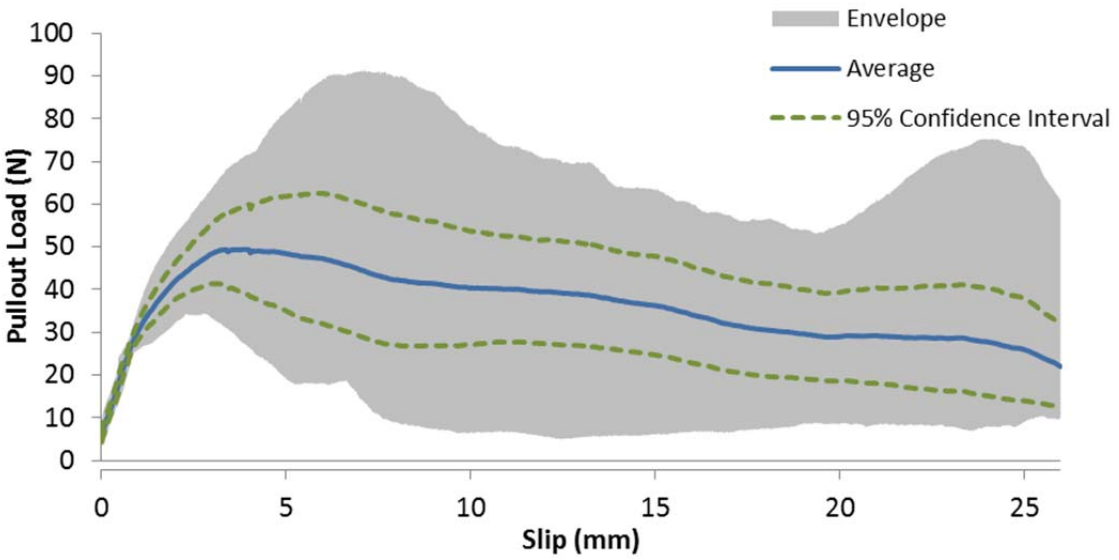

Figure B-71 - Load vs. slip curve for prototype macrofiber containing HDPE, 9% PVDF and 10% MAH: 15 degree inclination angle, 25.4 mm embedment length

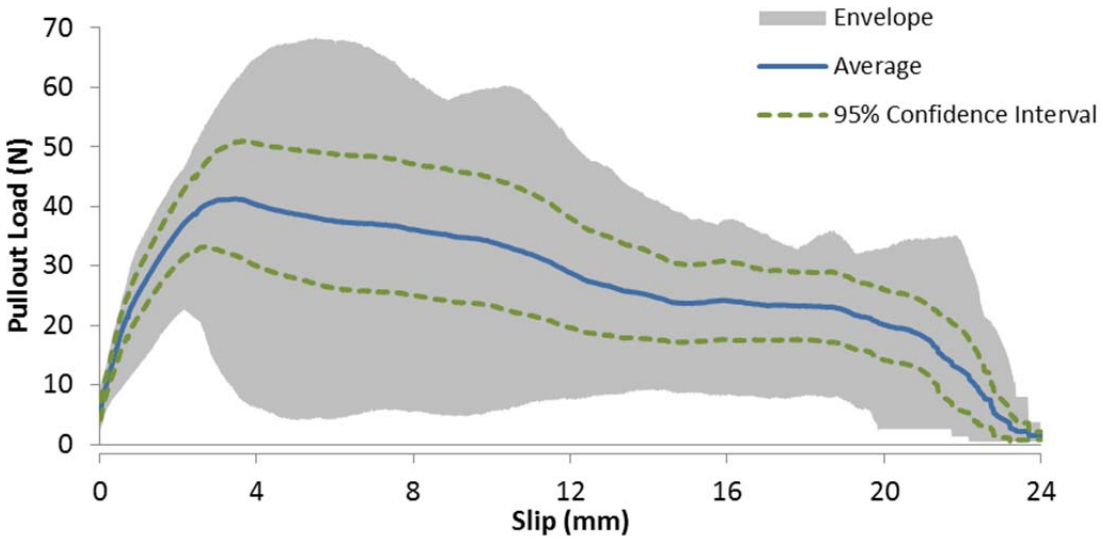

Figure B-72 - Load vs. slip curves for prototype macrofiber containing HDPE, 9% PVDF and 10% MAH: 15 degree inclination angle, 22.2 mm embedment length

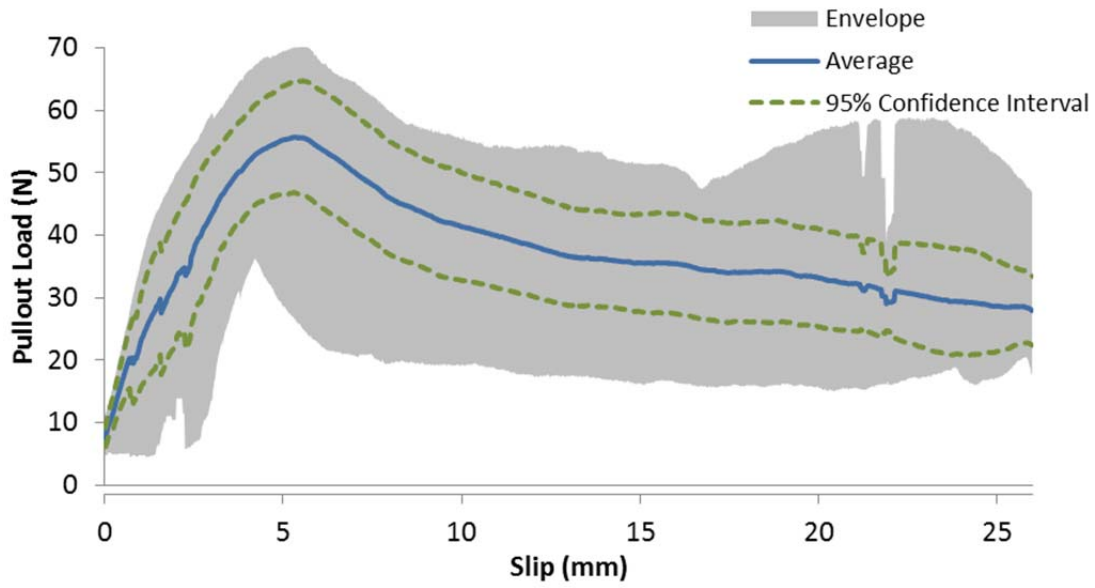

Figure B-73 - Load vs. slip curve for prototype macrofiber containing HDPE, 9% PVDF and 10% MAH: 30 degree inclination angle, 25.4 mm embedment length

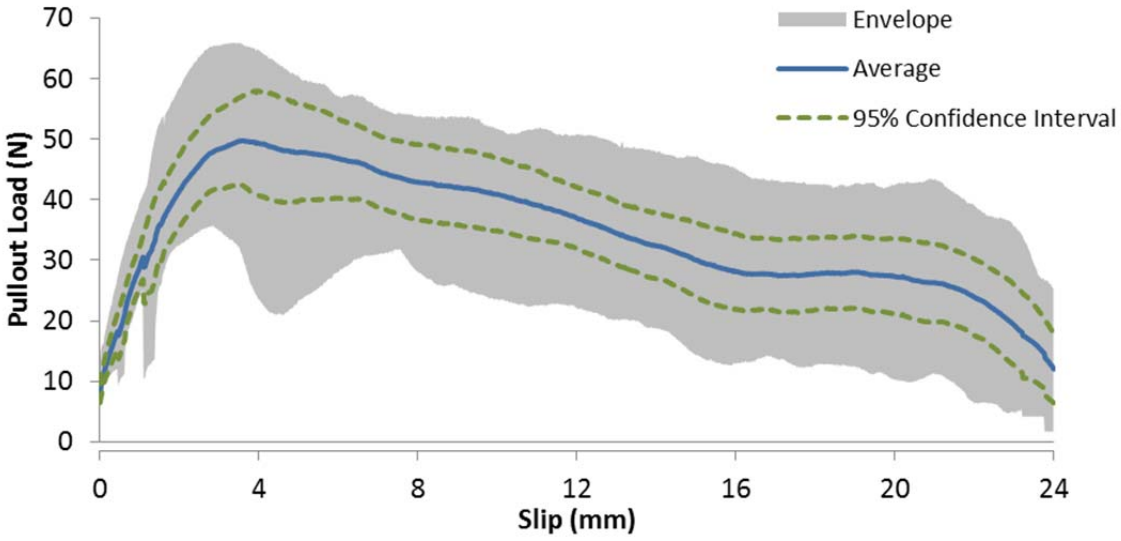

Figure B-74 - Load vs. slip curves for prototype macrofiber containing HDPE, 9% PVDF and 10% MAH: 30 degree inclination angle, 22.2 mm embedment length

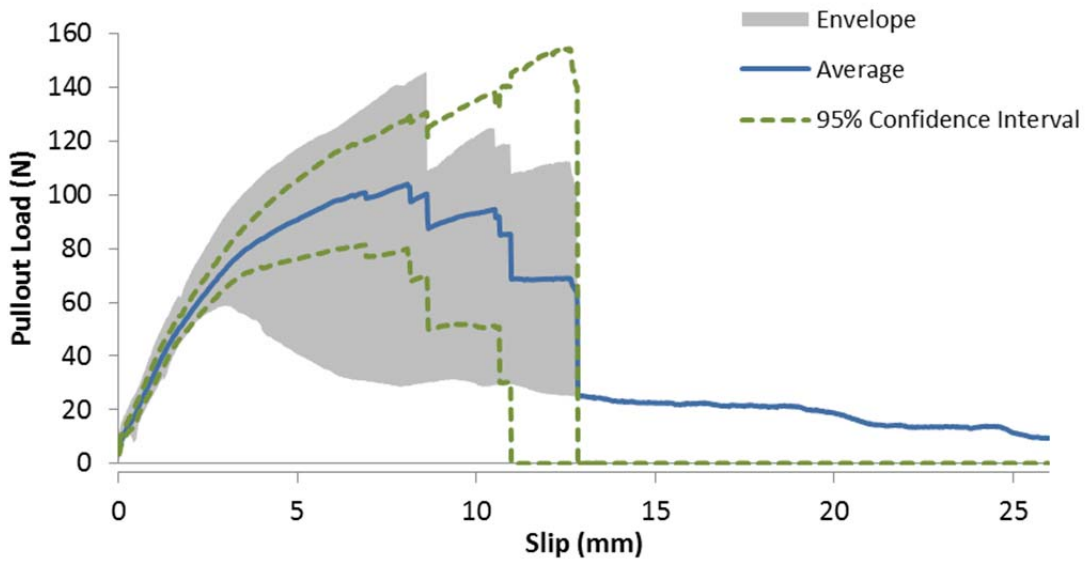

Figure B-75 - Load vs. slip curve for prototype macrofiber containing HDPE, 9% PVDF and 10% MAH: 45 degree inclination angle, 25.4 mm embedment length

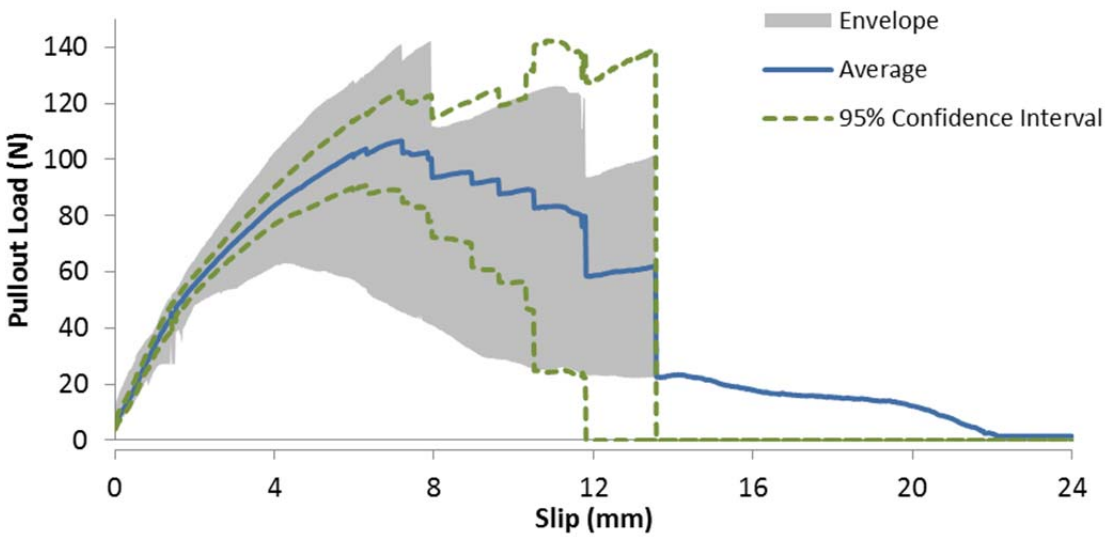

Figure B-76 - Load vs. slip curves for prototype macrofiber containing HDPE, 9% PVDF and 10% MAH: 45 degree inclination angle, 22.2 mm embedment length

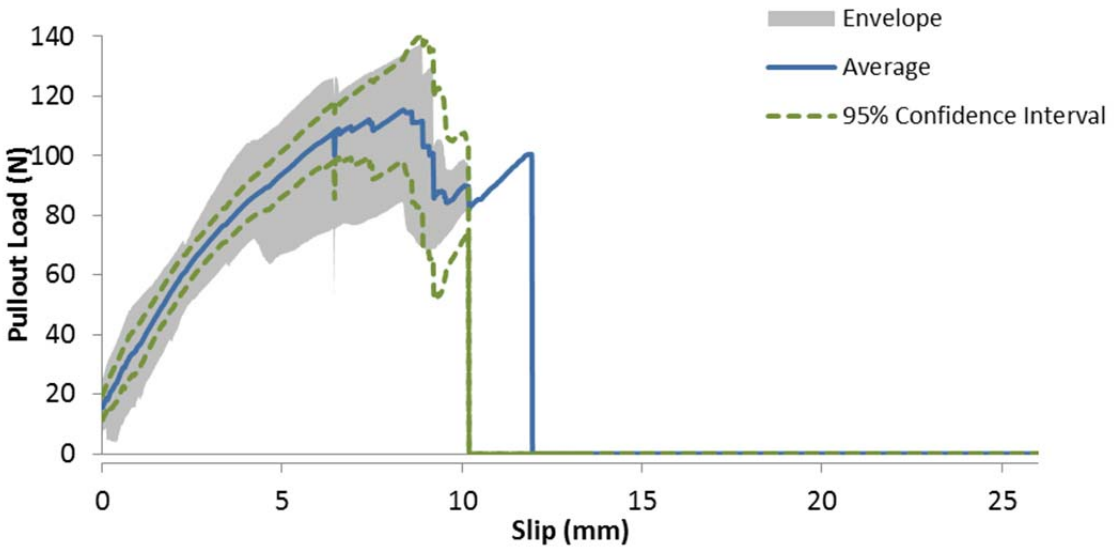

Figure B-77 - Load vs. slip curve for prototype macrofiber containing HDPE, 9% PVDF and 10% MAH: 60 degree inclination angle, 25.4 mm embedment length

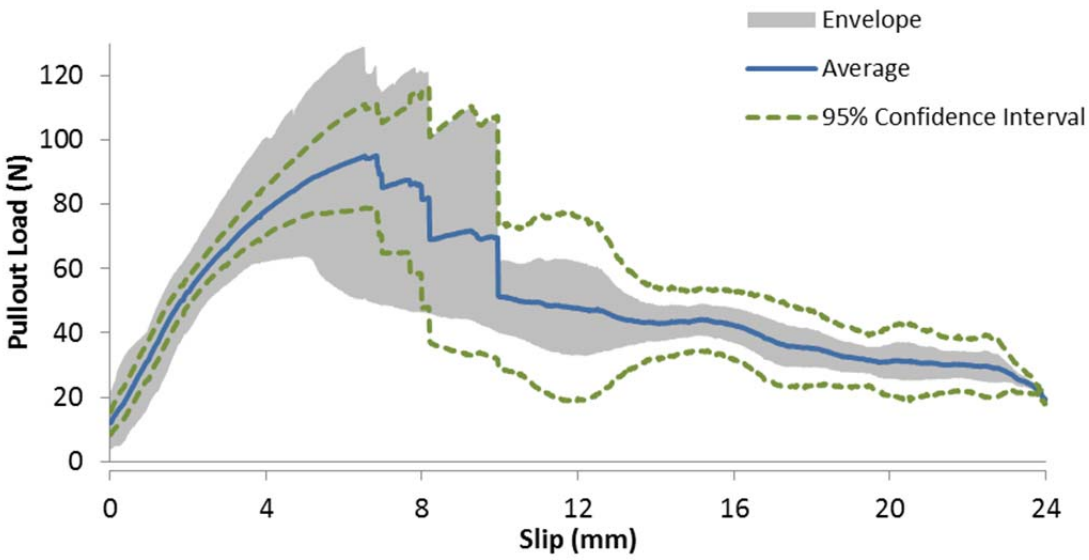

Figure B-78 - Load vs. slip curves for prototype macrofiber containing HDPE, 9% PVDF and 10% MAH: 60 degree inclination angle, 22.2 mm embedment length

B.8 - HDPE, 11% PVDF, 20% MAH PULLOUT CURVES

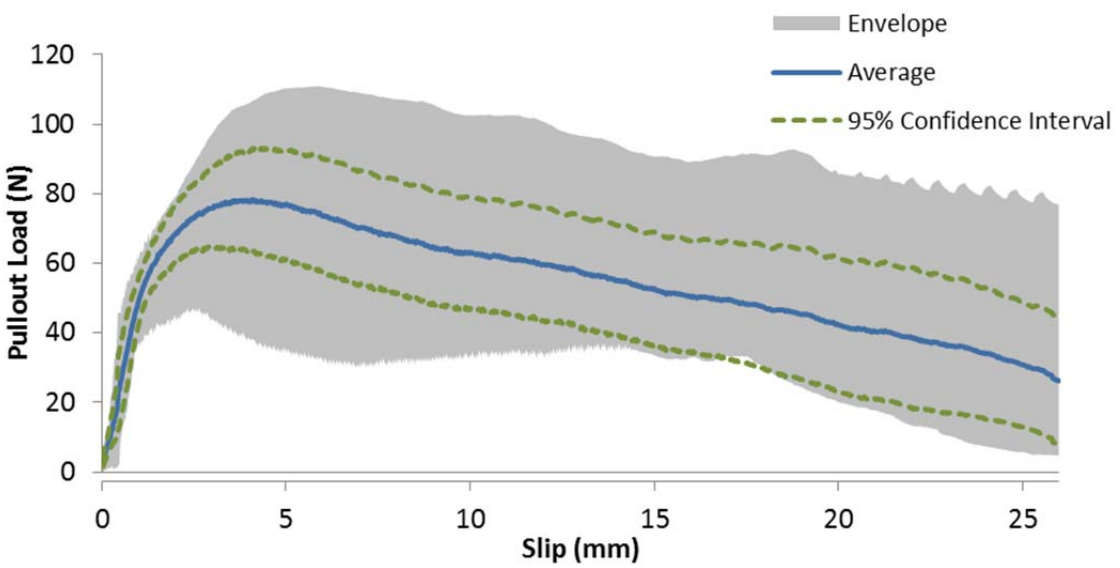

Figure B-79 - Load vs. slip curve for prototype macrofiber containing HDPE, 11% PVDF and 20% MAH: 0 degree inclination angle, 25.4 mm embedment length

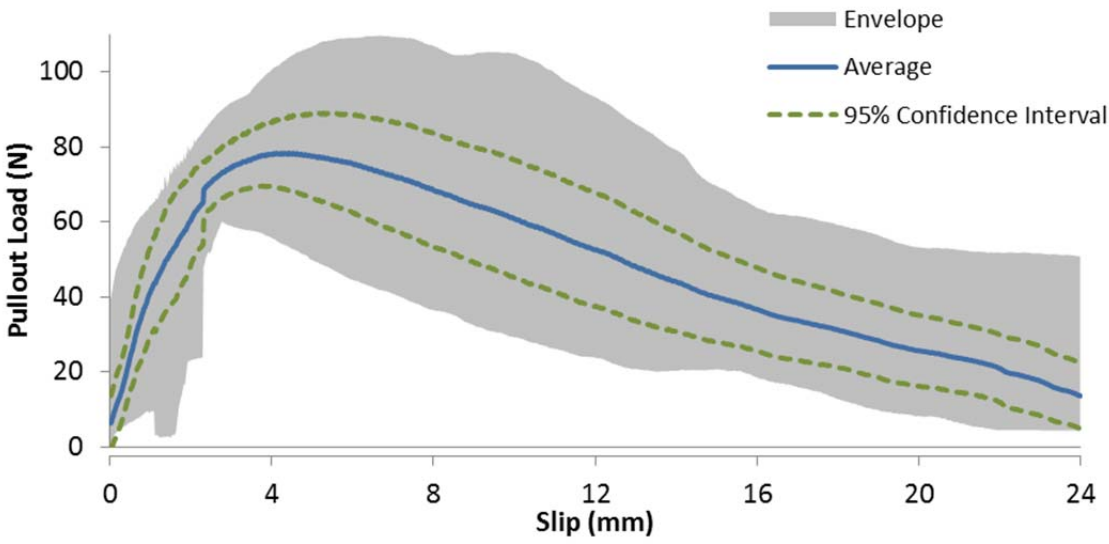

Figure B-80 - Load vs. slip curves for prototype macrofiber containing HDPE, 11% PVDF and 20% MAH: 0 degree inclination angle, 22.2 mm embedment length

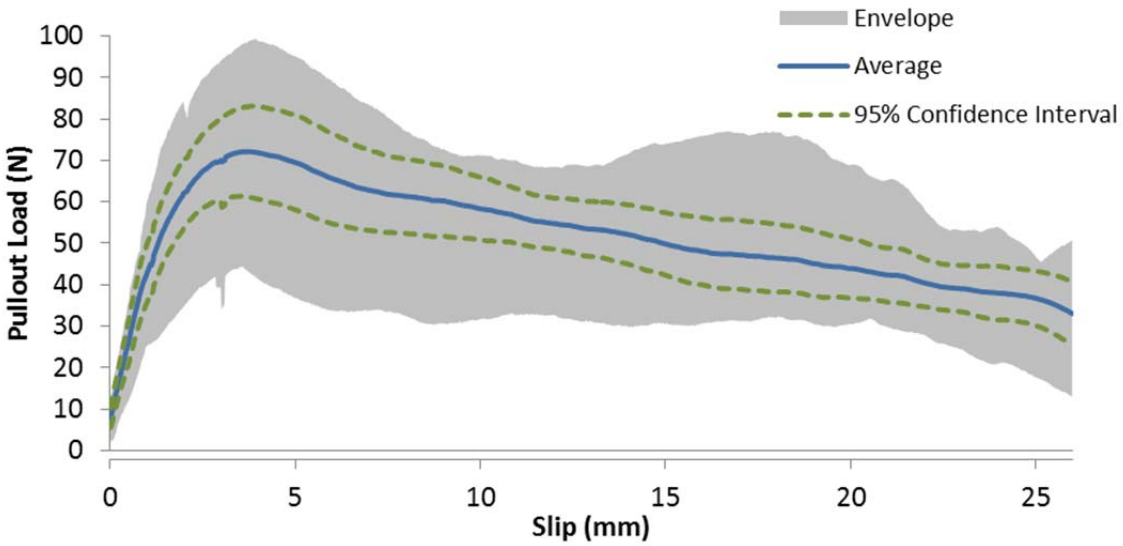

Figure B-81 - Load vs. slip curve for prototype macrofiber containing HDPE, 11% PVDF and 20% MAH: 15 degree inclination angle, 25.4 mm embedment length

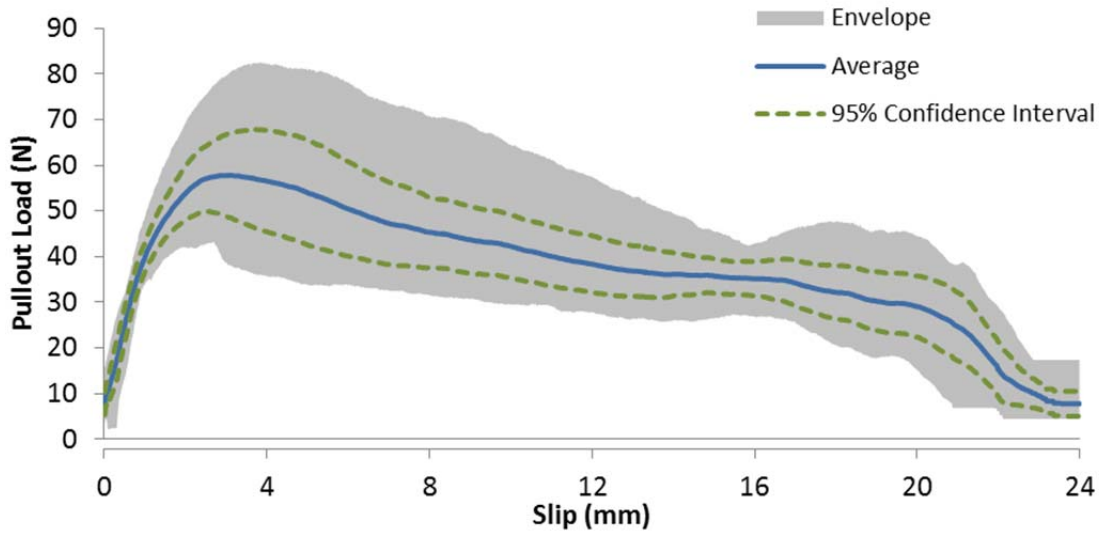

Figure B-82 - Load vs. slip curves for prototype macrofiber containing HDPE, 11% PVDF and 20% MAH: 15 degree inclination angle, 22.2 mm embedment length

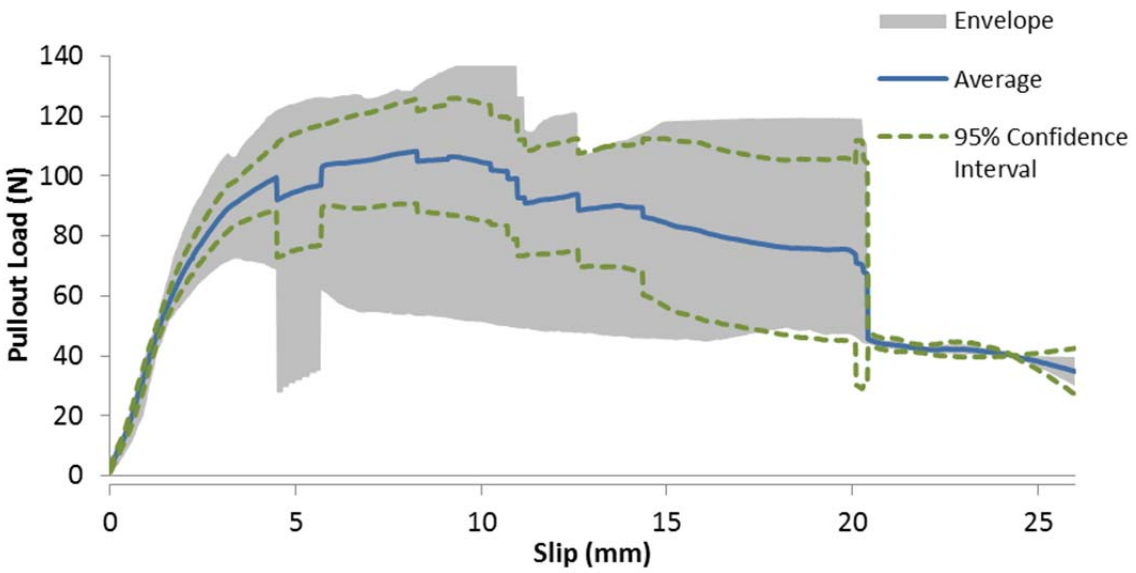

Figure B-83 - Load vs. slip curve for prototype macrofiber containing HDPE, 11% PVDF and 20% MAH: 30 degree inclination angle, 25.4 mm embedment length

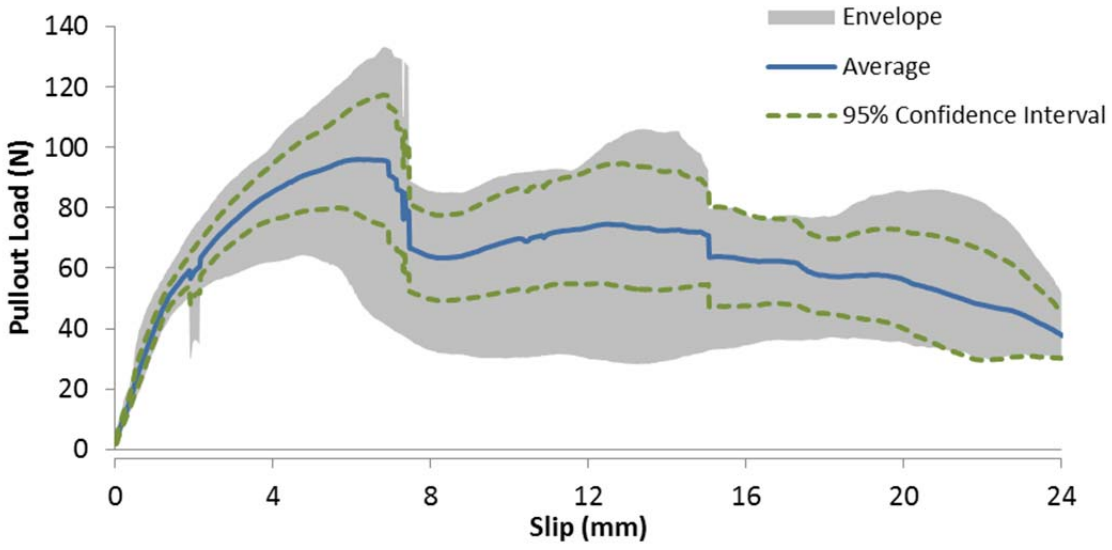

Figure B-84 - Load vs. slip curves for prototype macrofiber containing HDPE, 11% PVDF and 20% MAH: 30 degree inclination angle, 22.2 mm embedment length

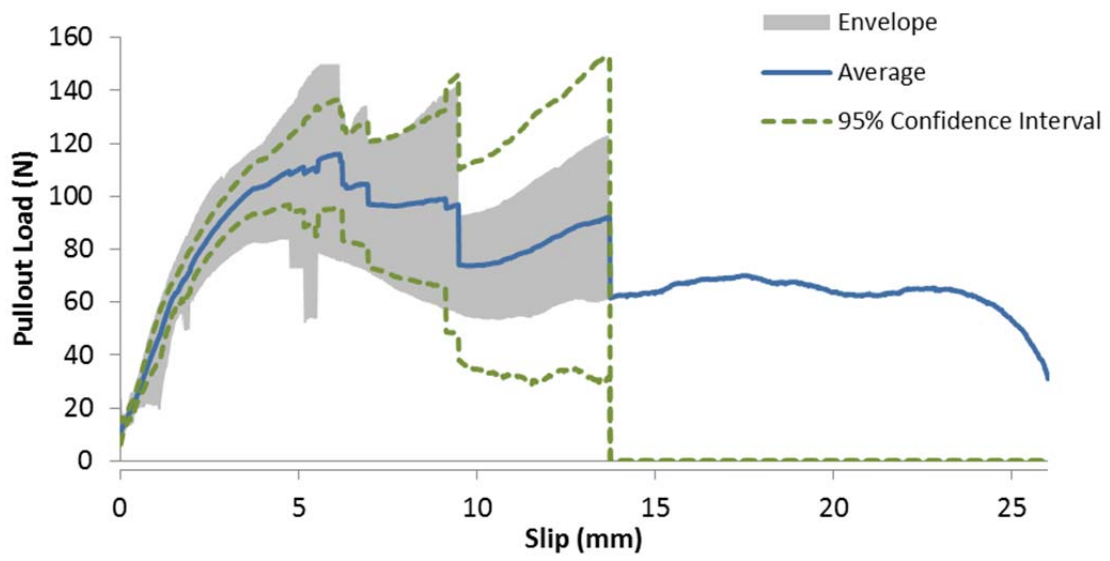

Figure B-85 - Load vs. slip curve for prototype macrofiber containing HDPE, 11% PVDF and 20% MAH: 45 degree inclination angle, 25.4 mm embedment length

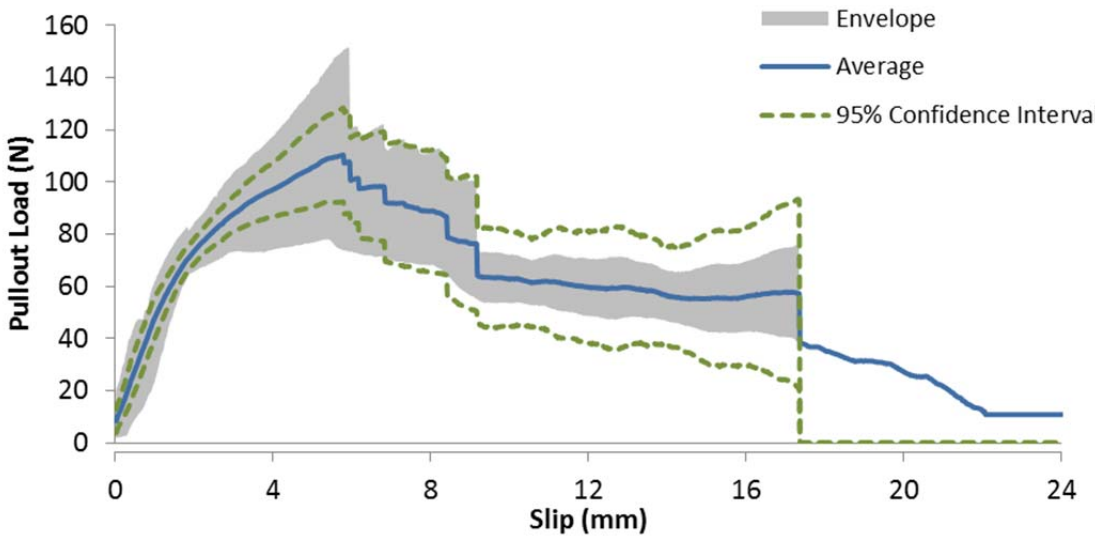

Figure B-86 - Load vs. slip curves for prototype macrofiber containing HDPE, 11% PVDF and 20% MAH: 45 degree inclination angle, 22.2 mm embedment length

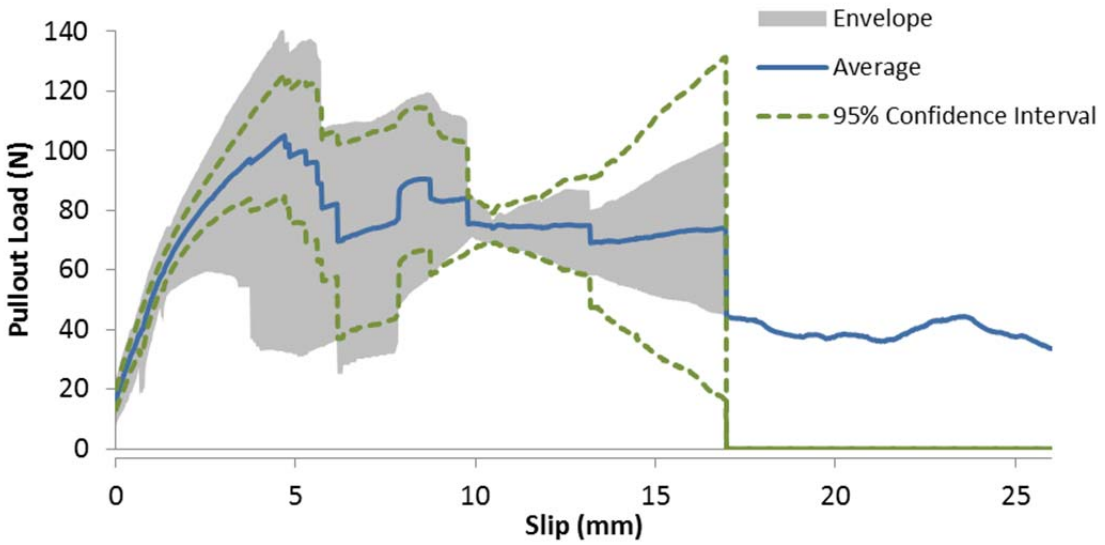

Figure B-87 - Load vs. slip curve for prototype macrofiber containing HDPE, 11% PVDF and 20% MAH: 60 degree inclination angle, 25.4 mm embedment length

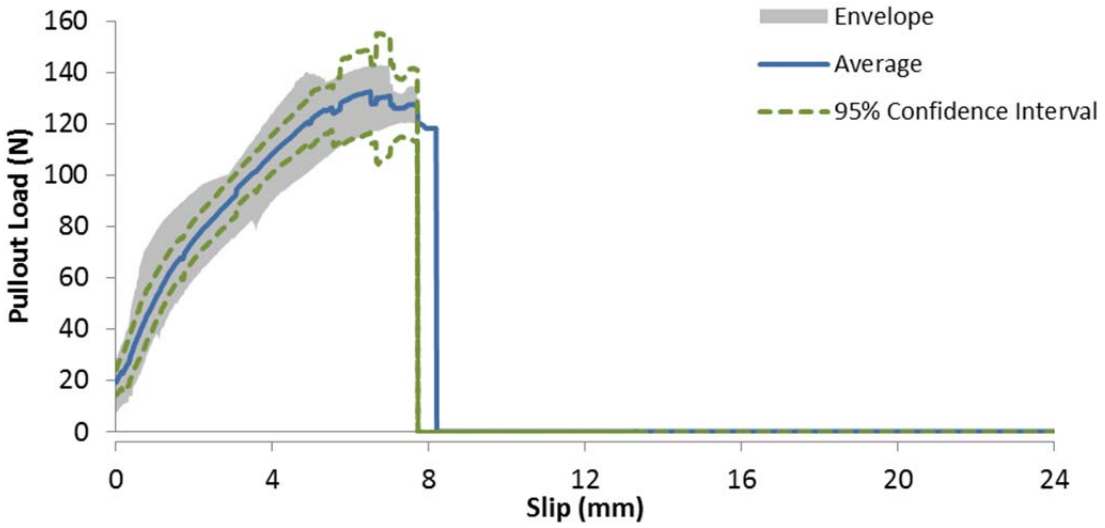

Figure B-88 - Load vs. slip curves for prototype macrofiber containing HDPE, 11% PVDF and 20% MAH: 60 degree inclination angle, 22.2 mm embedment length

B.9 - 100% PVDF PULLOUT CURVES

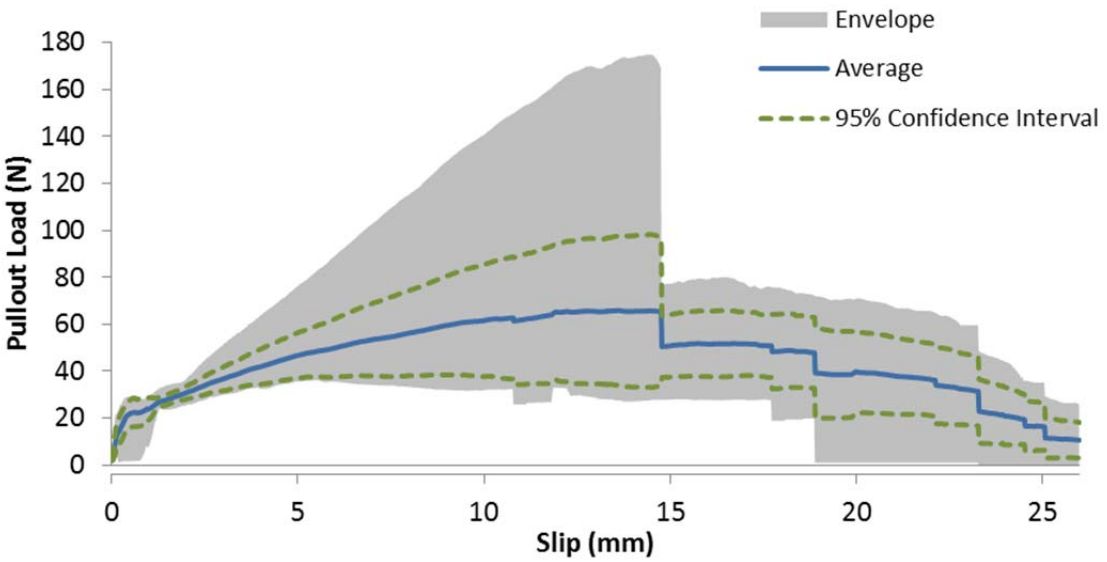

Figure B-89 - Load vs. slip curve for prototype macrofiber containing 100% PVDF: 0 degree inclination angle, 25.4 mm embedment length

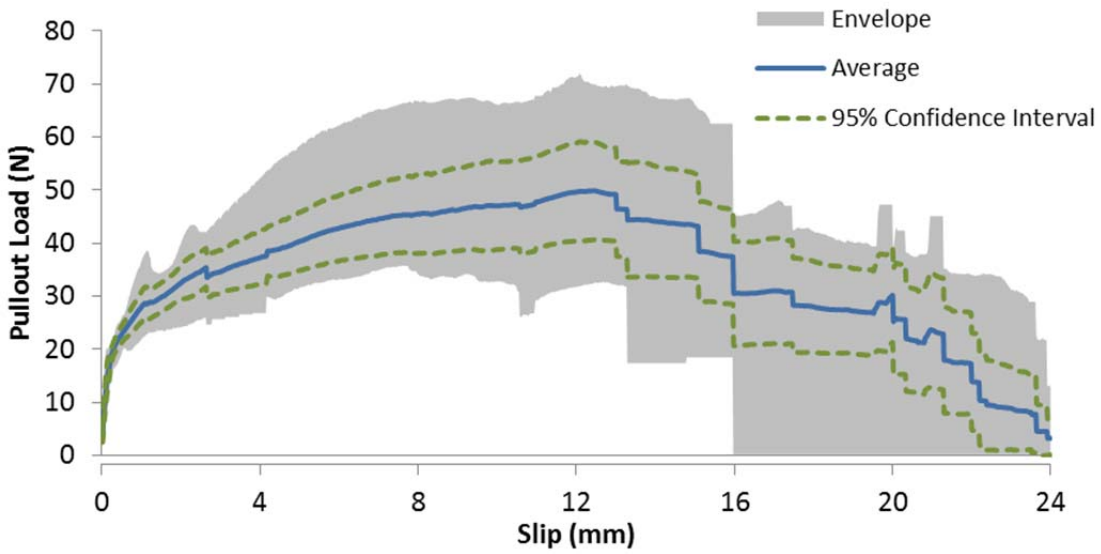

Figure B-90 - Load vs. slip curves for prototype macrofiber containing 100% PVDF: 0 degree inclination angle, 22.2 mm embedment length

B.10 - HDPE, 10% EVA PULLOUT CURVES

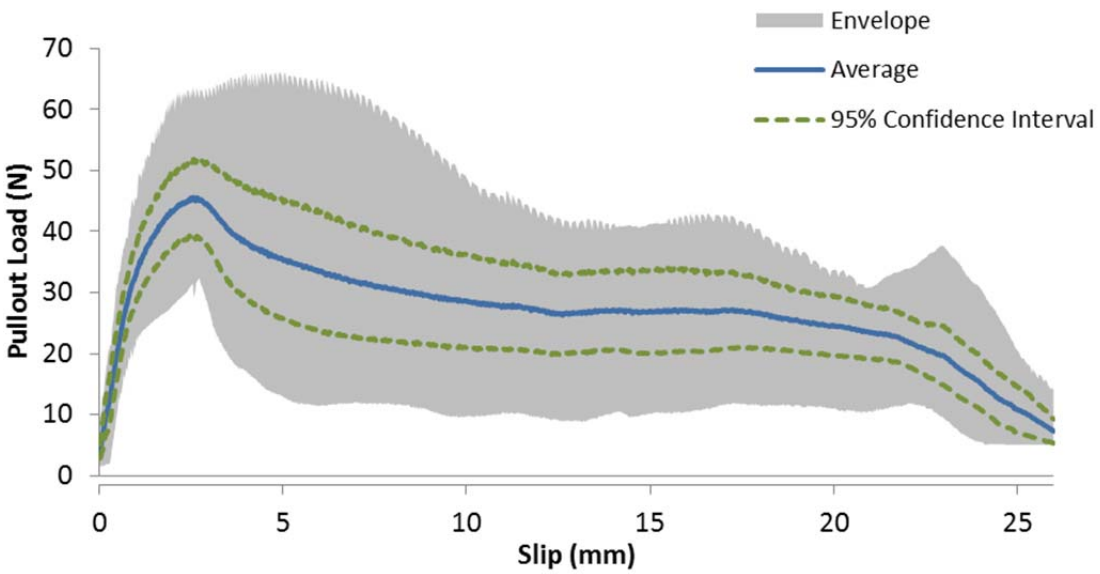

Figure B-91 - Load vs. slip curve for prototype macrofiber containing HDPE and 10% EVA: 0 degree inclination angle, 25.4 mm embedment length

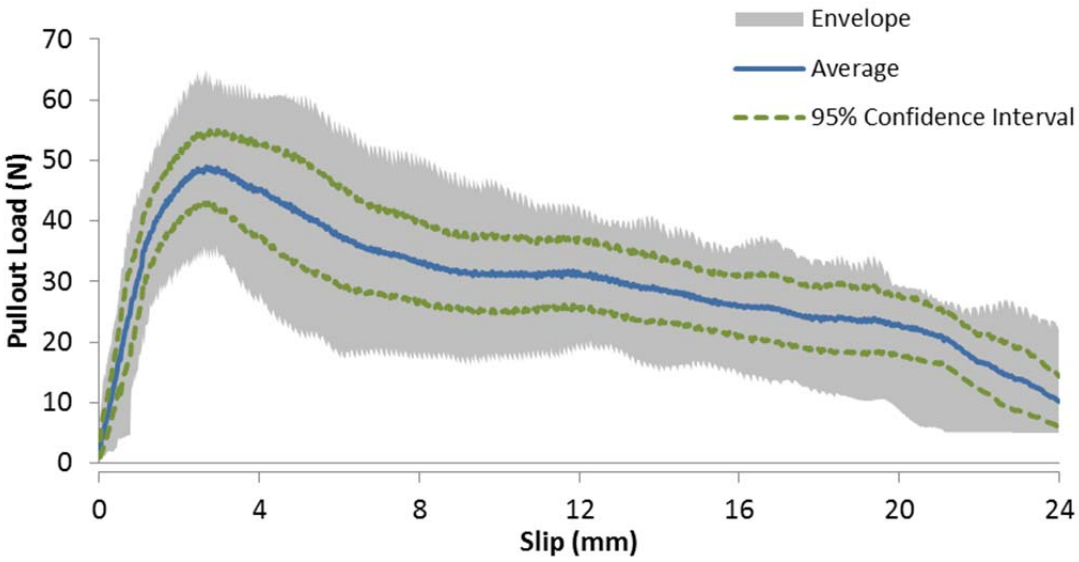

Figure B-92 - Load vs. slip curves for prototype macrofiber containing HDPE and 10% EVA: 0 degree inclination angle, 22.2 mm embedment length

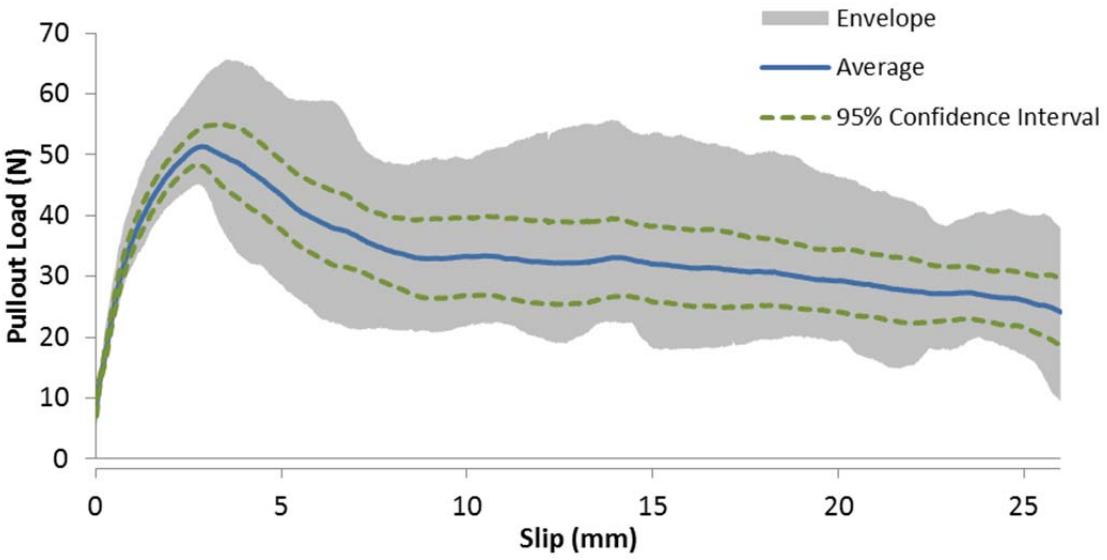

Figure B-93 - Load vs. slip curve for prototype macrofiber containing HDPE and 10% EVA: 15 degree inclination angle, 25.4 mm embedment length

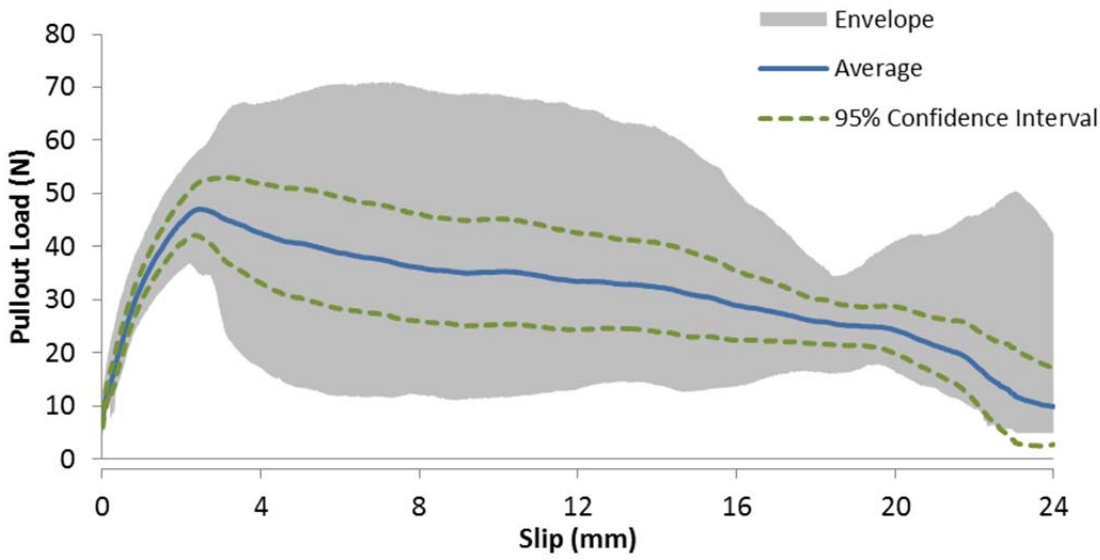

Figure B-94 - Load vs. slip curves for prototype macrofiber containing HDPE and 10% EVA: 15 degree inclination angle, 22.2 mm embedment length

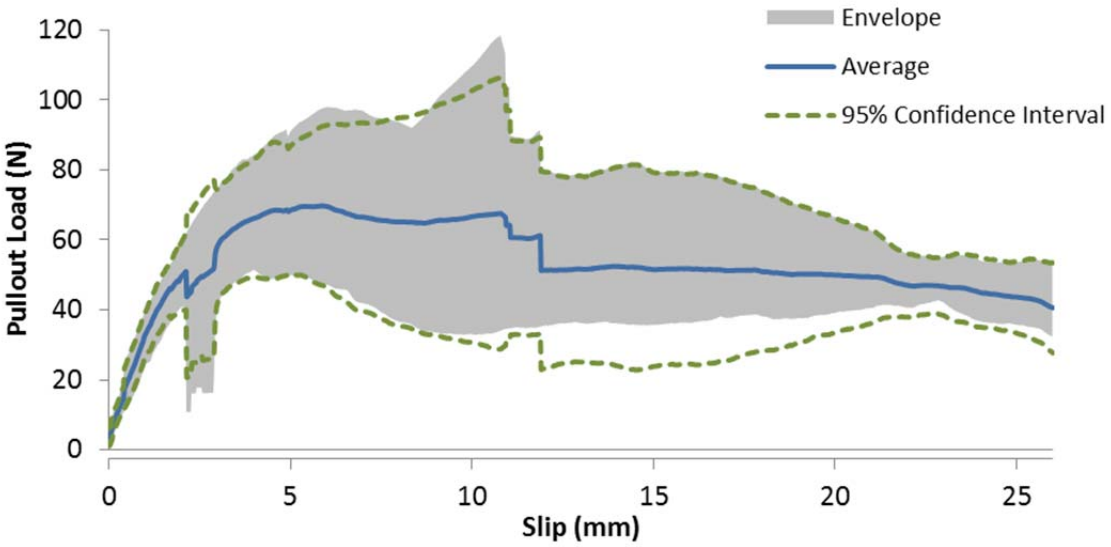

Figure B-95 - Load vs. slip curve for prototype macrofiber containing HDPE and 10% EVA: 30 degree inclination angle, 25.4 mm embedment length

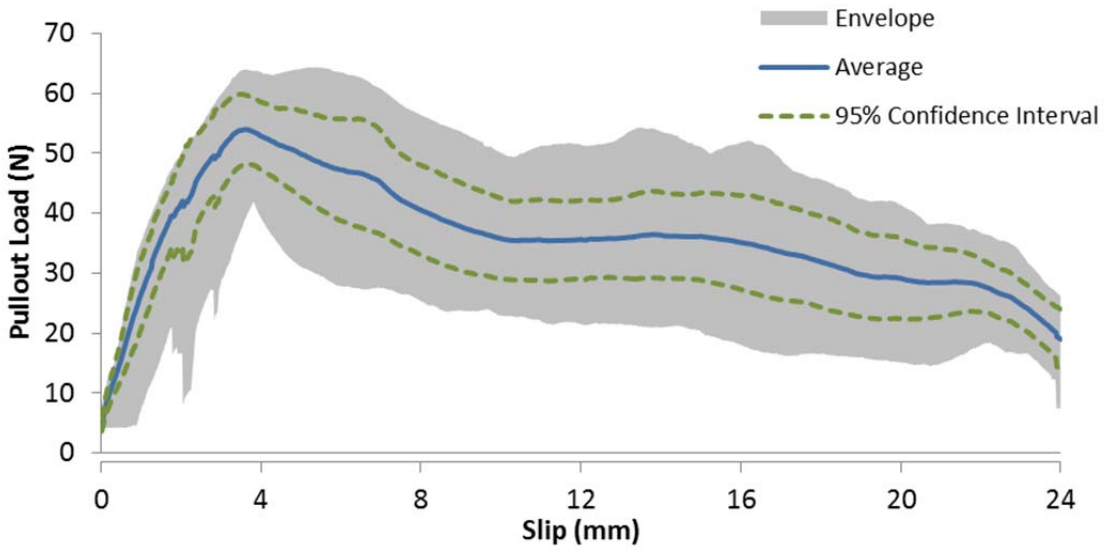

Figure B-96 - Load vs. slip curves for prototype macrofiber containing HDPE and 10% EVA: 30 degree inclination angle, 22.2 mm embedment length

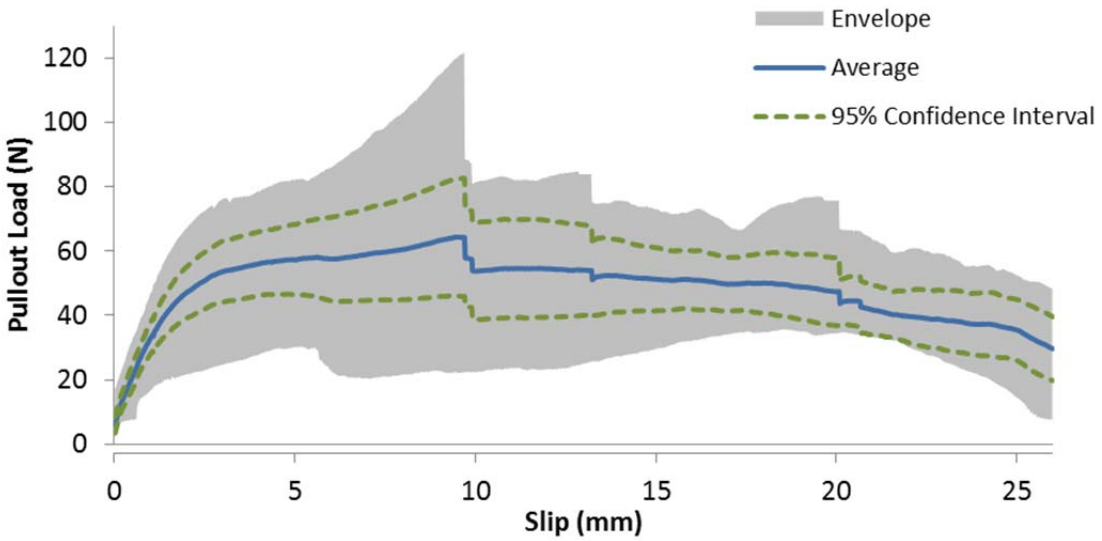

Figure B-97 - Load vs. slip curve for prototype macrofiber containing HDPE and 10% EVA: 45 degree inclination angle, 25.4 mm embedment length

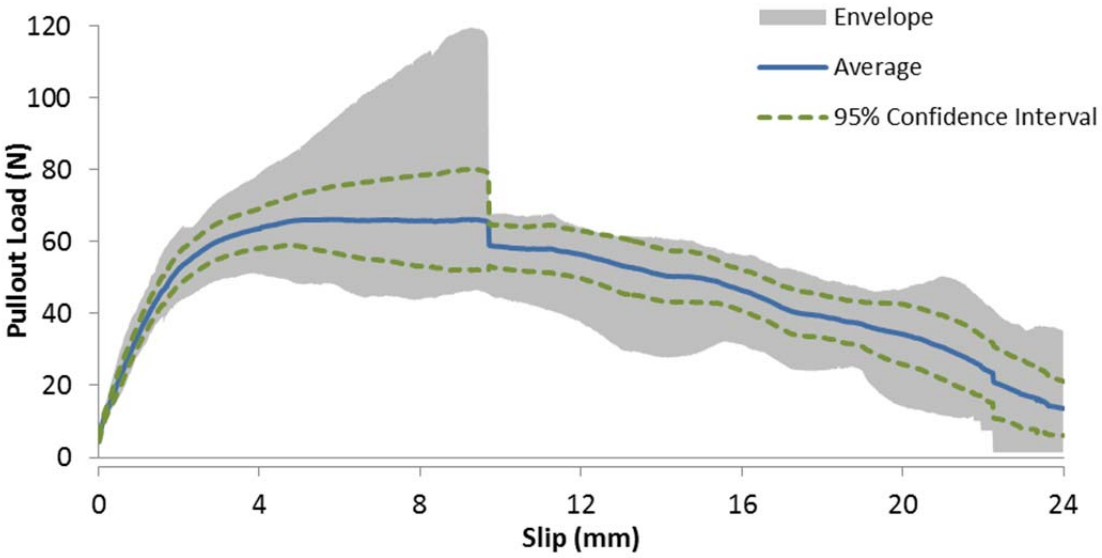

Figure B-98 - Load vs. slip curves for prototype macrofiber containing HDPE and 10% EVA: 45 degree inclination angle, 22.2 mm embedment length

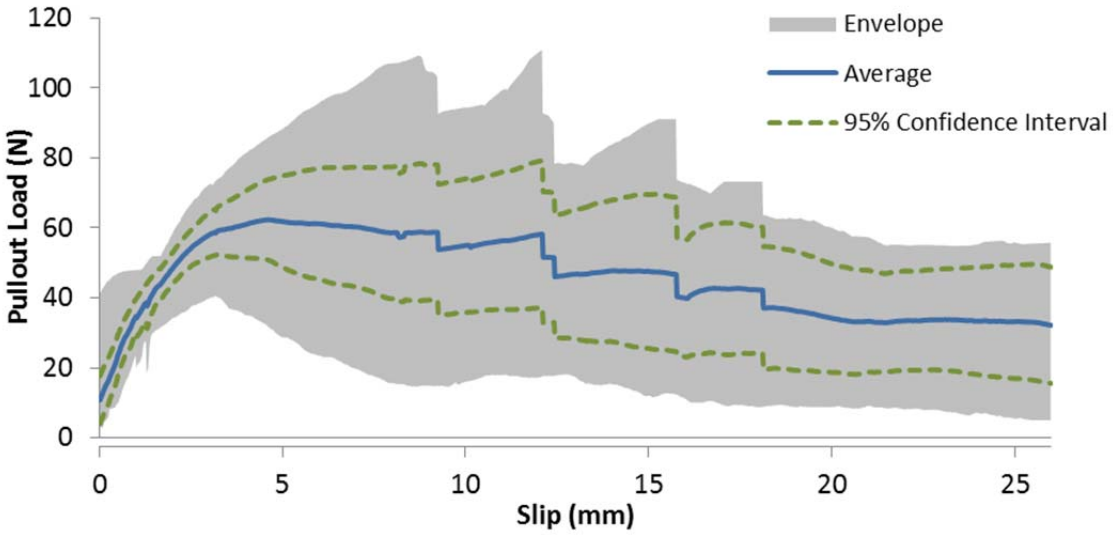

Figure B-99 - Load vs. slip curve for prototype macrofiber containing HDPE and 10% EVA: 60 degree inclination angle, 25.4 mm embedment length

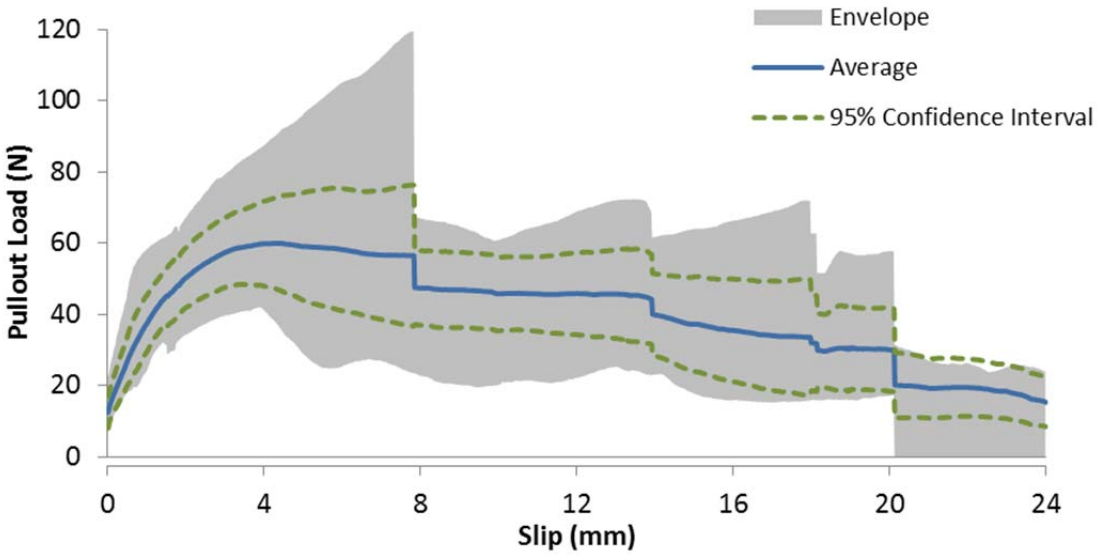

Figure B-100 - Load vs. slip curves for prototype macrofiber containing HDPE and 10% EVA: 60 degree inclination angle, 22.2 mm embedment length

B.11 - PP, 10% HDPE, 10% EVA PULLOUT CURVES

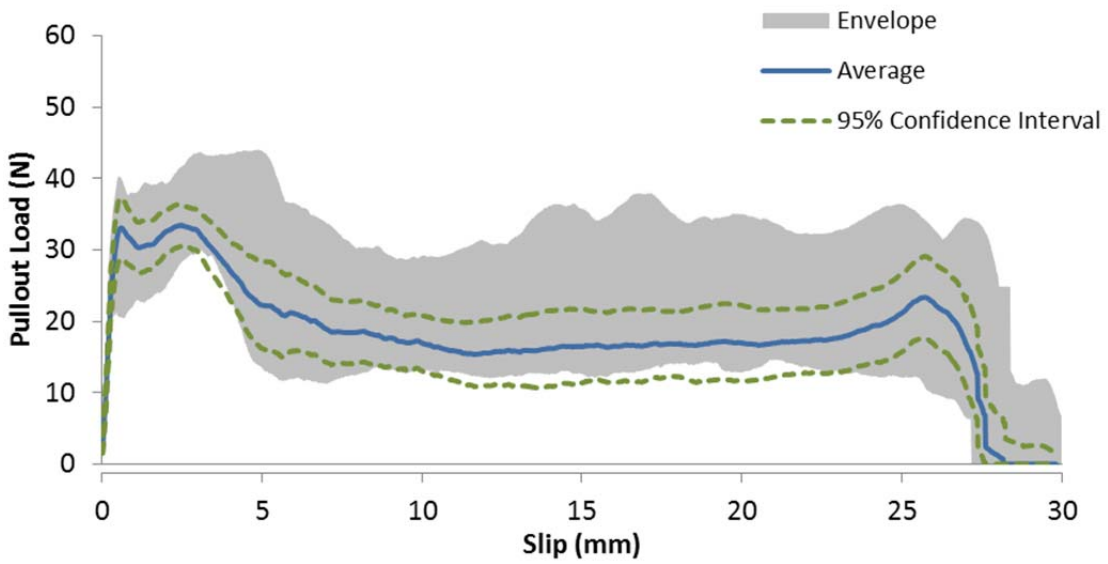

Figure B-101 - Load vs. slip curve for prototype macrofiber containing PP, 10% HDPE and 10% EVA: 0 degree inclination angle, 25.4 mm embedment length

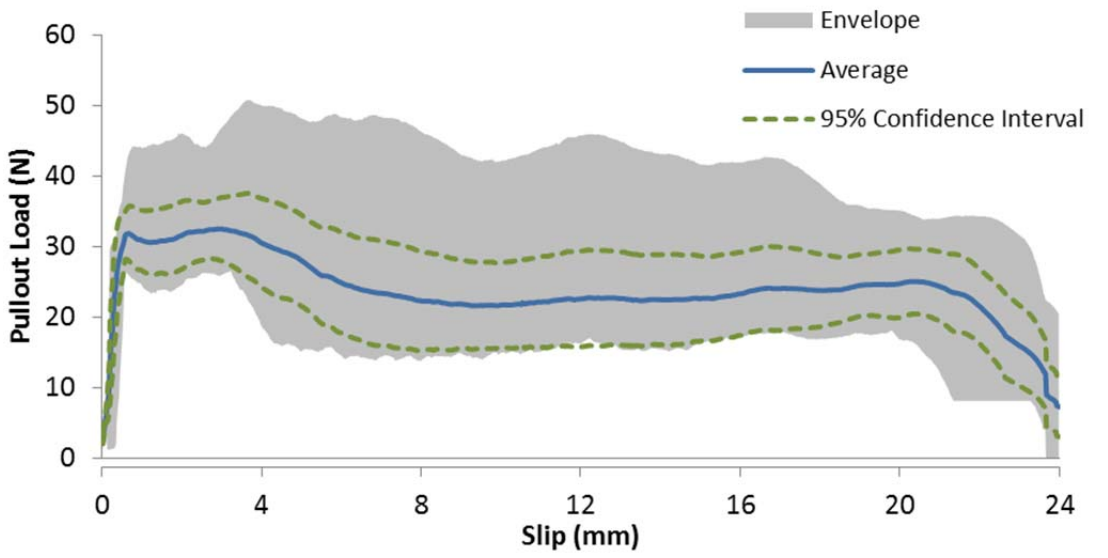

Figure B-102 - Load vs. slip curves for prototype macrofiber containing PP, 10% HDPE and 10% EVA: 0 degree inclination angle, 22.2 mm embedment length

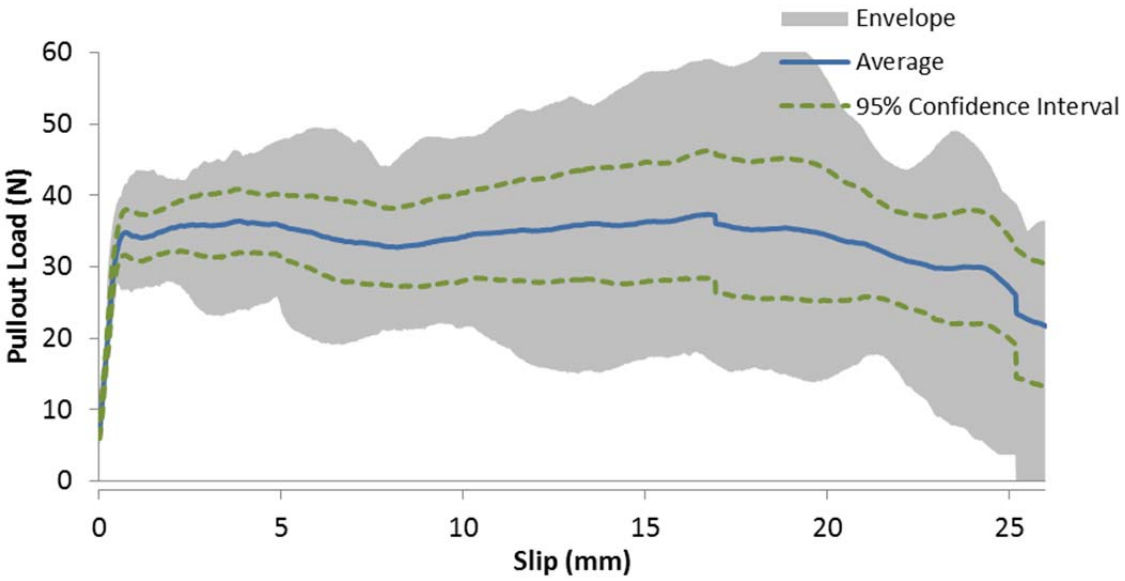

Figure B-103 - Load vs. slip curve for prototype macrofiber containing PP, 10% HDPE and 10% EVA: 15 degree inclination angle, 25.4 mm embedment length

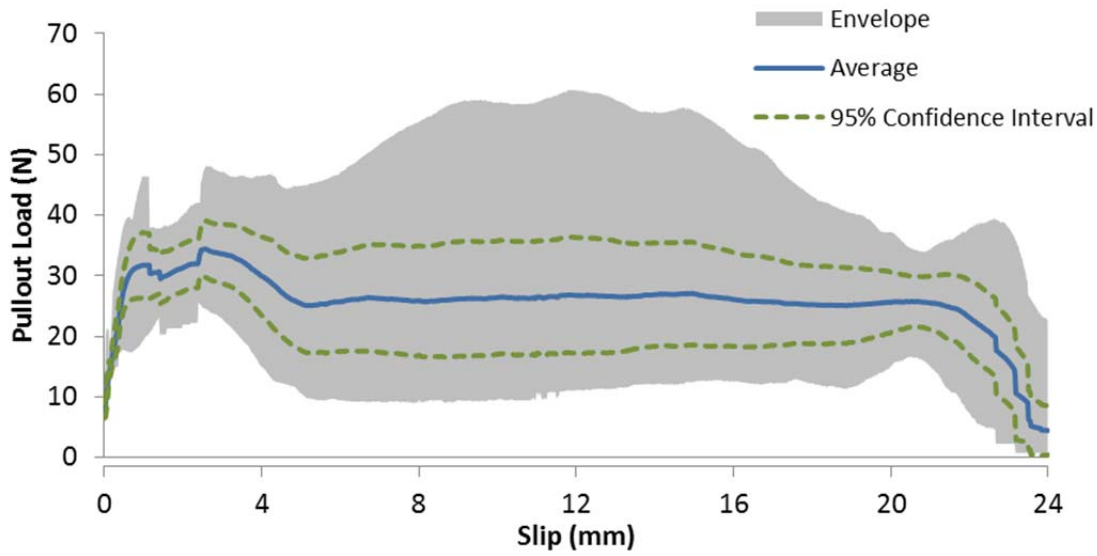

Figure B-104 - Load vs. slip curves for prototype macrofiber containing PP, 10% HDPE and 10% EVA: 15 degree inclination angle, 22.2 mm embedment length

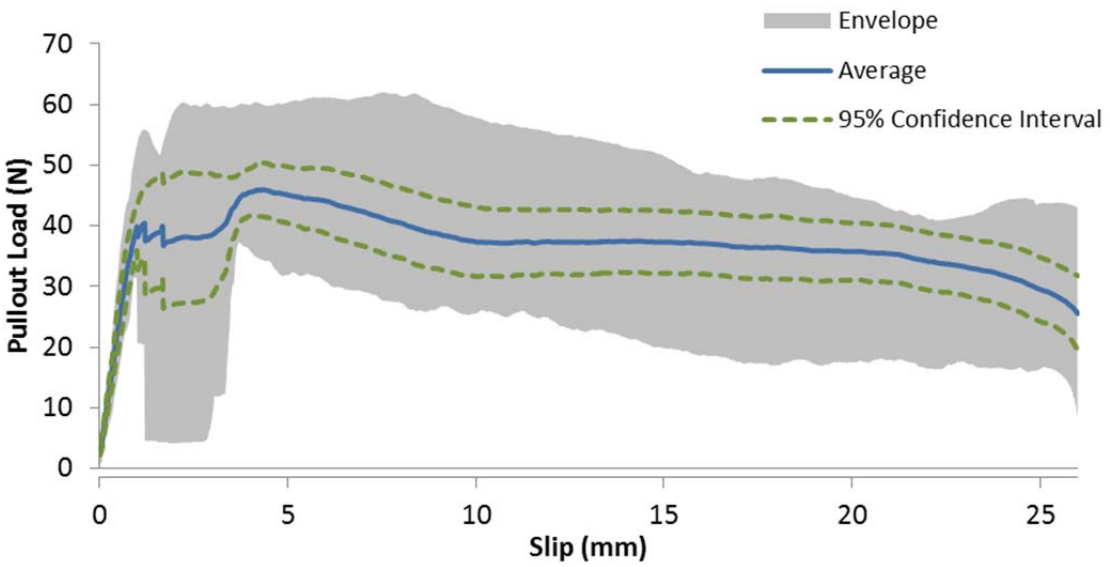

Figure B-105 - Load vs. slip curve for prototype macrofiber containing PP, 10% HDPE and 10% EVA: 30 degree inclination angle, 25.4 mm embedment length

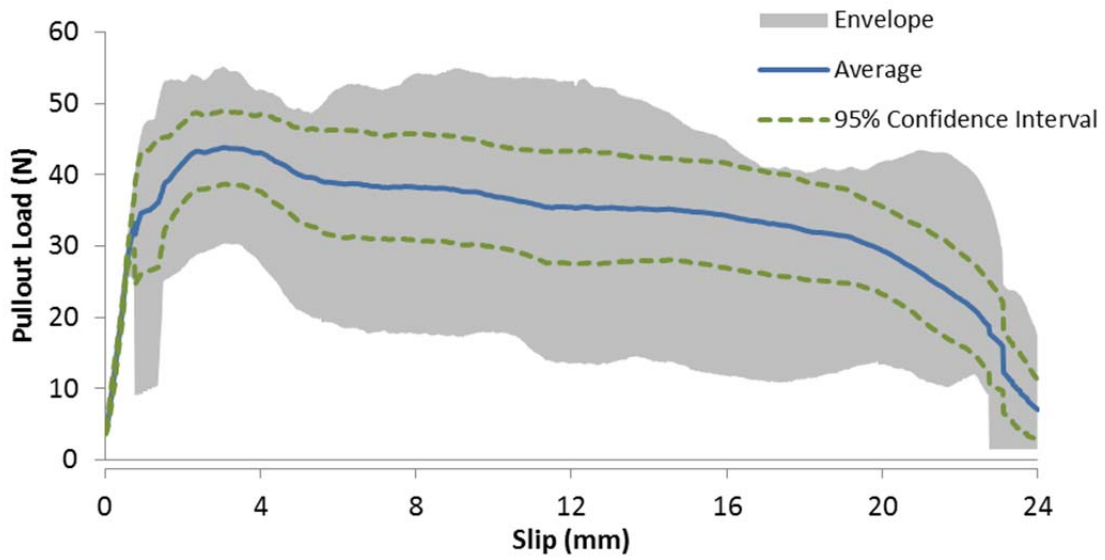

Figure B-106 - Load vs. slip curves for prototype macrofiber containing PP, 10% HDPE and 10% EVA: 30 degree inclination angle, 22.2 mm embedment length

B.12 - TUF-STRAND SF PULLOUT CURVES

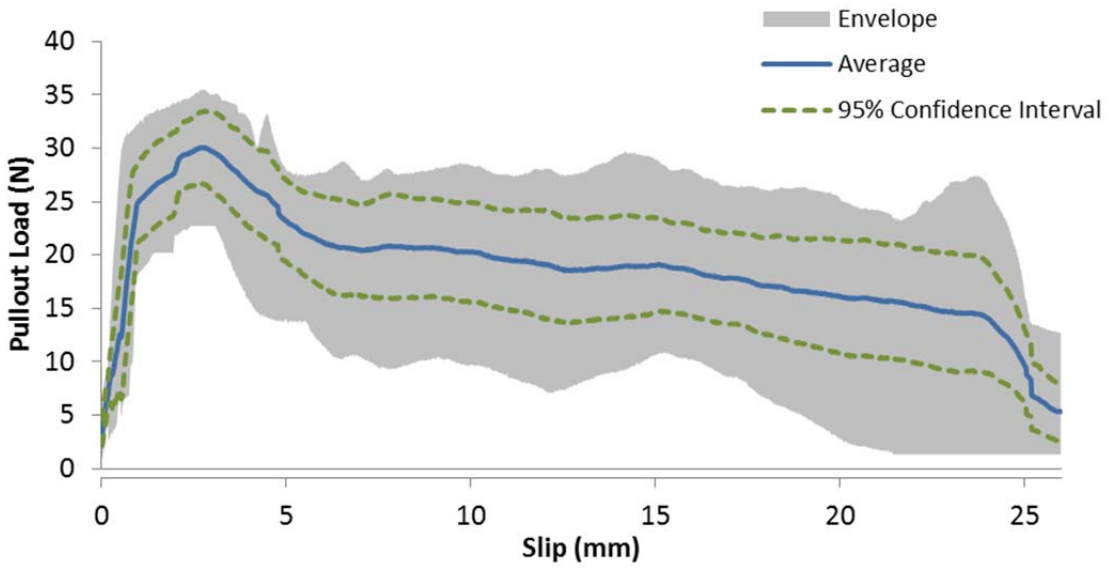

Figure B-107 - Load vs. slip curve for Tuf-Strand SF: 0 degree inclination angle, 25.4 mm embedment length

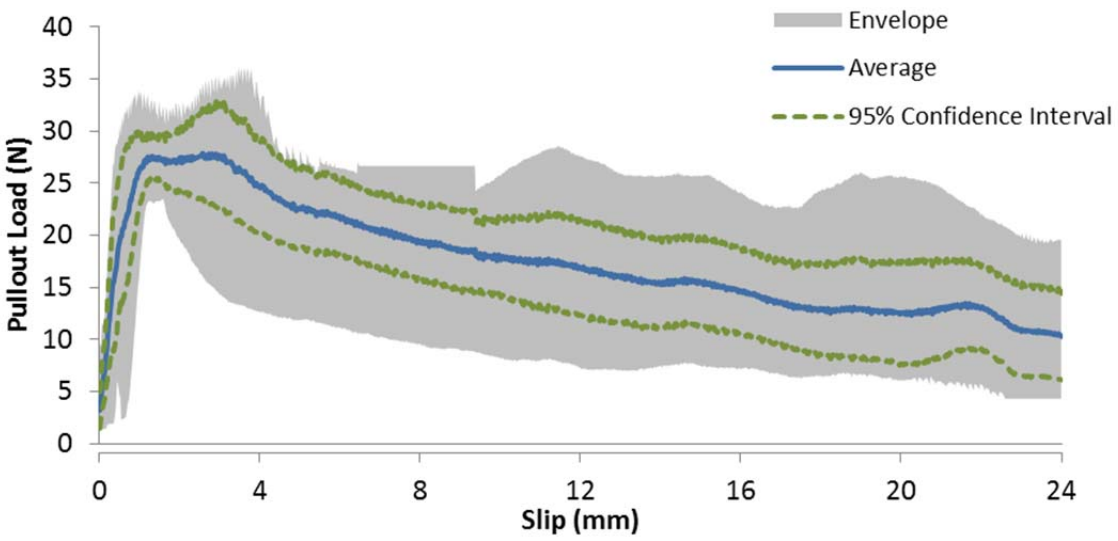

Figure B-108 - Load vs. slip curves for Tuf-Strand SF: 0 degree inclination angle, 22.2 mm embedment length

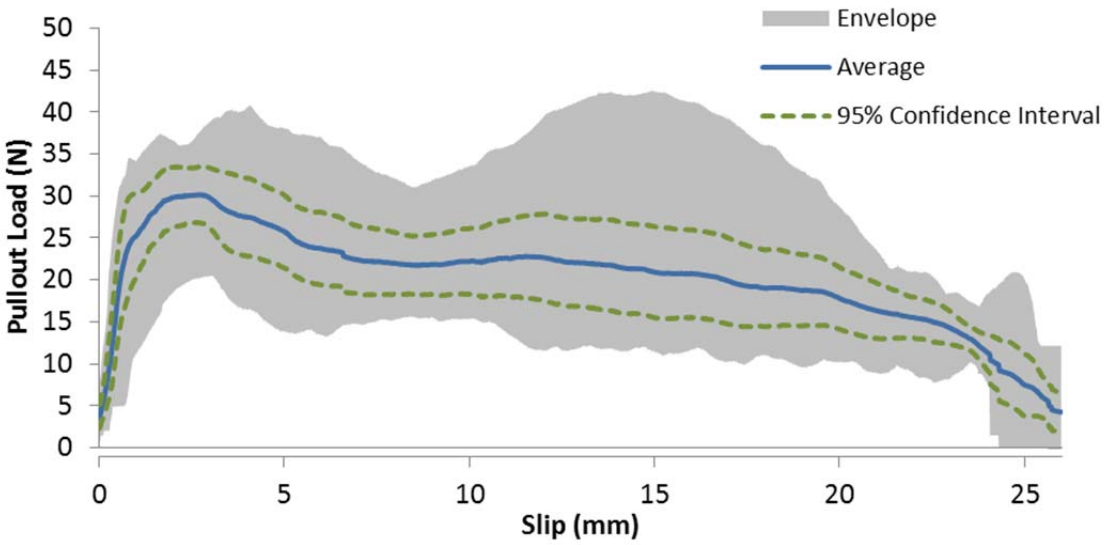

Figure B-109 - Load vs. slip curve for Tuf-Strand SF: 15 degree inclination angle, 25.4 mm embedment length

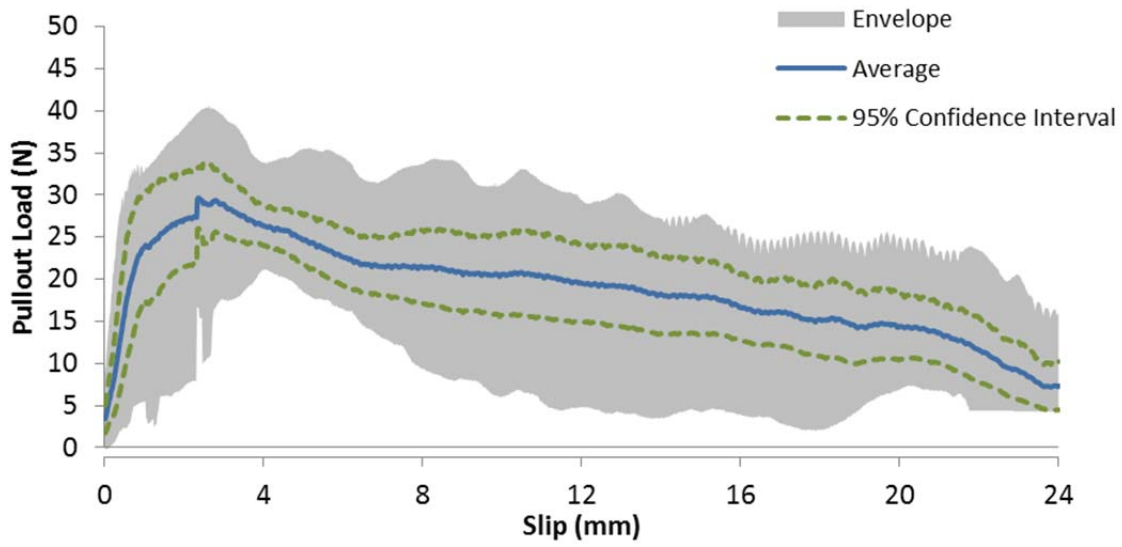

Figure B-110 - Load vs. slip curves for Tuf-Strand SF: 15 degree inclination angle, 22.2 mm embedment length

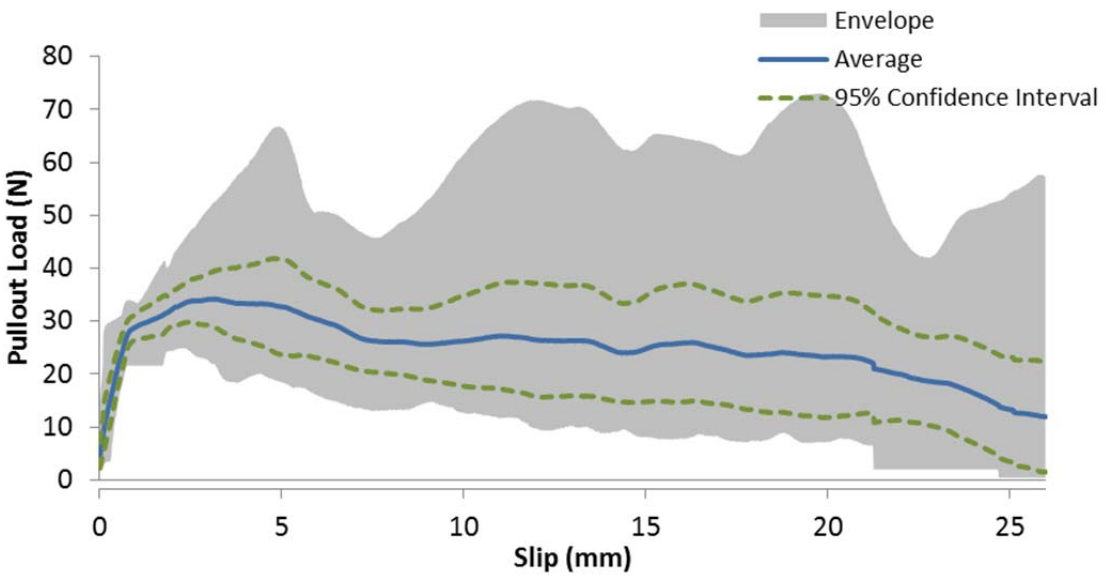

Figure B-111 - Load vs. slip curve for Tuf-Strand SF: 30 degree inclination angle, 25.4 mm embedment length

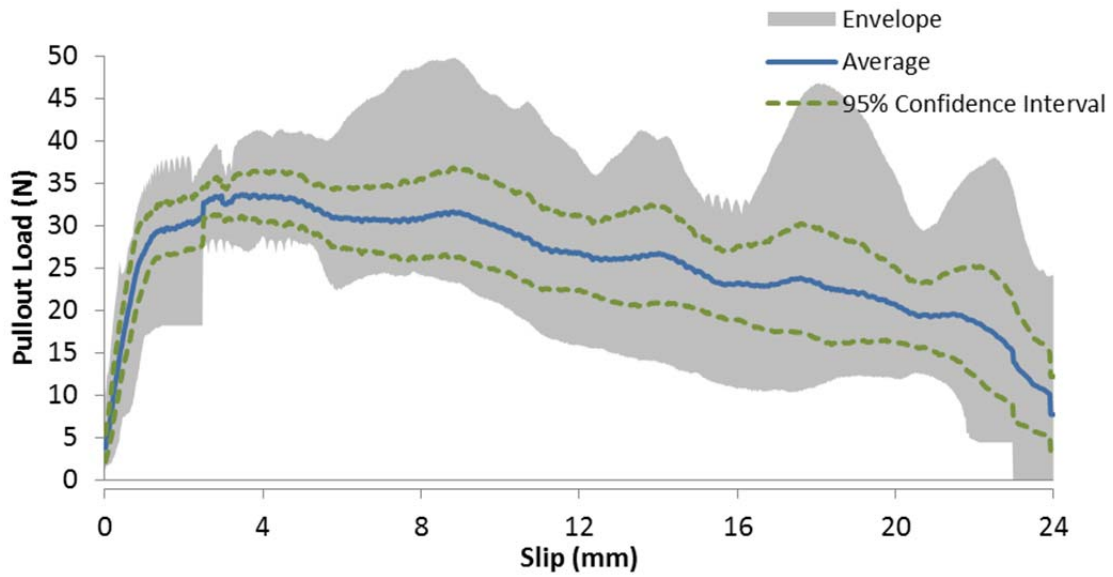

Figure B-112 - Load vs. slip curves for Tuf-Strand SF: 30 degree inclination angle, 22.2 mm embedment length

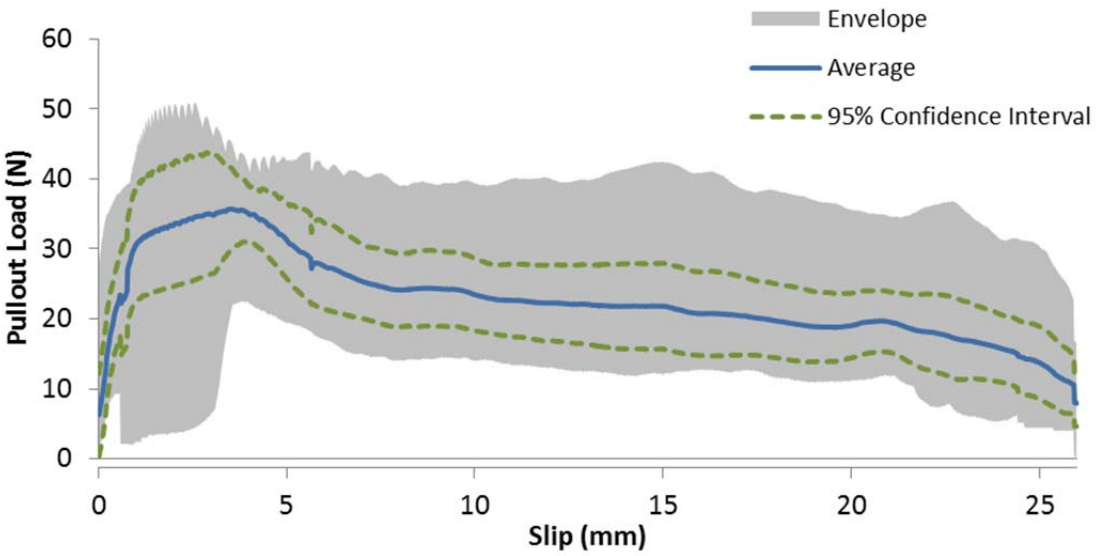

Figure B-113 - Load vs. slip curve for Tuf-Strand SF: 45 degree inclination angle, 25.4 mm embedment length

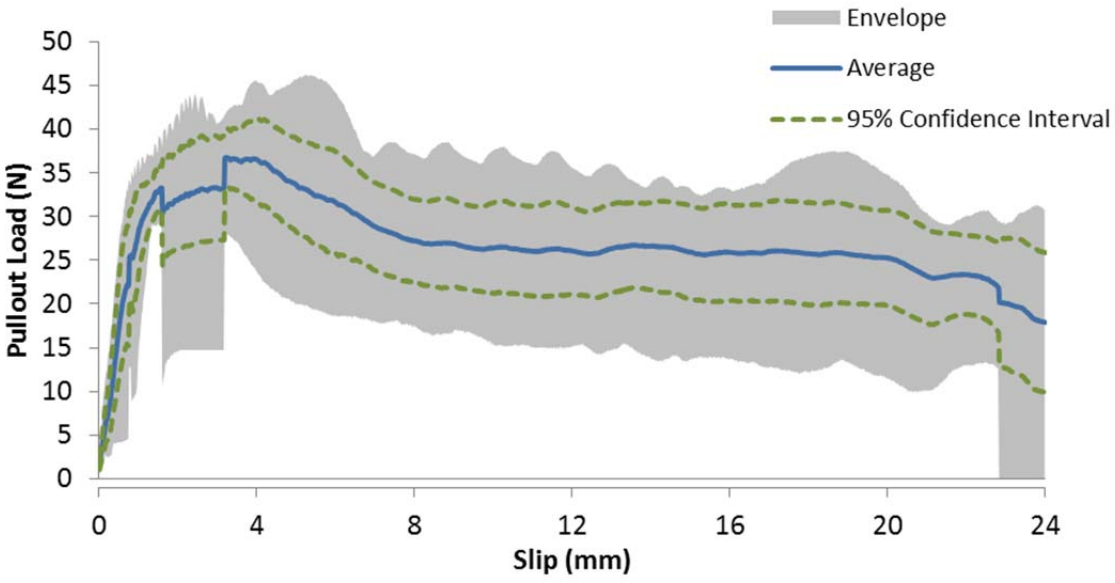

Figure B-114 - Load vs. slip curves for Tuf-Strand SF: 45 degree inclination angle, 22.2 mm embedment length

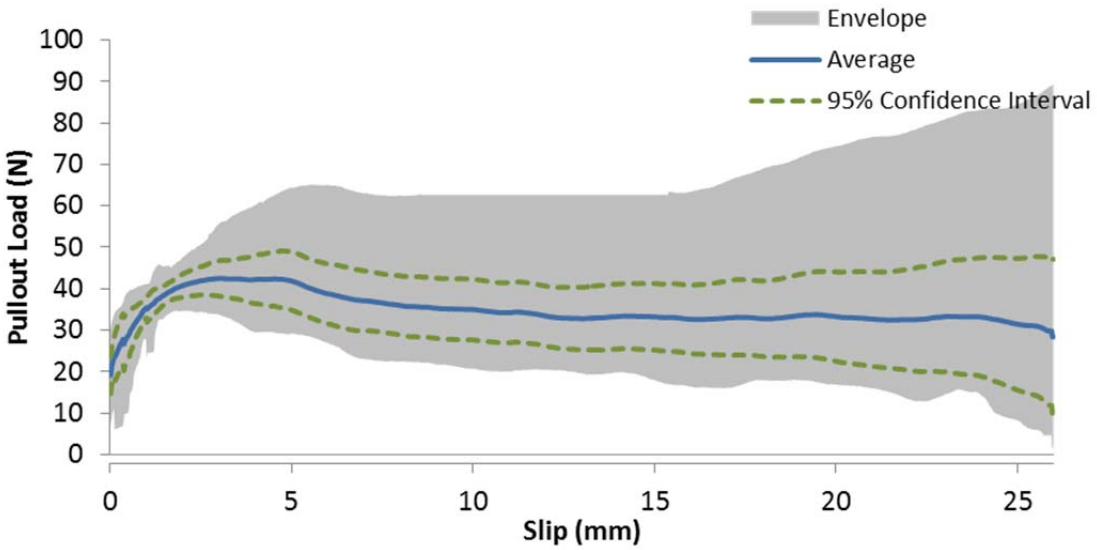

Figure B-115 - Load vs. slip curve for Tuf-Strand SF: 60 degree inclination angle, 25.4 mm embedment length

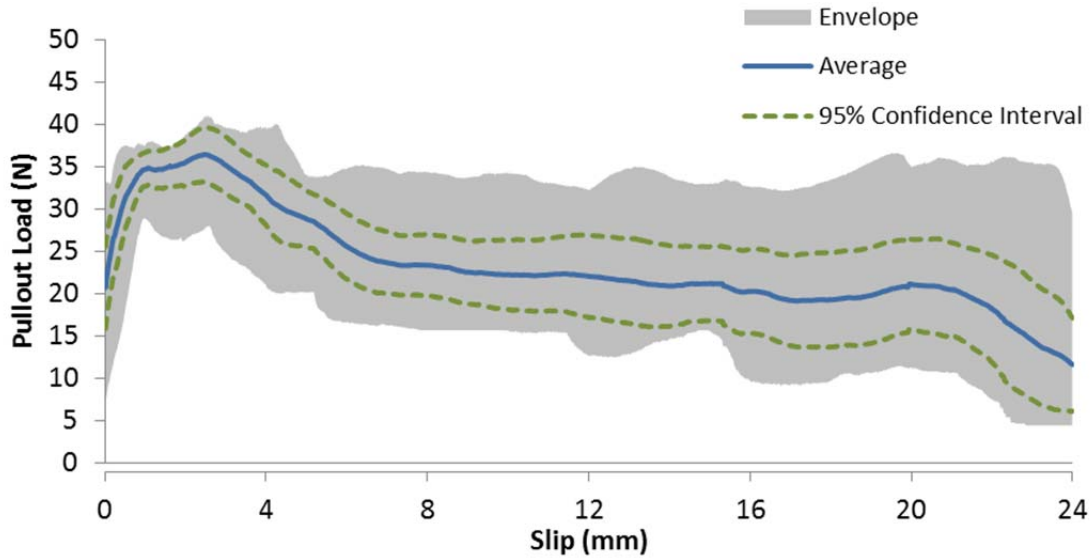

Figure B-116 - Load vs. slip curves for Tuf-Strand SF: 60 degree inclination angle, 22.2 mm embedment length

B.13 - HDPE 5906 MICROFIBER PULLOUT CURVES

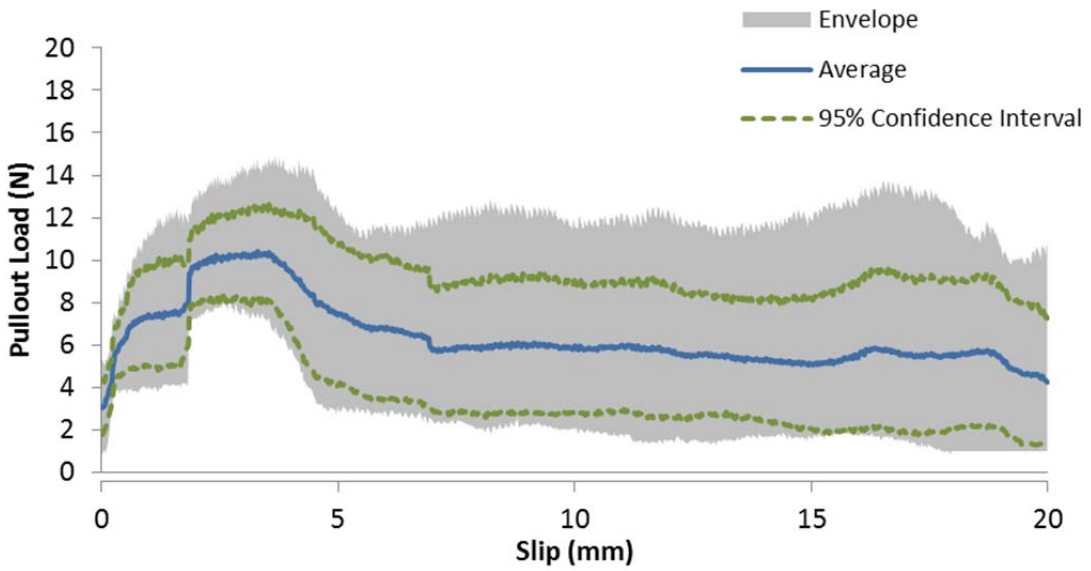

Figure B-117 - Load vs. slip curve for prototype microfiber containing HDPE 5906: 0 degree inclination angle, 19.1 mm embedment length

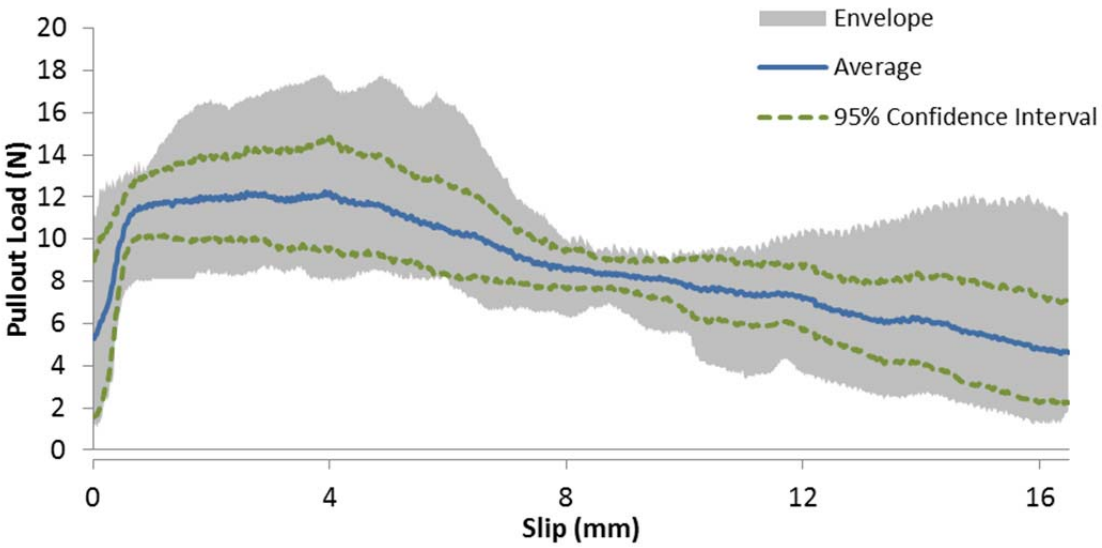

Figure B-118 - Load vs. slip curves for prototype microfiber containing HDPE 5906: 0 degree inclination angle, 15.9 mm embedment length

B.14 - HDPE 1288 MICROFIBER PULLOUT CURVES

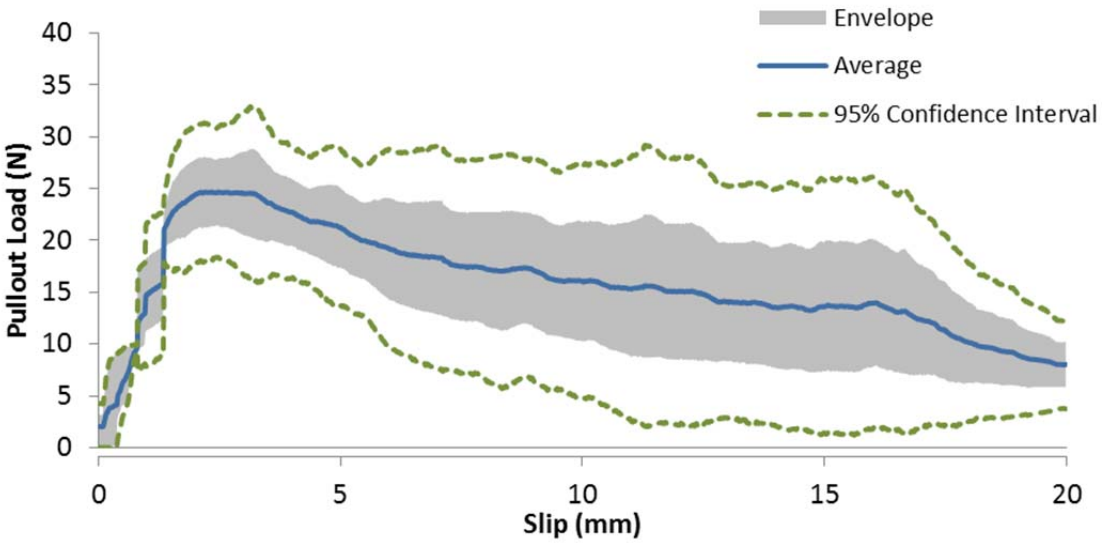

Figure B-119 - Load vs. slip curve for prototype microfiber containing HDPE 1288: 0 degree inclination angle, 19.1 mm embedment length

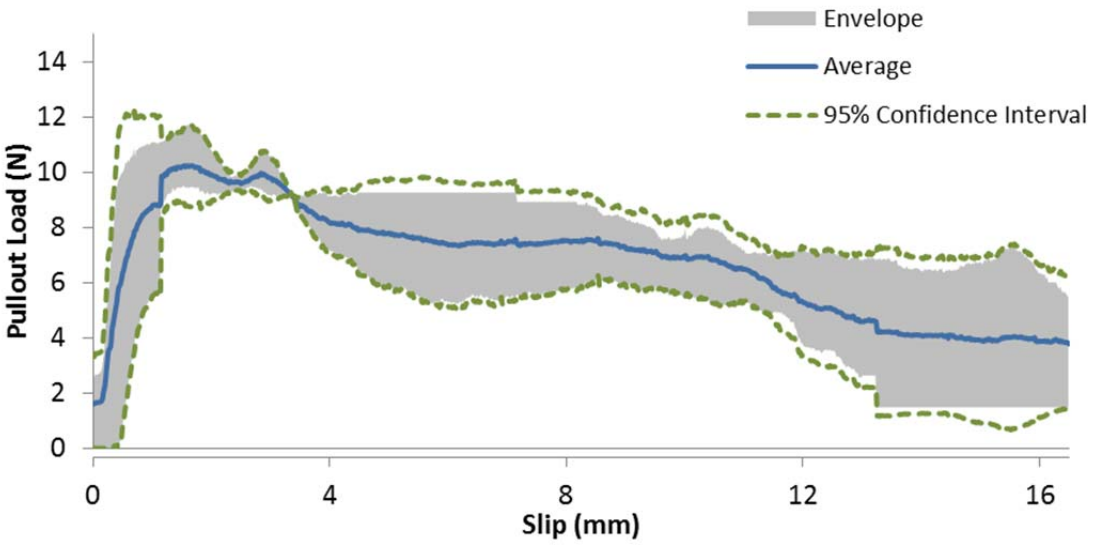

Figure B-120 - Load vs. slip curves for prototype microfiber containing HDPE 1288: 0 degree inclination angle, 15.9 mm embedment length

B.15 - HDPE, 10% PVDF, 20% MAH MICROFIBER PULLOUT CURVES

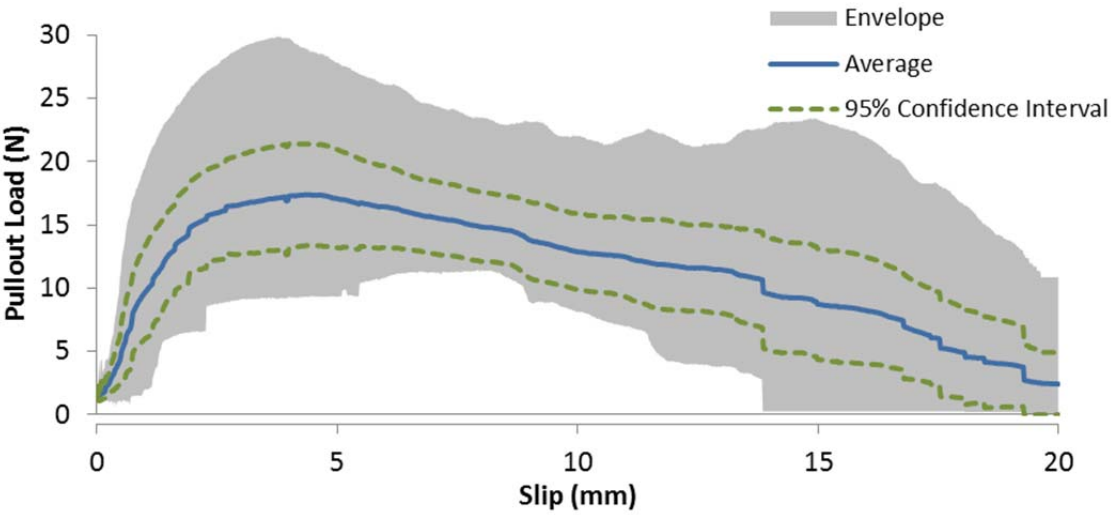

Figure B-121 - Load vs. slip curve for prototype microfiber containing HDPE, 10% PVDF and 20% MAH: 0 degree inclination angle, 19.1 mm embedment length

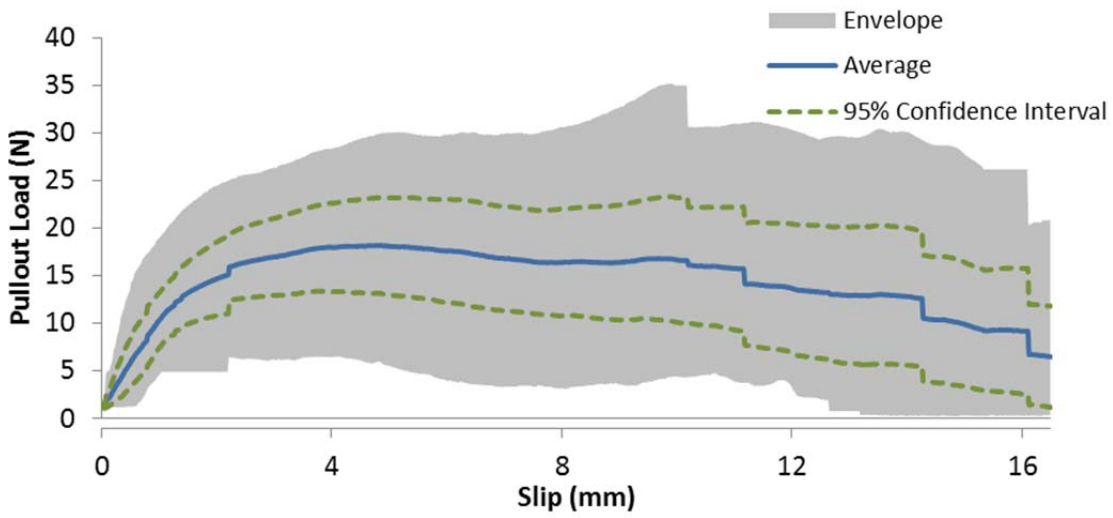

Figure B-122 - Load vs. slip curves for prototype microfiber containing HDPE, 10% PVDF and 20% MAH: 0 degree inclination angle, 15.9 mm embedment length

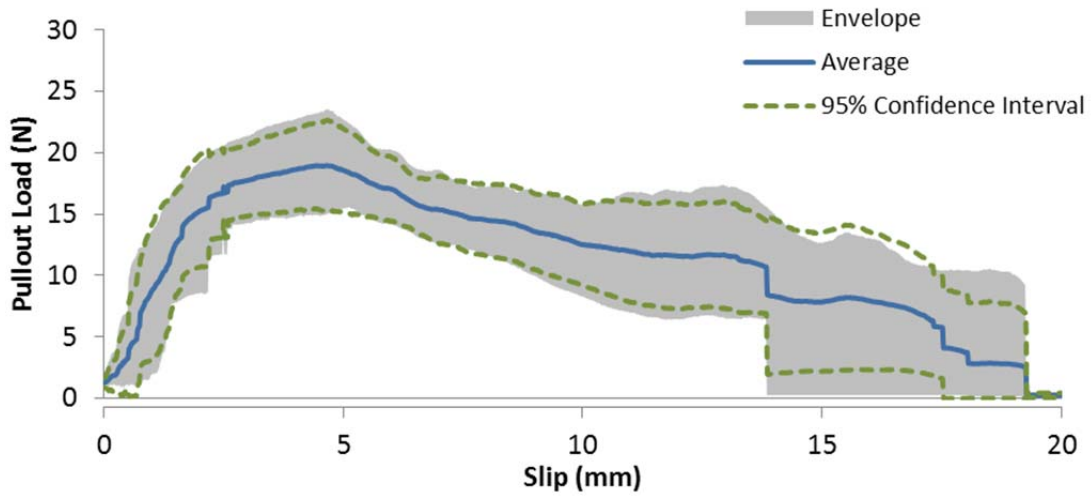

Figure B-123 - Load vs. slip curve for prototype microfiber containing HDPE, 10% PVDF and 20% MAH: 15 degree inclination angle, 19.1 mm embedment length

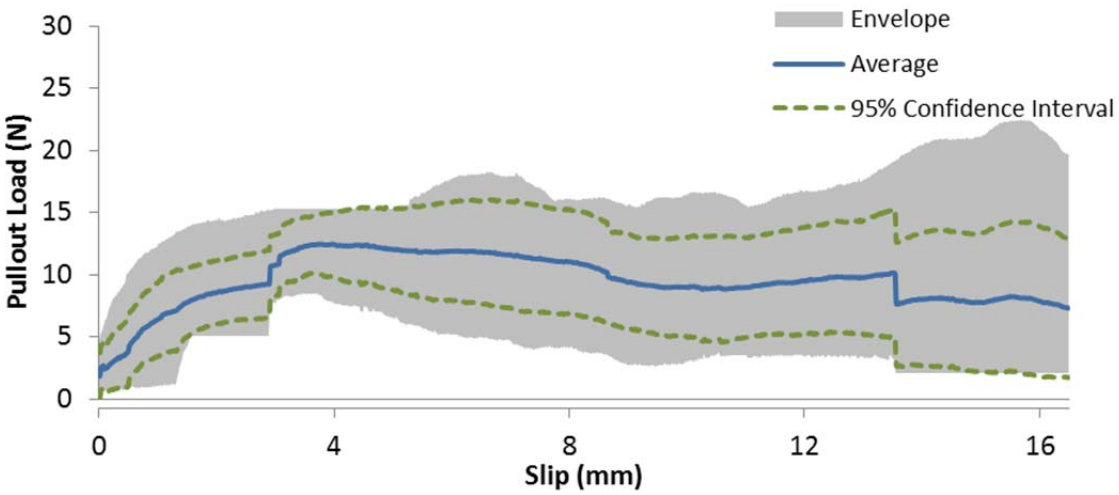

Figure B-124 - Load vs. slip curves for prototype microfiber containing HDPE, 10% PVDF and 20% MAH: 15 degree inclination angle, 15.9 mm embedment length

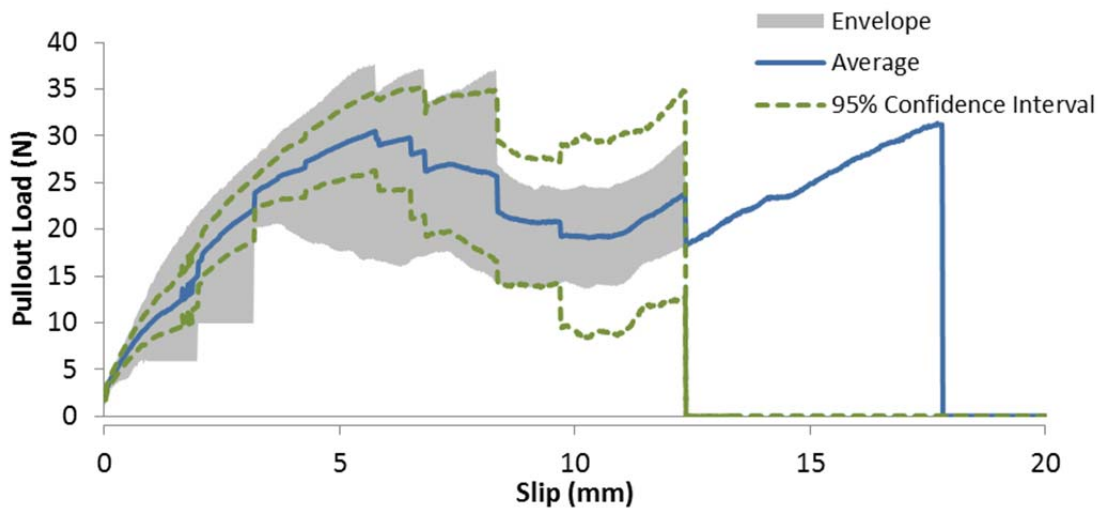

Figure B-125 - Load vs. slip curve for prototype microfiber containing HDPE, 10% PVDF and 20% MAH: 30 degree inclination angle, 19.1 mm embedment length

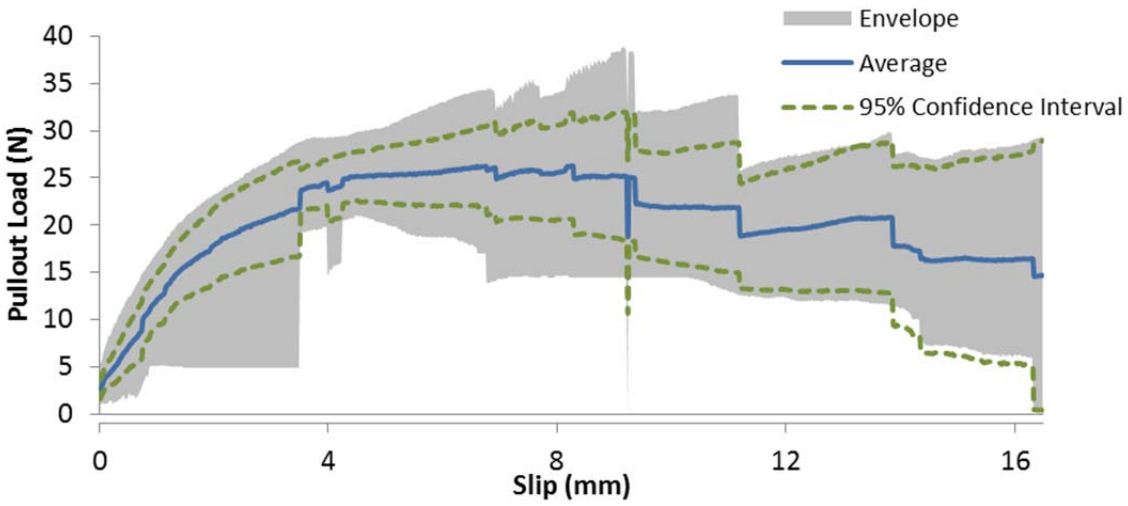

Figure B-126 - Load vs. slip curves for prototype microfiber containing HDPE, 10% PVDF and 20% MAH: 30 degree inclination angle, 15.9 mm embedment length

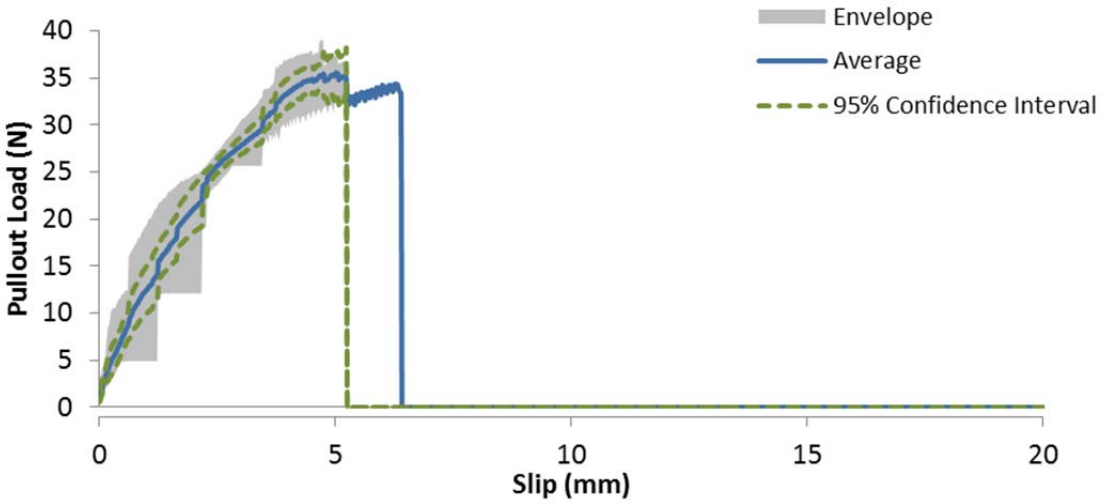

Figure B-127 - Load vs. slip curve for prototype microfiber containing HDPE, 10% PVDF and 20% MAH: 45 degree inclination angle, 19.1 mm embedment length

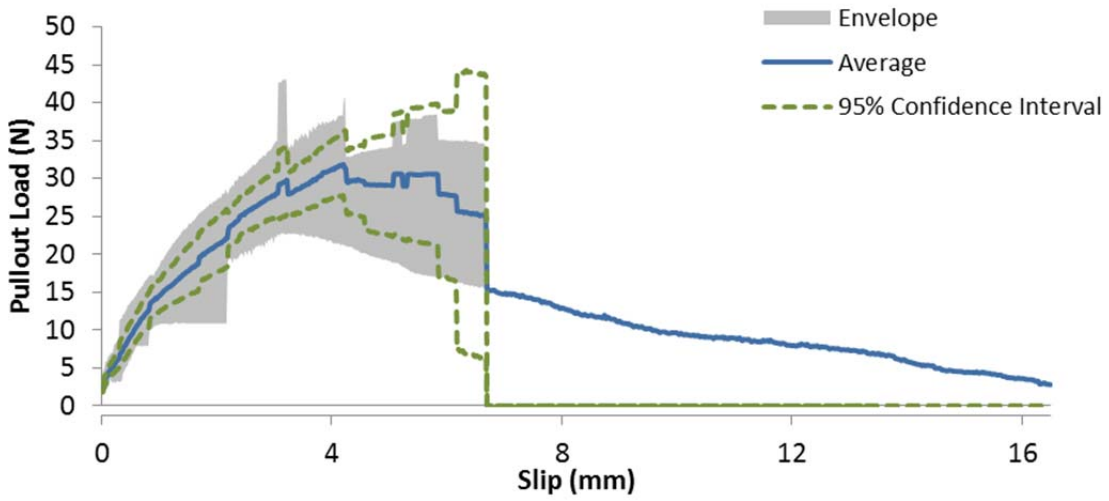

Figure B-128 - Load vs. slip curves for prototype microfiber containing HDPE, 10% PVDF and 20% MAH: 45 degree inclination angle, 15.9 mm embedment length

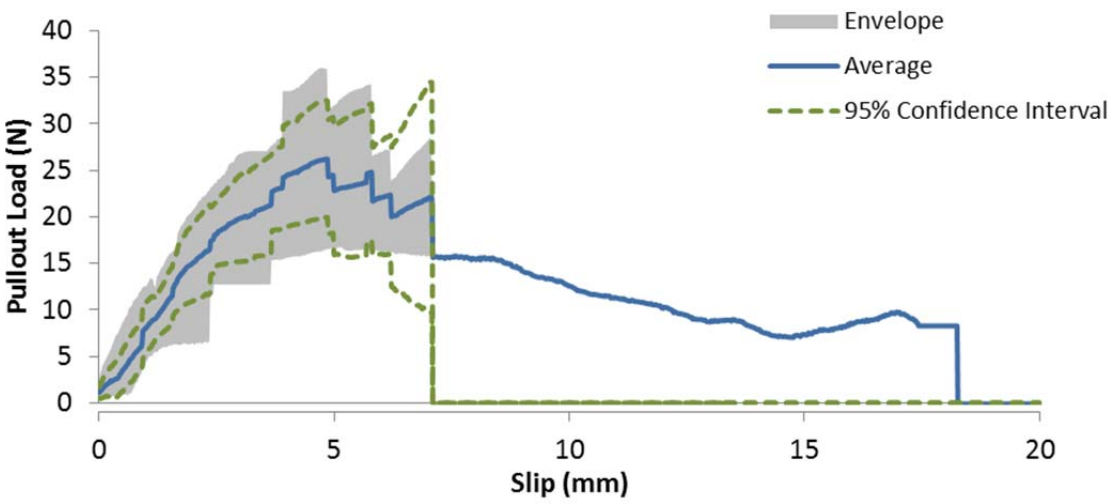

Figure B-129 - Load vs. slip curve for prototype microfiber containing HDPE, 10% PVDF and 20% MAH: 60 degree inclination angle, 19.1 mm embedment length

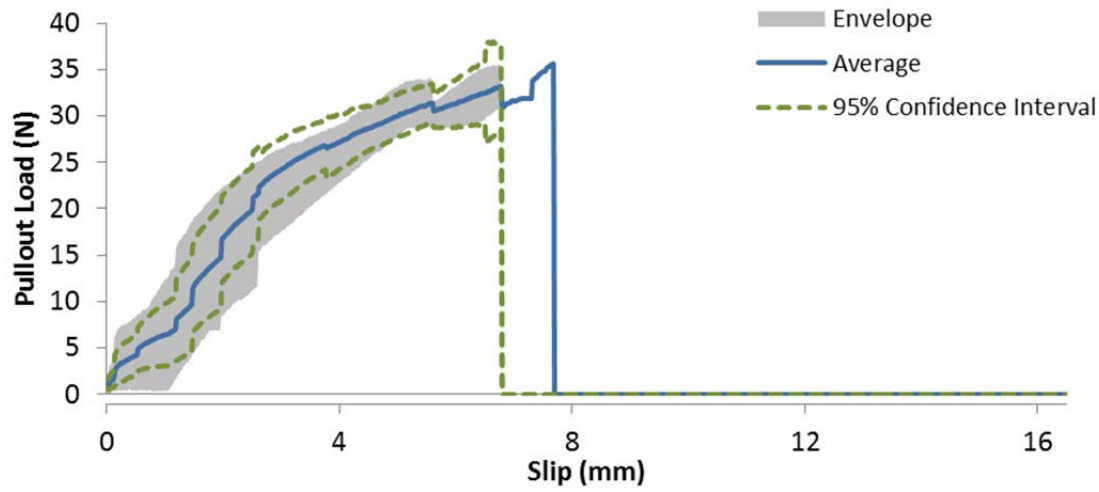

Figure B-130 - Load vs. slip curves for prototype microfiber containing HDPE, 10% PVDF and 20% MAH: 60 degree inclination angle, 15.9 mm embedment length

B.16 - HDPE, 10% EVA MICROFIBER PULLOUT CURVES

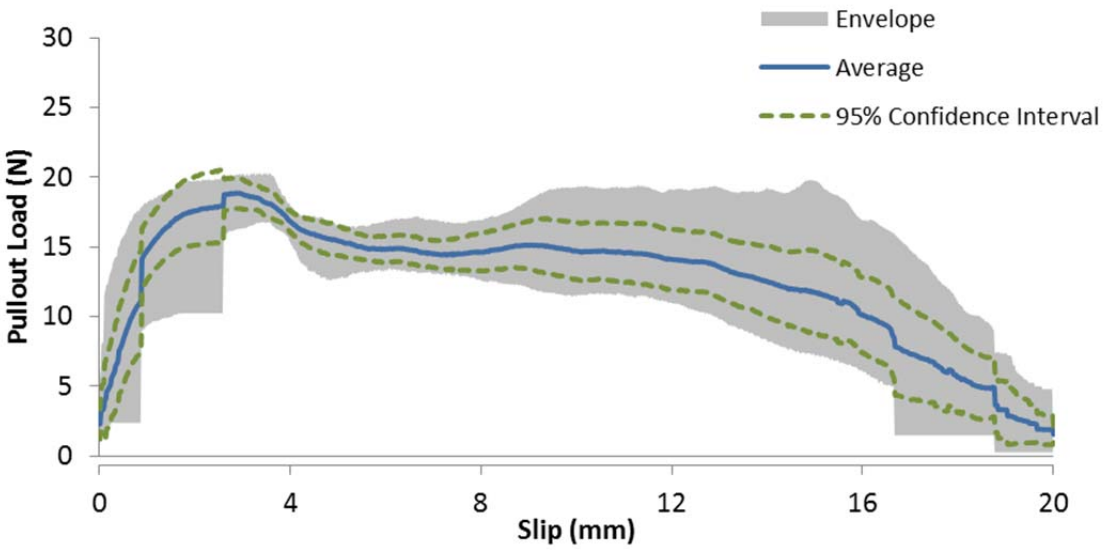

Figure B-131 - Load vs. slip curve for prototype microfiber containing HDPE and 10% EVA: 0 degree inclination angle, 19.1 mm embedment length

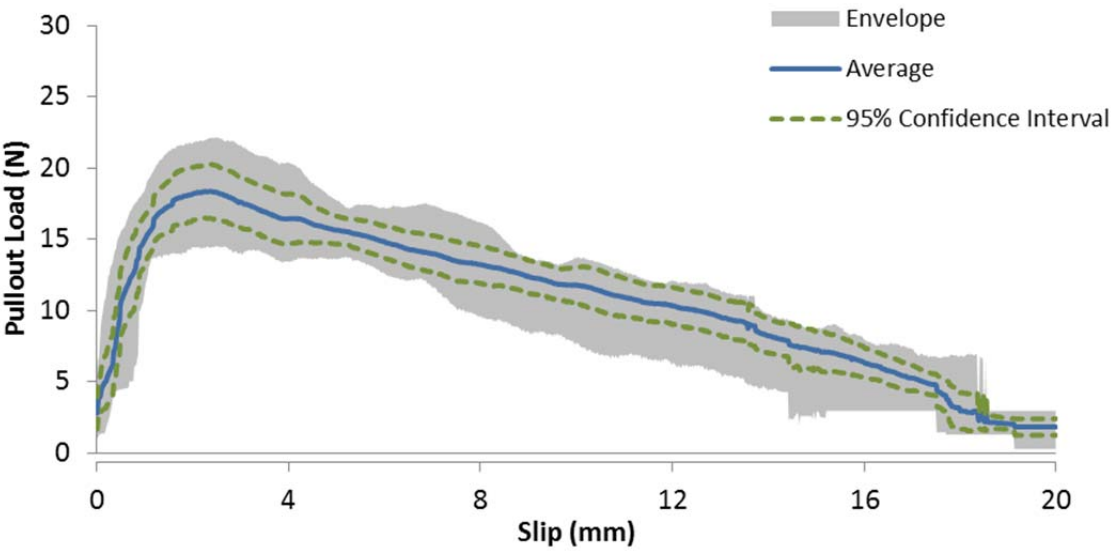

Figure B-132 - Load vs. slip curves for prototype microfiber containing HDPE and 10% EVA: 0 degree inclination angle, 15.9 mm embedment length

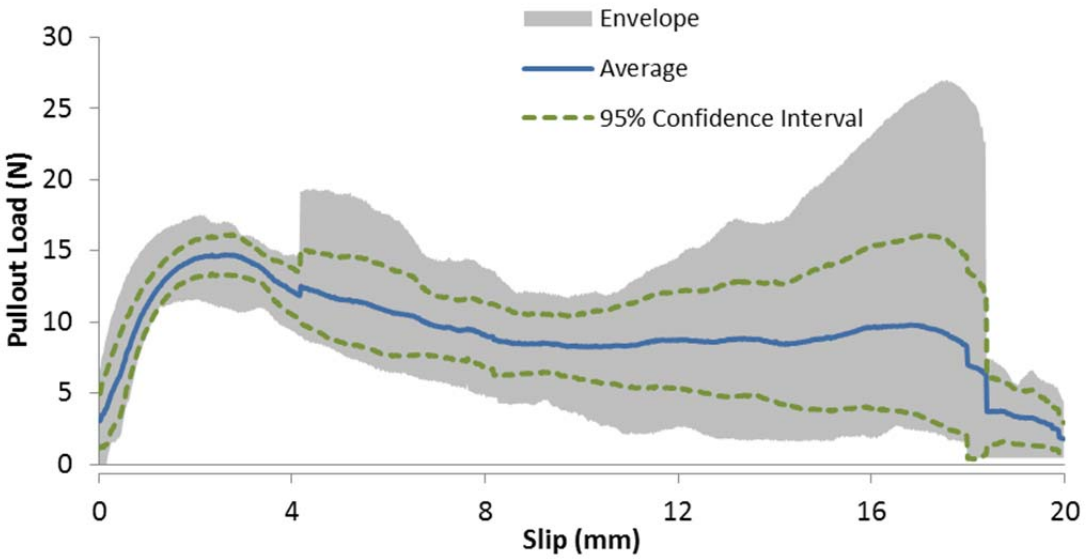

Figure B-133 - Load vs. slip curve for prototype microfiber containing HDPE and 10% EVA: 15 degree inclination angle, 19.1 mm embedment length

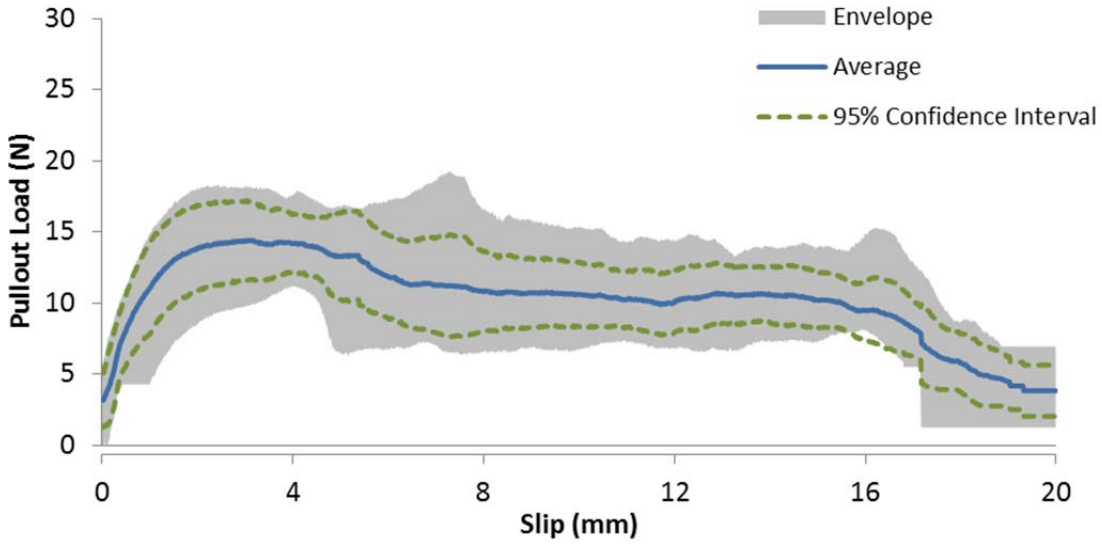

Figure B-134 - Load vs. slip curves for prototype microfiber containing HDPE and 10% EVA: 15 degree inclination angle, 15.9 mm embedment length

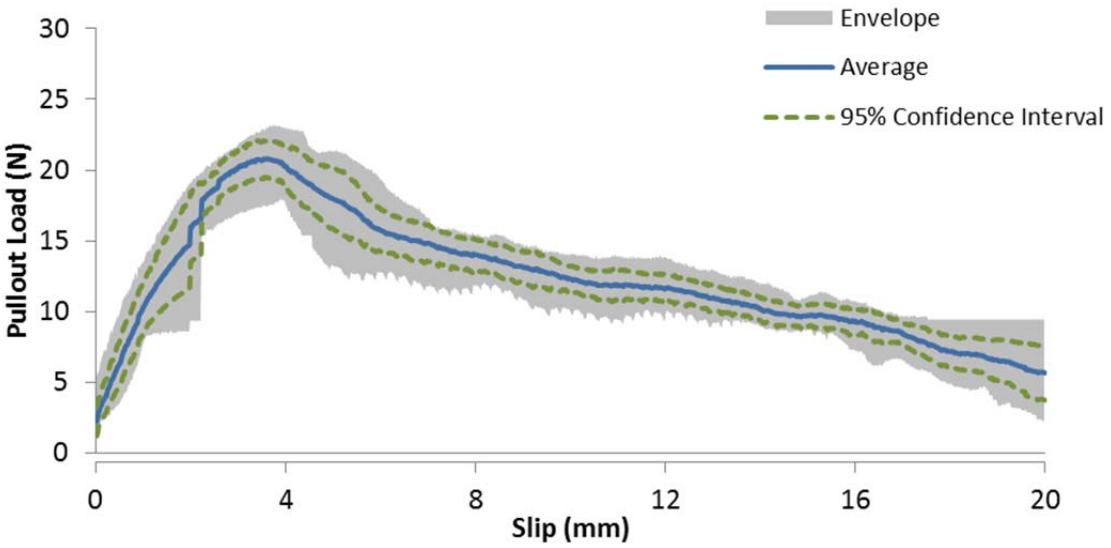

Figure B-135 - Load vs. slip curve for prototype microfiber containing HDPE and 10% EVA: 30 degree inclination angle, 19.1 mm embedment length

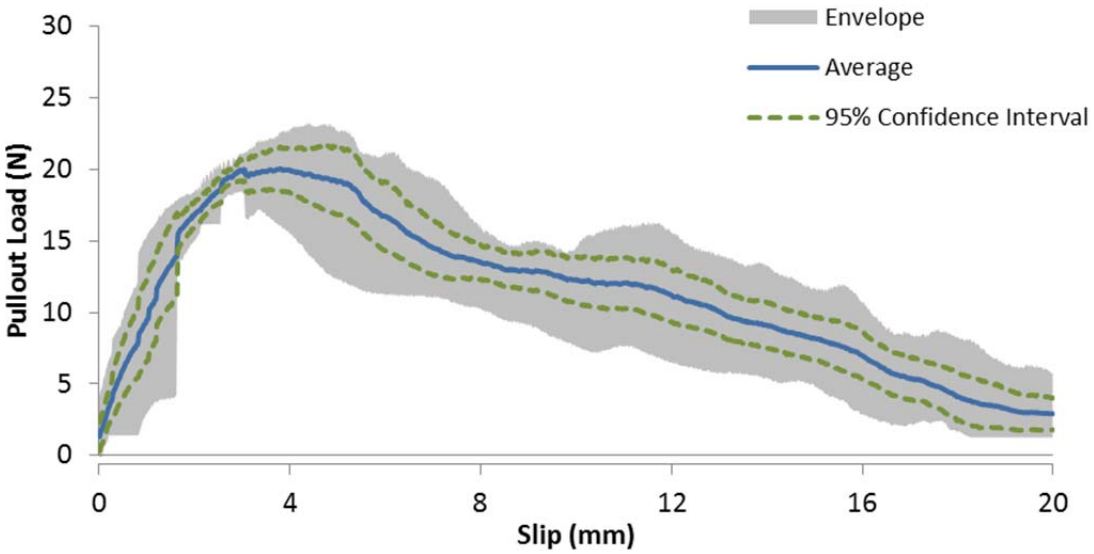

Figure B-136 - Load vs. slip curves for prototype microfiber containing HDPE and 10% EVA: 30 degree inclination angle, 15.9 mm embedment length

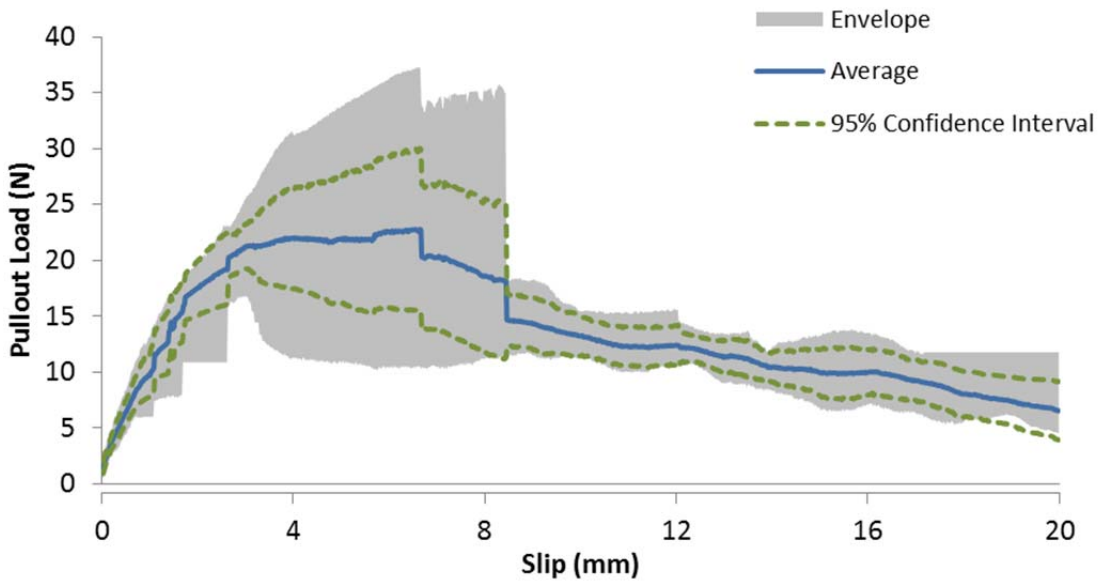

Figure B-137 - Load vs. slip curve for prototype microfiber containing HDPE and 10% EVA: 45 degree inclination angle, 19.1 mm embedment length

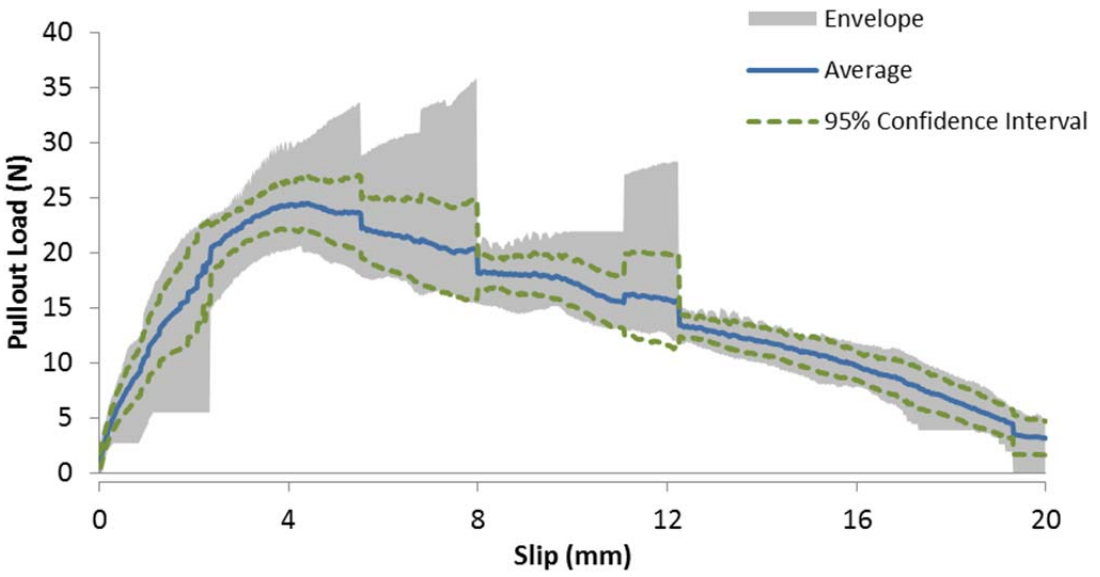

Figure B-138 - Load vs. slip curves for prototype microfiber containing HDPE and 10% EVA: 45 degree inclination angle, 15.9 mm embedment length

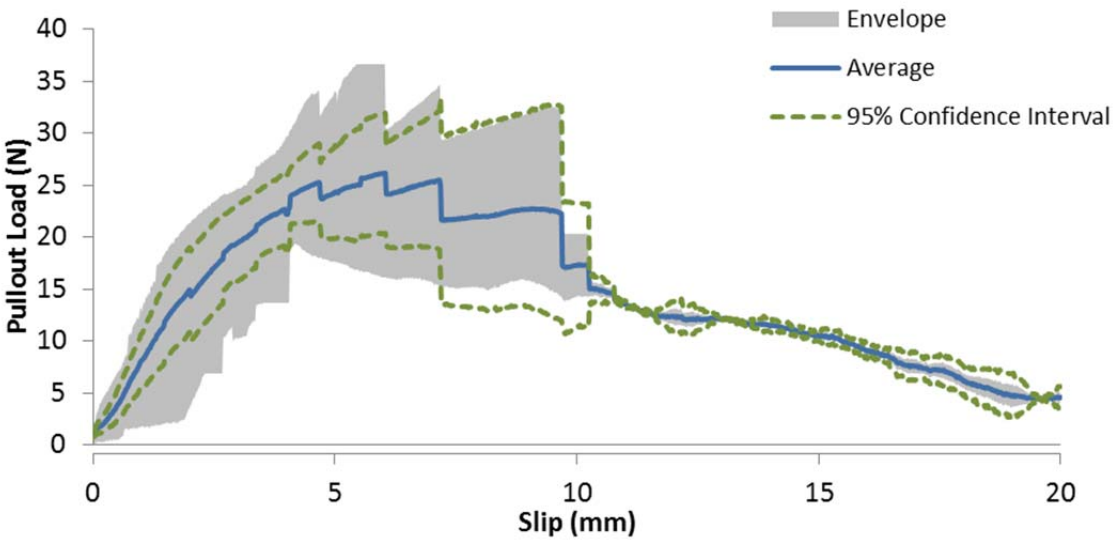

Figure B-139 - Load vs. slip curve for prototype microfiber containing HDPE and 10% EVA: 60 degree inclination angle, 19.1 mm embedment length

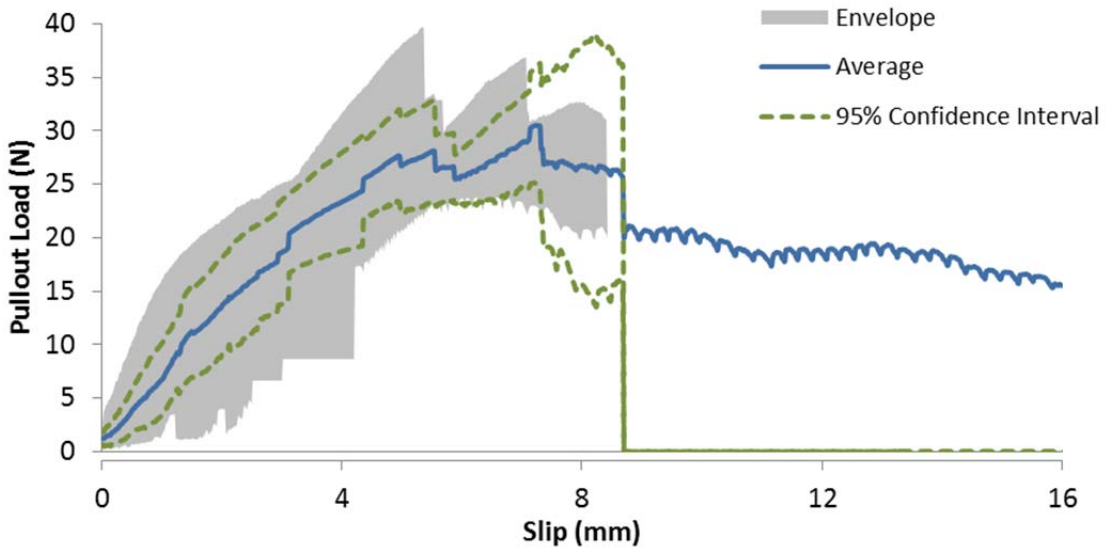

Figure B-140 - Load vs. slip curves for prototype microfiber containing HDPE and 10% EVA: 60 degree inclination angle, 15.9 mm embedment length

B.17 - NYLON PULLOUT CURVES

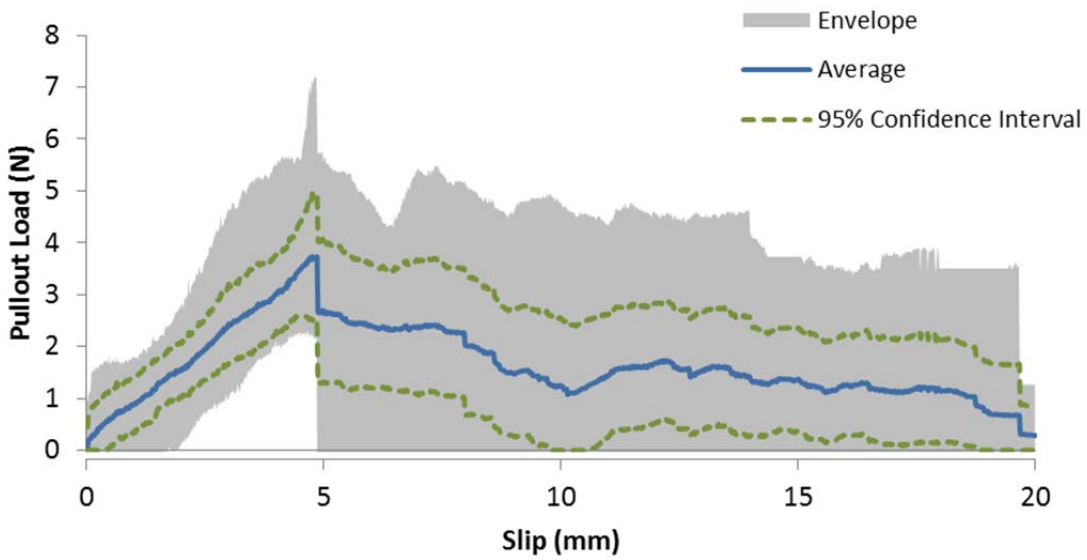

Figure B-141 - Load vs. slip curve for nylon: 0 degree inclination angle, 19.1 mm embedment length

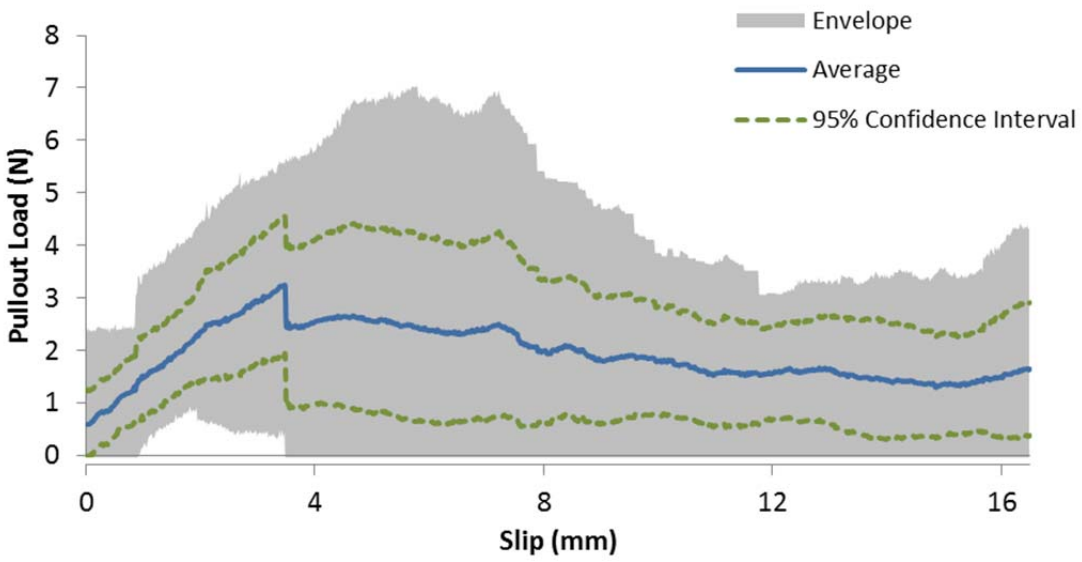

Figure B-142 - Load vs. slip curves for nylon: 0 degree inclination angle, 15.9 mm embedment length

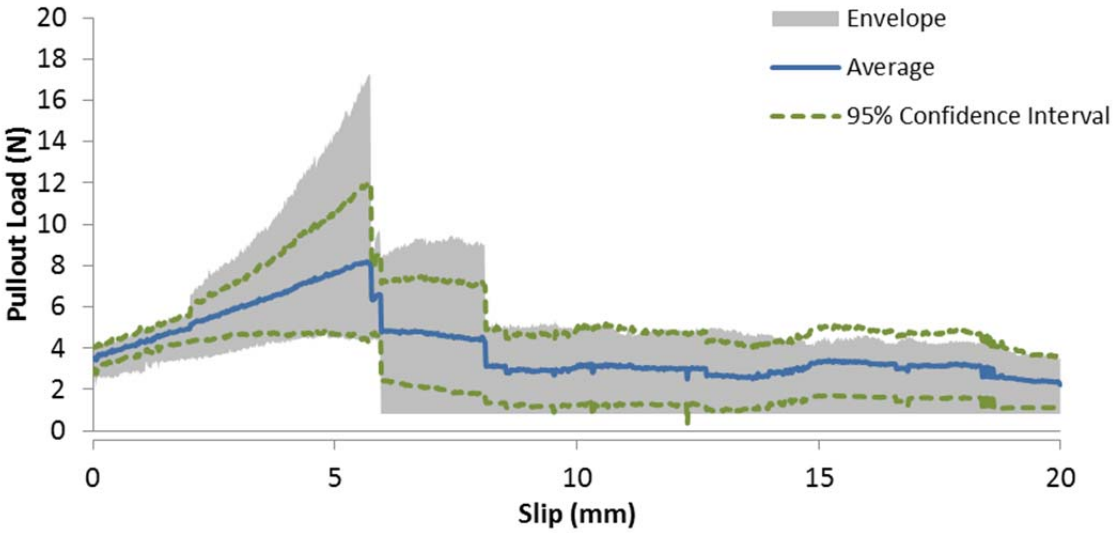

Figure B-143 - Load vs. slip curve for nylon: 15 degree inclination angle, 19.1 mm embedment length

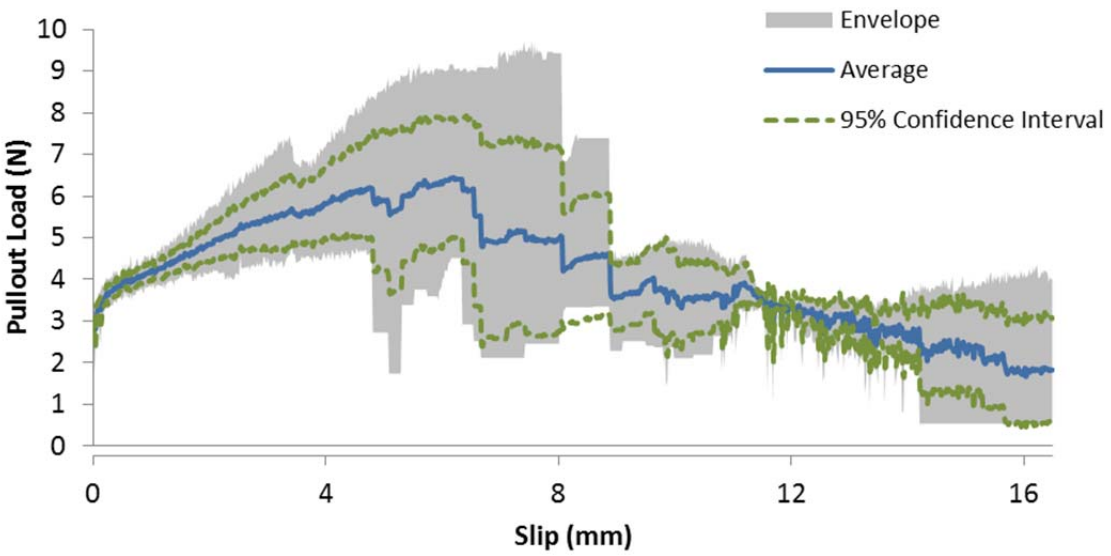

Figure B-144 - Load vs. slip curves for nylon: 15 degree inclination angle, 15.9 mm embedment length

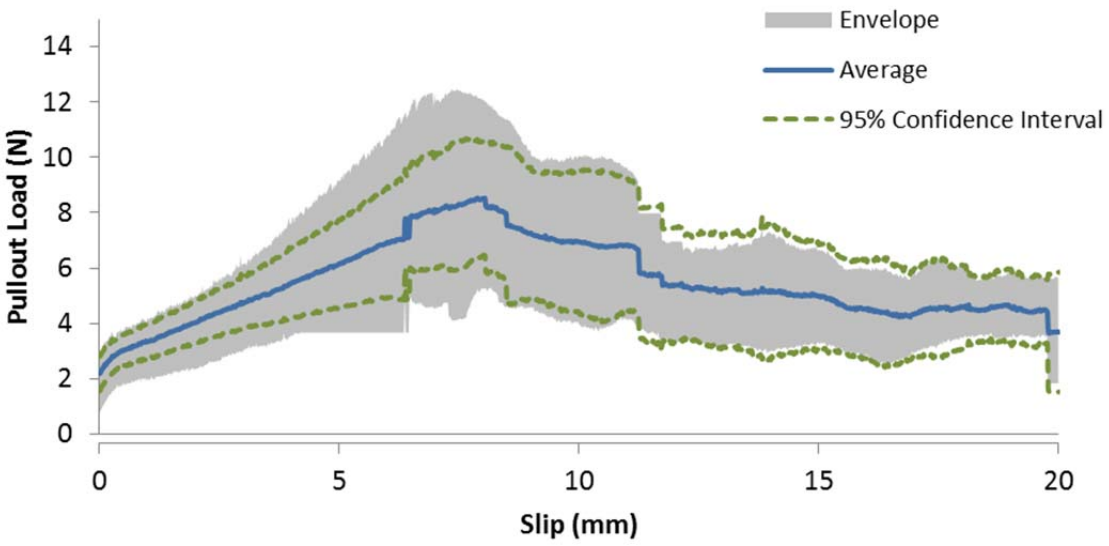

Figure B-145 - Load vs. slip curve for nylon: 30 degree inclination angle, 19.1 mm embedment length

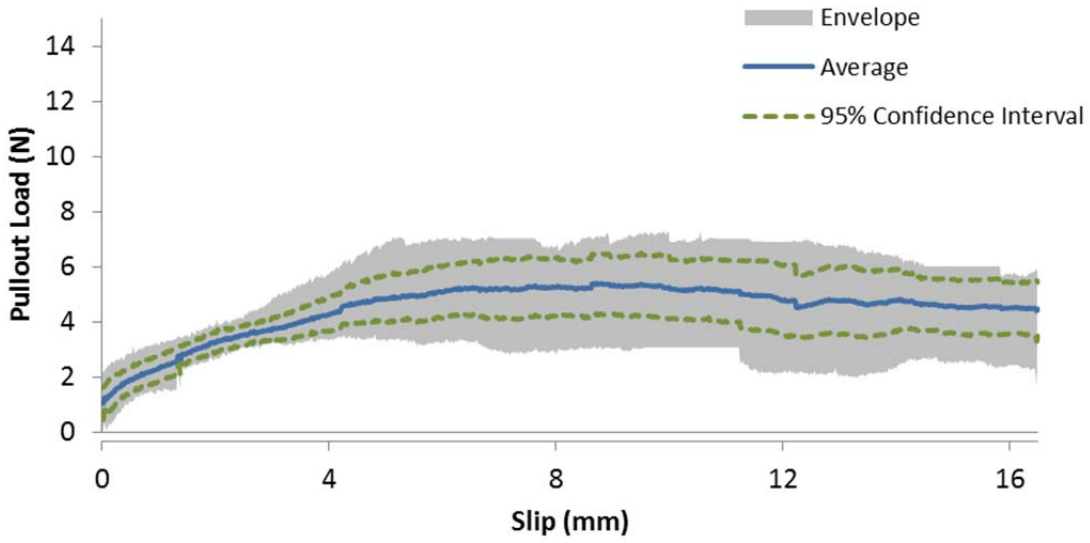

Figure B-146 - Load vs. slip curves for nylon: 30 degree inclination angle, 15.9 mm embedment length

B.18 - PVA PULLOUT CURVES

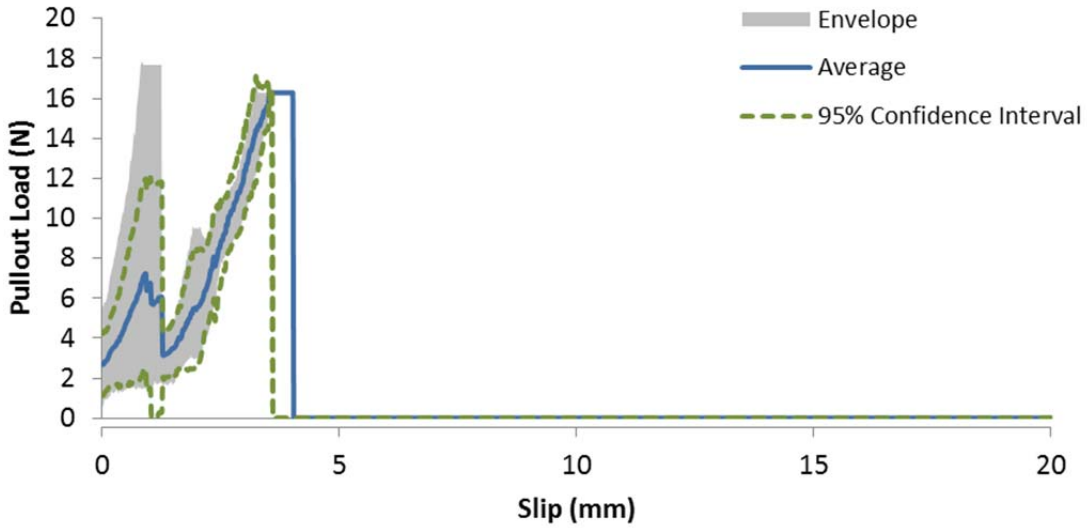

Figure B-147 - Load vs. slip curve for PVA: 0 degree inclination angle, 19.1 mm embedment length

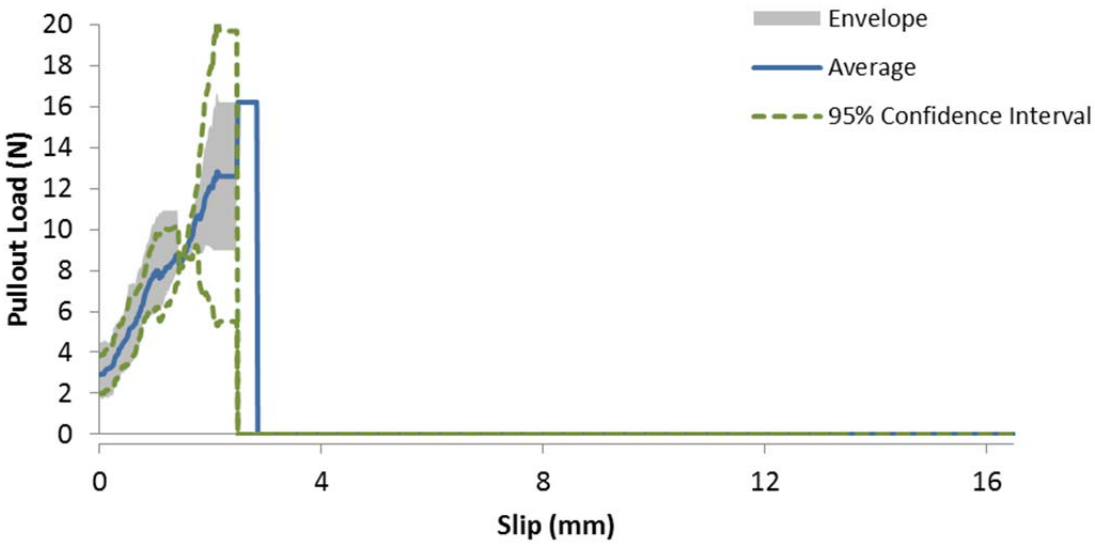

Figure B-148 - Load vs. slip curves for PVA: 0 degree inclination angle, 15.9 mm embedment length

APPENDIX C - RESULTS OF FRC MIXTURES FOR PERFORMANCE TESTING

Figure C-149 - Washout sample and virgin sample of prototype fiber containing 100% HDPE

Figure C-150 - Washout sample and virgin sample of cut prototype fiber containing HDPE and 1% PVDF

Figure C-151 - Washout sample and virgin sample of cut prototype fiber containing HDPE and 3% PVDF

Figure C-152 - Washout sample and virgin sample of cut prototype fiber containing HDPE, 5% PVDF and 10% MAH

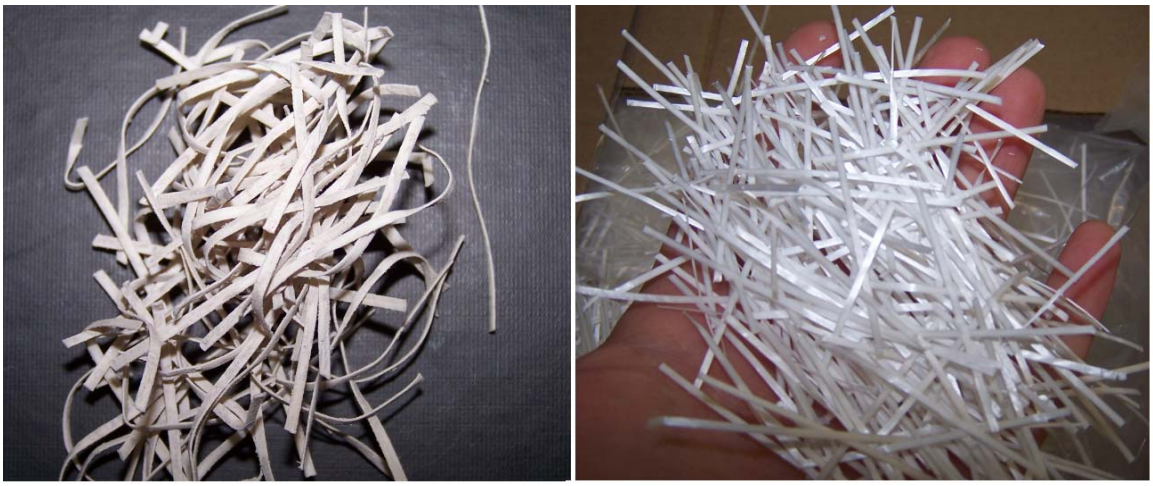

Figure C-153 - Washout sample and virgin sample of cut prototype fiber containing HDPE, 7% PVDF and 10% MAH

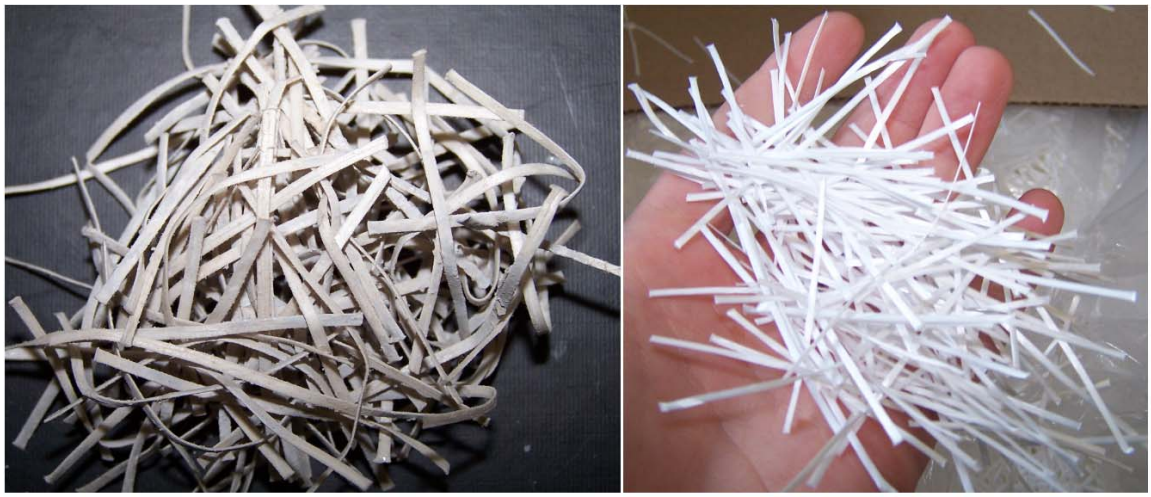

Figure C-154 - Washout sample and virgin sample of cut prototype fiber containing HDPE, 9% PVDF and 10% MAH

Figure C-155 - Washout sample and virgin sample of cut prototype fiber containing HDPE, 11% PVDF and 20% MAH

Figure C-156 - Washout sample and virgin sample of cut prototype fiber containing HDPE and 10% EVA

Figure C-157 - Washout sample and virgin sample of cut and twisted prototype fiber containing PP, 10% HDPE and 10% EVA

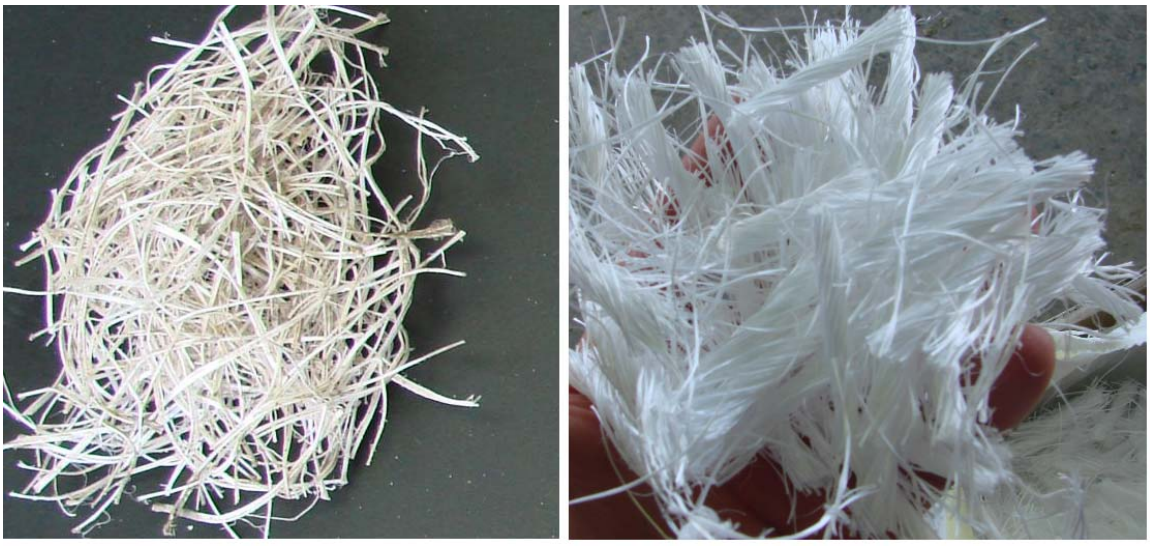

Figure C-158 - Washout sample and virgin sample of cut and twisted Tuf-Strand SF fiber

Table C-16 - Individual specimen results of compressive strength testing of FRC mixtures

Fiber	Sample ID	Load (N)	Compressive Strength (MPa)	Average Compressive Strength (MPa)
100% HDPE	SA-1	338532	41.8	**41.6**
	SA-2	342970	42.3	
	SA-3	329656	40.7	
HDPE, 1% PVDF	SA-1	369599	45.6	**43.9**
	SA-2	360723	44.5	
	SA-3	338532	41.8	
HDPE, 3% PVDF	SA-1	356284	43.9	**44.9**
	SA-2	367380	45.3	
	SA-3	369599	45.6	
HDPE, 5% PVDF, 10% MAH	SA-1	327437	40.4	**41.7**
	SA-2	347408	42.9	
	SA-3	338532	41.8	
HDPE, 7% PVDF, 10% MAH	SA-1	380694	47.0	**46.5**
	SA-2	391789	48.3	
	SA-3	358504	44.2	
HDPE, 9% PVDF, 10% MAH	SA-1	287495	35.5	**37.4**
	SA-2	318561	39.3	
HDPE, 11% PVDF, 20% MAH	SA-1	338532	41.8	**42.5**
	SA-2	342970	42.3	
	SA-3	351846	43.4	
HDPE, 10% EVA	SA-1	320780	39.6	**39.9**
	SA-2	329656	40.7	
	SA-3	320780	39.6	
80% PP, 10% HDPE, 10% EVA	SA-1	334094	41.2	**41.2**
	SA-2	338532	41.8	
	SA-3	329656	40.7	
BASF - Masterfiber MAC470	SA-1	331875	40.9	**39.0**
	SA-2	300809	37.1	
Strux 85/50	SA-1	249771	30.8	**36.1**
	SA-2	336313	41.5	
Tuf-strand SF	SA-1	240895	29.7	**32.2**
	SA-2	271962	33.5	
	SA-3	258648	31.9	
	SA-4	274181	33.8	

APPENDIX D - ADDITIONAL TABLES AND PLOTS FOR ASTM C1609 TESTING RESULTS

Table D-17 - Summary of results from ASTM C1609 testing, averages only

Fiber	Width (mm)	Height (mm)	f_p (MPa)	P_{900}^{150} (kN)	f_{900}^{150} (MPa)	P_{600}^{150} (kN)	f_{600}^{150} (MPa)	P_{400}^{150} (kN)	f_{400}^{150} (MPa)	P_{150}^{150} (kN)	f_{150}^{150} (MPa)	T_{150}^{150} (Joules)
100% HDPE	152.9	153.9	4.94	8.20	1.02	6.50	0.81	5.53	0.69	4.15	0.52	17.88
HDPE, 1% PVDF	155.8	153.1	4.6	8.9	1.1	7.1	0.9	6.4	0.8	4.7	0.6	21.7
HDPE, 3% PVDF	150.5	153.5	4.5	7.8	1.0	6.2	0.8	5.5	0.7	4.2	0.5	18.8
HDPE, 5% PVDF, 10% MAH	151.3	153.2	5.1	8.4	1.1	6.6	0.8	5.7	0.7	4.7	0.6	19.7
HDPE, 7% PVDF, 10% MAH	153.5	153.7	4.7	8.6	1.1	6.6	0.8	5.7	0.7	4.2	0.5	19.0
HDPE, 9% PVDF, 10% MAH	153.5	153.1	4.7	7.8	1.0	6.3	0.8	5.5	0.7	4.5	0.6	18.9
HDPE, 11% PVDF, 20% MAH	153.3	153.4	4.5	7.3	0.9	5.7	0.7	4.9	0.6	3.9	0.5	17.4
HDPE, 10% EVA	154.0	153.8	4.8	7.6	0.9	5.8	0.7	5.0	0.6	3.8	0.5	17.1
80% PP, 10% HDPE, 10% EVA	153.0	153.3	5.0	10.2	1.3	8.4	1.1	7.7	1.0	7.2	0.9	25.9
BASF - Masterfiber MAC470	152.8	153.3	5.0	9.6	1.2	7.7	1.0	6.6	0.8	4.6	0.6	20.9
Strux 85/50	152.5	152.3	4.5	9.6	1.2	8.3	1.1	8.0	1.0	8.1	1.0	23.1
Tuf-strand SF	150.0	150.0	4.4	11.1	1.4	9.6	1.2	8.7	1.1	8.3	1.0	28.9

Table D-18 - Individual specimen results for ASTM C1609 testing - 1 of 3

Sample ID	Width (mm)	Height (mm)	f_p (Mpa)	P_{900}^{150} (kN)	f_{900}^{150} (MPa)	P_{600}^{150} (kN)	f_{600}^{150} (MPa)	P_{400}^{150} (kN)	f_{400}^{150} (MPa)	P_{150}^{150} (kN)	f_{150}^{150} (MPa)	T_{150}^{150} (Joules)
100% HDPE-3.0-1	153.0	153.1	5.15	8.39	1.05	6.49	0.81	5.49	0.69	5.07	0.64	16.90
100% HDPE-3.0-2	150.9	153.5	4.67	8.01	1.01	6.36	0.80	5.57	0.71	4.36	0.55	18.96
100% HDPE-3.0-3	152.2	152.8	5.32	7.04	0.89	5.90	0.75	5.28	0.67	3.90	0.49	16.67
100% HDPE-3.0-4	155.7	153.6	4.92	7.03	0.86	5.49	0.67	4.82	0.59	3.44	0.42	16.50
100% HDPE-3.0-5	153.0	156.7	4.67	10.54	1.26	8.25	0.99	6.51	0.78	3.97	0.48	20.35
HDPE, 1% PVDF-3.0-1	155.7	153.2	4.99	10.88	1.34	8.33	1.03	7.23	0.89	4.75	0.58	23.97
HDPE, 1% PVDF-3.0-5	155.9	153.1	4.27	6.88	0.85	5.84	0.72	5.56	0.69	4.65	0.57	19.36
HDPE, 3% PVDF-3.0-1	148.1	153.6	3.94	8.61	1.11	6.36	0.82	4.99	0.64	3.22	0.41	16.26
HDPE, 3% PVDF-3.0-2	150.7	153.3	4.92	7.79	0.99	6.44	0.82	5.84	0.74	4.79	0.61	20.45
HDPE, 3% PVDF-3.0-3	147.7	153.7	4.79	6.88	0.89	5.67	0.73	5.12	0.66	3.97	0.51	17.34
HDPE, 3% PVDF-3.0-4	152.3	153.5	4.83	10.04	1.26	8.09	1.01	7.38	0.93	6.05	0.76	25.01
HDPE, 3% PVDF-3.0-5	153.9	153.4	4.03	5.64	0.70	4.66	0.58	4.22	0.52	3.17	0.39	14.71
HDPE, 5% PVDF, 10% MAH-3.0-1	149.2	151.9	5.27	9.03	1.18	6.85	0.90	5.38	0.70	4.04	0.53	17.68
HDPE, 5% PVDF, 10% MAH-3.0-2	150.1	153.0	4.88	7.30	0.94	5.72	0.73	4.71	0.60	3.52	0.45	16.71
HDPE, 5% PVDF, 10% MAH-3.0-3	152.1	154.2	5.14	8.08	1.01	6.87	0.86	6.29	0.78	5.54	0.69	21.56
HDPE, 5% PVDF, 10% MAH-3.0-4	154.1	153.5	5.27	9.16	1.14	6.72	0.83	5.43	0.67	4.03	0.50	18.98
HDPE, 5% PVDF, 10% MAH-3.0-5	150.8	153.5	4.95	8.48	1.07	6.98	0.88	6.58	0.83	6.46	0.82	23.70
HDPE, 7% PVDF, 10% MAH-3.0-1	155.0	153.5	4.27	7.39	0.91	6.48	0.80	6.19	0.76	4.95	0.61	20.51
HDPE, 7% PVDF, 10% MAH-3.0-2	152.1	153.7	4.39	11.30	1.41	8.48	1.06	7.27	0.91	5.31	0.66	23.66
HDPE, 7% PVDF, 10% MAH-3.0-3	152.5	153.8	4.82	7.91	0.99	5.74	0.72	4.70	0.59	3.53	0.44	16.67
HDPE, 7% PVDF, 10% MAH-3.0-4	153.9	153.8	5.10	7.97	0.99	6.29	0.78	5.44	0.67	3.45	0.43	16.76
HDPE, 7% PVDF, 10% MAH-3.0-5	153.9	153.6	5.12	8.61	1.07	6.21	0.77	5.09	0.63	3.97	0.49	17.50

Table D-19 - Individual specimen results for ASTM C1609 testing - 2 of 3

Fiber	Width (mm)	Height (mm)	f_p (Mpa)	P_{900}^{150} (kN)	f_{900}^{150} (MPa)	P_{600}^{150} (kN)	f_{600}^{150} (MPa)	P_{400}^{150} (kN)	f_{400}^{150} (MPa)	P_{150}^{150} (kN)	f_{150}^{150} (MPa)	T_{150}^{150} (Joules)
HDPE, 9% PVDF, 10% MAH-3.0-1	152.6	154.2	4.87	9.30	1.15	7.36	0.91	6.36	0.79	4.94	0.61	21.22
HDPE, 9% PVDF, 10% MAH-3.0-2	154.2	153.4	4.02	7.63	0.95	6.58	0.82	5.97	0.74	5.27	0.65	19.99
HDPE, 9% PVDF, 10% MAH-3.0-3	153.6	154.1	4.87	5.90	0.73	4.74	0.59	4.33	0.53	4.08	0.50	16.11
HDPE, 9% PVDF, 10% MAH-3.0-4	153.5	154.0	5.02	7.10	0.88	5.69	0.70	4.82	0.60	3.81	0.47	17.08
HDPE, 9% PVDF, 10% MAH-3.0-5	153.6	149.6	4.75	8.82	1.15	6.89	0.90	6.02	0.79	4.56	0.60	20.15
HDPE, 11% PVDF, 20% MAH-3.0-1	155.5	152.1	4.60	7.95	0.99	6.13	0.77	5.49	0.69	4.38	0.55	18.87
HDPE, 11% PVDF, 20% MAH-3.0-2	151.2	153.4	4.75	5.42	0.69	4.64	0.59	4.31	0.55	3.97	0.50	16.38
HDPE, 11% PVDF, 20% MAH-3.0-3	152.5	154.0	4.70	8.16	1.01	6.46	0.80	5.52	0.69	4.71	0.59	19.73
HDPE, 11% PVDF, 20% MAH-3.0-4	150.9	153.7	4.54	7.21	0.91	5.29	0.67	4.27	0.54	3.40	0.43	15.64
HDPE, 11% PVDF, 20% MAH-3.0-5	156.6	153.7	4.11	8.01	0.97	6.01	0.73	4.82	0.59	2.99	0.36	16.41
HDPE, 10% EVA-3.0-1	152.8	153.3	4.98	6.99	0.88	5.49	0.69	4.85	0.61	3.65	0.46	16.61
HDPE, 10% EVA-3.0-2	154.9	153.5	5.06	6.72	0.83	5.22	0.64	4.68	0.58	3.36	0.41	15.98
HDPE, 10% EVA-3.0-3	152.0	153.8	4.76	9.54	1.19	7.20	0.90	6.25	0.78	4.17	0.52	18.17
HDPE, 10% EVA-3.0-4	154.3	154.3	4.48	7.46	0.91	5.87	0.72	5.06	0.62	3.85	0.47	17.61
HDPE, 10% EVA-3.0-5	156.0	153.9	4.57	7.23	0.88	5.21	0.63	4.39	0.53	3.80	0.46	16.91
PP, 10% HDPE, 10% EVA-3.0-1	153.6	152.2	4.66	10.71	1.35	9.44	1.19	8.60	1.09	8.13	1.03	28.72
PP, 10% HDPE, 10% EVA-3.0-2	151.5	153.8	4.56	9.41	1.18	8.23	1.03	7.76	0.98	7.73	0.97	26.58
PP, 10% HDPE, 10% EVA-3.0-3	156.0	153.5	5.10	9.63	1.18	7.86	0.96	7.08	0.87	6.20	0.76	23.58
PP, 10% HDPE, 10% EVA-3.0-4	153.5	153.1	5.48	13.12	1.64	9.43	1.18	8.20	1.03	7.47	0.93	27.69
PP, 10% HDPE, 10% EVA-3.0-5	150.3	153.8	5.23	8.20	1.04	7.04	0.89	6.62	0.84	6.46	0.82	23.04

Table D-20 - Individual specimen results for ASTM C1609 testing - 3 of 3

Fiber	Width (mm)	Height (mm)	f_p (Mpa)	P^{150}_{900} (kN)	f^{150}_{900} (MPa)	P^{150}_{600} (kN)	f^{150}_{600} (MPa)	P^{150}_{400} (kN)	f^{150}_{400} (MPa)	P^{150}_{150} (kN)	f^{150}_{150} (MPa)	T^{150}_{150} (Joules)
BASF - Masterfiber MAC470-3.0-1	152.3	152.9	4.76	8.20	1.04	6.07	0.77	5.07	0.64	3.86	0.49	17.76
BASF - Masterfiber MAC470-3.0-2	150.6	153.4	5.06	8.57	1.09	6.86	0.87	5.82	0.74	4.06	0.52	18.67
BASF - Masterfiber MAC470-3.0-3	155.6	153.7	5.17	12.02	1.47	10.24	1.25	8.82	1.08	5.81	0.71	26.42
Strux 85/50-3.0-3	152.4	152.2	4.72	11.67	1.49	9.40	1.20	8.43	1.07	8.71	1.11	22.58
Strux 85/50-3.0-4	152.6	152.4	4.30	9.34	1.19	8.57	1.09	8.59	1.09	7.64	0.97	23.66
Strux 85/50-3.0-5	152.4	152.3	4.49	7.84	1.00	7.02	0.89	6.90	0.88	8.03	1.02	23.02
Tuf-Strand SF-3.0-1	153.1	153.5	4.74	8.99	1.12	8.19	1.02	7.89	0.99	8.57	1.07	27.34
Tuf-Strand SF-3.0-2	152.1	153.4	4.48	11.22	1.41	9.03	1.14	8.27	1.04	7.87	0.99	28.52
Tuf-Strand SF-3.0-3	154.4	155.9	4.17	14.04	1.68	12.31	1.48	11.02	1.32	9.67	1.16	34.96
Tuf-Strand SF-3.0-4	152.5	154.1	4.29	10.99	1.37	9.26	1.15	8.25	1.02	7.12	0.89	26.07
Tuf-Strand SF-3.0-5	152.6	153.3	4.55	10.30	1.29	9.01	1.13	8.23	1.03	8.13	1.02	27.47

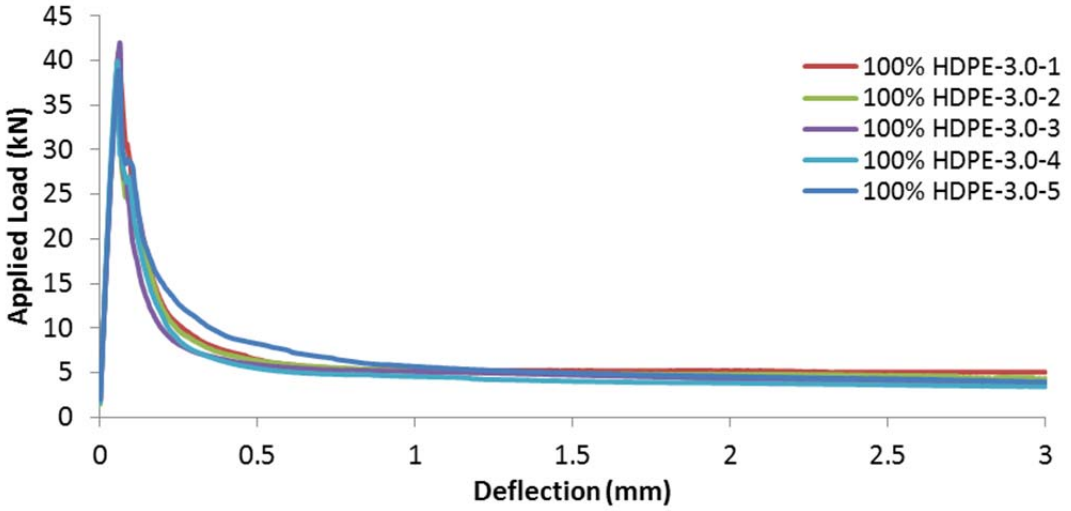

Figure D-159 - Load vs. deflection curves for ASTM C1609 testing using prototype macrofiber containing 100% HDPE

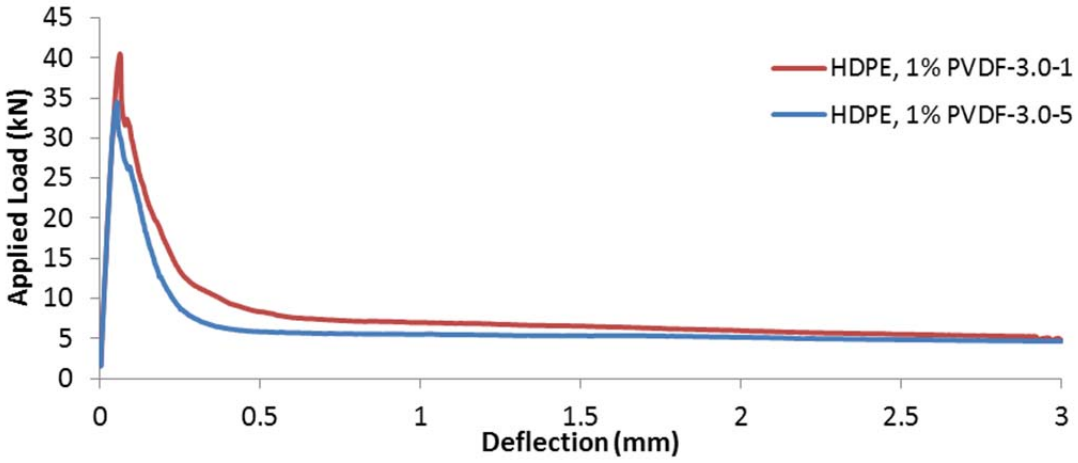

Figure D-160 - Load vs. deflection curves for ASTM C1609 testing using prototype macrofiber containing HDPE and 1% PVDF

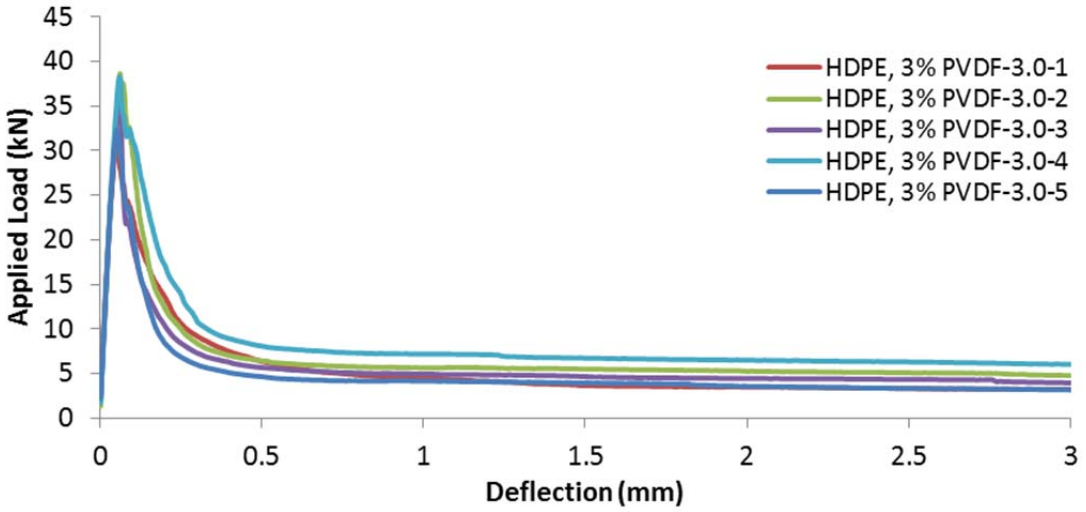

Figure D-161 - Load vs. deflection curves for ASTM C1609 testing using prototype macrofiber containing HDPE and 3% PVDF

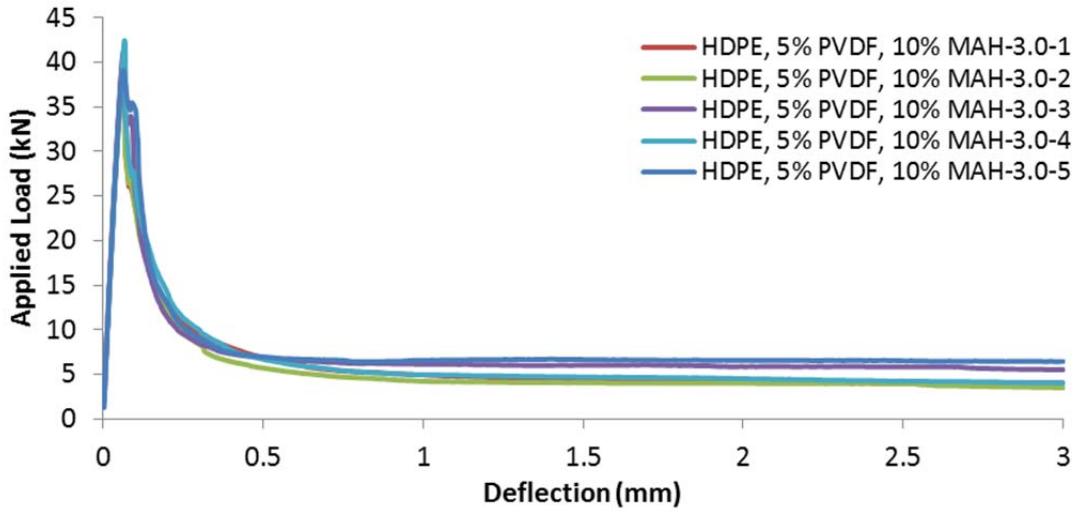

Figure D-162 - Load vs. deflection curves for ASTM C1609 testing using prototype macrofiber containing HDPE, 5% PVDF and 10% MAH

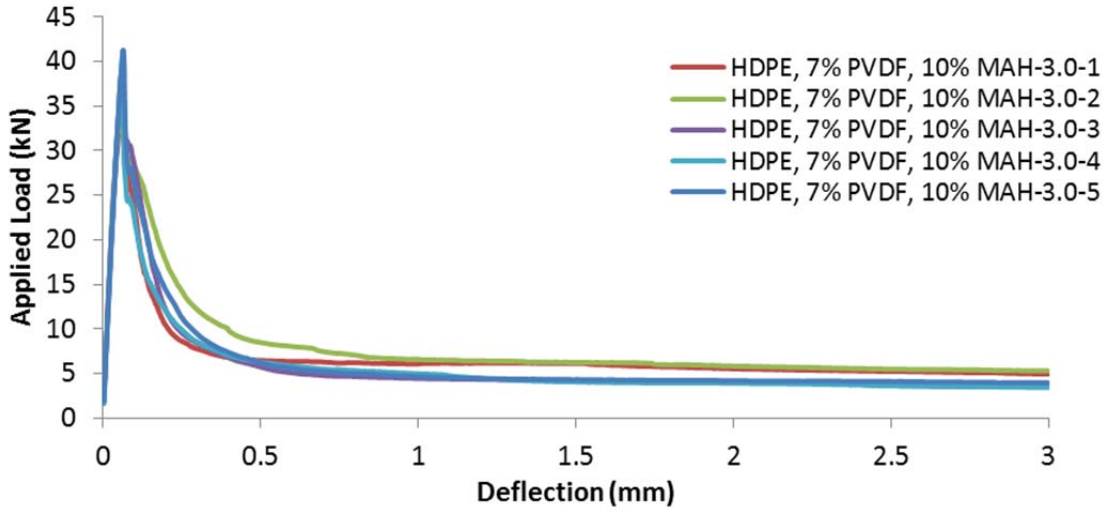

Figure D-163 - Load vs. deflection curves for ASTM C1609 testing using prototype macrofiber containing HDPE, 7% PVDF and 10% MAH

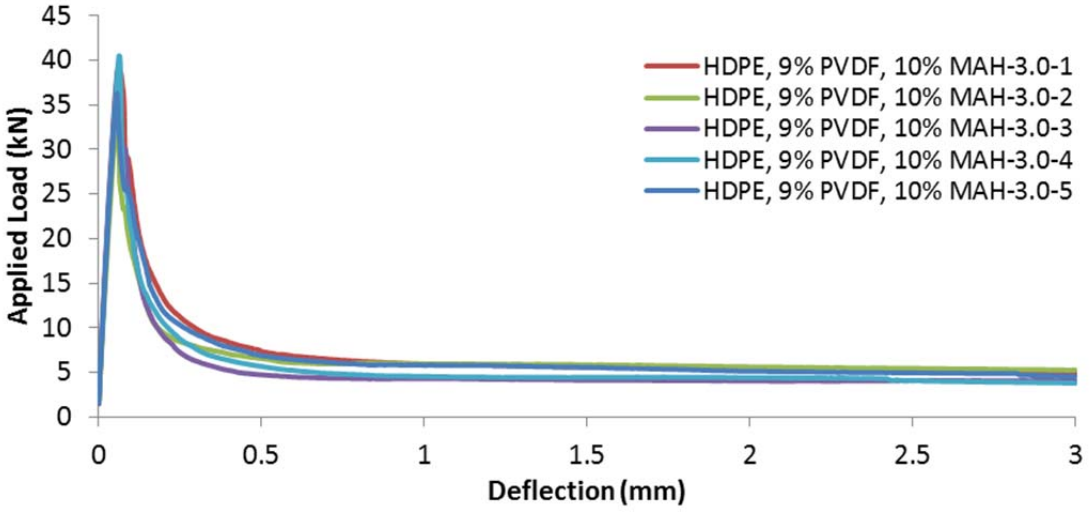

Figure D-164 - Load vs. deflection curves for ASTM C1609 testing using prototype macrofiber containing HDPE, 9% PVDF and 10% MAH

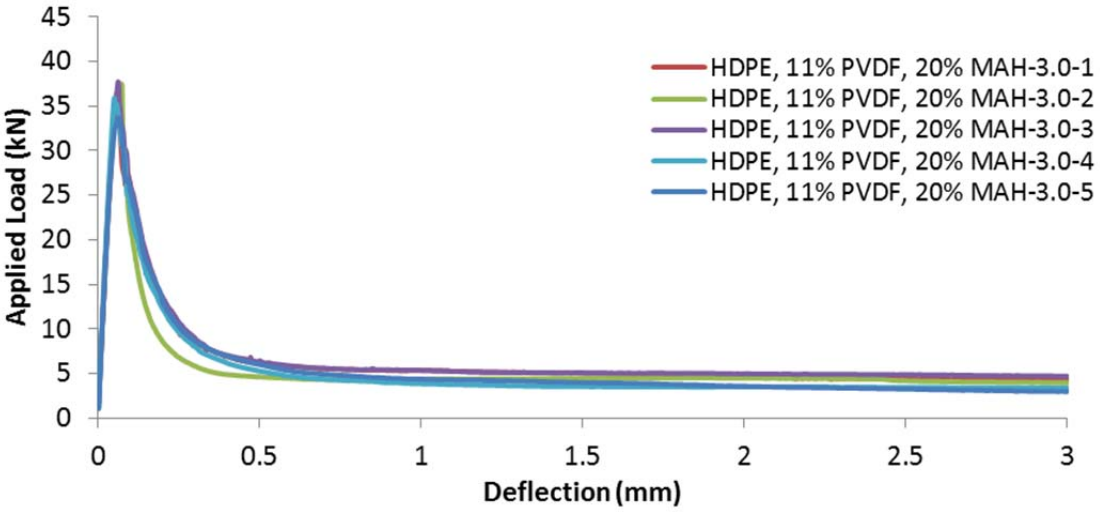

Figure D-165 - Load vs. deflection curves for ASTM C1609 testing using prototype macrofiber containing HDPE, 11% PVDF and 20% MAH

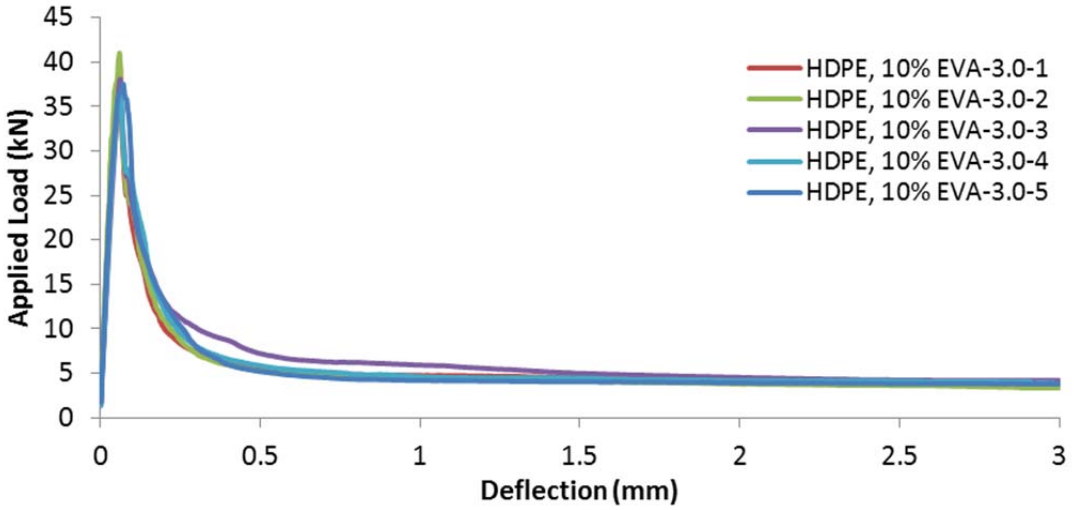

Figure D-166 - Load vs. deflection curves for ASTM C1609 testing using prototype macrofiber containing HDPE and 10% EVA

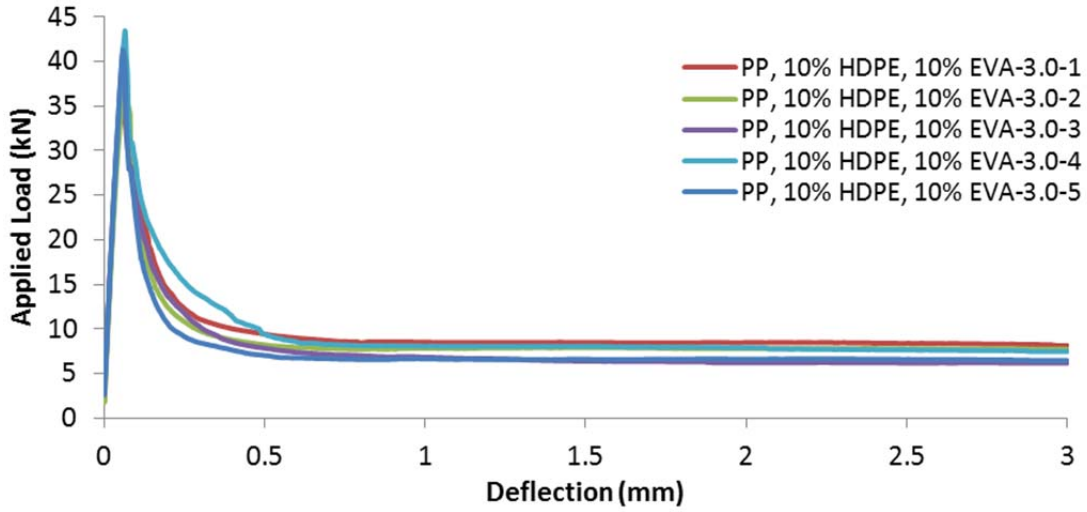

Figure D-167 - Load vs. deflection curves for ASTM C1609 testing using prototype macrofiber containing PP, 10% HDPE and 10% EVA

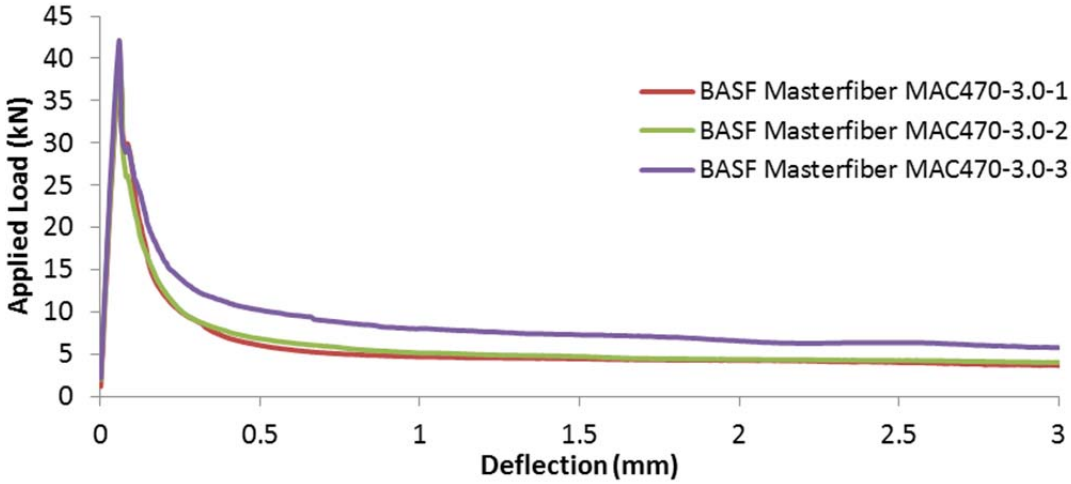

Figure D-168 - Load vs. deflection curves for ASTM C1609 testing using BASF Masterfiber MAC470

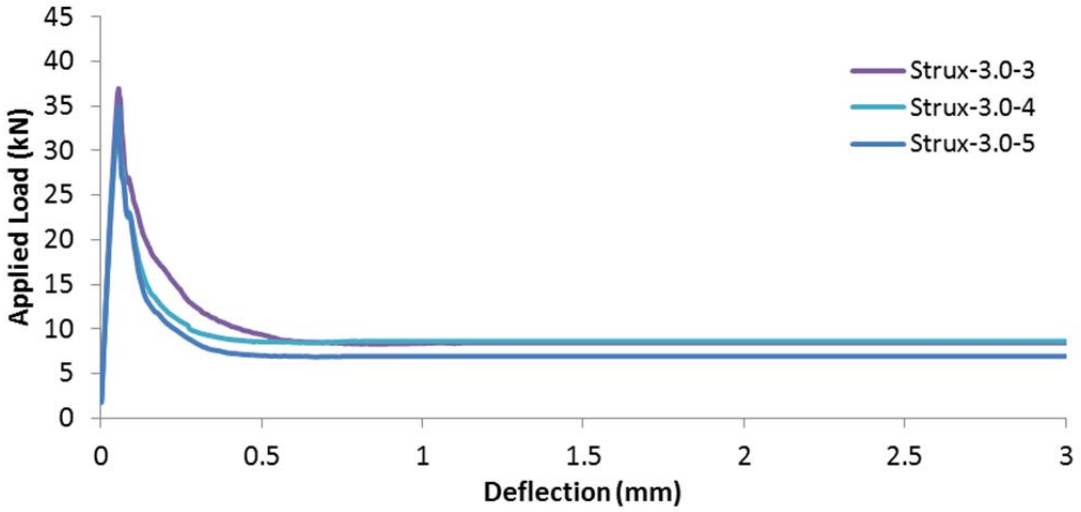

Figure D-169 - Load vs. deflection curves for ASTM C1609 testing using Strux 85/50

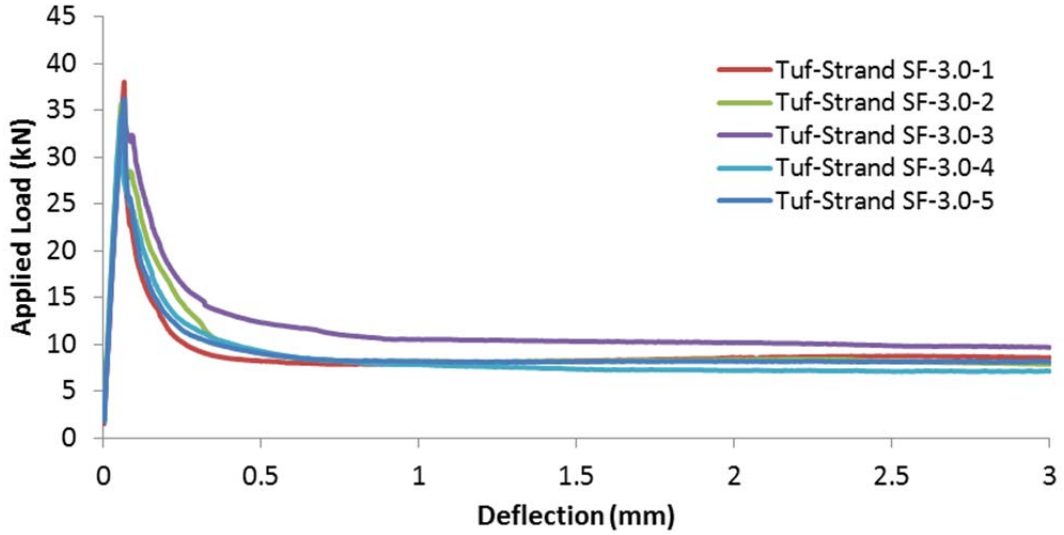

Figure D-170 - Load vs. deflection curves for ASTM C1609 testing using Tuf-strand SF

APPENDIX E - ADDITIONAL TABLES AND PLOTS FOR ASTM C1399 TESTING RESULTS

Table E-21 - Summary of results from ASTM C1399 testing, averages only

Fiber	Specimen Cross-Section		RSI (MPa)
	Base (mm)	Height (mm)	
100% HDPE	104.0	103.6	0.72
HDPE, 1% PVDF	105.0	103.5	0.94
HDPE, 3% PVDF	104.3	103.1	0.82
HDPE, 5% PVDF, 10% MAH	106.5	103.0	0.84
HDPE, 7% PVDF, 10% MAH	103.2	102.5	0.54
HDPE, 9% PVDF, 10% MAH	104.9	102.7	0.83
HDPE, 11% PVDF, 20% MAH	105.3	104.0	0.71
HDPE, 10% EVA	104.8	102.9	0.59
80% PP, 10% PE, 10% EVA	103.0	102.4	1.17
BASF Masterfiber MAC470	104.9	102.7	0.69
Strux 85/50	102.8	102.0	1.34
Tuf-strand SF	104.0	103.7	0.85

Table E-22 - Individual specimen results for ASTM C1399 testing - 1 of 2

Sample ID	Specimen Cross-Section		RSI (MPa)
	Base (mm)	Height (mm)	
100% HDPE-3.0-1	105.0	104.0	0.82
100% HDPE-3.0-2	102.8	102.3	0.40
100% HDPE-3.0-3	104.6	106.5	1.02
100% HDPE-3.0-4	103.6	101.5	0.64
HDPE, 1% PVDF-3.0-1	108.2	105.2	0.97
HDPE, 1% PVDF-3.0-2	103.7	102.7	0.86
HDPE, 1% PVDF-3.0-4	106	103.9	1.00
HDPE, 3% PVDF-3.0-1	100.4	101.8	0.44
HDPE, 3% PVDF-3.0-2	105.5	104.5	0.79
HDPE, 3% PVDF-3.0-3	105.6	103.7	0.89
HDPE, 3% PVDF-3.0-4	105.6	102.5	1.16
HDPE, 5% PVDF, 10% MAH-3.0-1	106.3	101.4	1.09
HDPE, 5% PVDF, 10% MAH-3.0-2	106.6	102.7	0.88
HDPE, 5% PVDF, 10% MAH-3.0-3	105.4	103.1	0.75
HDPE, 5% PVDF, 10% MAH-3.0-4	107.8	104.8	0.65
HDPE, 7% PVDF, 10% MAH-3.0-2	104.8	103.9	0.53
HDPE, 7% PVDF, 10% MAH-3.0-3	102.5	101.5	0.59
HDPE, 7% PVDF, 10% MAH-3.0-4	105.0	103.4	0.50
HDPE, 9% PVDF, 10% MAH-3.0-1	108.7	100.3	0.68
HDPE, 9% PVDF, 10% MAH-3.0-2	102.2	104.7	0.97
HDPE, 9% PVDF, 10% MAH-3.0-3	103.4	103.2	0.88
HDPE, 9% PVDF, 10% MAH-3.0-4	105.2	102.2	0.80
HDPE, 11% PVDF, 20% MAH-3.0-1	106.4	102.4	0.70
HDPE, 11% PVDF, 20% MAH-3.0-2	107.6	106.1	0.64
HDPE, 11% PVDF, 20% MAH-3.0-3	102.4	102.4	0.93
HDPE, 11% PVDF, 20% MAH-3.0-4	104.6	105.0	0.56
HDPE, 10% EVA-3.0-1	107.7	106.0	0.57
HDPE, 10% EVA-3.0-2	107.6	104.7	0.54
HDPE, 10% EVA-3.0-4	100.8	101.8	0.66
PP, 10% HDPE, 10% EVA-3.0-1	101.0	101.9	1.17
PP, 10% HDPE, 10% EVA-3.0-3	102.2	102.1	1.31
PP, 10% HDPE, 10% EVA-3.0-4	105.7	102.9	1.02

Table E-23 - Individual specimen results for ASTM C1399 testing - 2 of 2

Sample ID	Specimen Cross-Section		RSI (MPa)
	Base (mm)	Height (mm)	
BASF Masterfiber MAC470-3.0-1	108.7	100.3	0.68
BASF Masterfiber MAC470-3.0-2	102.2	104.7	0.68
BASF Masterfiber MAC470-3.0-3	103.4	103.2	0.34
BASF Masterfiber MAC470-3.0-4	105.2	102.2	1.08
Strux 85/50-3.0-1	102.9	103.1	1.33
Strux 85/50-3.0-2	104.6	102.9	1.43
Strux 85/50-3.0-3	104.8	100.2	1.25
Tuf-strand SF-3.0-1	104.7	104.7	0.82
Tuf-strand SF-3.0-2	104.4	103.2	0.93
Tuf-strand SF-3.0-4	102.9	103.2	0.81

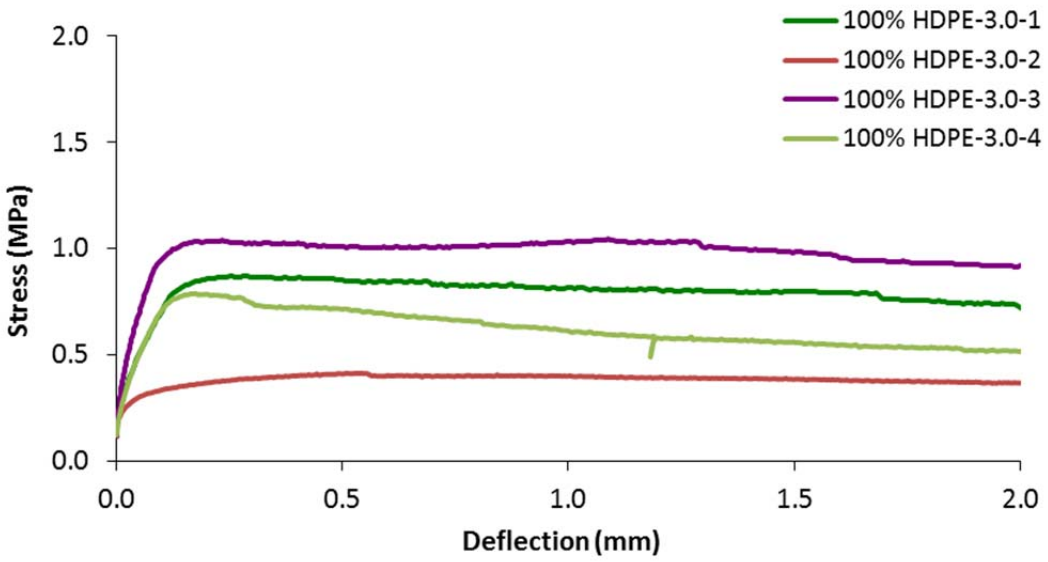

Figure E-171 - Stress vs. deflection curves for ASTM C1399 testing using prototype macrofiber containing 100% HDPE

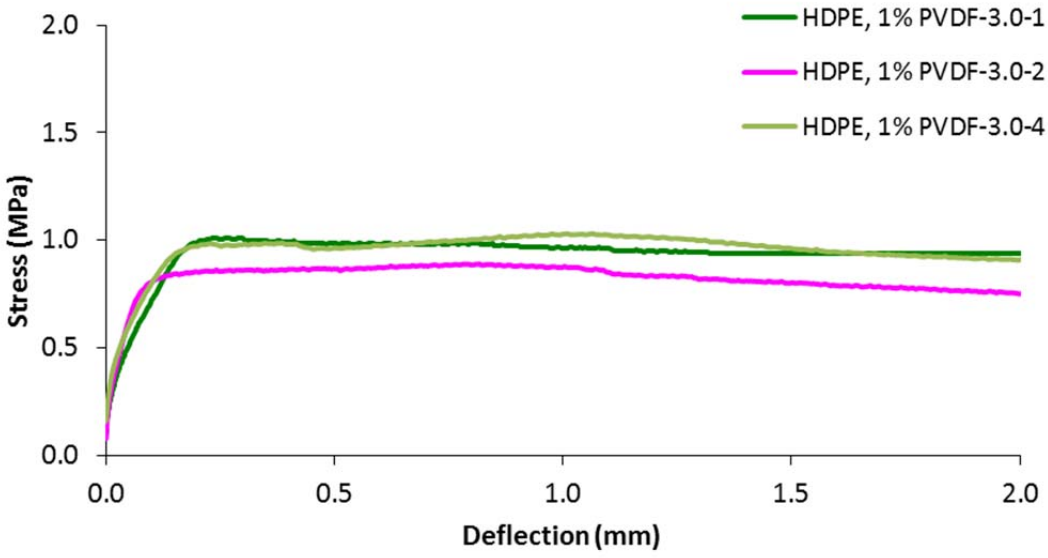

Figure E-172 - Stress vs. deflection curves for ASTM C1399 testing using prototype macrofiber containing HDPE and 1% PVDF

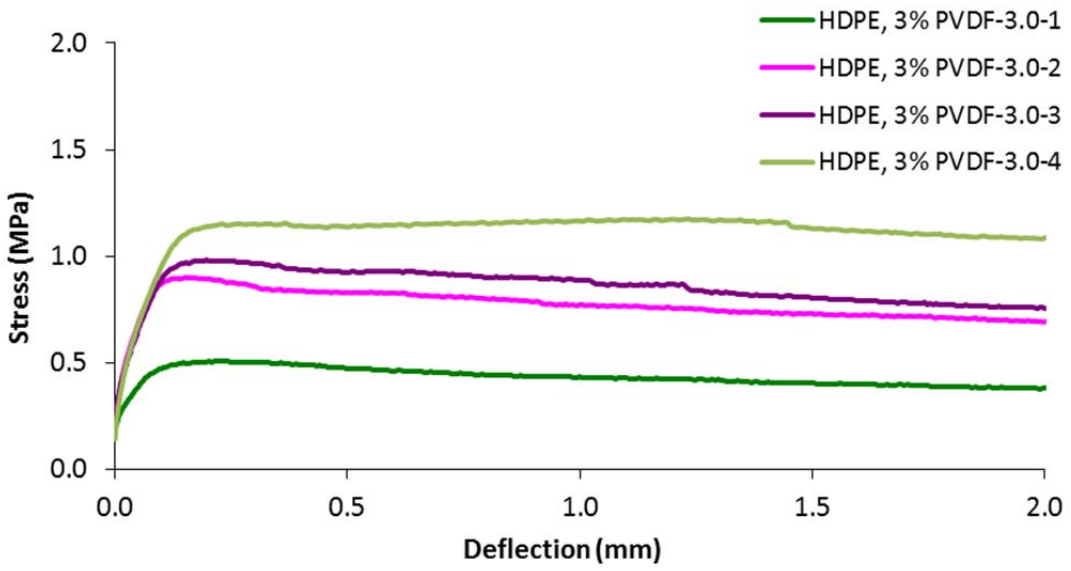

Figure E-173 - Stress vs. deflection curves for ASTM C1399 testing using prototype macrofiber containing HDPE and 3% PVDF

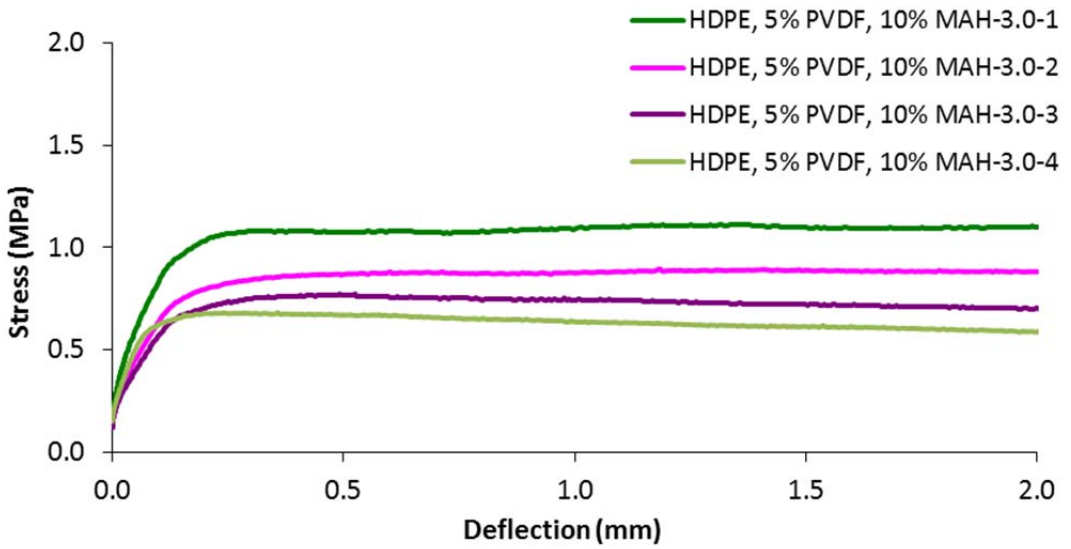

Figure E-174 - Stress vs. deflection curves for ASTM C1399 testing using prototype macrofiber containing HDPE, 5% PVDF and 10% MAH

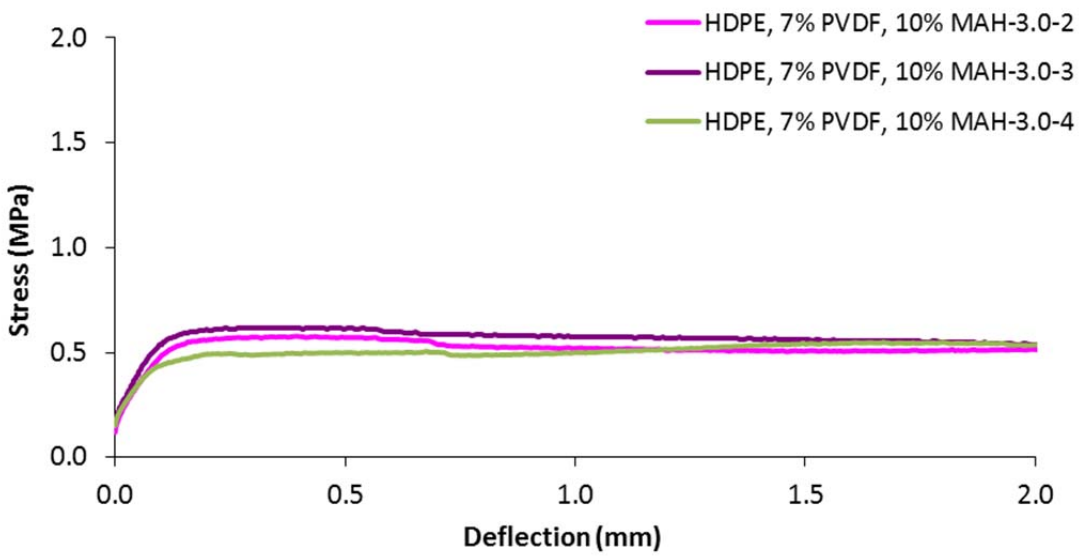

Figure E-175 - Stress vs. deflection curves for ASTM C1399 testing using prototype macrofiber containing HDPE, 7% PVDF and 10% MAH

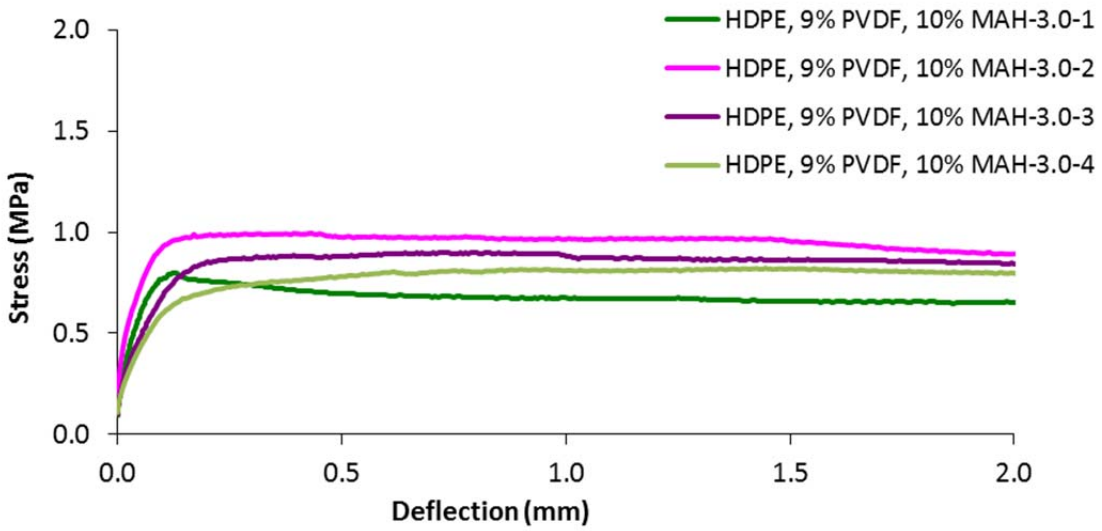

Figure E-176 - Stress vs. deflection curves for ASTM C1399 testing using prototype macrofiber containing HDPE, 9% PVDF and 10% MAH

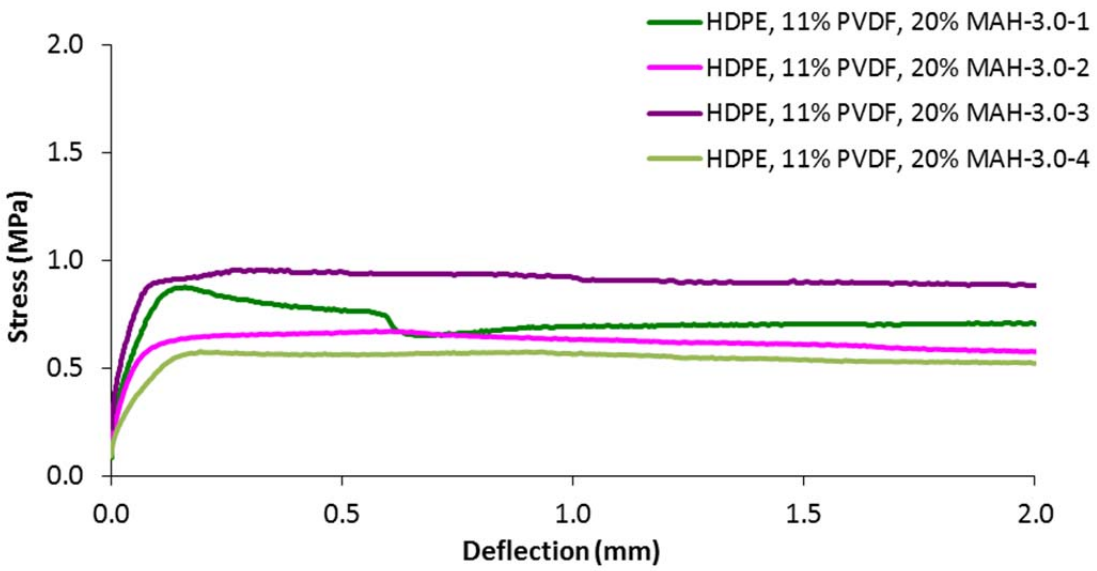

Figure E-177 - Stress vs. deflection curves for ASTM C1399 testing using prototype macrofiber containing HDPE, 11% PVDF and 20% MAH

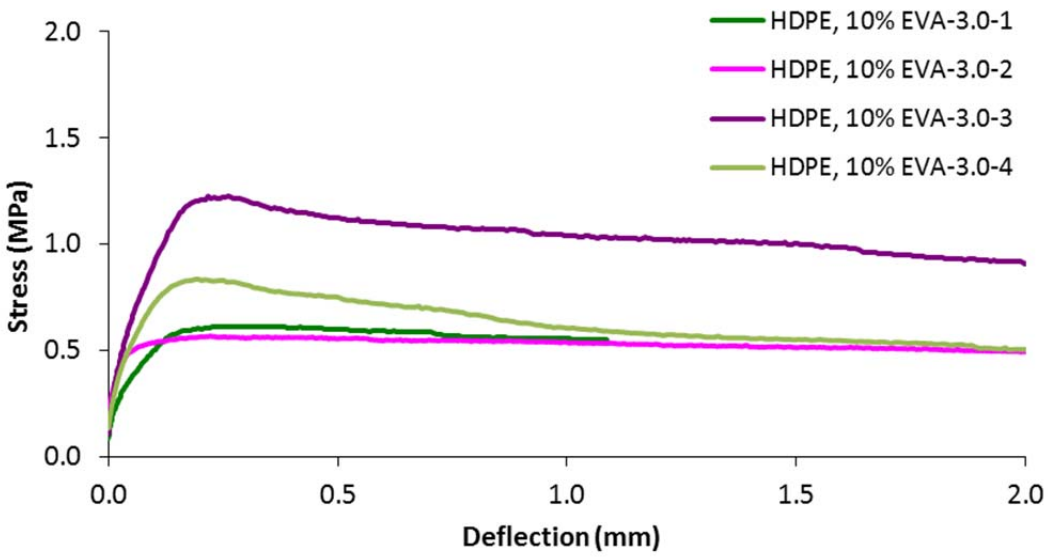

Figure E-178 - Stress vs. deflection curves for ASTM C1399 testing using prototype macrofiber containing HDPE and 10% EVA

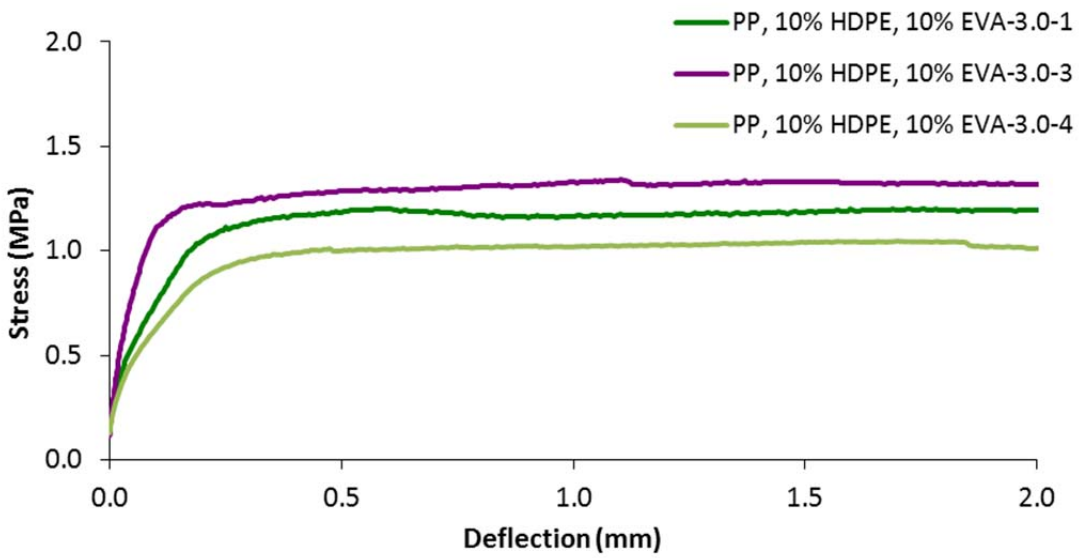

Figure E-179 - Stress vs. deflection curves for ASTM C1399 testing using prototype macrofiber containing PP, 10% HDPE and 10% EVA

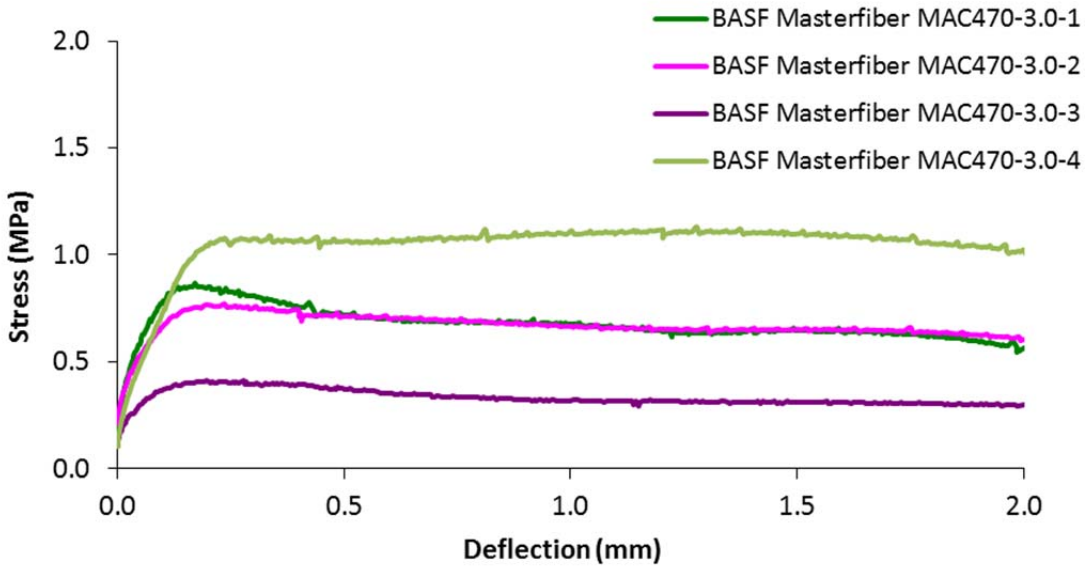

Figure E-180 - Stress vs. deflection curves for ASTM C1399 testing using BASF Masterfiber MAC470

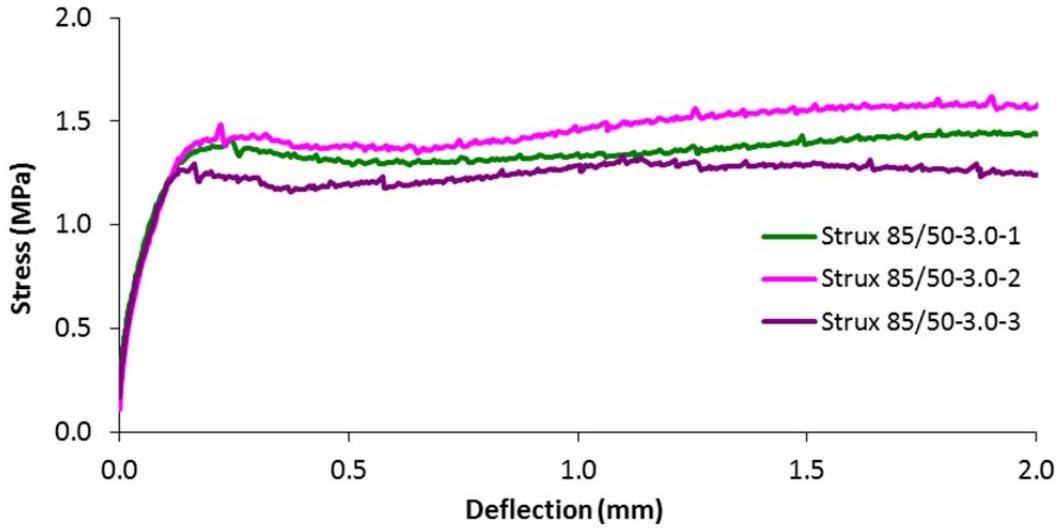

Figure E-181 - Stress vs. deflection curves for ASTM C1399 testing using Strux 85/50

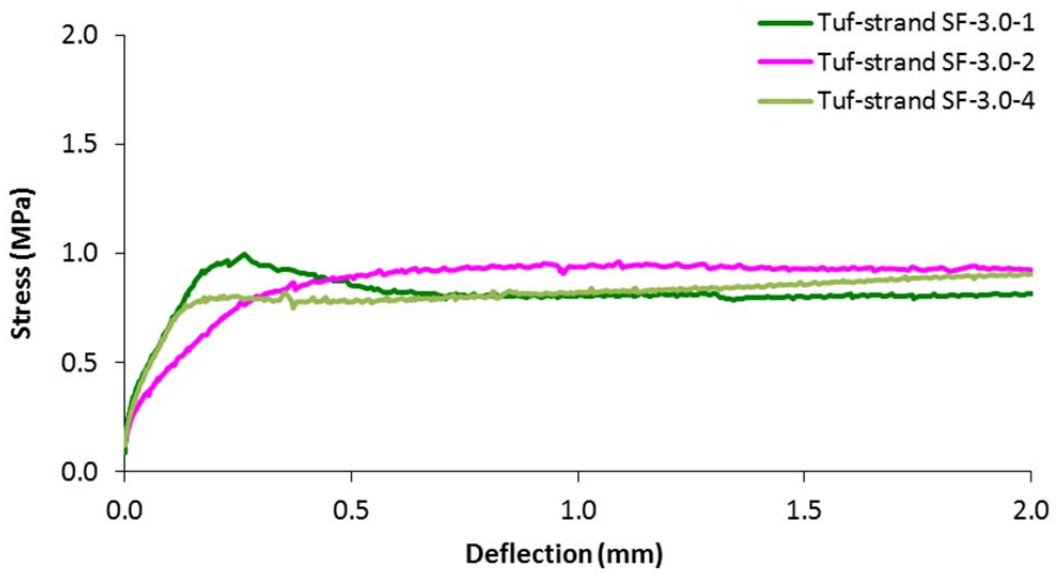

Figure E-182 - Stress vs. deflection curves for ASTM C1399 testing using Tuf-strand SF

APPENDIX F - ADDITIONAL TABLES AND PLOTS FOR ASTM C1550 TESTING RESULTS

Table F-24 - Summary of results from ASTM C1550 testing

Fiber	Thickness (mm)	Diameter (mm)	Peak Load (kN)	Energy at 40 mm (J)	Failure Description
100% HDPE	84.3	800	39.6	150	3
HDPE, 1% PVDF	82.7	800	35.8	160	3
HDPE, 3% PVDF	77.7	800	31.4	146	3
HDPE, 5% PVDF, 10% MAH	83.7	800	35.7	173	3
HDPE, 9% PVDF, 10% MAH	83.3	800	33.8	168	3
HDPE, 11% PVDF, 20% MAH	81.0	800	32.7	172	3
HDPE, 10% EVA	78.3	800	33.0	142	3
80% PP, 10% HDPE, 10% EVA	81.7	800	33.9	244	2
BASF Masterfiber MAC470	84.0	800	30.8	149	3
Strux 85/50	81.7	800	30.5	215	3
Tuf-Strand SF	78.3	800	28.0	281	3

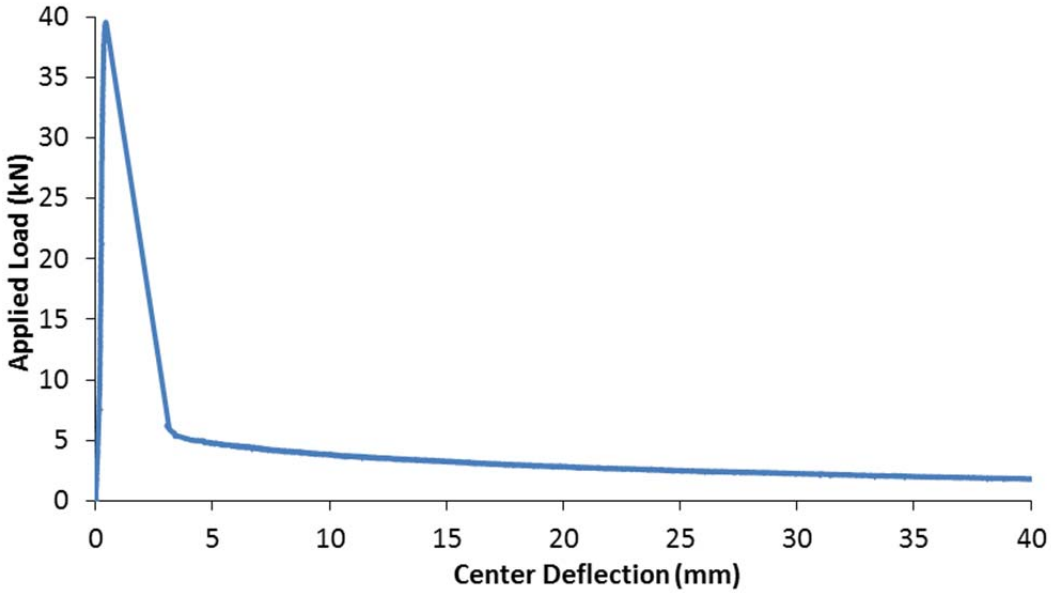

Figure F-183 - Load vs. deflection curve for ASTM C1550 testing using prototype macrofiber containing 100% HDPE

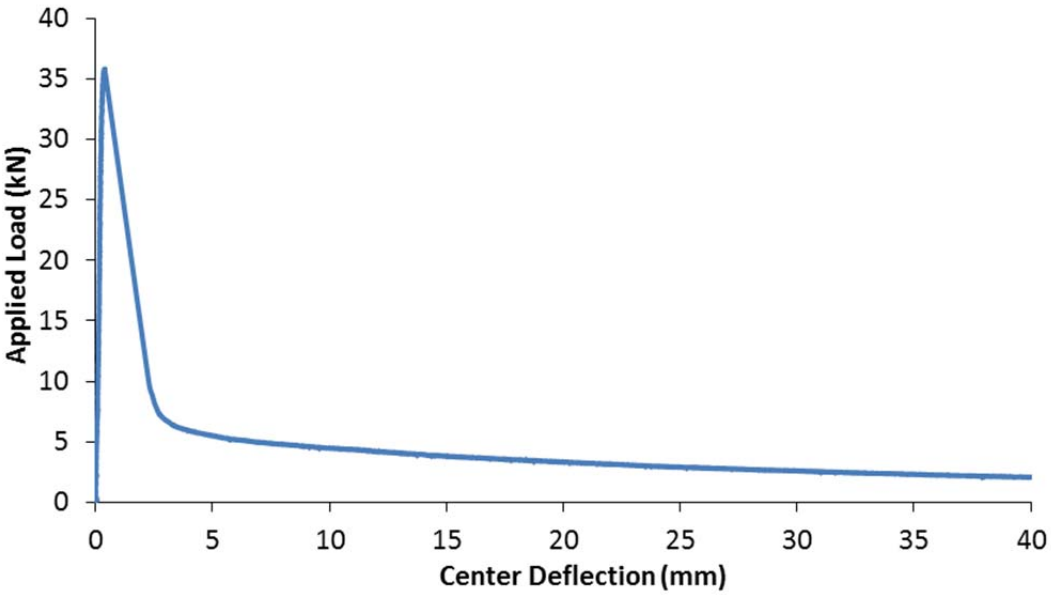

Figure F-184 - Load vs. deflection curve for ASTM C1550 testing using prototype macrofiber containing HDPE and 1% PVDF

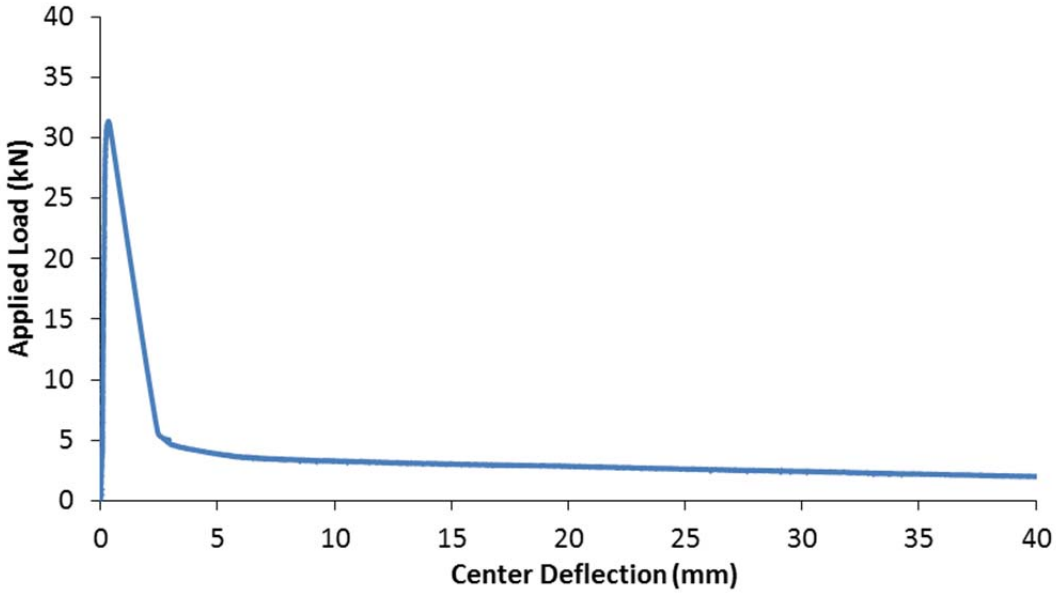

Figure F-185 - Load vs. deflection curve for ASTM C1550 testing using prototype macrofiber containing HDPE and 3% PVDF

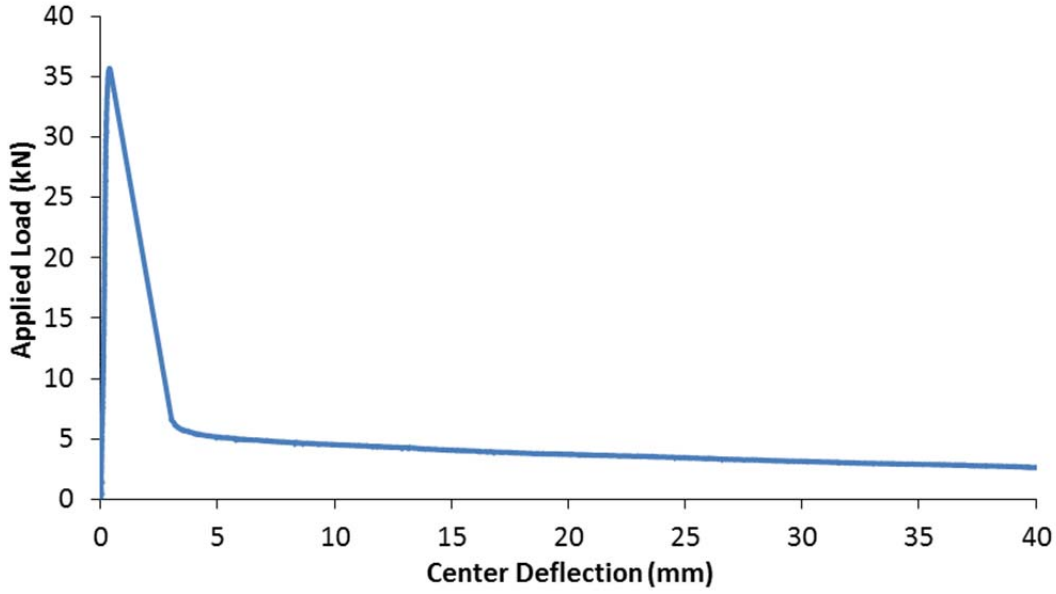

Figure F-186 - Load vs. deflection curve for ASTM C1550 testing using prototype macrofiber containing HDPE, 5% PVDF and 10% MAH

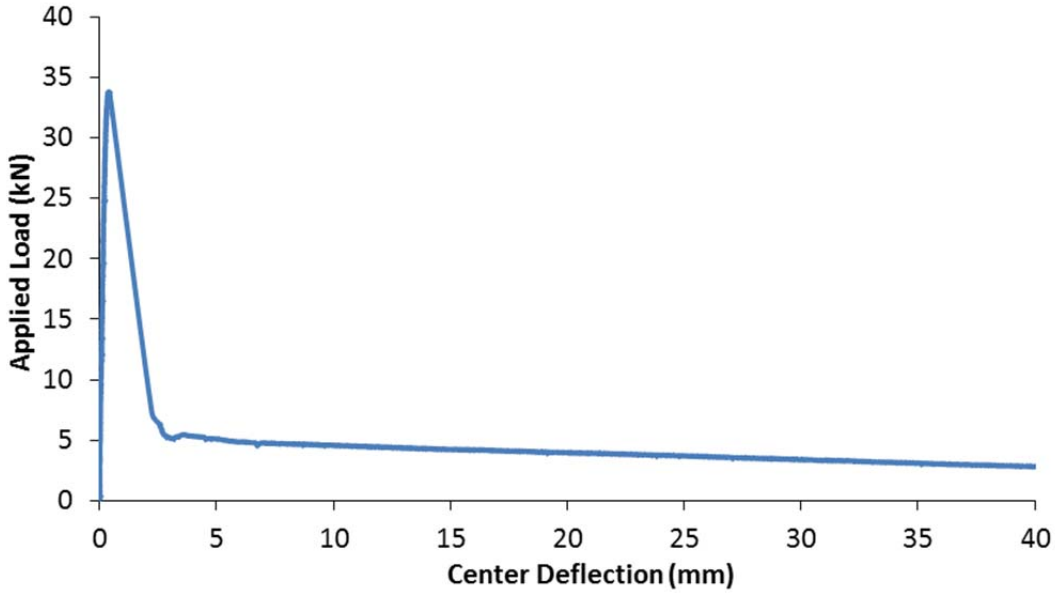

Figure F-187 - Load vs. deflection curve for ASTM C1550 testing using prototype macrofiber containing HDPE, 9% PVDF and 10% MAH

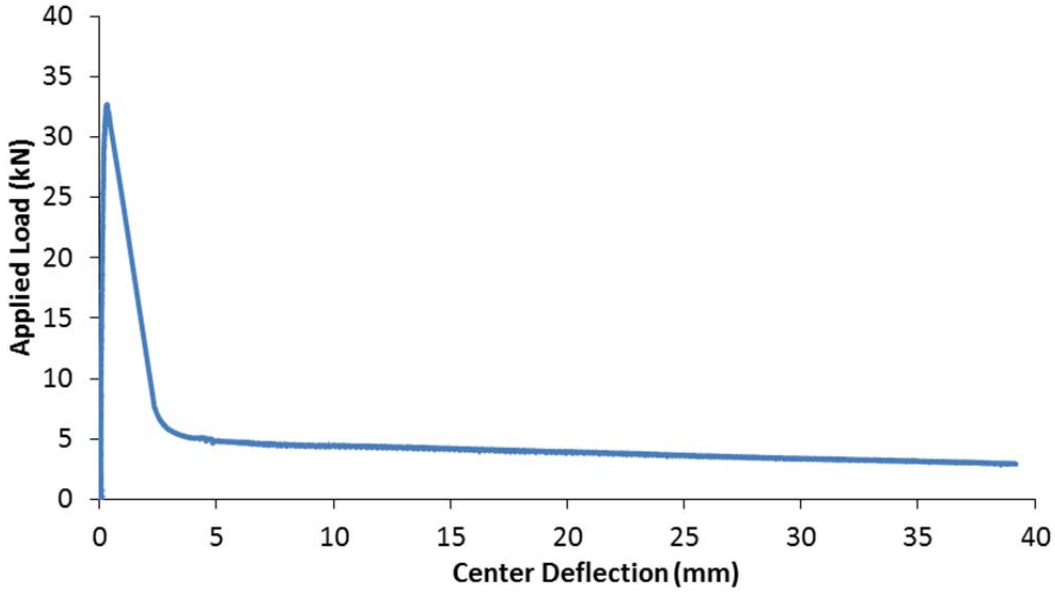

Figure F-188 - Load vs. deflection curve for ASTM C1550 testing using prototype macrofiber containing HDPE, 11% PVDF and 20% MAH

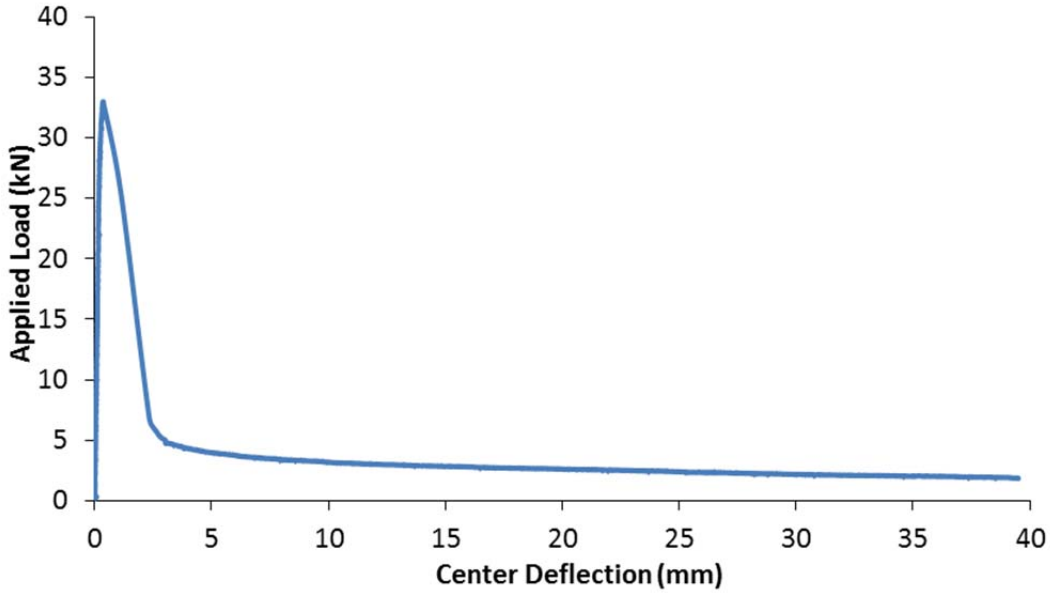

Figure F-189 - Load vs. deflection curve for ASTM C1550 testing using prototype macrofiber containing HDPE and 10% EVA

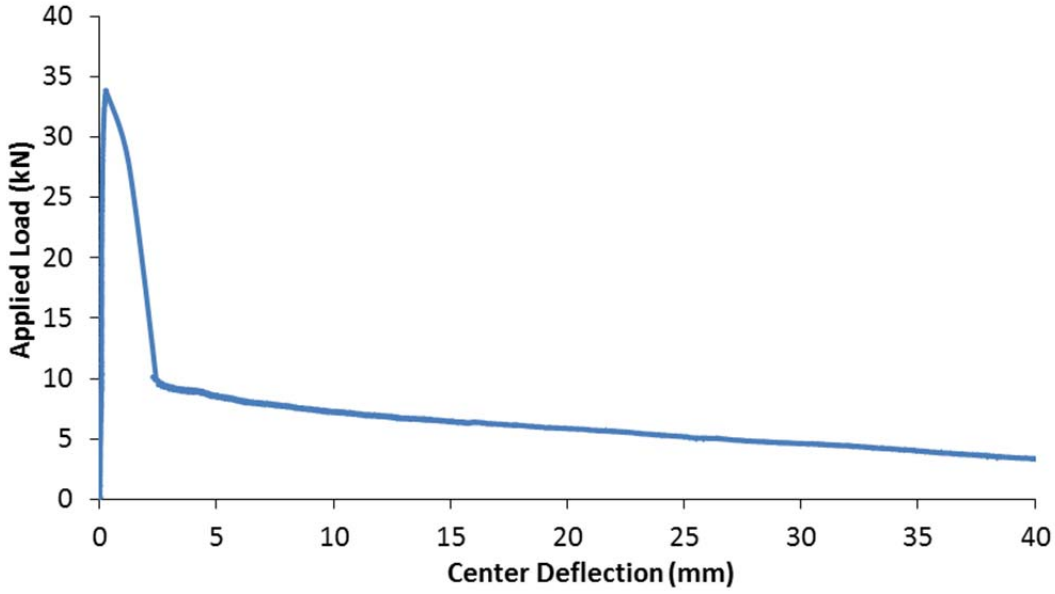

Figure F-190 - Load vs. deflection curve for ASTM C1550 testing using prototype macrofiber containing PP, 10% HDPE and 10% EVA

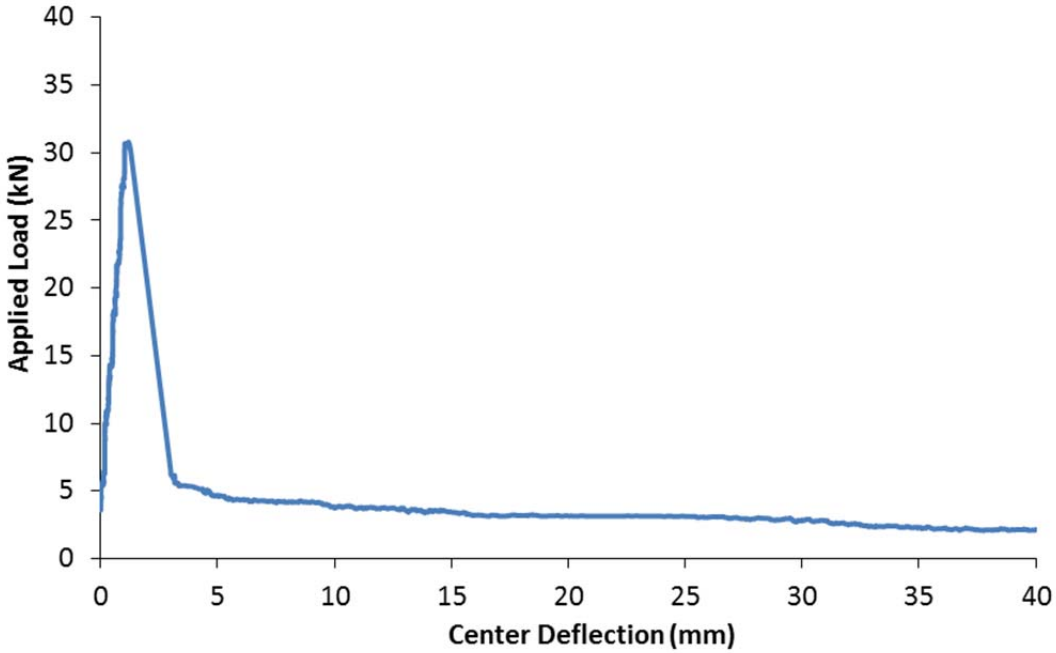

Figure F-191 - Load vs. deflection curve for ASTM C C1550 testing using BASF Masterfiber MAC470

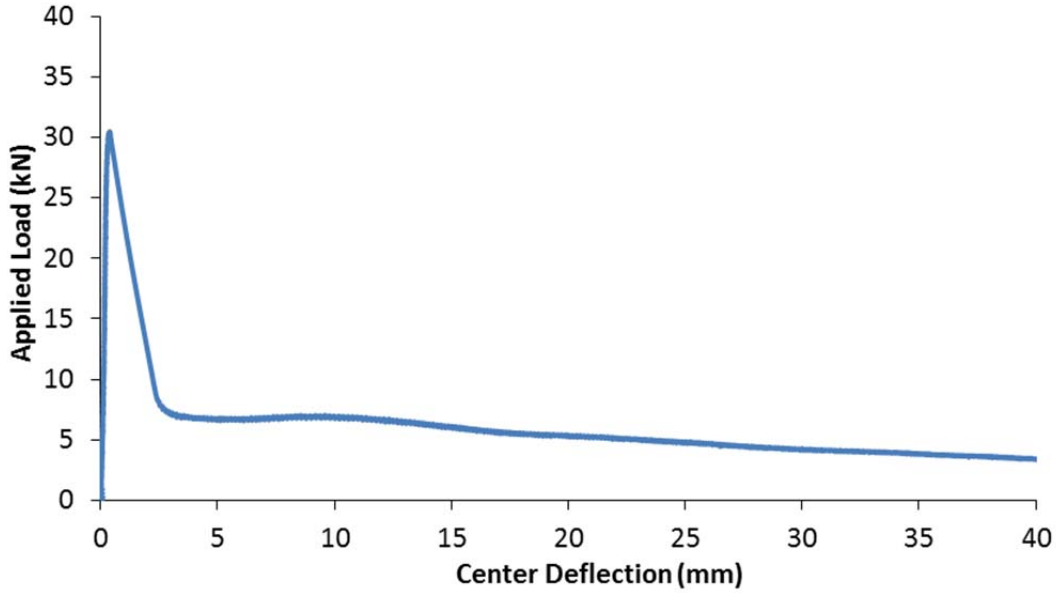

Figure F-192 - Load vs. deflection curve for ASTM C C1550 testing using Strux 85/50

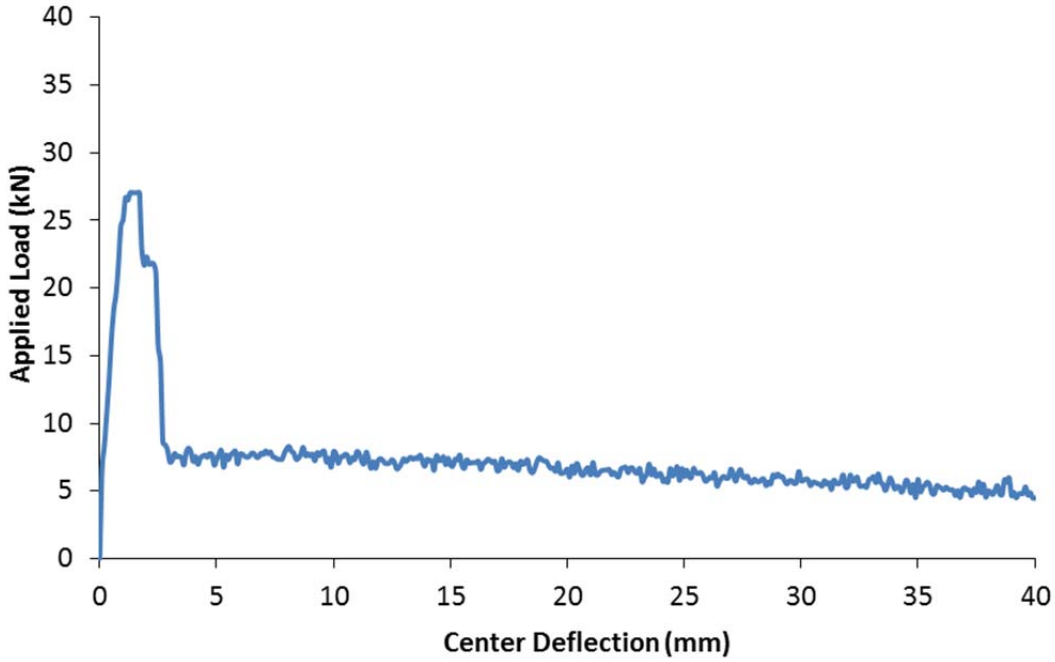

Figure F-193 - Load vs. deflection curve for ASTM C C1550 testing using Tuf-strand SF

APPENDIX G - ADDITIONAL PLOTS FOR RESULTS OF TENSILE CREEP TESTING

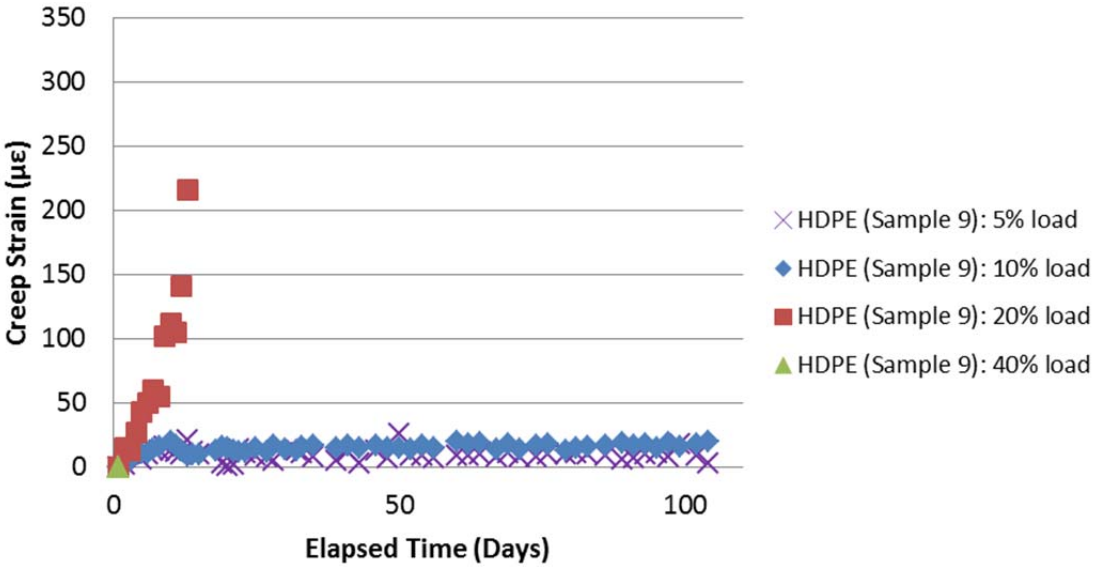

Figure G-194 - Creep strain vs. elapsed time plots for prototype macrofiber containing 100% HDPE (thick)

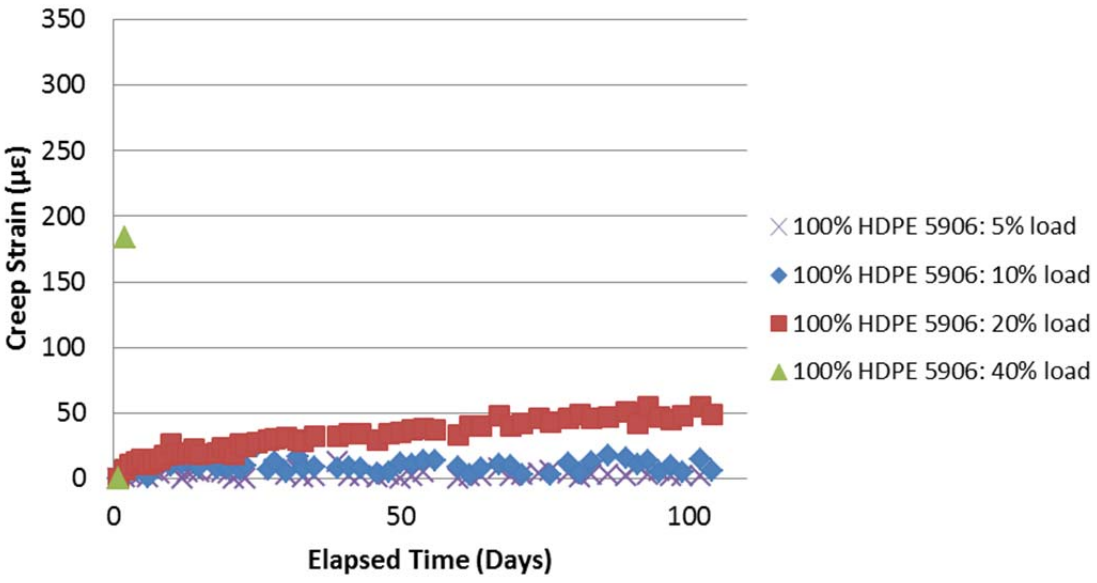

Figure G-195 - Creep strain vs. elapsed time plots for prototype macrofiber containing

100% HDPE

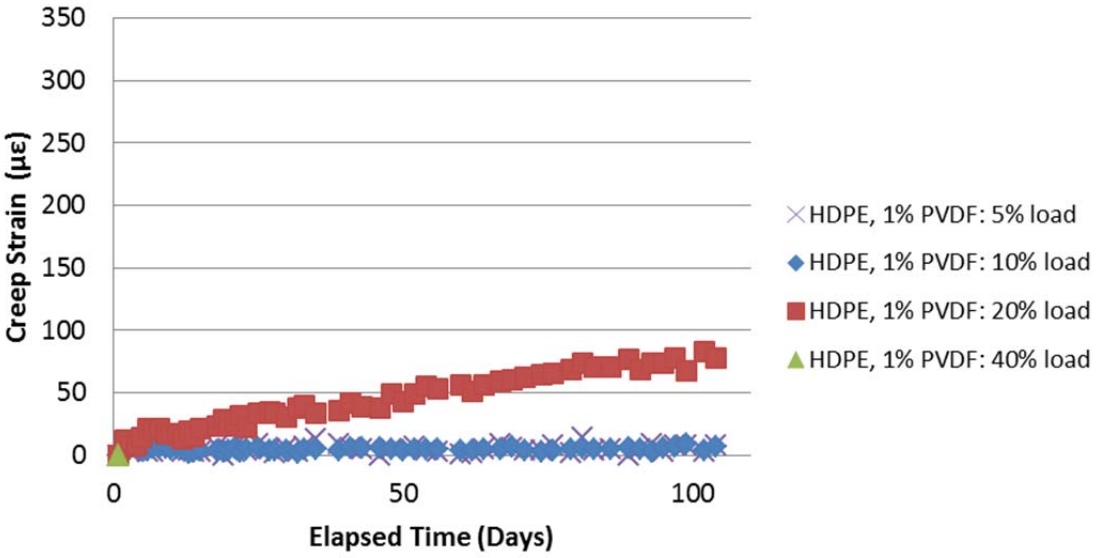

Figure G-196 - Creep strain vs. elapsed time plots for prototype macrofiber containing HDPE and 1% PVDF

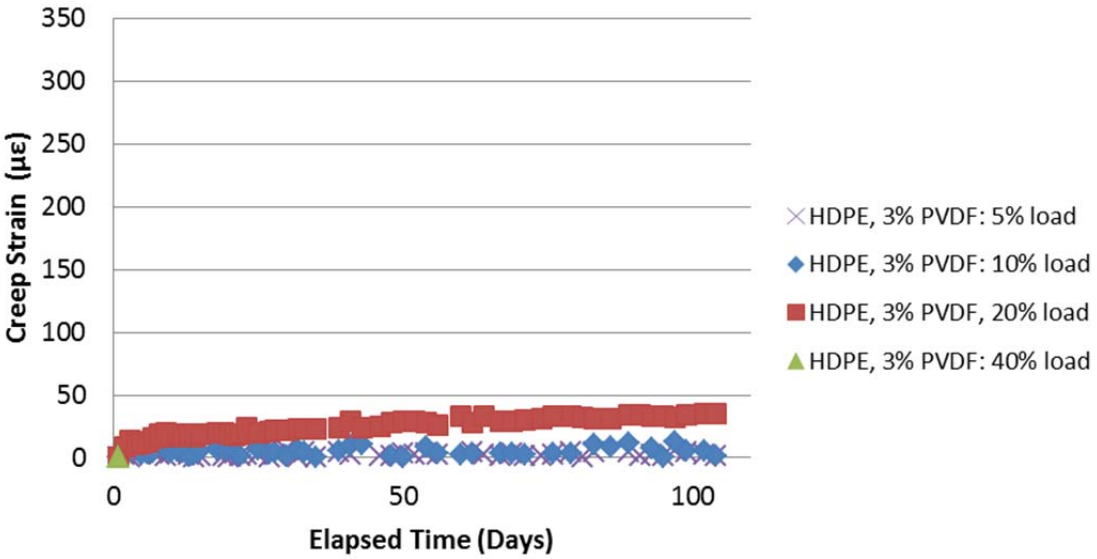

Figure G-197 - Creep strain vs. elapsed time plots for prototype macrofiber containing HDPE and 3% PVDF

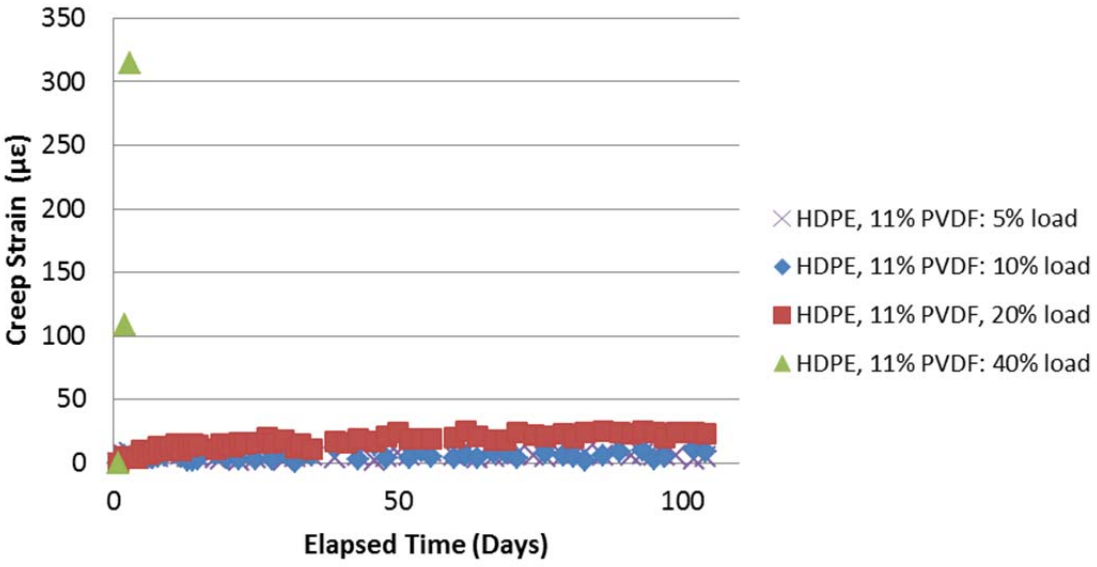

Figure G-198 - Creep strain vs. elapsed time plots for prototype macrofiber containing HDPE, 11% PVDF and 20% MAH

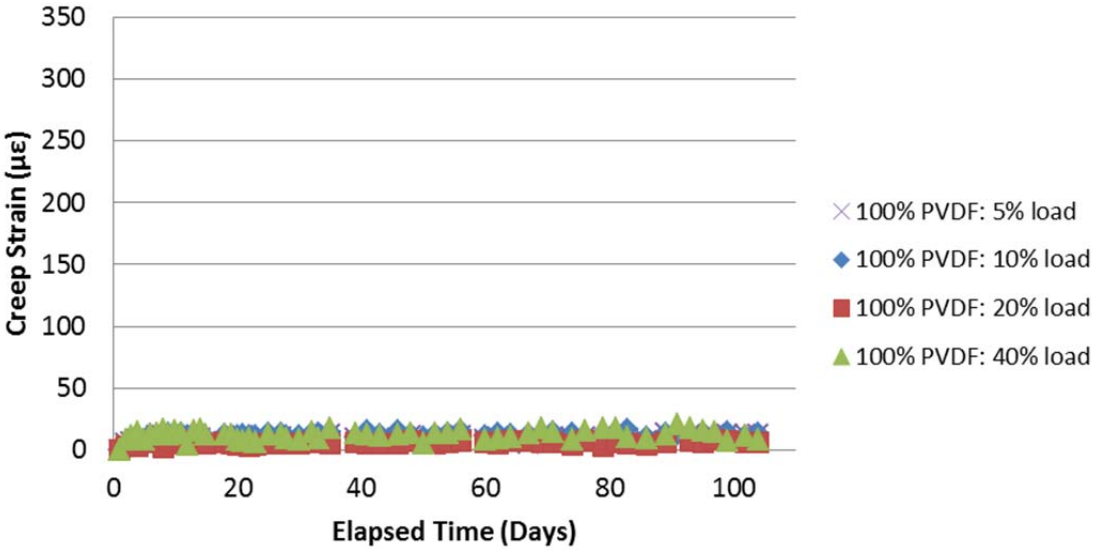

Figure G-199 - Creep strain vs. elapsed time plots for prototype macrofiber containing 100% PVDF

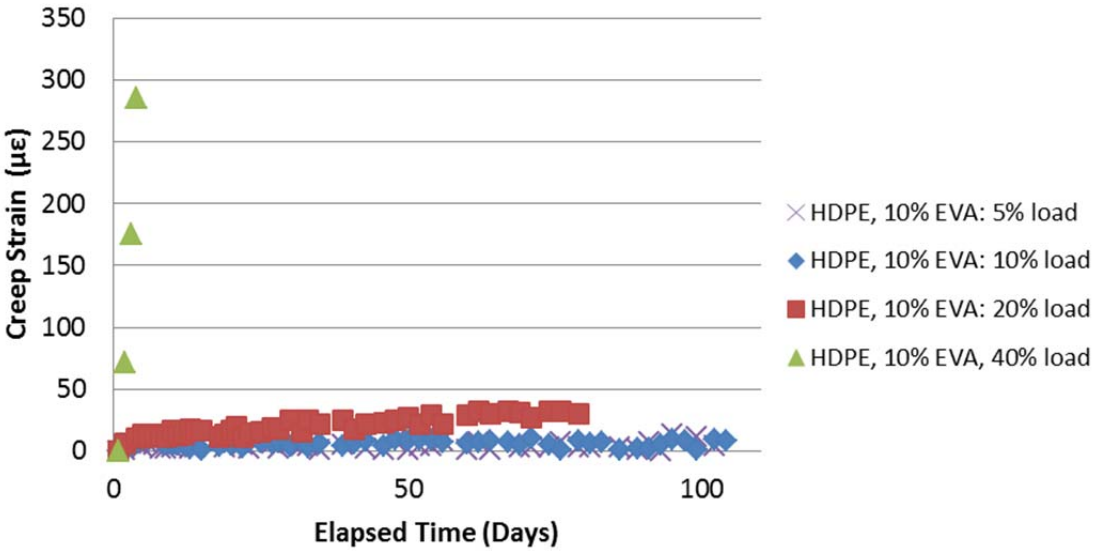

Figure G-200 - Creep strain vs. elapsed time plots for prototype macrofiber containing HDPE and 10% EVA

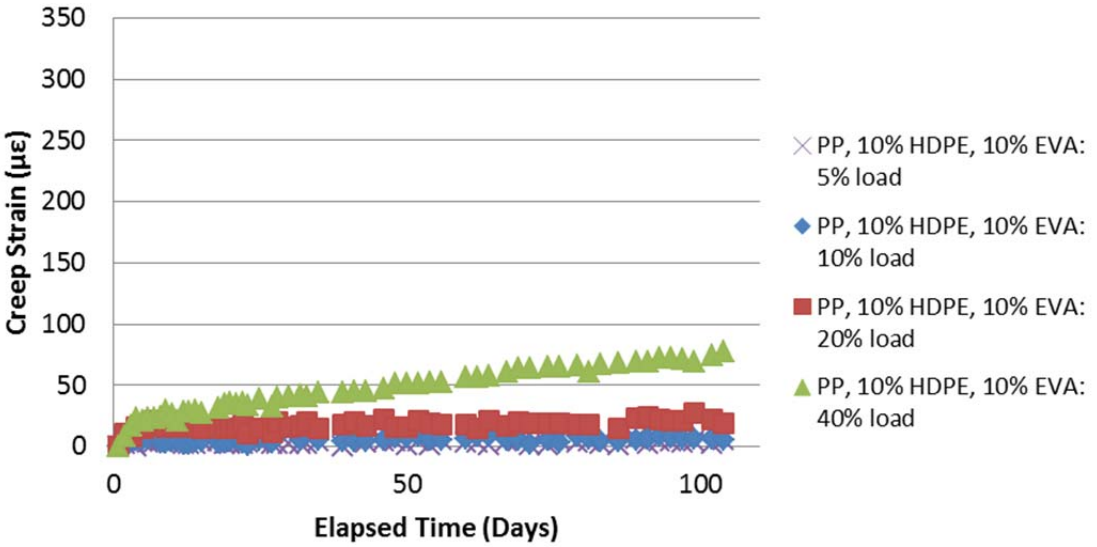

Figure G-201 - Creep strain vs. elapsed time plots for prototype macrofiber containing PP, 10% HDPE and 10% EVA

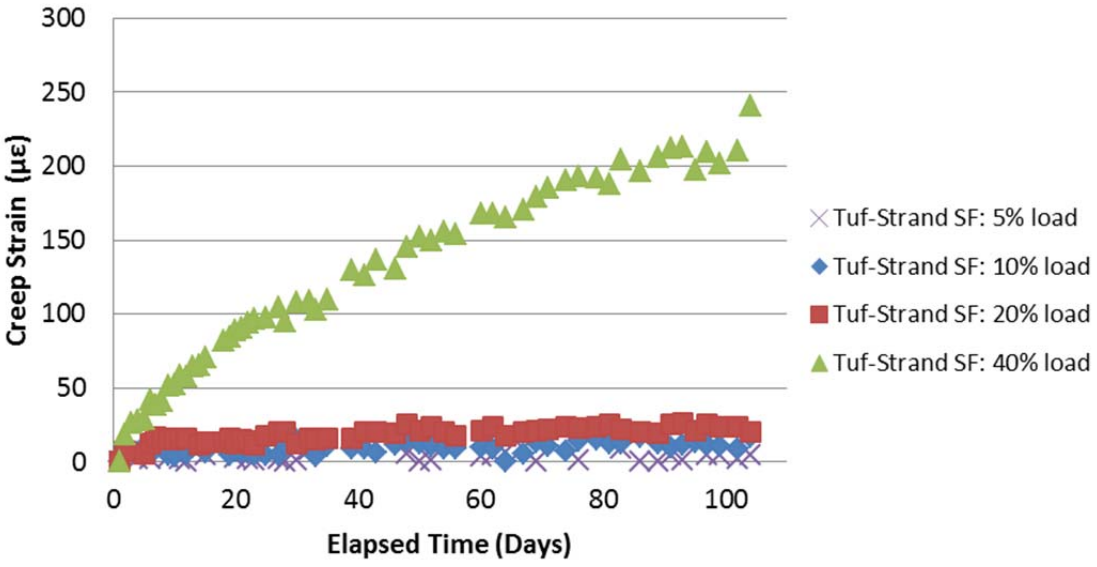

Figure G-202 - Creep strain vs. elapsed time plots for Tuf-strand SF

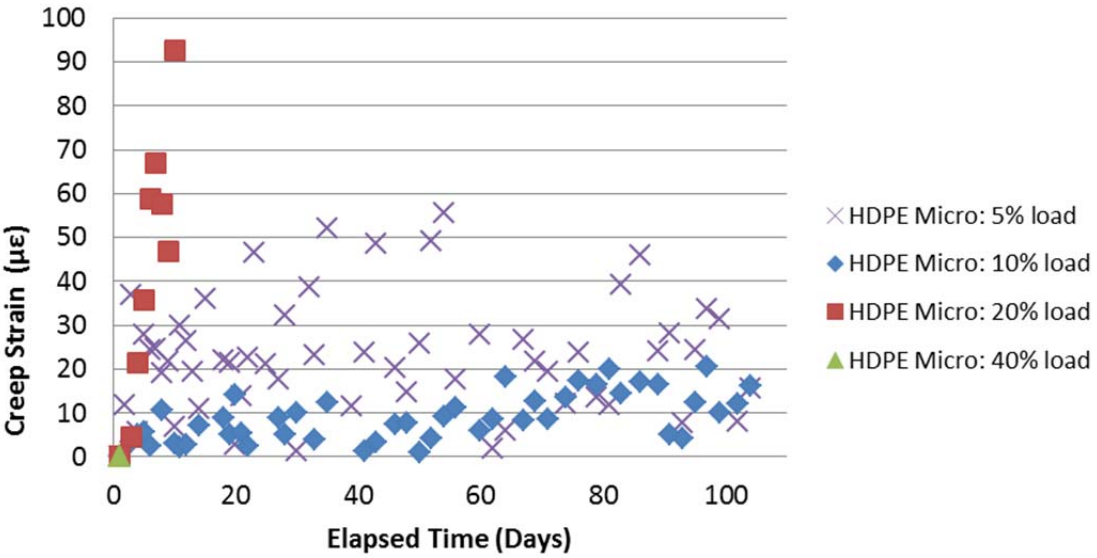

Figure G-203 - Creep strain vs. elapsed time plots for prototype microfiber containing 100% HDPE 5906

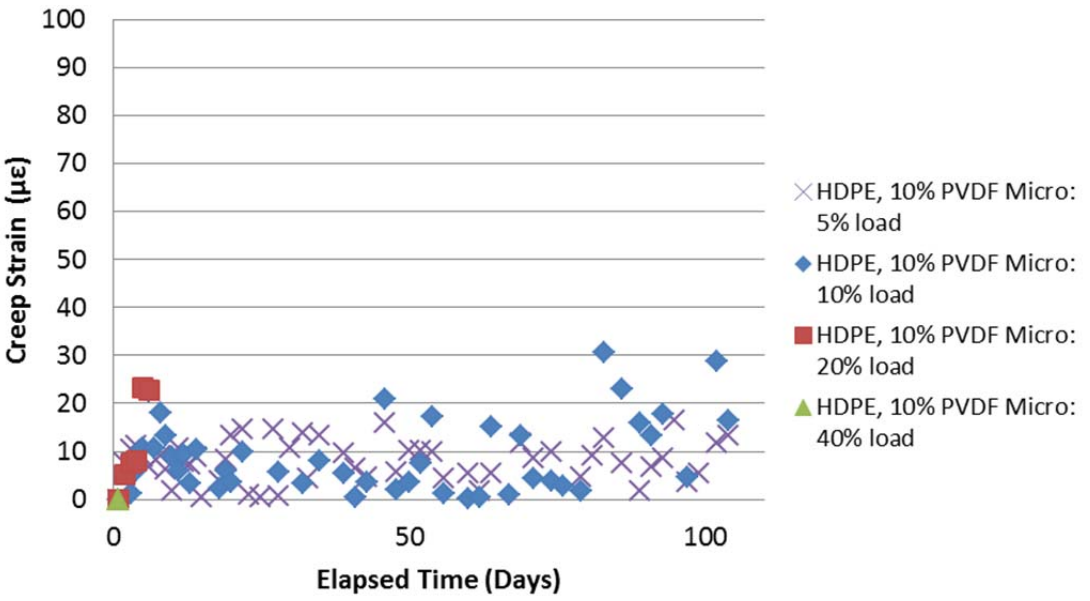

Figure G-204 - Creep strain vs. elapsed time plots for prototype microfiber containing HDPE, 10% PVDF and 20% MAH

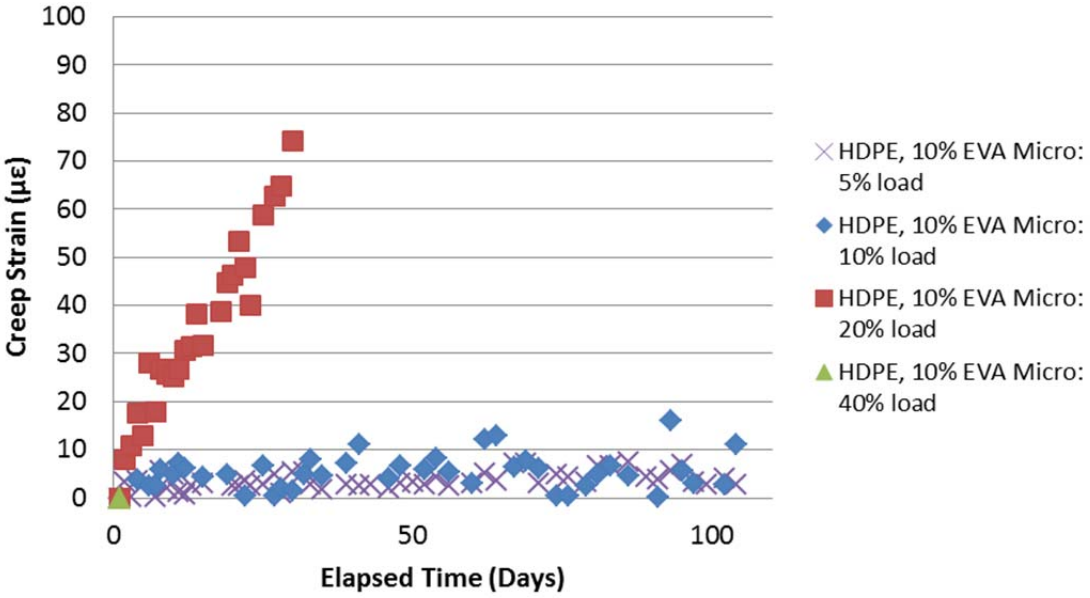

Figure G-205 - Creep strain vs. elapsed time plots for prototype microfiber containing HDPE and 10% EVA